HEAT PIPE TECHNOLOGY

Theory and Applications

Editors

J. H. Boo

K. W. Lee

Heat Pipe Section
Korean Society of Mechanical Engineers

HEAT PIPE TECHNOLOGY

Theory and Applications

HEAT PIPE TECHNOLOGY

Theory and Applications

Proceedings of The 7th International Heat Pipe Symposium,
Jeju, Korea, October 12-16, 2003

Editors

J. H. Boo

Hankuk Aviation University, Korea

K. W. Lee

Korea Institute of Energy Research

with the assistance of

S. Y. Park and W. B. Chung

Hankuk Aviation University, Korea

Principal Sponsor

Japan Association for Heat Pipes

HEAT PIPE TECHNOLOGY - Theory and Applications

Copyright ⓒ Heat Pipe Section, Korean Society of Mechanical Engineers

All Rights Reserved. No part of this publication may be reproduced, stored in a retrieval system or transmitted in any form or by any means; electronics, electrostatic, magnetic tape, mechanical photocopying, recording or otherwise, without prior permission in writing from the copyright holder.

First edition 2004

Heat Pipe Section, Korean Society of Mechanical Engineers
http://www.heatpipe.or.kr

ISBN 89-950046-3-0 93520

Printed in Korea

CONTENTS

Foreword xi
7IHPS Organization xii

Keynote Lectures

A Future Thermal Solution by Using the Family of Heat Pipe 1
M. Katsuta

The Effects of Non-condensable Gases on the Performance of Loop Thermosyphon Heat Exchangers 9
V. Dube, A. Akbarzadeh, J. Andrews, M. Mochizuki

History, Status Quo and Future of Heat Pipe Chemical Reactors 19
J. Zhuang, H. Zhang, Z. Wang

Loop Heat Pipes - Development and Application 31
Y. Maydanik

A Closed Look to a Closed-End Oscillating Heat Pipe 48
P. Terdtoon

Activity of Japan Association for Heat Pipe 63
T. Yamamoto, S. Matsumoto

Natural Flows - Its Nature and Applications – 70
J.H. Lee

Thermosyphons

A Simple Theoretical Model of a Thermosyphon 75
K.S. Ong

An Anti-Gravity Thermosyphon with a Switching Valve 83
H. Imura, Y. Koito, T. Ichinomiya

Experimental Investigation of a Two Phase Closed Thermosyphon 88
S.H. Noie, M.H. Kalaei, M. Khoshnoodi

A Comparison of the Heat Transfer Performance of Thermosyphon Using a Straight Groove and a Helical Groove 94
K.I. Han, D.H. Cho, J.U. Park, S.H. Lee

Creep Behavior of HDPE Thermosyphon under Long Term Operation 100
P. Kamonpet, K. Booddachan, P. Terdtoon, I. Preechawuttipong, Y. Kobayashi

An Experimental Study of a Closed Two-Phase Loop Thermosyphon with Two Evaporators in Parallel Arrangement 104
C.J. Kim, B.O. Yoo, Y.J. Park

Tensile Strength of HDPE Thermosyphon 110
K. Booddachan, P. Kamonpet, P. Terdtoon, T. Sutjaritakul, Y. Kobayashi

Heat Pipes

Analysis of the Optimal Mass of Working Fluid for Heat Pipe with Axially Grooved Wicks 114
J.S. Suh, G.S. Byun, C.H. Kang

Effect of Rotational Acceleration on Internal Flow Patterns of Radially Rotating Heat Pipe at Normal Operating Condition 119
T. Katpradit, N. Waowaew, P. Terdtoon, S. Maezawa, P. Kamonpet, T. Wongratanapaisarn

Study on the Heat Transfer Characteristics in a Copper-Water Variable Conductance Heat Pipe with Non-condensable Gas Reservoir 127
K.H. Park, K.W. Lee, W.H. Lee, K.J. Lee, J.S. Suh

Analysis of Thermal Control Performance of Variable Conductance Heat Pipe with Axially Grooved Wick 133
J.S. Suh, Y.S. Park, K.T. Chung, K.W. Lee, K.H. Park

Performance of Heat Pipes for Solar Collector Using Binary Mixture Working Fluid 140
E.G. Jung, W.B. Chung, J.H. Boo, H.Y. Kwak

A Study on the Heat Transfer Characteristics of Medium Temperature Heat Pipe 146
Y.S. Lee, K.C. Chang, J.R. Kim, Y.S. Jang

Loop Heat Pipes

Transient and Start-up Behavior of a Double-Condenser Design LHP for Monitor of All Sky X-ray Image(MAXI) 151
H. Nagai, M. Muto, M. Murakami, S. Ueno, M. Matsuoka

Miniature Loop Heat Pipes for CPU Cooling 157
V.M. Kiseev, A.S. Nepomnyashy, N.L. Gruzdova, K.S. Kim

Waste Heat Transportation by High-Speed Two-Phase Flow in a Closed Loop with a Vapor Accumulation Evaporator 163
K. Kadoguchi, M. Yamazaki

Heat Transfer Characteristics in an Evaporator Section of a Looped Parallel Thermosyphon 169
F. Kaminaga, C. Feroz, H. Watanabe, K. Matsumura

Heat Transfer Characteristics of Loop Thermosyphon Applied Heat Pump Dryer 175
W. Phaphuangwittayakul, P. Kamonpet, P. Terdtoon, W. Klongpanich, N. Vorayos, G.S.V. Raghavan

Startup and Operating of a Loop Heat Pipe at Different Evaporator Orientations 182
J. Cao, Z. Hou

An Experimental Study on the Operational Characteristics of Closed Loop Type Thermosyphon for Solar Hot Water Heater 187
M.C. Kang, Y.H. Kang, W.G. Chun

Heat Pipe Applications

Thermosyphon Kit for Conversion of Electrical Bakery Ovens to Gas 193
M.B.H. Mantelli, A. Lopes, G.J.M. Martins, R. Zimmerman, R. Baungartner, H.G. Landa

Development of Heat Pipe Heating Roller in Laser Printer 199
K.S. Kim, H.B. Kim, K.W. Lee

Overview Latest Technologies Using Heat Pipe and Vapor Chamber for Cooling of High Heat Generation Notebook Computer 204
M. Mochizuki, T. Nguyen, K. Mashiko, Y. Saito, T. Nguyen, X.P. Wu, V. Wuttijumnong

The Experimental Study on the Improvement of Enthalpy Efficiency of HPHE with Water Spray on Condenser Section 209
J.K. Hong, S.G. Choi, K.O. Yang, Y.S. Byun

Perspective Thermo Control System for a Spacecraft Having Onboard Equipment with Increased Heat Release 216
V. Dvirnyi, V. Dorokhov, V. Bartenev, A. Loganov

The Application of Heat Pipe Embedded Panel for the Transponder of Communication and Broadcasting Satellite (CBS) Payload System 220
J.H. Park, J.S. Choi, S.P. Lee, H.J. Woo

Heat Pipes Applied in Spacecraft 224
J. Miao, X. Shao, T. Li, J. Cao, M. Mi, W. Lv, H. Yang

Thermosyphon as an Energy Saver in Aeroponic System: A Case of Mathematical Modeling 232
N. Srihajong, S. Ruamrungsri, P. Terdtoon, P. Kamonpet, T. Ohyama

Numerical Simulation for the Thermal Design of 1U-2Way Server 238
M.H. Won, W.S. Moon, B.J. Baek, B.C. Pak

Development and Application of Evacuated Tube Solar Collectors with Heat Pipe in Korea 243
H.Y. Kwak, J.H. Boo, W.B. Chung

Cooling of Electric and Electronic Systems

Fundamental Investigations on Heat Transfer Characteristics of Heat Sinks with a Vapor Chamber 247
Y. Koito, K. Motomatsu, H. Imura, M. Mochizuki, Y. Saito

Research and Development of Heat Pipe Heat-sink for CDMA Base Station Power Module 252
J. Zhuang, H. Tao, H. Zhang

A Compact Cooling System with Triple Technologies 257
J.S. Bintoro, A. Akbarzadeh, M. Mochizuki, T. Nguyen

A Generalized Mathematical Model to Account for the Effect of Liquid-vapor Interfacial Shear Stress of a Heat Pipe with a Grooved Wick Structure: Modified Shah Method 264
J.K. Seo, S.J. Kim, K.H. Do

Micro and Miniature Heat Pipes

Theoretical Analysis of Two-phase Heat Spreaders with Different Cross-section Micro Grooves 269
F. Lefèvre, R. Revellin, M. Lallemand

Heat Transfer Characteristics in Flat Plate Micro Heat Pipe 276
M. Katsuta, Y. Homma, N. Hosoya, T. Shindo, J. Sotani, Y. Kimura, Y. Nakamura

Operating Performance of Micro Heat Pipe for Thin Electronic Packaging 282
S.H. Moon, G. Hwang, S.C. Ko, Y.T. Kim

Mathematical Model for Predicting the Transport Phenomena of the Evaporating Meniscus Region in a Capillary Channel 288
K.W. Park, K.S. Lee

Fabrication of Film Type Heat Pipe 294
S.W.Kang, M.C.Tsai, Y.H.Lin

Thermal Performance of a Grooved Flat-Strip Heat Pipe with Multiple Heat Source Locations 300
S.Y. Park, J.H. Boo

The Effects of Various Transverse Accelerations and Their Induced Body Forces on the Cooling Performance of Micro Heat Pipes 306
M. Katsuta, A. Jalilvand, Y. Homma

Mathematical Modeling and Thermal Optimization of a Micro Heat Pipe with Curved Triangular Grooves 312
K.H. Do, S.J. Kim, J.K. Seo

Forced Convective Flows in Microchannels for Cooling Electronic Devices 319
J.Y. Jung, H.Y. Kwak, S.W. Karng, Y.P. Lee

Oscillating Heat Pipes

Thermal Characterization of an Ammonia-charged Pulsating Heat Pipe 325
R.T. Dobson, G. Graf

Refrigerant Fluorinated Ethers and Self-Oscillating Heat Pipe Heat Exchanger for Peltier Cooling System 331
S. Maezawa, K. Gi, J. Sakiura, N. Yamazaki, T. Katoh, H. Akachi

Effects of Evaporator Section Lengths, Number of Turns and Working Fluid on Internal Flow Patterns of a Closed-End Oscillating Heat at Normal Operating Condition 337
S. Rittidech, P. Terdtoon, M. Murakami, P. Kamonpet, W. Jompakdee

Effect of Aspect Ratios and Internal Diameter on Performance Limit of a Closed-End Oscillating Heat Pipe Using Refrigerant Blend as Working Fluid 343
P. Anuchitchanchai, T. Wongratanapaisarn, P. Kamonpet, P. Terdtoon

Experimental Study on Hydration Heat Control of the Mass Concrete Using Oscillating Capillary Heat Pipe 348
J.S. Kim, B.N. Hung, T.H. Kim, J.H. Kim, S.J. Ha, M.S. Kim

Internal Flow Patterns of a Closed-End Oscillating Heat Pipe at Normal Operating Condition: Effect of Internal Friction 353
N. Srihajong, P. Terdtoon, P. Kamonpet, W. Jompakdee, R. Attabhanyo

Effects of Evaporator Lengths, Number of Turns and Working Fluids on Internal Flow Patterns of a Vertical Closed-Loop Oscillating Heat Pipe 360
P. Charoensawan, P. Terdtoon, P. Kamonpet, P. Ingsuwan

Effect of Number of Turns and Working Fluids on Heat Transfer Characteristics of a Closed-End Oscillating Heat Pipe at Critical State 368
T. Katpradit, T. Wongratanapaisarn, P. Kamonpet, P. Terdtoon, A. Akbarzadeh

Mathematical Modeling of a Closed-Loop Oscillating Heat Pipe at Normal Operating Condition 373
P. Sakulchangsatjatai, P. Kamonpet, T. Wongratanapaisarn, P. Terdtoon, M. Murakami

Keyword Index 381

Author Index 383

FOREWORD

The Seventh International Heat Pipe Symposium (7IHPS, in short) was held at Seogwipo KAL Hotel, Jeju-do, Korea from October 12 through 16, 2003. The Symposium was a sequel to a series of Heat Pipe Symposia that was initiated by the Japan Association for Heat Pipes (JAHP). The 7IHPS provided an excellent opportunity to exchange information and experience on the latest advances in heat pipe technology and its application.
Altogether 120 participants attended the 7IHPS from 14 countries, not only from the Asia-Pacific region but also from Russia, Europe, Middle East, South Africa, and South America. The total number of papers presented was 59 and the topic included virtually all aspects of heat pipe science and technology. During 4 days of intensive single-session operation, the participants went through various topics in the field of heat pipes. I believe the 7IHPS was a memorable gathering of academics and engineers who are the forerunners of knowledge in heat pipes.

I would like to express my thankfulness firstly to the Local Organizing Committee. The Committee had a difficult time to change the timetable of the Symposium due to the SARS disease that prevailed until late spring of 2004. The Committee Members were much delighted once the Symposium was held successfully after recovering from the unprecedented problem. However, I regret that quite a few people, who submitted papers and had planned to join the original schedule, were not able to take part in the re-scheduled Symposium at last. I would also like to express my gratitude to the International Advisory Committee of the 7IHPS for their contribution in peer review of the paper drafts and in major decisions we had to make.

On behalf of the Organizing Committee, I would like to express our sincere appreciation to our sponsors leaded by JAHP and KSME (Korean Society of Mechanical Engineers) Thermal Engineering Division. Several companies and institutions in the sponsor list made significant contributions.

I hope that The Proceedings of the 7IHPS will be an important resource for heat pipe scientists and a pleasing reminder of the enchanting time in Jeju-do.

Professor Joon Hong Boo, Chairman of the Symposium

7IHPS ORGANIZATIONS

International Advisory Board:

Prof. A. Akbarzadeh, Australia
Prof. A.A.M. Delil, Netherlands
Prof. M. Groll, Germany
Prof. S. Maezawa, Japan
Prof. K.S. Ong, Malaysia
Prof. P. Peterson, USA
Dr. F. Polasek, Czech Republic
Dr. R.J. Shyu, Taiwan
Prof. P. Terdtoon, Thailand
Dr. T. Yamamoto, Japan
Prof. J. Zhuang, China

Local Organizing Committee:

Prof. J.H. Boo (Chairman, *Hankuk Aviation Univ.*)
Dr. K.W. Lee (*Korea Institute of Energy Research*)
Prof. J.S. Kim (*Pukyong National Univ.*)
Dr. Y.S. Lee (*Korea Institute of Energy Research*)
Mr. S.S. Kim (*Daehong Enterprise Co., Ltd.*)
Dr. K.S. Kim (*Apack, Inc.*)
Dr. Y.P. Lee (*Korea Institute of Science and Technology*)
Prof. J.S. Suh (*Gyeongsang National Univ.*)
Prof. C.J. Kim (*Sungkyunkwan Univ.*)
Prof. K.H. Choi (*Cheju National Univ.*)

Secretariats, principal

Mr. S.Y. Park
Mr. W.B. Chung

Supporting Organizations:

Japan Association for Heat Pipes
Korean Society of Mechanical Engineers, Thermal Engineering Division
Daehong Enterprise Co., Ltd.
Apack, Inc.
DongHwa Entec
Seki Hi-Tech Co., Ltd.
Hankuk Aviation University
Ruytech Co., Ltd.
DF Tec.
Saewoon Sys-Tech

A Future Thermal Solution by Using the Family of Heat Pipe

Masafumi KATSUTA
Waseda University, 3-4-1 Ohkubo, Shinjuku-ku, Tokyo, Japan 169-8555
Tel/Fax: 03-5286-3251
e-mail:katsuta@waseda.jp

Abstract

Because of the rapid increase in the clock speed in high performance CPU and the integration density in a multi-function SOC (System on Chip), a new concept of cooling device instead of traditional heat pipe will be required in the near future.

In the present paper, newly developed oscillatory flow type heat pipe, in particular, the current research trend of the bubble driven heat pipes (so called LCHP, Pulsating or SEMOS Heat Pipe) are introduced as the candidates of micro and/or flexible heat transport device. Additionally, a unique application of SEMOS heat pipe in Korea is referred to prove the extremely high potential for application of this kind heat pipe.

Finally, the detailed characteristics of capillary pumped loop and/or loop heat pipe and future possibilities are discussed.

Key word: Future thermal Solution of CPU, Family of Heat Pipe, LCHP, SEMOS, CPL. LHP

1. INTRODUCTION

Recently, Fujikura news[1)], a commercial announcement published by Fujikura, one of the major heat pipe product companies in Japan, reported new products called “Composite wick type heat pipe”. According to this report, the rapid increase in the clock speed in high performance laptop PC becomes 2GHz and this clock level approaches almost the same level of desktop PC. Nowadays, the heat dissipation from the Pentium 4 Mobile processor reaches at more than 35W and the demand for thermal resistance of cooling system should be lower than 1.4K/W. There are two possible solutions, namely the development of a bland new cooling device (break-trough is needed instead of heat pipe with wick) and the improvement of maximum heat transport rate of a traditional heat pipe itself. They recognized that the latter was an important issue and they developed a composite wick type heat pipe having the heat transport capacity more than 50W and thermal resistance was successfully reduced more than 50% compared with the former cooling module. The examples of heat pipe packaging for the Pentium 4 Mobile processor and for laptop PC are shown in Photos 1 and 2 respectively. As shown in these photos, it is recognized that not only a couple of composite heat pipes are mounted on the module, but also various other technical innovations are made to ensure the severe cooling demand.

The above-mentioned article on the new product for processor cooling system symbolizes the present situation of heat pipe family (HTDS) application for semiconductor technology. Generally, the technical development of an advanced computing system has been directly in connection with as available cooling solution for its reliable operation. For PC, since the coolant is limited to air and the heat transfer coefficient of air is very small, the combination of high performance heat sinks and heat spreaders is necessary to cool efficiently the chips by air. In addition, since PC are rapidly becoming thinner, the heat sink should be more compact and the heat spreader should be thinner. The most crucial point is the rapid increase in the clock speed in high performance CPU and the integration density in multi-function Soc.(System on Chip), a new concept of cooling device is required in near future to overcome these situations. As an alternative candidates of a micro heat pipe, various kinds of new heat pipe concepts, here referred as term “family of heat pipe”, such as SEMOS heat pipe (Self-Exciting Mode Oscillating heat pipe), oscillating heat pipe, PHP (Pulsating heat pipe) and CPL (Capillary heat pipe) have been proposed and extensively studied. Among these, SEMOS heat pipe, Dream heat pipe, CPL and (flat plate micro heat pipe) are introduced in this paper and a comparison of performance of these devices is made.

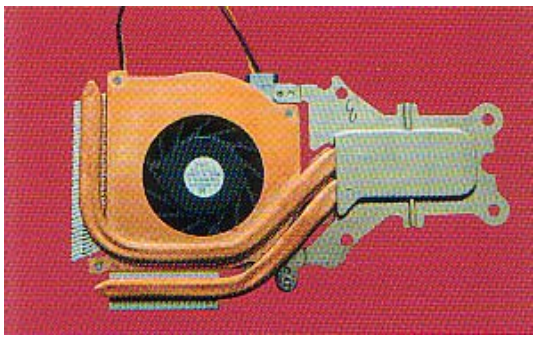


Photo 1 35W Cooling Module for Pentium 4 Mobile Processor

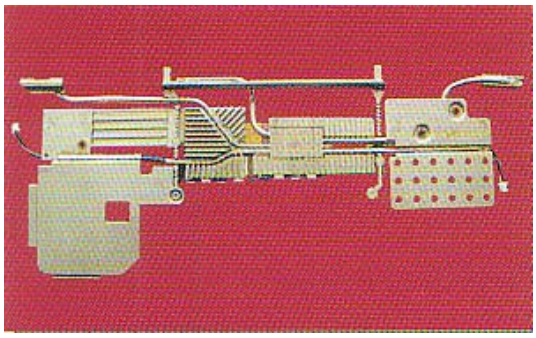


Photo 2 Heat Pipe Cooling Module for Note Book PC

2. OSCILLATORY FLOW TYPE HEAT PIPE

The oscillatory type heat pipe utilizing the forced oscillatory longitudinal flow of enclosed working fluid joined the family of heat pipe about 20 years ago. One is called Dream Pipe or Cosmos Heat Pipe (NISHIO)[2] , it consists of capillary bundle filled with working fluid and oscillation driving unit, which generates the forced sinusoidal oscillatory flow. The principle of heat transport in forced oscillatory flow type is the enhanced heat diffusion similar to the extraordinary mass diffusion in both steady and oscillatory viscous laminar flows within the tube which was first investigated by Taylor[3]. In 1984, Kurzweg and Zhao[4) 5)] invented the synchronized forced oscillatory type and it is called as “dream pipe”. Dream pipe attracted attention in heat pipe community and manufacturers to make up the weak point typical of the heat pipe with wick, namely their own limitation in heat transport rate such as capillary limit, sensitivities to the concentration of non-condensable gases and necessity of internal mechanism returning working fluid from the cold to hot section, even though dream pipe needs forced driving unit. The outstanding review on this oscillatory type heat pipe by Nisho was presented at 12th International Heat Pipe Conference held in Tokyo 1999. [6)]

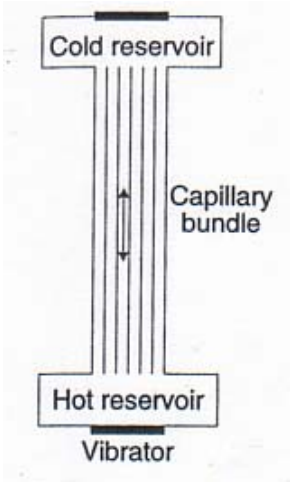


Fig. 1 Dream Pipe

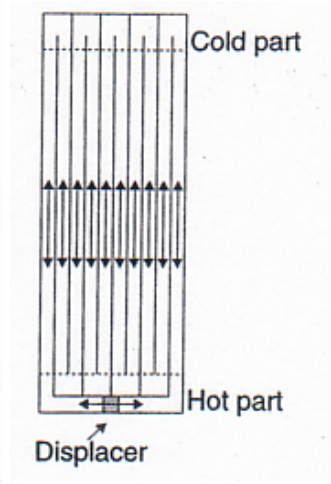


Fig. 2 COSMOS Heat Pipe

3. CLASSIFICATION OF HEAT PIPE FAMILY BY INTERNAL RETURNING MECHANISM OF WORKING FLUID

Basically, the heat transport mechanism of traditional heat pipe is attributed by the latent heat. Since the heat transport automatically terminates due to the lack of working fluid in the evaporation part if they have no mechanism for working fluid return, they need an internal mechanism returning the working liquid from the cold and hot section. Various kinds of these mechanisms have been proposed : gravity for two-phase thermo-syphon, centrifugal force for rotating heat pipe, capillary force for wick, groove, artery and composite wick heat pipe. In addition, osmotic pressure and bubble induced self-oscillating motion were recently suggested. These mechanisms should be selected depending on the structure and the application mode of heat pipe. The major and typical mechanisms in practical use are ①capillary pressure generated by wick, ②gravity and centrifugal force and ③ bubble induced self-oscillating motion. Among these mechanisms, the latest interest of heat pipe community focused on the third one, which is superior performance to compare with traditional heat pipe by using capillary pressure generated by wick. Nowadays, many researches on this novel heat pipe have been conducted in the last decade.

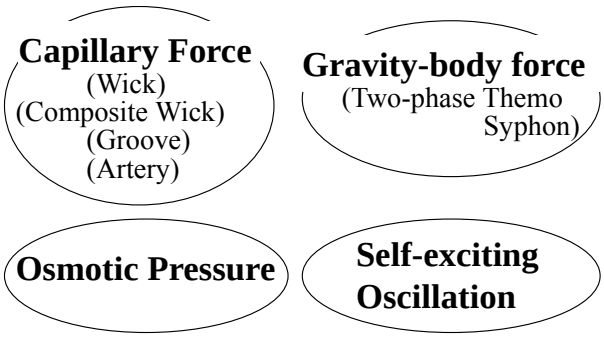


Fig. 3 The Major and Typical Mechanism for Woring Fluid

4. BUBBLE DRIVEN HEAT PIPE[7) - 11)] (LCHP, PULSATING OR SEMOS HEAT PIPE)

The bubble driven heat pipe is a novel heat transport device, which was invented by Akachi[12)] and originally named as the looped capillary heat pipe, LCHP. Other names as mentioned in this chapter's title are also used for this kind of heat pipe. In LCHP, the hot and cold sections are mutually connected by a closed loop of a meandering tube, and the working liquid of a volume fraction is enclosed in the meandering loop. The inner diameter of the tube is selected so small that vapor bubbles can grow up to vapor plugs in the tube. Because the distribution of the vapor plug is not uniform in the loop, pressure difference between high and low void regions is generated as follows; the evaporation heat transfer promotes in low void region, on the other hand in high void region the condensation heat transfer is enhanced, then the pressure difference induces the self exciting oscillatory motion.

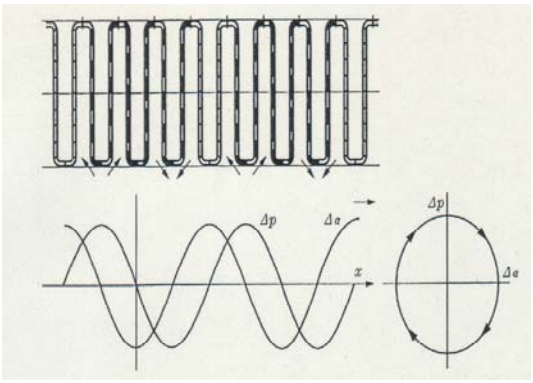


Fig. 4 Analyzing Model of Oscillating Heat Pipe

5. THE CHARACTERISTICS OF BUBBLE DRIVEN HEAT PIPE

As mentioned above, to a certain extent the small inner diameter tube is suitable, in order to fill up the vapor plug in the tube. This feature contributes to overcome the main problem in application of micro heat pipe for PC that is decreasing the inner diameter, the capillary limit in heat transport rate decreases rapidly below a value needed for the heat spreader. According to the recent experimental research by Nishio et al.,[13)] when R141b is applied as the working fluid, the SEMOS hear pipe is successfully operated from 0.5 to 5mm of inner diameter tube. They summarized the merit and characteristics of SEMOS heat pipe as follows:

(1) Since it is unnecessary to arrange an internal mechanism returning the working liquid, the structure of SEMOS heat pipe is extremely simple. The dependency of non-condensable gas, namely the initial degree of vacuum, on the performance is very weak.

(2) Based on their experimental results, the heat transport density (heat transport rate divided by cross sectional area) becomes higher with decreasing inner diameter of tube. When R141b is applied as the working fluid, this value with using 0.5mm inner diameter SEMOS heat pipe reaches at 1000W/cm^2 as shown in Fig.5.

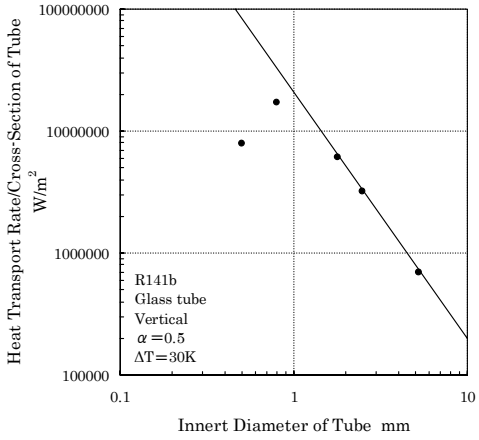


Fig. 5 Effect of Tube Diamiter on Heat Transfer Density

(3) This value corresponds to the maximum heat transport rate is sufficiently higher than that of traditional heat pipe with wick (50W/cm^2).

(4) An optimization of channel dimensions is performed (achieved), SEMOS heat pipe can operate in both directions, which means both of bottom and top heat modes and obtain the same performance.

Compared with the traditional wick type heat pipe, this SEMOS heat pipe has great advantageous characteristics for the micro heat pipe application. However, the state of

knowledge about this heat pipe is still insufficient. For example, an optimum design (material for channel, number of turn, length of hot and cold section) is not made clear in experimental results and the model for numerical analysis is not established. An application area of SEMOS heat pipe very wide as micro heat pipe and the possibility expands not only thermal management of semiconductor device but also heat recovery system for waste heat at low temperature level.

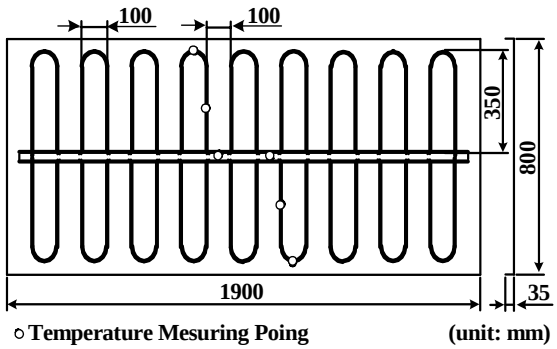
6. INTERESTING APPLICATION OF SEMOS HEAT PIPE FOR HEATING SYSTEM IN KOREA

Ondoru is a Korean original traditional floor heating system[14] and this system has following advantages: this is a system without a radiator (the floor is used as radiator), in addition dust and noise free system. Even at low room temperature, thermal amenity is much higher to compare with other heating system. In Korea, because this floor heating system is used 5 or 6 months per year and most of energy source are LPG or fossil fuels, the improvement of performance directly affects the saving energy and heating cost.

Kim proposed a real application of SEMOS heat pipe (he refers this heat pipe as OCHP) for Ondoru, this floor heating, namely this application seems to be technical innovation for native Korean culture. As shown in Fig. 6, they developed an OCHP floor-heating panel, being 9 turns flexible heat pipe with 100mm in interval and 350mm in length. Its inner and outer diameter is 3.1 and 4.0mm respectively. Hot water line made of rectangular copper channel is placed on centerline of this OCHP.

They carried out a feasibility field test of this floor heating panel installed to urban apartment located in central Buzan in Korea. Experimental results obtained from feasibility test are represented in Figs. 7 and 8 compared with popular heating system until now in Korea (denoted as PE pipe type). The comparison between floor surface temperature and room temperature history during unsteady state are made in Fig. 7. Based on the both results, the thermal response of OCHP heating is superior to that of PE pipe heating. They also measured the circulated hot water flow rate and LPG consumption rate during same period as mentioned above to confirm the energy saving of OCHP system and the results are shown in Fig. 8. Until 60mins from start up, the almost same tendency was observed in both system, however beyond this period consumed energy, i.e. both indices, gradually decreases and achieved approximately 24% (LPG consumption rate base) energy saving. Under the steady state, they confirmed that this new system has 30% energy saving potential to compare with PE pipe system. They concluded that the OCHP type heating system can be operated with the smaller flow rate, less electric power and LPG consumption than those of PE pipe type heating system.

Kim successfully established a venture company (named 3R) selling this OHP type floor heating panel in his university. This is an unique example of SEMOS heat pipe application and, in fact, this is proving the extremely high potential for application of this heat pipe and the application is not limited to cooling of semiconductor.

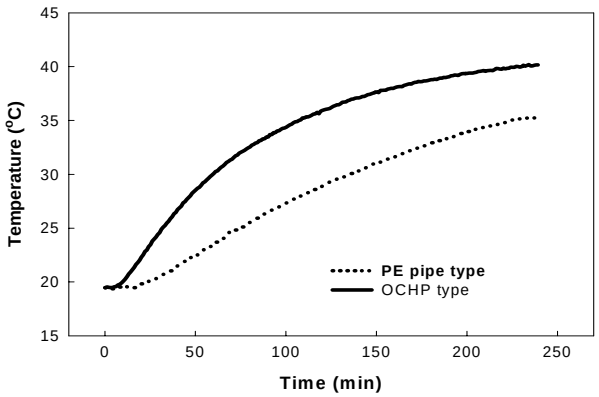


(a) Schematics of Feasibility Test Apparatus

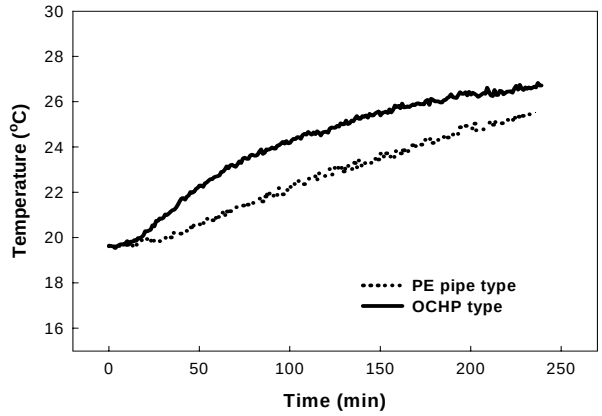


(b) Photograph

Fig. 6 Heat Pipe Type Panel for Floor Heating

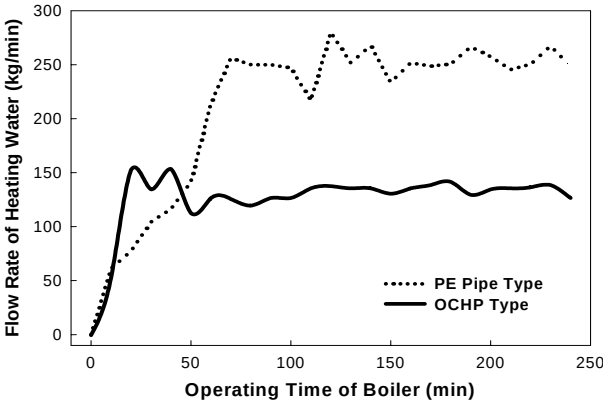


(a) Floor Surface Temperature

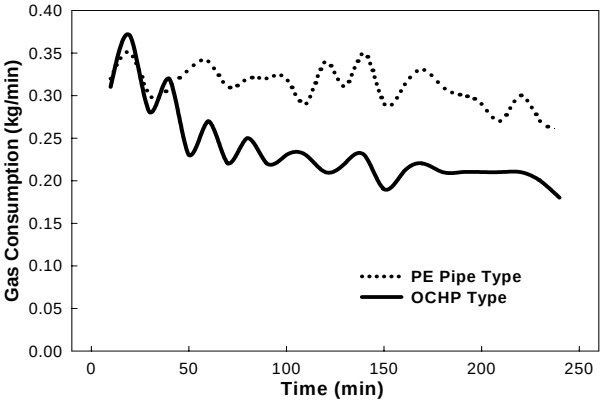


(b) Indoor Ambient Temperature

Fig. 7 Temperature Variation during Transit State



(a) Flow Rate of Hot Water



(b) Consumed LP Gas at Boiler

Fig. 8 Variations of Hot Water Flow Rate and Energy Consumption Rate during Transient State

7. OTHER CANDIDATES HAVING A POTENTIAL FOR WIDE APPLICATION-CAPILLARY PUMPED LOOP-

Author's Group has designed CPL for Japanese Satellite[15) 16)], named Users (as shown in Photo 3), which was launched in September 2002, and is accumulating CPL performance data in space. Photo 4 represents the radiator of the CPDR (Capillary Pumped Deployable Radiator). This radiator can be deployed in space like a solar paddle. The CPDR mainly consists of the control unit, the power supply unit and CPL unit as shown right side of Photo 4. Until now, data from Users are favorite condition and, hopefully, CPL experiment will be successfully finished. These data can be presented on the symposium site.

Taking the possibility of wide application beside semiconductor cooling into consideration, this CPL and Loop type heat pipe seem to be other candidates of traditional family of heat pipe. The CPL consists of evaporator pump, a condenser, a reservoir which functions as an inside pressure regulator, an isolator with wick structure to prevent the inverse flow from the evaporator pump to a liquid line at the start up stage, a liquid line and a vapor line connecting the evaporator pump and condenser. Fig. 9 and 10 shows a prototype of CPL for space use. It is well-known fact that the principal of heat transport mechanism of CPL is almost same as that of heat pipe with wick, however, wick structure for CPL is only installed in evaporator section and other components can be appropriately selected. Our experimental results on performance limit of the above-mentioned CPL are shown in Fig. 11 to 13.

Because detailed numerical analytical model has developed and completed, CPL and Loop heat pipe have an ability of downsizing by using multi-evaporator and condenser accompanied with the development of high performance wick. This possibility appeals to an attractive attention of an application for low temperature region, also semiconductor cooling and other wide areas in near future.

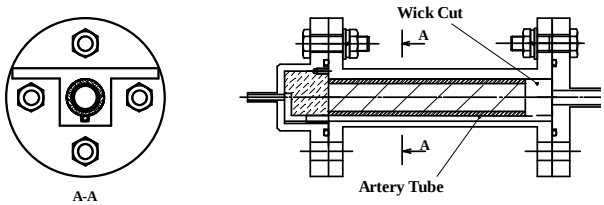


Fig. 9 Details of Evaporator

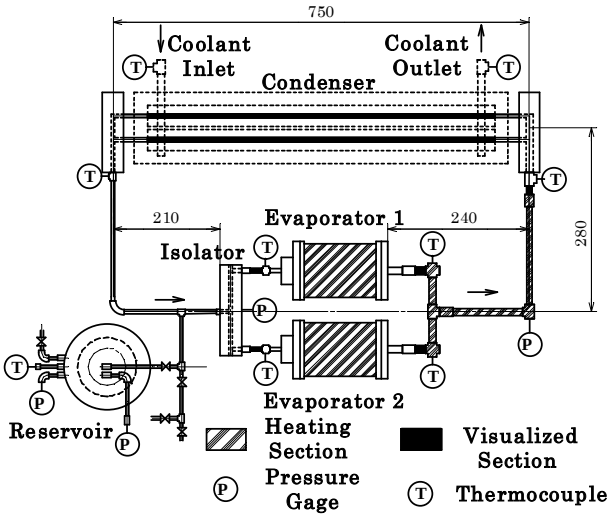


Fig. 10 Schematics of Experimental Set Up

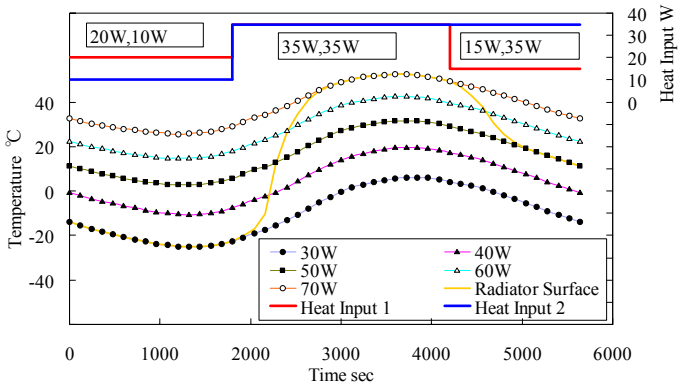
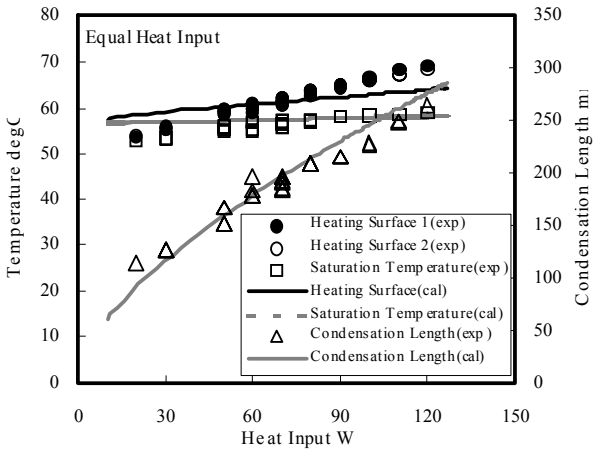
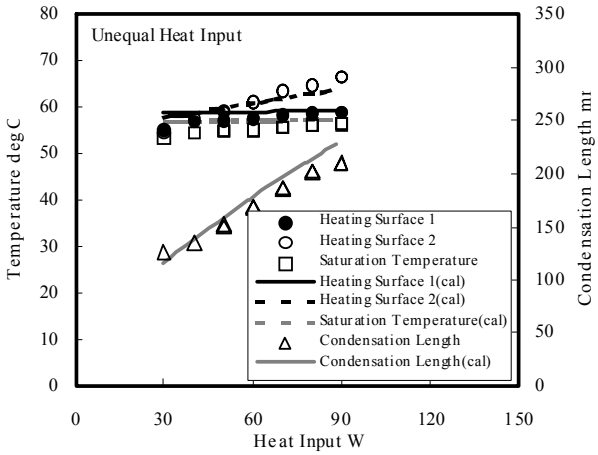


Fig. 12 Simulation of the Operating Conditions for USERS' CPL



(a) Equal Heat Input



(b) Unequal Heat Input

Fig. 11 Predicted and Experimental Results of Steady-state Condition

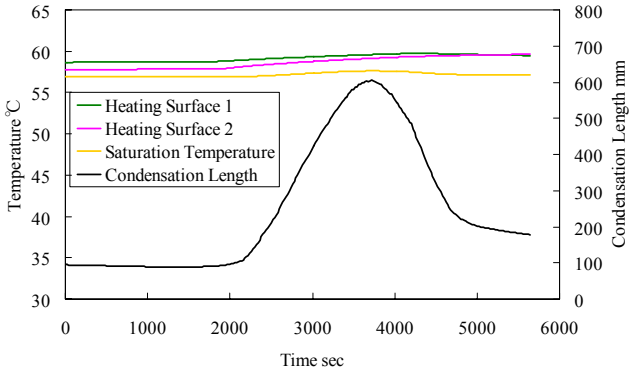


Fig. 13 Predicted Results of Loop Response for USERS' CPL

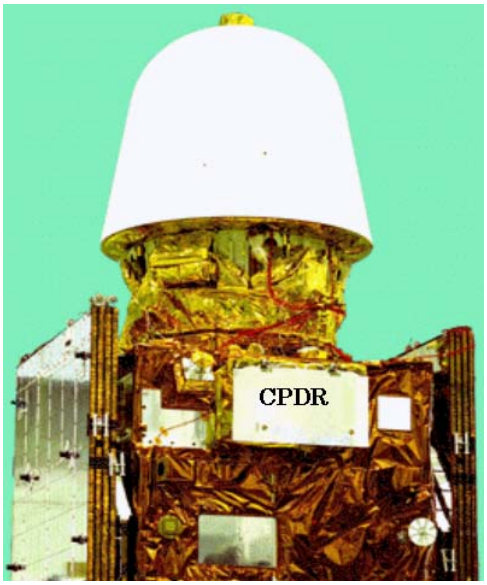


Photo 3 USERS (CPDR on the Orbiter)

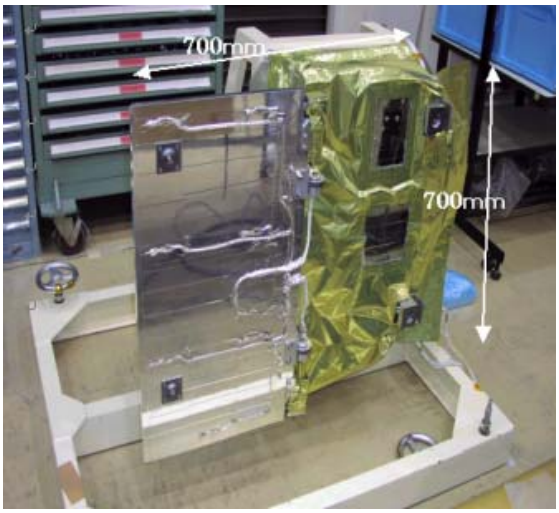


Photo 4 CPDR Configuratior (Open Radiator)

8. CONCLUSIONS

Bubble driven oscillatory heat pipe, an original technology from Japan, is now progressing the fundamental researches and developments as the candidates for micro and flexible heat-transport devices. Experiments for operation (working confirmation) confirmation are conducting under systematically changed principal parameters and the establishment of design method and the model for numerical analysis are still required.

Additionally, the performance of heat transport, operational temperature range, the suitable working fluid and the optimum filling ratio and so on should be make clear.

On the other hand, the fundamental researches and developments stage on CPL and LHP has almost finished. In particular, the development of optimum design method and investigation of reliability will be the next subject for research on CPL and LHP.

Reference

1) Fujikura News, No.261, April 2003 (email : netsu-info@fujikura.co.jp)
2) S. Nishio, Fine Diameter Heat Pipe by using Oscillatory Flow, The Energy Conservation, Vol.55, No.4, P.22-23,(2003-5). (In Japanese).
3) G.I. Taylor, Dispersion of Soluble Matter in Solvent Flowing Slowly Through a Pipe, Proc. Roy. Soc. London, A219, PP.186-203, (1953).
4) U.H. Kurzweg and L. Zhao, Heat Transfer by High Frequency Oscillations: A New Hydrodynamic Technique for Achieving Large Effective Thermal Conductivities, Phys. Fluids, Vol.27,pp.2624-2627,(1984).
5) U.H. Kurzweg, Enhanced Heat Conduction in Fluids Subjected to Sinusoidal Oscillations, J. of Heat Transfer, ASME, Vol.106, pp.459-462, (1985).
6) S. Nishio, Oscillatory-Flow Heat-Transport Device (Forced Oscillatory Flow Type and Bubble Driven Type), Heat Pipe Science and Technology, JAHP, p.39-49, (1999).
7) S. khandekar, M.Groll, P.Charoensawan and P.Terdtoon Pulsating Heat Pipe: Thermo-fluidic Characteristics and Comparative Study with Single Phase Thermosyphon, Heat Transfer 2002, Grenoble, P.308
8) M. Hosoda, S. Nishio, R.Shirakashi, Study of Meandering Closed-Loop Heat –Transport Device (Vapor-plug Propagation Phenomena), JSME International Journal, Series B, Vol.42, No.4, PP737-744,1999
9) N. Nishio, S. Nagata, S. Baba and R.Shirakashi, Thermal Performance of SEMOS Heat Pipes, Heat Transfer 2002, Greoble, p.311
10) Y. Miyazaki and F. Polasek, Operating Limit of Oscillating Heat pipe, Heat Transfer 2002, Grenoble P.312
11) K. Gi, F. Sato and S. Maezawa, Flow Visualization Experiment on Oscillating Heat Pipe, Proc. 36th National Heat Transfer Symposium of Japan, Vol. Ⅲ, pp.659-660,(1999). (In Japanese).
12) H. Akachi, Looped Capillary Heat Pipe, Japanese patent, No. Hei6-97147,(1994). (In Japanese).
13) S. Nisho, S. Nagata and T.Kubota, Study on Thermal Performance of SEMOS Heat Pipe, Proc. 39th National Heat Transfer Symposium of Japan, Vol. Ⅰ,p.127-128,(2002-6). (In Japanese).
14) J. Kim and S. Bae, Floor heating system using self oscillating type heat pipe, The Energy Conservation, Vol.55, No.4, P.74-76,(2003-5). (In Japanese).
15) M. Katsuta, T.Arai, N.Hosoya and K.Tanaka, Design of capillary pumped loop to be boarded on the artificial satellite (Users) and development of its application heat transport model, Heat Transfer 2002, 12th International Heat Transfer Conference, P.305, (2002-8)
16) K. Tanaka, A. Okamoto, M. Katsuta, K. Ichiji and A. Wakabayashi, Thermal performance of the capillary pumped loop deployable radiator, Heat Transfer 2002, 12th International Heat Transfer Conference, P.306, (2002-8)

Appendix

Author present another paper entitled “Heat Transfer Characteristics in Flat Plate Micro Heat Transfer Characteristics in Flat Plate Heat Pipe” in this symposium. Tables 1 and 2 show the maximum performance data of brand new μHP together with cooling demand of CPU. Judging from these Tables, it is easy to understand that the other technical innovations are required to ensure the severe cooling demand of CPU for mobile use.

Table 1 Maximum Performance of μHP

μHP Type	Maximum Heat Transport [W]	Heat Flux [kW/m^2]
μHP 118mm	10.87	30.19
μHP 200mm	6.55	18.19
μHP 250mm	6.33	17.58

Table 2 Thermal Specifications of CPU

CPU Type	Clock/Voltage	TDP (Max) [W]	Heat Flux(Max) [kW/m^2]
Mobile PentiumIII	500MHz/1.10V	5.0 (8.1)	51.54(83.49)
Mobile PentiumIII	750MHz/1.35V	12.4 (17.2)	127.8(177.2)
Mobile Celeron	750MHz/1.60V	15.8 (24.6)	160.8(253.6)
Mobile PentiumIII	1GHz/1.70V	24.8 (34.0)	234.8(350.4)

The Effects of Non-condensable Gases on the Performance of Loop Thermosyphon Heat Exchangers

V. Dube, A. Akbarzadeh, J. Andrews.
Energy Care Group, School of Aerospace, Mechanical and Manufacturing Engineering,
Bundoora East Campus, RMIT University. PO Box 71, Bundoora, Victoria 3083, Australia
Phone + 613 99256079, Fax: +613 99256108, Email: aliakbar.akbarzadeh@rmit.edu.au

M.Mochizuki
Thermal Engineering Department, Fujikura Ltd.
1-5-1, Kiba, Koto-Ku, Tokyo 135, Japan

Abstract

The effects of 'Non-Condensable Gases' (NCG) on the performance of 'Loop Thermosyphon Heat Exchangers' (LTHE) used in industrial waste heat recovery systems are investigated experimentally and theoretically. The optimum location for installing a reservoir to trap NCG and minimise their adverse effect on effectiveness is identified. A procedure to calculate the size of a reservoir such that all the NCG present in the LTHE system can be trapped in it at a predetermined working fluid temperature is presented. For an NCG-loaded LTHE the temperature determining the onset of heat recovery, the optimum operating temperature and the maximum operating temperature are determined.

Key Words: Loop Thermosyphon Heat Exchangers (LTHE), Non-Condensable Gases (NCG), Waste heat recovery

1. INTRODUCTION

The indiscriminate use of fossil fuels is likely to cause irreversible and deleterious climate change by increasing global greenhouse gas emissions, and is also responsible for polluting air, water and land environments. To minimise these harmful effects, the idea of energy conservation has been brought forward and discussed in many international forums. In the 1997 Kyoto Protocol many countries agreed to reduction targets for greenhouse gas emissions, and hence there has been increasing interest in a wide range of energy efficiency technologies. One such technology is the use of heat exchangers to recover heat formerly wasted in higher temperature industrial processes, for use in lower-temperature heating applications. The present paper focuses on the 'Loop Thermosyphon Heat Exchanger', which potentially has a role to play in industrial waste heat recovery systems. The Loop Thermosyphon Heat Exchanger (LTHE) is a highly-efficient energy-transfer device capable of transferring heat between a heat source and a heat sink separated by a distance of up to 30 m. Since there is no contact between the hot gases in the heat source and the medium to be heated, an LTHE allows heat to be safely recovered even from contaminated exhausts, a capability particularly important in food and pharmaceutical industries [1]. The LTHE works without a pump on the principle of a thermosyphon, and is a device of very high thermal conductance.

In the conventional thermosyphon heat exchanger, the evaporator and condenser sections form a single integrated unit [2]. In the LTHE, however, the evaporator and condenser sections are located some distance apart (Figure 1). The evaporator can be located near the heat source and the condenser near the heat sink. The need for complex and expensive ducting to bring the hot gas stream and the cooler gas stream to be heated close together is therefore eliminated.

In an LTHE at operating temperature, there a number of gases mixed with the working fluid vapour, including in particular nitrogen, oxygen and carbon dioxide. These gases condense at a much lower temperature than that of the condenser, and remain in the gas phase in an LTHE during its operation. Consequently they are described as 'Non Condensable Gases' or NCG. If proper care is not taken these gases can adversely affect the performance of a LTHE. NCG in LTHEs come from the following sources:

- The release of gases dissolved in the working liquid when it boils.
- Gases produced by reactions between the working fluid and the material of the container walls.

- Leakage of atmospheric gases inwards through joints and fittings.

In addition, NCG are sometimes deliberately introduced into LTHEs to change their working characteristics [3]. The present paper focuses on this practice.

The presence of NCG in LTHEs has both disadvantages and advantages. On the one hand NCG reduce the range of applications of LTHEs. On the other hand they introduce some new heat transfer characteristics that can be utilised to advantage in specific applications. Interaction between the non-condensable gases and the condensable gases present in the system, and the resulting change in the flow field in the heat transfer loop, are of prime importance. This paper investigates such interactions by experimental study of the flow mechanisms for condensable and non-condensable gases, and the consequent impact on the thermal characteristics of heat exchangers operating in the 100 – 250°C range (sections 2-4). A theoretical derivation of the temperature determining the onset of heat recovery in an LTHE, the optimum operating temperature, and the maximum operating temperature are presented in section 5. The overall findings of the experimental and theoretical investigations are summarised in section 6.

2. EXPERIMENTAL APPARATUS AND INVESTIGATIONS

A series of experiments were performed to identify the optimum location of reservoirs to trap NCG in an LTHE, and to investigate the relationship between the effectiveness of an LTHE and the quantity of NCG present in the system.

In an inactive LTHE (Figure 1) at room temperature, the NCG present in the system are equally spread throughout the system except for the space occupied by the liquid. When the temperature in the evaporator section increases and the liquid reaches its saturation temperature, the rate of vapour generation increases and this vapour pushes the NCG towards the condenser. We would therefore expect that the NCG would accumulate in the condenser region of the LTHE not the evaporator. Our earlier experimental work also indicated that NCG initially start accumulating at the ends of the condenser headers that were not in the flow path of saturated vapour.

Hence in the experimental apparatus (Figure 1), a reservoir with the associated fittings was installed at each corner of the upper and lower headers of the condenser, that is, four reservoirs in total (labelled A to D), to collect NCG. Reservoirs A and B were located at the left and right ends of the lower header of the condenser, while reservoirs C and D were located at the right and left ends of the upper header. The evaporator and the condenser sections of the LTHE used were identical, each having two rows of twelve tubes. The tops of the 24 tubes in each section were welded to an upper header, and the bottoms to a lower header. To form a loop, the upper header of the evaporator was connected to the upper header of the condenser, and the lower header of the condenser connected to the lower header of the evaporator through adiabatic pipes.

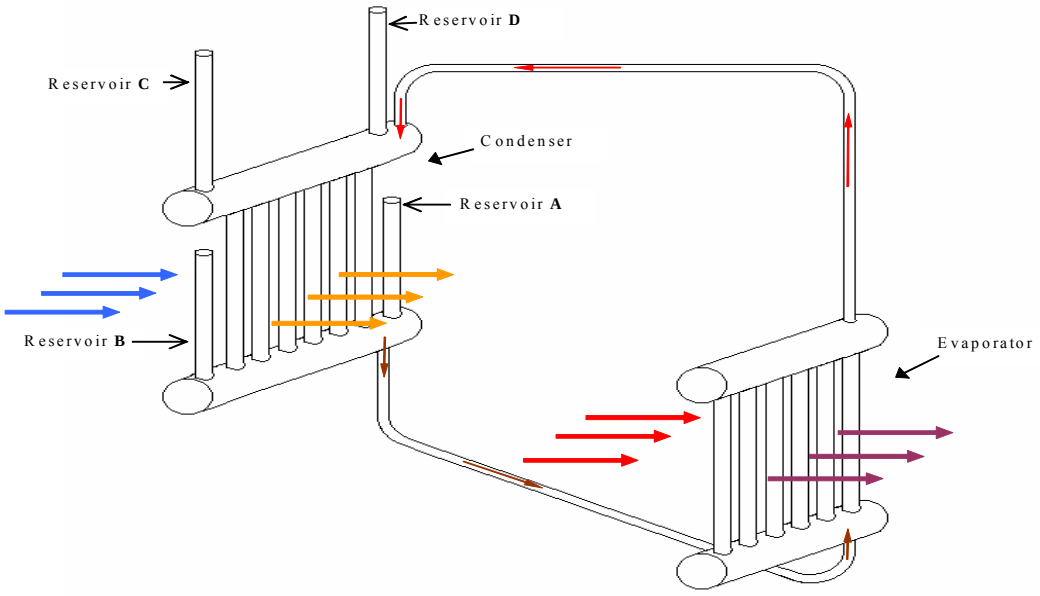


Figure 1 Sketch of an LTHE showing flow direction of working fluid and the location of reservoirs A, B, C, and D

The concentration of NCG in each reservoir was measured indirectly by taking the temperature of its outer surface using a thermocouple. It was assumed that a flat front existed between the working fluid vapour and the NCG, thus neglecting diffusion (and hence mixing) between vapour and NCG. Since the NCG act as a good thermal insulator, as the thickness of the NCG layer between the thermocouple and the working fluid vapour increases the temperature recorded by that thermocouple decreases. Hence the lower the recorded temperature, the higher the concentration of NCG in the reservoir.

A test rig was designed, constructed, thermally insulated and instrumented to measure the effectiveness of LTHEs with differing amounts of NCG present in the system over the specified temperature range 100 – 250 ºC (Figure 2). Evaporator and condenser sections were separated as required in the LTHE configuration, and the working fluid (water) was circulated through headers and adiabatic pipes connecting these sections.

Six experiments were carried out using the test rig to measure the concentrations of NCG in the four reservoirs for different total quantities of NCG – and hence differing pressures at room temperature – within the system, and also the effectiveness of the LTHE under each condition (Table 1). The parameters held constant in all the conditions are also listed in Table 1. The only variable was the air pressure in the inactive LTHE system at room temperature – and hence the amount of NCG present – which was varied progressively from 'maximum possible vacuum' (experiment 1) to 'atmospheric pressure' (experiment 6). The vacuum was created for experiment 1 using a vacuum pump to extract air through a valve located at the top of reservoir A. For the subsequent experiments, ambient air was progressively induced by slowly opening a drain valve located at the lowest point of the LTHE system.

The temperatures of air, vapour, and condensate in and out of the evaporator and condenser were measured by thermocouples placed in the air-stream flow paths within the test rig ducts, and on the outer surface of LTHE tubes and headers. In addition, bimetal analog thermometers were placed at the air inlet and outlet of condenser and evaporator as a second source of data on air-stream temperatures.

Thermograph images of the four NCG reservoirs and condenser face area were taken to measure their temperatures by using an infrared thermal imaging camera as an independent measure of surface temperatures. Temperatures measured by thermograph images were compared with those taken by thermocouples. The temperature discrepancy of within $\pm 3\,\%$ was considered acceptable for these experiments. On the basis of the thermograph images, temperature profiles were thus drawn to obtain the temperature distribution along the surfaces of NCG reservoirs and condenser face area.

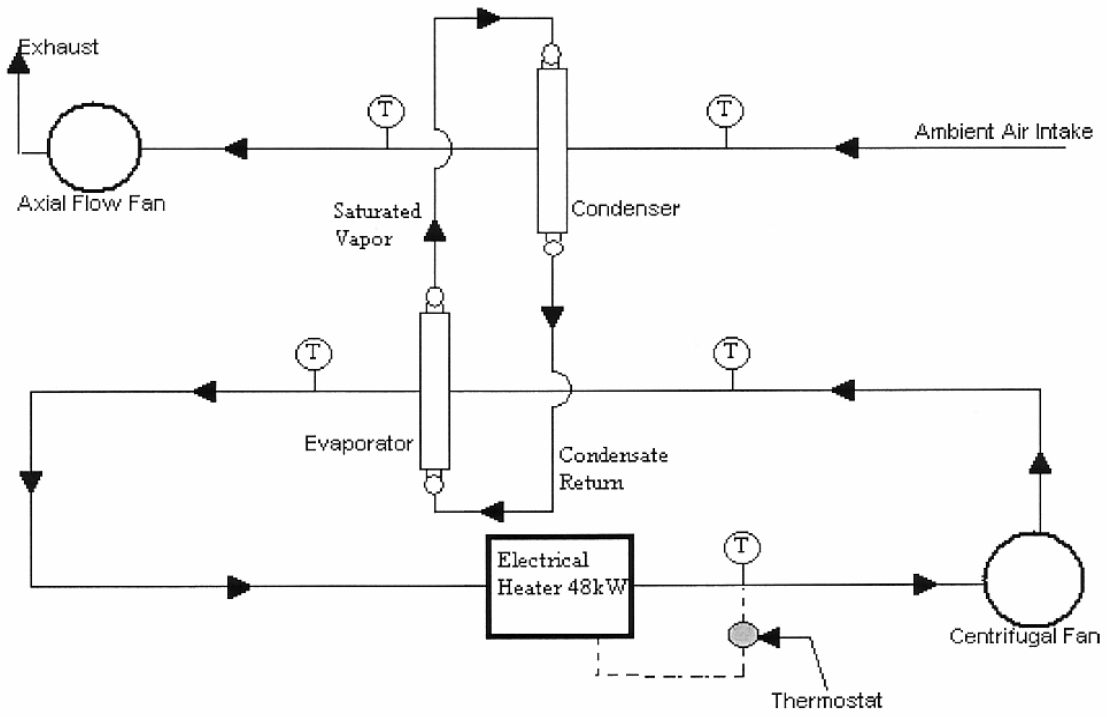


Figure 2 Flow diagram of the double air stream test rig

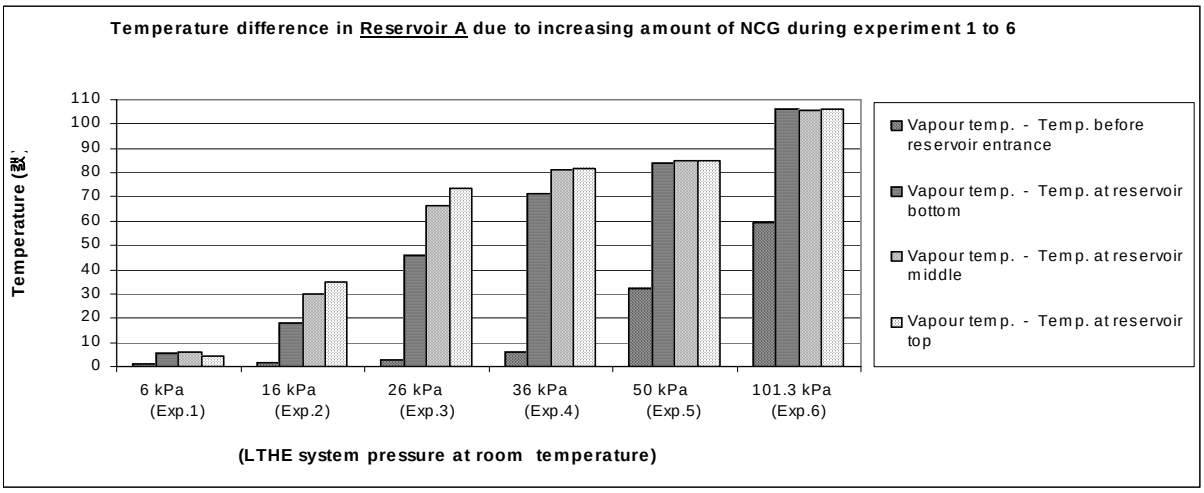
Table 1 The six experimental conditions, and parameters held constant across all experiments

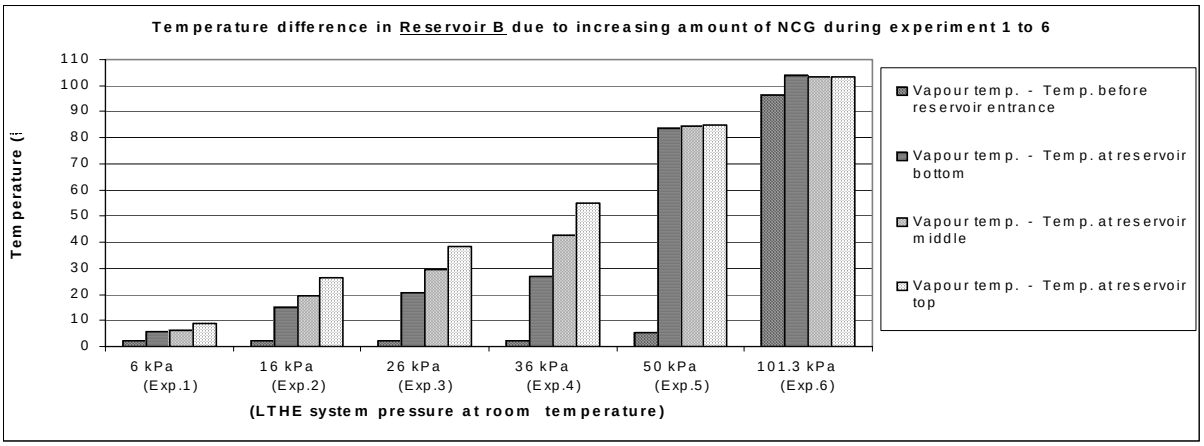
Experiment	**Absolute pressure in system at room temperature**	**Procedure**
1	6 kPa	Maximum available vacuum in the system
2	16 kPa	Absolute pressure in the system increased by 10 kPa by inducing air in the LTHE system.
3	26 kPa	Absolute pressure in the system increased by another 10 kPa by inducing additional air
4	36 kPa	Absolute pressure in the system was increased by further 10 kPa by inducing additional air
5	50 kPa	Absolute pressure in the system was increased by further 14 kPa by inducing additional air
6	101.325 kPa	System pressure equal to atmospheric pressure
Constant parameters		
Inlet air flow velocity to the evaporator		2 m/s
Inlet air flow velocity to the condenser		2 m/s
Inlet air temperature to the evaporator		200°C (approx.) (Varied between 194.7°C and 206.3°C)
Inlet air temperature to the condenser		Room temperature (Varied between 15.1°C and 31.9°C)
Working fluid		Distilled water
Quantity of the working fluid		Sufficient to fill 60% of evaporator section

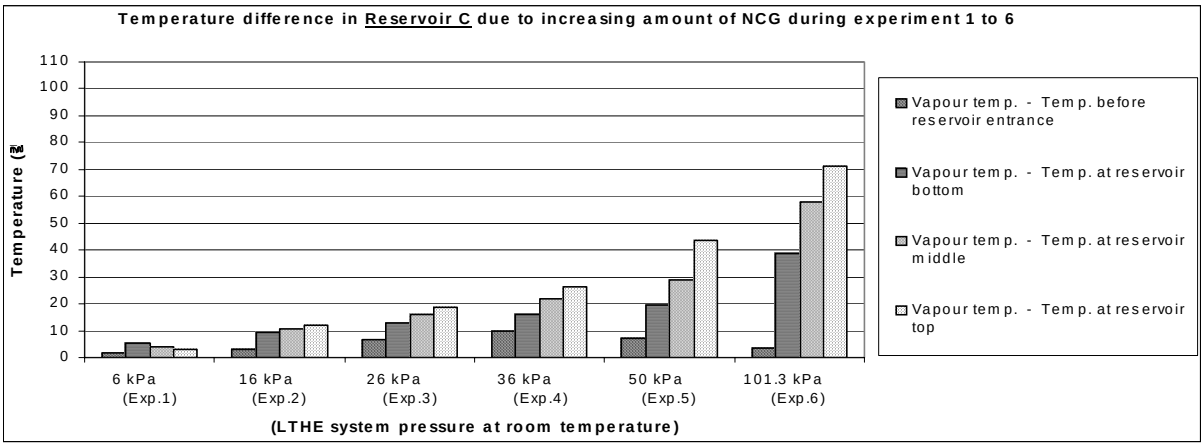
3. EXPERIMENTAL RESULTS

The temperature difference between saturated vapour and the surface of each individual reservoir recorded during experiment 1 was compared with the similar temperature differences recorded during experiments 2 to 6. The variation of these temperature differences with the gradual introduction of NCG into the LTHE system during successive experiments is presented graphically in Figure 3 for reservoirs A to D.

Experimental results for the variation of the effectiveness of an LTHE with increasing concentrations of NCG in the system, reflected in increasing system pressures, are presented in Figure 4. Between experiments 1 and 6, the effectiveness based on the condenser heat output fell from 26.34% to 20.49%, while the effectiveness based on evaporator heat input decreased from 33.16% to 26.88%. In all experiments the measured effectiveness based on evaporator heat input was higher than that based on condenser heat output.







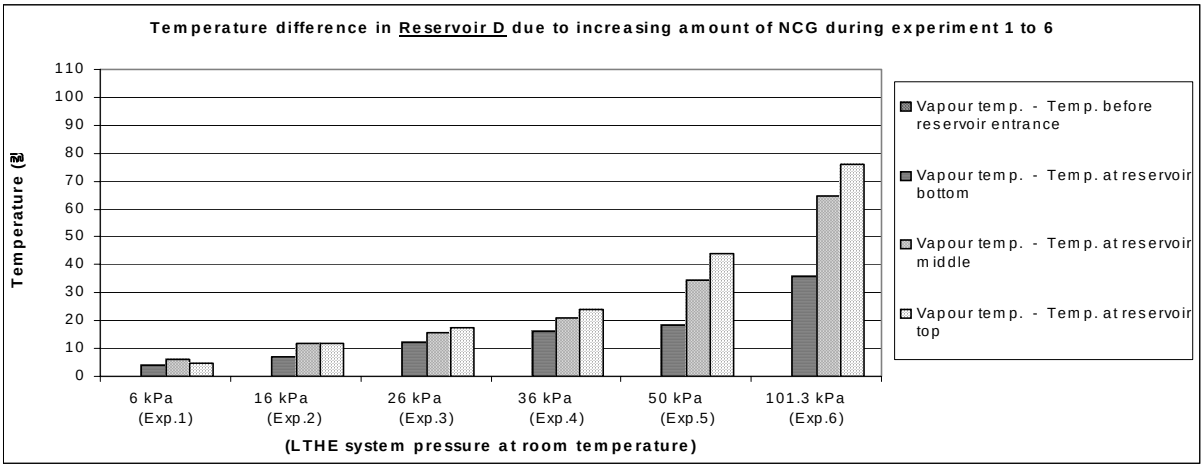


Figure 3. Temperature differences in reservoirs A, B, C, and D during experiments 1 to 6.

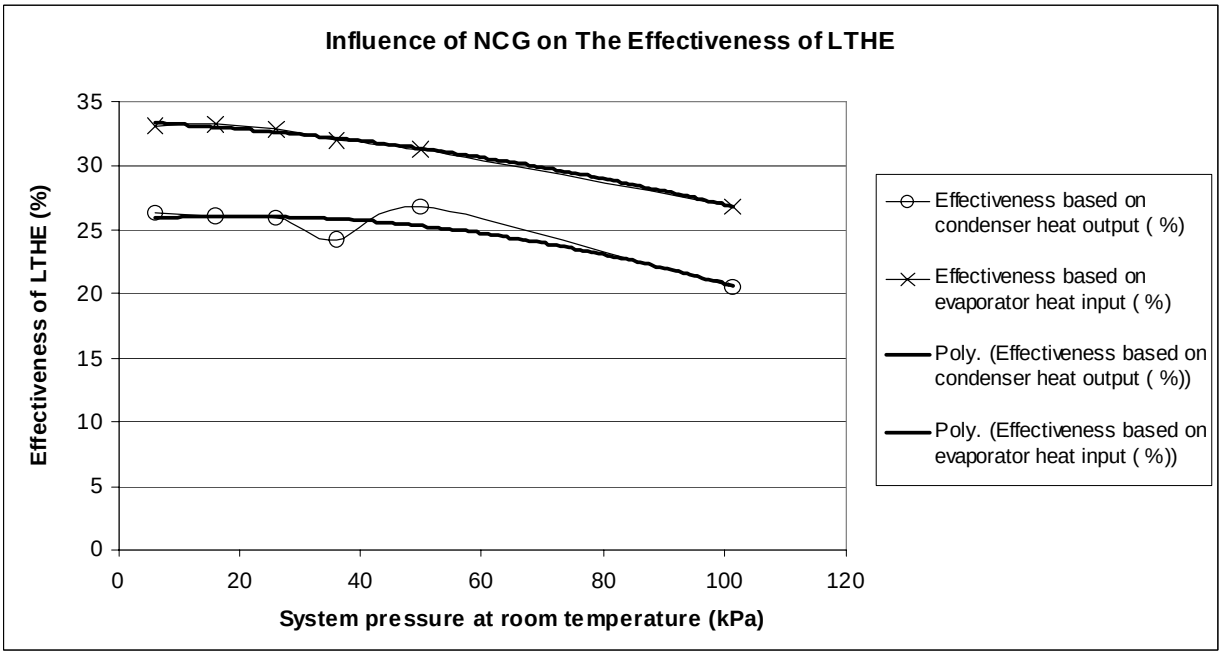


Figure 4 Influence of NCG variation on the effectiveness of LTHE

4. ANALYSIS

The following trends in the temperature differences between saturated vapour and reservoir surface temperatures can be observed in Figure 3:

1. As the quantity of the NCG in the LTHE system increased, the temperature difference for each reservoir increased accordingly. This observation is consistent with the explanation offered in section 2 that increasing concentration of NCG in a reservoir increases the thermal resistance between vapour and the reservoir surface, so that the temperature drop across this surface will be enlarged.

2. In experiments 2 to 6, the temperature difference for reservoir A was always greater than those for the other reservoirs.

For further analysis, the average of the temperature difference pertaining to the top, middle and bottom of each reservoir in all six experiments was calculated. These averages are presented graphically in Figure 5. It can be seen that the temperature difference in reservoir A was higher than that in reservoir B, which in turn was always higher than those in reservoirs C and D. In addition, these temperature differences increased with increasing amounts of NCG in the system.

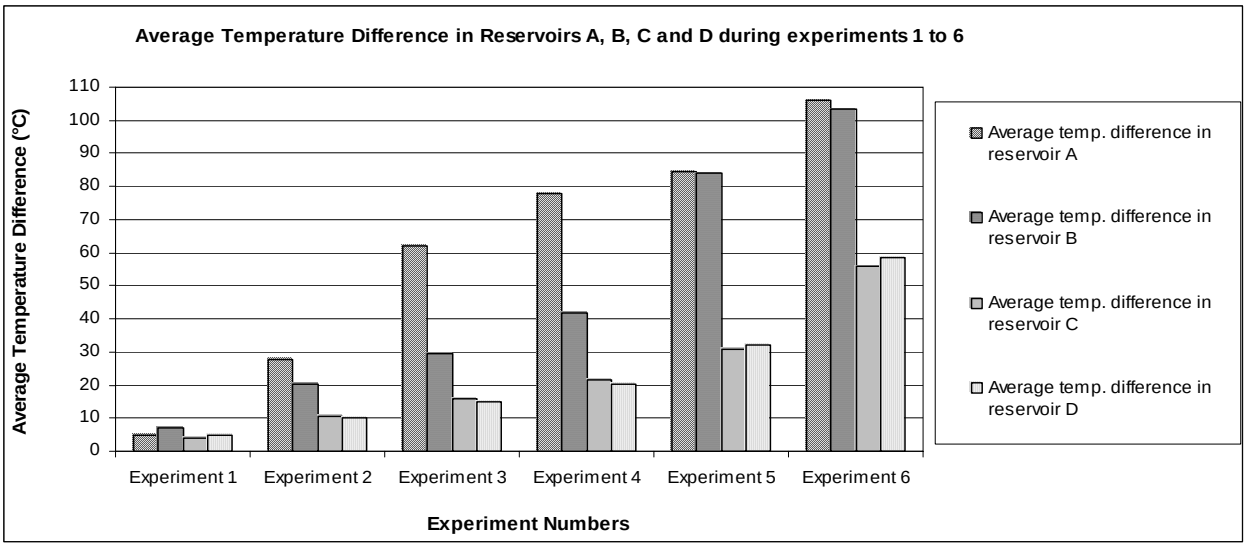


Figure 5 Average temperature difference in reservoirs A, B, C, and D during experiments 1 to 6

From Figures 3 and 5, we can conclude that in each experiment the maximum temperature difference between condenser vapour and reservoir surface was in reservoir A. This finding suggests that the intensity of concentration of the induced NCG was highest in reservoir A. Noting the location of reservoir A (Figure 1), we can therefore propose on the basis of this experimental study that the most suitable location for a gas reservoir to collect NCG in an LTHE is on the bottom header of the condenser where the condensate exits to the evaporator through adiabatic pipe. Pioro [4] has discussed industrial two-phase thermosyspons, and Mori and Konishi [5] described a 'Loop Thermosyphon Heat Exchanger' for heating the combustion air of a blast furnace. A container was provided in this heat exchanger for receiving non-condensing gases that are released in the course of operation. The container was positioned at the condenser bottom header, opposite to the condensate exit from the condenser. The unit was operated for 40 000 hours and found to be very reliable and efficient.

This optimum location for a reservoir to collect NCG is also consistent with the following theoretical analysis of the flow of NCG in an LTHE based on the principles of vapour and gas flow. Contrary to thermosyphons, the NCG in an LTHE enter from the top of the condenser and are pushed by vapour towards the bottom. After entering the condenser, the NCG pass through the upper header, and then enter the condenser tubes that form the condenser face area. Here vapour condenses and creates a pressure gradient that enables the continuous flow of incoming vapour into the condenser. The incoming vapour to the condenser continues to push the NCG towards the bottom header. After reaching the bottom header, the condensed vapour in the form of condensate exits from the condenser and flows under gravity towards the evaporator through adiabatic return tubes. The NCG are pushed down by the incoming vapour towards the condensate exit until the buoyancy of the liquid-vapour mixtures prevents the gases descending any further. The NCG thus accumulate in the bottom header of the condenser, where reservoir A was located in the experimental apparatus.

The graph of effectiveness versus pressure, which in turn is directly and positively related to the amount of NCG in the system (Figure 4), shows that the effectiveness of an LTHE slowly declines with increasing NCG concentration. This relationship can be explained by the adverse effect on the rate of heat transfer to the cold air passing over the condenser tubes of the partial accumulation of NCG inside these tubes. It can therefore be concluded that to achieve maximum effectiveness the NCG in the system must be trapped in a reservoir of suitable volume installed at the condensate exit end on the condenser bottom header. At a predetermined temperature, which can be designated as the 'LTHE maximum operating temperature', all the NCG can accumulate in this reservoir and are thus prevented from having an adverse impact on the operation of the condenser.

5. THE DETERMINATION OF OPERATING TEMPERATURES AND RESERVOIR VOLUME FOR AN LTHE LOADED WITH NON-CONDENSABLE GASES

A number of critical temperatures relating to the use of LTHEs loaded with NCG can be derived theoretically:

- *The starting point operating temperature,* at which the non-condensable gases are pushed by working fluid vapour up to the upper boundary of condenser face area. With a slight increase in this temperature, the working fluid vapour begins to enter the tube within the condenser face area and the process of heat transfer from condenser commences.
- *The optimum operating temperature,* at which the working fluid vapour pushes the non-condensable gases just below the lower boundary of the condenser face area and the condenser tubes within the condenser face area get filled with the working fluid vapour. At this stage the whole condenser face area is utilised for heat transfer. A slight decrease in this temperature allows the non-condensable gases to return to the condenser face area, thus reducing the active condenser face area for heat transfer and decreasing the rate of heat transfer.
- *The maximum operating temperature,* at which the working fluid vapour pushes the non-condensable gases to the entrance of the NCG reservoir. At this stage all the non-condensable gases are confined within the NCG reservoir. With a slight increase in this temperature the working fluid vapour enters into the reservoir and occupies a portion of it, enabling heat loss to the atmosphere through the uninsulated reservoir walls. This heat loss reduces the effectiveness of the LTHE. By considering the heat recovery conditions the maximum operating temperature is predetermined during the design of LTHE system.

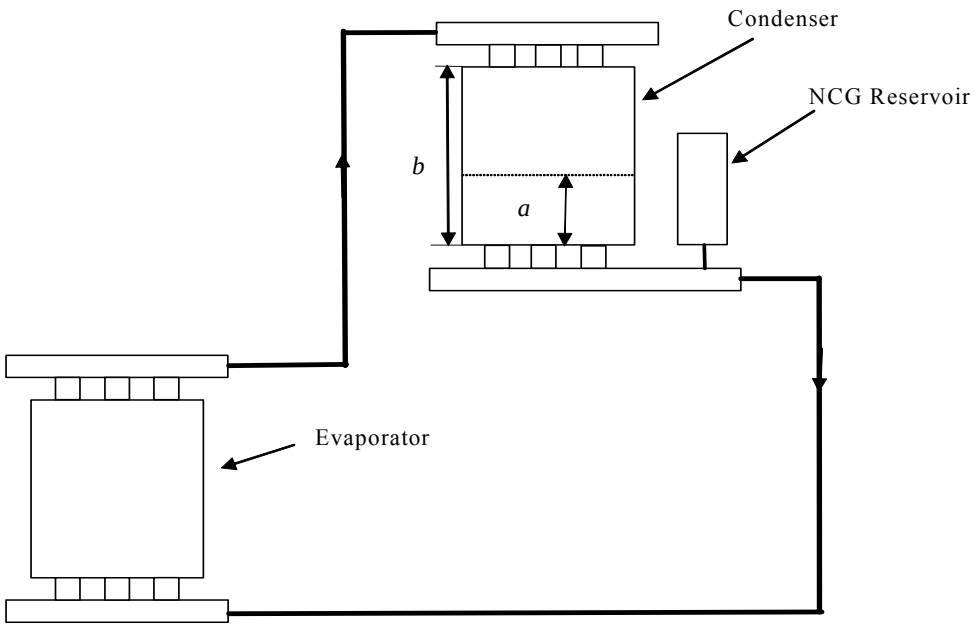


Figure 6: Schematic of an LTHE with a NCG reservoir

For maximum heat exchange through the condenser face area, the LTHE operating temperature should be equal to or greater than 'optimum operating temperature', and be equal to or lower than 'maximum operating temperature', that is:

$$Optimum\ \ Operating\ \ Temperature \leq Operating\ \ Temperature \leq Maximum\ \ Operating\ \ Temperature$$

For a loop thermosyphon heat exchanger loaded with NCG, the proper selection of the volume of a reservoir to collect NCG is very important for its effective operation. During normal operating conditions, an oversized reservoir volume may cause the working fluid vapour to enter into the reservoir leading to additional heat loss to the atmosphere; or an undersized reservoir may lead to NCG partially or fully occupying the tubes within the condenser face area, thus reducing heat transfer from the condenser. In both cases the effectiveness of the LTHE is reduced.

An LTHE operates at its maximum effectiveness when its volume is filled with the working fluid only, and the NCG initially present in the system, are trapped in the appropriately sized and located reservoir. Based on the experiments conducted during this study, the recommended location of the reservoir is near the exit of condensate from the condenser.

The following theoretical analysis of an LTHE system is based on the conditions in which the initial pressure of the LTHE system is the standard atmospheric pressure (101.325 kPa), water as the working liquid, and air as the NCG. The saturation pressure of the working fluid corresponding to the maximum operating temperature is considered the maximum operating pressure of the LTHE for the given size of the NCG reservoir. At this stage, all the NCG are confined within the reservoir and the pressure of the NCG in the reservoir is equal to the maximum operating pressure of the LTHE.

The following additional assumptions are made:

- Initially the LTHE system is at ambient temperature and pressure.
- After vapour formation, a flat front exists between 'vapour' and the NCG.
- There is no heat exchange between vapour and NCG.
- The NCG reservoir is not insulated and the temperature of the NCG is equal to the ambient temperature.

On the basis of the above assumptions, the isothermal compression of NCG in the LTHE can be expressed as:

$$P_{Ambient}\left(V_{NCG@LTHE} + V_{Reservoir}\right) = P_{Maximum\ Operating}\ \ V_{Reservoir} \qquad \text{(Equation 1)}$$

Or:

$$V_{Reservoir} = \frac{P_{Ambient}\ V_{NCG@LTHE}}{P_{MaximumOperating} - P_{Ambient}} \qquad \text{(Equation 2)}$$

where

$P_{Ambient}$ The absolute ambient pressure (kPa)

$V_{NCG@LTHE}$ The volume occupied by the NCG, in the LTHE system (excluding the volume of reservoir) at ambient pressure and temperature (m^3)

$V_{Reservoir}$ The volume of NCG reservoir (m^3)

$P_{Maximum\ Operating}$ The absolute pressure in the LTHE system at which all the NCG from the LTHE is pushed into the reservoir (kPa).[1]

In a LTHE system using water as working fluid, the 'starting point operating temperature' and 'optimum operating temperature' for an NCG-loaded LTHE are determined in two steps:

1. Calculate the 'starting point operating pressure' and 'optimum operating pressure'.
2. Find the saturation temperature corresponding to the 'starting point operating pressure' by using steam tables. This saturation temperature is considered to be the 'starting point operating temperature'. Similarly the saturation temperature corresponding to the 'optimum operating pressure' is found, which is considered to be the 'optimum operating temperature' for the NCG-loaded LTHE.

At a LTHE operating pressure, when the volume of NCG is greater than the volume of the NCG reservoir (Figure 6), then Equation 1 can be expressed as following:

$$P_{Operating}\left(\frac{a}{b}\ V_{CFA}\ +\ V_{CBHA}\ +\ V_{Reservoir}\right) = P_{MaximumOperating}\ \ V_{Reservoir}$$

Or:

$$P_{Operating} = \frac{P_{MaximumOperating}\ V_{Reservoir}}{\left(\frac{a}{b}V_{CFA} + V_{CBHA} + V_{Reservoir}\right)} \qquad \text{(Equation 3)}$$

where

a Height of condenser face area occupied by NCG (m)(see Figure 6)

b Total height of condenser face area (m)(see Figure 6)

V_{CFA} LTHE volume within the condenser face area (m^3)

$\frac{a}{b}V_{CFA}$ Volume of NCG within the condenser face area (m^3)

V_{CBHA} Volume of condenser bottom header assembly (m^3), (including 'condenser bottom header', 'part of condenser tubes between bottom header and condenser face area' and 'connecting tube between reservoir and bottom header')

$V_{Reservoir}$ Volume of NCG reservoir (m^3)

$P_{Operating}$ Operating pressure of the LTHE (kPa)

$P_{MaximumOperating}$ Maximum operating pressure of the LTHE (kPa).

To determine the operating pressure of the LTHE ($P_{Operating}$) for a predetermined maximum operating pressure ($P_{MaximumOperating}$), there are five unknown parameters in Equation 3, four of which can be determined as below:

- $V_{Reservoir}$ is calculated by using Equation 2. This volume is constant for a particular maximum operating temperature.
- Values of dimension b, V_{CFA} and V_{CBHA} can be found from the LTHE geometry and these values are also constant.

Hence in Equation 3, the dimension 'a' is the only variable determining the operating pressure. A zero value of dimension 'a' makes the value $\frac{a}{b}V_{CFA} = 0$. So the volume of NCG within the condenser face area is zero and the full condenser face area is available for heat exchange. That is why this operating pressure is considered the *optimum operating pressure.*

In Equation 3, when dimension $a = b$, then $\frac{a}{b}V_{CFA} = \frac{b}{b}V_{CFA} = V_{CFA}$, which means that the total volume within the condenser face area is filled with NCG. In other words, there is no heat exchange from the condenser face area. Any further increase in operating pressure will push the NCG front down within the condenser face area, thus making that portion of the condenser face area available for heat exchange. Thus operating pressure calculated under this condition is considered to be the *starting point operating pressure*.

In summary, the following relationship is established:

$$P_{Operating} = \frac{P_{MaximumOperating}\ V_{Reservoir}}{\left(\frac{a}{b}V_{CFA} + V_{CBHA} + V_{Reservoir}\right)}$$

When
a = 0 then
$P_{operating}$ *= Optimum Operating Pressure*

[1] In an LTHE where the working liquid is water, for a predetermined maximum operating temperature, the corresponding saturation pressure of the working liquid is found by using a 'Steam Table'.

When
a = b then
$P_{operating}$ *= Starting Point Operating Pressure*

After establishing the 'starting point operating pressure' and 'optimum operating pressure', steam tables are used to find the 'starting point operating temperature' and 'optimum operating temperature':

- The saturation temperature corresponding to the 'starting point operating pressure' is considered to be the *starting point operating temperature* for the NCG-loaded LTHE.
- The saturation temperature corresponding to the 'optimum operating pressure' is considered to be the *optimum operating temperature* for the NCG-loaded LTHE.

6. CONCLUSION

In this study, it has been shown experimentally and theoretically how NCG affect the performance of the LTHE and reduce their effectiveness. The effects of the NCG are more pronounced at low temperatures, and as the operating temperature increases the performance of LTHEs improves. The adverse effects of NCG can be minimised by installing a reservoir of the appropriate size in the region where condensate exits from the condenser and flow of vapour is least. In an LTHE loaded with NCG, the condenser face area becomes available for heat exchange when the LTHE operating temperature exceeds the 'starting point temperature'. With rising operating temperature, the condenser face area becomes increasingly available for heat exchange, and the effectiveness of the LTHE increases, until the 'LTHE optimum operating temperature' is reached. To attain maximum effectiveness, the operating temperature must be equal to or more than the 'LTHE optimum operating temperature' but it should not exceed the 'LTHE maximum operating temperature'.

References

1. Dube, V., Noie-baghban, S. H., Awasthi, B., and Akbarzadeh, A., "Waste Heat Recovery Using a Loop Thermosyphon Heat Exchanger in a Bakery", 6 International Heat Pipe Symposium, Chiang Mai, Thailand, Dept. ME. CMU. 001/2544, 5-9 November 2000, page 174-183
2. Dunn, P. D. and Reay, D. A., *Heat Pipes*, 4th ed. 1994, Oxford, England; Tarrytown, N. Y. U.S.A., Pergamon. ix, 348.
3. Dube, V., "The Development and Application of a Loop Thermosyphon Heat Exchanger for Industrial Waste Heat Recovery and Determination of the Influence of Non-Condensable Gases on its Performance", Ph.D Thesis, RMIT University Melbourne Australia, 2003.
4. Pioro, L.S.P.I.L., *Industrial Two - Phase Thermosyphons*, 1997: Begell House, inc. New York.
5. Mori, T. and Kinishi, J., "Waste Heat Recovery by Large Capacity Heat Pipes in Iron and Steel Works", Proceedings of 6th Heat Pipe Conference, May 1987, Grenoble, p 744-747.

History, Status Quo and Future of Heat Pipe Chemical Reactors

Zhuang Jun[*] Zhang Hong[**] Wang Zhiliang[***]

*Nanjing HETE Energy Conservation & Environmental Protection Co., Ltd.
Zhongshan Science and technology Development Zone,
Nanjing Dachang District,
Nanjing, Jiangsu 210048 China
E-mail: jzhuang@heatpipe.com.cn

** Mechanical & Power Engineering Department of Nanjing University of Technology
No.5 Xinmofan Road, Nanjing, 210009 China
E-mail: hzhang@hotmail.com

***Engineering and Technological Development Center of
Qilu Petrochemical Research Institute
Linzi, Zibo, Shandong, 255400 China
E-mail: wangzhl@riqpc.sina.net

Abstracts

Heat pipe chemical reactor follows the principle to control the catalyst bed temperature variation by means of the homogeneous temperature characteristics and high heat conductivity of heat pipes, so as to approach the optimum reaction temperature with minimized by-reaction. It can not only raise product output and quality, but also lower raw materials and energy consumption. Although many researchers in different countries over the world have developed a number of heat pipe chemical reactors, very few of them have been really put into operation in industrial production. In this article, the authors gave a brief presentation of the development history of heat pipe chemical reactors over the recent two decades or more and the latest industrial achievements in this field, and proposed a new concept of design. Facts have proven that heat pipe chemical reactors have bright prospects.

Key words: heat pipe chemical reactor.

1. FOREWORD

Chemical reactors are the heart equipment of chemical industry. In industrial application, many chemical reactors are packed with a catalyst bed, and when reacting materials flow through this bed, chemical reaction takes place under given temperature and pressure conditions. In the chemical reaction, not only products are converted, many byproducts also appear. Temperature has a major bearing on the results of chemical reaction, and the optimum reaction temperature for a given chemical reaction is the temperature at which maximum products are obtained with the minimum by-products, thus raising the product yield and quality to the maximum extent with the minimum raw materials and energy consumption. Chemical reactions can be classified into two types: endothermic reaction and exothermic reaction. In case of an endothermic reaction, heat should be supplied into the reactor continuously while the reaction is in progress, to keep the reaction going on, while in case of an exothermic reaction to the contrary, heat should be removed continuously from the reacting bed, to make sure that the chemical reaction is going on at the optimum temperature. How to ensure that the reaction temperature approaches the optimum reaction temperature in the reacting bed and how to input or remove the heat required by the

chemical reaction into or from the catalyst reaction bed, are important factors to be taken into consideration in the research and design of chemical reactors.

The heat pipe technology has the following advantages when used in chemical reactors:

(1) The isothermal surface of heat pipe can keep a more homogeneous temperature in the catalyst bed inside the chemical reactors;

(2) The heat flow density variation of heat pipe is beneficial to the removal and input of heat out of and into the bed;

(3) The rapid start and close of heat pipe is beneficial to the temperature rise and shutdown of chemical reactors;

(4) Other characteristics of heat pipe, such as passive operation performance, no mechanical power required for transmission of heat flow, thermal diode characteristics for mono-directional heat transfer and varying conductivity characteristics, are all beneficial to the control of chemical reaction temperature.

2. HISTORICAL REVIEW OF DEVELOPMENT OF CHEMICAL REACTORS:

The first paper on research of heat pipe chemical reactors was published in 1974. [1]Strimbek, P.C., et a1 reported the application of heat pipe in a fluidized coal gasifier. In 1976, William A.Ranken [2] reported indirect coal gasifier and methane conversion reactor operating with heat pipes, the working principle of the former is as shown in Fig. 1, [2]

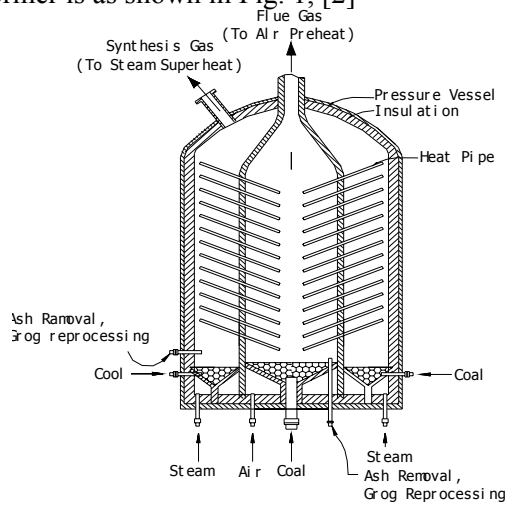


Fig.1.Possible configuration of heat pipe indirect gasifier showing central combustion region thermally connected by heat pipes to concentric high pressure gasification region.

the reactor consists of two concentric cylindrical vessels, the inner vessel is a combustion chamber, into which coal and air is fed from outside, and the heat produced by combustion is transferred via the high temperature sodium heat pipe to the outer vessel, the reaction chamber, where the steam and coal fed from outside receive the heat input from the sodium heat pipe, so that coal and steam react chemically to generate synthesis gas. The advantages are: ① the generated gas contains no nitrogen and therefore has a high heat value; ② it has reduced the conveying pipe diameter, therefore saving the conveying cost; and ③ the equipment features simple structure, full utilization of energy with minimum consumption. The most difficult point preventing its industrial application is the material of the high temperature sodium heat pipe. It must withstand the corrosion and wearing of materials such as sulfur, alumina, silicon carbide and limestone under a high temperature (1255~1370K), in particular, hydrogen must be prevented from permeating into the heat pipe via the pipe wall to damage the operation of the heat pipe.

This article also reported the second heat pipe chemical reactor – heat pipe methane conversion reactor. It is an exothermic chemical reactor, and the key to its successful design is how to lead out the chemical reaction heat for utilization. The schematic structure diagram is as shown in Fig. 2. [2]

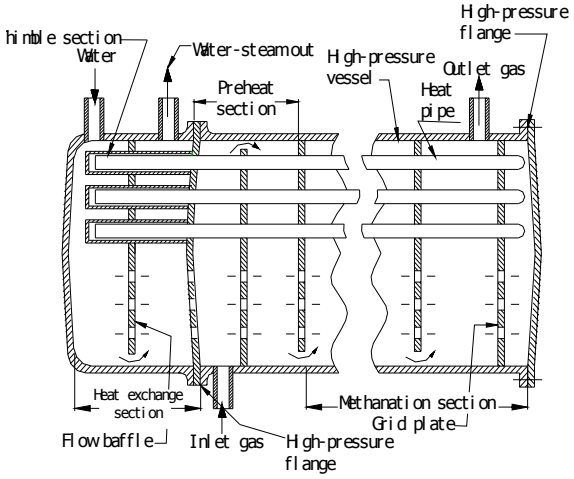


Fig.2.Schemtic representation of a heat pipe methanator showing merging of methanator preheated and steam generator in one unit. In operation, the heat exchanger would be tilted several degrees above horizontal to enhance gravity return of the heat pipe working fluid.

The total production capacity of methane in this plant was 7.06×10^6m3/day, and totally 9 reactors were required, each sized as 11m long and 2.5m in diameter, containing 2000 heat pipes of 51mm in diameter. Each heat pipe transferred heat of 17kW, at the reaction temperature of 670K (397℃). The main advantages: ① the heat pipes can transfer the chemical reaction heat to the energy recovering system at a very small temperature difference, while maintaining the optimum reaction temperature in the catalyst layer; ② the reaction heat led out by heat pipes can preheat the raw material gas entering the reaction bed to the reaction temperature; ③ the reaction heat led out by heat pipes can be used to produce steam; and ④ in case of fluctuation in the raw material gas flow entering the reactor, heat pipes can quickly adjust the reaction temperature in the reactor catalyst bed. Despite of these obvious advantages with this reactor, it is rather difficult to realize industrialized application for this design, the main reason being that a working medium suitable for this type of heat pipe can hardly be found. Mercury would be the most suitable working liquid, but there is great difficulty to make a mercury heat pipe with such big dimensions, and the price would be far beyond affordable.

In 1979, Kengo Uematsu[3] proposed a patent on heat pipe catalyst reactor, its structure is as shown in Fig. 3.

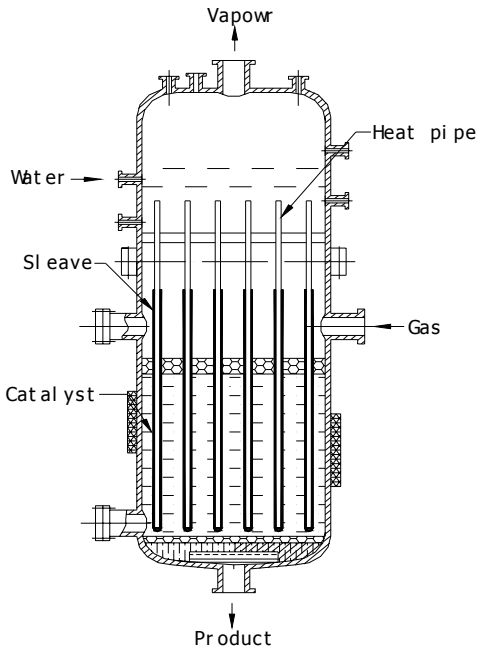


Fig.3. heat pipe reactor

It is envisaged that many sleeves are arranged in the catalyst bed of the reactor, and the evaporating segments of the heat pipes are inserted into the sleeves, while the condensing segment of heat pipes extend into the steam generator above the reactor. The heat pipe evaporating segments absorb reaction heat in the reaction bed and transfer it to the water in the evaporating zone to turn water into steam. The result is poor as heat pipes do not directly absorb heat from catalyst bed, and there are also many difficulties to insert the heat pipes and to load and replace catalyst.

In 1981, Humphreys & Glasgow Ltd [4] proposed the heat pipe gas – solid fluidizing reactor, the structure is sketched in Fig. 4.

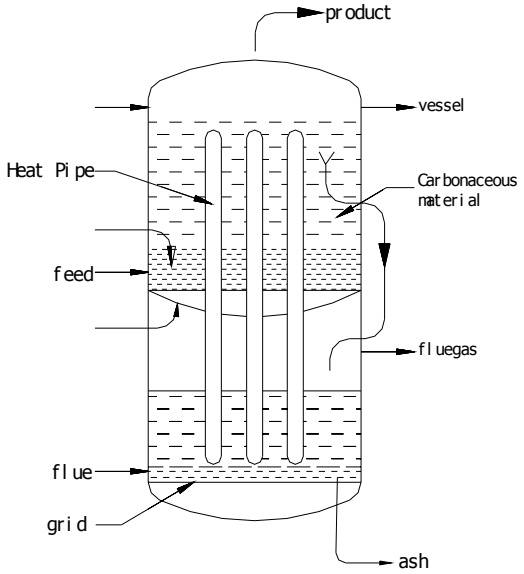


Fig.4. Fluidized bed reactor with heat pipes

This equipment can be used in catalytic cracking, catalyst regeneration and carbonaceous fuel oxidation.

The equipment is divided into two parts in one vessel, and each part being loaded with solid carbon particles, which are loaded on partition plates with airflow distribution holes. The lower chamber works as the combustion bed and upper chamber as reaction bed, and heat pipes transfer the combustion heat from combustion bed into the reaction bed to supply the heat required by reaction. A design example was given, the combustion bed operates at 900℃, and the heat pipe diameter being 80mm and sodium is used as working medium in the heat pipes. The effective height in the reaction bed is 3m. A total of 300 heat pipes are used. Whether this patent can be realized also depends if the heat pipe material can withstand the high temperature corrosion and

wearing under the high temperature conditions.

In 1982, Hide Kimura and Seiji Nishinwra [5] proposed the heat pipe reactor for hydrocarbon conversion reaction, with the structure schematic shown in Fig. 5.

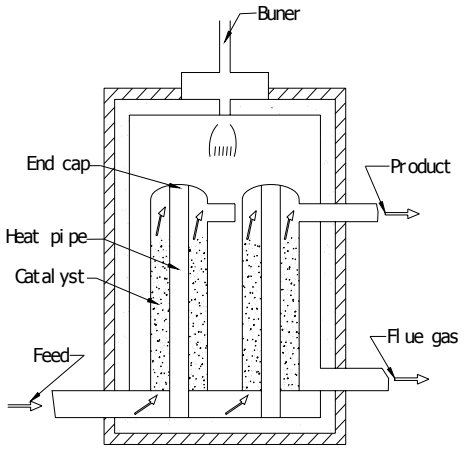


Fig.5. Homogenous temperature reactor with heat pipes

Heat is supplied to the reactor by nozzles, and catalyst is loaded inside the reaction pipes, and heat pipes are arranged in the center of the catalyst layer. Within the reaction pipes, the catalyst receives radiated heat from outside the pipe from the pipe outer surface, and on the other hand, it receives heat introduced from the heat pipe ends, to provide heating from the center of pipes. This envisage would not be easy to realize industrially, as input of heat is only possible when the heating end of heat pipe is located outside the bottom of the reaction pipe.

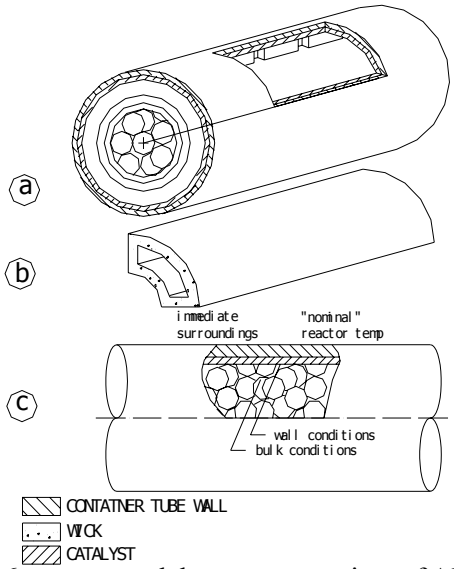


Fig6.reactor model: a. cutaway view of AHP reactor; b. basic AHP wick channel element; c. reactor tube model (packing is inert)

In 1983, Y.O.Parent[6] et al developed annular heat pipe reactor, used as an oxidizing reactor to generate Phthalic anhydride from naphthalene by oxidization, as shown in Fig. 6.

The catalyst is packed in the inner tube of the radial heat pipe, and the reaction heat is removed by heat pipe from inner pipe wall to outer pipe wall. The advantages of this type of reactor are: the inner surface of reactor is basically the isothermal surface of the heat pipe (the evaporating segment of heat pipe), the heat resistance between the two is very small, and there is homogeneous heat flow density on the outer surface of the heat pipe (the condensing segment of heat pipe). In a radial heat pipe, the outer surface area is greater than the inner surface area, which is beneficial to heat dissipation. The result of computer simulation calculation is shown in Fig. 7. [6],

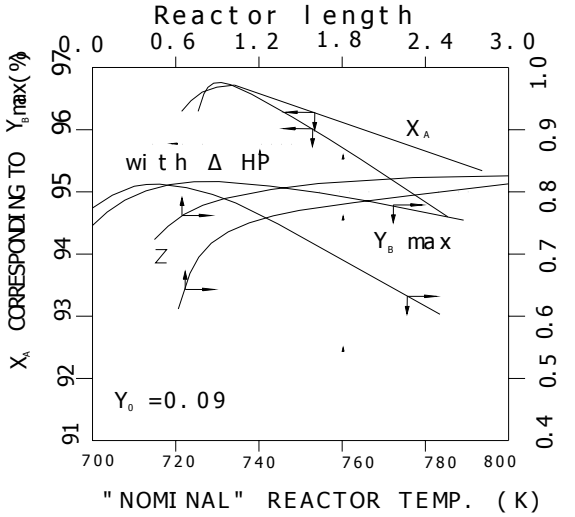


Fig7. Maximum yield of (B) with corresponding position of occurrence and conversion of (A)

which shows that the conversion rate and yield of radial heat pipe reactor are both higher than those with a conventional reactor. More important, the heat pipe reactor has a very wide operation range, which is extremely important to chemical reaction. The difficulties to realize this type of reactor are: ① it is difficult to make a radial potassium heat pipe; and ② a radial heat pipe reactor requires larger space than ordinary reactors.

In 1988, J.T. Richardson, S.A. Paripatyadar, J.C.She[7] reported the analysis and test results of a sodium heat pipe chemical reactor, this test was steam reforming of methane, with the following reaction formulas:

$$CH_4+H_2O = CO+3H_2 \quad (1)$$

$$CO+H_2O = CO_2+H_2 \quad (2)$$

The test device is as shown in Fig. 8,

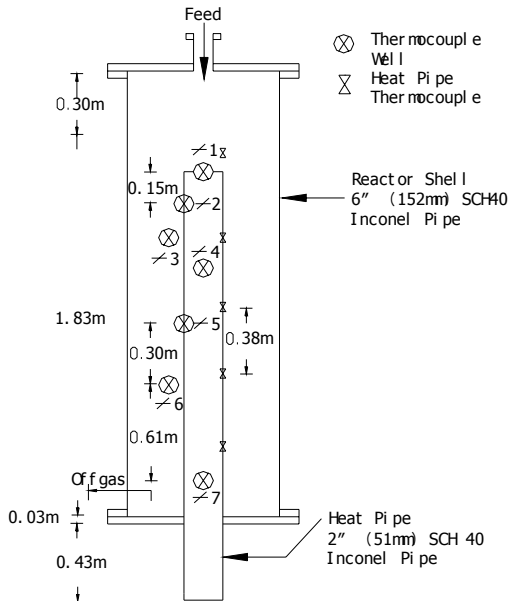


Fig.8. Sodium heat pipe reactor

and the test was performed with two different heat pipe operation temperatures (952K and 1043K). The test results and model calculation results for two different temperatures are shown in Fig. 9 and 10.

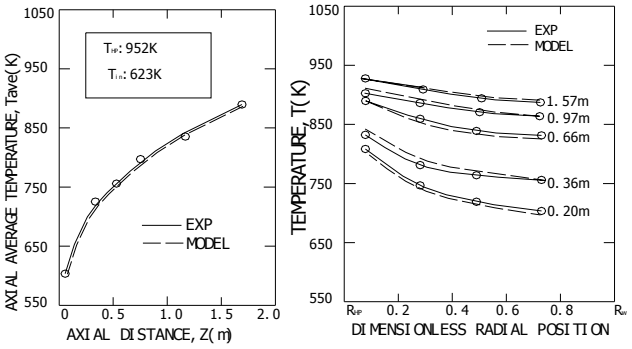


Fig.9 Axial and radial temperature profiles
T_{mp}-1.043k;CH_4flow-47.7mol/h;H_20/CH_4-2064;pr-132kpa;power-3.07kw

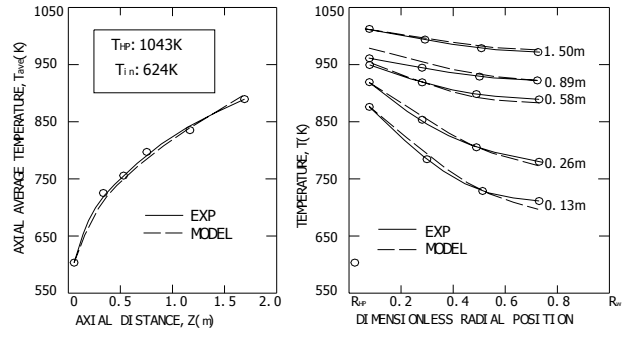


Fig.10. Axial and radial temperature profiles
T_{MP}-952k; CH_4 flow-40.8mol/h; H_20/CH_4-2.79; Pr-131kpa; power-2.34kw

The measured axial temperature and radial temperature well agreed the model calculation results. The reaction result also quite approached the theoretical calculated values. The greatest difficulty to prevent industrial application of this achievement is the hydrogen permeation of sodium heat pipe. As under the condition of high temperature and a certain pressure difference, the hydrogen generated from reaction will permeate into the heat pipe via the heat pipe wall, to hinder the normal operation of heat pipe. This has been proved by the test.

In 1997, John H.Rosenfeld, et al published an article on improving the chemical process unit operation with heat pipe technology [8], the article presented the isothermal batch reactor and isothermal tube reactor, their structures are as shown in Figs. 11 and 12.

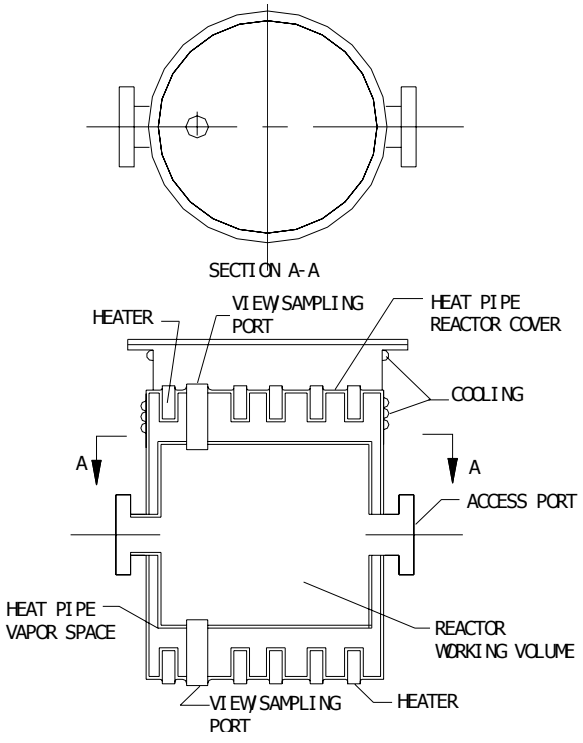


Fig.11. Isothermal batch reactor

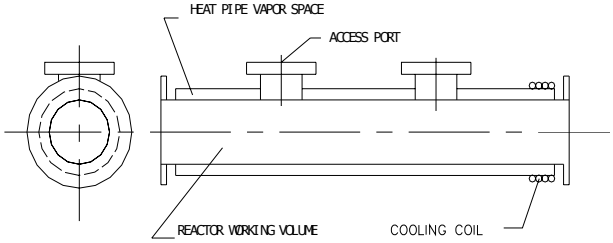


Fig.12. Isothermal tube flow reactor

It also mentioned the application of potassium, sodium and lithium heat pipes in high temperature chemical reactors, and the

temperature homogeneity could reach 0.5℃, with an operation temperature up to 1500℃. An isothermal reactor of 1m in diameter and 3m in length has been built, but no design or experimental data has been reported.

Most of the above developments are conceptual design or theoretical model calculation, with very few experimental data, and almost no successful example of real industrial operation. The reasons are twofold: ① chemical industry is usually in large scale with continuous production, so test risk and loss would be great, therefore it is very difficult to get an opportunity in industrial test; ② heat pipe housing materials that are resisting against corrosion and wearing without hydrogen permeation under conditions of high temperature and high pressure are still to be developed; and ③ it is difficult to make a high temperature liquid metal heat pipe (mercury, potassium and sodium) with a working temperature higher than 400℃, and the price would be expensive.

3. DEVELOPMENT, RESEARCH AND ACHIEVEMENTS OF HEAT PIPE CHEMICAL REACTOR IN CHINA

Researchers of Nanjing University of Technology (formerly Nanjing University of Chemical Technology) started the industrial development and application research of heat pipe chemical reactor from 1983. They performed the conceptual design, model calculation, small scale test and industrial test for endothermic chemical reactor (dehydrogenation reaction) [9][10], exothermic chemical reactor (oxidizing and synthesizing reactors) [11] [12] over a period of 20 years, until 2003 when the first solid – liquid bi-phase heat pipe chemical reactor was successfully put into operation in Taizhou Petrochemical Plant with good results. Now some typical development tests are presented as follows:

(1)Heat pipe chemical reactor for dehydrogenation of cyclohexanol

To make cyclohexanone by dehydrogenation of cyclohexanol is an endothermic reaction, and the chemical reactor requires ① reaction heat be supplied externally to maintain the reaction heat required by chemical reaction; ② the bed axial and radial temperature be homogeneous to avoid by-reaction; and ③ the optimum reaction temperature on the reaction bed be 360~390℃. The heat pipe chemical reactor can well meet the above requirements.

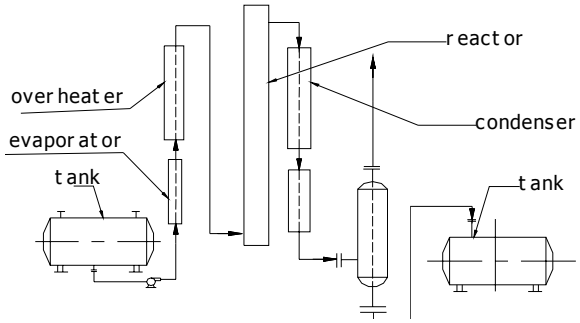


Fig.13. Process plant for dehydrogenation of cyclohexanol

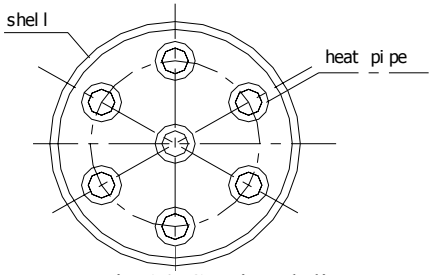


Fig.14. Sectional diagram

Fig. 13 is the test flow diagram, and Fig. 14 the sectional diagram of the heat pipe reactor. In this reactor, 7 mercury heat pipes are used, which are 6.4m in length and 32mm in diameter, made with 1Gr18Ni9Ti.

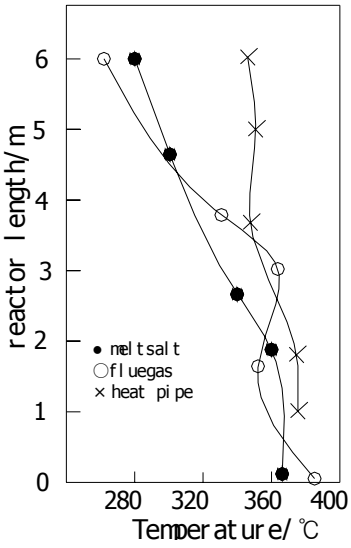


Fig.15. Reactor temperature distribution with different heat source.

Fig.15 shows a comparison of the axial temperature distribution in the reactor with different heating methods. Table 1 shows the

comparison of test results with production plant, and it can be seen that the energy consumption per ton of product in the heat pipe chemical reactor is only 60% of the production plant.

Table 1. Comparison of pilot test results with production plant data

Item	Thermal industrial test	Production plant
Catalyst type	Type Zn/Ca	Type Zn/Ca
Reactor type	Heat pipe heating	Flue gas heated tube type
Scale (t/a)	500	3000
Liquid phase speed (h-1)	0.6~0.7	0.2~0.3
Reaction temperature (℃)	355~390	355~390
Cyclohexanone conversion rate per pass (%)	65~80	60~75
Cyclohexanone yield (%)	80~90	80~93
Energy consumption (kJ/t of cyclohexanone)	3,812,493	6,485,420

(2)Heat pipe chemical reactor for dehydrogenation of ethyl benzene

As the above reaction, this reaction is also an endothermic reaction, requiring supply of heat externally to the bed. The difference from dehydrogenation of cyclohexanol is that the optimum reaction temperature in the reaction bed is 600~650℃, for which potassium or sodium heat pipes can be used. Fig. 16 shows the schematic diagram of the ethyl benzene reactor, Fig. 17 is the temperature distribution inside the heat pipe reactor in axial direction.

Fig. 18 gives the experimental results with different water to hydrocarbon ratio, and Table 2 lists the comparison between heat pipe chemical reactor and other two chemical reactors. It can be seen from the table that the single pass conversion rate of heat pipe reactor is slightly lower than that of the other two reactors, but the product yield (output) is higher than both of them, this is because heat pipe will permit reaction to take place close to the optimum temperature condition.

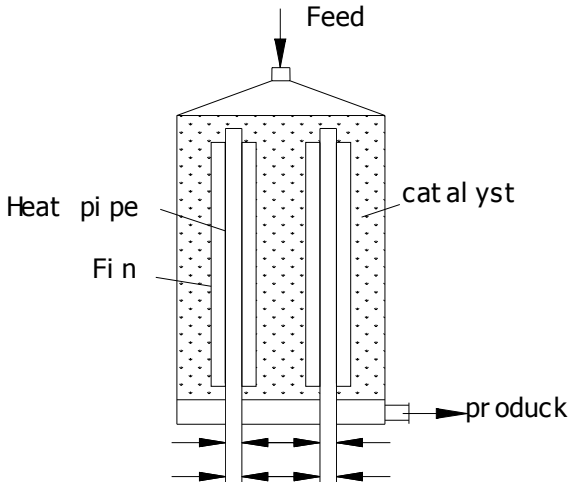


Fig.16. Heat pipe reactor

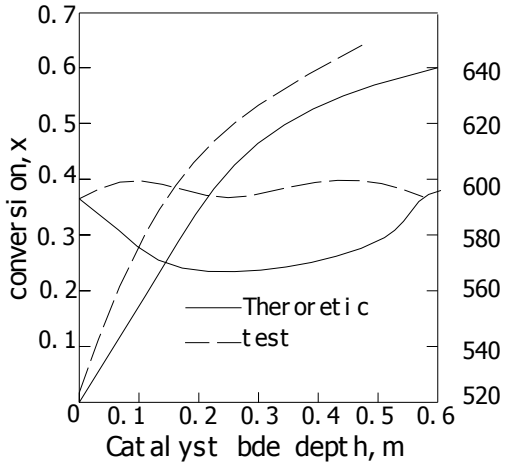


Fig.17. Conversion and temperature profiles

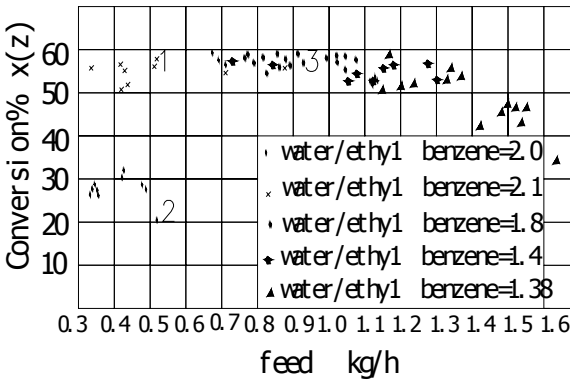


Fig18 Experimental results

Table 2. Comparison of different types of dehydrogenation reactors

Type of reactor	Ethyl benzene/ Water /weight ratio	Reaction temperature /℃	Single pass conversion rate /%	Styrene selectivity with the same conversion rate /%	Production capacity /kg styrene / (h·m3 catalyst)
Adiabatic	1/2~3	630~650	35~60	90~94	650~675
External heated	1/1~1.5	580~610	40~60	92~94	210
Heat pipe	1/1.2~1.4	Close to optimum reaction temperature	50~58	95~97	355

(3)Oxidization reactor with heat pipes

This is an intensive exothermic reaction, with the reaction temperature at 420~460℃. The structure of the loop heat pipe reactor developed by Hu Jiazhen [11] is shown in Fig. 19.

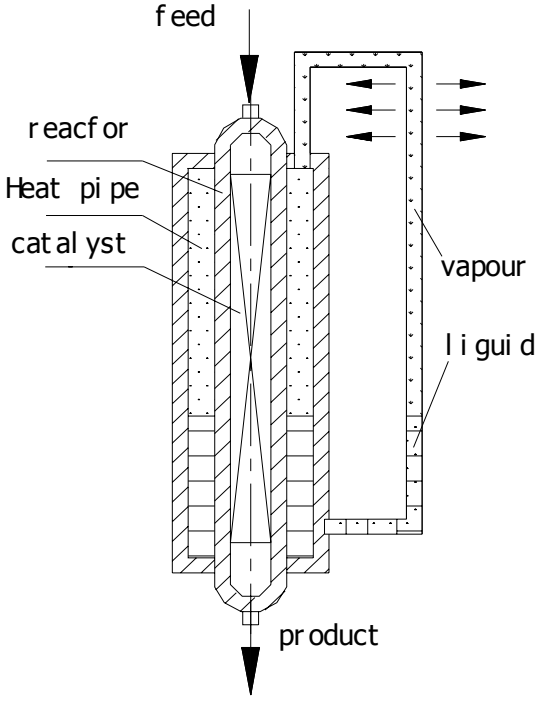


Fig.19. Heat pipe oxidization reactor

The reactor consists of the primary heat pipe, the catalyst is packed inside the pipes, and materials enter the reactor from top and are discharged from the bottom after passing the catalyst bed. The chemical reaction heat released during reaction is carried away by the heat pipe working liquid (mercury) in the gaps of circuit outside the pipes in the form of phase change. The outer wall of reaction pipes are covered with stainless steel screen as a liquid absorbing core, and the working liquid vapor is condensed outside the circuit. The condensate is refluxed from the bottom back to the gap to continue to absorb the heat to evaporate. The test results show:

(i) The maximum temperature zone distributed along the reactor axis in a heat pipe reactor is much wider than that of a tube reactor, the hot spot of a tube reactor appears at 1/3—1/6 of the top of the reaction bed, while the hot spot temperature of a heat pipe reactor moves downwards along the bed by 4cm (the total length of bed layer being 10cm). This has greatly increased the length of the chemical reaction zone, therefore increasing the utilization rate of the catalyst. The temperature distribution comparison is shown in Fig. 20.

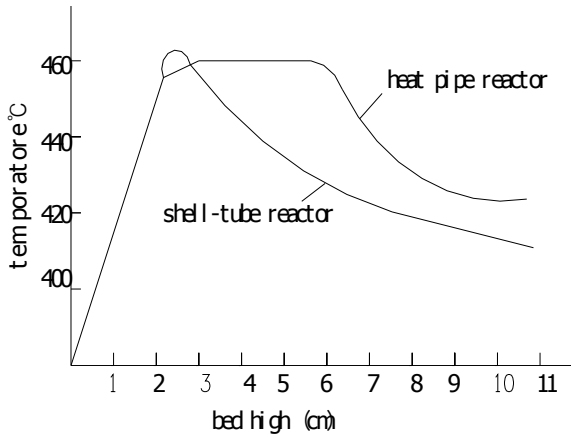


Fig.20. Temperature distribution in bed

(ii) The airspeed of a heat pipe reactor is 30% lower than that of a tube reactor, which not only greatly saves energy consumption, but also reduces the volume of the trap.

(iii) Under the same reaction conditions, the production capacity of the heat pipe reactor is increased by 60% as compared with a tube reactor, the specific data are as shown in Table 3.

Table 3. Comparison of airspeed for two types of reactors (30ml of catalyst and hot spot temperature being 440~460℃)

Items	Airspeed (hr^{-1})	Product concentration (g/m3)	Product yield (%)	Product purity
Heat pipe type	6100	22.64	103.37	84.97
Tube type	8800	11.10	102.95	91.59

(4) Development and research of heat pipe ammonia synthesizing column [11]

Ammonia synthesizing reactor is the heart for synthesized ammonia production. Hydrogen and nitrogen enter the reactor at a give proportion (3:1) to reactor with the presence of catalyst (reaction temperature 400~480℃ at a pressure of 30Mp). In the synthesizing reaction of ammonia, there is an optimum reaction temperature zone in the axial direction of reactor. Zhang Hong [11] has designed a loop heat pipe-synthesizing reactor, with the concept of sectional adiabatic reaction, to take heat indirectly by sections by means of heat pipes, so that the synthesizing temperature infinitely approaches the optimum reaction temperature curve. The structure is shown in Fig. 21.

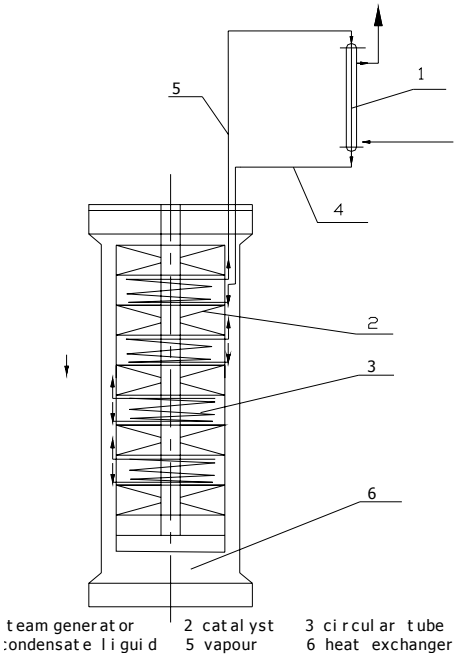


Fig.21. Ammonia synthesizer with heat pipe

In the synthesizing reactor, there are four layers of threaded pipes as the evaporating segments of heat pipes. The media inside the threaded pipes absorb the reaction heat in the catalyst layer, and flow upward along the circuit through the top cover to enter the steam generator outside the reactor. In the steam generator, the working media in the heat pipes release the heat and become condensed, while the water in the generator is heated and becomes steam. The condensed media return to the reactor along the down comer to continue to absorb heat. With computer simulation calculation, the reaction temperature inside the catalyst layer can infinitely approach the optimum reaction temperature, to get a high ammonia yield. Fig. 22 shows the calculation result of sectional approaching mode, and Fig. 23 gives the calculation result of infinite approaching mode. In both modes, the net yield of synthesized ammonia can be increased by 60%.

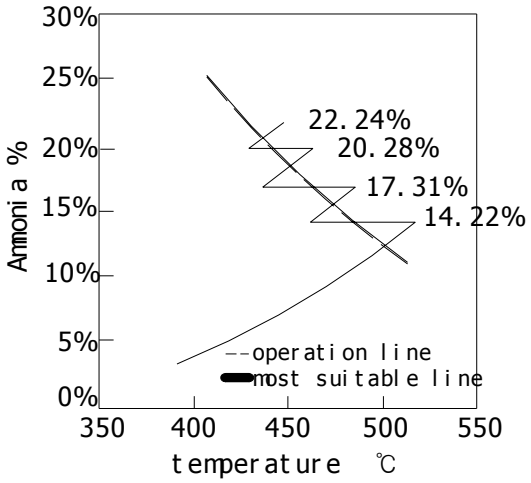


Fig.22. Limited sections calculation results

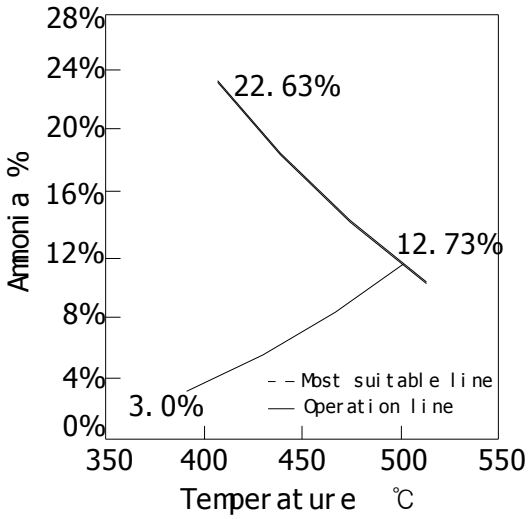


Fig.23. Infinite approach calculation results

(5)Heat pipe liquid – solid phase invertible chemical reactor

This type of reactors currently in use in industrial plants is mostly fixed bed circulating reactors, as shown in Fig. 24.

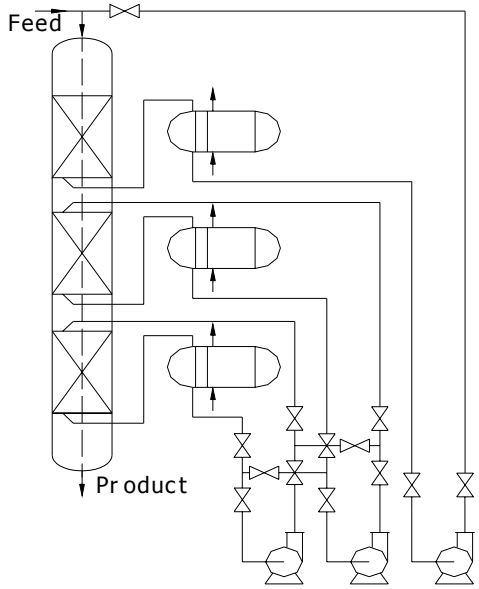


Fig24 Liquid- solid reactor

The disadvantages are: ① large amount of materials from the reactor are returned and mixed, with reduced utilization rate of catalyst; ② large amount of kinetic energy is consumed; and ③ leakage is likely to take place in the materials circulating system due to high pressure in the reactor. In July 2003, two heat pipe reactors were used in a 20000 t/a MTBE plant in Taizhou Petrochemical Plant in Jiangsu Province, China[13] (1m in diameter and 15m high, and 1.4m in diameter and 15m high), as shown in Fig. 25.

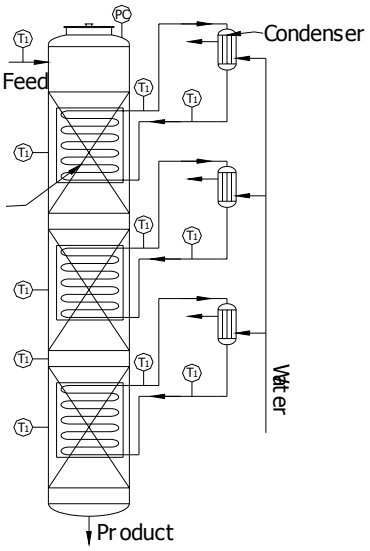


Fig25.Reactor with loop heat pipe

The operation results showed that, compared with plants of the same scale, the catalyst utilization rate in the heat pipe reactor increased by 40%, circulating power reduced by 62kW, the reaction bed temperature lowered by 5℃~8℃, the conversion rate increased by 2~3 percentage points, the byproducts reduced from the previous 0.43%~0.6% to present 0.2~0.35%, and the product quality was also improved. The successful operation of this plant has proved that the design concept and inherit advantages of heat pipe chemical reactor can be realized in industrial mass production.

4.FUTURE OF HEAT PIPE CHEMICAL REACTORS

In the above, the history of heat pipe chemical reactor development in various countries in the world since 1976 was reviewed. Due to the complication and engineering risk of heat pipe chemical reactors, there have been many difficulties in this development work, and there has been almost no report of real realization of industrial application. The main reason is that it is quite difficult to adapt the conventional heat pipe technology to the needs in chemical projects. Especially, under high temperature reaction conditions, high temperature heat pipes with great length to transfer very high power are required, and such heat pipes are not only difficult to make, but also very expensive, very difficult to meet the needs of industrial application. In recent years, a chemical reactor design with a new type of heat pipe structure may bring new hopes to the development of heat pipe chemical reactors.

In this new heat pipe chemical reactor design, heat pipes of small size are used as fins to penetrate the vessel or pipe walls, to enhance the heat transfer on their both sides, to achieve rapid control of chemical reaction temperature.

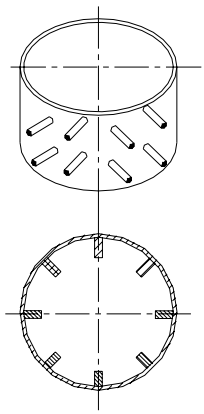


Fig.26(a)SRT-VI furnace tube

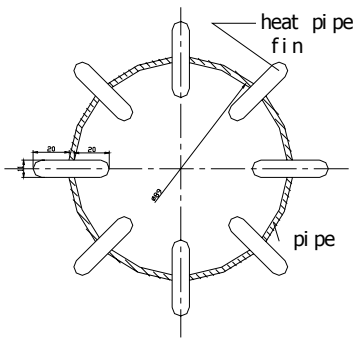


Fig.26(b)Heat pipe fin furnace tube

Fig. 26 shows a set of cracking furnace pipes

fitted with high temperature heat pipe fins. Inside the pipes is the hydrocarbon to be cracked (such as naphtha), and combustion takes place outside the pipes to supply heat required by the cracking reaction inside the pipes. The cracking temperature is 800~900℃, the working medium inside the heat pipe fins is metal sodium, and they are sized at Ø25×50mm. Table 4 gives a comparison of the parameters of a heat pipe finned furnace pipes and ordinary industrial furnace pipes. It shows that the unit volume, the ratio of pipe internal to external heat transfer area (s/v) and heat flux of heat pipe finned furnace pipes are all greater than those of an ordinary finned furnace pipe. Table 4

Table4 comparison of tubes

Type	SRT-VI	Heat pipe fin tube
Di/ mm	89	89
Do/mm	101	101
Si/v	58	121
So/v	73	128
Inside expansion	1.27	2.25
outside expansion	1.42	1.99
Heat flux increase	1.42	2.98

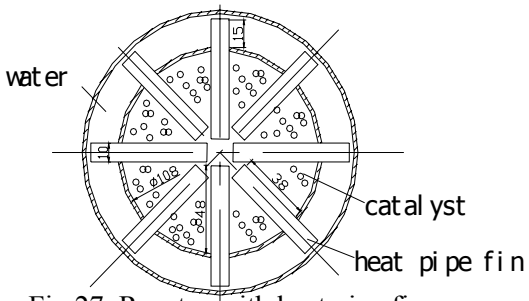


Fig.27. Reactor with heat pipe fin

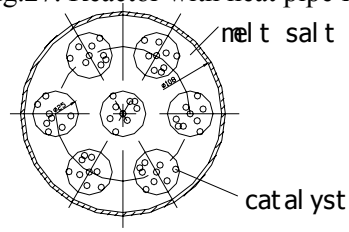


Fig.28. shell-tube reactor

Fig. 27 shows the sectional view of heat pipe fins used in intensive oxidizing chemical reactors. In a chemical reactor with intensive oxidization, as it is necessary to reduce radial temperature difference, tube bundles with small diameter Ø25mm are used and catalyst is loaded inside. It is quite difficult to control the axial temperature of the reactor. The sectional view is as shown in Fig. 28. Table 5 presents a comparison of parameters of two types of reactors, and it shows that with the same diameter and height conditions, the catalyst loaded in a heat pipe fin reactor is 1.64 times that of a tube reactor, and the heat exchange area is increased by 1.69 times. More important, as the internal flow pattern in the reactor is changed, the heat exchange coefficient between the reacting gas and the heat pipe fins is also increased, and the result is the heat taking ability is over 5 times that of the tube reactor. This has not only increased the production capacity of the oxidizing reactor, but also greatly increased the utilization of catalyst.

Talbe5 Comparison of parameters

Type	Shell-tube	Heat pipe fin
High/ m	2	2
Di/ m	0.108	0.108
Fill of catalyst/ m^3	0.0067	0.011
Heat transfer surface/ m^2	1.1	1.859
Rate of heat transfer	1	5
Cooling medium	Melt salt	water

5. CONCLUSION

The development and research of heat pipe chemical reactors now has a history of over 20 years. Although there are only few successful examples of application, the many advantages of heat pipe chemical reactors and the major effect that they may bring to the chemical engineering have attracted researchers all the time in their continuous pursuit and exploration. With the advance of heat pipe technology and the continual efforts by the scientific workers in all countries, heat pipe chemical reactors will surely have their bright future.

References

[1] Strimbeck,D.C.,et al "Process Environment Effects on Heat Pipes in Fluid-Bed Coal Gasification" 9th Intersociety Energy Conversion Engineering Conference, San Francisco, Calif.,august 26~30,1974,Los

Alamos scientific Laboratory Report LA-UR-74-984(1974)
[2] William A. Ranken “The Potential of The Heat Pipe in Coal Gasification Processes” 11th IECEC sep. 1976 p876~882
[3] Patent 54-107903(JP)
[4] Patent 1 599 398(GB)
[5] Patent 57-127443(JP)
[6] Y. O. Parent, H. S. Caram, R. W. Coughlin “Tube-wall Catalytic Reactor cooled by an Annular Heat Pipe. AICHE J. V29 N3. 1983
[7] J. T. Richardson, S. A. Paripatyadar, J. C. Shen “Dynamics of a Sodium Heat Pipe Reforming Reactor” AICHE Journal May 1988 vol. 34,No.5 P743-752
[8] John H. Rosenfeld, Peter C. Cologer, Amon Ducao, and Peter M. Dussinger, “Heap Pipe, Applications for improved Chemical Process Unit Operations” Thermacore, lnc. February 7. 1977
[9] Zhuang Jun: The final report for heat pipe chemical reactor of dehydrogenation.1984.N1CT 840017
[10] Qiu Yuantao Zhuang Jan, “Experimental Study of Heat Pipe Reactor for Catalytic Dehydrogenation of Ethyl Benzene” 3rd IHPS-TSUKUBA Preprints,sep. 1988,p261-265
[11] Hu Jia-zhen: Development on oxygenation reactor with heat pipe 1984,N1CT 80-019.
[12] Zhang Hong: Research on heat pipe ammonia reactor, thesis for doctor NUCT 1999.
[13] Wang Zhiliang et al, The final report for liquid-solid reversible chemical reactor with Loop heat pipes, May 2003,NUCT, 0305.

The 7th International Heat Pipe Symposium, 12-16 October, 2003, Jeju, Korea

Loop Heat Pipes - Development and Application

Yu. F. Maydanik

Institute of Thermal Physics, Ural Branch Russian Academy of Sciences

Ural Branch / Institute of Thermal Physics (ITP)

Contents

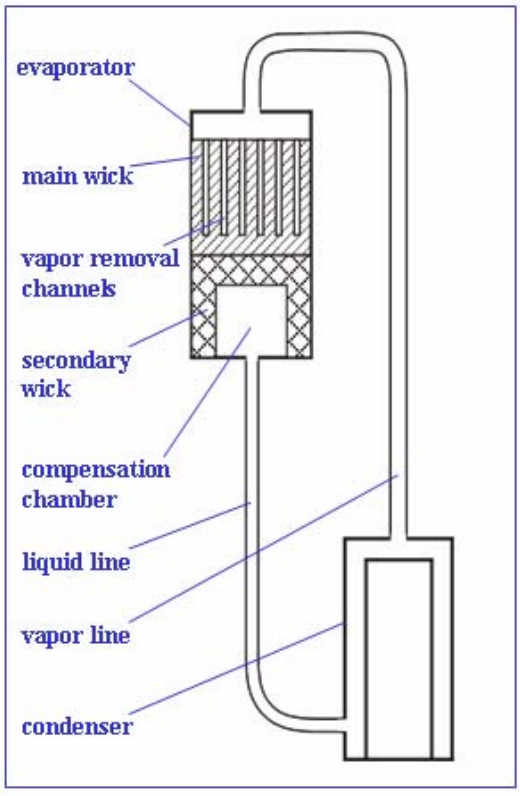
- **Identifications of a Loop Heat Pipe**
- **Historical background**
- **Theoretical foundations of the LHP operation**
- **Materials and working fluids**
- **Classification of LHPs**
- **Different types of LHPs and the main results of their investigations**
- **Application of LHPs**
- **Conclusion**

Brief historical background

- The LHP creation was a response to the challenge to develop a heat-transfer device operating on the principle of a heat pipe and possessing all its advantages, but at the same time capable of transferring heat for distances up to 1 m and more at different orientations in the gravity field.
- Such a device was first invented in 1972 by Yu. Gerasimov and Yu. Maydanik at the Ural Politechnical Institute.
- The first name of the device was "a heat pipe". Later the names "a heat pipe with separate channels" and "an antigravitational heat pipe" were used.
- In 1989, when these devices came into use in space engineering, there appeared a new name "a Loop Heat Pipe", which is now generally recognized.

Ural Branch / Institute of Thermal Physics (ITP)

The first LHP scheme



Specification

Total length, mm	≈ 1000
Evaporator diameter,mm	≈ 30
Active zone length, mm	≈ 60
Body material	ss
Wick material	nickel
Working fluid	water
Capacity, W	≈ 500
Year of development	1972
USSR certification 449 213	1974

Identifications of the Loop Heat Pipe (LHP)

1. By the principle of operation

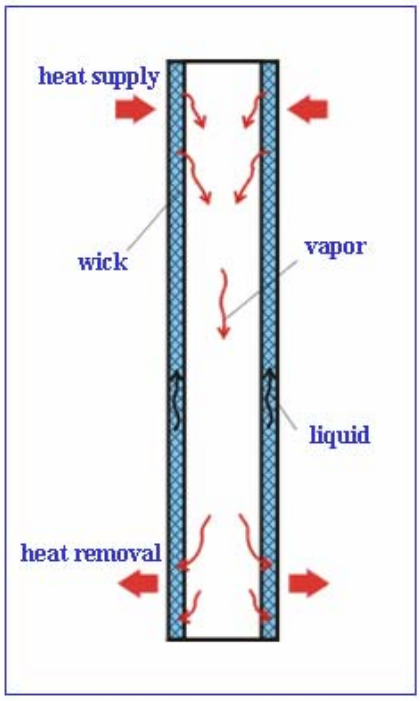
A loop heat pipe is a hermetic heat-transfer device operating on a closed evaporation-condensation cycle, in which the circulation of vapor and liquid flows in the transportation section is realized along separate smooth-walled tubing, and the capillary structure (wick), localized in the heat-supply zone, acts simultaneously as a capillary pump, a thermal and a hydraulic gate.

2. By design

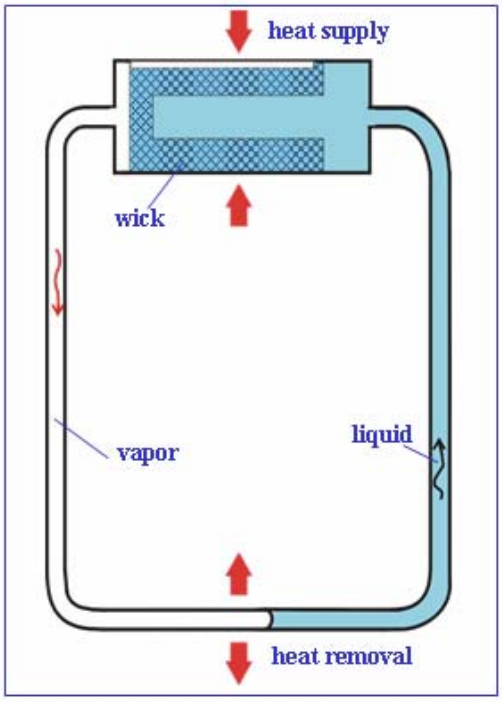
A loop heat pipe is a hermetic heat-transfer device made in the form of a closed loop filled with a working fluid in the vapor and in the liquid phase containing an evaporator with a capillary structure (wick) combined with a compensation chamber and a condenser connected to the evaporator by means of separate smooth-walled tubing of a relatively small diameter.

Ural Branch / Institute of Thermal Physics (ITP)

Scheme of a traditional heat pipe



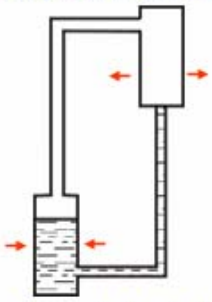
Scheme of a LHP



Ural Branch / Institute of Thermal Physics (ITP)

Scheme of classification of heat-transfer devices by the main design features

Loop Thermosyphon



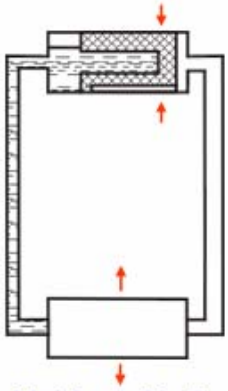
- the condenser is located above the evaporator
- separate smooth-walled tubing for vapor and liquid

Conventional Heat Pipe



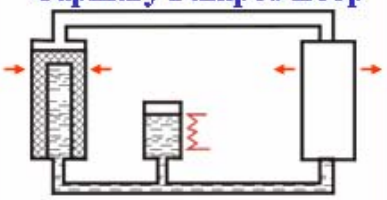
- single body
- the wick is located along the whole length

Loop Heat Pipe



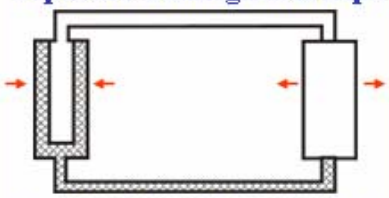
- the wick is located in the evaporator
- separate smooth-walled tubing for vapor and liquid
- the compensation chamber (reservoir) is combined with the evaporator

Capillary Pumped Loop



- the wick is located in the evaporator
- separate smooth-walled tubing for vapor and liquid
- separate reservoir with an additional heater

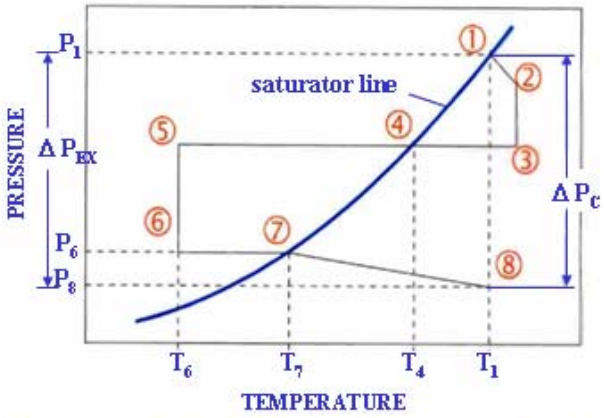
Separate Tubing Heat Pipe

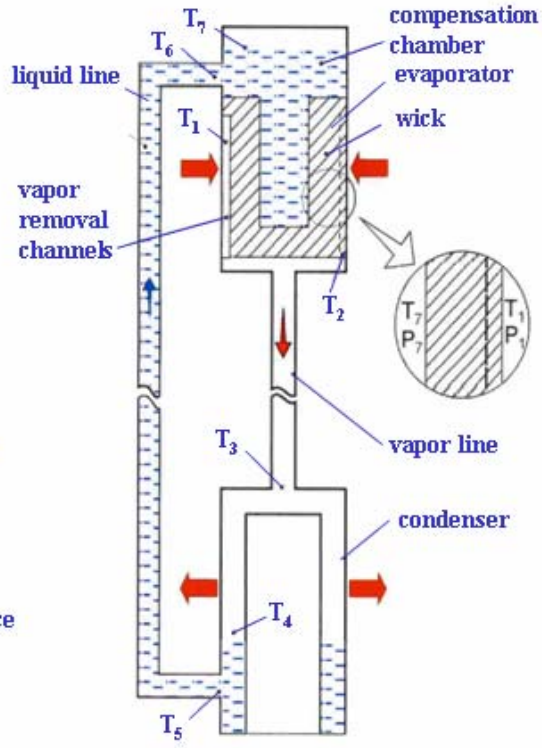


- the wick is located along the whole length
- separate tubing for vapor and liquid

Ural Branch / Institute of Thermal Physics (ITP)

Scheme and diagram of working cycle of an LHP





1, vapor state over the evaporating menisci in a wick
1-2, vapor motion in vapor-removal channels with superheating
2-3, adiabatic vapor motion in vapor line
3-4, vapor cooling and condensation in a condenser
4-5, liquid supercooling in a condenser
5-6, adiabatic liquid motion in a liquid line with allowance for the hydrostatic resistance
6-7, liquid motion in a compensation chamber
7-8, liquid motion in a wick

RAS Ural Branch / Institute of Thermal Physics (ITP)

Conditions of an LHP serviceability

1. Condition of balance of the capillary head and the sum of pressure loses in all sections of the working fluid circulation (hydrodynamic condition):

$$P_C = \Sigma P_{1\text{-}8} = \Delta P_L + \Delta P_V + \Delta P_G$$

2. Condition of correlation between the temperature and the pressure of saturated vapor above the surface of menisci in the evaporation zone and above the surface of the interface in the compensation chamber (start-up condition):

$$dP/dT\ (T_1 - T_7) \approx P_1 - P_7$$

3. Condition of liquid supercooling (thermodynamic condition):

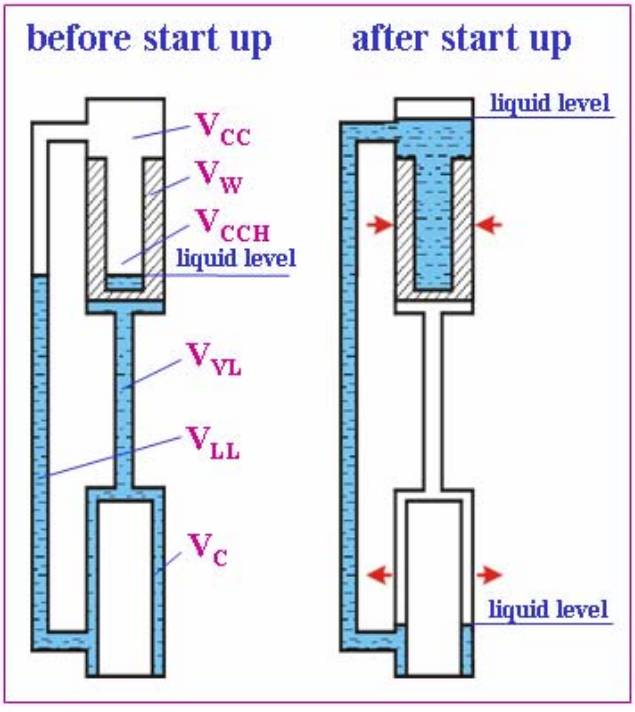
$$dP/dT\ (T_5 - T_4) \approx P_5 - P_6$$

4. Condition of relationship between the internal volumes and the volume of a liquid:

$$\begin{cases} V_{CC} \geq V_{VL} + V_C \\ V_L = V_W + V_{LL} + V_{CC} + V_{CCH} \end{cases}$$

RAS Ural Branch / Institute of Thermal Physics (ITP)

Correlation of volumes in an LHP



1. The volume of the compensation chamber V_{CC} must be equal to or exceed the sum of the volumes of the vapor line V_{VL} and the condenser V_C

$$V_{CC} \geq V_{VL} + V_C$$

2. The volume of the liquid V_L in an LHP must be equal to the sum of the volumes of the liquid in the wick V_W, the liquid line V_{LL}, the compensation chamber V_{CC} and the central channel V_{CCH}

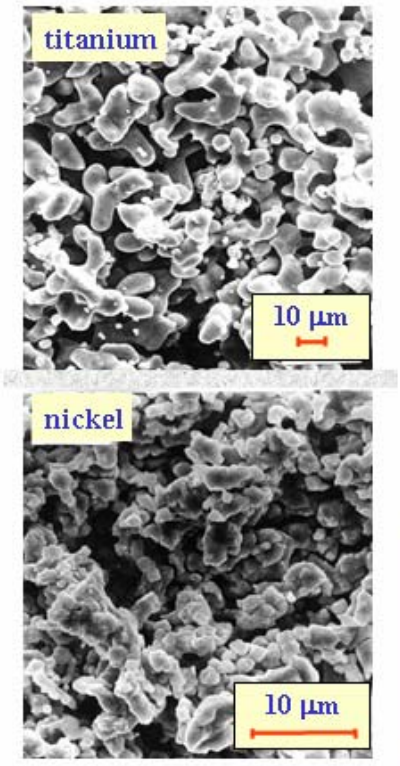
$$V_L = V_W + V_{LL} + V_{CC} + V_{CCH}$$

Classification of LHPs

LHP design	LHP dimensions	Evaporator shape	Evaporator design
• conventional (diode) • reversible • flexible • ramified	• miniature • all the rest	• cylindrical • flat disk-shaped • flat rectangular	• one butt-end compensation chamber • two butt-end compensation chambers • coaxial
Condenser design	**Number of evaporators and condensers**	**Temperature range**	**Operating-temperature control**
• pipe-in-pipe • flat coil • collector	• one • two and more	• cryogenic • low-temperature • high-temperature	• without active control • with active control

RAS Ural Branch / Institute of Thermal Physics (ITP)

Metal-theramic wicks for LHPs





Specification

Material	Nickel	Titanium
Effective pore radius, μm	0.5 - 2	3 - 10
Porosity, %	65 - 75	55 - 70
Permeability, m^2	10^{-14}	10^{-13}
Year of development	1972	1978

RAS Ural Branch / Institute of Thermal Physics (ITP)

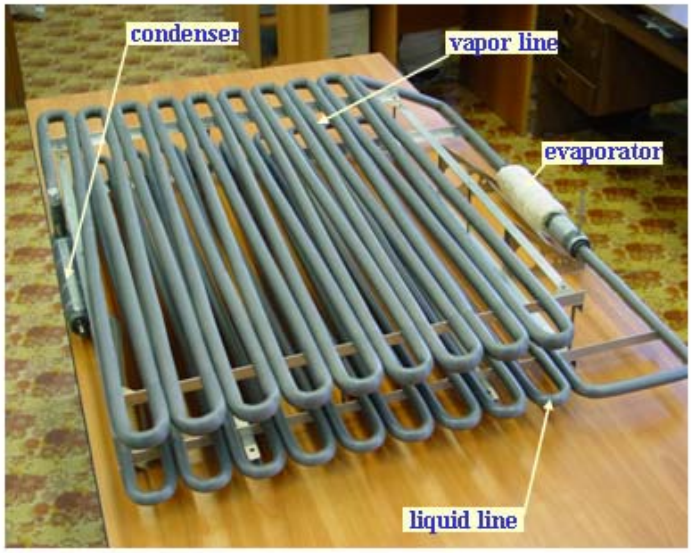
Tested LHPs material- working fluid combinations

Body	Wick	Working fluid
stainless steel	nickel	water, ammonia, acetone, pentane, freon-152A, freon 11, propylene
stainless steel	titanium	water, ammonia, acetone, pentane, freon-152A, toluene
stainless steel	stainless steel	ammonia
nickel	titanium	ammonia
nickel	nickel	ammonia
copper	copper	water

RAS Ural Branch / Institute of Thermal Physics (ITP)

LHPs with a high heat-transfer capacity

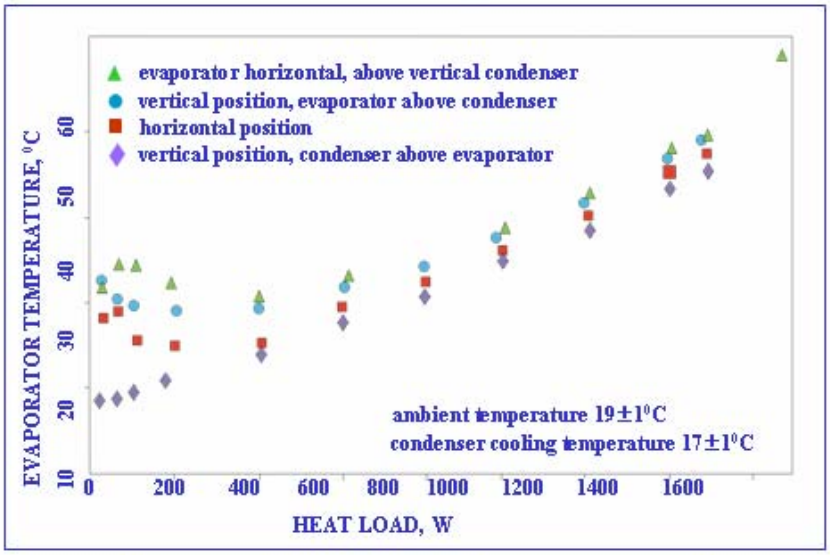




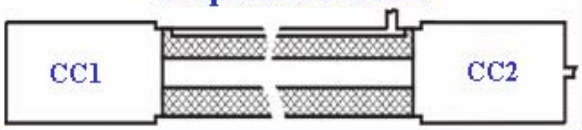
Ural Branch / Institute of Thermal Physics (ITP)

Ammonia two-meter LHP with two butt-end compensation chambers





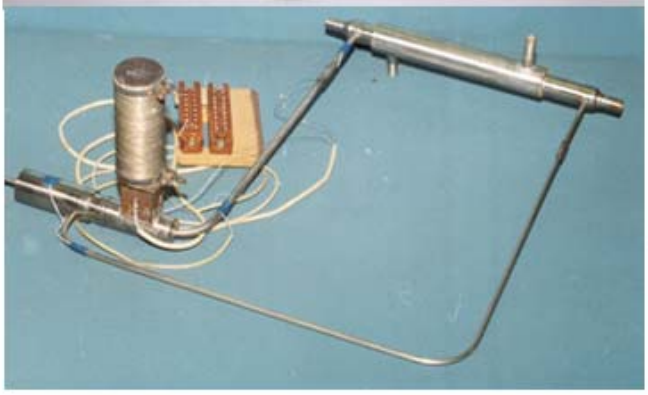
Evaporator scheme



Ural Branch / Institute of Thermal Physics (ITP)

Ammonia High-Heat Flux LHP



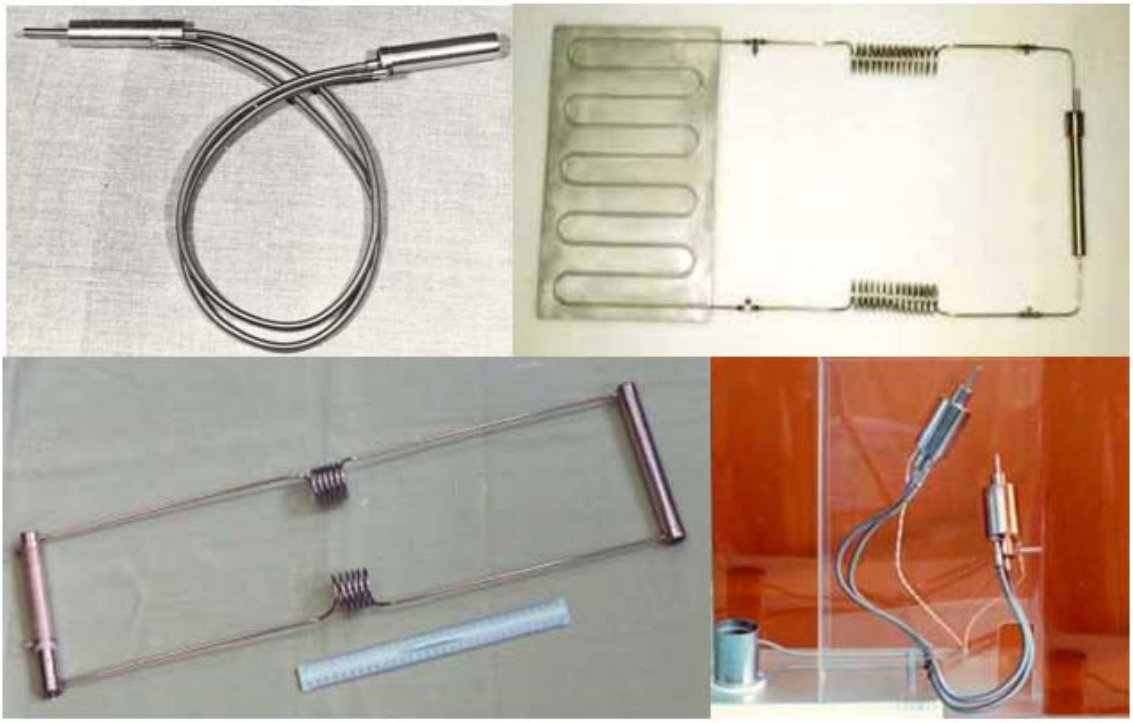


Specification

Effective length, mm	450
Evaporator diameter, mm	20
Vapor line diameter, mm	6/4
Liquid line diameter, mm	4/3
Heating zone area, cm^2	4.25
Max heat flux, W/cm^2	130
Max heat transfer coef., W/m^2 K	30 000
Year of development	1997

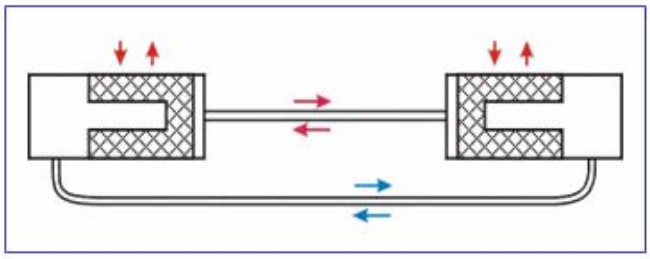
Ural Branch / Institute of Thermal Physics (ITP)

Flexible LHPs



Ural Branch / Institute of Thermal Physics (ITP)

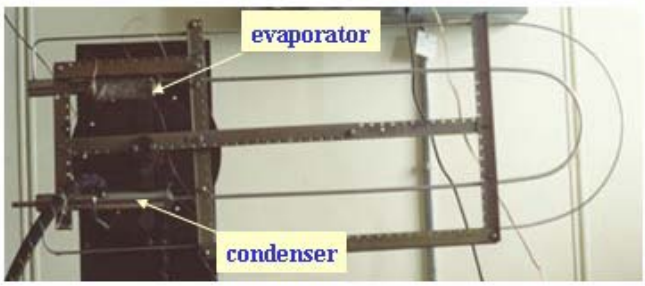
Reversible LHP scheme



Specification

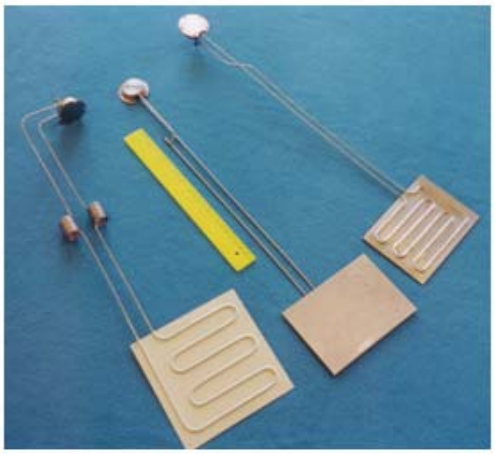
Total length, mm	2000
Evaporator diameter, mm	24
Active zone length, mm	100
Vapor line diameter, mm	6
Liquid line diameter, mm	4
Max capacity, W	900
Min thermal resistance, ^{0}C/W	0.02
Year of development	2000

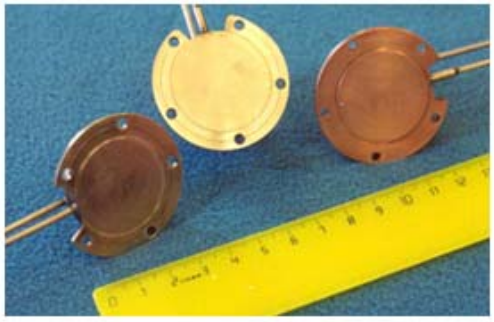
General view of ammonia RLHP



Ural Branch / Institute of Thermal Physics (ITP)

LHPs with flat evaporators



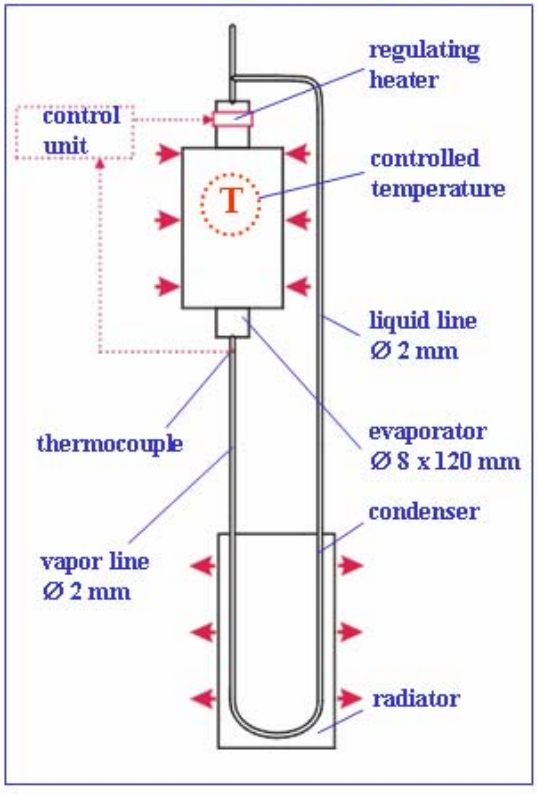


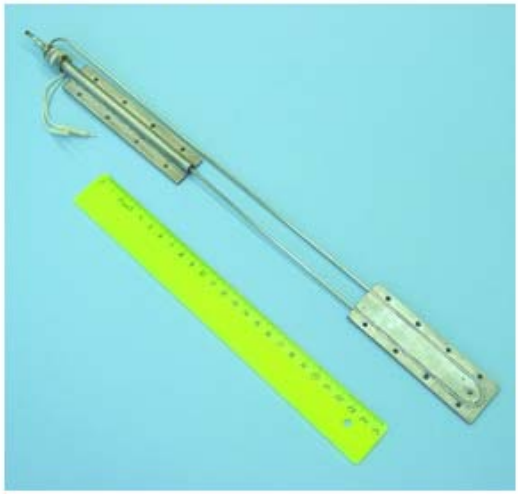
Specification

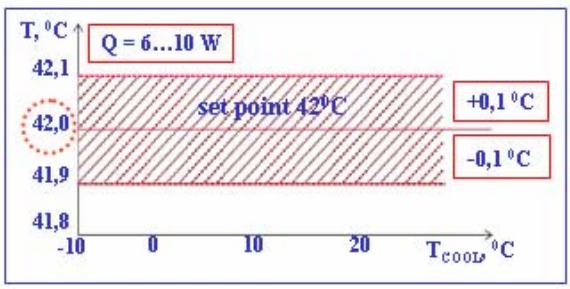
Total length, mm	865
Evaporator diameter, mm	30
Evaporator thickness, mm	13
Vapor/Liquid line diameter, mm	2/1.2
Condenser length, mm	720
Body material	ss
Wick material	nickel/titanium
Working fluid	ammonia
Total mass, g	167
Max capacity, W	110/90
Min thermal resistance, ^{0}C/W	0.30/0.41
Year of development	1999 - 2001

Ural Branch / Institute of Thermal Physics (ITP)

LHP with temperature active control

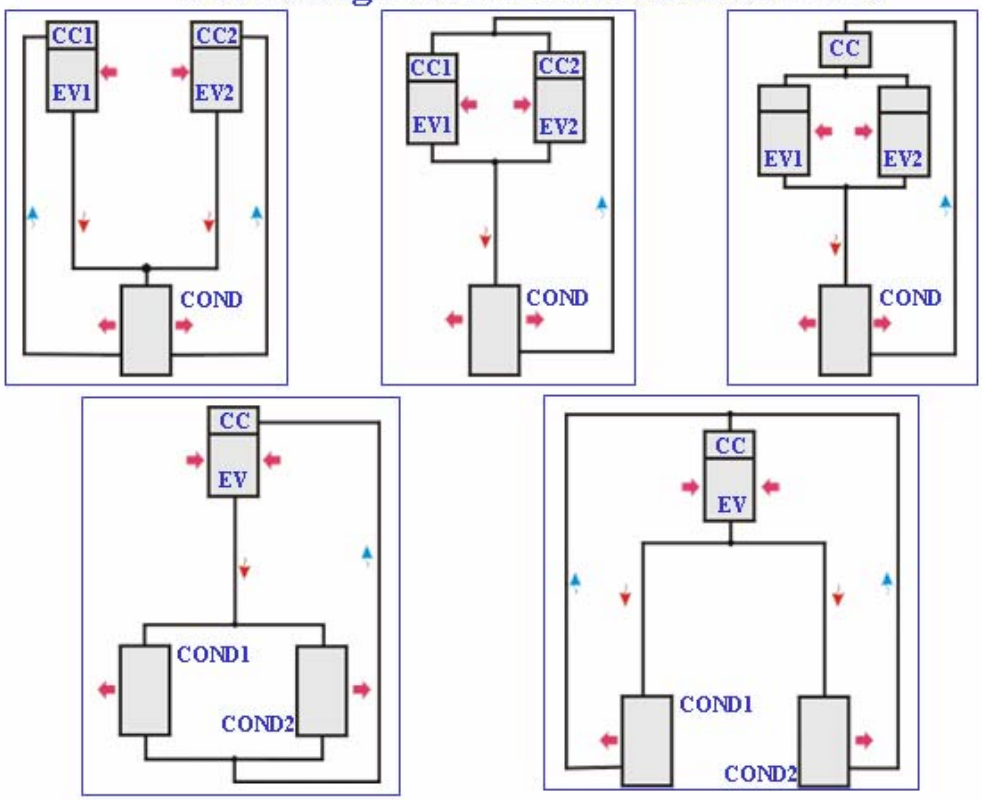






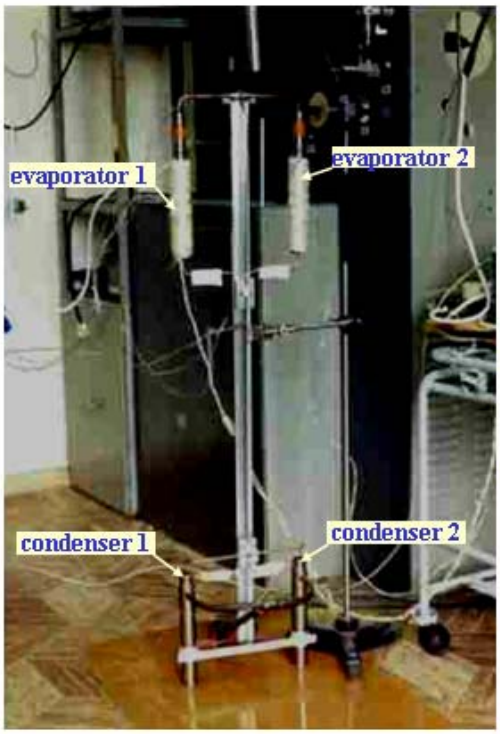
Ural Branch / Institute of Thermal Physics (ITP)

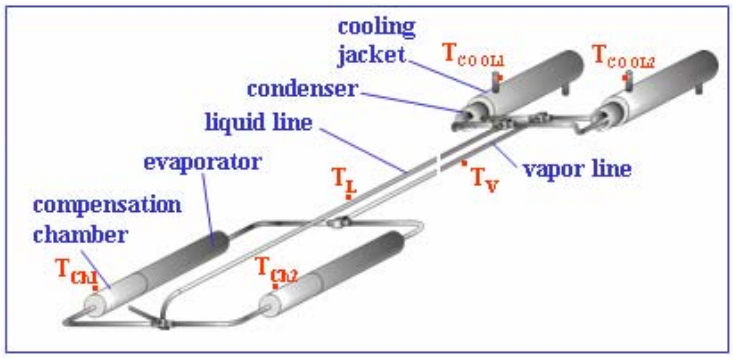
Base design variants of ramified LHPs



Ural Branch / Institute of Thermal Physics (ITP)

Two evaporator-condenser LHP

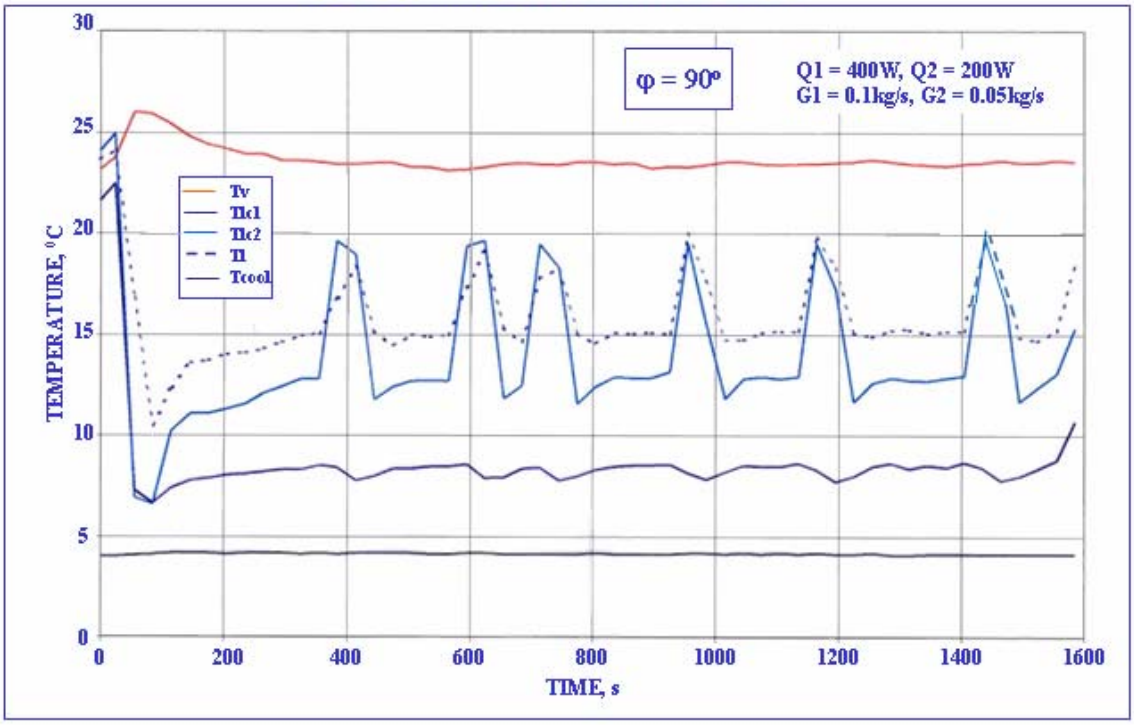




Specification

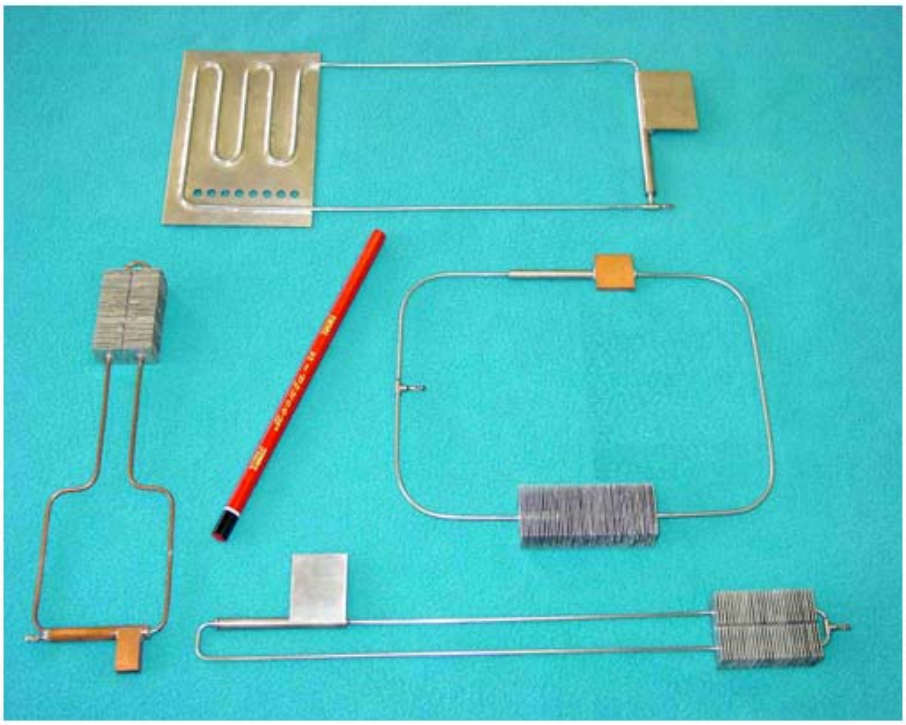
Total length, mm	1000
Evaporator diameter, mm	24
Vapor line diameter, mm	6/4
Liquid line diameter, mm	4/3
Max capacity, W	1400
Year of development	2002

Test results of ramified LHP



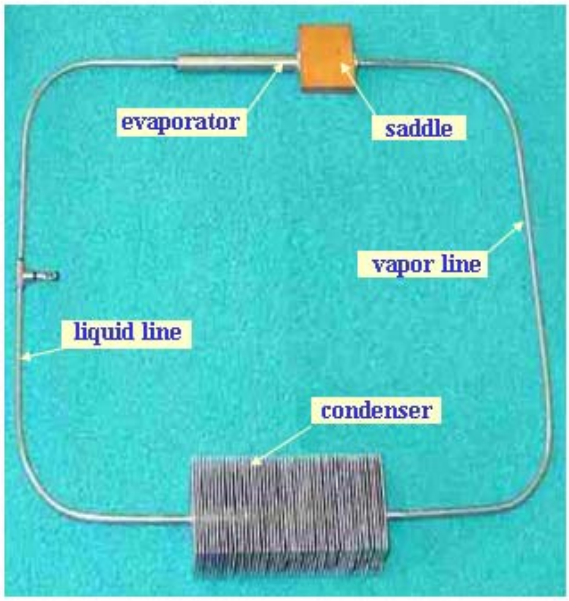
Ural Branch / Institute of Thermal Physics (ITP)

Miniature LHPs



Ural Branch / Institute of Thermal Physics (ITP)

General view of MLHP

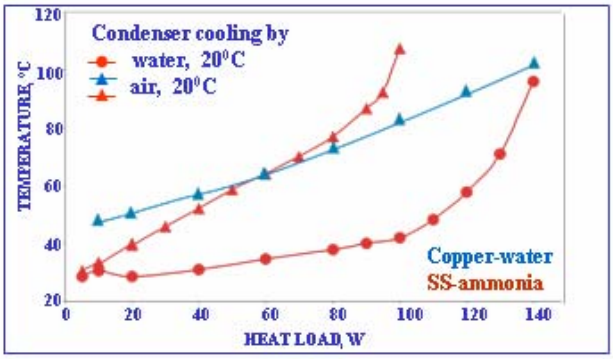


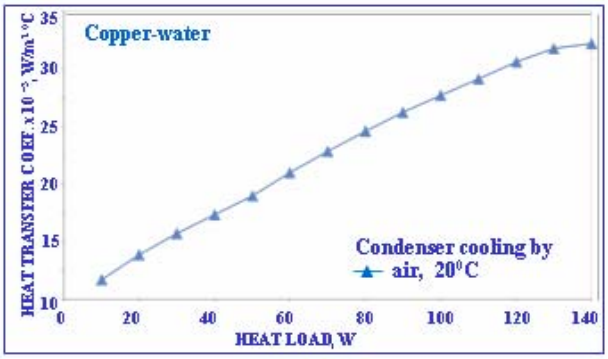
Specification

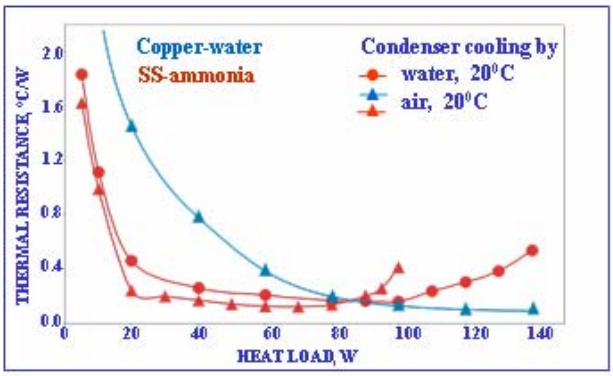
Body-working fluid	Copper- water	SS-ammonia
Effective length, mm	300	230
Evaporator diameter, mm	6	5
Lines diameter, mm	2.5	2
Active - zone length, mm	20	20
Condenser length, mm	60	60
Thermal interface, mm	20 x 20	20 x 20
Heat load, W	130	70
Evaporator temperature	98	70
Own thermal resistance, ^{0}C/W	0.10	0.12
Total thermal resistance - (evaporator-ambient), ^{0}C/W	0.59	0.68
Year of development	2003	2002

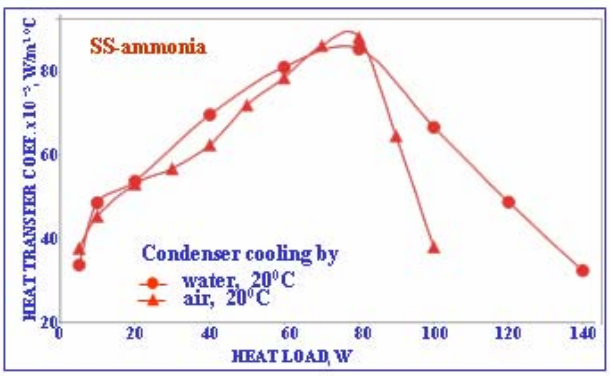
Ural Branch / Institute of Thermal Physics (ITP)

Tests results of miniature LHPs



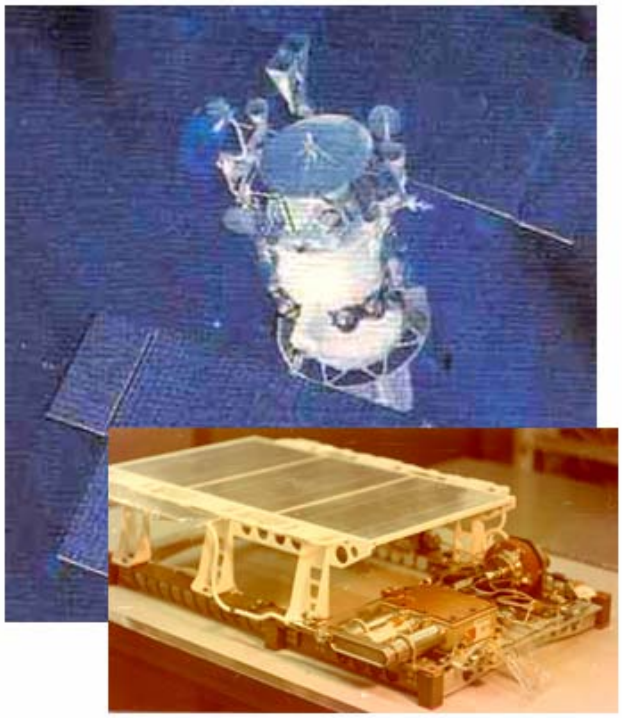






Ural Branch / Institute of Thermal Physics (ITP)

The first flight experiment with an LHP aboard the spacecraft «GORISONT» in 1989

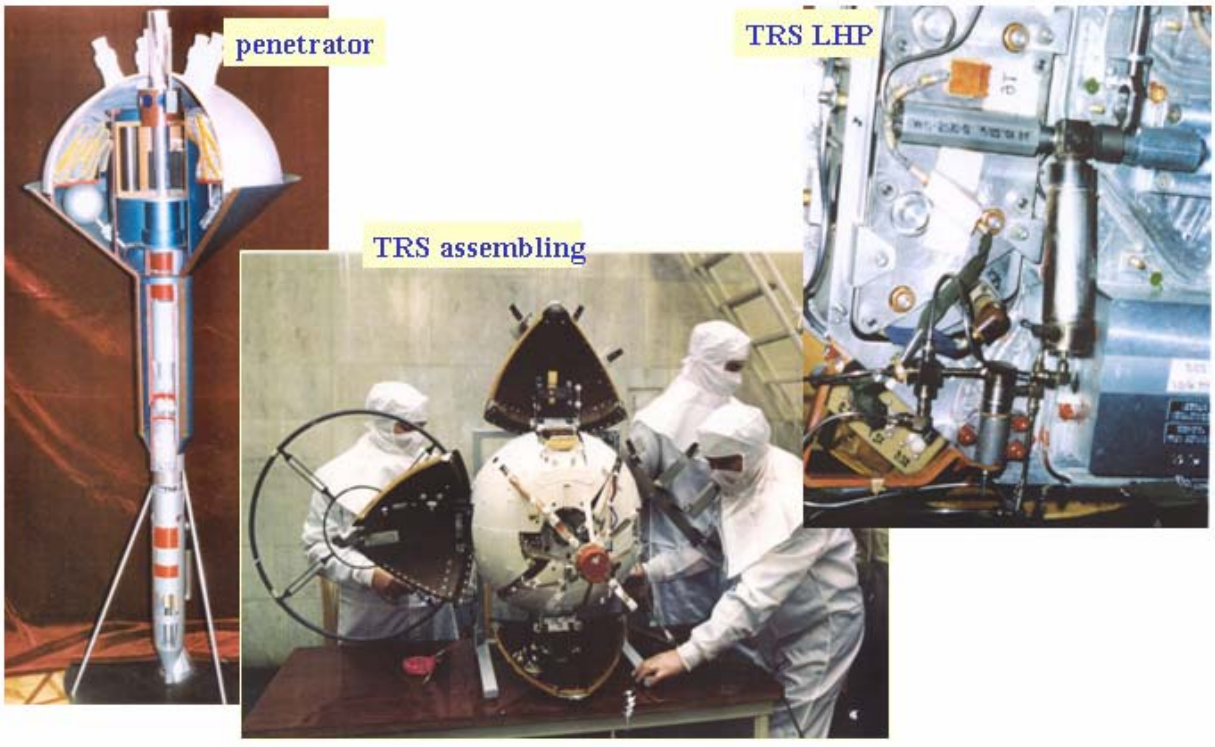


The first application of an LHP aboard the spacecraft «OBZOR» in 1994



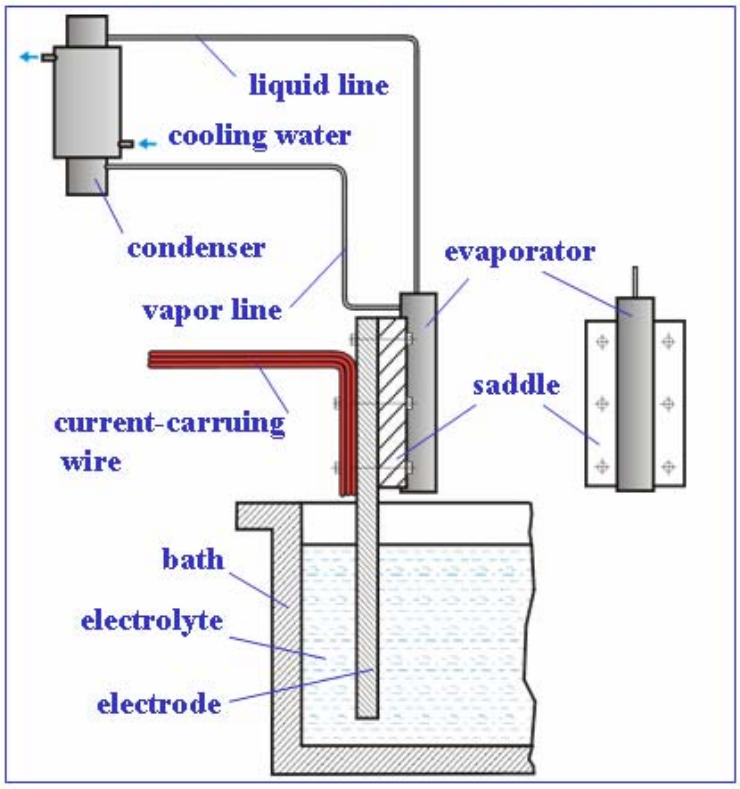
Ural Branch / Institute of Thermal Physics (ITP)

Thermoregulation system with LHPs for the international program «MARS-96»



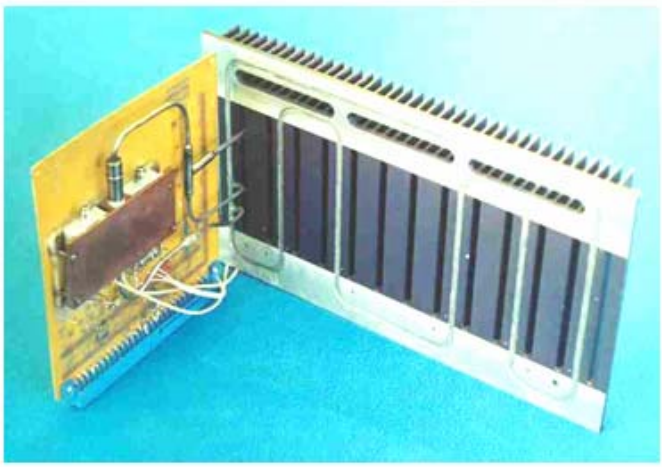
RAS Ural Branch / Institute of Thermal Physics (ITP)

Cooling of the copper bus of an electrolysis-bath electrode

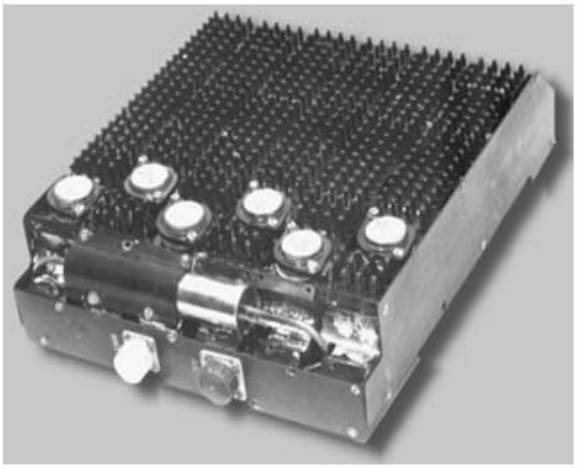


RAS Ural Branch / Institute of Thermal Physics (ITP)

Cooling of quantum-electronic converters

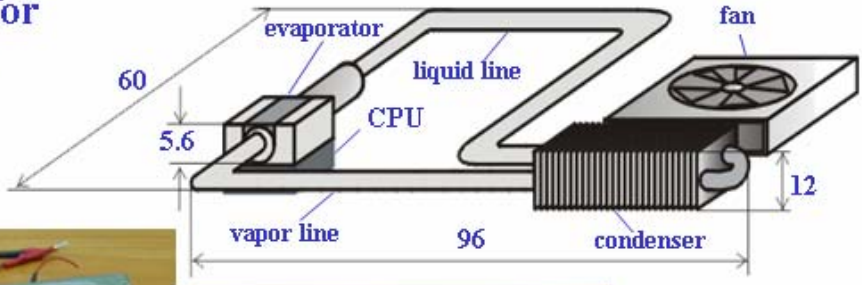


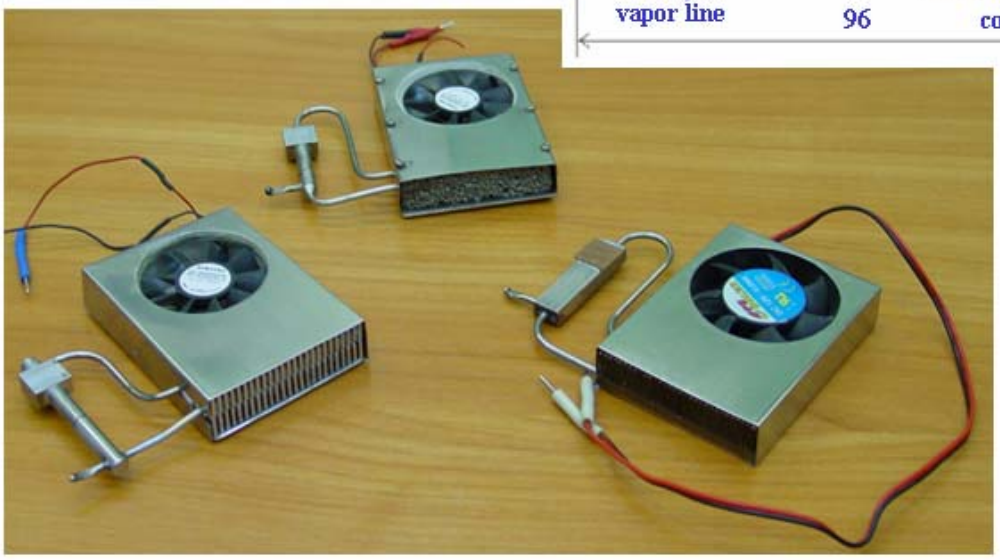
Cooling of powerful transistors



RAS Ural Branch / Institute of Thermal Physics (ITP)

25 W CPU coolers for a mobile computer

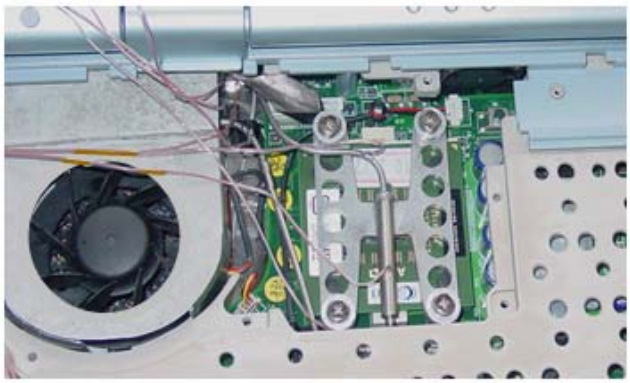


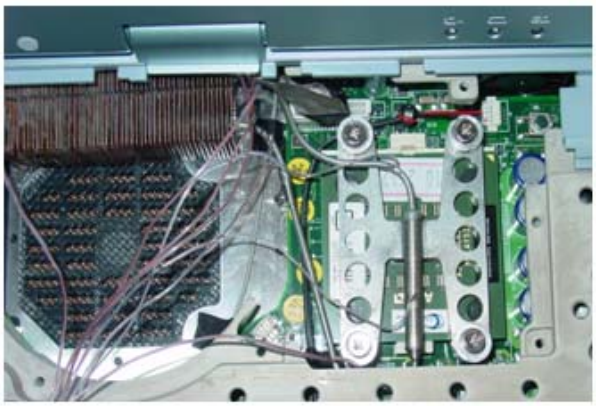


RAS Ural Branch / Institute of Thermal Physics (ITP)

45 W CPU Cooler for a Mobile PC









Conclusion

Loop Heat Pipes are very promising and universal heat-transfer devices, whose potential of development and application has not been used in full measure.

A Closed Look to a Closed-End Oscillating Heat Pipe

Pradit TERDTOON

Department of Mechanical Engineering, Faculty of Engineering
Chiang Mai University, Chiang Mai 50200, Thailand
Tel. +66-5394-4151 ext. 911, Fax. +66-5322-6014, E-mail: pradit@eng.cmu.ac.th

Abstract

Heat pipe is a device with very high thermal conductance. The heat pipe employs evaporating and condensing process of working fluid (Dunn and Reay, [1]). Generally, it is a closed end tube which comprised of an air-evacuated hollow tube and some amount of working fluid sealed with in the tube. The heat pipe components, classified by their functions are; evaporator, adiabatic and condenser sections. The heat pipe can be utilized in many ways such as a heat transfer device in heat recovery system, heat exchanger and stabilizer temperature of electronics devices. In order to ultimately enhance the performance of the heat pipe, the understanding of type, working principle and thermal performance of the heat pipe must be thoroughly gained. The heat pipe can be divided into two main types; conventional heat pipe and oscillating or pulsating heat pipe which is a new evolution of heat pipe technology with very high heat transfer, compact size and lightweight.

1. CONVENTIONAL HEAT

The conventional heat pipe can be divided into two main groups; without internal wick or thermosyphon, and with internal wick. The conventional heat pipe without internal wick, schematically shown in Figure 1, consists of a container and some working fluid. It can be separated into 3 parts as evaporator, adiabatic and condenser sections. When the evaporator receives heat, the fluid vaporizes and flows to the condenser section, where surrounding temperature is decreased, and condenses there. The condensate returns to the evaporator section by gravitational force. This group of conventional thermosyphon must operate only at vertical position because it employs the gravitational force to return the condensate to the evaporator section. Figure 2 shows the conventional heat pipe with wick structure.

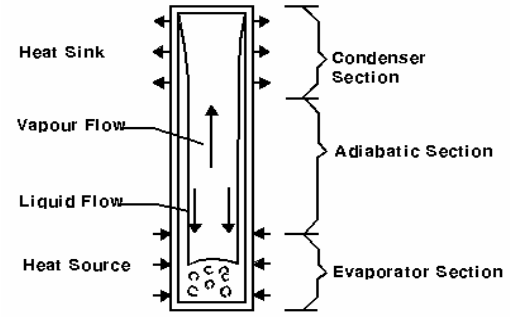


Figure 1: Thermosyphon

It consists of a container, some working fluid and a wick structure. The wick attaches with the inner wall of the container. The principle of operation is similar to that of the conventional thermosyphon. The difference is the method to return the condensate from the condenser section to the evaporator section. In this type of the heat pipe, the condensate returns to the evaporator section by capillary effect instead of the gravitational effect. So it can operate in any direction.

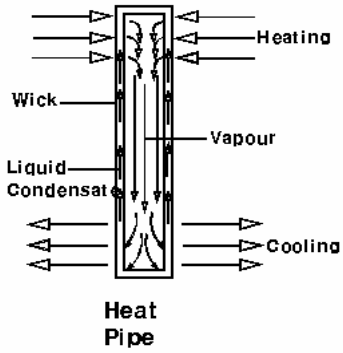


Figure 2: Conventional heat pipe

However, the heat pipe with or without wick structure has its own operating limits. This may be caused since the wick structure cannot sufficiently promote the flow of liquid from the condenser to the evaporator. These limits occur when the different temperature between heat source and heat sink is increased to a specific condition. The heat transfers rate at this point is called critical heat flux. According to ESDU [2], these limits are;

- Vapor pressure limit. When operates a heat pipe at a pressure substantially below atmospheric, the pressure drop of the vapor may be significant compared with the pressure in the

evaporator and the heat transfer cannot be transferred.

- Sonic limit. At low operating pressure, the vapor velocity may be appreciable compared with the sonic velocity in the vapor. This causes the limit in the heat pipe at higher operation.

- Dryout limit. This limit can be occurred due to volume of the liquid fill is not sufficient. When high heat flux is added to the evaporator section, temperature of tube wall in evaporator section will rise due to drying of liquid.

- Countercurrent flow limit. Even when there is sufficient liquid in heat pipe, the overall rate of heat transfer is subjected to another limit. This occurs when the rate of entrainment of liquid by the vapor prevents the downward flow of liquid and it is called flooding limit.

- Boiling limit. The boiling limit occurs when high heat flux is supplied to evaporator section and vapor bubble occurs. The vapor bubble will immediately mix in the vapor film at wall. This vapor film is a heat insulator between tube wall and liquid and accumulates heat at the wall. Temperature at wall, accordingly, increases and hot spot occurs as resistor in circulating of fluid.

2. OSCILLATING OR PULSATING HEAT PIPE, OHP

When diameter of tube is too small (e.g. when heat pipe is applied with cooling of electronic device), the problems of conventional heat pipe are capillary limit and countercurrent flow limit. A new type of heat pipe which is called oscillating heat pipe (Akachi et al., [3]) has been developed to solve this problem by connecting bundle of parallel capillary tubes into a single undulating in series and without internal wick structure. In this undulating pipe, the formation of the slugs and bubbles gives rise to the oscillating motion of the working fluid plus the phase change phenomena. The oscillation of slugs and bubbles in the OHP is self- sustained by the evaporation of the liquid slugs and the condensation of the bubbles in the pipes. The driving force is sustained by the interaction between nucleate boiling and liquid slug of working fluid. It can transfer the heat from high temperature section to another section with lower temperature. The OHP has advantages as follow, it can be easily made with low cost, has good heat transfer performance, fast thermal response, capability of operation in any position and operational flexibility. Although the OHP is widely adopted, the internal phenomena of OHP are very complicated. Many researchers are not quite sure to identify the internal movement pattern of the OHP, some might adopt this movement as “Pulsating” or “Oscillating”. In this case, the OHP can be classed as the Pulsating (PHP) or Oscillating Heat Pipe. Some, however, point out that the internal movement pattern of the vapor slug is rather “Chaotic” so they reason that this should be identified as the Chaotic Heat Pipe (CHP).

2.1 Types of oscillating heat pipe

The OHP can be divided into three main types as shown in Figure 3 (Maezawa et al., [4])

- Closed-loop oscillating heat pipe, CLOHP. It consists of a long capillary tube forming closed loop. Heat is transferred by oscillating the working fluid in the direction of the pipe’s longitudinal axis causing it to circulate slowly in either direction.

- Closed-loop oscillating heat pipe with check valves. This made of very long of capillary tube, coiled with their ends joined to form closed loop. It incorporates one of more check valves in the loop so that the working fluid that carries the heat quickly circulates in the specified direction.

- Closed-end oscillating heat pipe, CEOHP. is made from long capillary tube has no check valves and no closed loops. In this case, heat transfer could be occurred by the oscillating which may be driven by fast fluctuating pressure waves caused by nucleate boiling in the working fluid. This paper will concentrate on the heat transfer characteristic of the CEOHP.

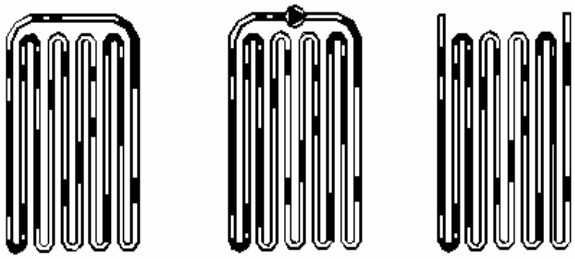


Figure 3: Three types of meandering capillary tube.

2.2 Working principle of OHP

Akachi et al. [3] studied the principle, feature and application of the OHP. It was found that basic operational principle of heat transfer of OHP was that, the liquid plugs and vapor bubbles must co-exist inside the tube along its length. This can be achieved by vacuuming the tube and then partially filling it with some working fluid. During the operation, the driving force of a pulsating heat pipe is the pressure force generated by evaporation at the high temperature end. The evaporation at the high- temperature end increases

the vapor pressure which causes the bubbles in the evaporator to grow. This pushes the liquid columm toward the low-temperature end (condenser). The condensation at this end will further enhance the pressure difference between the two ends. Because of the inter-connection of the tube, the motion of liquid slugs and vapor bubbles at one section of the tube towards the condenser also leads to the motion of slugs and bubbles in the next tube section towards the high-temperature end in the next section. This works as the restoring force. The inter-play between the driving force and the restoring force leads to oscillation of the vapor bubbles and liquid slugs in the axial direction.

There are not many works concerning its performance limit. Maezawa et al. [4] reported only few limits of performance and Lin et al. [5]showed the effect of filling ratio on the performance limit of the FC-72 OHP. In order to clarify the phenomena of this limitation, this paper aims at the basic investigation of the limited and determine the correlation to predict the occurrence of such limit.

2.3 Researches of heat transfer characteristics of OHP

Maezawa et al. [4] investigated the heat transfer characteristic of OHP. The OHP is made of a long capillary tube with an inner diameter of 1 mm. The tube is meandered with 20 turns and the 24 m total length. The R142b was used as working fluid. Heat was transferred to the working fluid through the tube wall by means of resistive electric flat type heaters sandwiched around the outer wall of evaporator. The A.C. power supplied to the heaters was controlled through variable transformers and measured with wattmeter. At the condenser section, heat was released by means of water jacket, which were installed in the condenser section. Water flow rate and the inlet/outlet temperature were measured by 4 copper-constantan thermocouples at evaporator, condenser and adiabatic in each sections. A schematic diagram of experimental apparatus is shown in Figure 4.

The results obtained are, the unlooped meandering capillary tube is able to transfer heat by the fluctuant phenomenon of working fluid. The source of this heat by the fluctuation may be the process of bubble formation by nucleate boiling, growth, broken in the evaporator and lapsed in the condenser. The fluctuation character in the meandering capillary tube is very complex, and affected by heat transfer rate, filling ratio of working fluid, operation mode, tube diameter and the number of meandering turns. Also, presented to internal flow pattern which has slug and vapor bubbles flow, it can be shown in Figure 5

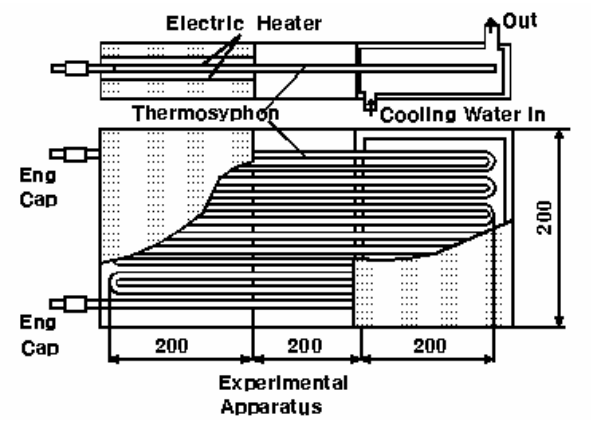


Figure 4: Experimental apparatus of OHP. (Maezawa et al., [4])

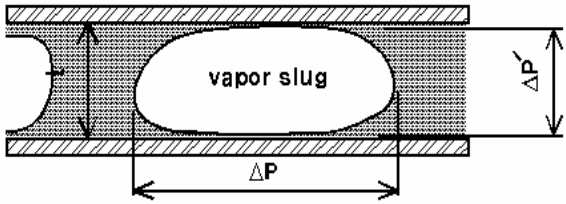


Figure 5: Slug flow. (Maezawa et al., [4])

Figure 5 shows radial pressure $(\Delta P')$ and axis pressure (ΔP) of the OHP. For the condition of $\Delta P > \Delta P'$, the slug exists inside tube. The working filling ratio of 50% will result in thermal resistance of lower than that of filling ratio 30% and 70%. The minimum inner diameter of the capillary tube can be defined as;

$$d_{\max} < 2\sqrt{\frac{\sigma}{\rho_L g}} \qquad (1)$$

Rittidech et al. [6] investigated the effect of inclination angles, evaporator section lengths and working fluid properties on heat transfer characteristics of a closed-end oscillating heat pipe at normal operation. The CEOHPs were made of copper tubes with inside diameter of 2.03 mm. It was one continuous beaded long without joints having a sealed by welding at each end. The length of evaporator, adiabatic and condenser sections varied as 15 and 5 cm. The total length was 10 m. R123, ethanol and water were used as working fluids with a filling ratio of 50%. The evaporator section was heated by hot water, while the condenser section was cooled by a solution of water and ethylene glycol 50:50 by volume, the temperature at evaporator and condenser section are 80 ^{o}C and 20 ^{o}C respectively. Figure 6 showed an experimental setup.

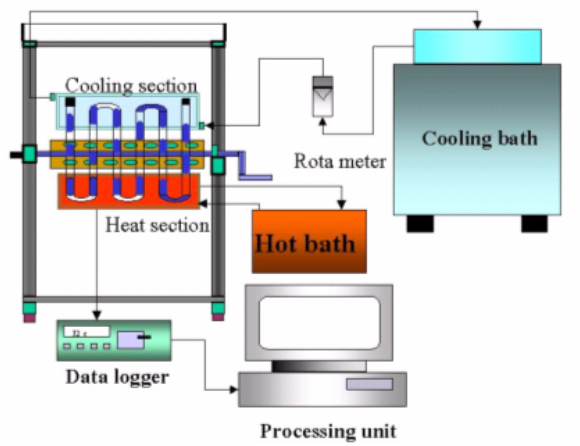


Figure 6 Experimental setup of CEOHP. (Rittidech et al., [6])

Figure 7 shows the effect of an inclination angle on Q/Q_0. The Q/Q_0 increases with the decrease of the inclination angles from vertical to 80-85 degree. The maximum values of Q/Q_0 for R123, ethanol and water are 2.19, 2.15 and 1.98 respectively.

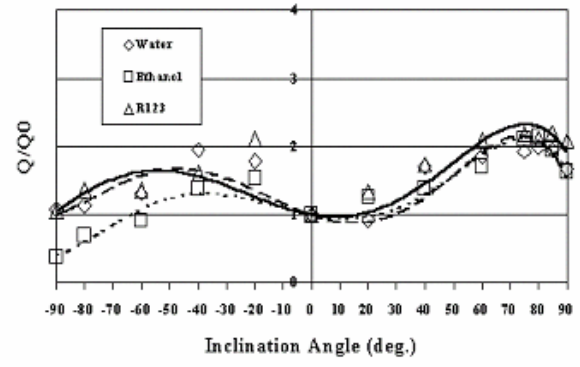


Figure 7: Effect of inclination angle on Q/Q_0at any angles of CEOHP (Rittidech et al., [6])

The relationship of Q_{max}/Q_0 and evaporator section lengths of the CEOHP can be seen in Figure 8. The controlled parameters are 2.03 ID, evaporator section length of 5 and 15 cm, filling ratio 50%, total length 10 m. and R123, Ethanol and water are working fluids. It can be observed that, the evaporator section lengths affect the Q_{max}/Q_0 such that the longer evaporators section lengths, the higher Q_{max}/Q_0. The following correlation is found;

$$Q_{max}/Q_0 = 1.80 + 0.06Le \qquad (2)$$

In addition, it was found the latent heat of vaporization affects the Q_{max}/Q_0. The working fluid with the lower latent heat of vaporization exhibits a higher Q_{max}/Q_0. Moreover, They proposed their correlation to predict heat transfer rate of the CEOHP as;

$$Ku_0 = 0.0052\left[\left(\frac{D_i^{4.3}L_t^{0.1}}{L_e^{4.4}}\right)n^{0.5}\left(\frac{\rho_v}{\rho_l}\right)^{-0.2}Pr_v^{-25}\right]^{0.116} \qquad (3)$$

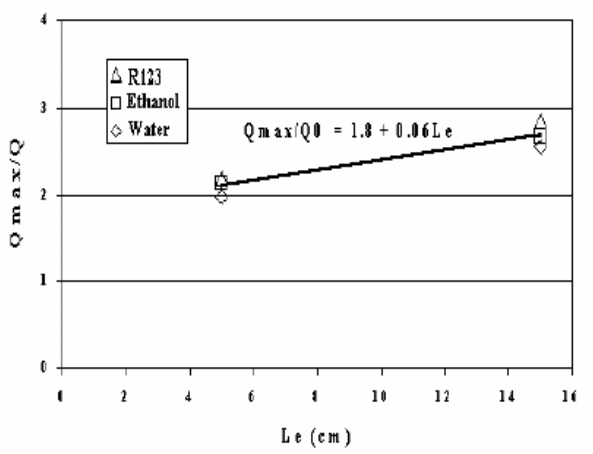


Figure 8: Effect of evaporator section length on Q_{max}/Q_0, (Rittidech et al., [6])

With the comparison of experimental results as in Figure 9.

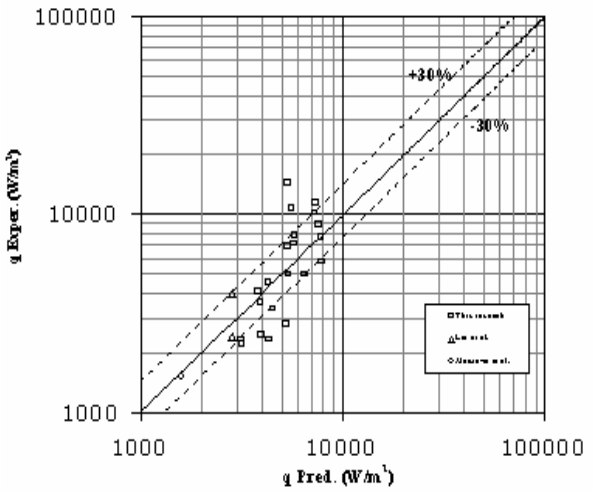


Figure 9: Accuracy of prediction from the correlation of Rittidech et al. [6].

Lin et al. [5] investigated the OHP. The OHP is made of a small copper tube with an inner diameter of 1.75 mm. Outer diameter is 3.18 mm. The tube is bent into a multitube array having 40 turn and a length of 446 mm. There are one evaporator in the middle of the OHP and two condensers on the top and bottom of the OHP. Lengths of the evaporator, adiabatic and condenser section are 125 mm., 51.5 mm. and 109 mm. respectively. Due to their non-flammability feature, FC-72 and FC-75 are employed as the

OHP working fluid. The filling ratio of the fluorocarbon fluids is varied from 32% to 50%. In the range of the present OHP operating temperature are 25 to 85 ^{o}C. The schematic diagram of the OHP is shown in Figure 10. The heater contains four aluminum thermal conduction plates. The thermal conduction plates are machined, on their contact side with the OHP tube array, into semicircle grooves having the same radius as the OHP tube. Two electric resistors are installed in the thermal conduction plates. In condenser section, water is used as the coolant. In addition, the coolers can adjust flow rate of fluid which controlled by the two control valves. The thermocouples are used to measure the inlet and outlet temperature and nineteen thermocouples of type T are placed on the OHP wall among which five are located in the evaporator, six in the adiabatic section and eight in the condensers. It is found from the experiments that, no dryout on any tube wall of the evaporator of the vertical FC-72 OHP with the filling ratio of 50% operating at the temperature of 75 and 85 ^{o}C and the total heat rates up to 2040 W. However, the fluorocarbon OHP with the 32% filling ratio cannot operate appropriately even at the low input power of 200 W due to the occurrence of the dryout in the evaporator. Figure 11 shows the relationship between thermal conductance of the evaporator and condenser with total heat rate.

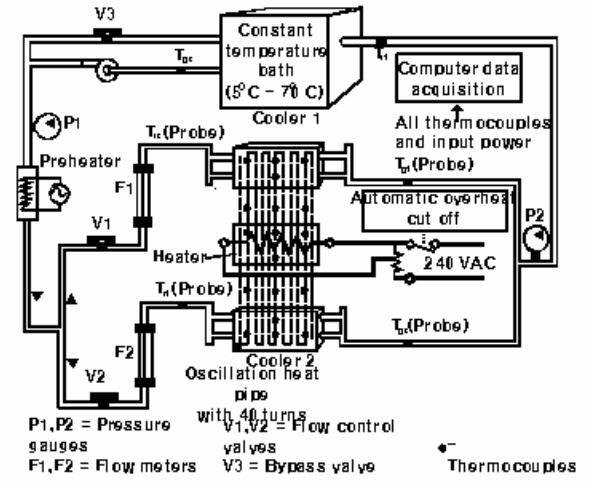


Figure 10: Experimental setup of Lin et al. [5].

For the FC-72 OHP at vertical and horizontal operation, the thermal conductance of the evaporator and condenser is found to be a function of the heat rate. At operating temperature of 75 ^{o}C and filling ratio of 50%, The thermal conductance increases with the heat rate. In addition to, Lin et al. [5] compared the thermal conductance of the FC-72 with those of the FC-75 and acetone OHP. The thermal conductance of evaporator of the FC-72 OHP is lower than that of the acetone OHP but higher than that of the FC-75 OHP.

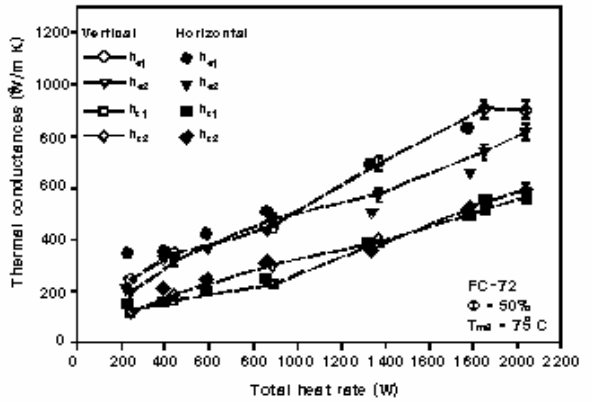


Figure 11: Relationship between thermal conductance of the evaporator and condenser with total heat rate (Lin et al., [5]).

2.4 Researches of internal flow patterns of OHP

Gi et al. [7] studied the flow visualization in looped and closed-end oscillating heat pipes. The tubes used in the experiment were made of Teflon with an internal diameter of 2 mm, and a total length of 8.2 m. each tube was made into one heat pipe with 10 meandering turn and 400 mm in length. The lengths of the heating, the adiabatic and the cooling sections were 15 cm, 100 mm and 150 mm respectively. The R142b was used as the working fluid. The water tank was installed at the heating section and the cooling section to visualize the flow pattern inside the heat pipe. The heat pipe was operated by passing hot water and cold water through water jackets. The flow patterns of the working fluid was monitored and recorded by an 8 mm vide camera. During the experiment, heat pipes were operating at a nearly constant temperature of 35-45 ^{o}C on the adiabatic section. Figure 12 shows the experimental apparatus.

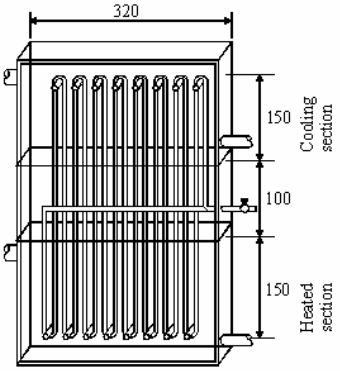


Figure 12: Experimental apparatus of Gi et al. [7].

From their experimental results, it can be concluded that, the working fluid was not able to circulate, the heat was transferred by the driving force of the oscillation between the heating and cooling section. The oscillation inside the unlooped heat pipe easily occurs at a small inclination angle and small-medium fill charge ratio. When comparing the looped type to the unlooped type, the looped heat pipe is better than the unlooped heat pipe for heat transfer performance. This is shown in Figure 13.

The effects of filling ratio can be explained as: in case of 30-50% filling ratios, vapor slugs and liquid slugs were suitably distributed, and their absolute quantity of vapor and slugs and the flow pattern were slightly different. In the case of large fill charge ratio of 70%, vapor and liquid slugs were not homogenous. At some tubes, vapor slug was not occupied all region of its tube. The circulation velocity increased as increasing of filling ratio and reached maximum velocity at 50-60% filling ratio. Thereafter the velocity decreased over 60% filling ratio.

The effects of operating temperature, which is defined as the adiabatic temperatures, can also be described as follows. At the higher operating temperature, the lengths of vapor and liquid slugs that were velocity with high operating temperature is faster than one with low operating temperature. Because at 45^{o}C operating temperature, much vapor bubbles were generated and grew to small size of vapor slugs.

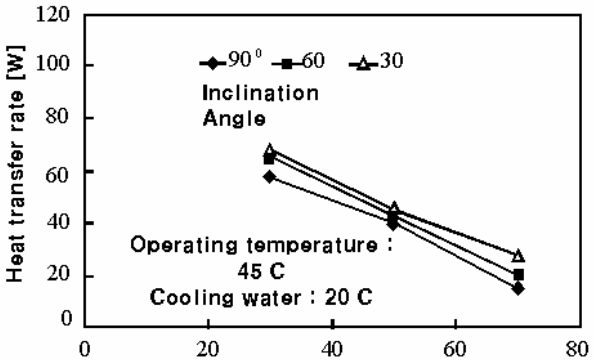


Figure 13: Effect of filling ratio on heat transfer rate of the CEOHP (Gi et al., [7]).

The effects of inclination angle can be explained as in case of small filling ratio of 30%, at the small inclination angle, the oscillation intensely occurred. When the inclination angle of 90^{O}, i.e. vertical, vapor slugs which rose to cooling section broke and collapsed with the condensation and the oscillation of working fluid decreased. The circulation velocity gradually increased with increasing the inclination angle to vertical position. Furthermore, the working fluid in the CLPHP could possibly to oscillate between heating and cooling sections, and circulate with an unsteady flow. On the other hand, the working fluid in the CEPHP was not able to circulate but the heat was transferred by driving force of only vapor oscillation.

Miyazaki et al. [8] studied the oscillatory flow in an PHP. The visualization model consisted of a base plate of copper and a window plate of polycarbonate. The base plate had provided with a rectangular groove, which was turned repeatedly to form 50 parallel grooves and the groove ends were connected as a loop. On the grooved surface, the window plate was attached by bonding to form a channel. A silicone rubber heater was attached to the heating section and a water-cooled plate was attached to the cooling section. The working fluid was R142b. The PHP operated at a top heat mode. The flow pattern of the working fluid was recorded by a digital video camcorder at 30 frames per second. It was seen that liquid and vapor were almost separated into two parts in the individual turns. The flow of liquid in the heating section and of vapor in the cooling section were accomplished by the oscillation of column. As the heat load increased, the oscillation of the liquid column increased and the liquid overflowed into neighboring turns. It can be fully observed from the past researches that, the exact phenomena and model to explain inclination angle function of the CEPHP at normal operating conditions are not fully understood. Therefore, the purposes of this research are clearly effect of inclination angle on heat transfer characteristics of a CEPHP.

Rittedech et al. [9] studied the flow visualization of internal flow patterns inside a CEOHP at normal operating conditions for several evaporator section lengths, number of turns and working fluids. The CEOHPs used employed a glass tube with inside diameter of 2 mm. The lengths of evaporator, adiabatic and condenser sections were 150 and 50 mm. Number of turn were 10 and 28 turns. The working fluids used were R123 and R141b with a filling ratio of 50% of the total volume of the tube. The CEOHPs operated at horizontal heat mode and a vapor temperature was maintained at 50 ^{o}C. The heat source temperature was controlled of 80 ^{o}C while the heat sink temperature was controlled at 20 ^{o}C. The evaporator section was heated by silicon oil and the condenser section was cooled by distilled water. The photographs of flow patterns at specific times were recorded at evaporator section by digital cameras. Figure 4 shows the flow pattern of the CEOHP with all same condition.

Figure 14(A), shows the inside flow pattern of the CEOHP at the 150 mm evaporator length. It can be seen that slug flow is the main flow pattern with annular flow as frequently seen flow pattern . The length of vapor bubbles is approximately 1-10 mm. The annular flow tends to develop and flows separately from the lower to upper part at the right side of the evaporator with the length of vapor bubbles of 50-57 mm. However, bubble flow slightly occurs. The vapor bubbles oscillate from the left to right side with the frequency of 0.40 Hz. The total oscillation period cannot be clearly identified. The velocity of vapor bubbles at right side is about 0.52 m/s. The amplitude of temperature at the right side is about 2.7 and heat flux is 4578 W/m^2. The slug flow with very few nucleation sites appears at the bottom part of the evaporator. These vapor slugs subsequently expand to the middle parts of evaporator before moving up to the condenser section where they collapse and the heat is released. Figure 14(B), shows the inside flow pattern of the CEOHP with Le of 50 mm It can be seen that slug together with bubble flow still be the main flow pattern. The length of vapor bubbles is approximately 30-35 mm. At the middle part, bubble flow increasingly occurs with the length of vapor bubbles of 1-3 mm. The annular flow cannot be observed. The vapor bubbles oscillate from the left to right side with frequency of 0.48 Hz. However, the total oscillation period cannot be clearly identified. The velocity of vapor bubbles is about 0.50 m/s. The amplitude of temperature is about 0.32 and heat flux is 18189 W/m^2. The slug flow with very few nucleation sites appears at the bottom part of the evaporator. These vapor slugs subsequently expand to the middle parts of evaporator before moving up to the condenser section where they collapse and the heat is released. From this study, it can be explained that the heat can be transferred by the following mechanism: as heat is supplied at the evaporator, the vapor bubbles originates in the evaporator section. Firstly the flow pattern of working fluid in the CEOHP is slug flow as the vapor bubbles is short. The bubbles grows irregularly. These bubbles move to condenser with very high speed. The frequency of temperature oscillation is very high but the amplitude is low. Most of the bubbles that flow into the condenser section collapse there where the absorbed latent heat is released, resulting in the lower void faction. The heat flux is, thus, transferred by this mechanism. These results agree with the results of Gi et al. [7]. From which the results show that at 150 mm evaporator length, the vapor bubble grows to long vapor slug and the oscillation is low.

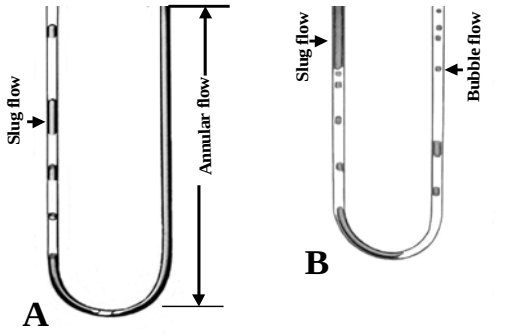


Figure	Le (mm)	Main flow plattern	Lv (mm)	Vs (m/s)	ω (Hz)	λ (°C)	q (W/m²)
A	150	Slug + Annular	50-57	0.40	0.31	3.22	4578
B	50	Slug + Bubble	1-35	0.45	0.38	0.36	18189

Figure 14: Internal flow pattern of CEOHP at Di 2.03mm, 10 Turns, Tv 50 ^{o}C, R123 and 90^{O}(Rittidech et al., [9]).

Figure 15 shows the flow pattern of the 2 CEOHPs with same condition. Figure 15(A), shows the inside flow pattern of the CEOHP at the 28 turn. It can be seen that slug and bubble flow is the main flow pattern. The length of vapor bubbles is approximately 30-38 mm. At the middle part, the bubble flow increasingly occurs with the length of of 2-3 mm. The vapor bubbles oscillate from the left to right side with the frequency of 0.48 Hz. However, the total oscillation period cannot be clearly identified. The velocity of vapor bubble is about 0.53 m/s. The amplitude of temperature is about 0.33 ^{o}C and heat flux is 18102 W/m^2. The slug flow with very few nucleation sites appears at the bottom part of the evaporator. These vapor slugs subsequently expand to the middle parts of evaporator before moving up to the condenser section where they collapse and the heat is released. Figure 15(B), shows the inside flow pattern of the CEOHP at the 10 turn. It can be seen that slug together with bubble flow still be the main flow pattern. The length of vapor bubbles is approximately 30-35 mm. At the middle part, the bubble flow increasingly occurs with the length of vapor bubbles is approximately 1-3 mm. The annular flow cannot be observed. The vapor bubbles oscillate from the left to right side with the frequency of 0.48 Hz. However, the total oscillation period cannot be clearly identified. The velocity of vapor bubbles is about 0.50 m/s. The amplitude of temperature at right side is about 0.32 and heat flux is 18189 W/m^2. The slug flow with very few nucleation sites appears at the bottom part of the evaporator. These vapor slugs subsequently expand to the middle parts of evaporator before moving up to the condenser section where they collapse and the heat is released.

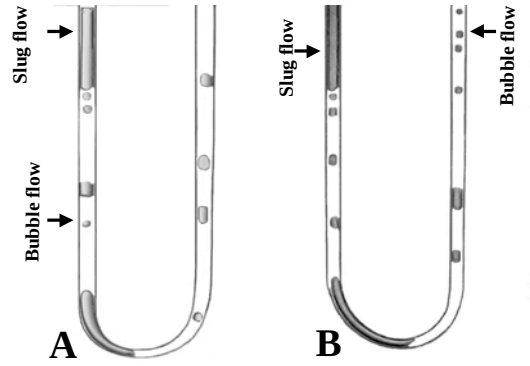


Figure	Turn	Main flow plattern	Lv (mm)	Vs (m/s)	ω (Hz)	λ (°C)	q (W/m²)
A	28	Slug + Bubble	2-38	0.43	0.41	0.33	18102
B	10	Slug + Bubble	1-35	0.45	0.38	0.36	18189

Figure 15: Internal flow pattern of CEOHP at Di 2.03mm, Le 50 mm, Tv 50 °C, R123 and 90°(Rittidech et al., [9]).

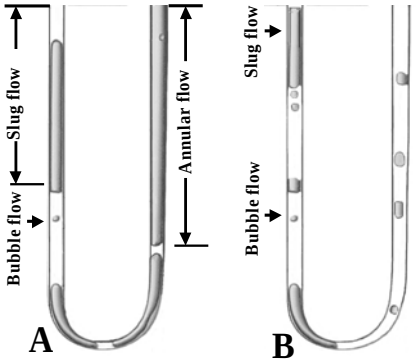


Figure	Hfg (kJ/kg)	Main flow plattern	Lv (mm)	Vs (m/s)	ω (Hz)	λ (°C)	q (W/m²)
A	213	Slug + Annular	1-50	0.35	0.38	2.02	10840
B	160	Slug + Bubble	2-38	0.43	0.41	0.33	18102

Figure 16: Internal flow pattern of CEOHP at Di 2.03mm, Le 50 mm, 28 Turns, Tv 50 °C, and 90°(Rittidech et al., [9]).

Figure 16 shows the flow pattern of the CEOHP with working fluids of R141b and R123. It can be observed from Figure 16(A) in which R141b is employed that, slug flow is the main flow pattern with annular flow some times seen. The length of vapor bubbles is approximately 10 mm. The annular flow tends to develop and flows separately from the lower to upper part at the right side of the evaporator with the length of vapor bubbles of 50 mm. At the middle part, bubble flow slightly occurs. The vapor bubbles oscillate from the left to right side with the frequency of 0.28 Hz. However, the total oscillation period cannot be clearly identified. The velocity of vapor is about 0.20 m/s. The amplitude of temperature is about 3.01 °C and heat flux is 10804 W/m^2. The slug flow with very few nucleation sites appears at the bottom part of the evaporator. These vapor slugs subsequently expand to the middle parts of evaporator before moving up to the condenser section where they collapse and the heat is released. Figure 16(B), shows the inside flow pattern of the CEOHP with R123 (Hfg of 160 kJ/kg, σ of 0.012 N/m). It can be seen that slug and bubble flow still be the main flow pattern. The length of vapor bubbles is approximately 30-38 mm. At the middle part the bubble flow increasingly occurs with the length of vapor bubbles is approximately 2-3 mm. The vapor bubbles oscillate from the left to right side with the frequency of 0.48 Hz. The velocity of vapor bubbles is about 0.53 m/s. The amplitude of temperature is about 0.33 °C and heat flux is 18102 W/m^2. The slug flow with very few nucleation sites appears at the bottom part of the evaporator.

2.5 Researches on modeling of operational phenomena

Dobson et al. [10] studied the lumped parameter analysis of closed and open oscillatory heat pipe. Used simple mathematical models of two simplified geometrical configurations in which this behavior might be simulated were employed. In case of an open oscillatory heat pipe the pipe is not sealed but open the one end as shown in Figure 17.

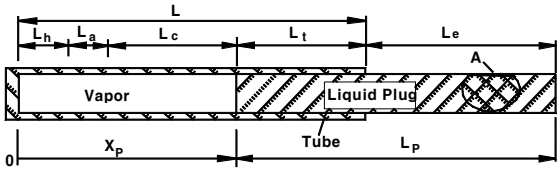


Figure 17: Dimensional variables of a one-dimensional model of an open oscillatory heat pipe (Dobson et al., [10]).

The pipe is heated along a length, L_h, and exposed to a cooling environment along a length, L_c, with an adiabatic length L_a between the heated and cooled lengths. As the closed end is heated liquid vaporized, the pressure increases and the liquid plug moves toward the open end. As the plug move towards the open end, more and more of the vapor is exposed to the cooling length, more and more vapor is condensed and a position will be reached when the rate at which vapor is condensing exceeds the rate at which it is being generated. At this point the pressure of the vapor will start to decrease. The pressure continues to decrease (to well below that of the environment) and the liquid plug comes to rest. The higher

environment pressure is now able to push the plug back towards the closed end where it again comes to rest with a vapor pressure higher than the environment. In this way the oscillatory motion of the liquid is supplied to the surface of the pipe wall as the plug moves out of the heated length towards the open end. As the plug moves, The trailing edge of the plug leaves a thin liquid film on the pipe wall. It is observed that this thin film tends to break up into little droplets that cling to the wall and has influent to decrease the heat transfer rate. Another factor to consider is that the liquid plug does not move all the way back to the beginning of the closed end in a single pipe oscillatory heat pipe. To ensure adequate supply of liquid to the heated end, the heat pipe is manufactured as shown in Figure 18.

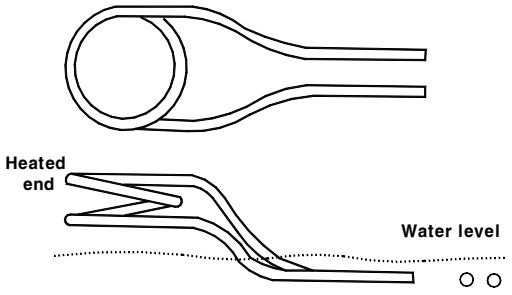


Figure 18: Dimensional variables of a one-dimensional model of an open oscillatory heat pipe (Dobson et al., [10]).

The operation of the open oscillatory heat pipe is modelled by assuming a single control volume of vapor between the closed end and the plug, a single plug of length of length L_p and a restraining force is;

$$R = \left(P_v - P_e\right)A \qquad (4)$$

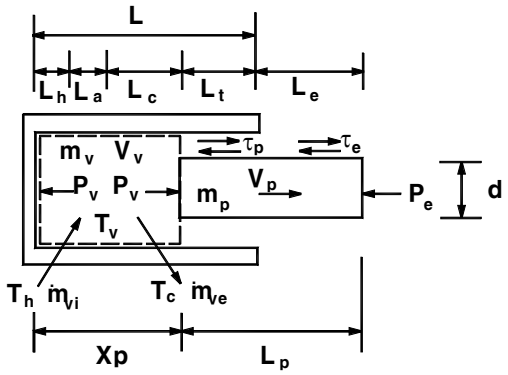


Figure 19: Vapor and plug of a one-dimensional model of an open oscillatory heat pipe (Dobson et al., [10]).

The vapor is assumed to be saturated and at the same temperature as the heated liquid film and hence there is no heat transfer from/to the liquid film lining the inside of the tube to/from the vapor. The mass flow rate of vapor entering the control volume in the heated length is given by;

$$\dot{m}_{vi} = \dot{Q}_i / h_{fg} \qquad (5)$$

where $\dot{Q}_i = U_i A_i \left(T_h - T_v\right)$

and $A_i = \pi d L_h$

For the portion of the vapor control volume exposed to the cooled length

$$\dot{m}_{ve} = \dot{Q}_e / h_{fg} \qquad (6)$$

where

$$\dot{Q}_e = U_e A_e \left(T_c - T_v\right)$$

and

$$A_e = \pi d L_e$$

The liquid plug will be assumed to be incompressible relative to the vapor. It will also be assumed that there is no heat transfer between the liquid plug and its surroundings. Making these simplifying assumptions the equation of motion of the liquid plug only needs to be considered and may be given as;

$$m_p \frac{dv_p}{dt} = \left(P_v - P_e\right)A - \pi d\left(L - x\right)\tau_p - \pi d L_e \tau_e \qquad (7)$$

The mass of the vapor will be small and the change in momentum can therefore be neglected. The continuity equation for the vapor is;

$$\frac{dm_v}{dt} = \dot{m}_{vi} - \dot{m}_{ve} \qquad (8)$$

The energy equation for the vapor control volume is;

$$\frac{dU}{dt} = \dot{m}_i h_i - \dot{m}_e h_e - \frac{PdV}{dt} \qquad (9)$$

The vapor assumed to be an ideal gas with equation of state

$$PV = mR\left(T + 273.15\right) \qquad (10)$$

Letting $u = c_vT$ and $h = c_pT$ equation (8) may be written as;

$$mc_v \frac{dT}{dt} = (\dot{m}_e - \dot{m}_e)c_P T - PA\frac{dx}{dt} \qquad (11)$$

An explicit finite difference scheme was used to solve the equation of change; the basic steps of the solution procedure being as follows. Depending on the position of the plug relative to the closed end x_P, the length of the vapor exposed to the heated L_h, the adiabatic L_a and the cooled L_{ce} portions of heat pipe, and the length of the plug L_P in contact with the pipe wall $L_t = L\text{-}X_P$ and the environment L_e are determined. The volume of the vapor is;

$$V_v = \pi d^2 x_P / 4 \qquad (12)$$

and mass of the plug vapor is;

$$m_P = \rho_l \pi (L_t + L_e) d^2 / 4 \qquad (13)$$

Assuming appropriate values for the overall heat transfer coefficients between the heated pipe wall and the vapor U_h and the cooling environment U_c the vapor mass flow rates into and exiting the control volume are given by

$$\dot{m}_{vi} = U_h(\pi d L_{hi})(T_h - T_v)/h_{fg}$$

$$\dot{m}_{ve} = U_c(\pi d L_{ce})(T_v - T_c)/h_{fg} \qquad (14)$$

Depending on the Reynolds number.

It was assumed that the friction factor between the length of the plug and the surrounding $C_p = C_{fP}$. The shear stress acting between the plug and the pipe and the plug and the surrounding are determined from

$$\tau_P = C_{fP}\rho_l v_P^2 / 2 \quad \text{and} \quad \tau_e = C_{fe}\rho_l v_P^2 / 2 \qquad (15)$$

The sum of the forces acting on the plug is given by

$$\sum F_p = (P_v - P_e)A - \pi d L_t \tau_P - \pi d L_e \tau_e \qquad (16)$$

The new values at time step t+Δt are determined from the known old values at time t. The old values are replaced by the new values and the procedure repeated for the next time step and so on.

$$m_v^{new} = m_v + (\dot{m}_{vi} - \dot{m}_{ve})\Delta t \qquad (17)$$

$$T_v^{new} = T_v + \frac{(\dot{m}_{vi} - \dot{m}_{ve})c_P T_v - P_v A \Delta x}{m_v c_v}\Delta t \qquad (18)$$

$$P_v^{new} = \frac{m_v R_v (T_v + 273.15)}{V_v} \qquad (19)$$

$$v_P^{new} = v_P + \frac{\sum F_P}{m_P}\Delta t \qquad (20)$$

$$x_P^{new} = x_P + v_P \Delta t \qquad (21)$$

$$\Delta x_P^{new} = x_P^{new} - x_P \qquad (22)$$

A simple closed oscillatory heat pipe as shown in Figure 20 was also considered. An exactly similar analysis as for the open case was done except that there were now two-vapor control volume. Although the 2 simple mathematical models do not exhibit the exact behavior of the OHP at least the general tendencies of the thermal and fluid mechanics of oscillatory heat pipes, the thrust developed by an experimental open heat pipe could be reasonably calculated. The model will be extended to include multiple liquid plugs in order to more accurately simulate the behavior in an oscillatory looped heat pipe.

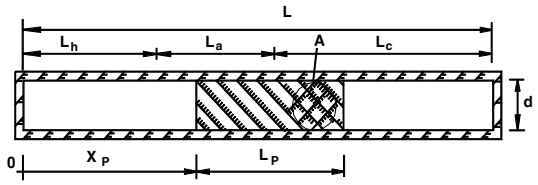


Figure 20: Dimensional variables of a one-dimensional model of a simple closed oscillatory heat pipe (Dobson et al., [10]).

Wong et al. [11] studied theoretical model of OHP by formulation based on the Lagrangian method. The capillary heat pipe is mmodeled under adiabatic condition and a sudden pressure pulse is applied to a plug at the evaporator. The OHP are made from capillary tube. The working fluid inside the OHP will arrange itself into a slug train system. Therefore the fluid flow inside a OHP can be described as a two phase slug flow regime. The hydrodynamic characteristics of a slug train can be described by a set of first order, non-linear differential equations, formulated based on the Lagrangian frame of reference, by considering the mass and momentum balance

across the control volumes for both the slugs and plugs. The set of first order ordinary differential equations are solved using the 4th order Runge Kutta technique. In solving differential equations 1st order and the definitions for the slug – train system used in the mathematical formulation is shown in Figure 21. The Figure 22 shows schematic diagram for capillary heat pipe.

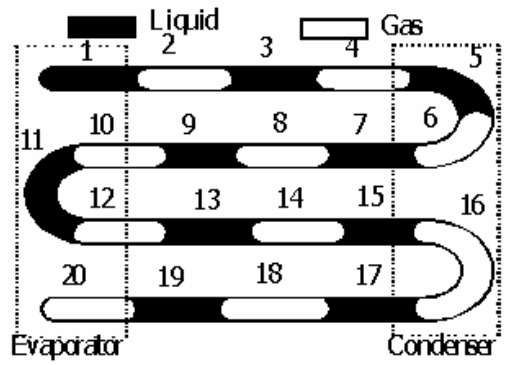


Figure 21: Nomenclature of a slug trains (Wong et al., [11]).

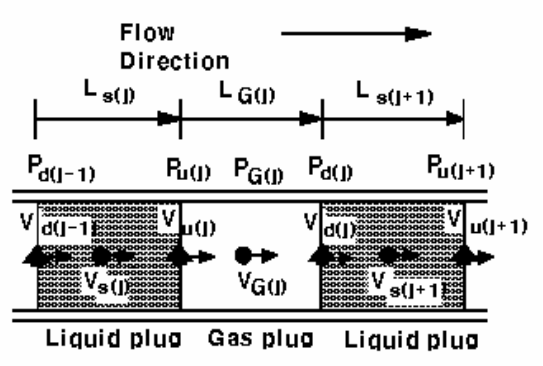


Figure 22: Schematic diagram for capillary heat pipe (Wong et al., [11]).

The assumptions in this model are as follows;

- there is no picking up and shedding of liquid masses and liquid film.
- the layer of liquid film is not considered.
- the liquid slug is completely free from any bubbles and there is no liquid entrainment in the gas plug.
- the liquid is assumed to be incompressible and the vapor plug assumed to behavior as ideal gas.
- the losses at the bends are not considered.
- the OHP is horizontal orientation and there is no gravitational effect.

From the momentum equation the following expression for the rate of change of slug velocity is deduced;

$$\left[\frac{dV_s}{dt}\right]_j = \frac{1}{\rho_s L_{sj}}\left[\left(P_{d(j-1)} - P_{u(j)}\right) - \frac{\tau_L \pi D L_{sj}}{A}\right] \tag{23}$$

The wall shear stress on the liquid slug is;

$$\tau_L = \frac{f}{8}\rho_s \overline{V}_{sj}\left|\overline{V}_{sj}\right| \tag{24}$$

when f = 64/Re if Re < 2000
f = 0.0056+0.5Re$^{-0.32}$ if Re > 2000

The liquid slug is also assumed incompressible. As such the upstream and downstream velocities of the liquid slug are the same as the translation velocity as;

$$\left[\frac{dV_d}{dt}\right]_{j-1} = \left[\frac{dV_u}{dt}\right]_j = \left[\frac{dV_s}{dt}\right]_j \tag{25}$$

In case of vapor, governing equations for gas plug control volume. The rate of change for plug length is expressed as;

$$\left(\frac{dL_G}{dt}\right)_j = V_{dj} - V_{uj} \tag{26}$$

The rate of change for the plug translation velocity is;

$$\left[\frac{dV_G}{dt}\right] = \frac{1}{\rho_G L_{Gj}}\left[\left(P_{uj} - P_{dj}\right) - \frac{\tau_G \pi D L_{Gj}}{A}\right] \tag{27}$$

The equation of state, the ideal gas equation is;

$$P_G V_{OG} = M_G R T_G \tag{28}$$

Differentiating Eqn. (27) and the following equation is obtained.

$$V_{OG}\left[\frac{dP_G}{dt}\right]_j + P_{Gj}\left[\frac{dV_{OG}}{dt}\right]_j = RT_{Gj}\left[\frac{dM_G}{dt}\right] + RM_G\left[\frac{dT_G}{dt}\right]_j \tag{29}$$

As the flow is modeled under adiabatic condition and it is assumed that there is no phase change involved, Eqn. (28) is further simplified as;

$$\left[\frac{dT_G}{dt}\right]_j = \frac{T_{Gj}}{P_{Gj}}\left[\frac{dP_G}{dt}\right]_j + \frac{T_{Gj}}{V_{OG}}\left[\frac{dV_{OG}}{dt}\right]_j \quad (30)$$

The plug pressure is expressed as;

$$P_{Gj} = \frac{P_{uj} + P_{dj}}{2} \quad (31)$$

$$\left[\frac{dP_G}{dt}\right]_j = \frac{1}{2}\left(\left[\frac{dP_u}{dt}\right]_j + \left[\frac{dP_d}{dt}\right]_j\right) \quad (32)$$

The plug velocity is expressed as;

$$V_{Gj} = \frac{V_{uj} + V_{dj}}{2} \quad (33)$$

$$\left[\frac{dV_G}{dt}\right]_j = \frac{1}{2}\left(\left[\frac{dV_u}{dt}\right]_j + \left[\frac{dV_d}{dt}\right]_j\right) \quad (34)$$

An OHP, which is 0.3 m. long measured from the evaporator to the condenser, is simulated using the model. The slugs and plugs have equal length and each measures 0.06 m long. Based on the schematic diagram in Figure 16. When has pressure acting on slug and plug at one end, the plug that is next to the non-moving end will experience a higher-pressure surge. Due to the presence of friction. If the plug and vapor bubbles length is changed to 0.12 m., it is found that, a longer plug length will result in a lower frequency in the pressure oscillation.

Shafii et al. [12] developed a very detailed theoretical model to accurately simulate the behavior of liquid slugs and vapor plugs in both unlooped and looped PHPs at top heat mode. Heat transfer due to the phase change was also considered. It was found that the effect of gravity on the performance of top heat mode unlooped PHP was insignificant. The effects of diameter, filling ratio and heating wall temperature on the performance of looped and unlooped PHPs were also investigated. The results also show that heat transfer in both looped and unlooped PHPs was due mainly to the exchange of sensible heat. This analytical models for both unlooped and looped PHPs with multiple liquid slugs and vapor plugs because the concept of this model is fairly close to the practical working more than two models mentioned above. The governing equations are solved using an explicit finite difference scheme to predict the behavior of vapor plugs and liquid slugs.

Sakulchangsatjatai et al. [12] studied theoretical model of PHPs by formulation based on the explicit finite element method. Although the previous model, i.e. Shafii et al. [11] and Dobson et al. [10], can be used with some degree of prediction, they deal with very few meandering turns, e.g. 2 turns. It is widely accepted that, the higher the number of turns, the better the heat transfer characteristics of the PHPs. For the top heat mode, the number of turns must be more than 40. The mathematical model was applied to the PHPs, which has higher number of turn and modeled under adiabatic condition. The parameters affecting the heat transfer of PHPs at top heat mode were analytically investigated. The principles and theories of internal friction flow, basic governing equations and finite difference scheme were applied to evaluate the heat transfer rate. As a result, by using this model the heat transfer rate of the CEPHP and CLPHP were predicted and compared with the experimental data. It was found that the parameters, which affected the heat transfer rate, and the data from experimental were satisfied to predict the heat transfer of PHPs. The PHPs with ethanol exhibited the highest heat flux, while those with R123 and water were save less heat flux, respectively. The heat flux was proportional to inner diameter of tube and inversely proportional to the evaporator length.

2.6 Performance limit of the CEOHP

When the CEOHP is heated to some degrees, internal thermal resistance will rapidly increase. The heat flux from the evaporator to condenser section cannot accordingly be transferred, and the outside surface temperature subsequently increases to unlimited level. The inside vapor pressure is subsequently high. This high vapor pressure will retard the liquid slug from returning back to the evaporator section. The liquid quantity in the evaporator section is accordingly small and this caused the dryout at some part of the evaporator or even dry patch. After that, burnout at the dry patch will occur as shown in Figure 23. The state at which the burnout occurs is called " Critical State" which is our main interest.

2.6.1 Occurrence of the critical state

The reason why the critical state occurs cannot be clearly explained but a brief explanation might be as follows; at normal operating condition the CEOHP operates by the simultaneous oscillation of bubble slug and liquid

plug inside the capillary tube. When heat is added to the evaporator section, liquid will boil and vaporize into vapor. Such vapor accumulates in the nearby vapor slug making its size larger. The slug density is subsequently lower which leads to the driving force of the above liquid plug. This makes both liquid plug and vapor slug move to the condenser section where some part of the vapor plug condenses resulting in size reduction and lower temperature. The released latent heat of vaporization will be transferred from both liquid plug and vapor slug to the heat sink. Some part of the condensate will return to the original evaporator while some part might flow further to the next meandering tube. This causes the inside oscillation phenomena. If the heat flux at the evaporator section is increased to very high level, the violent boiling will occur with very high evaporation rate. The oscillation phenomena will also be violent. At a specific condition, the size of vapor bubble will be too large compares to the capillary size of the tube such that it cannot move to the condenser section. The above-accumulated heat in the evaporator section results in very high outside wall temperature and the burnout eventually occurs at this state. This is defined as critical state. Figure 24(A) shows the heating condition of the normal operating condition. Figure 24(B) shown the occurrence of the critical state and Figure 24(C) shows the post – critical state observed by the burnout at the evaporator section.

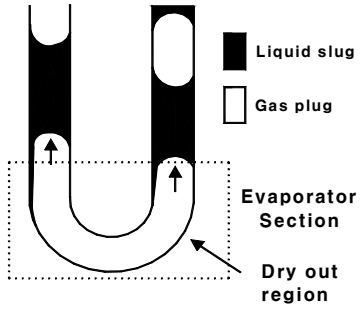


Figure 23: Dryout occur at evaporator section.

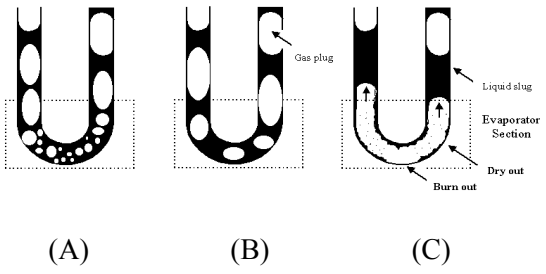


Figure 24: Operation state of OHP.

2.6.2 Detection of the critical state

If the evaporator section of the CEOHP is heated by using the electric heater plate, the critical state can be detected as in Figure 25. The evaporator at lower part will be heated by thermal conduction plate attached to the electric heater. The heating temperature can be controlled by adjusting the voltage and current of the supply power. Heat will be removed at the condenser section by calorific jacket with water as cooling substance. Temperature sensor probes will be applied at heater plate, outside surface of the evaporator, adiabatic and the condenser section. Calorimeter is used to monitor the heat transfer rate at the condenser section. When the heat is supplied to the CEOHP, the temperatures will increases to some degree and will be constant if the steady state is reached. Figure 26 shown the temperature of the heater (solid line) and evaporator section (dashed line). When heat is increased in the normal operating condition, the evaporator temperature will be definitely lower than that of the heater due to heat conduction from electric heater through evaporator and the condenser section. However, after the critical state is reached, since the dryout occurs inside the evaporator, the temperature of the evaporator will

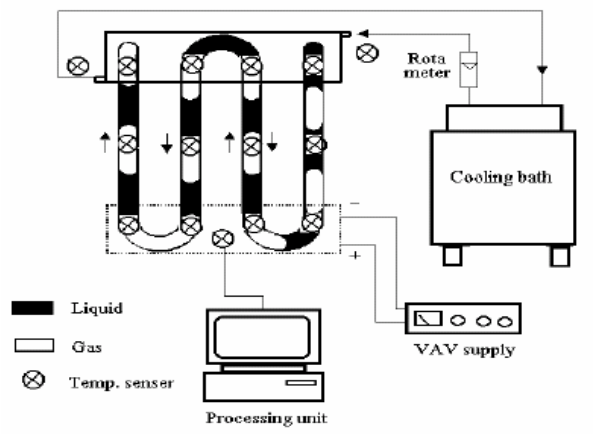


Figure 25: Apparatus to detect the critical state of the CEOHP.

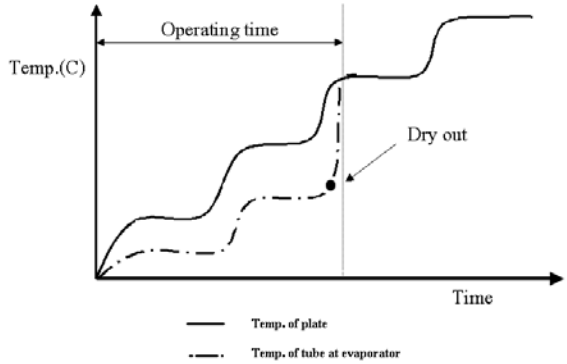


Figure 26: The pattern of the system temperatures with normal electric heater.

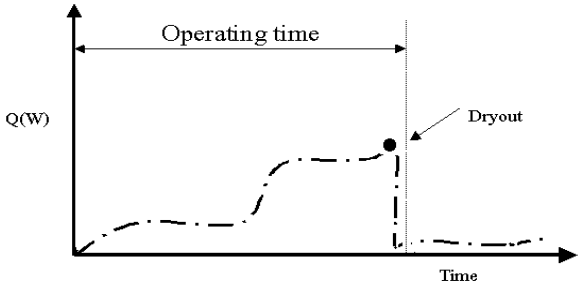


Figure 27: Heat transfer rate at the critical state.

be much higher than the electric heater. This implies that the heat cannot be transferred to the condenser section. The heat transfer rate just before the rapid increase of the evaporator temperature is defined as "critical heat flux". Figure 27 shows heat flux of any CEOHP up to the critical state.

Figure 28 shows the pattern of the system temperatures to which the electric heater is employed. However, if the metal tube of the CEOHP is employed as the heater itself, the temperature pattern will not be the same. In this case the electric heater will be passed through the metal tube only at the evaporator section (grounded at adiabatic section to ensure that there is no short circuit at condenser section). Heat will be generated by means of electrical resistance of the evaporator tube itself. Figure 27 shown the temperature of the evaporator section with respect to time. It can be seen that, at normal operating condition the temperature pattern seems to be the same as Figure 28. On the other hand, at the critical state the evaporator temperature will drastically increase without limitation since the electrical power is continuously supplied to the tube. This temperature will be much higher than that of Figure 28 and confirm that the critical state is reached.

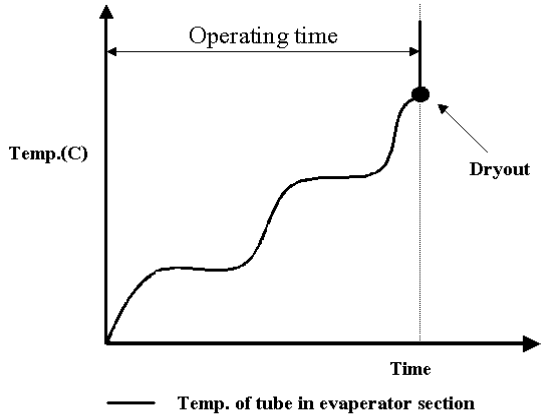


Figure 28: Temperature of tube will drastically increase without limitation since the electrical power is continuously supplied to the tube.

2.6.3 Hypothesis of the occurrence of the critical state

Due to lacking of information about the critical state, the possible way to explain the occurrence of the critical state might be as follows;

(A) When the heat is supplied to the CEOHP to a specific condition, the above liquid plug cannot return to the evaporator beneath because its weight is much less than the buoyancy force of the growing vapor bubble underneath. This causes the dryout in the evaporator section because the liquid quantity in the evaporator is not sufficient. The vapor bubble beneath still be growing in its size resulting in the sudden increase of the evaporator temperature since there is on heat transferred to the condenser section. Figure 29(A) shows the detail of such hypothesis. Another hypothesis is;

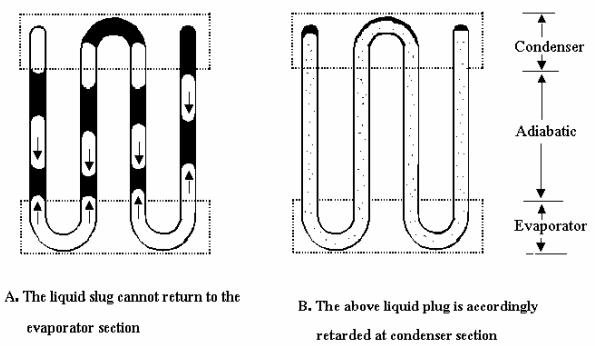


Figure 29: Hypothesis of the occurrence of the critical state.

(B) When the heat is supplied to the CEOHP to a specific condition, the vapor bubble underneath instantaneously grows in its size such that its surface tension force capture itself in the evaporator section. The above liquid plug is accordingly retarded at condenser section. The heat cannot be transferred through the CEOHP resulting in the dryout and burnout of the evaporator section. Figure 29(B) shown such hypothesis.

2.6.4 Researches on the critical state

Since the CEOHP is newly invented, many researchers are, at present, not realized the existing of its critical state. Very few papers have reported on these phenomena such as;

Maezawa et al. [4] observed that, at a specific condition of their experimental works, the dryout occurred and the CEOHP did not operate. The cause of such phenomena was not completely reported.

It was also observed from the experimental works of Miyazaki et al. [14] that, the dryout occurred by the insufficient supply of liquid into

the evaporator section. It was also suggested that, installing of the check valve into the CLOHP could alleviate such phenomena even at top heat mode.

Lin et al. [5] studied the relationship of the fill ratio and the heat flux of the CEOHP by using the FC-72 and FC-75 CEOHP. There were two condenser sections with only one evaporator section (located at the middle section) in their experimental setup. The working temperature was 75-85 ^{o}C. It was found from their experiments that, in case of FC-72 CEOHP, the fill ratio of only 32% would cause the dryout condition even with the very low heat input of 200 W. In case of FC-75, this was much higher (800 W at 38% of fill ratio). Inadequate fill ratio easily led to the dryout condition because it was caused by the insufficient quantity of liquid inside the evaporator section.

In order to establish the complete knowledge of the CEOHP, urgent researches on the CEOHP must be basically conducted. The significance of these researches will be definitely beneficial for all scientists and engineers who are now involving with development of the CEOHP for the future of the heat pipe technology of the world.

References

1. Dunn, P. and Reay, D. A., *Heat Pipe*, Pergamon Press Ltd., 3rd edition, 1982.
2. Engineering Science Data Unit. *Heat pipe – performance of two phases closed thermosyphons.* Item No.81038 U.K, 1981.
3. Akachi, H., Polasek, F., and Stulc, P., *Pulsating Heat Pipe*. Procs. of the 5th International Heat Pipe Symposium, Melbourne Australia, Nov, 1996.
4. Maezawa, S., Gi, K.Y., Minamisawa, A., and Akachi, H., *Thermal Performance of Capillary Tube Thermosyphon*. Procs. of the 4th International Heat Pipe Conference, Albuquerque, USA. Vol. II, May, 1996.
5. Lin, L., Ponnappan, R. and Leland, J., *Experimental Investigation of Oscillating Heat Pipe*, Procs. Of 35th Energy Conversion Engineering Conference and Exhibit, Vol. 2, 2000.
6. Rittidech, S., Terdtoon, P., Tantakom,P., Murakami, M., and Jompakdee, W., *Effect of Inclination Angles, Evaporation and Working Fluid Properties on Heat Transfer Characteristic of A Closed-End Oscillating Heat Pipe.* Procs. of the 6th International Heat Pipe Symposium, Chiang Mai, Thailand, 2000.
7. Gi K., Sato F. and Maezawa S., *Flow Visualization Experiment on Oscillating Heat Pipe*, Proc. 11th Int. Heat Pipe Conf., Tokyo, Japan, pp. 373-377., 1999.
8. Miyazaki Y. and Arikawa M., *Oscillatory Flow in the Oscillating Heat Pipe*, Proc. of the 11th Int. Heat Pipe Conf., Tokyo, Japan, pp.367-372, 1999.
9. Rittidech, S., *Heat Transfer Characteristics of Closed – End Oscillating Heat Pipe.* Thesis for Doctor of Philosophy in Mechanical Engineering, Chiang Mai Unibersity, 2002.
10. Dobson, R. T., and Harms, T. M., *Lumped Parameter Analysis of Closed and Open Oscillatory Heat Pipe.* Proceedings of 11th International Heat Pipe Conference, Tokyo, Japan, pp. 137-142,1999.
11. Wong, T. N., Tong, B. Y., Lim, S. M., and Ooi, K. T., *Theoretical Modeling of Pulsating Heat Pipe*, Proceedings of 11th International Heat Pipe Conference, Tokyo Japan, pp. 159-163, 1999.
12. Shafii, B., Faghri, A., and Zhang,Y., *Thermal Modeling of Unlooped and Looped Pulsating Heat Pipe*. Int. J. Heat Transfer. 123 pp. 1159-1172, 2001.
13. Sakulchangsatjatai, P., Kamonpet, P., Wongratanaphisan, T., and Terdtoon, P., *Operation Modeling of Closed-End and Closed-Loop Oscillating Heat Pipes*, Submit.
14. Miyazaki, Y., Polasek, F. and Akachi, H., *Oscillating Heat Pipe with Check Valves.* Procs. of the 6th International Heat Pipe Symposium. Chiang Mai Thailand., 2000.

Activity of Japan Association for Heat Pipe

Tadashi YAMAMOTO* (Chairman of JAHP), Seiji MATSUMOTO**

* Advanced Research Institute for Science and Engineering (RISE), Waseda University
Sanyo 2nd Building 2F, 1-10-12, Higashi-Ueno, Taito-Ku, Tokyo, 110-0015, JAPAN
Tel: +81-3-3832-5333, Fax: +81-3-3855-4807, e-mail: yamat@beige.ocn.ne.jp

** Thermal Energy Applications Research Group, Institute for Energy Utilization
National Research Institute for Advanced Industrial Science and Technology (AIST)
AIST Tsukuba-West, 16-1, Onogawa, Tsukuba, Ibaraki, 305-8569, JAPAN
Tel: +81-29-861-8234, Fax: +81-29-861-8209, e-mail: s.matsumoto@aist.go.jp

Abstract

In this paper, the activity of the Japan Association for Heat Pipe(JAHP), especially, outline of the activity on establishment of heat transfer rate measurement method for standardization will be introduced.

Key words: The Japan Association for Heat Pipe, Measurement method for standardization, Publications.

1. INTRODUCTION

The JAHP is a nationwide organization of the Japanese Heat pipe researchers, engineers and the various companies related to heat-pipe. Its membership consists of about 150 persons as individual member and 10 of the leading companies in the field of heat pipe companies, electrical equipment companies, etc as corporation member.

The JAHP was established June 1982.and the JAHP is the academic party that has been authorized by Japanese government as a result of our efforts of research and technology activities. The Objectives of JAHP is to contribute to the overall advancement of the heat pipe research, technology, heat pipe industry etc.

The first Chairman of JAHP was Prof. Kouichi Oshima. The foundation of the JAHP was laid by his strong leadership and we can not also forget the effort of late Mr. Honda Ichiro.

The position of Chairman has been changed by 4 persons through a period of about 20 years. The numbers of Members decreased with the times in both the individual member and corporation members.

Until about 10 years ago, main product of heat pipe industry was heat pipe type heat exchanger. That age was Golden age.

But after that, the current of product has shifted to the production of **mini** heat pipe.

The diameter of round type heat pipe is changing from 3mm to 8 mm larger with increasing in power of CPU and the shape of the heat pipe is changing to flat type.

The Organization figure is as follows

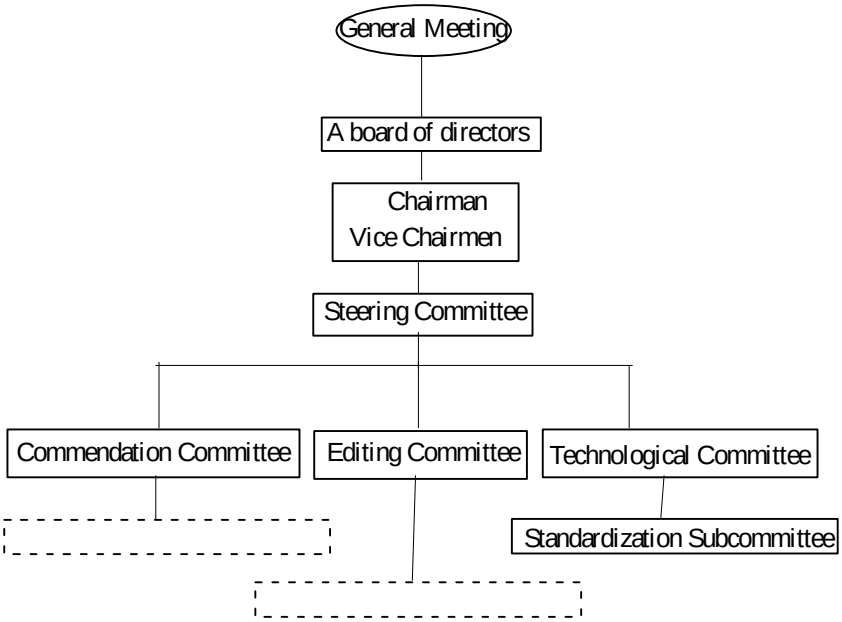


Fig.1 The Organization figure of JAHP

2. THE ACTIVITIES OF JAHP

The JAHP has continued to fulfill its original objectives through the following activities.

2.1 Publication Activity

a) Publication of 2 Journals
Journal of the Japan Society for Heat Pipes
Heat Pipe Heat Pipe Science and Technology



Fig.2 Journal of the Japan Society for Heat Pipes

b) Publication of Text book of Heat pipes.



Fig.3 Heat Pipe (2nd edition)

2.2 Educational Activity

Open of Heat pipe seminar for the engineers etc once every year.



Fig.4 The text book for seminar (Title: Heat pipe and Carbon Nanotubes)

2-3 Awards

1) Paper Prize for excellent paper published in Journal of Heat Pipe Science
2) Technical Prize for excellent devices.
3) Prof. Oshima Kouichi Prize to persons who is contributing the excellent result about Development of Heat Pipe science and Technology, and development of devices using heat pipe, etc.

2-4 Coordinate activities with similar and related organizations, both domestic and international.

2-5 Activity for Standardization for mini heat pipe

Making the standard for measurement method of heat transfer rate of mini heat pipes and activity to our government in order to make government recognize it as the official standard.
Before explaining the activity of technology group, something on the heat pipe industry in Japan will be introduced.
2-5-1 The circumstance of heat pipe industry in Japan considered from Patent application Number [1].

The trend of heat pipe application is shown in Fig.5. The patent numbers applied from 1990 year to 2001 year are 3223 in total. The 1986 numbers of them are related to applications. 34% is occupying the field of the cooling for semiconductor. 33% is the cooling for electric devices, 12% is the cooling for computers, 13% is the uniform-heating and cooling for the copy machine and the image forming device and 8% is for the
On the other hand, the companies related to heat pipe are doing business activities according to their plans. Such examples are shown in Fig.6. For example, RICOH is showing only the application of Image forming devices.
2-5-2 Development of thin heat pipe (vapor chamber) [2]
This heat pipe has been developed in order to replace it instead of conventional flat type heat pipe. This heat pipe is a high heat transfer element with thin thickness like as paper and high flexibility.
This heat pipe was developed to use as the thin vapor chamber as shown in Fig.7. The thickness is less than 1mm and the heat conductivity is more than one of the copper with 10mm.
The performance of heat discharge rate is 10 W when the vapor chamber is 0.6 mm in thickness, 20 mm in width and 150 mm in length.
2-5-3 Activity of Japan Association for Heat Pipe.
In order to make standard for heat transfer rate measurement method of mini heat pipe we have opened the new division for it under the technical committee.
Output of mini heat pipe in Japan is higher compared to other heat pipes, but it has been under strict competition on the world market. In order to win the International Competition, we must offer the mini heat pipes with high quality and low cost. For the purpose, we are trying to make the excellent standard that is accepted by the person concerned. In future, we would like to make the overall standard for the heat pipes including mini heat pipe, but at present we have being carried out to make the measurement method of the heat transfer rate for mini heat pipe. Therefore, our final target is to be recognized by our government as JIS.
At starting this project, the temperature measurement method, measurement method for heat transfer rate etc being used at corporation members were examined as shown in Table1.
On base of the result of table1, the discussion of temperature method and the development of apparatus for heat transfer rate measurement were started.
The development of the apparatus has been carried out at the University. The new measurement apparatus has been developed by Prof. Takamura's group（3）.
This apparatus can measure easily the heat transfer rate of mini heat pipe under unsteady state condition.
After we will carry out the test of the apparatus for reliability more, we will recommend it to the subcommittee as standard apparatus of the heat transfer rate measurement.
But at the moment, we have not yet enough data through it.
As future image, JAHP will have the apparatus as a standard for heat transfer rate measure managed by group of specialists. On the other hand, the companies will have the copy apparatus.
The JAHP will send a standard heat pipe to the companies at regular intervals to check their apparatuses as shown in Fig. 8.
By this system, we are expecting that the quality of heat pipe will be kept.

Table1 the temperature and Heat transfer rate measurements method of each company

Companies		Sort of Thermo-couple	Fitting method of T.C	Heating method	Cooling method
A		*	#	$	@
B		* *	# #	$ $	@ @
C		* * *	# # #	$ $ $	@ @ @
D		* * * *	# # # #	$ $ $ $	@ @ @ @
E		* * * *	# # # # #	$ $ $ $ $	@ @ @ @ @
F	Flat type H.P	* * * * *	# # # # # #	$ $ $ $ $ $	@ @ @ @ @ @
	Round type H.P	* * * * * *	# # # # # # #	$ $ $ $ $ $ $	@ @ @ @ @ @ @

Marks:

*: Sort of thermo-couple

T and K type thermo-couples are being used, but the diameters are different. In some cases, very thin sheath thermo-couple is also being used.

#: Fitting method of thermo-couple.

These are very important subject at each company and the matter that is belong to Know-how.

$&@: Heating method and cooling method

Besides conventional and basic methods, special method is being used.

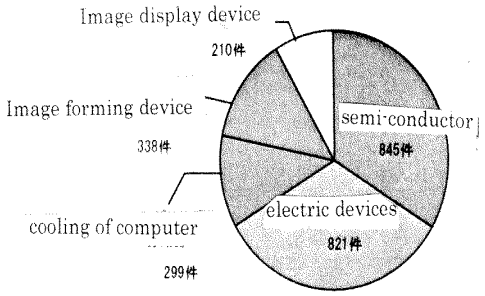
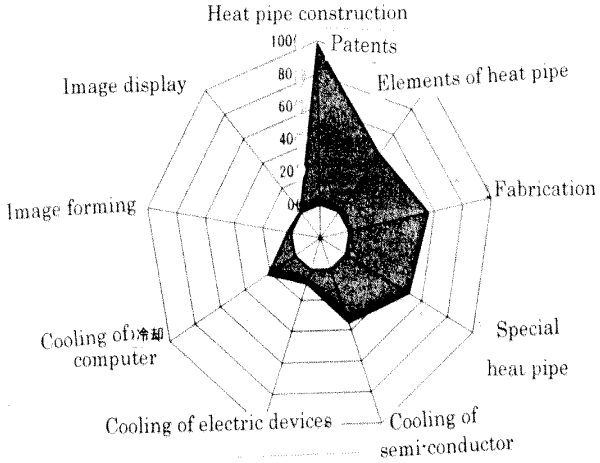
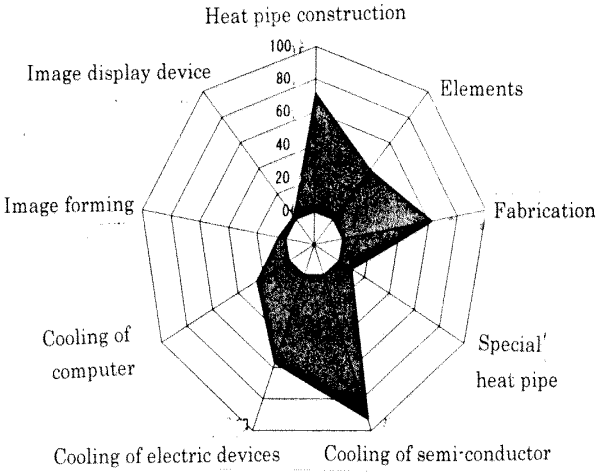


Fig.5 The trend of patent application in the application field.



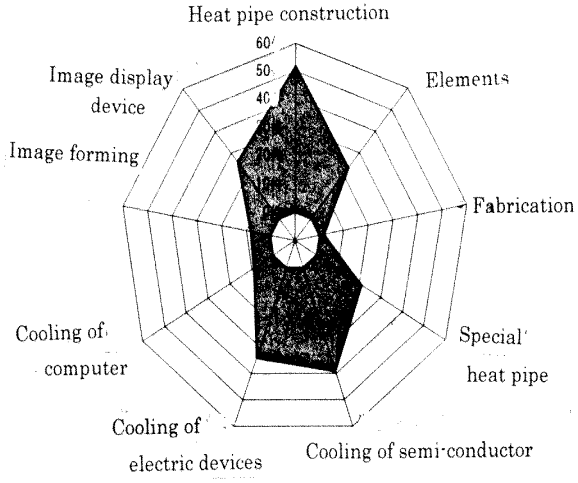
FUJIKURA

Fig6 (a) The trend of patent application of typical companies (Fujikura)



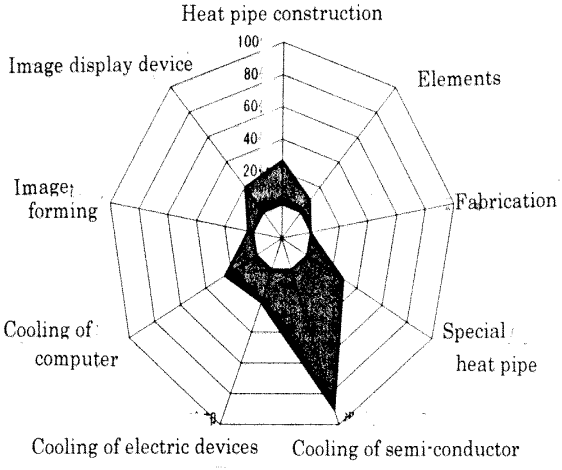
FURUKAWA

Fig6 (b) The trend of patent application of typical companies (Furukawa)



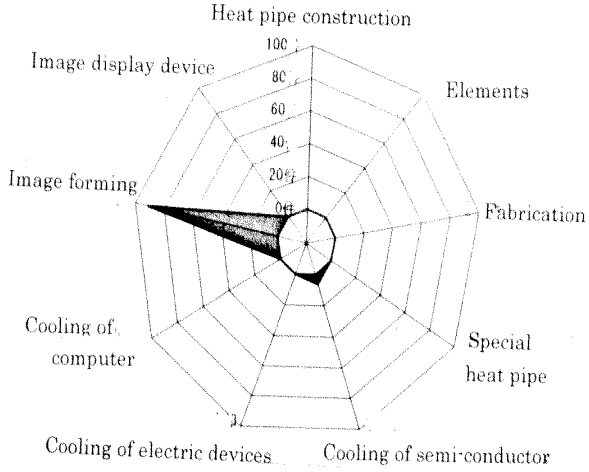
MITSUBISHI

Fig6 (c) The trend of patent application of typical companies (Mitsubishi)



TOSHIBA

Fig6 (d) The trend of patent application of typical companies (Toshiba)



RIKO

Fig6 (e) The trend of patent application of typical companies (Riko)

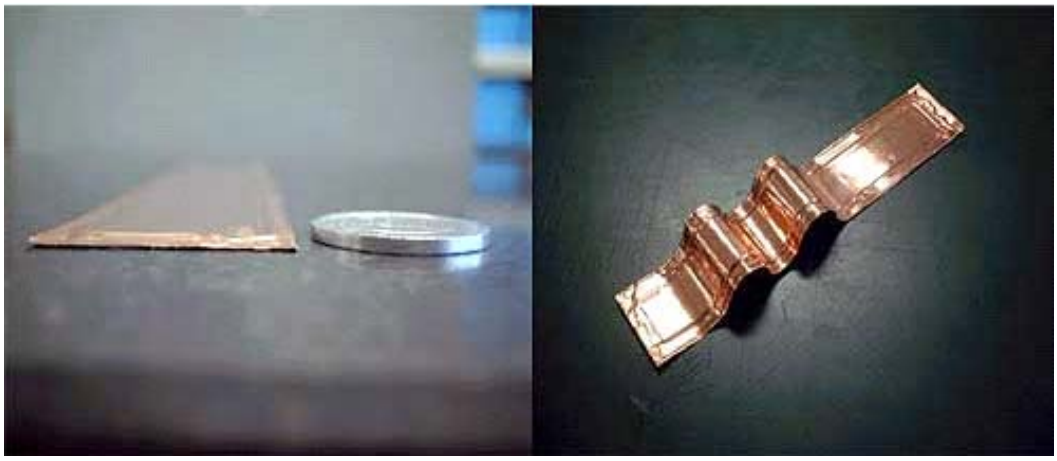


Fig.7 Thin vapor chamber (The Furukawa Electric Co. LTD)

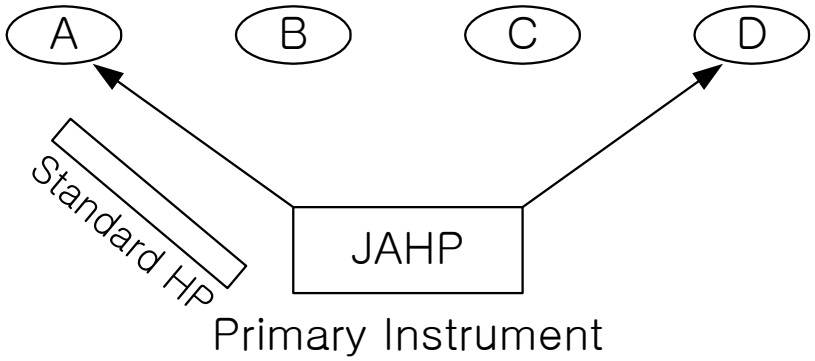


Fig.8 Future image figure of standard apparatus system

3. CONCLUSION

We have thought that our project is very important to promote the heat pipe industry, but the speed of our project is slow.

As the above-mentioned, the demand for the **mini** heat pipe is changing daily. When our project for the measurement method was started, our target was heat pipe with 3 mm in diameter. But at present, the diameter of the round type heat pipe is mainly from 7mm to 8 mm, and the sharp is flat

References

1) Patent Distribution Support Chart, Heat Pipe (Machine-4), National Center for Industrial Property, 3(2002).

2) Furukawa Electric Technical Information, 4(2003)

3) Ichikawa Tomohiro et al, Tokyo Denki University Bachelor's thesis, The study on Performance Evaluation Method for Small Size Heat Pipe, 2003.3.

Natural Flows
- Its Nature and Applications -

Jinho Lee

School of Mechanical Engineering, Yonsei University,
134 Sinchon-dong, Seodaemun-gu, Seoul 120-749, KOREA
Tel. : +82-2-2123-2816, Fax : +82-2-312-2159,
E-mail : jinholee@yonsei.ac.kr

Abstract

Natural convection due to combined buoyancy forces by temperature gradient and concentration gradient is generally referred to as "thermosolutal convection" or "double-diffusive convection." Flow induced by surface tension gradient due to free surface with tangential temperature gradient is called thermocapillary flow. Double-diffusive convection or surface-tension driven flow may produce unusual, complex flow phenomena which are very difficult to resolve. In the following, two most common natural flows, i.e., natural convection due to combined temperature and concentration gradients and thermocapillary flow, and their flow characteristics and mathematical treatment are identified and delineated. Three examples of related problems are given to help one understand the physical nature of natural flows.

Key words: Combined Buoyancy, Double-Diffusive Convection, Surface Tension Gradient Flow, Thermocapillary Convection, Marangoni Convection

1. INTRODUCTION

Natural flow simply means that the flow is not occurred by any forced means such as fans, blowers, or pumps, etc. The flow, instead, is induced naturally when proper physical conditions are met. Two good examples can be given; One, natural (or free) convection by buoyancy due to density gradient under the body force field such as gravity and the other, the surface-tension driven flow due to free surface with tangential temperature and/or concentration gradients.

In many transport processes in nature and technology, there are both temperature and concentration gradients in the fluids that can lead to buoyancy-driven flows. Natural convection due to these combined buoyancy forces is generally referred to as "thermosolutal convection" or "double-diffusive convection" and has various modes of convection depending on how both gradients are oriented relative to each other as well as to the gravity.

Gradients in surface tension can drive convective flows, that are sometimes known by the eponym "Marangoni convection." These phenomena include thermocapillary convection and solutocapillary convection, wherein the surface tension gradient arises from a gradient of temperature and a gradient of solute concentration, respectively [1, 2]. With rare but important exceptions (e.g., crystal growth from a melt [3]) these flows are mere curiosities under terrestrial conditions. The marked reduction of buoyancy-driven convection in microgravity greatly amplifies their relative importance. For instance, in proposed large containerless processing systems, surface tension-driven convection velocities can take on extreme magnitudes.

In many cases, double-diffusive convection or surface-tension driven flow may produce unusual, complex flow phenomena which are very difficult to resolve. In the following some of its basic and important flow characteristics will be delineated and some descriptions will be followed regarding how to treat such unusual, complex problems effectively.

2. NATURAL CONVECTION DUE TO COMBINED BUOYANCY FORCES

Problems that involve the interaction of temperature and concentration gradients are considerably more complicated than ones in which the driving force is due only to one of them. Sometimes the combined mechanism yields unusual phenomena, for example, such as "salt

fingers" and "salt fountains" [4, 5] in deep ocean wherein thermal and salinity gradient are important.

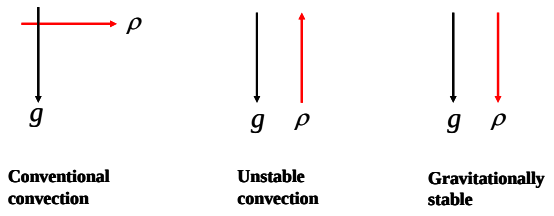


Fig. 1. Two modes of natural convection

In the case where the driving force is due to one of them, two distinct modes of convection can be identified as is shown in Fig. 1. When a component of the density gradient is perpendicular to the body-force direction, a flow ensues immediately and is called conventional convection. On the other hand, if the body force and the density gradient are parallel and opposed, the configuration is unstable (heavier fluid above lighter) and convection occurs only after a critical value of the density gradient is exceeded. Of course, if the density gradient and the body force are aligned and in the same direction, the flow is stably stratified and no convection is possible.

Clearly, with the simultaneous action of both temperature and concentration gradients, many more configurations are possible because the two gradients can have different orientations relative to each other as well as relative to the body force direction. In the situation in which both the gradients are paralleled to the body force direction (as in the thermally unstable mode), four distinct cases are identified by Turner and Stommel[6] in water with a combined vertical temperature gradient and solinity gradient as is shown in Fig. 2.



CASE		T	C	ρ	REMARKS
1		↑	↓	↓	Stable
2	a	↑	↑	↓	Salt finger
	b	↑	↑	↑	unstable
3	a	↓	↓	↓	Oscillatory instability
	b	↓	↓	↑	unstable
4		↓	↑	↑	Unstable

Fig. 2. Unstable natural convection mode due to combined buoyancy

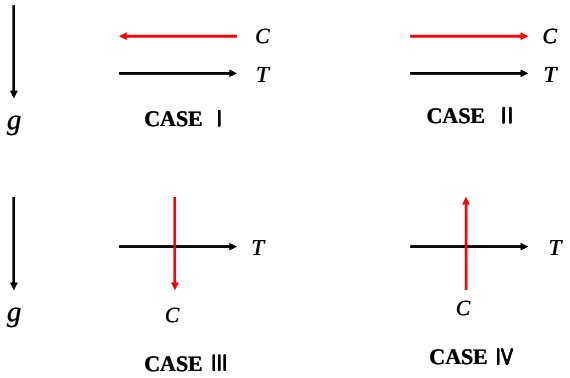


Fig. 3. Conventional natural convection mode due to combined buoyancy

Four distinct cases are also identified corresponding to the conventional convection mode by Ostrach[27] in Fig. 3. The fundamental dimensionless parameters derived by Ostrach are Grashof number, $Gr \equiv \frac{\beta g \Delta T L^3}{\nu^2}$, Prandtl number, $\Pr \equiv \frac{\nu}{\alpha}$, Schmidt number, $Sc \equiv \frac{\nu}{D}$, and the buoyancy ratio, $N \equiv \frac{\bar{\beta}\Delta c}{\beta \Delta T}$, where β and $\bar{\beta}$ are the thermal and concentration volumetric coefficients, and ΔT and Δc are the imposed temperature and concentration differences, respectively. Also g is the acceleration due to gravity and ν, α and D, the kinetic viscosity, thermal diffusivity and the diffusion coefficient. Note for N positive, the combined driving forces enhance the flow and for negative N they retard it. Various ratios or products of these fundamental parameters are used in existing work. Thus, four parameters describe the phenomena due to combined buoyancy forces as compared to two for a simple driving force. This is another of the complexities associated with problems of this type. It should be noted also that there exist three distinct boundary layers in problems of this type, viz., those of velocity, temperature, and concentration and their relative extents are determined by the relative orders of $\Pr$ and Sc.

In double-diffusive convection, the basic problem is governed by the combined buoyancy effects arising from the simultaneous diffusion of thermal energy and of chemical species. Therefore, the continuity, momentum, energy and mass diffusion equations are coupled through the buoyancy terms alone, if the other effects, such as Soret and Defour effects, are neglected.

In dealing with new and complex problems, it

was pointed out by Ostrach[8] that dimensionless parameters are most useful for obtaining qualitative features of the flows and for estimating flow velocity. They also indicate the dominant physical factors, mathematical simplifications, data correlations, and proper theoretical and experimental models.

The parameters can be obtained in several ways, but, to obtain all of the information from them, it is best, to the author's knowledge, to derive them from the basic equations and boundary conditions that describes the phenomena. This is done by making all variables not only dimensionless, but also of unit order of magnitude. The normalization of the variable is not an automatic process, but require sufficient physical information or insight to choose the proper reference quantities.

3. SURFACE-TENSION GRADIENT FLOWS

Free surfaces with tangential temperature and/or concentration gradients are often encountered in many crystal growth situations, e.g., in Czochralski growth and in floating zone techniques. Since surface-tension is a function of temperature, composition, and electrical potential, gradients of any one of these or combinations of them can lead to surface-tension gradients which inevitably cause movement in the fluid interface due to the variations in tangential stresses. Hydrodynamical phenomena driven (or partly driven) by such gradients of surface tension are called Marangoni effects.

When surface-tension flows were considered under terrestrial conditions, the relative importance of gravity and surface-tension forces was thought to be determined by the 'static" Bond number, $Bo = \dfrac{\rho g d^2}{\sigma}$, where σ is the surface-tension. On this basis it was concluded that gravity suppresses surface-tension except in configurations with very small dimensions, such as thin film, capillary tubes, and droplet and bubbles. Only recently, the importance of surface-tension driven flow in crystal growth system was realized among crystal growers because of the possibility of growing crystals under reduced gravity in an orbiting spacecraft, wherein buoyancy-driven convection would be diminished and surface-tension driven convection of importance.

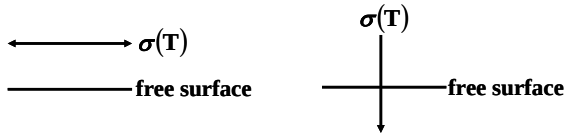


Fig. 4. Two modes of thermocapillary flow

There are essentially two modes of flow generated by surface-tension flows that are analogous to those induced by buoyancy[9]. As is shown in Fig. 4., if the gradients are along the interface, the surface-tension gradients act like shear stresses applied by the interface to the adjoining fluids and, thereby, induce flows or affect existing ones. These flows are analogous to conventional (stable) convection and are called thermocapillary or diffusocapillary flows according to whether they are caused by temperature or concentration gradients, respectively. These flows can, of course, affect transport processes.

If one of the aforementioned gradients is perpendicular to the interface a "Marangoni instability" can occur under proper conditions that can lead to cellular flows. This situation is analogous to the thermally unstable type of buoyancy flows. Problems of this type have received more attention than those with gradients along the interface.

Although a physically reasonable reference velocity for surface-tension gradient flow was indicated or implied by Levich[10], Kenning[11], and Stanek and Szekely[12], no explicit derivation of the fundamental dimensionless parameters was made until recently by Ostrach[13]. It is shown therein that, in analogy to buoyancy flows, there are different reference velocities from the tangential stress balance, e.g., for viscous-type thermocapillary flows the characteristic velocity is

$$U_R = \frac{\left|\partial\sigma/\partial T\right|\Delta T}{\mu}\frac{D}{L}$$

where μ is the absolute viscosity and D and L are two different characteristic lengths. For boundary-layer flows

$$U_R = \left[\frac{\left(\partial\sigma/\partial T\right)^2 \Delta T^2 \nu}{\mu^2 L}\right]^{1/3}$$

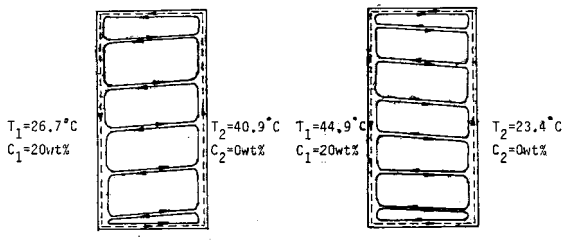
Note that both reference velocities are given in terms of the physically important variables for establishing thermocapillary flows. The relevant dimensionless parameters based on those reference velocities that appear in the basic equations are the surface-tension Reynolds number, $\mathrm{Re}_\sigma = \left[\left(\partial\sigma/\partial T\right)\Delta T \cdot D\right]/\mu\nu$, the

Marangoni number, $Ma = \Pr \mathrm{Re}_\sigma$, and aspect ratio, $A = D/L$, a dynamic bond number, $\mathrm{Re}_\sigma = \rho g L^2 / [(\partial\sigma/\partial T)\Delta T]$, and the relative temperature variation, $\beta\Delta T$. The surface-tension Reynolds number plays the same role as the conventional Reynolds number in that it appears in the equations of motion and indicates the nature of the flows. The Marangoni number is equivalent to the conventional Peclet number and appears in the energy equation to give an indication of the heat transfer. The proper influence of buoyancy is determined by the coefficient of the buoyancy term which for viscous-type flows is $Bd(\beta\Delta T)$ and for boundary-layer flows is $Bd(\beta\Delta T)(A/\mathrm{Re}_\sigma)^{2/3}$. Thus, it can be seen that the dynamic Bond number, Bd, and not the static one, Bo, is the correct parameter for that purpose. From the above criteria it is clear that in a sufficiently low gravitational environment surface-tension gradient flows will be significant.

4. EXAMPLES OF RELATED PROBLEMS

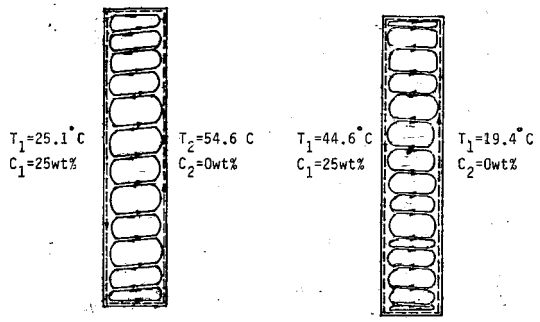
(1) Double-diffusive Convection in Confined Fluids

Experimental results will be given for steady-state natural convection of a salt-water solution in confined fluids due to the combined horizontal temperature and concentration gradients. There appears to be two types of global fluid motion, i.e. a unicell flow pattern and a multi-layer flow pattern depending on the relative magnitude of the buoyancy ratio. Formation and growth of a layered flow structure is visually observed. A lager number of layers appear in the case of the opposing thermal and solutal buoyancy forces than that of the cooperating case. Due to the double-diffusive nature of heat and salt, interesting temperature and concentration profiles are obtained in the multi-layer flow regime.



(a) (b)

Fig. 5(a)(b). Cellular Flow Pattern due to Combined Buoyancy Force (a) ΔT=14.2°C, ΔC=20wt%, (b) ΔT=21.5°C, ΔC=20wt%



(c) (d)

Fig. 5(c)(d). Cellular Flow Pattern due to Combined Buoyancy Force (c) ΔT=29.5°C, ΔC=25wt%, (d) ΔT=25.2°C, ΔC=25wt%

(2) Thermocapillary Convection in a Simulated Floating Zone

Experimental results will be given for the unstable oscillatory thermocapillary flow and its associate temperature characteristic in a simulated floating zone. Oscillatory flow, which is three dimensional and has an azimuthal directional velocity, appears when the Marangoni number is greater than a certain critical value. The flow patterns in the liquid zone are classified with mode numbers according to the oscillatory flow characteristics. It is determined that the mode depends on the aspect ratio but not on Marangoni number. Also, the thermal oscillation frequency is observed to be equal to the rotation frequency of the flow. Flow oscillation, temperature oscillation and the free surface deformation are found to be closely coupled and these frequency are equal.

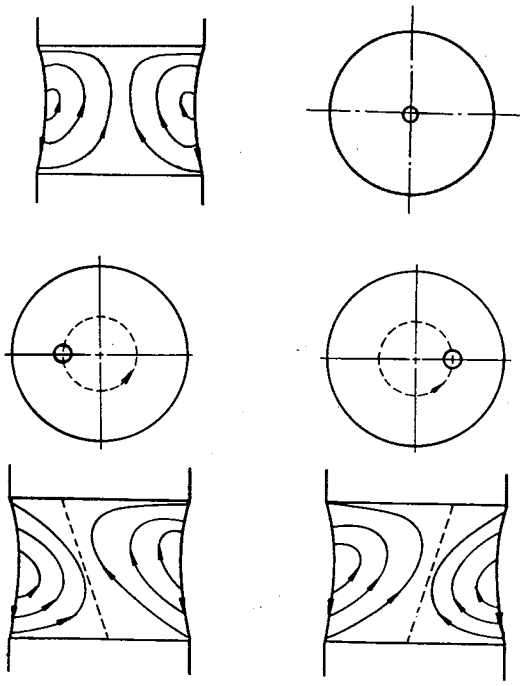
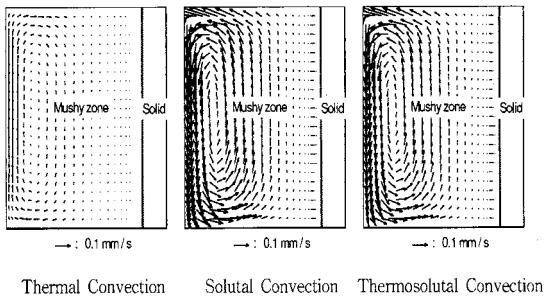


Fig. 6. Sketch of the streamlines in horizontal cross section of the liquid column (a) steady thermocapillary flow, (b) asymmetric oscillatory thermocapillary flow

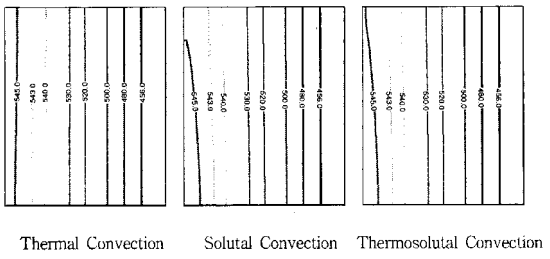
(3) Effect of Thermosolutal Convection in Alloy Solidification

Numerical results will be given for the effects of thermosolutal convection on the formation of macrosegregation in a Pb-Sn alloy solidification process in a two dimensional confined rectangular mold. The basic equations are solved using the Continuum Model theory with the SIMPLE algorithm during the solidification process. In addition, to track the liquid-solid interface with time variations, the moving boundary conditions was adopted and moving irregular interface shape were treated with the time-dependent, boundary-fitted coordinate system. As the temperature reduces from the liquidus to the solidus, the liquid concentration of Sn, the lighter constituent, increase. Then the buoyancy-driven flow due to temperature and liquid composition gradients occurs in the mushy region and forms the complicated macrosegregation maps. Related to this phenomena, effects on the macrosegregation formation depending on the cooling condition and gravity values are examined.



(a) Velocity Profile

(b)



(b) Temperature Profile

Fig. 7(a)(b). Effect of Thermosolutal Convection on Velocity and Temperature Profiles

5. SUMMARY

Two most common natural flows, i.e., natural convection due to combined temperature and concentration gradients and surface-tension gradient flow, and their flow characteristics and mathematical treatment are identified and delineated. Three examples of related problems are given to help one understand the physical nature of natural flows.

References

1. S.H. Davis, Themocapillary Instabilities, Ann. Rev. Fluid Mech. 19(1987) 403.
2. G.F. Teletzke, H.T. Davis and L.E. Scriven, Wetting Hydrodynamics, Rev. Phys. Appl. 23(1988).
3. D. Schwabe, Surface-tension Driven Flow in Crystal Growth Melts, in Crystals, Growth, Applications and Properties, ed. H.C. Freyhardt, Vol. 11, p. 75(Springer Verlag, Berlin 1988)
4. C.L. Strong, Scientific-American 224-6 (1971) 124.
5. J. Walker, Scientific-American 237-4 (1977) 142.
6. J.S. Turner and H. Stommel, Proc. Nat'l. Acad. Sci. 52 (1964) 49.
7. S. Ostrach, PhysicoChemical Hydrodynamics 1 (1980) 233.
8. S. Ostrach, Role of Analysis in the Solution of Complex Physical Problems, Proc. 3rd Int. Heat Transfer Conf., Chicago, IL, 1966, Vol. 6, pp. 31-43.
9. S. Ostrach, Motion Induced by Capillarity, in: PhysicoChemical Hydrodynamics, Vol. 2, Ed. D.B. Spalding (Advanced Publication Ltd., London, 1979).
10. V.G. Levich, PhysicoChemical Hydrodynamics (Prentice-Hall, 1962).
11. D.B.R. Kenning, Appl. Mech. Rev., Vol. 21 (1968) 1101.
12. V. Stanek, and J. Szekely, Chem. Eng. Sci., 25 (1964) 699.
13. S. Ostrach, Convection Due to Surface-Tension Gradients in: Proc. COSPAR Space Research, Vol. Ⅷ, Innsbruck, Austria, 1978.

A Simple Theoretical Model of a Thermosyphon

K. S. Ong

Monash University Malaysia, 2 Jalan Kolej, Bandar Sunway, 46150 Petaling Jaya, Malaysia.
Tel: +603 56360600, Fax: +603 56329314, Email: Ong.Kok.Seng@engsci.monash.edu.my

Abstract

A simple theoretical model of a thermosyphon operating under steady-state condition is proposed. The evaporator section is assumed immersed in a pool of hot water and heat transfer from the hot water to the thermosyphon is via natural convection. The condenser section is surrounded by a concentric-pipe water-cooled jacket. Forced convection is assumed. The theoretical model assumes heat transfer to take place from the hot pool (evaporator) to the coolant water (condenser) via a series of thermal resistances. These resistances are assumed contributed by the water film heat transfer coefficients external to the thermosyphon, the pipe metal wall, internal and external fouling resistances on the pipe wall and the evaporating and condensing film coefficients along both evaporator and condensing sections of the thermosyphon. The temperatures at the various interfaces along the thermosyphon are considered. An equivalent thermal network is established based on the interface temperatures. Since interface temperatures and heat transfer are inter-related, the former are not determined explicitly. Instead, an iterative process was established to determine their steady-state values. In the calculations, fluid properties are not assumed constant, but dependent upon the prevailing corresponding interface temperatures. Heat transfer correlations are obtained from existing literature. Experimental data for water-filled thermosyphons from previous investigations showed that the performance of the thermosyphon was independent of fill ratio at the relatively high fill ratios studied and a minimum operating temperature difference of around 5 to 7^{o}C was required before it could begin to function.. Comparison between predicted and experimental results showed that the present theoretical model under-predicted the performance.

Key words: Heat pipe, thermosyphon, water-filled thermosyphon, theoretical model thermosyphon.

1. INTRODUCTION

The evaporating and condensing heat transfer coefficients affect the performance of a thermosyphon. The analysis of boiling heat transfer in the evaporator section of a thermosyphon is very complex. In most cases the evaporator section consists of a falling liquid film portion and the liquid pool portion. The different lengths of these two sections will affect the mean evaporation heat transfer coefficient at the evaporator section. A smaller fill ratio has a longer liquid film in the evaporator section. Since the liquid film heat transfer coefficient is higher than that of the liquid pool section, smaller fill ratio results in higher mean heat transfer coefficients.

Andros and Florschuetz [1] made a visual study and reported various flow regimes in the evaporator section. At low evaporator heat flux, a continuous film with evaporation was found. Convective boiling and evaporation dominate here. At high evaporator heat flux, nucleate boiling was observed. Nucleate boiling also dominates as fill ratio increases.

Shiraishi et. al. [2] obtained experimentally, heat transfer coefficients for both condenser and evaporator sections using water, ethanol and Freon 113 and developed a simple mathematical model to predict the performance of the thermosyphon. For the liquid film in the evaporator section at high heat flux, they proposed to use the boiling heat transfer coefficient. At low heat flux, they proposed to use the laminar film evaporation model which is essentially the reverse of Nusselt's condensate theory. Their predictions underestimated their experimental results especially at low fill ratios.

Chen et. al. [3] showed that with increasing heat flux, this effect of filling ratio disappeared as the height of the liquid pool expands with increasing

heat flux. Yong et. al. [4] showed that the effect of fill ratio on evaporator heat transfer coefficients was nearly negligible in the heat flow rate between 50 – 600 W and 10 – 70% fill ratio.

The objective of the present paper is to present a theoretical model for a thermosyphon based on the thermal resistance network analysis.

2. THEORETICAL MODEL AND NALYSIS

The model is illustrated in Fig. 1. The thermosyphon is assumed to consist of three sections, the evaporator section of length L_e, the adiabatic section L_a, and the condenser section, L_c. The amount of liquid in the evaporator section is represented by the length L_p. The evaporator section is exposed to a hot fluid at a uniform temperature T_e and the condenser section to a cold fluid at a uniform temperature T_c.

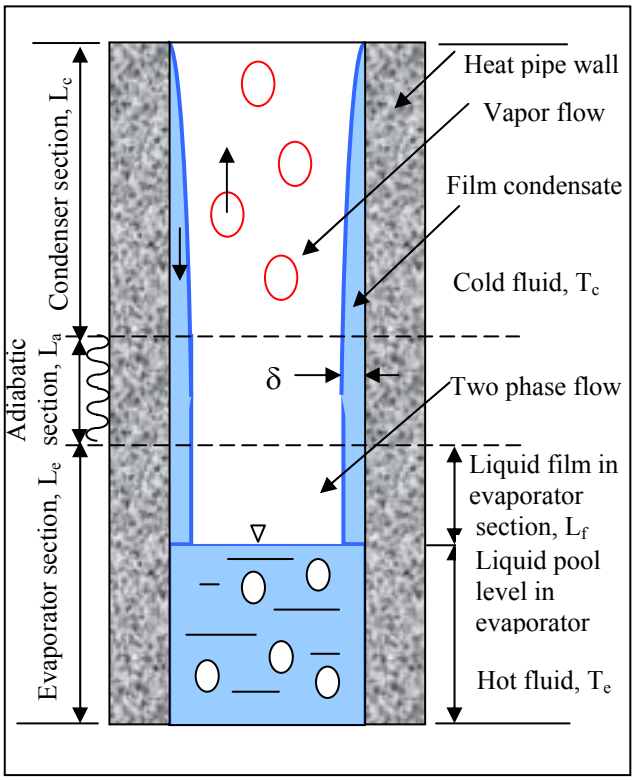


Fig. 1. Vertical thermosyphon.

2.1 Heat transfer rate

The heat transfer and the temperatures at the associated locations in a simple heat pipe set-up are shown in Fig. 2. The overall heat transfer rate is given by

$$\dot{q} = U\,\Delta T_m \qquad (1)$$

where

$$\Delta T_m = T_e - T_c \qquad (2)$$

The mean condenser temperature, T_c, could be approximated by

$$T_c = \frac{T_{ci} + T_{co}}{2} \qquad (3)$$

In the absence of any heat losses from the pipe, the heat absorbed at the evaporator section equals the amount of heat rejected at the condenser section, viz.,

$$\dot{q} = \dot{m}_c\, C_p\, (T_{co} - T_{ci}) \qquad (4)$$

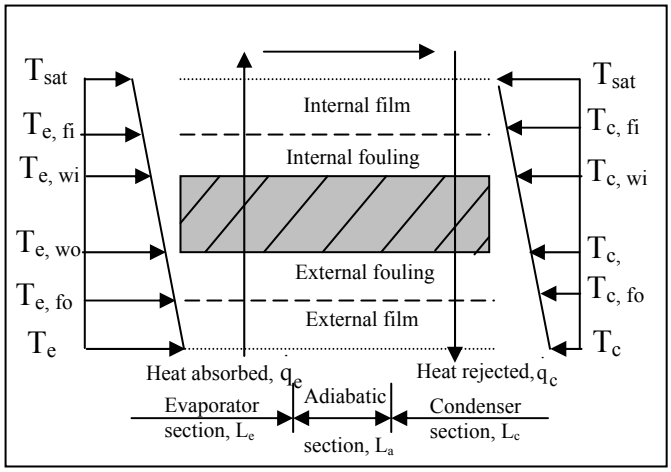


Fig. 2. Temperature distribution across thermosyphon.

2.2 Heat transfer resistance

The total resistance to heat transfer, ∑R, is found by adding up the individual resistances to heat flow. The equivalent thermal network for the heat transfer is shown in Fig. 3. It is assumed that there is no heat transfer along the wall of the pipe, viz., $R_{wall} = 0$. The individual resistances are defined and calculated as follows:

Ext film at evap: $R_e = 1/(\pi D_o L_e h_e)$ (5)
Ext fouling at evap: R_f
Evap wall: $R_{e,wall} = \ln(D_o/D_i)/(2\pi k_{wall} L_e)$ (6)
Int fouling of evap: R_f
Boiling at evap: $R_{evap} = 1/(\pi D_i L_e h_{evap})$ (7)
Vapour resistance: $R_v \approx 0$
Condensation at cond: $R_{cond} = 1/(\pi D_i L_c h_{cond})$ (8)
Int fouling of cond: R_f
Cond wall: $R_{c,wall} = \ln(D_o/D_i)/(2\pi k_{wall} L_c)$ (9)
Ext fouling at cond: R_f

Ext film at cond: $R_c=1/(\pi D_o L_c h_c)$ (10)

For clean smooth pipes filled with distilled water, fouling coefficient R_f is small, about 0.0001 kW^{-1}.

The overall heat transfer coefficient is equal to

$$U = \frac{1}{\Sigma R} \quad (11)$$

2.3 Interface temperatures

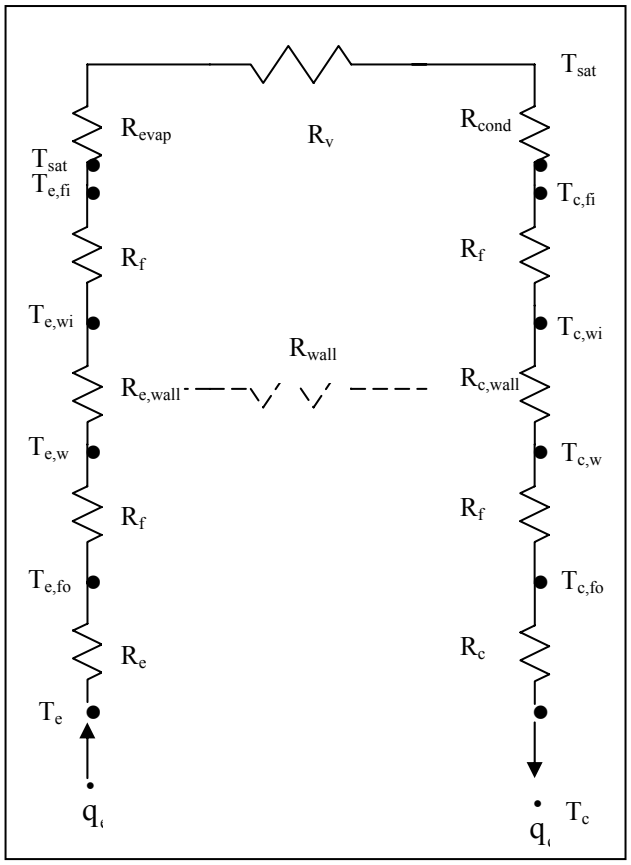


Fig. 3. Thermal network for thermosyphon.

From Fig. 3, the temperatures at the respective interfaces may be calculated from the following expressions

$$T_{e,fo} = T_e - \frac{R_e}{\Sigma R}\Delta T_m \quad (12)$$

$$T_{e,wo} = T_e - \frac{R_e + R_f}{\Sigma R}\Delta T_m \quad (13)$$

$$T_{e,wi} = T_e - \frac{R_e + R_f + R_{e,wall}}{\Sigma R}\Delta T_m \quad (14)$$

$$T_{e,fi} = T_e - \frac{R_e + R_f + R_{e,wall} + R_f}{\Sigma R}\Delta T_m \quad (15)$$

$$T_{sat} = T_e - \frac{R_e + R_f + R_{e,wall} + R_f}{\Sigma R} - \frac{R_{evap}}{\Sigma R}\Delta T_m \quad (16)$$

$$T_{c,fi} = T_e - \frac{R_e + R_f + R_{e,wall} + R_f}{\Sigma R} - \frac{R_{evap} + R_{cond}}{\Sigma R}\Delta T_m \quad (17)$$

$$T_{c,wi} = T_{c,fi} - \frac{R_e + R_f + R_{e,wall} + R_f}{\Sigma R} - \frac{R_{evap} + R_{cond} + R_f}{\Sigma R}\Delta T_m \quad (18)$$

$$T_{c,wo} = T_e - \frac{R_e + R_f + R_{e,wall} + R_f}{\Sigma R} - \frac{R_{evap} + R_{cond} + R_f + R_{c,wall}}{\Sigma R}\Delta T_m \quad (19)$$

$$T_{c,fo} = T_e - \frac{R_e + R_f + R_{e,wall} + R_f + R_{evap}}{\Sigma R} - \frac{R_{cond} + R_f + R_{c,wall} + R_f}{\Sigma R}\Delta T_m \quad (20)$$

$$T_c = T_e - \frac{R_e + R_f + R_{e,wall} + R_f + R_{evap}}{\Sigma R} - \frac{R_{cond} + R_f + R_{c,wall} + R_f + R_c}{\Sigma R}\Delta T_m \quad (21)$$

2.4 Natural convection heat transfer coefficient

McAdams [5] recommended for a vertical isothermal plate or cylinder the mean Nusselt number

$$Nu = m\,(Gr_L\,Pr)^n \quad (22)$$

The constants m and n are given in Table 1.

Table 1. Values of m and n

Flow	Range Gr_L Pr	m	n
Laminar	$10^4 - 10^9$	0.59	¼
Turbulent	$10^9 - 10^{13}$	0.10	1/3

The above heat transfer correlation is employed to determine h_e, the external film heat transfer coefficient in the evaporator section. Fluid properties are evaluated at the average film temperature $(T_{e,fo} + T_e)/2$.

2.5 Forced convection heat transfer coefficient

Sieder and Tate [6] proposed the following correlation taking into account wall viscosity for laminar flow in the entrance region of a circular tube at constant wall temperature

$$Nu = 1.86\,(Re\,Pr\,D/L)^{1/3}\left[\frac{\mu}{\mu_{wall}}\right]^{0.14} \quad (23)$$

for $0.48 < Pr < 16{,}700$, $0.0044 < \mu/\mu_{wall} < 9.75$, and $(Re\ Pr\ L/D)\ (\mu/\mu_{wall})^{0.14} > 2$.
For flow in concentric-tubes, the pipe diameter is replaced by the equivalent diameter

$$D_h = (D_c - D_o) \qquad (24)$$

The above heat transfer correlation is employed to determine h_c, the external film heat transfer coefficient in the coolant jacket. Except for μ_{wall}, which is evaluated at the wall temperature, all physical properties are evaluated at the coolant fluid mean temperature, T_c.

From Nusselt [7], the condensate film thickness at the bottom of the condenser section for laminar film condensation is

2.6 Condensation heat transfer coefficient

$$\delta = \left[\frac{4\,k\,\mu\,(T_{sat} - T_{c,fi})\,L_c}{g\,\rho\,(\rho - \rho_v)\,h_{fg}} \right]^{1/4} \qquad (25)$$

Rohsenow [8] suggested that subcooling of the film be accounted for by replacing the latent heat of vaporization with

$$h_{fg}' = h_{fg} + 0.68\,C_p\,(T_{sat} - T_{c,fi}) \qquad (26)$$

The average condensation heat transfer coefficient is given by

$$\overline{h_{cond}} = 0.943 \left[\frac{g\,\rho\,(\rho - \rho_v)\,h_{fg}'\,k^3}{\mu\,(T_{sat} - T_{c,fi})\,L_c} \right]^{1/4} \qquad (27)$$

and the average Nusselt number is

$$\overline{Nu_{cond}} = 0.943 \left[\frac{g\,\rho\,(\rho - \rho_v)\,h_{fg}'\,L_c^3}{\mu\,k\,(T_{sat} - T_{c,fi})} \right]^{1/4} \qquad (28)$$

From experimental results, McAdams [5] recommended that the above condensation Nusselt's number be multiplied by a factor of 1.2 to give

$$\overline{Nu_{cond}} = 1.13 \left[\frac{g\,\rho\,(\rho - \rho_v)\,h_{fg}'\,L_c^3}{\mu\,k\,(T_{sat} - T_{c,fi})} \right]^{1/4} \qquad (29)$$

For most practical cases, since $\rho_v << \rho$, the following approximation may be applied

$$\rho\,(\rho - \rho_v) \approx \rho^2 \qquad (30)$$

For the condensing heat transfer coefficient h_{cond}, fluid properties are evaluated at the mean condensate film temperature $(T_{sat} + T_{c,fi})/2$ while h_{fg} is evaluated at the saturation temperature T_{sat}.

2.7 Fill ratio

The interval volume of the evaporator section in a heat pipe is given by

$$V_e = \frac{\pi\ D_i^2\ L_e}{4} \qquad (31)$$

The fill ratio F_R is defined as the ratio of the initial total volume of fluid contained in the heat pipe to the internal volume of the evaporator section of the heat pipe. In terms of initial height of liquid in the evaporator section of the pipe

$$F_R = \frac{L_{p,in}}{L_e} \qquad (32)$$

The total mass of fluid in the pipe is

$$M = \rho_{in}\ F_R\ V_e \qquad (33)$$

Initially, the fluid is in its liquid state and fills the bottom (evaporator) section of the pipe. During operation, this fluid exists as a liquid film of condensate running down the condenser and adiabatic sections of the pipe, a pool of liquid in the evaporator section and in the gaseous state throughout the non-liquid filled portions of the pipe as shown in Fig. 1. The actual amount of fluid in each section would depend upon the fill ratio and operating condition of the pipe.

The total volume of the condensate film running down the wall of the condenser section of the pipe may be obtained by integrating the condensate thickness equation over the length of the condenser section to give

$$V_c = \frac{4}{5} \left[\frac{4\,k\,\mu\,(T_{sat} - T_{c,fi})}{g\,\rho\,(\rho - \rho_v)\,h_{fg}'} \right]^{1/4} L_c^{5/4} \qquad (34)$$

In the adiabatic section, the condensate film thickness is assumed uniform and equal to the thickness of the condensate at the bottom of the condenser section, δ.

Hence the total mass of condensate in both condenser and adiabatic sections is approximately

$$m_{c+a} = \rho_c \left(V_c + \pi\,D_i\,L_a\,\delta \right) \qquad (35)$$

If we assume that the fill ratio is large enough so that the evaporator section never runs dry, then the mass of the pool of liquid remaining in the evaporator section during operation is given by

$$m_e = M - m_{c+a} \quad (36)$$

and the height of this liquid pool in the evaporator section during operation can be determined from

$$L_p = \frac{4\, m_e}{\pi D_i^2 \rho} \quad (37)$$

2.8 Boiling heat transfer coefficient

For pool boiling, Shiraishi et. al. [2] proposed the following average nucleate boiling heat transfer coefficient in the pool region

$$\overline{h_p} = 0.32\left[\frac{\rho^{0.65} k^{0.3} C_p{}^{0.7} g^{0.2}}{\rho_v{}^{0.25} h_{fg}{}^{0.4} \mu^{0.1}}\right]\left(\frac{P}{P_a}\right)^{0.23} \dot{q}_e''^{0.4} \quad (38)$$

and for the falling liquid film in the evaporator, the laminar convection heat transfer coefficient similar to the reverse of Nusselt's condensation theory at low heat flux, viz.,

$$\overline{h_f} = 0.943\left[\frac{g \rho^2 h_{fg}' k^3}{\mu L_f (T_{sat} - T_{e,fi})}\right]^{1/4} \quad (39)$$

In this paper where the evaporator section consists of a liquid pool and a falling liquid film, an equivalent heat transfer coefficient is proposed, viz.,

$$\overline{h_e} = \frac{\overline{h_p} L_p + \overline{h_f} L_f}{L_e} \quad (40)$$

For the evaporation film heat transfer coefficient equations above, fluid properties are evaluated at the average film temperature equal to $(T_{sat} + T_{c,fi})/2$.

2.9 Physical properties

The physical properties for water are based on tabulated data from Incropera and DeWitt [9]and assumed to vary linearly with temperature between 300 – 360 K, except for viscosity.

3. EXPERIMENTAL INVESTIGATION

The 28.2 mm O/D and 25.5 mm I/D copper tube thermosyphon constructed is shown in Fig. 4. It measured 780 mm long. The copper tube was plugged at one end and provided with a screwed end cap and an 'O' ring seal at the other. A compound pressure gauge was fitted via a 6.3 mm O/D copper "T" piece to measure the working pressure in the pipe. A type K thermocouple in a stainless steel sheath was also fitted through the plug to measure the saturation temperature of the working fluid. The pipe was filled with water. Experiments were conducted with fill ratios 0.6, 0.7 and 0.8.

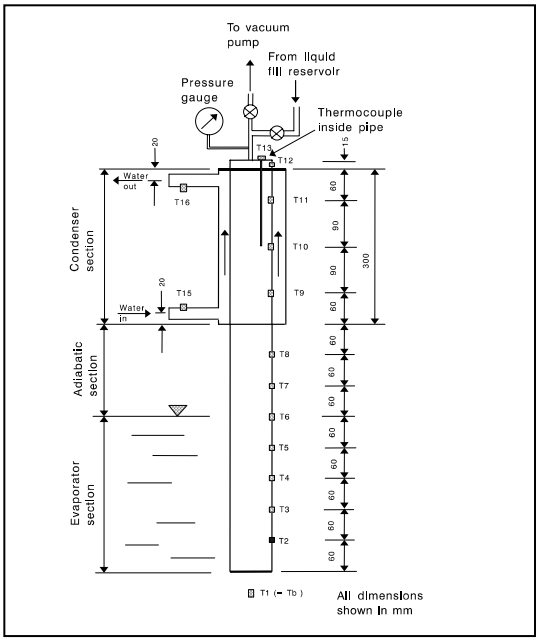


Fig. 4. Schematic diagram of thermosyphon.

a water-cooled jacket constructed from 45 mm I/D copper pipe surrounding the pipe. Two 12 mm O/D inlet and outlet connections were brazed diagonally across each other to induce swirl at the inlet. Temperature distribution along the external surface of the thermosyphon in the evaporator and adiabatic sections were measured by Cu/Con thermocouples mechanically attached by wire twisted onto the surface of the pipe. Temperature distribution in the condenser section was measured using Cu/Con thermocouples mounted on the water jacket but pressed against the external surface of the inner pipe of the thermosyphon through screwed connections on the outer wall of the jacket. Coolant water and bath temperature were measured using Cu/Con thermocouples. All the thermocouples were connected to a multi-point temperature monitor and connected to a data acquisition system. Temperature measurements were accurate to $\pm$ 0.5°C and water mass flowrate to within $\pm$ 3% of measured value.

The test facility is shown schematically in Fig. 5. The thermosyphon was immersed in a water bath which was provided with two electrical immersion heating elements of 0.75 kW each. One of the elements was provided with a thermostat to maintain a pre-set bath temperature. The element without the thermostat

was utilised in the event a heat input greater than 0.75 kW was required. The bath was stirred slowly to ensure no temperature stratification within the bath. Temperature difference between the top and bottom of the bath was less than 0.5°C. Coolant water was supplied via a constant-head tank device. Coolant water flow rate was measured using a variable area flow meter. Experiments were performed using water flowrates at 0.0020, 0.0039, 0.0058 and 0.0077 kg s^{-1}. Water inlet temperature was about 30°C.

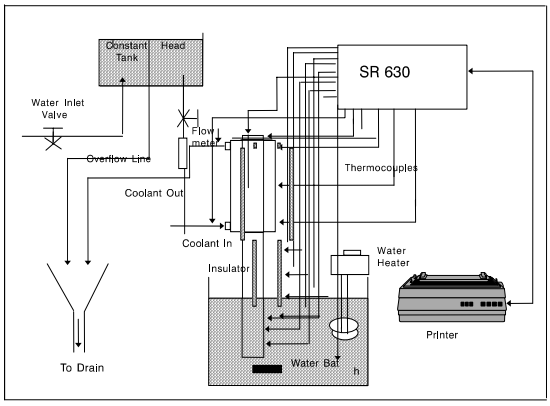


Fig. 5. Schematic diagram of apparatus.

For each experiment, the thermosyphon was immersed in the water bath initially at ambient temperature. The bath temperature was then progressively increased in steps until steady state was achieved at the temperature level desired. Steady state was considered to be achieved when four sets of temperature readings taken at 3-minute intervals showed less than 0.5°C variation. The procedure was then repeated for the next temperature setting. The bath temperature was controlled from 40 - 90°C. The resultant heat transferred for the pipe ranged from 34 – 630 W. Further details of the equipment are available in Haider [10] and Lau [11]. The experimental data for the present discussion is taken from Lau [11].

4. DISCUSSION OF RESULTS

A typical set of results showing the axial temperature distribution on the outer surface of the thermosyphon is shown in Fig. 6 for a fill ratio of 0.7 and coolant water flowrate at 0.0077 kg s^{-1}. The temperatures at the evaporator and adiabatic sections decreases slightly as we progress towards the condenser section indicating some heat transfer along the pipe wall. However, the temperature differences are small. In the theoretical model we have assumed no heat transfer along the wall. Further, the temperatures along the outer condenser wall are not uniform. The portion of condenser wall immediately adjacent to the coolant water inlet exhibits a lower temperature than at the other locations. The saturation temperature is slightly higher than the wall temperature at the top of the thermosyphon, as expected.

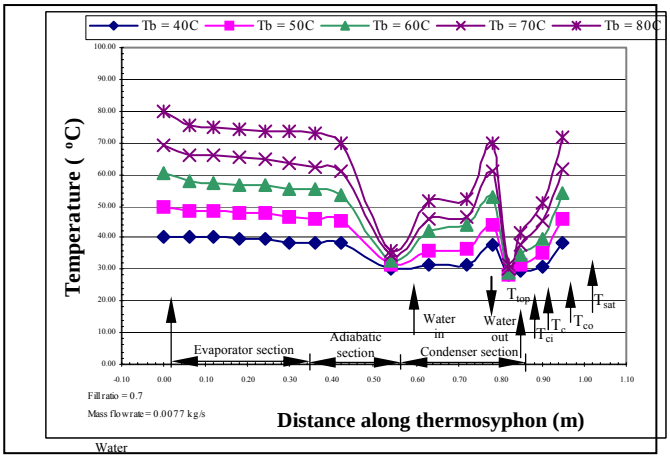


Fig. 6. Temperature distribution along thermosyphon.

gure 7 shows the heat transfer rate obtained at a fill ratio of 0.7 with the various coolant flowrates employed plotted against the operating temperature difference between bath and mean coolant temperatures. As expected, greater operating temperature differences result in higher heat transfer rates. The results also shows that the overall heat transfer coefficient increases with increase in coolant water flowrate due to increased convection heat transfer in the coolant jacket. An almost linear relationship between heat transfer rate and operating temperature difference is observed. Extrapolating the heat transfer rate to zero values shows that the thermosyphon requires a minimum operating temperature difference of around 5 to 7°C before it could begin to function. Considering this minimum starting temperature difference and looking at the gradient of the lines it could be said that the experimentally obtained values of overall heat transfer coefficient were thus higher than the values that could result if the lines had started from the origin, ie. with no minimum temperature difference.

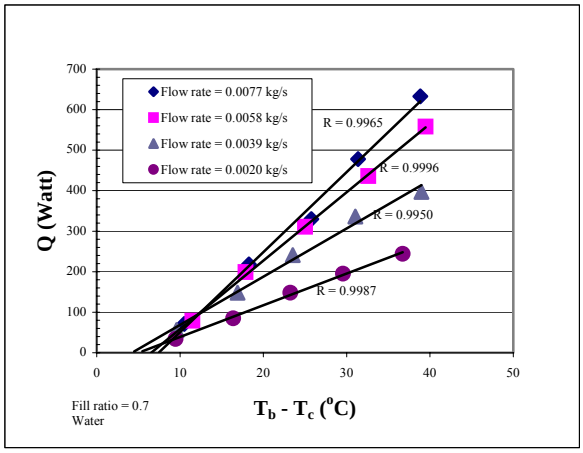


Fig. 7. Effect on heat transfer rate due to different mass flowrates.

Figure 8 shows the heat transfer rates obtained at a coolant flowrate of 0.0077 kg s^{-1} for the various fill ratios of 0.6 to 0.8 plotted against the operating temperature difference between bath and mean coolant temperature. In addition to the observations made previously, the results also show that the performance of the thermosyphon is independent of fill ratio at the relatively high fill ratios studied.

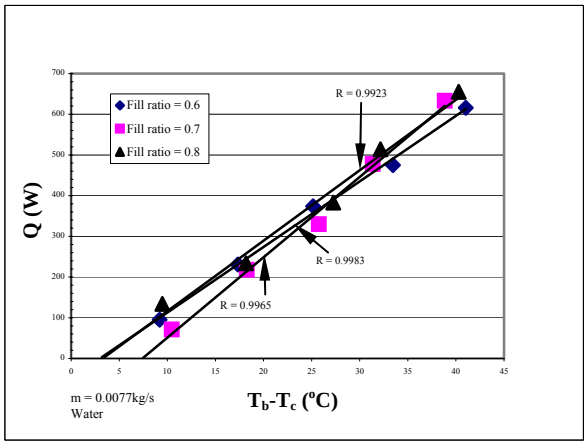


Fig. 8. Effect of fill ratio on heat transfer rate.

Figure 9 compares the predicted overall heat transfer coefficient results and the experimental data for fill ratio equal to 0.6. The simple theoretical model under-predicted the thermosyphon performance. This is attributed to the minimum starting temperature difference as explained previously. Further and due consideration should be given to this phenomena in order to improve the model.

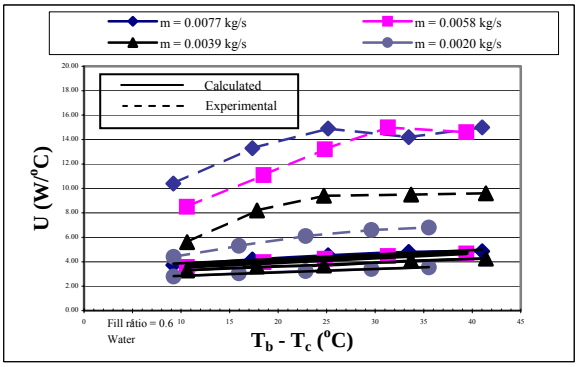


Fig. 9. Experimental and theoretical U.

5. CONCLUSIONS

A simple theoretical model of a thermosyphon was presented. Experimental data showed that the performance of the thermosyphon was independent of fill ratio at the relatively high fill ratios studied and a minimum operating temperature difference of around 5 to 7°C was required before it could begin to function. The present theoretical model under-predicted the performance.

Nomenclature

A	pipe surface area (m^2)
C_p	specific heat (J kg^{-1} K^{-1})
D	diameter (m)
D_h	equivalent diameter (m)
F_R	fill ratio
g	gravitational constant (9.8 m s^{-2})
h	heat transfer coefficient (W m^{-2} K^{-1})
h_{fg}	latent heat of vaporisation (J kg^{-1})
k	thermal conductivity (W m^{-1} K^{-1})
L	length (m)
m	mass (kg)
M	total mass of fluid in pipe (kg)
P	Operating pressure in the thermosyphon (bar)
P_a	Atmospheric pressure (bar)
$\dot{q}$	heat transfer rate (W)
$\dot{q}''$	heat flux (W m^{-2})
R	thermal resistance (K W^{-1})
T	temperature (°C, K)
ΔT_m	mean temperature difference (K)
U	overall heat transfer coefficient (W K^{-1})
u	velocity (m s^{-1})
V	volume (m^3)

Greek letter symbols

β	coefficient of thermal expansion (K^{-1})

δ condensate film thickness (m)
σ surface tension (N m^{-1})
μ absolute (dynamic) viscosity (N s m^{-2})
ν kinematic viscosity (m^2 s^{-1})
ρ density (kg m^{-3})

Subscripts

a adiabatic section
c condenser section
cond condensate
ci, co inlet and outlet condenser coolant sections
d liquid pool in evaporator
e evaporator section
evap evaporation
f fouling, film
i, o inner and outer pipe diameters
in initial
max maximum
m, n constants in Eq (28)
p liquid pool
sat saturation
v vapor
wall pipe wall

Dimensionless terms

Gr_L Grashof No. $\left[\frac{g\,\beta\,(T_w - T_\infty)\,L^3}{\nu^2}\right]$

Gz Graetz No. $\left[Re\,Pr\,\frac{D}{L}\right]$

Ja Jacob No. $\left[\frac{C_p\,(T_\infty - T_w)}{h_{fg}}\right]$

Nu Nusselt No. $\left[\frac{h\,L}{k}\right]$

Re Reynolds No. $\left[\frac{\rho\,u\,D}{\mu}\right]$

Pr Prandtl No. $\left[\frac{C_p\,\mu}{k}\right]$

Acknowledgements

Thanks are extended to Abdesselam Hamlaoui for his assistance and corporation in making the data from Lau's thesis available in the present analysis.

References

1. Andros F. E. and Florschuetz L. W., "The two-phase closed thermosyphon: An experimental study with flow visualization", Veziroglu T. N. and Kakak S. (Ed): Two-phase transport and reactor safety, 4, Hemisphere Publishing Corporation, Washington, 1231 - 1267, 1978.
2. Shiraishi M., Kikuchi K. and Yamanishi T., "Investigation of heat transfer characteristics of a two-phase closed thermosyphon", Proc. 4th Int heat Pipe Conference, London, 95 - 104, 1981.
3. Chen Z. Q., Zhang Z. and Ma T. "Heat transfer correlation of the evaporator section in a two-phase closed thermosyphon", Proc. 8th Int Heat Pipe Conference, Beijing, 354 - 359, 1992.
4. Yong J. P., Hwan K. K. and Chul J. K., "Heat transfer characteristics of a two-phase closed thermysyphon to the fill charge ratio", Int. J. Heat and Mass Transfer, 45, 4655 - 4661, 2002.
5. McAdams W. H., "Heat Transmission", 3E, McGraw-Hill, 1954.
6. Sieder E. N. and Tate G. E., "Heat transfer and pressure drop of liquids in tubes", Ind. Eng. Chem., 28, 1963.
7. Nusselt W., "Die oberflachenkondensation des wasserdampfes", ZVDI, 60, 541, 1916.
8. Rohsenow W. M., "Heat transfer and temperature distribution in laminar film condensation", Trans ASME, 78, 1645, 1956.
9. Incropera F. P. and DeWitt D. P., "Introduction to heat transfer", 3E, Wiley, 1996.
10. Md. Haider E. Alahi., "Performance of a wickless heat pipe (thermosyphon)", MSc Thesis, University of Malaya, 1998.
11. Lau Henry S. K., "Theoretical and experimental study of thermosyphon using water", Graduation Thesis, Engineering Faculty, University, 2002.

An Anti-Gravity Thermosyphon with a Switching Valve

Hideaki Imura, Yasushi Koito, and Takuya Ichinomiya
Department of Mechanical Engineering and Materials Science,
Faculty of Engineering, Kumamoto University,
2-39-1 Kurokami, Kumamoto, 860-8555, Japan
Tel and Fax: 81-96-342-3752, E-mail:imura@gpo.kumamoto-u.ac.jp

Abstract

There exist several types of top-heated thermosyphons and heat pipes. They are operated by a capillary force, a buoyancy force due to liquid-vapor density difference, an osmotic pressure and a vapor pressure as a driving force. The present thermosyphon transports heat from higher to lower positions by making use of the vapor pressure which is controlled by opening and shutting an electromagnetic switching valve. The present experimental study was carried out to examine if this top-heated thermosyphon works properly without trouble and to investigate the pressure and temperature variations with time at several main points. As a result, it was verified that this anti-gravity thermosyphon possessed very practical probability.

Key words: Thermosyphon, Anti-gravity, Top-heated, Switching valve

1. INTRODUCTION

This paper describes heat transport from higher to lower positions using an anti-gravity loop-type thermosyphon with an electromagnetic switching valve. These thermosyphons and heat pipes are utilized to store the solar heat irradiated on roads in underground soil during summer[1]. The stored heat is used to melt snow on roads and roofs, to prevent water from icing on the road surface, and also to grow vegetables and the other farm products in winter[2]. In the anti-gravity thermosyphons and heat pipes, a condensed liquid in a condenser must be pumped up by some driving forces[3][4]. As representative ones, a capillary force[5], a vapor-lift pump[6],[7], an osmotic pressure [8],[9] and a vapor pressure[10] have been used, and the study on the heat transport rates has been investigated.

Kawabata et al.[10] have tested on the heat transport rates of the anti-gravity heat pipe with a switching chamber in which a float box worked to open and close valves for controlling the vapor pressure. It was shown that their apparatus with the effective height of 10 m transported up to 3500 W. The apparatus in the present study was replaced the switching chamber by the switching valve because the switching valve could securely open and shut a valve for controlling vapor flow.

2. EXPERIMENTAL APPARATUS AND PROCEDURES

The experimental apparatus is shown in Fig.1. It consists of an evaporator, a condenser, a reservoir, a switching valve, two check valves, and tubes connecting the above components. The dimensions of the evaporator and reservoir made of stainless steel are 200×200 mm^2 of the cross area and 250 mm high, so that both of the volumes are 10 liters. A sheathed heater of 2 kW is set up at the bottom of the evaporator. These vessels have respectively a water level indicator to see the quantity of water in them. The electromagnetic switching valve is usually closed by force of a spring and is made open when it is delivered electricity. The opening and shutting of the switching valve is made by a time switch. The condenser is double-tube type and the length is 540 mm. The inside tube made of copper is 10 mm ID and 12 mm OD. The outside tube made of brass is 24 mm ID and 30 mm OD. The tubes connecting the components is made of copper with 10 mm ID and 12 mm OD. Therefore, the inner diameter of the inside condenser tube is the same as that of the connecting tubes. One check valve is fitted on the liquid passage between the evaporator and the reservoir. The liquid is only flow through this valve from the reservoir to the evaporator. The other one is fitted on the passage at the bottom of the apparatus. Through this valve, the condensate can flow only from the condenser to the reservoir. This apparatus is

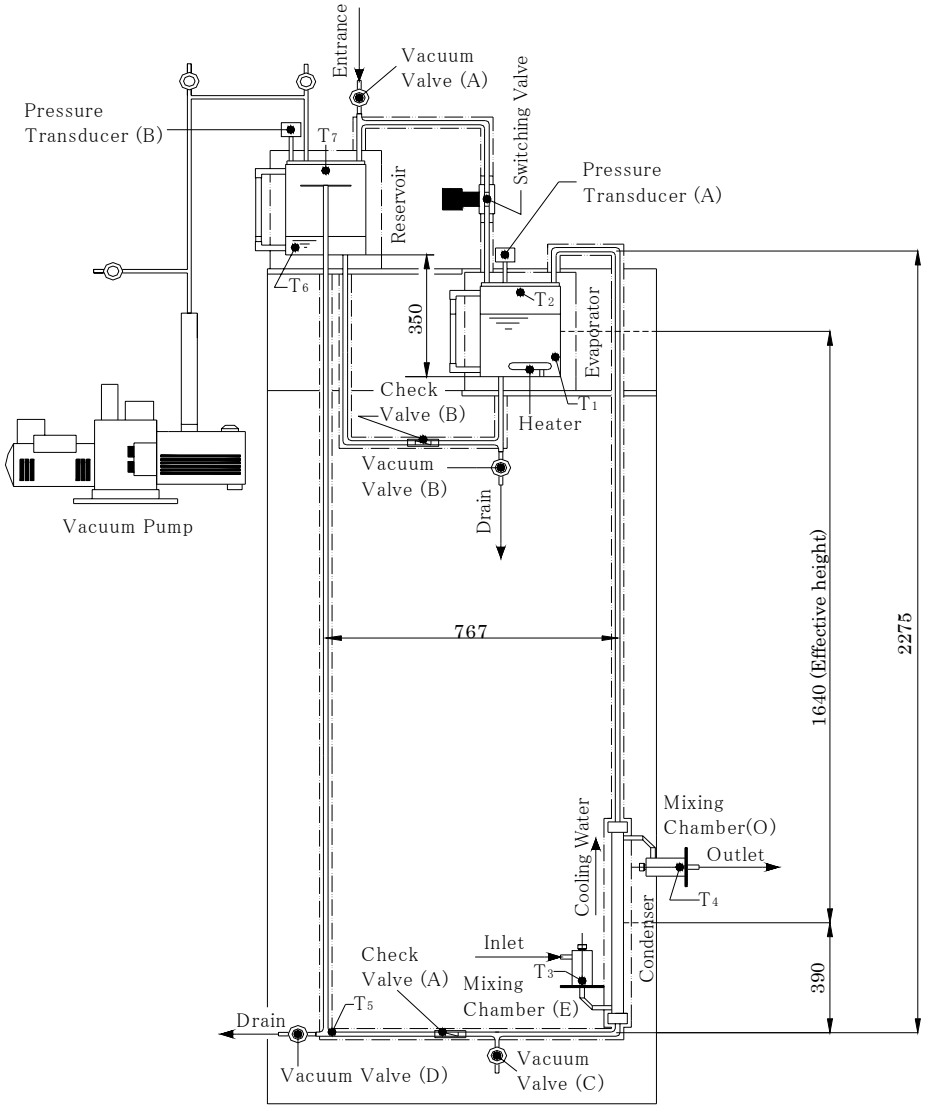


Fig.1 Schematic diagram of experimental apparatus

sealed by soldering and using O rings, so that the air in the apparatus may be evacuated by a vacuum pump. The leak test for keeping vacuum was performed. The vacuum pressure evacuated by the vacuum pump reached 7.4 Pa (0.074 mbar) when the inside of the apparatus was empty. After 48 hours from the time when the vacuum valves were completely closed and the vacuum pump was stopped at the same time, the vacuum pressure became 760 Pa (7.6 mbar). The effective height between the middles of the evaporator and condenser was 1640 mm. Water was used as the working fluid.

The experiments were performed as follows. Distilled water of 7 liters was poured into the evaporator. After that, the air was evacuated from the apparatus and the heat input was loaded with shutting the switching valve. The temperature of water in the evaporator rose and boiling occurred when the temperature reached the saturated one. The generated vapor flowed into the condenser through the vapor passage. The vapor condensed there and the generated condensate accumulated in the bottom connecting passage. When the condensate accumulated further, the upper level of the condensate reached the top of the condenser. In such a situation, the pressure of vapor rose because the vapor could not condense. Thus, the pressurized vapor pushed down the condensate into the condenser, and then the same quantity of condensate was pumped up into the reservoir. Thus, condensation again took place in the pushed-down surface at the top of condenser, and the condenser was again filled with the condensate. Through such a mechanism, the condensate was pumped up to the reservoir and accumulated in it. During such process, water in the evaporator evaporated and reduced in quantity, and the generated vapor transported

heat to the condenser as a latent heat.
When most of the liquid was pumped up to the reservoir from the evaporator (or condenser), the switching valve was opened and then the vapor flowed from the evaporator into the reservoir. Therefore, the pressure in the reservoir became almost the same as or even higher than that in the evaporator. At the same time, the liquid in the reservoir flowed down into the evaporator under the action of the gravity force. After that, when the temperature in the evaporator rose up to the saturated temperature, boiling again started and the generated vapor flowed to the condenser.

The temperatures were measured with thermo-couples at the positions of T_1 to T_7 shown in Fig.1. Also, the pressures were measured with pressure transducers A and B installed at respectively the evaporator and reservoir. Cooling water to cool the condenser was made flow from a overhead tank which was settled on the roof of the laboratory building. The transported heat was calculated from the mass flow rates measured by a float-type flowmeter and the temperature differences measured in mixing chambers fitted at the inlet and outlet of the condenser.

3. EXPERIMENTAL CONDITIONS AND RESULTS

The heat input was raised from 400 W to 2000 W with 200 W heat increment. Sixty minutes was chosen as the length of one cycle. In one cycle, the switching valve was shut for 58.5 min and opened for 1.5 min. Therefore, 58.5 min was the time for vapor condensation and liquid pumping, and 1.5 min is that for the switching valve opening and liquid flowing down from the reservoir to the evaporator. However, when the heat input was 1600 W to 2000 W, the valve was opened for 2 min because much more condensate was pumped up and then longer time was needed for liquid to flow down to the evaporator. Since the flowing-down liquid was subcooled, the boiling stopped for some time and started when the temperature reached the saturated one.

Figure 2 shows the pressure and temperature variations with time after the heat input was loaded. In Fig.2, the heat input was 1400 W. After 3 or 4 cycles, all pressure and temperature variations indicated almost the same variations.

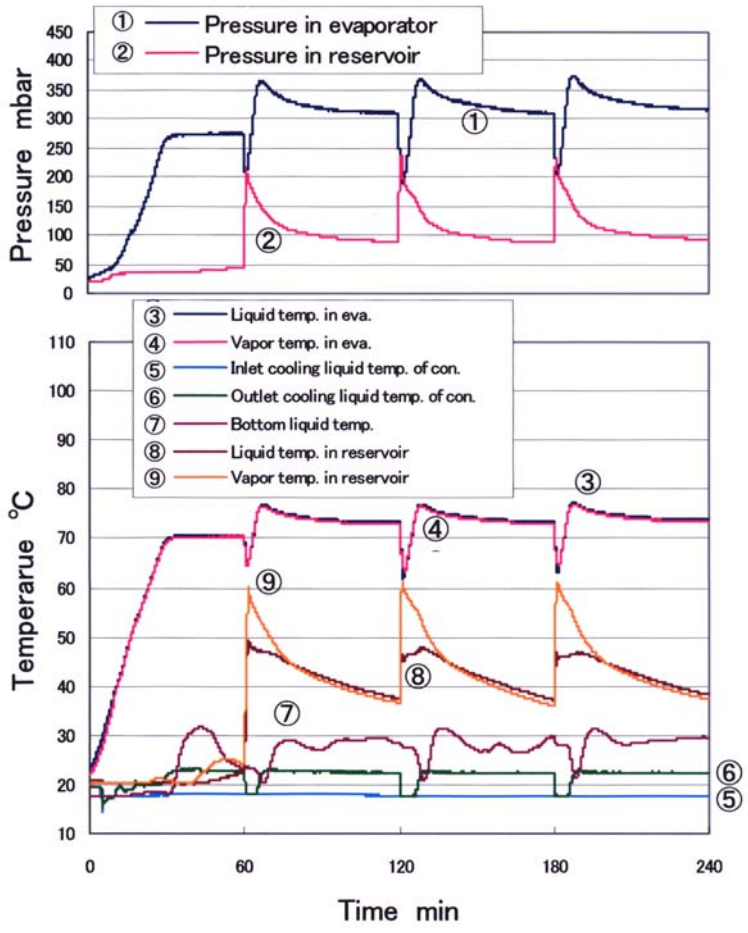


Fig.2 Pressure and temperature variations with time (Heat input=1400 W)

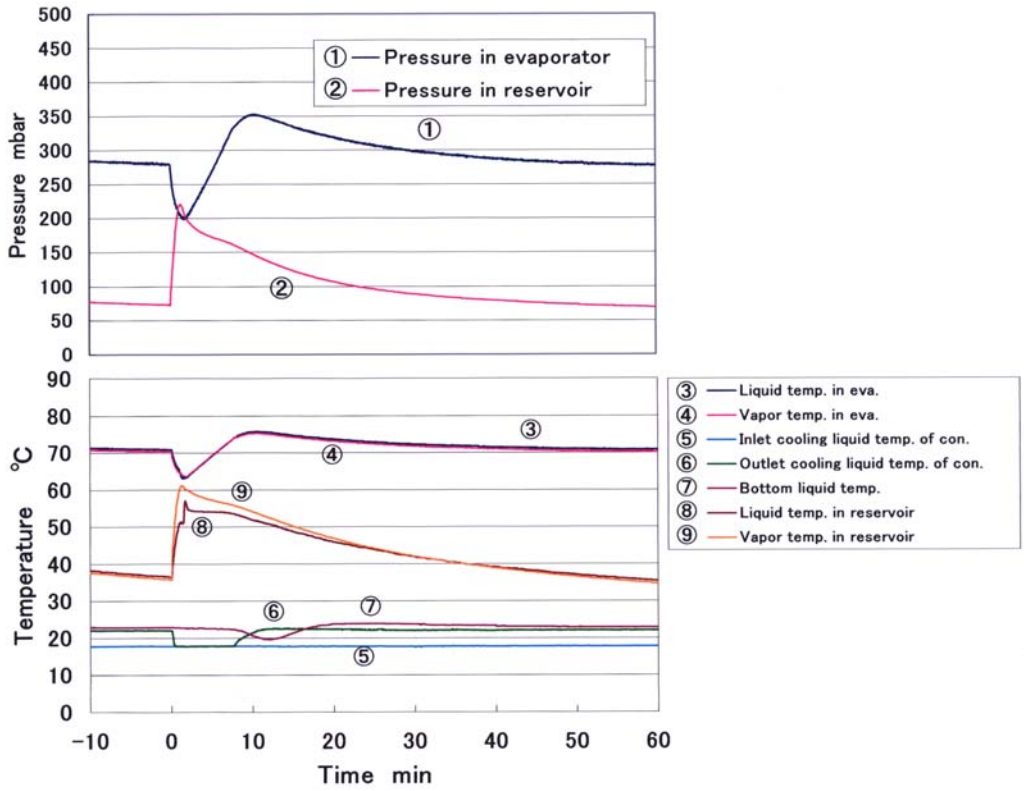


Fig.3 Pressure and temperature variations with time (Heat input=1000 W, at the 4th cycle)

Figure 3 shows the pressure and temperature variations at the forth cycle for the heat input of 1000 W. When the switching valve was opened, the pressure ① and temperatures ③ and ④ in the evaporator suddenly decreased. To the contrary, the pressure ② and temperatures ⑧ and ⑨ in the reservoir suddenly increased and the pressure in the reservoir slightly exceeded that in the evaporator. Therefore, the liquid in the reservoir flowed smoothly down to the evaporator. The temperatures in the reservoir rose abruptly as shown by ⑧ and ⑨. The liquid temperature in the reservoir was lower than the vapor temperature for some time after opening the switching valve. The cooling water temperature at the inlet ⑤ was constant as seen. On the other hand, the cooling water temperature at the outlet ⑥ was the same as that at the inlet while the liquid temperature in the evaporator ③ was lower than the saturated temperature because the subcooled liquid flowed down into the evaporator from the reservoir and then the boiling did not take place for some time. After the boiling commenced, the condensation also commenced in the condenser, so that the temperature difference between the outlet and inlet emerged. The temperature of the condensate shown by ⑦ was affected by the flow rate of the cooling water and the heat input to the evaporator. The condensate temperature became high as the flow rate of the cooling water decreased and the heat input increased.

Figure 4 shows the heat transport efficiency (defined by the heat transport rate divided by the heat input). These values were between 79 % and 96 %. Therefore, it was thought that the rest of heat was lost from the evaporator, the reservoir and the connecting tubes to the environment through heat insulation materials.

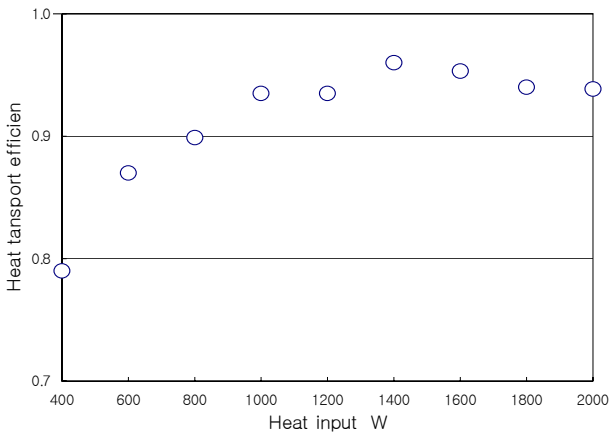


Fig.4 Heat transport efficiency vs. heat input

Finally, the power consumed by the switching valve and the time switch was measured. The switching valve consumed 10.7 W when it was opened and 0 W when closed. The time switch consumed 0.9 W when the switching valve was shut and 0.7 W when it was opened. Thus, the sum of the consumed power was 11.4 W when the switching valve was opened and 0.9 W when it was shut. From these values, the mean consumed power during one cycle was around 1.2 W.

4. CONCLUSIONS

(1) The experimental investigation was carried out on the heat transport rates of top-heat mode loop thermosyphon with a switching valve. It was verified that this thermosyphon possessed very practical probability.
(2) The heat transport efficiencies were 79%~96%.
(3) The consumed power by the switching valve and the time switch were very small.
(4) The merit of this top-heat mode thermo-syphon is the simplicity of the structure.

Acknowledgement

The authors thank Mr. Masahiko Hoshi for his active cooperation in performing this experiment.

References

1. Hirashima, M. et al., “Experimental Study of Top Heat Mode Thermosyphon (On the Lifting Mechanism of Working Fluid Effects on the Extension of Stable Working Range”, Trans. of the Japan Assoc. Ref., Vol.10, No.2, 1993, pp.247-256 (in Japanese).
2. Mizuno, S. et al., “Long-Term Storage of Solar Energy under Ground and Use for Vinylhouse Heating”, Refrigeration, Vol.57, No.654, 1982, pp.349-357 (in Japanese).
3. Roberts, C. C., “A Review of Heat Pipe Liquid Delivery Concept”, Proc. 4th Int. Heat Pipe Conf., 1981, pp.693-702.
4. Imura, H. et al., “A Review of Anti-Gravity Thermosyphons and Heat Pipes”, Proc. 6th Int. Heat Pipe Symp., 2000, pp.50-60.
5. Maidanik,Yu. F. et al., “Development, Analytical and Experimental Investigation of Loop Heat Pipes “, Proc.7th Int. Heat Pipe Conf., Vol.Ⅱ, 1990, pp.539-546.
6. Chisholm, D., “The Anti-Gravity Thermo-syphon”, Multi-Phase Flow Systems, Vol.Ⅱ, I. Chem. E. Symp. Series, No.38, 1974, I. Ch. E. & I. Me. E., pp.1-17.
7. Kadoguchi, K. and Yamazaki, M., “Experimental Study on the Improvement of the Self-Operative Heat Transport Characteristics”, 39th National Heat Trans. Symp. of Japan, Vol.Ⅰ, 2002, pp.129-130 (in Japanese).
8. Minning, C. P. et al., “Development of an Osmotic Heat Pipe”, Proc. 3rd Int. Heat Pipe Conf., 1978, pp.327-334.
9. Basiulis, A et al. “Design, Development, and Test of a 1000 W Osmotic Heat Pipe”, Proc. AIAA 15th Thermophysics Conf., 1980, pp.324-344.
10. Kawabata, K. et al., “Anti-Gravity Heat Pipe”, Proc. 5th Int. Heat Pipe Symp., 1996, pp.168-175.

Experimental Investigation of a Two Phase Closed Thermosyphon

S.H. Noie*, M.H. Kalaei**, M. Khoshnoodi**
* Chem. Eng. Dept., Engineering Faculty, Ferdowsi University of Mashhad,
Mashhad, P.O. Box. 9177948944-1111, I.R.IRAN
Tel: +98511 8615100, Fax: +98511 8612295 and E-mail: noie@ferdowsi.um.ac.ir
**Chem. Eng. Dept., Engineering Faculty, Sistan and Baluchestan University, I.R.IRAN. Tel: +98451 2440901, Fax: +98451 2443391 E-mail: Kalaei@hotmail.com

Abstract

In this paper the heat transfer characteristics of a two-phase closed thermosyphon with various heat transfer rates, system pressure, aspect ratios and filling ratios have been studied. The experiments focused on the boiling and condensation heat transfer characteristics of the thermosyphon with copper tube having 25 and 32 mm inside and outside diameters. Distilled water was used as the working fluid. The experimental boiling and condensation heat transfer inside the thermosyphon has been compared with the existing correlations. A good agreement between the experimental results of boiling heat transfer coefficient and condensation heat transfer of the thermosyphon and the empirical correlations were obtained. In addition, the optimal working fluid filling and the overall heat transfer coefficient was evaluated for the practical operation.

Key words**:** Aspect ratio, Two-phase closed thermosyphon, Thermal characteristics, Boiling heat transfer coefficient, Condensation heat transfer coefficient

1. INTRODUCTION

Two-phase closed thermosyphon has many advantages such as a large amount of heat transfer through a small cross-sectional area over a considerable distance with no additional power input to the system, small end-to-end temperature drops, fast heat response, extremely wide temperature application range (4-3000K), and minimum maintenance [1,2,3]. However, the thermodynamic behaviors of thermosyphon are quite complicated.

Over the past years a number of experimental works and researches have been performed to get correlations which may be used to calculate the boiling and condensation heat transfer coefficients in a two-phase closed thermosyphon. Researches of boiling focused on pool boiling in evaporator section, liquid film boiling and working principle of thermosyphon based on its flow pattern, needs the improvement and the estimation of heat transfer coefficient. Imura [5] and Skirashi et al. [6] have studied heat transfer in pooling liquid, falling film, and mechanism of flooding of the boiling phenomena independently. Kaminaga et al. [1] proposed an empirical correlation for the boiling heat transfer in wide ranges of pressure, heat flux, and filling ratio.

Condensation heat transfer in a two-phase closed thermosyphon has been a subject of active analytical study. Many investigations and contributions to this problem area have been reported [1-5]. Lee and Bedrossian [6] derived a simple condensation equation that was similar to that of Nusselt's condensation model. However, the characteristics of the condensation in thermosyphon are much complex than that of Nusselt's condensation model. In particular, the interfacial shear due to the countercurrent liquid and vapor flow obstructs the condensation heat transfer. As a consequence, the Nusselt's condensation model cannot apply to this case. Spendel [7] developed a model with laminar film and vapor flow, and the computed results showed that local Nusselt number differ considerably from the Nusselt's solution (up 27%), but both the mean values are consistent. Such condensation problems have also been investigated by several researchers [8-12], with the consistent conclusions that the interfacial shear stress does have strong effect on the condensation and reflux film inside a thermosyphon. Hashimoto et al. [10] reported that the non-condensable gas might cause the considerable decrease of condensation heat transfer.

The present research is an experimental study the thermal performance of a two-phase closed thermosyphon by changing the various experimental parameters. The main objective the present paper is to evaluate the actual boiling and condensation heat transfer coefficients of a

thermosyphon experimentally and compare with the empirical correlations.

2. EXPERIMENTAL APPARATUS AND PRODURE

A schematic diagram of the experimental apparatus is shown in figure (1). The main parts of test rig are test section, a liquid reservoir for charging, an electric heater, cooling water circulation, high vacuum system, and temperature measurement using data acquisition system. The thermosyphon is made of a smooth copper tube with outside diameter of 32 mm and a total length of 98 cm. The condenser section is 38 cm long, while the evaporator and adiabatic section length is variable according to values of the aspect ratio (Le/D). A copper jacket with diameter 50 mm surrounds the condenser section, and cooling water flows through the annular passage that is measured by Rota-meter with accuracy of ± 3. The temperature outputs are recorded on a data logger and it is connected to personal computer to analyze recorded data. The saturation temperature of water and vapor are being read by thermocouples installed at the beginning and end of pipe, respectively. A rotary vacuum pump and a diffusion pump with a rating to 10^{-6} Torr are used to remove air and other non-condensable gases.

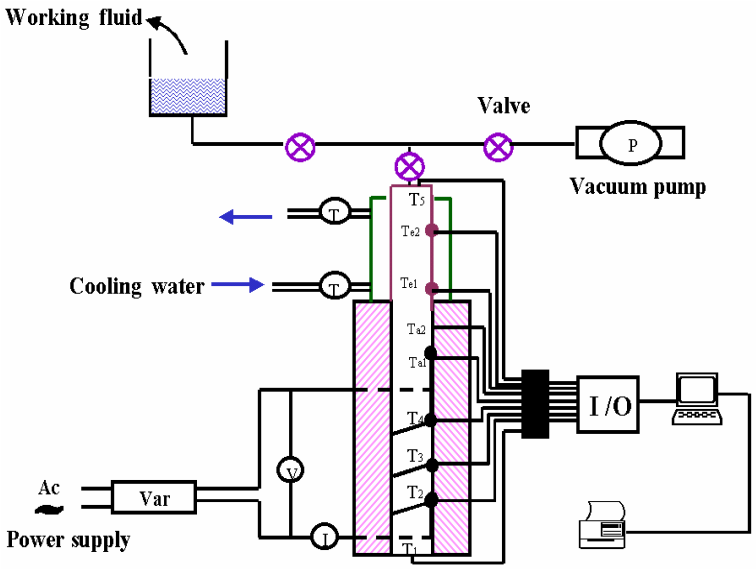


Figure 1 Schematic of diagram of the experimental apparatus

3. CALCUATION PROCEDURE

Heat transfer rate added to the evaporator section by electric elements is calculated from the following relation:

$$\dot{Q}_{in} = \mathrm{VI}$$

The rate of heat removal from the condenser section is obtained from the following relation:

$$\dot{Q}_{out} = \dot{m} c_p (T_o - T_i)$$

From the measurement data on wall temperature distribution, vapor temperature and value of thermal load, the heat transfer coefficients of boiling and condensation could be evaluated using the following equations respectively:

$$h_e = \frac{\dot{Q}}{\pi D L_e (T_{e,m} - T_v)}$$

$$h_c = \frac{\dot{Q}}{\pi D L_c (T_v - T_{c,m})}$$

where $T_{e,m}$ and $T_{c,m}$ denote area-average-mean values of the wall temperatures at the evaporator and condenser, respectively.

3-1. Correlations of boiling

In the previous study, it was found out that nucleate boiling is the dominant mechanism in the evaporator, when the filling ratio is higher than 30% [12]. Therefore, the following two correlations based on nucleate boiling was chosen to compare with experimental data.

Rohsenow's correlation [14]:

$$h_e = \frac{q^{2/3}}{\frac{C_{sf} h_{fg}}{C_{p,l}} \left\{ \frac{1}{h_{fg} \mu_l} \left(\frac{\sigma}{g[\rho_l - \rho_v]} \right)^{1/2} \right\}^{0.33} Pr}$$

Imura's correlation [15]:

$$h_e = 0.32 Z \left(\frac{P_{sat}}{P_{atm}} \right)^{0.3}$$

where

$$Z = \frac{\rho_l^{0.65} k_l^{0.3} c_{pl}^{0.7} g^{0.2} q_e^{0.4}}{\rho_v^{0.25} h_{fg}^{0.4} \mu_l^{0.1}}$$

3-2. Correlation of condensation

In general, the dominant flow regime inside a condenser of a thermosyphon is known to be a counter current annular flow, with a condensate film flowing downward on the wall surface and vapor flow moving upward through the tube core. The correlation described below is based on the analysis of falling condensate films, and will be compared with present data.

Nusselt's model [2]:

Nusselt derived the expression of condensation heat transfer coefficient described in the following equation from a theoretical analysis of laminar condensate flow.

$$h_c = 0.943 \times \left\{ \frac{\rho_l g k_l^{\,3} (\rho_l - \rho_v)[h_{lv} + 0.68 C_{p,l}(T_{sat} - T_w)]}{\mu_l L_c [T_{sat} - T_w]} \right\}^{1/4}$$

4. RESULTS AND DISSCUSIONS

4-1. Wall temperature profile in evaporator and condenser sections

To find the average temperature of outer wall of the evaporator and condenser sections the temperature along the surface of the thermosyphon was measured by K thermocouples. The thermocouples were mechanically attached to the surface of pipe. Figure (2) shows axial profiles of outer wall temperatures of the evaporator, adiabatic, and condenser sections calculated from the measured data for various heat rates.

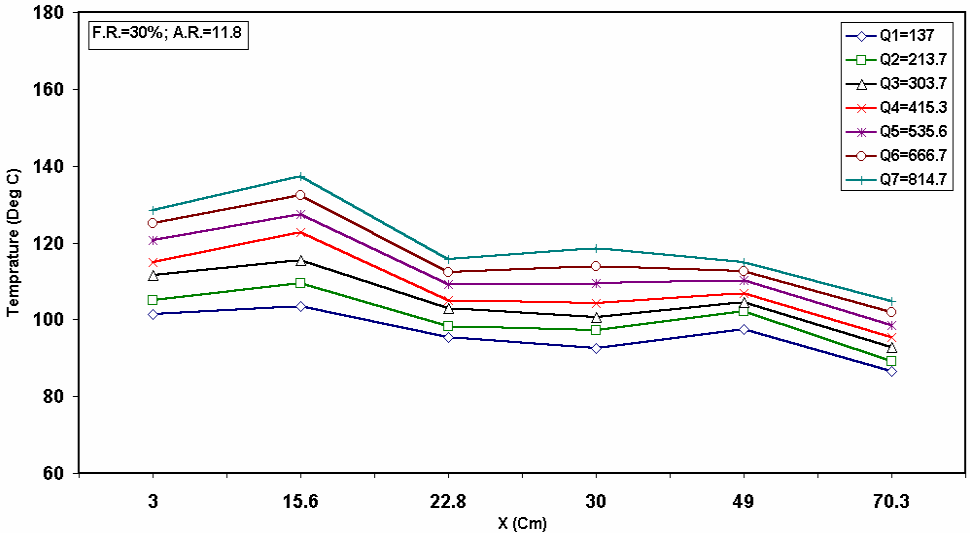


Figure 2 Outer wall temperature profiles along thermosyphon

4-2. Boiling heat transfer coefficient

Boiling heat transfer coefficients with respect to average temperature of evaporator surface are shown in Figure (3) for aspect ratio of 11.8 and filling ratio 30% and compared with empirical correlations. As shown in the Figure, the Rohsenow's correlation gives better predictions to the experimental results.

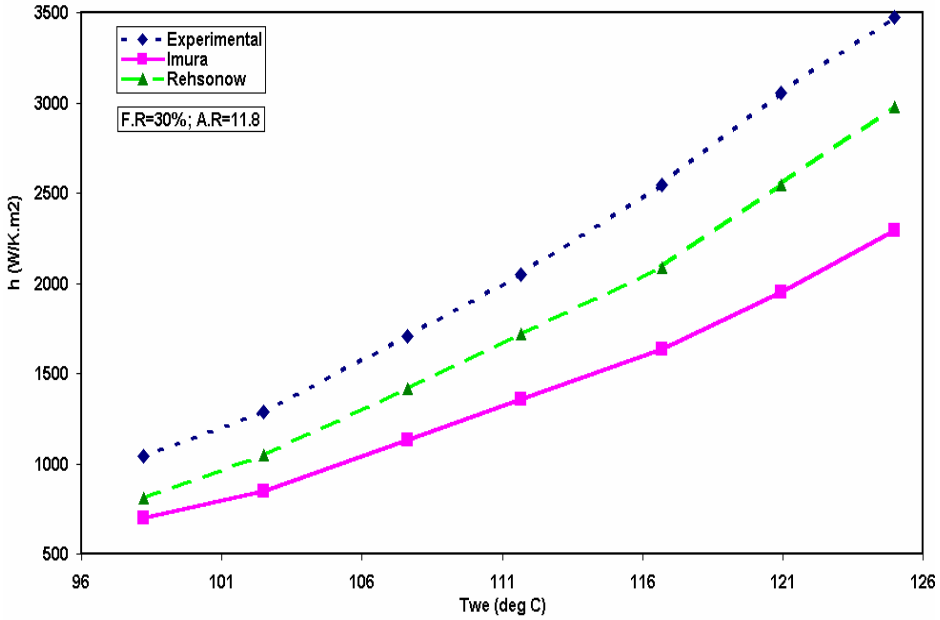


Figure 3 Comparison of boiling heat transfer coefficient with empirical correlations for A.R=11.8 & F.R=30%

4-3. Condensation heat transfer coefficient

Figure (4), shows the variation of inlet vapor temperature of the condenser with respect to surface temperature of evaporator section of the thermosyphon for A.R=11.8 and F.R=30%. The results have been compared with Nusselt's theory [2]. A good agreement between the experimental results and Nusselt's correlation has been observed. The Nusselt's theory is used for analysis of condensing rate on flat plate at the temperature constant by considering the following assumptions: laminar flow on plate, saturation temperature in vapor and negligible shear between falling film and raised vapor. In this system, surface temperature increasing of evaporator conduces to enhance shear stress. This phenomenon probably is one of the reasons of difference between experimental data and Nusselt data.

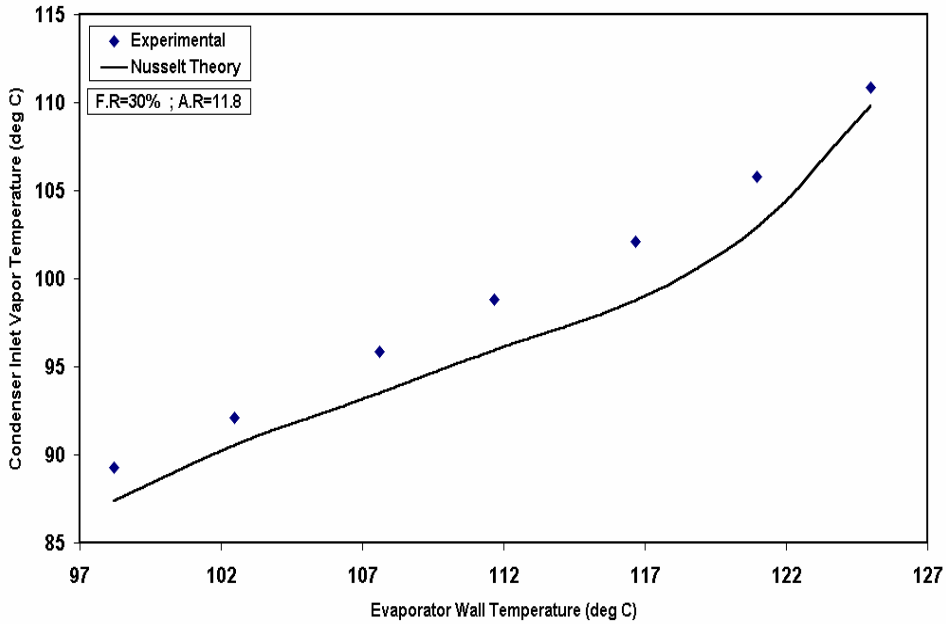


Figure 4 Variation entering vapors temperature of the condenser

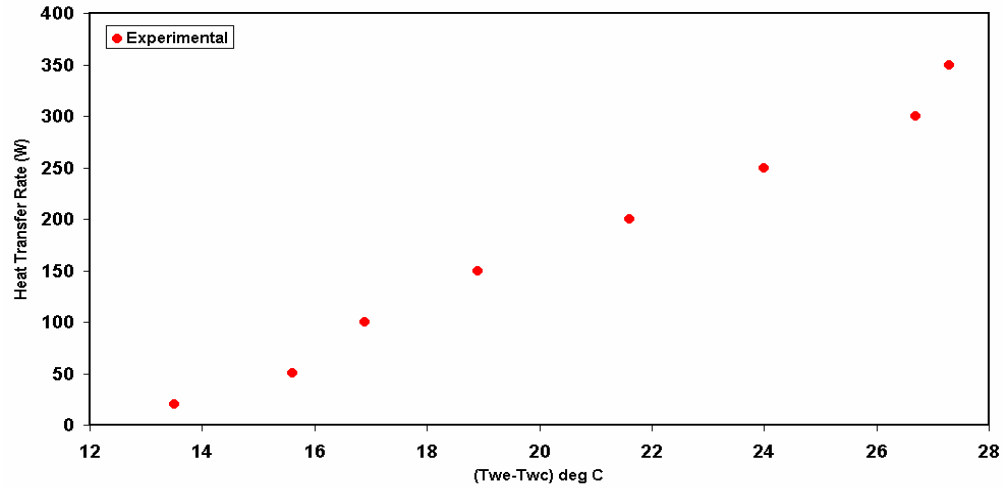


Figure 5 Variation entering power VS difference temperature of The evaporator and condenser

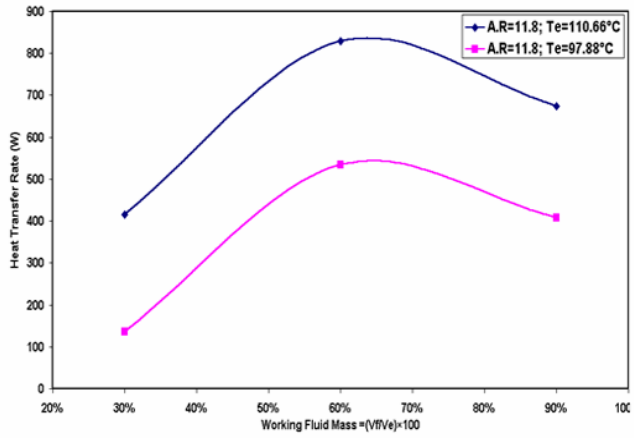


Figure 6 Optimum working fluid in A.R=11.8

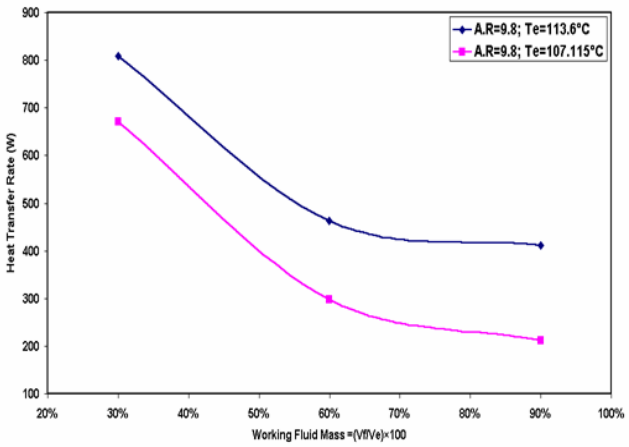


Figure 7 Optimum working fluid in A.R=9.8

4-4. Overall heat transfer coefficient

We can calculate average thermal conductivity of thermosyphon (per cross-section unit) by using Figure (5).

This overall heat transfer coefficient is about 96000 $W/m^2.^oC$ that is about 250 times of copper thermal conductivity. This is one of the important advantages of thermosyphon.

4-5. Optimum working fluid

In A.R=11.8, optimum mass for maximum power is in the F.R=60% that is equal to 182gr water (Figure 6). In the steady state, if quantity of working fluid in pooling water is minimum, temperature of ending pipe has remarkable fluctuation and then its temperature will suddenly increase. If quantity of working fluid is less than above mentioned, the dry out phenomenon will be occurred. Hydrostatic pressure increasing in pooling liquid is simultaneously with increasing depth of pooling liquid. This phenomenon causes that heat transfer and boiling point to be increased. By increasing working fluid, rising boiling point effect will be dominant and heat transfer will be decreased. Maximum heat transfer rate in A.R=9.8 occurs in F.R=30% because the effect of rising boiling point is affecting from the beginning of the boiling process (Figure 7).

5. CONCLUSION

Experimental studies for boiling and condensation heat transfer in a vertical two-phase closed thermosyphon using water as working fluid gave the following conclusions.

1. Maximum heat transfer rates for each aspect ratio occurs at different filling ratio. For aspect ratio of 9.8 the maximum heat transfer rate occurs when filling ratio is 60%, while for aspect ratio of 11.8 occurs at filling ratio 30%.

2. The Nusselt theory isn't good for prediction of pipe behavior (because negligible shear between falling film and raised vapor).
3. Overall and boiling heat transfer coefficients are approximation constant and considerable in interval of experiments.
4. The comparison between experimental results and empirical correlations show good agreement.

Nomenclature

A.R aspect ratio
C_{sf} constant, determined from experimental data
c_p specific heat of water (j/kg.°C)
g gravitational acceleration (m/s^2)
F.R filling ratio
k_l thermal conductivity of liquid(W/m.°C)
h_e boiling heat transfer coefficient ($W/m^2.°C$)
h_{fg} latent heat of vaporization (J/kg)
I current (A)
ID inside diameter of tube (m)
L_a length of adiabatic section (m)
L_c length of condenser section (m)
L_e length of evaporator section (m)
$\dot{m}$ mass flow rate of water in condenser (kg/s)
OD outside diameter of tube (m)
Pr Prandtl number
P_{atm} atmospheric pressure (Pa)
P_{sat} saturated pressure (Pa)
q heat flux (W/m^2)
$\dot{Q}_{av}$ heat transfer rate (W)
$\dot{Q}_{in}$ inlet heat by evaporation (W)
$\dot{Q}_{out}$ outlet heat by condensation (W)
$\dot{Q}_{av} = \frac{\dot{Q}_{in} + \dot{Q}_{out}}{2}$ average of heat transfer rate (W)
$T_{e,m}$ average temperature of evaporator section (°C)
$T_{c,m}$ average temperature of condenser section (°C)
T_i inlet water temperature of condenser (°C)
T_o outlet water temperature of condenser (°C)
V voltage (V)
R resistance (Ω)
ρ_l density of liquid (kg/m^3)
ρ_v density of vapor (kg/m^3)
μ_l viscosity of liquid (kg/m.s)
σ surface tension (N/m)

References

1. Dunn, P. D. and Reay, D. A, "Heat pipes", 3rd. ed. Pergamon Press, (1994)
2. Faghri, A., "Heat Pipe Science and Technology," Taylor & Francis, USA, (1995).
3. Dobran, F., "Heat pipe research and development in the America", Heat Recovery Systems, CHP 9, pp. 67-100, (1989).
4. Lock, G.S., "The tubular thermosyphon", Chaps 1 and 3, Oxford University Press, (19992).
5. Imura, H., et. al., "Critical heat flux in a closed two-phase thermosyphon", Int. J. Heat and Mass, 26, pp. 11811-1188 (1983).
6. Shirashi, M., et. al., "Investigation of heat transfer characteristics in Heat pipe technology", (Edited by Reay), pp. 95-104, Pergamon Press, New York, (1981).
7. Imura, Heat al., "Heat transfer in two-phase closed thermosphere", Heat transfer Japanese Research, Vol. &, No. 2, (1979), P.P. 41-53.
8. Incorporate, F.P., Darid, D., P., Fundamentals of Heat and Mass transfer, chap.10, John Wiley and sons, New York, (1990).
9. Noie, S.H., Kalaei, M.H., "Thermal Characteristics of a Tow-Phase Closed Thermosyphon", The 12th International Heat Pipe Conference (12IHPS), Moscow, Russia, (2002).
10. Hong. S.E. et al. "An experimental study on the heat transfer characteristics of a FC-72 thermosyphon", 12th International Heat Pipe Conference, Moscow, pp. 308-314, (2002).
11. Rohsenow, W. M., "A method of correlating heat transfer data for surface boiling curves", Int. J. of Heat Trans. ASME, Vol. 84, p. 969. (1962).
12. Imura, H., Kusada, H., Oyata, J., Miyazaki, T., and Sakamoto, N., "Heat transfer in two-phase closed-type thermosyphon' Trans. of Japan Soc. of Mech. Engrs, pp. 485-493, (1977).
13. Kaminaga et al., "Study on boiling heat transfer correlation in a two-phase closed thermosyphon," Proc. of 8th IHPC. Pp. 317-322, (1992).

A Comparison of the Heat Transfer Performance of Thermosyphon Using a Straight Groove and a Helical Groove

K. I. Han, D. H. Cho*, J. U. Park, S. H. Lee
School of Mechanical Engineering, Pukyong National University, San 100, Yongdang-Dong, Nam-Gu, Busan, 608-739, Korea
Tel: (+82)-51-620-1581, Fax: 620-1574, and E-mail: kihan@pknu.ac.kr
*Department of Mechanical Design Engineering, Daejin University, Pocheon-Gun, Kyonggi-Do, 487-711, Korea
Tel: (+82)-31-539-1973, Fax: 539-1970, and E-mail: chodh@road.daejin.ac.kr

Abstract

This study is focused on the comparison of heat transfer performance of two thermosyphons having 60 straight and helical internal grooves. Distilled water has been used as working fluid. Liquid fill charge ratio defined by the ratio of working fluid volume to total internal volume of thermosyphon, the inclination angle and operating temperature were used as experimental parameters. The heat flux and heat transfer coefficient are estimated from experimental results. The conclusions of this study may be summarized as follows; Liquid fill charge ratio, inclination angle and geometric shape of grooves were very important factors for the operation of thermosyphon. The optimum liquid fill charge ratio for the best heat flux were 30%. The heat transfer performance of helically grooved tube was higher than that of straight grooved tube in low inclination angle(less than 30˚), but the results were opposite in high inclination angle(more than 30˚). As far as optimum inclination angle concerns, range of 25˚ ~ 30˚ for a helically grooved tube and about 40˚ for a straight grooved tube are suggested angles for the best results.

Key words: Thermosyphon, Internal Groove, Liquid Fill Charge Ratio, Heat Flux, Operating Temperature, Condensation, Evaporation

1. INTRODUCTION

One of The effective management and application of energy is the usage of heat transfer by latent heat exchange caused by phase change. The typical closed heat transfer mechanisms using this principle are heat pipe and thermosyphon named as a wickless heat pipe. The heat pipe transfers large amount of heat even with a small temperature difference under boiling and evaporation of working fluid.

Gaugler[1] first designed the heat pipe in 1944, and many other researchers conducted this kind of researches in many fields. Also, Schmidt[2] developed the thermosyphon for the cooling of turbine blade, and its effectiveness is highly evaluated. Especially, the research of heat transfer performance of thermosyphon is conducted continuously by Cohen and Bayley[3], Larkin[4], Lee and Mital[5], Stet'tsov[6]. They all insisted that the heat transfer performance of the thermosyphon is effected by the parameters such as the type of working fluid, quantity of working fluid, inclination angle, internal diameter of tubes, heat flux, working fluid pressure, geometric shape of internal surface. And better heat transfer coefficient of thermosyphon exists in the inclined position compared to vertical position because the thermosyphon is effected by a gravitational force as well as a frictional force caused by inclination angle.

Tu et al.[7] did an experiment using a thermosyphon with 1000mm in length and 25mm in diameter and water as a working fluid. His result showed that the maximum heat transfer coefficient is obtained by the inclination angle between 50° and 55°. Hahne and Gross[8] carried out an experiment using a steel thermosyphon with 2000mm in length, 40mm in diameter and CFC-115 as a working fluid and came up with a result showing that the maximum heat transfer coefficient is obtained by the inclination angle between 45° and 50°. Cho and Kwon[9] had an experiment with a thermosyphon that has an outer surface of low fin using distilled water and CFC-30 as a working fluid with the tube length of 1200mm, diameter of 15mm. His result said that the most heat transfer rate is obtained by the inclination angle between 20° and 45°.

Recently, Park[10] made a thermosyphon with the tube length of 1200mm, 15.8mm in diameter and a plain copper tube and came up with a result

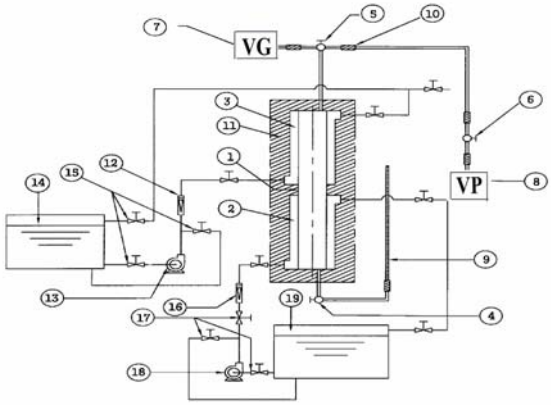
that showed the maximum heat transfer rate is obtained by 30° of inclination angle. The experiments conclude that the inclination angle having maximum heat transfer coefficient varies by different conditions given to the experiment and importantly the selection of the working fluid along with the liquid fill charge ratio affects the efficiency of the thermosyphon. But these researches were mostly done by using a plain tube and only several researches were done by using grooved tubes. The usage of the triangular grooved tube was performed in Peterson and Ma's heat transfer research[11], and Hong[12] also performed a thermosyphon experiment using a heat pipe with an inner groove. Recently, researches for the heat transfer characteristics done by differences in number of grooves were reported by Han[13] and Yee[14] but more research is still necessary.

In this study, straight and helically grooved copper tube were chosen to make the thermosyphon with other different parameters that effect heat transfer performance. And the experiment is done by using the distilled water working under low temperature region. Its heat transfer performance is compared by the parameter variation of liquid fill charge ratio and inclination angle.

2. EXPERIMENTAL APPARATUS AND METHOD

Fig. 1 shows the schematic diagram of experimental apparatus. It consists of five parts such as test section, cooling water circulation line, system, temperature measurement and recording system. The total length of test section is 1200mm and it consists of boiling and evaporation section with 550mm in length respectively and 100mm of adiabatic section. The test tube has a 14.35mm of internal diameter and a 15.85mm of a outer diameter and material is copper. The outer surface of the tube is smooth(plain) and internal surface has grooves. Two types of internal grooved tube are used One is straight in axial direction and the other is 18 degree of helically grooved tube from axial direction. Geometric specifications of two grooved tubes and internal surface configurations are shown in Table 1 and Fig. 2, respectively.

Two 550mm long annular shaped water jackets (38mm of internal diameter and 42mm of outer diameter) are set on both ends of the test tube. One is used as a heating jacket for an evaporator and the other is used as a cooling jacket for a condenser. Outside of thermosyphon is perfectly insulated with 50mm of glass wool insulator. The thermosyphon can be positioned with any inclination angle from 0° to 90° with respect to the horizontal position.

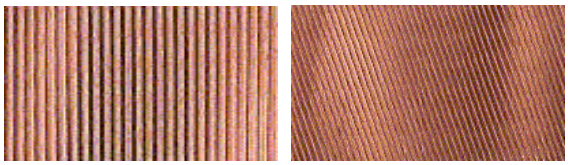


1. Test Tube 2. Heating Water Jacket 3. Cooling Water Jacket 4. Vacuum Valve 5. Vacuum Valve 6. Vacuum Rubber Hose 7. Vacuum Gauge 8. Vacuum Pump 9. Measuring Device for Liquid Level 10. Vacuum Rubber Hose 11. Insulation 12. Coolant Flow Meter 13. Coolant Pump 14. Coolant Constant Temperature Bath 15. Coolant Control Valve 16. Heating Water Flow Meter 17. Heating Water Control Valve 18. Heating Water Pump 19. Heat Water Constant Temperature Bath

Fig. 1 Schematic diagram of the experimental apparatus

Table 1 Geometric specifications of two grooved thermosyphons

Classification	Tube		Groove		
	Do (mm)	Di (mm)	Skew Angle (°)	Depth (mm)	Angle (°)
Straight Groove	15.85	14.35	0	0.29	42
Helical Groove	15.85	14.35	18	0.29	42



(a) Straight groove (b) Helical groove

Fig. 2 Internal surface configuration of two grooved tubes

Nine thermocouples(T type Cu-CuNi) are soldered on the outside surface of the tube along its length to measure surface temperatures. Another nine thermocouples(K type NiCr-Ni) are inserted into the inside of thermosyphon to measure inside vapor temperatures. Four more Pt 100 temperature sensors are placed at the inlets and the outlets of two water jackets. The location of thermocouples is shown in Fig. 3. The temperature outputs are recorded on a data logger and it is connected to personal computer to analyze recorded data.

A rotary vacuum pump is used first and a diffusion pump with a rating of 10^{-6} Torr is used

to remove air and other non-condensable gases. Distilled water is chosen as working fluid. The working fluid is injected into the tube after evacuating air. After injecting the working fluid, heating and cooling water flow into the evaporator and the condenser jackets, respectively. A small amount of non-condensable gas was collected at the end of the condensation section after a few minutes of operation. This gas is removed again by vacuum pump for perfect operation of thermosyphon. All of the residual working fluid in the test tube was collected after each run of experiment and its volume was measured to compare the exact quantity of working fluid. Only a data with no volumetric difference of working fluid before and after each test was taken.

The experimental conditions are set as follows. The heating and cooling water temperature are varied. Two constant water temperature baths support hot or cool water continuously within ±0.2˚C difference of each setting temperature. The capacity of constant water temperature bath for heating water is 100 liter and that for cooling water is 130 liter and temperature control range is 0˚C to 100˚C.

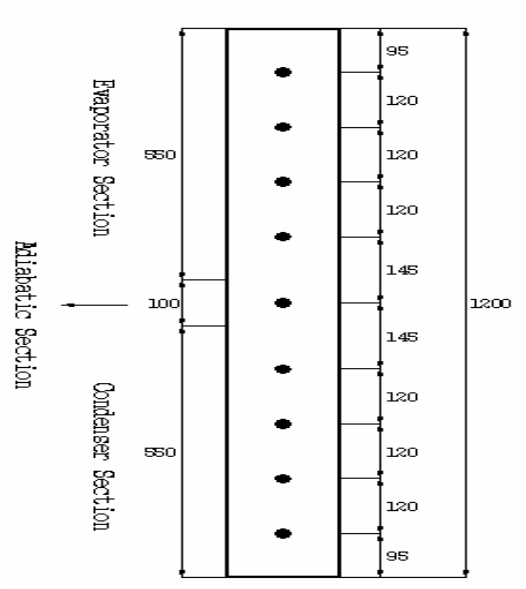


Fig. 3 Location of thermocouples

3. RESUSTS AND DISCUSSON

3-1 Equilibrium of Energy for Thermosyphon

Preliminary test has been done for the test of energy equilibrium on the evaporation and condensation zone of the test section. All of the data is obtained after steady state condition is reached. Energy balance for the heat loss of heating water and the heat gain of cooling water is well maintained within 10% of error as represented in Fig. 4. Heat loss and heat gain for both sections are calculated using eq. (1) and eq. (2), respectively.

$$Q_{cool} = \dot{m}_{cool} C_{p,cool} \left(T_{out} - T_{in}\right)_{avg} \quad (1)$$

$$Q_{cool} = \dot{m}_{hot} C_{p,hot} \left(T_{in} - T_{out}\right)_{avg} \quad (2)$$

Where, $\dot{m}_{cool}$, $\dot{m}_{hot}$ shows the mass flow rate of cooling water and heating water and T_{in} and T_{out} represent the inlet and outlet water temperature.

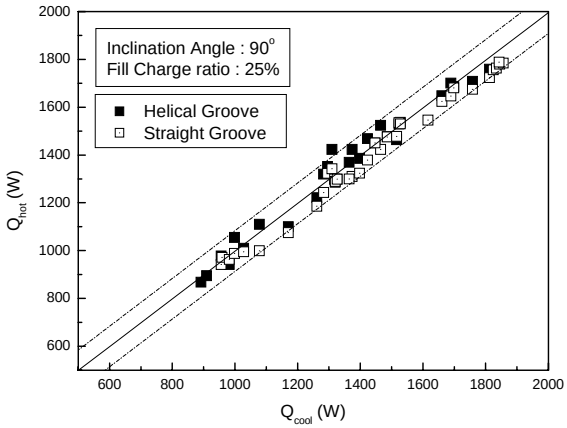


Fig. 4 Heat balance of two thermosyphons

3-2 Temperature Distribution of Outside wall of Thermosyphon

Fig. 5 through Fig. 7 show the distributions along the length of two thermosyphons using straight and helically grooved tube at the 80℃ of operating temperature. Fig. 5 represents the profile based on the data of 90˚ of inclination angle and 25% of fill charge ratio. Temperature distribution of straight grooved tube moves close to the adiabatic temperature compared to that of helically grooved tube. This means that more saturated working fluid flows to the evaporation section from condensation section because of the lower frictional force in the straight groove compared to that in the helical groove.

Fig. 6 and Fig. 7 show the temperature distribution with 30% of fill charge ratio and 4 cases of inclination angle(10˚, 30˚, 40˚, 70˚) for two types of thermosyphon(straight and helical). Highest heat transfer performance is 30˚ of inclination angle for helically grooved tube and 40˚ for straight grooved tube. More temperature fluctuation in the condensation section compared to evaporation section is caused by the turbulence wave of the interface of condensing liquid flowing downward on the internal surface and evaporating vapor flowing upward through the core of the tube.

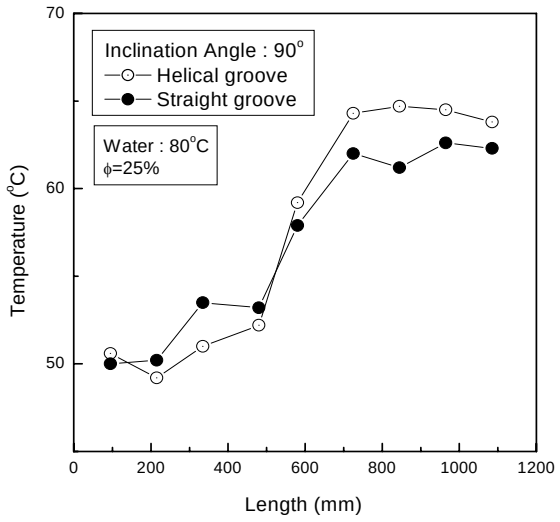


Fig. 5 Temperature distribution along the length of two grooved thermosyphons

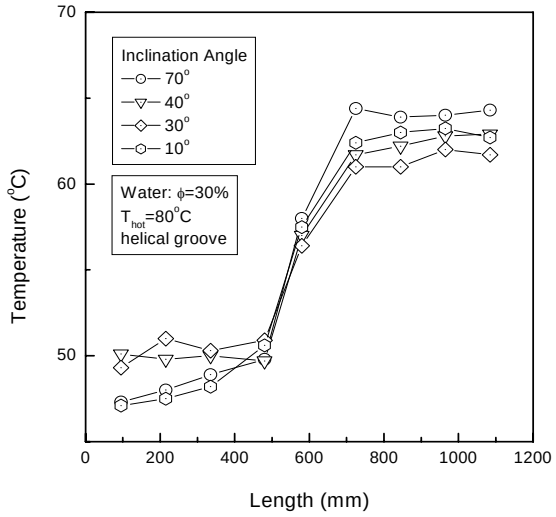


Fig. 6 Temperature distribution along the length of helical grooved thermosyphon

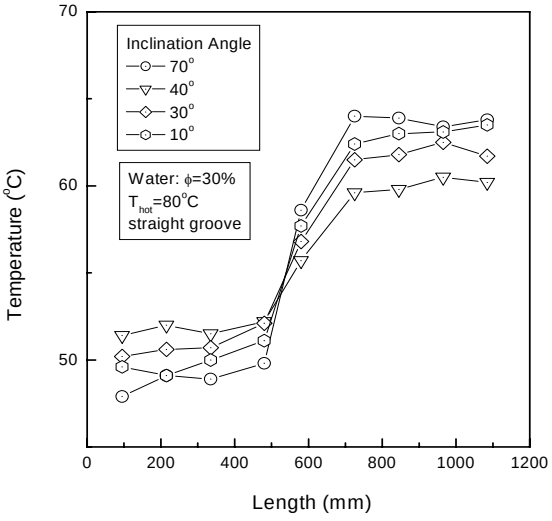


Fig. 7 Temperature distribution along the length of straight grooved thermosyphon

3-3 Heat Flux and Heat Transfer Coefficient

Fig. 8 is showing the variation of the boiling heat flux with respect to the temperature difference of average internal wall temperature and average saturated vapor temperature on the evaporation section. The fill charge ratio is 30% and inclination angle is 90° in this case. The boiling heat flux increases as the excess temperature increases. Heat transfer performance for the straight grooved tube is higher than that for helically grooved tube in all of the range and it can be justified by the slope difference of two lines.

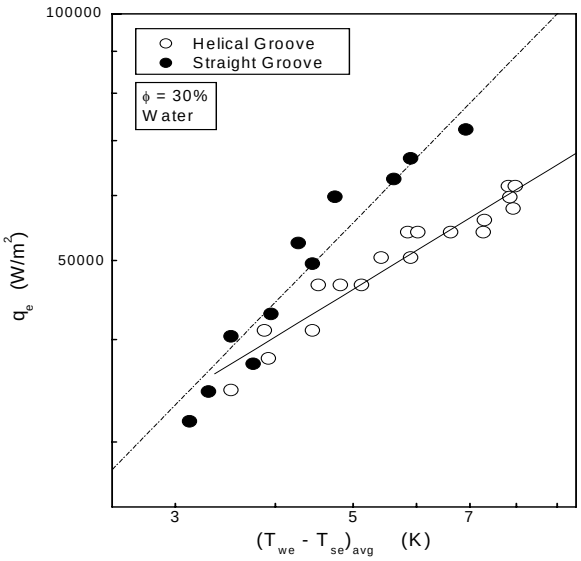


Fig. 8 Plot of boiling heat flux vs. excess temperature

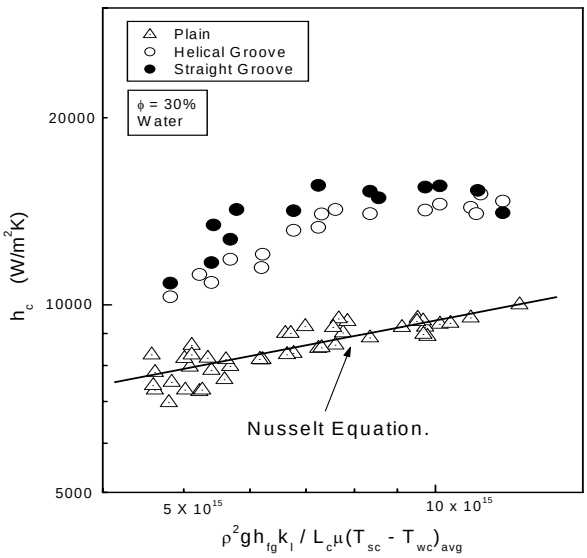


Fig. 9 Comparison of the experimental data with Nusselt's equation

Fig. 9 shows the condensation heat transfer coefficient for grooved tubes and plain tube at the 30% of fill charge ratio. Nusselt's equation

matches well with the data of plain tube. The coefficient for the grooved tube is higher than that of plain tube in all of the experimental range. The condensation heat transfer coefficient is calculated by the eq. (3). The eq. (4) represents Nusselt's equation of condensation theory.

$$h_c = \frac{(Q_{cool} + Q_{hot})}{A_o (T_{wc} - T_{sc})_{avg}} \tag{3}$$

$$h_c = 0.943 \left[\frac{\rho_l^{\,2} g\, h_{hg} k_l^{\,3}}{L_c \mu_l (T_{sc} - T_{wc})} \right]^{1/4} \tag{4}$$

3-4 Heat Transfer Rate as the Function of Inclination Angle and Fill Charge Ratio

Fig. 10 and Fig. 11 show the variation of condensation heat flux against inclination angle for two types of grooved tubes. Data is obtained using two heating water temperature of 60° C and 80° C. As shown in two Figures, between 35° and 40° of inclination angle is the approximate region at which the trend of heat transfer rate is changing. This means that the heat transfer rate in the case of helically grooved tube has higher value at lower than these range of angle and the value of heat transfer rate is reversed after these range of angle. The highest condensation heat transfer rate is obtained at about 30° of inclination angle for the case of helically grooved tube and at about 40° in the case of straight grooved tube.

Fig. 12 shows the condensation heat flux against the fill charge ratio. Five cases of fill charge ratio (10%, 20%, 25%, 30%, 40%) are used. Heat flux is low at 10% of fill charge ratio because of the dry out of working fluid. And heat flux is increasing until the fill charge ratio reaches to about 30%.

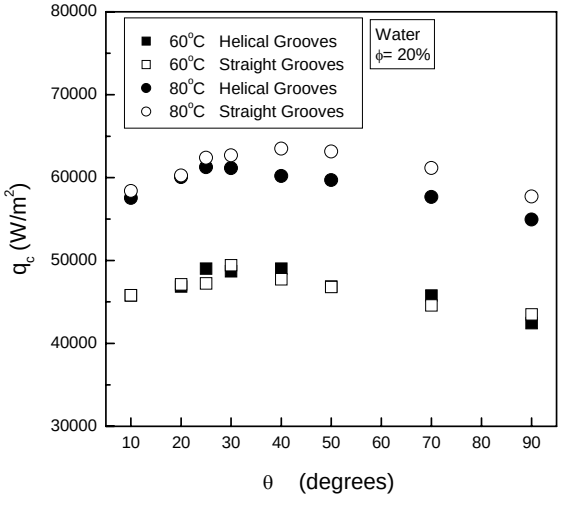


Fig. 10 Plot of Heat Flux against inclination angle (Ø=20%)

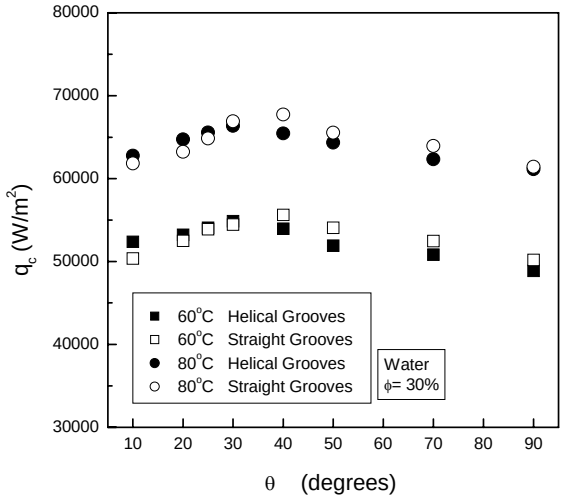


Fig. 11 Plot of Heat Flux against inclination angle (Ø=30%)

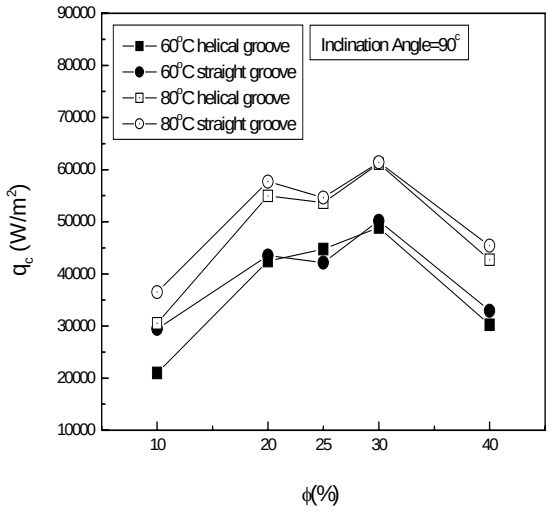


Fig. 12 Plot of heat flux against fill charge ratio

The heat flux is decreasing after 30% of ratio. This is considered that if the volume of working fluid increases to the certain limit, two phase flow mixed with liquid and vapor reaching to the condensation section results in decreasing the condensation heat transfer performance.

4. CONCLUSION

The experimental results are summarized as follows.

1) The thermosyphon using grooved tube has the higher heat transfer rate compared to the thermosyphon using plain tube. This is well verified by using Nusselt's condensation theory.

2) The heat transfer performance is tested by changing of inclination angle between 10° and 90° with respect to the horizontal position. The highest result is obtained at about 25° ~ 30° in

case of helically grooved tube and at about 40° in case of straight grooved tube.
3) The highest heat flux is obtained at 30% of fill charge ratio regardless of the types of grooved tube.

Nomenclature

A_c surface area on condensation section $[m^2]$
C_{pw} specific heat of cooling water [kJ/kgK]
D_i internal diameter [m]
h_c condensation heat transfer coefficient $[W/m^2K]$
h_{Nu} Nusselt's condensation heat transfer coefficient $[W/m^2K]$
L_c length of condensation section [m]
$\dot{m}_c$ mass flow rate of cooling water [kg/s]
P_s internal saturation pressure [Pa]
P_{atm} atmospheric pressure [Pa]
Q_{cool} heat gain of cooling water [W]
Q_{hot} heat loss of heating water [W]
q heat flux $[W/m^2]$
T_{we} surface temperature of evaporation section [K]
T_{wc} surface temperature of condensation section [K]
T_{sc} vapor temperature of condensation section [K]
T_{in} inlet temperature of cooling water [K]
T_{out} outlet temperature of cooling water [K]
Ø liquid fill charge ratio
θ inclination angle

References

1. Gaugler, R.S., 1994 Heat Transfer Device, Us Patent NO.2350348, Applied December 21, 1942. Published June 6
2. Schmidt, E., Proc. Inst. Mech. Eng. ASME Cong. Proc., 1951, pp. 361-363
3. Cohen, H., Bayley, F.J., "Heat Transfer Problems of Liquid Cooled Gas Turbine Blades", Proc. Inst. Mech. Eng., 169-20, 1995, pp. 1063~1080
4. Larkin, B.S., Trans. Canada. Soc. Mech. Eng., 14-B6, 1971, pp. 1-8
5. Lee, Y. and Mital, V., Int. J. of Heat and Mass Transfer. 15-9, 1707, pp. 1695-1707
6. Stret'tsov, A. I., Heat Transfer, Soviet Research. 7-1, 1975, pp. 23-27
7. Tu, C., Xie, G., Hu, C., Gao, Z. and Hong, R., "The Two Phase Closed Thermosyphon: an Experimental Study with Flow Pattern and Optimum Fill Charge", China-U.S. Seminar on Two-flows and Heat Transfer, Sian, 1984, pp. 395-405
8. Hahne, E. and Gross, U., "The Influence of the Inclination Angle on the Performance of a Closed Two-Phase Thermosyphon", 4th IHPC, London, 1981, pp. 125-135
9. Cho, D. H., Kwon, H. H., "Experimental Study on Heat Transfer Inside Inclined Thermosyphon", J. of SAREK, Vol. 11, No. 2, 1998, pp. 165-172
10. Park, S.H., "A Study on the Improvement of Heat Transfer Performance in Low Temperature Two-Phase Closed Thermosyphon", Pukyong National University Master Thesis, 2001
11. Peterson, G. P. and Ma, H. B., "Experimental Investigation of the Maximum Heat Transport in Triangular Groove," ASME J. of Heat Transfer, Vol. 35, No. 3, 1996, pp. 740-746
12. Hong, J., Boo, J. and Jung, Y, "Experimetns on the Thermal Performance of a Thermosyphon in Inner Grooved Copper Tube," Proc. SAREK Summer Conf., 1998, pp. 313-317
13. Han, K.I., Lee, S.H., Cho, D.H., Lee, S.J., "Characteristics of Condensing Heat Transfer in an Inclined Thermosyphons with Micro Grooves," Proc. SAREK Summer Conf., 2001, pp. 1364-1371
14. Yee, S.S., "A Study on the Heat Transfer Performance of the Thermosyphon with Internal Micro Grooves", Pukyong National University Ph. D. Dissertation, 2001

Creep Behavior of HDPE Thermosyphon under Long Term Operation

P. Kamonpet, K. Booddachan, P. Terdtoon, I. Preechawuttipong, and Y. Kobayashi*
Department of Mechanical Engineering, Faculty of Engineering, Chiang Mai University,
Chiang Mai, 50200, Thailand. Tel. +66-53-944151, Fax. +66-53-226014
E-mail: patrapont@yahoo.com
*Institute of Space and Astronautical Science, 3-1-1 Yoshinodai, Sagamihara 229-8510, Japan.
Tel. +81-42-7598362, Fax. +91-42-7867588

Abstract

Creep behavior of thermosyphon made from High Density Polyethylene (HDPE) pipe with R113 and R123 as working fluids under 15,000 operating hours was investigated. The evaporation temperature was set as 40 °C, 60 °C, and 80 °C; while the condensation temperature was the ambient temperature which was around 30-35 °C. During the test, there were no sign of failure or crazing and cracking. The nonlinear creep data and the creep compliance were presented for further design purposes.

1. INTRODUCTION

In searching for a new pipe material which has better chemical resistance, heat pipe Laboratory at Chiang Mai University has been investigating the performance and lifetime of HDPE thermosyphon since the year 1999. Generally, when the pipe functions as a thermosyphon container, it must be able to maintain pressure different across the wall and to transfer heat to and from the working fluid. Thus, during a selection of the pipe material for the container, there are several factors that are needed to be considered, i.e. the conductivity, the strength of the material; and the compatibility of the material and the working fluids. Terdtoon et. al. [1] and Boondachan et. al. [2] conducted the tests on the performance and thermal behavior of HDPE thermosyphons and found that they had good performance and thermal behavior. Jirawatsiwaporn, Nontacamjun, and Rohitacani [3] applied the HDPE thermosyphons for reducing soil temperature and the result was quite optimistic. Sooksom and Trikesornmaskul [4], Buddachan et. al. [5], and Prakaiwit [6] did some studies on the compatibility of the HDPE pipe material and the working fluids and showed that the HDPE pipe is chemically compatible with R113, R123 and R141b under the testing time of 1080, 1000, and 3000 hours, respectively. Boodachan et. al. [7] inspected the short-term mechanical property, tensile strength, of the HDPE pipe material when exposed to R113 and R123 and when working as thermosyphon with the same working fluids and found that the tensile strength of the HDPE pipes for both cases drastically decreased during the first period of operation and then leveled out.

The basic difference between metal pipe and plastic pipe operated as thermosyphon is that plastic pipes are being used very close to their melting temperatures, consequently, the pipe will be subjected to creep. Kamonpet et. al. [8] investigated the creep property of the HDPE pipe material when working as thermosyphon with R113 and R123 as working fluids for 3000 hours and concluded that this pipe material was capable for working as thermosyphon under the test conditions and time. They also presented the extended creep data up to 10000 hours by using time-temperature equivalent principle for design proposes. However, the extended creep data were for only the working temperature of 40 °C, and 60 °C. Since it is necessary to caution against extrapolation of creep data beyond more than one order of magnitude of time, the creep data for HDPE thermosyphon with R113 and R123 as working fluids is now valid only about 1 year of working hours which is considered short for this type of application. Therefore, there is a need to conduct long-term creep testing to identify the longevity of the material when works as the thermosyphon under specified operating conditions. The test time conducted in this study was 15000 hours, which when extrapolation for one decade of time, we can obtain the creep data of the HDPE thermosyphon up to approximately 11 years for the working temperature of 40 °C, 60 °C, and 80 °C.

2. EXPERIMENTAL PROCEDURE

The test pipes were made from HDPE (HDPE-BS HEAVY, Asia Pipe Co. Ltd.) with the inner diameter of 15 mm., the length of 400 mm., and the aspect ratio of 10. R113 and R123 were used as working fluids with the filling ratio of 50% of the evaporator volume. During the test the evaporator sides of the HDPE thermosyphons were submerged in the hot sand baths. The temperature of the sand bath was controlled at three levels: 40 °C, 60 °C, and 80 °C. The condenser sections of the thermosyphons were exposed to the ambient temperature for free convection. Fig. 1 shows the experimental setup. The creep data of the thermosyphon in the evaporator section in both diametral and longitudinal directions were measured by the modified depth micrometer as shown in Fig. 2. The number of samples in each test condition was five.

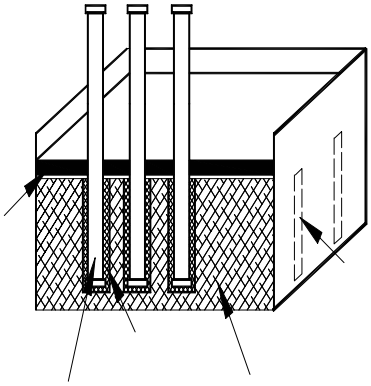


Fig. 1. Experimental setup.

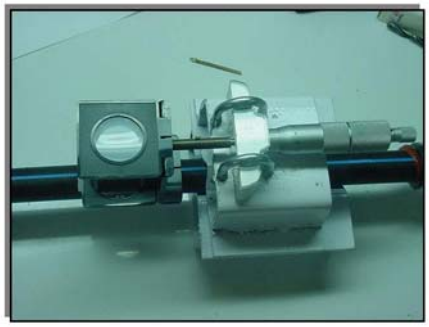


Fig. 2. The modified depth micrometer.

3. RESULT AND DISCUSSION

Fig. 3 and Fig. 4 show the diametral and longitudinal creep data, respectively, for HDPE thermosyphon with R113 as the working fluid for 15000 hours of operating time, whereas Fig. 5 and Fig. 6 show the diametral and longitudinal creep data, respectively, for HDPE thermosyphon with R123 as the working fluid for the same duration of operating time. The time axes of all the figures were extended for one decade of time for the purpose of extrapolation. The non-linear fits in all of the figures were obtained by using the Zener model coupled with the principle of distribution of the retardation times [9] which can be represented by the Prony series [10] as:

$$D(t) = D_0 + \sum_{i=1}^{N} D_i \left[1 - \exp\left(-\frac{t}{\tau_i} \right) \right] \qquad (1)$$

while the creep strain can be formulated as:

$$\varepsilon_c(t) = \left[L(t) - L_0 \right] / L_0 \qquad (2)$$

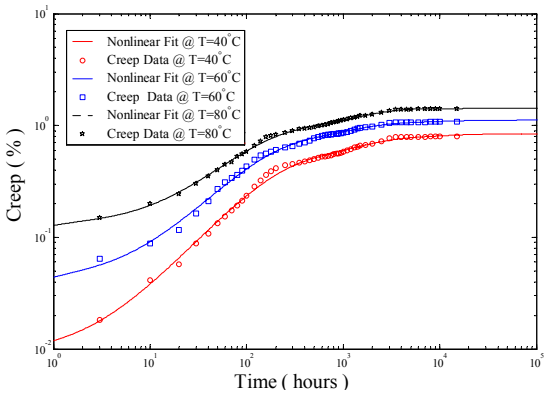


Fig. 3. Diametral creep of HDPE thermosyphon with R113 as the working fluid.

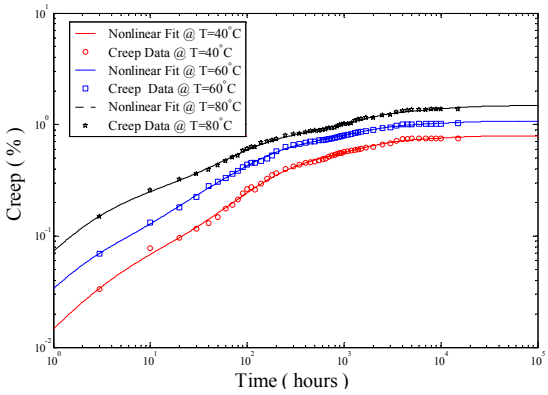


Fig. 4. Longitudinal creep of HDPE thermosyphon with R113 as the working fluid.

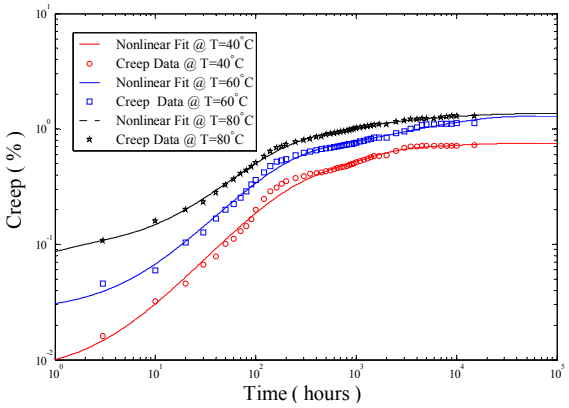


Fig. 5. Diametral creep of HDPE thermosyphon with R123 as the working fluid.

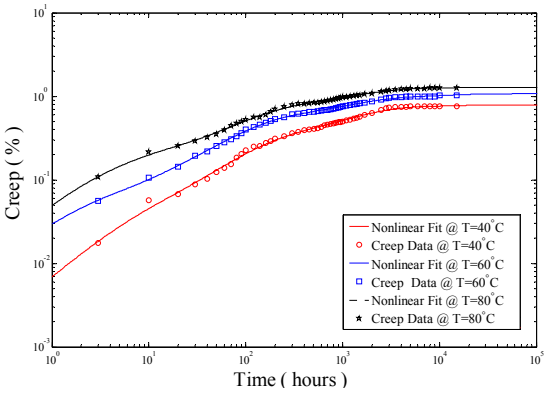


Fig. 6. Longitudinal creep of HDPE thermosyphon with R123 as the working fluid.

Fig. 7 and Fig. 8 show the diametral and longitudinal creep compliance, respectively, for HDPE thermosyphon with R113 as the working fluid for 15000 hours of operating time, whereas Fig. 9 and Fig. 10 show the diametral and longitudinal creep compliance, respectively, for HDPE thermosyphon with R123 as the working fluid for the same duration of operating time. The time axes of all the figures were extended for one decade of time for the purpose of extrapolation.

The non-linear curves fitted by using Prony series can fit quite well with the data obtained. The RMS error for each case was approximately 5%. There was no sign of any failure, including the crazing and cracking when observing the outside surface quality of the pipe, and the thermosyphon was still able to transfer heat. The effects of temperature and working fluids on the creep behaviors of HDPE thermosyphons are corresponding to those explained Kamonpet et. al [8].

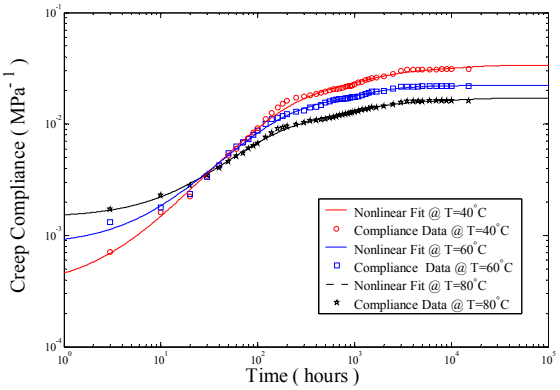


Fig. 7. Diametral creep compliance of HDPE thermosyphon with R113 as the working fluid.

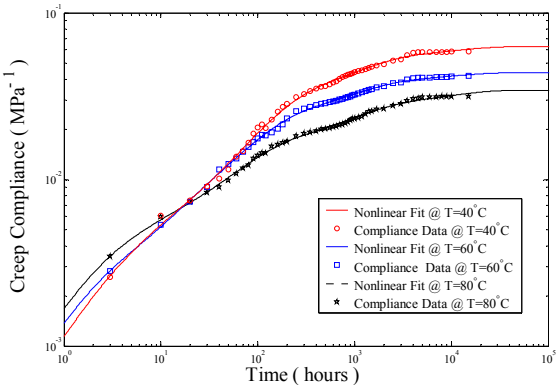


Fig. 8. Longitudinal creep compliance of HDPE thermosyphon with R113 as the working fluid.

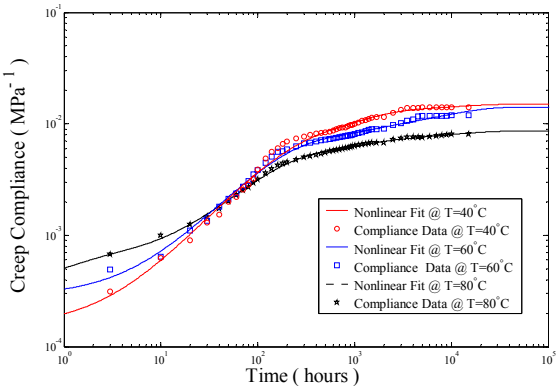


Fig. 9. Diametral creep compliance of HDPE thermosyphon with R123 as the working fluid.

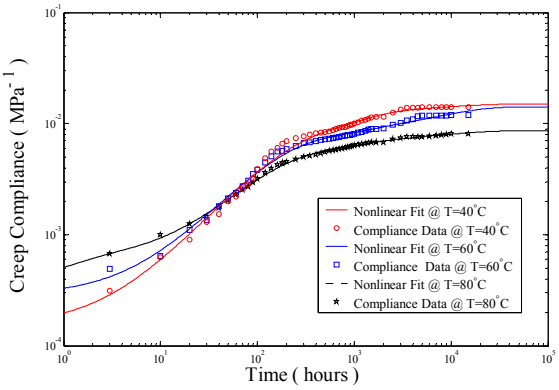


Fig.10. Longitudinal creep compliance of HDPE thermosyphon with R123 as the working fluid.

4. CONCLUSION

The creep strain and creep compliance data for the HDPE thermosyphon working under the testing temperature of 40 °C, 60 °C, and 80 °C for 15000 operating hours were obtained for further design proposes. The extrapolated data up to 11 years were also included in the paper. These data were obtained by the Zener model coupled with the principle of distribution of the retardation times which can be represented by the Prony series and the RMS error was around 5%.

Acknowledgement

This paper was conducted under the supports from National Science and Technology Development Agency of Thailand (NSTDA). The authors would like to show their sincere appreciation for all the support provided.

Nomenclature

$D(t)$	creep compliance (Pa^{-1})
D_0, D_i	Prony series coefficience
$L(t)$	length as a function of time (mm)
L_0	original gage length (mm)
t	operating time (hrs)
ε_c	creep strain
τ	retardation time (hrs)

References

1. Terdtoon, P., Tantakom, P., and Buddajan, K., "Plastic Thermosyphon", Proc. of 11th IHPC, Tokyo, Japan, 1999, pp. 193-196.
2. Boodachan, K., Tantakom, P., Terdtoon, P., and Polchai, A., "Thermal Behavior of a HDPE Thermosyphon", Proc. of 6th IHPS, Chiang Mai, Thailand, 2000, pp. 288-293.
3. Jirawatsiwaporn, K., Nontacamjun, K., and Rohitacani, A., "Application of Plastic Thermosyphon for Soil Temperature Reducing", Undergraduate Project, Chiang Mai University, Chiang Mai, Thailand, 2000.
4. Sooksom, C., and Trikesornmaskul, J., "A Study of Chemical Resistance of HDPE Pipe on R123 and R141b", Undergraduate Project, Chiang Mai University, Chiang Mai, Thailand, 2000.
5. Booddachan, K., Tantakom, P., Terdtoon, P., Kobayashi, Y., and Sucharitkul, T., "Corrosion of a HDPE Thermosyphon under Long-Term Operation", Proc. of 6th IHPS, Chiang Mai, Thailand, 2000, pp. 431-436.
6. Prakaiwit, S., "The Compatibility of HDPE Plastic Thermosyphon with R113 and R123 Refrigerants", Master Thesis, Chiang Mai University, Chiang Mai, Thailand, 2001.
7. Kamonpet, P., Anuchitanukul, Y., Terdtoon, P., and Sucharitkul, T., "Creep Property of HDPE Thermosyphon", Proc. of 12th IHPC, Moscow-Kosroma-Moscow, Russia, 2002, pp.553-557.
8. Booddachan, K., Kamonpet, P., Terdtoon, P., "Tensile Strength of HDPE Themosyphon", to be present at the 7th IHPS, Jeju, Korea, 2003.
9. McCrum, N.G., Buckley, C.P., and Bucknall, C.B., Principles of Polymer Engineering, Oxford Science Publications, New York, 1994, Chapter 4.
10. Lai, J. and Bakker, A., "Analysis of the Non-Linear Creep of High-Density Polyethylene", Polymer, 36(1), 1995, pp.93-99.

An Experimental Study of a Closed Two-Phase Loop Thermosyphon with Two Evaporators in Parallel Arrangement

Chul Ju Kim, Byoung Ok Yoo*, Yong Joo Park*

School of Mechanical Engineering, Sungkyunkwan University Suwon 440-746, South Korea

Tel: +82-31-290-7434, Fax: +82-31-290-5849, cjkim@me.skku.ac.kr

*Heat Transfer Lab. Graduate School of Mechanical Engineering, Sungkyunkwan University

Suwon 440-746, South Korea, Tel: +82-31-290-7474, Fax: +82-31-290-5849

yetiman@korea.com, yjpark@skku.edu

Abstract

The Present study was conducted to investigate the operational problems occurring at the heated area of the evaporator, related to the dry-out phenomenon, when a closed two-phase loop thermosyphon cooling system, designed to have two evaporators, was put in operation under diverse different conditions such as changing power at each evaporator or fill charge ratio. Temperature distributions on the walls of evaporators and condenser, inside the liquid and vapor lines of the system were measured, and not only the performances of the evaporator and condenser but also the appearance of hot dry patch and its effect were examined. It was observed that those multi-evaporator systems would work properly, if the power were distributed evenly to the evaporators. If not, the difference in powers among evaporators has to be contained within a certain limit, a value yet to investigate. The present system was found out to have a capacity of cooling of 650W per unit evaporator at a fill charge ratio of 130%. The value of critical limit, mentioned above, was around 100W, 15% of the power per unit evaporator, when operated under conditions of maximum allowable power.

Key words: Closed two-phase loop thermosyphon, Heat transfer coefficient, Thermal resistance, Fill charge ratio

1. INTRODUCTION

In general, a closed two-phase loop thermosyphon consists of one evaporator, one condenser and two insulated lines of vapor and condensate liquid flows, and the evaporator has to be placed lower than the condenser within their vertical plane. That is an inevitable measure required to let the condensate liquid flow from the condenser to the evaporator with the assistance of the gravity force field. [1],[2]

Lots of studies [3],[4] have been performed to investigate the matters related on design and performances of these systems so far, but it still seems to be uncertain whether a loop thermosyphon could be designed to have multiple evaporators due to operational complications. These kinds of loop thermosyphon cooling systems will be especially useful for some electronic equipment, where several circuit boards with heat sources are in parallel arrangement. Our interest of the present study lies on studying the possibility of a multi-evaporator loop thermosyphon cooling system and understanding diverse phenomena, arising inside evaporators. It would be expected for those systems to encounter some problems, probably related to inequalities of boiling temperatures and corresponding vapor pressures for each evaporator when its powers of each are not evenly distributed

It is worth noting here that a capillary pumped loop heat pipe (CPL) had been developed to respond to these problems and its usefulness was successfully verified by flight test on board of a satellite. [5],[6] However, these systems are far more sophisticated in structure and cost demanded than any types of loop thermosyphons.

For the present study, we designed and fabricated a closed two-phase loop thermosyphon, consisting of two evaporators in parallel arrangement and being able to transport about 1 kW. It was supposed that this system was to remove heat from electronic equipment, where thermal sources were distributed on several circuit boards in shapes of rectangular plate.

2. EXPERIMENTAL APPARATUS AND PROCEDURES

Fig. 1 shows a schematic drawing of the experimental model designed and fabricated for the present study. The system was consisting of

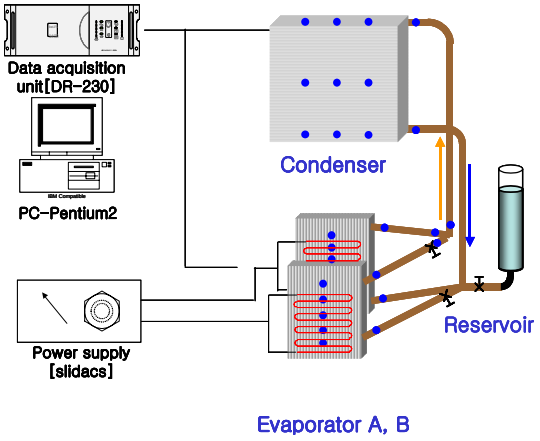


Fig. 1 Schematic diagram of a closed two–phase loop thermosyphon with two evaporators in parallel arrangement.

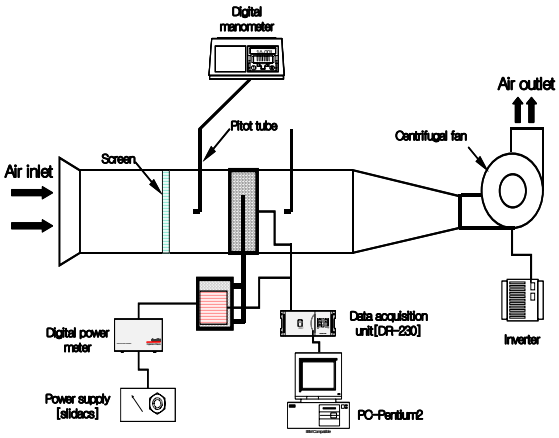


Fig. 2 Schematic diagram of an assembled system for the experiment

two evaporators in parallel arrangement, a single condenser and two adiabatic lines of vapor and condensate flows. The evaporators were in shape of a plate with a parallelogram cavity at its center, and the condenser was made of a conventional compact-heat-exchanger of a fin-tube structure. A liquid reservoir was attached to the condensate line at the bottom of it to serve as a measure to control a fill charge ratio of working fluid inside.

Fig. 2 represents a scheme of the assembled equipment for performance tests of the system in Fig1, that consisted of a loop thermosyphon with dual evaporators, a wind tunnel for supplying air flow to the condenser, two power suppliers and a data logger system, etc. The air velocity was kept constant at 3m/sec., and its intake temperature was at room temperature ranging 20-25C. The velocity and temperature of the airflow were measured at two planes, in front and behind of the condenser. For each evaporator, wall temperature was measured at several points arranged along its centerline of the heated surface. The wall temperature distributions for each evaporator provide lots of information about boiling regime, flow patterns, existence of dry patch, etc. In contrast, to measure the working fluid temperatures, four thermo proves (T-type; 1ϕ×10L) were placed inside the each line of condensate and vapor flow.

For the first three cases, the fill charge ratio ψ was kept constant at 100 %. The fill charge ratio ψ was defined as being 0 % if the free line of liquid column inside the evaporator touched the bottom line of its heated section, and 100% if touching its top, when measured at the moment the system was at rest. For the case of ψ >100%, the value of ψ was determined by the expression described below:

$$\Psi = 100 + \frac{(m - m_0)}{m_0} \times 100, \quad [\%]$$

where, m is the quantity of charged working fluid in mass and m_0 is that at ψ = 100 %.

3. FLOW PATTERNS AND HEAT TRANSFER COEFFICIENTS

From their definitions, the evaporating and condensation heat transfer coefficients of the system can be determined by the expression (1) and (2), respectively. Those values obtained from the experiment were compared to the predictions that had been calculated from some correlations listed below. For the prediction of evaporating heat transfer coefficient, the correlations written in Eqs. (3) and (4), developed on the basis of nucleate boiling by Rohsenow and Imura et al., respectively, were chosen. For the condensation heat transfer coefficient, the expressions, described in Eqs. (5) through (8), were chosen. They had been formulated by Nusselt, Traviss et al. and Boyko & Kruzhilin, respectively, for a condensation in a vertical tube.

$$\overline{h_e} = \frac{Q}{A_e (T_{pv,e} - T_{v,e})} \tag{1}$$

$$\overline{h_c} = \frac{Q}{A_c (T_{v,c} - T_{pl,c})} \tag{2}$$

where, A_e is the heated surface area of the evaporator and A_c is the total surface area of the condenser.

Rohsenow's correlation [7]:

$$\overline{h_e} = \frac{q^{2/3}}{\frac{C_{sf} h_{fg}}{C_{p,l}} \left\{ \frac{1}{h_{fg} \mu_l} \left(\frac{\sigma}{g[\rho_l - \rho_v]} \right)^{1/2} \right\}^{0.33} \Pr^{1.7}} \tag{3}$$

Imura's correlation [8]:

$$\bar{h}_e = 0.32\left[\frac{\rho_l^{0.65} k_l^{0.3} C_{p,l}^{0.7} g^{0.2} q^{0.4}}{\rho_v^{0.25} h_{fg}^{0.4} \mu_l^{0.1}}\right]\left(\frac{p_{sat}}{p_a}\right)^{0.3} \quad (4)$$

Nusselt's model [9]:

$$\bar{h}_c = 0.943 \times\left\{\frac{\rho_l g k_l^3 (\rho_l - \rho_v)[h_{fg} + 0.68 C_{p,l}(T_{sat} - T_w)]}{\mu_l L_c (T_{sat} - T_w)}\right\}^{1/4} \quad (5)$$

Taking account of the subcooling effect of condensate, h_{fg} in Eq. (5) has to be replaced by h'_{fg} in Eq. (6).

$$h'_{fg} = h_{fg} + \left(0.683 - \frac{0.228}{\mathrm{Pr}_l}\right) c_{pl}(T_{sat} - T_e) + c_{pv}(T_{sat} - T_e) \quad : \mathrm{Pr} \rangle 0.6 \quad (6)$$

Traviss et al. Model [10]:

$$h_T = \left(\frac{k_l}{D}\right)\frac{0.15\,\mathrm{Pr}_l\,\mathrm{Re}_l^{0.8}}{F_T}\left(\frac{1}{X_{tt}} + \frac{2.85}{X_{tt}^{0.476}}\right) \quad (7)$$

Boyko & Kruzhilin model [11]:

$$h_{BK} = 0.021\left(\frac{k_l}{D}\right)\left(\frac{GD}{\mu_l}\right)^{0.8} \times \mathrm{Pr}_b^{0.43}\left(\frac{\mathrm{Pr}_b}{\mathrm{Pr}_w}\right)^{0.25}\left[(1-x) + x\left(\frac{\rho_l}{\rho_v}\right)\right]^{0.5} \quad (8)$$

4. RESULTS AND DISCUSSION

4.1 Single evaporator mode of operation (Q_a = vari, Q_b = 0)

In this mode of operation, the evaporator A was activated only. Prior to start the system, the two valves connecting the evaporator B to the main loop line were closed. Fig. 3 shows the temperature distributions of the loop thermosyphon along the distance from the bottom of the evaporator A.

As was noted in the previous section, temperatures in the zones of both the evaporator and the condenser were wall surface temperatures, but those values in the vapor and liquid zones are temperatures of the fluids.

The sum of temperature drops, that the fluid had gained during their passage through both the adiabatic lines of vapor and liquid, was found to be contained within 0.5-2C, small enough to be neglected when compared to total temperature drop of the system. When the heat load to the evaporator was raised to a certain value, a peak temperature appeared at the top of heated section, an evidence of a dry-out due to a lack of liquid on the surface. In this early stage of the dry-out, a large part of the heated area was observed to be still wet and involved in the evaporation process,

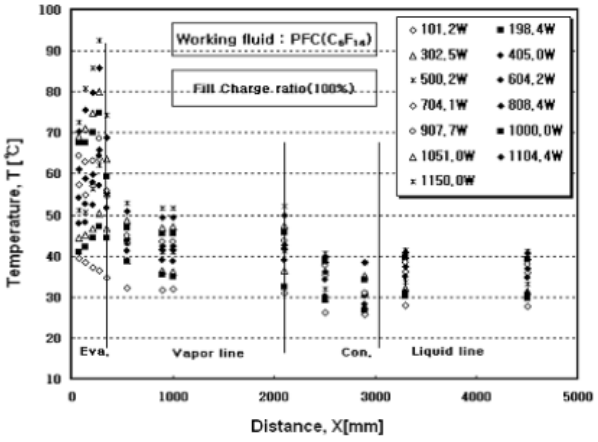


Fig. 3 Temperature distributions of the loop Thermosyphon starting from the bottom of the evaporator along the fluid flow for the operation mode of single evaporator.(Q_b=0)

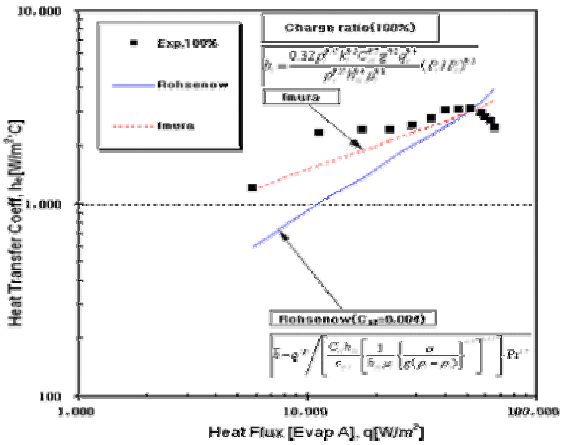


Fig. 4 Evaporating heat transfer coefficient vs. heat flux, when the system was operated at the single evaporator mode.

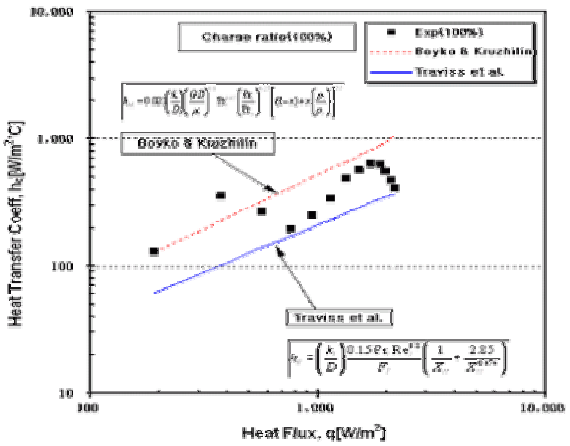


Fig. 5 Condensation heat transfer coefficient vs. heat flux, when the system was operated at the single evaporator mode.

keeping the wall temperature distribution relatively flat over that wet area.

As a consequence, the total rise of wall temperature at the evaporator had been contained within 10 °C, a value of tolerable rise that we admitted for this system, for a power up to 900W-1000W. However, an additional raise of heat load led to a different pattern of wall temperature distribution, a linear increase over most of the heated area, a phenomenon that we recognized as a dangerous sign of dry-out.

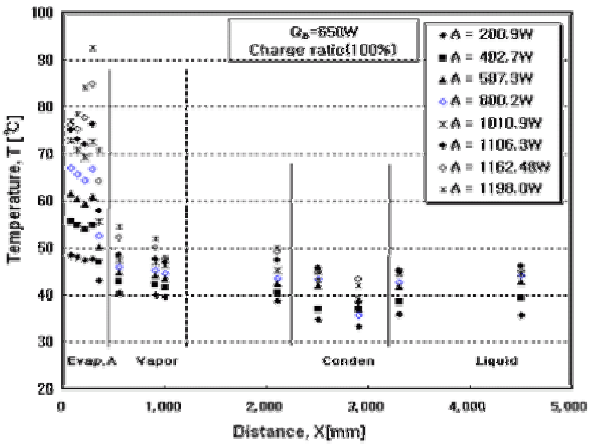
Figs. 4, 5 show the relationship between the heat transfer coefficient and the heat flux for the evaporator and condenser, respectively. In each of the figures, the experimental data were compared with the predictions calculated from the corresponding correlations described in the previous section.

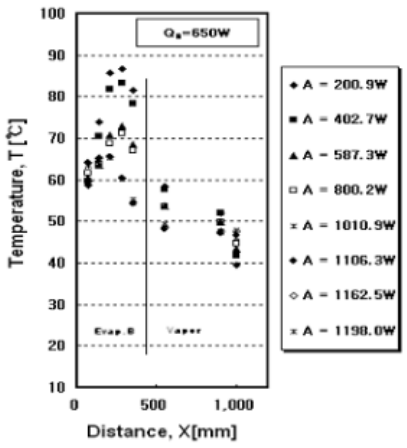
In Fig. 4, the experimental data showed favorable agreement with the prediction by Imura et al. for most of the heat inputs under 60kW/m^2, the allowable maximum power, at which the hot dry dispatch seemed to grow and start to ruin the performance of the evaporator, resulting in a decrease of heat transfer coefficient.

For the condensation heat transfer coefficient in Fig.5, the experimental data were observed to fall between either of the two predictions by Boyko & Kruzhilin and Travis et al., respectively. Interestingly, a similar trend was observed for heat flux over 60kW/m2. This phenomenon seems to be related to the fact that the vapor enters the condenser and start to condensate not at a saturated state but superheated state.

4.2 Dual evaporators mode of operation with uneven heat load to each evaporator. (200W < Q_a < 1200W, Q_b = const.)

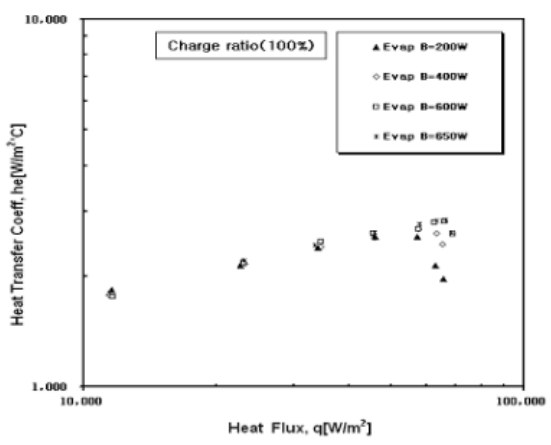
Fig. 6(a) shows the temperature distributions obtained while operating at the mode of dual

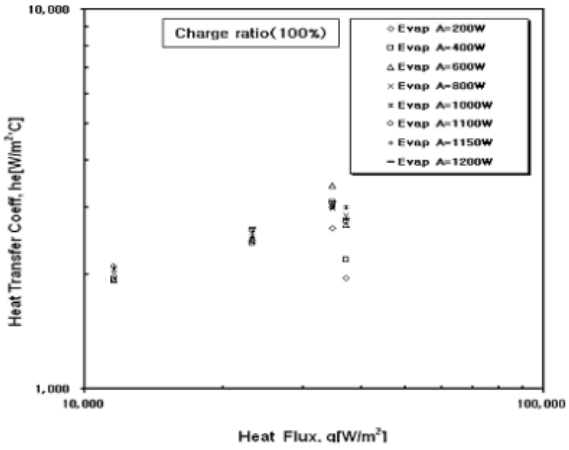




(a) Evaporator A **(b) Evaporator B**

Fig. 6 Temperature distributions of the loop thermosyphon, starting from the bottom of the evaporator along the fluid flow, for an operation mode of dual evaporators.





(a) Evaporator A **(b) Evaporator B**

Fig. 7 Evaporating heat transfer coefficients vs. heat flux for an operation mode of dual evaporators with different power at each evaporator. ($Q_a \neq Q_b$)

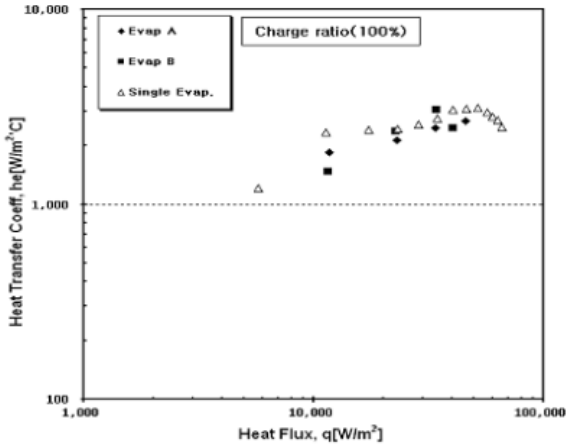


Fig. 8 Evaporating heat transfer coefficient vs. heat flux when equal heat load was provided ıch of the evaporators A and B.

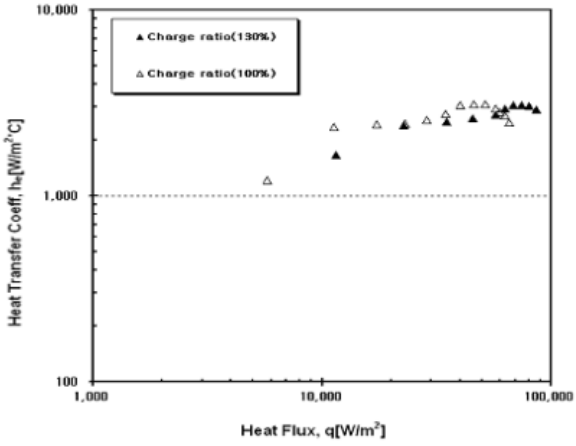


Fig.9 Evaporating heat transfer coefficient vs. heat flux for two different values of fill charge ratio of working fluid.

evaporators. The power Q_a was changed from 200W to 1200W by an increment of 100W, but the power Q_b was kept constant at 650W, the maximum allowable power per unit evaporator.

Fig. 6 showed some interesting phenomena. The two evaporators featured different temperature distributions from each other, i.e. a higher temperature profile was marked for the higher powered evaporator of the two; moreover, it stuck out with an appearance of a peak temperature when the difference of power between the two was over a certain limit. This gap of temperature between the two evaporators was observed to decrease to zero as the amount of the two powers approached to be equal. For the present study, the critical value of power difference between the two evaporators was about 100W, equivalent to 15% of Q_b = 650W, the maximum allowable power per unit evaporator.

From the above observation, it can be said that a closed two-phase loop thermosyphon with multi-evaporator in parallel arrangement could work without any hazards like a local overheating, if any differences of power among evaporators were contained within a certain limit. To understand the characteristics of this critical power gap and predict its value seem to be crucial for such a cooling system as the one presented in Fig.1 to operate in a proper way, and that needs to be investigated more.

Fig. 7(a), (b) show the experimental results of heat transfer coefficient for the evaporator A and B, respectively, calculated on the basis of the temperature distributions obtained for four different values of Q_b. As was mentioned above, the evaporating performance of evaporator is different one another, being more stable and featuring higher value of heat transfer coefficient for the lower powered evaporator of the two.

4.3 Dual evaporators mode of operation with equal heat load to each evaporator. ($Q_a = Q_b$)

Fig.8 shows the experimental relationship between the heat transfer coefficient vs. the heat flux for each of the evaporators A and B, to which an equal amount of heat load was supplied. In the same figure, the data in Fig. 6, the result of experiment performed at a mode of single evaporator, was enlisted for comparison. All the data were observed to collect within 10 % of error, and this result represented that the number of evaporators would not impose any substantial effects on boiling performance, if the power were evenly distributed to each evaporator.

4.4 Changing the fill charge ratio (Q_a=200W~1400W, Q_b = 0)

For the simplicity of work, the experimental procedure of single evaporator mode of operation, discussed previously in the case of Fig.5, was revived here, but the fill charge ratio, ψ had been raised from 100 % to 130 %. Fig. 9 shows the resultant change in heat transfer coefficient of the evaporator in association with the change in fill charge ratio. The peak point of the curve for ψ = 130 % shifted to the right side of that point for ψ =100%. Considering that the peak point represented the fact that the hot dry patch on heated zone started to harm the evaporator performance, increasing the fill charge ratio from 100 % to 130 % resulted in expending the maximum allowable heat load from 1000W to 1300W.

5. CONCLUSION

It can be concluded that a closed two-phase loop thermosyphon with multi-evaporator in parallel arrangement could work properly, only if the power were evenly distributed to all the evaporators. The following are a summary of some important phenomena observed through a performance test of a loop thermosyphon cooling system designed to imply two evaporators.

1. If there exist any difference in power among the evaporators, it should be contained within a certain limit for the system to avoid any problems related to overheating heat sources. To know exactly the critical value of that limit seems to be crucial for proper operations of a given loop thermosyphon cooling system with multi-evaporator, and yet to be studied a lot.
2. The evaporating heat transfer coefficient was found to be in good agreement with the prediction by Imura et al. for the heat flux under 60kW/m2, where the dry-out phenomenon started to affect the evaporating performance.
3. Increasing fill charge ratio from 100% to 130% resulted in expanding the maximum allowable power per unit evaporator from 500W to 650W by around 30%.

Nomenclature

A	*surface area or cross-section area*, [m^2]
c_p	*specific heat at constant pressure*,[J/kgK]
c_v	*specific heat at constant volume*, [J/kgK]
D	*diameter*, [m]
g	*gravitational acceleration*, [m/s^2]
h	*heat transfer coefficient*, [$W/m^2℃$]
h_{fg}	*enthalpy of vaporization*, [J/kg]
k	*thermal conductivity*, [W/mK]
L	*length*, [m]
p	*absolute pressure*, [N/m^2]
Q	*rate of heat transfer into a system*, [W]
q	*heat flux* , [W/m^2]
R	*thermal resistance,* [m^2k/W]
Re	*Reynolds number*
T	*temperature*, [℃]
$\overline{T_w}$	*average wall temperature*, [K or℃]
u	*velocity*, [m/s]

GREEK SYMBOLS

δ	*liquid film thickness*, [mm]
μ	*dynamic viscosity*, [kg/ms]
ν	*kinematics viscosity*, [m^2/s]
ρ	*density*, [kg/m^3]
σ	*surface tension*, [N/m]
Ψ	*fill charge ratio*, [%]

Subscripts

a	*adiabatic*
c	*condenser*
crit	*critical*
e	*evaporator*
f, l	*fluid or fin/liquid*
max	*maximum*
sat	*saturation*
tot	*total*
v, g	*vapor/gas*
w	*wall*

References

1. Dunn, P. B. and Reay, D. A., *Heat Pipes*, 4th Edition, Pergamon Press, Oxford, 1993.
2. Faghri, A., *Heat Pipe Science and Technology*, Tayler & Francis, Washington, 1995.
3. Chengming, s., Mingdao, X. and Yuanguo, c., Analysis of Three-Fluid Separate Type Heat Pipe Exchanger, *Heat Recovery Systems & CHP*, Vol. 12, No. 4, pp. 317-322, 1992.
4. Shi, C. M. and Xin, M. D., Design and operation of large scale separate type heat pipes, *Proc. of Sixth Int. Heatpipe Conf*., France, Vol. 3, pp. 624, 1987.
5. Maidanik, Y. F., Fershtater, Y. G. and Solodovnik, N. N., Loop Heat Pipe : Design, Investigation, *Prospects of Use in Aerospace Technics*, Warrendale, Pennsylvania, USA SAE, 1994.
6. Stenger, F. J., Experimental Feasibility Study of Water-Filled Capillary-Pumped Heat Transfer Loops, *NASA TM-X-1310*, Lewis Research Center, Cleveland, Ohio, 1966.
7. Rohsenow, W. M., Heat Transfer and Temperature Distribution in Laminar Film Condensation, *ASME J. Heat Transfer*, Vol. 78, pp. 1645-1648, 1956
8. Imura, H., Kusada, H., Oyata, M., Miyazaki, T. and Sakamoto, N., Heat Transfer in the Two-Phase Closed Thermosyphon, *Trans. JSME*, Vol. 45, pp.712-722, 1979.
9. Nusselt, W., Die Oberflachen Kondensation des Wasser Dampfes, *Zeitschrift der Vereins Deutscher Ininuere*, Vol. 60, pp. 541-575, 1916.
10. Traviss, D. P., Rohsenow, W. M., and Baron, A. B., Forced convection condensation in tubes: A heat transfer correlation for condenser design, *ASHRAE Trans*., Vol. 79, part I, pp. 157-165, 1973.
11. Boyko, L. D., and Kruzhilin, G. N., Heat transfer and hydraulic resistance during condensation of stream in a horizontal tube and in a bundle of tubes, *Int. J. Heat Mass Transfer*, Vol. 120, pp. 361-373, 1967.

Tensile Strength of HDPE Thermosyphon

K.Booddachan*, P. Kamonpet*, P. Terdtoon*, T. Sutjaritakul* and Y. Kobayashi**

*Department of Mechanical Engineering, Faculty of Engineering, Chiang Mai University
Chiang Mai Thailand, 50200 Tel. +66+53+944151 Fax. +66+53+226014
**Institute of Space and Asttonautical Science, 3-1-1 Yoshinodai, Sagamihara 229-8510 Japan
Tel. +81+42+759-8362 Fax. +91+42+786-7588

Abstract

This paper presents the experimental data of tensile strength of high density polyethylene (HDPE) thermosyphon under long term operation. The HDPE pipe was selected as a container. The HDPE thermosyphons, with aspect ratio of 10 and employed R113 and R123 as working fluids were filled by 50% of the evaporator volume. The operation was conducted with 40, 60, and 80^{o}C of working temperature. The tensile testing samples were prepared according to the ASTM D2290-90. They were divided into 2 groups. The first group was the samples that were prepared from the HDPE thermosyphon that were tested for 15,000 hours. The second was the samples of the HDPE pipes which was cut to testing dimension and submerged into the working fluid. Both groups were tested at the controlled operating temperature. It was found that the tensile strength of the HDPE thermosyphon was drastically decreased by 17-22 % at the first 3000 hours of operating time then tended to be constant until 15000 hours. The R123-HDPE thermosyphon retained higher tensile strength than R113-HDPE thermosyphon because the difference in solubility function between R123-HDPE is more than that of R113-HDPE one.

Key word**:** HDPE thermosyphon, tensile strength

1. INTRODUCTION

A thermosyphon is a simple heat pipe which utilizes gravity to return condensate from the condenser to the evaporator section. It is widely used because of its simple structure and high heat transfer performance. It has been used in many applications such as heat recovery devices and thermal stabilizer. Most of thermosyphon were made of metal pipes such as copper, steel, and aluminum pipes because of their good thermal conductivities. However these metal pipes are easily corroded and when installed at large-scale application, their weight are high. The high density polyethylene (HDPE) heat pipes had been firstly proposed by Tantakom et al.[1]. It has acceptable performance. Although its strength is comparatively low, its lighter weight and anti-corrosion property give its advantage to the metal pipe. HDPE was chosen to be a container of plastic heat pipe so it was called HDPE-Thermosyphon [1, 2, 3].

It is necessary to know the mechanical properties such as tensile strength of the material when selecting of pipe material for thermosyphon applications. The material ought to have high enough strength to withstand the operating pressure inside the pipe along the course of operation. However, up to present, there is no information about the tensile strength of the HDPE pipe when working, with working fluids, as the thermosyphon.

This paper presents the experimental investigation of tensile strength of the long-time-operated HDPE thermosyphon. These results can be utilized as basic data of choosing this new type of heat pipe in many applications.

2. EXPERIMENT SET UP AND PROCEDURE

The tested pipes were made from HDPE pipe (ASTM 1248) [4] with inside diameter of 15 mm and the length of 400 mm. The ratio of evaporator length to the diameter was 10. R113 and R123 were used as the working fluids because of their suitable operating pressure for HDPE thermosyphon at the required temperature. The filling ratio of 50% of the evaporator volume was selected. The operating temperature was controlled at 40, 60, and 80^{o}C. The evaporator section was heated by the hot sand in the controlled-temperature test tank as shown in Figure 1. The condenser section was freely exposed to the environment in order to use the natural convection to release the heat that was transferred from the evaporator section. The

operation time was 15,000 hours. The surface temperature of the evaporator section was detected by 2 thermocouple sensors (type K) at the distances of 50 and 120 mm from the bottom of the pipe. The infrared thermometer was used to detect the surface temperature of the condenser section at the position of 10, 30, 50, 75, 110 and 200 mm from the top end of the pipe. As the operation was conducted, the temperature difference was used to calculate heat transfer performance. The tensile strength of the test pipe was measured from 2 sample groups that were prepared according to the ASTM D2290-92. The first group was the samples that were prepared from the HDPE thermosyphon that were tested for 15,000 hours. The second was the samples that were prepared from the HDPE pipes which submerged into the working fluid inside the test bottles. Figure 2 shows the shape and dimension of the prepared sample. The tensile strength was measured by the universal tensiometer (Mizzui R1250) which showed the result as a stress & strain curve.

The reason of choosing the two different groups of samples was that, the first group which was the thermosyphon operated under the operating temperature and pressure had a direct contact to the working fluid. While the second group, though was tested under the same level of temperature, did not expose to the operating vapor pressure. However this sample group was still inside the pressurized bottle at the same temperature level. In the experiment, the same conditions of these 2 groups were temperature and testing duration. The data, then were compared with the tensile strength of fresh pipe. In order to be certain of only the effect of temperature or time, 2 adding sample groups were also tested. These two additional sample groups were prepared in the same dimensions and then the first additional sample was directly submerged into the same test tank. While the other (or the second additional group) was put into the test bottle filled up with working fluid, and left at room temperature.

In order to compare with the experimental results of Booddachan et al. [2,5], the experiment was conducted for 15,000 hours. They have found that heat transfer performance of the HDPE thermosyphon drastically changed at the first 1000-3000 hours. If there are any relationships between these studies, drastic change in the tensile strength should be easily observed within this range of operating duration. The condition of the samples was checked at 500, 1000, 3000, 10000 and 15000 hours. Figure 3 shows the sample before and after tensile testing. Data from the first two sample groups were compared with those of the fresh sample to find the change in pipe property (as thermosyphon).

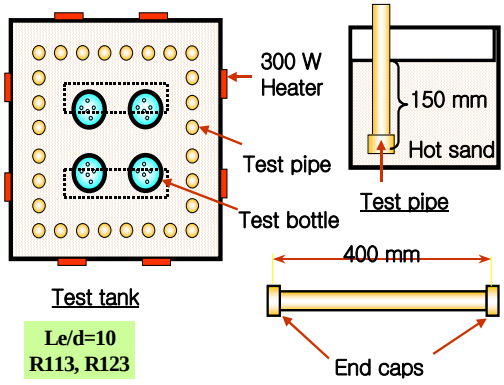


Figure 1: Experimental setup.

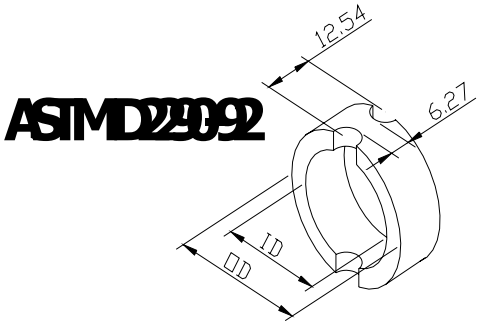


Figure 2: Standard sample base on ASTM D2290-92

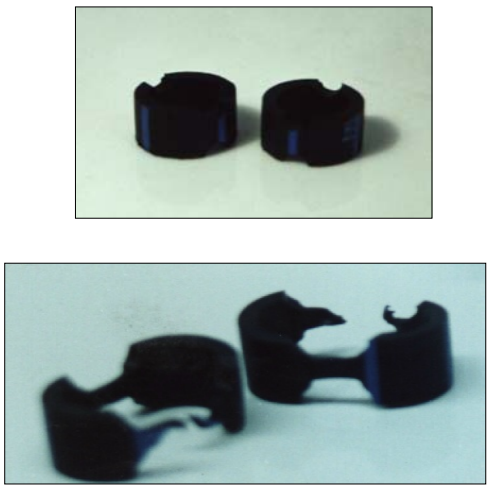


Figure 3: The samples before and after test

The whole parameters and the groups of the experiments were shown in Table 1.

Table 1: Parameters and groups of experiments

Group	Treatment	Activity				
		A	B	C	D	E
1	Tested pipe*	/	/	/	/	/
2	Submerged in the bottle and put in test tank*	/	/	/	/	/
Adding 1	Put in the test tank*	/		/		/
Adding 2	Submerged in the bottle at room temperature*			/	/	/
Standard	Non-treatment					/

*tested at 500, 1000, 3000, 10000, and 15000 hours

- A Temperature
- B Pressure
- C Duration
- D Direct contact
- E Tensile strength test

3. RESULTS AND DISCUSSION

Figure 4 shows the stress and strain diagram of the sample. The curve in Figure 4 is the result of the fresh sample, which will be called 'standard sample' hereafter. Figure 5 and 6 show the stress & strain curve of R123-HDPE thermosyphon and R113-HDPE thermosyphon over 3000 hours.

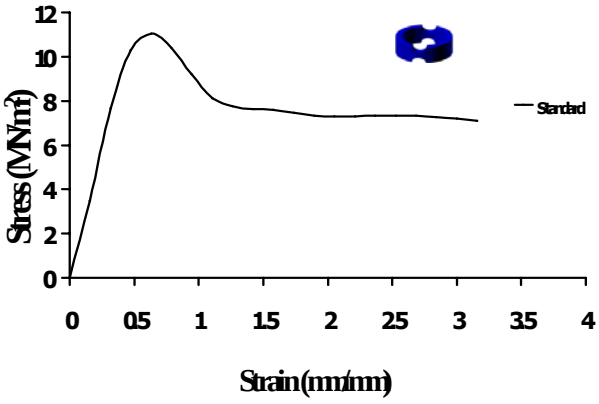


Figure 4: Stress and strain curve of fresh or standard samples

The fresh sample of HDPE pipe had the tensile strength of 11.25 MPa as shown in Figure 4 and also represented by a dotted line marked as 'sample standard' in both Figures 7 and 8. This value is the hoop stress of the pipe and all of the tests were conducted with this type of stress. The longitudinal tensile stress of the pipe, which is 20.15 MPa, is also shown as a dash line on the top of both Figures. In both figure, there are the two types of legend that represent 2 groups of the sample. The clear legend represented the data from the samples that prepared from the operated thermosyphon while the other, solid legend, represent the data of the samples that submerge in the test bottle.

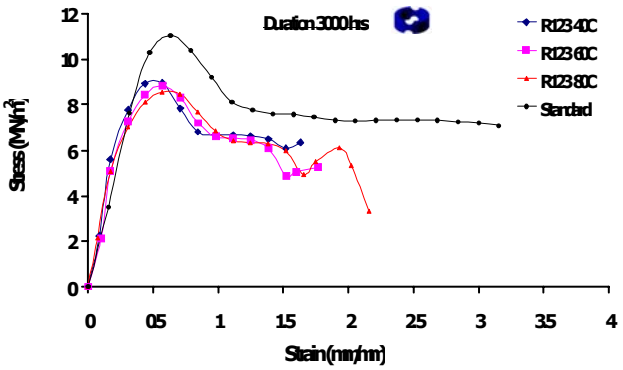


Figure 5: Stress & strain curve of the R123 HDPE thermosyphon over 3000 hours of operation

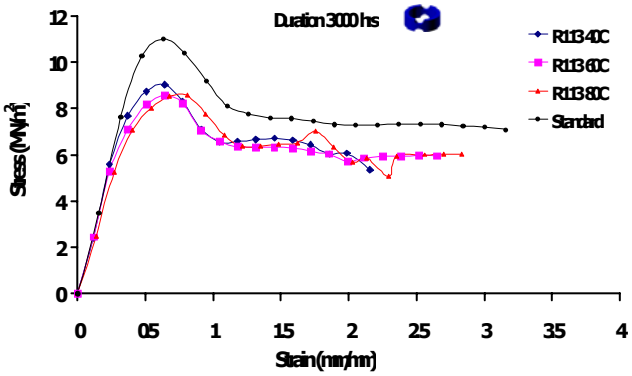


Figure 6: Stress & strain curve of the R113 HDPE thermosyphon over 3000 hours of operation

By using the statistical method, it was found that, both of working fluids similarly affected tensile strength. The tensile strength of the R113-HDPE thermosyphon drastically decreased from a starting value to 10.75 MPa at the first 500 hours to 8.4 MPa at 3000 hours. After that it tended to be constant at this level up to the end of the experiment. While the result of the R123-HDPE thermosyphon also drastically decreased from a starting value of 10.15 MPa at the first 500 hours to 8.4 MPa at 3000 hours. Then

the same trend can be observed until the end of the test.

These experimental data also supported the fact that found by Prakaiwit, S. 2000 [5] that the solubility factor between a pair of R113 and HDPE pipe are closer than the pair of R123 and HDPE pipe. The closer the values between the pair, the easier the pipe material absorbs the fluid, and lowering its strength. As a result, it directly affects the tensile strength of the container.

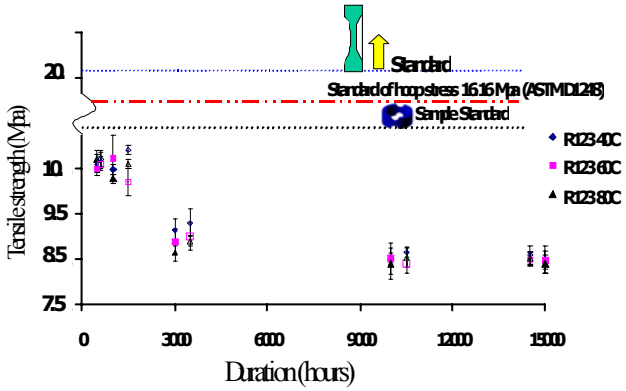


Figure 7: Tensile strength of R123 HDPE thermosyphon over 15000 hours of operation

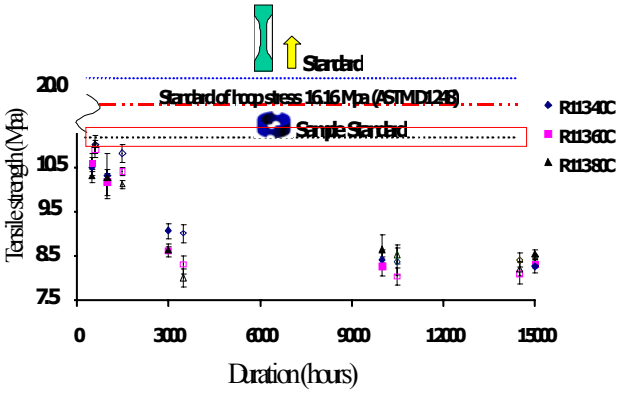


Figure 8: Tensile strength of R113 HDPE thermosyphon over 15000 hours of operation

The result of the additional group 1 and 2 are shown as the rectangular block in Figure 8. It was found that tensile strength of these groups were at the same level with the standard sample (11.25 MPa). It can be clearly concluded that, "*Neither merely temperature nor merely working fluids affected the tensile strength of the pipe*". This ensures that the tensile strength of the HDPE thermosyphon decreases with its operation (with continuous evaporation and condensation). A container under this condition continuously confronted with the fluctuated operating pressure and temperature all over the operation.

4. CONCLUSION

The experimental data of the tensile strength of the R113- and R123-HDPE thermosyphon have been presented in this paper. Its was found that the tensile strength of R113-HDPE thermosyphon was lower than those of R123-HDPE thermosyphon. The tensile strength of the R113-HDPE drastically decreased by 22% at 3000 hours of operating time. After that it tended to be constant at this level up to the end of the experiment. While that of the R123-HDPE system also decreased. It decreased by 17% at 3000 hours of operating time and then tended to be constant at that level up to the end of the operating duration. The difference in tensile strength between R113-HDPE thermosyphon and the R123-HDPE one was due to the difference in the solubility function between the pipe material and the working fluid. The R123-HDPE thermosyphon retained higher tensile strength than R113-HDPE thermosyphon because the difference in solubility function between R123-HDPE is more than that of R113-HDPE one.

Acknowledgement

This paper was conducted under National Science and Technology Development Agency of Thailand (NSTDA). The authors would like to show their sincere appreciation for all of the support provided.

Reference.

1. Tantakom P., Buddajan K., and Terdtoon P. (1999). *Plastic Thermosyphon*., Proc. The 11th Int. Heat Pipe Conf., Tokyo, Japan.
2. Booddachan K., Kamonpet P., Terdtoon P., and Sucharitakul T. (2000) *Thermal Behavior of HDPE Thermosyphon* Proc., The 6th Int. Heat Pipe Symp., Chiang Mai, Thailand.
3. Booddachan K., Kamonpet P., Terdtoon P., and Sucharitakul T. (2000) *Corrosion of HDPE Thermosyphon under Long-Term Operation* Proc., The 6th Int. Heat Pipe Symp., Chiang Mai, Thailand.
4. Annual book of ASTM standards(1993) *Test method for tensile property of plastic*.D2290-92 Vol.08.01, Easton, USAS.
5. Prakaivit S. (2001) *The Compatibility of HDPE Plastic Thermosyphon with R113 and R123 Refrigerant*, Master Thesis, Chiang Mai University. Chiang Mai Thailand

Analysis of the Optimal Mass of Working Fluid for Heat Pipe with Axially Grooved Wicks

Jeong-Se Suh, Gil Sung Byun, and Chang Ho Kang

School of mechanical and aerospace engineering and ReCAPT, GyeongSang Nat'l Univ.,
Jinju 660-701, Korea
Tel: +82-55-751-5312, FAX: +82-55-757-5622, E-mail: jssuh@gsnu.ac.kr

Abstract

In this study, analysis is made for optimum filling quantity in grooved heat pipes. The mathematical models of two-phase flow in grooved heat pipe are presented for an optimum filling quantity of working fluid in steady state. Heat pipe used in this study has one evaporator, condenser and adiabatic section respectively. Generally the quantity of working fluid is determined by considering only a geometrical shape condition but required less than that under ideal condition owing to the meniscus recession phenomena of working fluid in the evaporator region. Therefore optimal filling quantity of working fluid is recommended to be calculated by considering capillary pressure, radius of curvature and wetting angle with the aid of the proposed model.

Key words: Heat Pipe, Capillary Limitation, Capillary Pressure, Meniscus, Radius of Curvature, Wetting Angle

1. INTRODUCTION

Since heat pipe with grooved type wick uses the hole as a liquid passage, it has very low frictional coefficient for liquid flow and it also very low heat resistance because of using metal having same characteristic of pipe as a fin inside between hole and hole. And it is also safety for the fraction of wick in the device of high pressure and long time usage. In this reason recently we use axial grooved wick heat pipe commonly. Axial grooved heat pipe is used in the field of spacecraft industry and many industrial applications very widely. Since space industry such as satellite require not only highly heat transfer characteristic but also structure simplicity and safety most of all, we use grooved heat pipe. Heat pipe controls constant temperature to retain each component of satellite and structure supplying heat in the opposite side in the course of emission and sun radiation. And it is also used in the wide areas such as high precision machines, energy related industry and cooling of electric and electronic devices. Today, heat pipe is highly respected as heat transfer devices because of ease of manufacturing due to its simplicity of structure and since it has no heat resistance, it can transfer much quantity of heat with small temperature difference.

Heat pipe researches have been implemented as different approaches. Kemme[1] reviewed operation limit of heat pipe and verified several types of capillary limit, Tathgir et al.[2] studied heat transfer according to working fluid quantity of grooved stainless steel heat pipe using water as a working fluid. Ogushi et al.[3] studied capillary limit and heat transfer quantity of condenser according to working fluid quantity and angle of grooved aluminum heat pipe using Freon as a working fluid and Shin[4] experimentally studied optimal working fluid quantity of heat pipe with screen mesh wick and Jung[5] studied heat transfer characteristic according to elevation, working fluid quantity, and cooling water quantity of heat pipe in using solar heat conservation. And Lee et al.[6] presented heat transport factor through performance experiment and analyzed according to operating temperature, elevation and heat load of axial grooved heat pipe.

Performance of heat pipe is determined by the wick structure and working fluid quantity. If working fluid quantity is injected in the heat pipe so small, dry out happens in the evaporator region, but if this quantity is so much, this may lead to diminish heat transfer of heat pipe because of condenser blockage by the liquid slug. Thus it is required proper quantity to maintain optimal operation states. Despite working fluid quantity affecting overwhelm effects on the performance of heat pipe, we only depend on try and error method which based on individual experiences.

Thus, in this paper we determine optimal quantity of working fluid through the performance analysis of axial grooved heat pipe. Generally the quantity of working fluid is determined by considering only a geometrical shape condition[7] but the quantity is required less than that under ideal condition owing to the meniscus recession phenomena of working fluid in the evaporator region.[4] Therefore optimum filling quantity of working fluid is recommended to be calculated by considering capillary pressure, radius of curvature and wetting angle with the aid of the proposed model.

2. OPTIMAL MASS OF WORKIN FLUID

2.1 Capillary pressure

Figure 1 shows the block diagram of circulation of working fluid inside of heat pipe forming grooved wick and Table 1 shows the specification of grooved heat pipe model in this study. During steady state operation of a heat pipe as shown in Fig. 1, the working fluid in the vapor phase flows continuously from the evaporator section to the condenser, and it returns to the evaporator in the liquid phase.

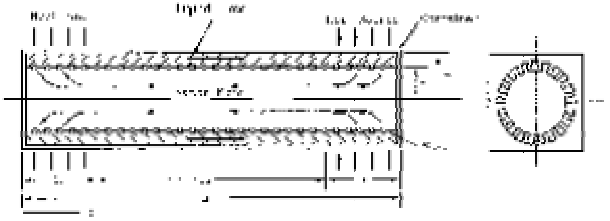


Fig. 1 Schematic of a heat pipe showing circulation of working fluid

Table 1 Specification of variable conductance heat pipe used in this study

Properties	Values
Pipe Material	Aluminium
Working Fluid	Ammonia
Groove Width(w)	0.46 mm
Base Groove Width	0.97 mm
Vapor Core Diameter(D_v)	7.43 mm
Groove Depth	1.05 mm
Number of Grooves(N)	21
Groove Wick Porosity(ε)	0.363
Cross Section Area of Heat Pipe	11.68×14.73mm^2
Condenser Length(L_c)	300 mm
Adiabatic Length(L_a)	449 mm
Evaporator Length(L_e)	140 mm

As the vapor flows from the evaporator to the condenser, there exists a vapor pressure gradient along the vapor flow passage. There also exists a liquid pressure gradient as the condensed liquid flows back from the condenser to the evaporator. For the required balance of pressure it is necessary that along the entire length of the heat pipe the pressure at the liquid side of the liquid-vapor interface is different from that at the vapor side. Thus, the capillary pressure exists to support this pressure difference between the two sides of the liquid-vapor interface. Since there does exist a maximum possible capillary pressure for any liquid-wick combination, capillary pressure available for axial transport of fluid will be smaller than the maximum capillary pressure. To operate a heat pipe in the normal condition without dry out of wick, the capillary pressure must satisfy the following condition.

$$\Delta P_{cm} - \Delta P_n \geq \Delta P_c(x) \tag{1}$$

Where ΔP_{cm} is a maximum capillary pressure and ΔP_n is a normal hydrostatic pressure, which can be expressed as follow

$$\Delta P_n = \rho_l g d_\upsilon \cos\varphi \tag{2}$$

$$\Delta P_{cm} = \frac{2\sigma\cos\theta}{r_c} \tag{3}$$

Thus, using the condition of Equation (1), the capillary pressure can be calculated from the following expression

$$\Delta P_c(x) = \int_{x_{\min}}^{x}\left(\frac{dP_\upsilon}{dx} - \frac{dP_l}{dx}\right)dx = \int_0^x\left[(F_l + F_\upsilon)Q - D_\upsilon\frac{dQ^2}{dx} + \rho_l g\sin\varphi\right]dx \tag{4}$$

in condenser region ($0 \leq x \leq L_c$)

$$Q = \frac{x}{L_c}Q_{c,\max} \tag{5}$$

in adiabatic region($L_c \leq x \leq L_c + L_a$)

$$Q = Q_{c,\max} \tag{6}$$

in evaporator region ($L_c + L_a \leq x \leq L_t$)

$$Q = \frac{L_t - x}{L_e}Q_{c,\max} \tag{7}$$

For turbulent flow, capillary pressure of heat pipe can be calculated from the previous study[7,8].

$$f_\upsilon = \frac{0.079}{\mathrm{Re}_\upsilon^{0.25}} \quad \text{(Blasius correlation)} \tag{8}$$

$$F_v = \frac{0.039\mu_v}{r_v^2 A_v \rho_v \lambda}\left(\frac{2r_v Q}{A_v \mu_v \lambda}\right)^{0.75} \quad (9)$$

$$D_v = \frac{1.33}{A_v^{\,2}\rho_v \lambda^2} \quad (10)$$

$$\Delta P_c(x) = F_l \int_0^x Q dx + \int_0^x \rho_l g \sin\varphi dx + \frac{0.039\mu_v}{r_v^2 A_v \rho_v \lambda}\left(\frac{2r_v Q}{A_v \mu_v \lambda}\right)^{0.75} \int_0^x Q^{7/4} dx - D_v \int_0^x \frac{dQ^2}{dx} dx \quad (11)$$

2.2 Theoretical optimal mass of working fluid

Generally, the quantity of working fluid is determined by considering only a geometrical shape condition as follows [7],

$$m_{th} = A_v L_t \rho_v + A_w L_t \varepsilon \rho_l \quad (12)$$

But Fig. 2 shows that the quantity of working fluid is required less than that under ideal condition owing to the meniscus recession phenomena of working fluid in the liquid-vapor

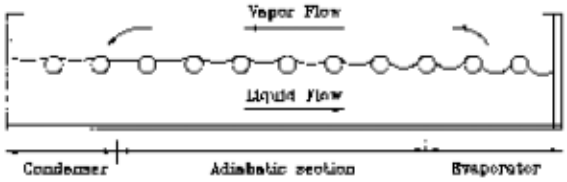


Fig. 2 Schematic diagram of meniscus curvature variation as a function of axial position

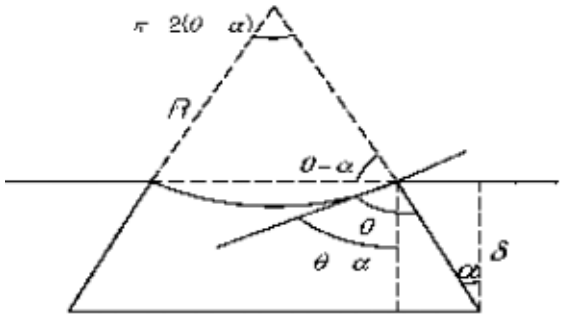


Fig. 3 Sketch of meniscus in cylindrical pore

interface. Feldman et al.[9] suggested that curvature radius became to be small by liquid amount reduced as the liquid-vapor interface moves toward wick by evaporation in the evaporator region but almost approached infinitely great in the condenser region.

Figure 3 describes the recession of meniscus of heat pipe in real operation by capillary pressure. The curvature radius is changed by axial pressure distribution. Thus, according to capillary pressure along with axial position, the curvature radius can be calculated from Laplace-Young equation and wetting angle is determined by following equation with the notation of Fig. 3.

$$\theta(x) = \cos^{-1}\left(\frac{wP(x)}{2\sigma}\right) + \alpha \quad (13)$$

As shown in Fig. 3, the quantity of working fluid removed in one groove by capillary pressure is a area of nail subtrating the triangle area from the sector area. Removed working fluid quantity by capillary pressure in total length of heat pipe can be calculated by following equation.

$$V_{re} = \int_0^{L_t}\left[\frac{1}{2}R(x)^2(\pi - 2\theta(x) + 2\alpha) - \frac{w}{2}R(x)\sin(\theta(x)-\alpha)\right]Ndx \quad (14)$$

$$m_{re} = V_{re}(\rho_l - \rho_v) \quad (15)$$

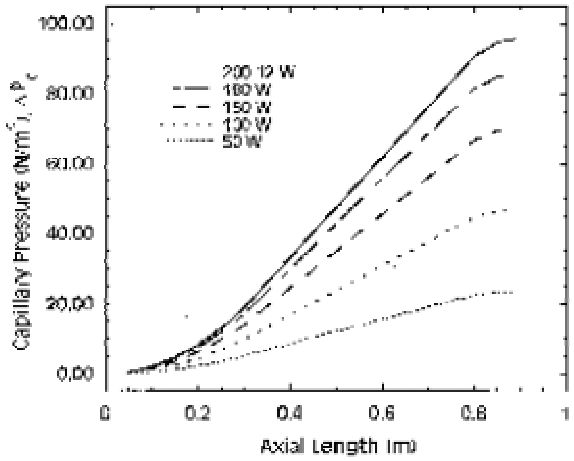


Fig. 4 Capillary pressure variation along with axial position on the operating temperature of 290K

Thus, optimal working fluid quantity is determined by following equation.

$$m_{opt} = m_{th} - m_{re} \quad (16)$$

3. RESULTS AND DISCUSSION

Figure 4 shows the distribution of capillary pressure with increasing heating of evaporator in the operation temperature of 290K. In this figure, the capillary pressure is varied slowly in the end ports of both evaporator and condenser and increases linearly in the adiabatic region due to the small mass flux of working fluid. The capillary pressure also grows with the increasing of heat flux in the evaporator and reaches the

maximum value at the heat flux of 200.12W in the heat pipe used in this study. The trend of distribution of capillary pressure shown in this figure is similar to a typical tendency of that appeared in a long heat pipe.

In Fig. 5, when the temperature of liquid-vapor is maintained in 310K, the pressure distributions of vapor and liquid are depicted for the operating temperature of 290K and the heating flux of 200.12W, and the distribution of capillary pressure obtained from the difference of pressure between vapor and

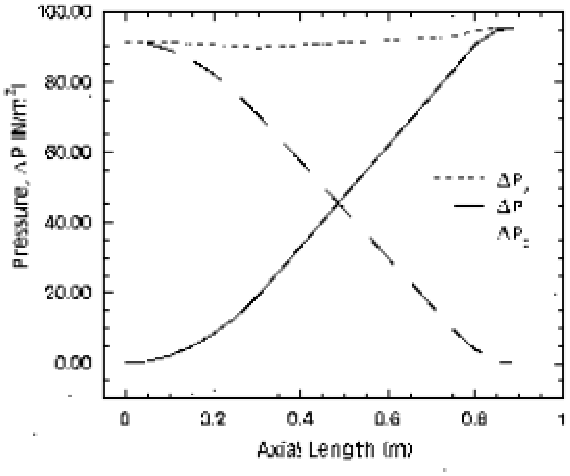


Fig. 5 Pressure distribution along with axial position on the operating temperature of 290K and the liquid-vapor interface temperature of 310K in evaporator region

liquid also presented. This figure shows that the pressure drops rapidly in the liquid but increases slowly toward the evaporator of heat pipe. This behavior of pressures of vapor and liquid comes from the difference of working fluid density between vapor and liquid. It can be also seen from this figure that the variation of pressure in the liquid is greatly dependent of liquid density, while small in vapor. The result from Fig. 5 is the good agreement with that of a heat pipe, which has the long length of condenser or operates under the high pressure, in the case of considering only the pressure drop by the viscous friction, neglecting the inertial force for low liquid and vapor velocity [10].

The variation of curvature radius of meniscus with increasing heat flow toward evaporator is shown in Fig. 6 for the operating temperature of 290K. As illustrated in Fig. 6, the curvature of meniscus formed in the axial groove of heat pipe becomes small with increasing of heat flow rate and by the high pressure with approaching the evaporating region. For this behavior of curvature of liquid, Feldman et. al.[9]

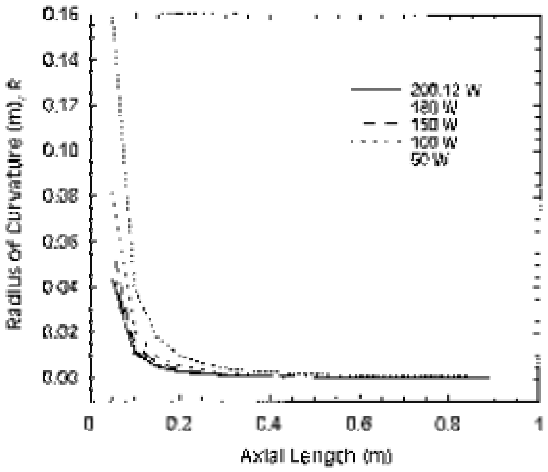


Fig. 6 Variation of curvature of radius along with axial position on the operating temperature of 290K

have shown the result that the curvature of meniscus decreases in the vapor-liquid interface of a evaporator due to the reduction of working fluid resulted from evaporating, but increases and approaches the limit to the infinite radius in the condenser region. It is shown that the results from the present study is good agreement with those of Feldman et. al[9].

Figure 7 shows the variation of wetting angle along with axial position on the operating temperature of 290K. From this figure, it can be seen that an increase of heat flow rate in the evaporator region raises the capillary pressure and decreases the radius of curvature, and thus makes a recession of liquid-vapor interface and results in the decrease of wetting angle. It can be also seen that the wet angle decreases in the evaporator.

Figure 8 shows that the heat flow in the evaporator region varies with the quantity of working fluid charged in the heat pipe. From this figure, it is shown that in the operating temperature of 290K, the heat transfer rate is the

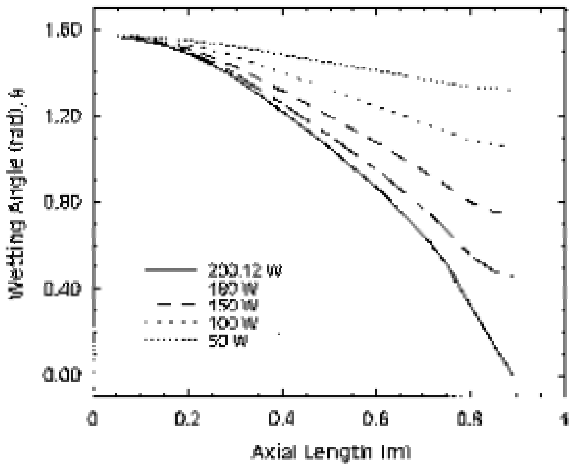


Fig. 7 Variation of wetting angle along with axial position on the operating temperature of 290K

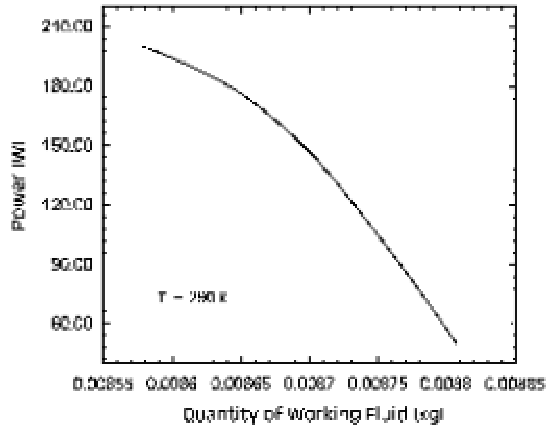


Fig. 8 Power versus quantity of working fluid

maximum value of 200.12 W for the working fluid quantity of 8.578g and decreases monotonically with an increasing quantity of working fluid. But the quantity of working fluid can be calculated easily from the Chi model[7] and is the analytical value of 8.854 g for the groove geometry of heat pipe. Therefore, it can be seen that for the maximum heat transfer rate, the working fluid quantity from this study is lower than that of Chi model[7]. And thus, when considering the recession of meniscus caused by the capillary pressure, the optimal quantity of working fluid has to be not calculated by Chi model[7] but by the estimation method of determining working fluid quantity of heat pipe suggested in the present study.

4. SUMMARY

In this study, the optimal mass of charging working fluid is carried out analytically for the axial grooved heat pipe using the working fluid of ammonia, and the concluding remarks are as follows.

1) As the heat flow rate in the evaporator increases, the capillary pressure rises and a decrease of the curvature radius and wet angle is confirmed in this study.

2) The optimal quantity of working fluid can be obtained by considering the recession of liquid-vapor interface caused by the capillary pressure and is the value of 8.578 g for the case of the grooved heat pipe used in the present work in the operating temperature of 290K. it can be seen that for the maximum heat transfer rate, the working fluid quantity from this study is lower than that of Chi model[7].

3) When considering the recession of meniscus caused by the capillary pressure, the optimal quantity of working fluid has to be not calculated by Chi model[7] but by the estimation method of determining working fluid quantity of heat pipe suggested in the present study.

Acknowledgements

This work is partially supported by Brain Korea 21 Projector, and ReCAPT.

References

1. Kemme, Josep E., 1969, "Heat Pipe Design Considerations", *Report LA-4221-MS*, Aug. 1, 1969, of the Los Alamos Scientific Laboratory of the University of California, Los Alamos, N. Mex., pp.1-8.

2. Tathgir, R. G. and Singth, G., 1984, "Performance Characteristics of a Stainless Steel Gravity Assisted Grooved Water Heat Pipe at Low Temperature", *the Proceeding of 5IHPC Part I*, pp.18-23.

3. Tetsuro Ogushi and Goro Yanmanaka, 1986, Heat Transfer Performance of Axial Grooved Heat Pipes, Trans. JSME , No.86-0252A, pp.600-607.

4. Shin, D. S, 1987, “An Experimental Study on the Optimal Quantity of Working Fluid in the Heat Pipe," *M.D.thesis*, Seoul National University.

5. Jung, J.Y., 1994, “An Experimental Study on the Characteristic of Heat Transfer in the Heat Pipe," *M.D.thesis*, Kyungbuk National University.

6. Lee, W., Park, Y.J., Suh, J.-S. and Kim, M.-G., 1997, "Analysis and Experiment for Thermal Performance of Grooved Heat Pipe," *Proci. the Air-Conditioning and Refrigeration Engng 1997 Summer Annual Meeting*, Vol. 2, pp.512-517.

7. Chi, S. W., 1976, *Heat Pipe Theory and Practice*, McGraw-Hill, NewYork.

8. B. H. Kim and C. J. Kim, 1995, "Design Optimization for the Performance Enhancement of Large Scale Thermosyphone", *KSME Journal*, Vol.9, No.3, pp.286 ~ 297

9. Feldman Jr, K. T. and Whiting, G. H., 1967, *The heat pipe*, Mechanical Engineering, pp.30-33.

10. Ivanovskii, M. N., Sorokin, V. P. and Yogodkin, I. V., 1982, *The Physical Principles of heat pipes*, Clarendon Press Oxford, pp.86-107

Effect of Rotational Acceleration on Internal Flow Patterns of Radially Rotating Heat Pipe at Normal Operating Condition

T. Katpradit*, N. Waowaew*, P. Terdtoon*, S. Maezawa**, P. Kamonpet*
and T. Wongratanapaisarn*

*Department of Mechanical Engineering, Faculty of Engineering, Chiang Mai University , Chiang Mai, Thailand 50200. Tel. +66-53-944151 Fax. +66-53-226014
Email: wao_narong @ hotmail.com
**Department of Mechanical Engineering, Faculty of Engineering, Seikei University , Kijijoji-Kitamachi Musashino-shi,Tokyo, Japan.

Abstract

The effects of rotational accelerations on the internal flow patterns of a radially rotating heat pipe (RRHP) at normal operating condition are considered in this paper. The RRHP used, employed a glass tube for the evaporator and half of the adiabatic section, and a copper tube for other half of adiabatic section and the condenser. The internal diameter of the RRHP was 11 mm. The aspect ratio was 20. The horizontal RRHP lay on the radial axis of rotation. R123 was used as the working fluid with a filling ratio of 60 % of evaporator volume. The selected rotational acceleration corresponded to 1g and 7g. The working temperature was 90 C. The experiments were conducted at inclination angles of 90, 50 and 0 degrees from the horizontal axis. Heat was removed from the condenser section by natural convection, while electrical heating was employed to supply heat to the evaporator section. A video camera was used to record all the flow patterns, while a still camera was used to record the internal flow patterns at specific times. Heat transfer rate was obtained by means of the input electrical power and from the heat loss at the evaporator section. It was found from the experimental results that the inclination angle had an effect on the internal flow patterns of the RRHP. For example, at the upper part of the evaporator section, the flow pattern was annular flow, and the film thickness decreased when the inclination angle decreased. In the middle and lower parts, when the inclination angle increased from 50 to 90 degrees, the flow pattern was bubble flow and the vapor sizes decreased i.e. Bond number decreased. In the middle and lower parts, when the inclination angle decreased from 50 to 0 degrees, the flow pattern was annular flow. The effect of the rotational acceleration on the internal flow patterns was that the internal flow patterns were bubble flow and annular flow. But at high rotational acceleration, the condensate quickly returned to the evaporator section and swept the liquid film at all times. These reasons give support for a high heat transfer rate of the RRHP.

Moreover, all the experimental results support the correctness of the correlation of Waoweaw et al.[3] as seen in equation (1) for the practical application of a RRHP.

Key words: Radially rotating heat pipe; Heat transfer characteristic

1. INTRODUCTION

Radially rotating heat pipe (RRHP) is an appropriate device for the rotary equipment. The RRHP employs evaporating and condensing process of working fluid, which uses the centrifugal force that generated by the rotation of the RRHP for the return of the liquid condensate from the condenser to evaporator section.

$$q^*_{90}=6x10^7\left(\left(\frac{Le}{d}\right)^{-0.65} Fr^{0.5} Bo^{-0.85} Ek^{0.1} Ja^{-0.15} Pr_l^{-0.35}\left(\frac{Cp_v}{Cp_l}\right)^{4.6}\left(1-\left(\frac{\rho_v}{\rho_l}\right)\right)^{0.19}\right)^{0.57} \quad (1)$$

The advantages of RRHP are, its properties of transferring heat in any types of rotary equipments, any orientations, its quicker response, and simple construct since its ithout
the internal wick structure. The heat transfer characteristics of the RRHP depend greatly on the internal flow patterns. Such as, slug flow has the heat transfer rate more than bubble flow [1]. Geometry, filling ratio, some working fluid and an inclination angle of a RRHP results in changes internal flow patterns and heat transfer characteristics. Moreover, the rotational

acceleration has affected heat transfer characteristics of the RRHP [2].

At present, the internal flow patterns of RRHP still cannot be clearly explained by any investigator.

It is our objectives to experimentally investigate the following aspects of RRHP. To clarify the internal flow phenomena and confirm many parameter in correlation of the RRHP [2];

- Effect of inclination angle on the internal flow patterns of RRHP at normal operating condition.
- Effect of rotational acceleration on the internal flow patterns of RRHP at normal operating condition.

2 EXPERIMENTAL SETUP AND PROCEDURE

Figure 1 shows an experimental setup of the RRHP. The electric power was employed to heat by means of silicone oil at the evaporator section and at the condenser section heat was naturally released by air. The evaporator and a half of adiabatic section were made of glass tube, and copper tube for condenser and a half of adiabatic section. The operating temperature of RRHP was controlled at 90 ^{Q}C.

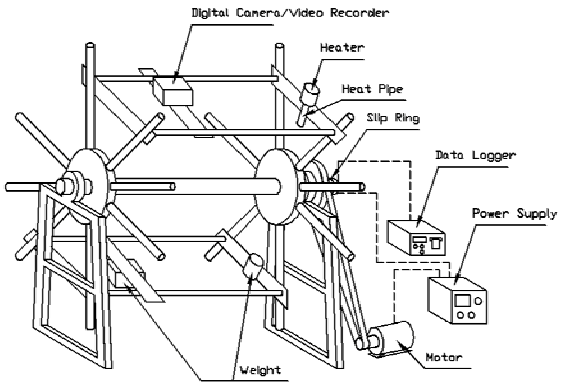


Figure 1 Experimental setup

A still camera was used to record the internal flow patterns at specific times, while a video camera was used to record the continuous internal flow patterns of the RRHP. The data logger (Comark C8510 with $\pm$0.2 % accuracy, 10 channel input and -100 °C to 1300 °C measurement temperature range) was used with type K thermocouples (Omega with $\pm$1°C accuracy) with one point attached to silicone oil at the evaporator section, one point to adiabatic section, two points to the condenser section and five points to the heat loss at the evaporator section. Ohm's law was used to calculate the heat transfer rate that had already been minuses the heat loss. The inverter (Omron 3G3JV, maximum applicable motor capacity 3.7 kW, frequency control range 0.1 to 400 Hz, frequency precision $\pm$0.01%) was used to adjust the motor speed. The rotational speed detector (Photo Type DT245P $\pm$ 0.05 % accuracy) was used to measure the rotational speed. During the experiment, the angle was adjusted between to 90^0, 50^0 and 0^0degree with respect to a rotating radial axis. When steady state was achieved, the temperature, rotational speed, DC voltage, DC Ampere and internal flow patterns were recorded. They were used to calculate the heat transfer and also the thermal resistance of the test RRHP by using the Ohm's law, as the following equations;

$$Q_{Transfer} = Q_{in} - Q_{loss} \quad (2)$$

$$Q_{in} = EI \quad (3)$$

and the Q_{loss} of evaporator section of RRHP was evaluated from the Fourier's law of conduction.

In order to thoroughly study, the effect of all parameters to internal
flow patterns, the controlled parameters were as follow:

- working temperature of 90^0C
- working fluid of R123
- filling ratio of 60% (by evaporator volume)
- internal diameter of 11 mm.
- Aspect ratio (Le/d) of 20

The variable parameters were as follow;

- inclination angle of 0^0, 50^0 and 90^0. (respect to the horizontal axis) rotational acceleration of equal to gravitational acceleration and seven times of gravitational acceleration were selected to obviously observe the effect of rotational acceleration on the flow patterns of the RRHP. However, there occur some superimposed phenomena different, such as merging, breaking, expanding, collapsing and swaying of the vapor bubbles with the flow patterns. These flow patterns can be observed and defined from the pattern that often occured in video movie.

Although, the heat transfer rate of the RRHP results were somewhat higher than the experimentally results of the RRHP performance [2]. But the heat transfer rate of the RRHP in this result has the same trend and based on the same experimental standard. So, it can be used to compare with each other. However, the flow patterns were obtained, there occur some superimposed phenomena different, such as merging, breaking, expanding, collapsing and

swaying of the vapor bubbles, these flow patterns can be observed and defined from often occur in video movie.

Although, the heat transfer rate of the RRHP results were somewhat higher than the experimentally results of the RRHP performance [2]. But the heat transfer rate of the RRHP in this result has trend to be the same and base on the same experimental standard. So, it can be compared.

3. RESULTS AND DISCUSSIONS

To clarify the effect of inclination angle and rotational acceleration on internal flow pattern of the RRHP, experiment results of di = 11 mm, Le/d = 20, inclination angle of 90^0, 50^0 and 0^0, rotational acceleration = 1 and 7 times of gravitational acceleration will be considered. In order to clearly understand, the part of vertical will be designated as lower, middle and upper parts corresponding to such parts, while the positions of the inclined RRHP will be called as the wind buffet and wind trailing side. In order to clearly understand the different angle and quadrant will be defined as in Figure 2. The photographs were selected at nearly inclination of 90 degree.

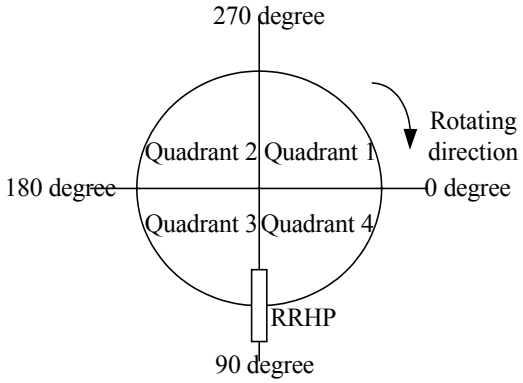


Figure 2 The angle reference of RRHP

The effect of inclination angle on internal flow patterns of RRHP will be firstly discussed.

3.1 Effect of inclination angle on internal flow patterns of RRHP.

Figure 3 shows internal flow patterns of the RRHP with a di = 11 mm, Le/d = 20, inclination angle of 0^0, 50^0 and 90^0, rotational acceleration of 7 times of gravitational acceleration. From the visualization results, it was found that, the flow patterns could be mainly divided into 2 categories.

3.1.1 At inclination angle of 90 to 50 degree

Figure 3A. shows the internal flow patterns of the RRHP. It can be observed that at vertical position, and a heat flux of 23.6 kW/m^2, the flow pattern in the lower and middle parts of the evaporator was bubble flow while that of the upper part of the evaporator was annular flow. The boiling was violent and small-sized vapor bubbles occupied the majority of the evaporator section and quickly swayed from the wind buffet to the wind trailing side at about 1.6 times/sec, due to the effect of inertia force of the liquid. At the upper part, although the annular flow dominated, it can be observed that the liquid film of the condensate that returns to the evaporator from the condenser section was not smooth. Droplets fell directly onto the liquid pool because of the effect of rotational acceleration as shown in Figure 3A.

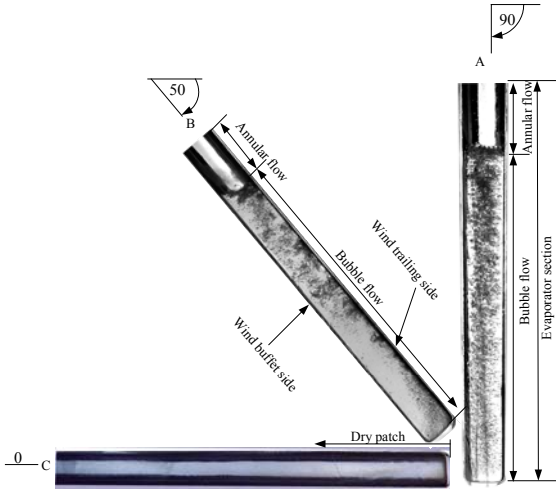


Figure	A	B	C
β degree	90	50	0
Tv (^{o}C)	90	90	90
q (kW/m^2)	23.6	19.2	-

Figure 3 Internal flow patterns of RRHP at 7g

At an inclination angle of 50 degrees, it can be observed that, the flow pattern in the lower and middle parts of the evaporator was bubble flow while at the upper part of the evaporator, annular flow dominated. At a heat flux of 19.22 kW/m^2, the boiling was violent and small-sized vapor bubbles collapsed at the wind trailing side of the lower part of the evaporator section. After that, vapor bubbles were found all over the middle part of the evaporator section. But the vapor bubbles were large and the liquid-vapor interface

was not smooth when compared to the middle part of the evaporator section at vertical position as shown in Figure 3B.

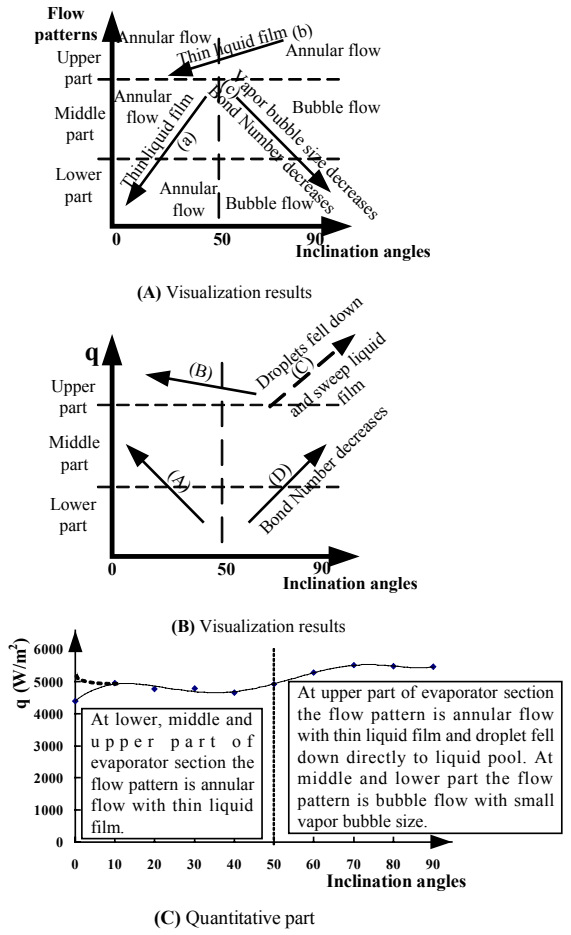


Figure 4 Comparison qualitative and quantitative part

3.1.2 At inclination angle of 50 to 0 degree

At an inclination angle of 0 degrees, it can be observed that there was no liquid in the evaporator section. Dryout occurred at the upper end of the lower part of the evaporator section as shown in Figure 3C. The flow pattern was annular flow. The heat transfer of the RRHP could not be measured because the vapor temperature continually decreased. The cause of the dryout was due to inertia force of liquid being smaller than the rotational acceleration force. The liquid at the evaporator totally evaporated, but the condensate could not return to the evaporator section. It can be illustrated as a graph as shown in Figure 4.

Comparing this qualitative result with the obtained correlation or the quantitative research of Waowaew et al.[3] as in equation (1), it can be seen that the inclination angle affects the heat transfer of a RRHP. The inclination angle affects the liquid film thickness and the rate of return to the evaporator section or Bond number as shown in Figure 4A-4C.

Figure 4A shows the effect of the inclination angle on the flow pattern of the RRHP. The x-axis shows the inclination angle from 0 to 90 degrees. The inclination angle of 50 degrees was selected for this study due to this angle corresponding to the flow pattern as shown in Figure 3B. The y-axis represents the flow pattern; it is divided into three regions of the evaporator section. At the upper part of the evaporator section, the flow pattern was annular flow with a slightly decreased film thickness. Arrow line b shows the decrease in the inclination angle. At the middle and lower parts, when the inclination angle increased from 50 to 90 degrees, the flow pattern was bubble flow with a decreased vapor size i.e. Bond number $\left(Bo = d\left[\frac{g(\rho_l - \rho_v)}{\sigma} \right]^{\frac{1}{2}} \right)$, which is shown in the right hand third term of the equation, (1) slightly decreases, which is indicated as arrow line c due to it being directly proportional to the diameter of the vapor bubble. As the inclination angle decreased from 50 to 0 degrees, the flow pattern at the middle and lower parts of the evaporator section was annular flow where the film thickness at the upper side quickly decreased as shown in Figure 4A. Figure 4B connects the flow patterns in Figure 4A to the heat flux corresponding to each flow pattern. The effects of the inclination angle on the heat flux were plotted on a graph. At the upper part of the evaporator section, the heat flux increased when the inclination angle decreased from 50 to 0 degrees as shown by arrow line B, and the heat flux increased when the inclination angle increased from 50 to 90 degrees. Droplets fell directly onto the liquid pool and swept the liquid film at the upper part of the evaporator section. This caused an increase in the heat flux. It is represented by light arrow line C as shown in Figure 4B. The A and B lines indicate increasing heat flux that correspond to a and b lines in Figure 4A. The thin liquid film easily evaporated, this caused a high heat transfer. Line D indicates the increasing heat flux, which was affected by decreasing vapor bubble diameter i.e. Bond number decreases. Figure 4C shows the effect of the inclination angle on the heat flux of the RRHP, which is in agreement with the experimental results of Waowaew et al [3]. It can be seen that, when the inclination angle increased from 40 to 90 degrees, the heat flux increased from 4.8 to 5.2 kW/m^2 and when the inclination angle decreased from 40 to 10 degrees, the heat flux increased from 4.8 to 4.9

kW/m^2. But at an inclination angle of 0 degrees, the heat flux was lower than 10 degrees because initial dryout occurred, which can be seen from the fact that the condenser temperature decreased by 12 ^{o}C.

By comparing figure 4B and 4C, it can be seen that the effect of the inclination angle on the heat flux has a similar trend. For example, when the inclination angle increased from 40 to 90 degrees, the heat flux increased from 4.8 to 5.2 kW/m^2 and when the inclination angle decreased from 40 to 10 degrees, the heat flux increased from 4.8 to 4.9 kW/m^2. From figure 4C, it can be seen that at an inclination angle of 0 degrees the heat flux was lower than 10 degrees. If initial dryout does not occur, the heat flux increases as shown by the dotted or light line. It can be seen that the qualitative results, as shown in Figure 4B, support the previous quantitative conclusion.

3.2 Effect of rotational acceleration on internal flow patterns of the RRHP

Figure 5 shows internal flow patterns of the RRHP with a di = 11 mm, Le/d = 20, inclination angle of 90^0, rotational acceleration of 1 and 7 times of gravitational acceleration. From the visualization results, it is found that,

3.2.1 At low the rotational acceleration

Figure 5A shows the internal flow pattern of a RRHP at a rotational acceleration of 1 time that of gravitational acceleration. It can be observed from the video taken that the flow patterns in the lower and middle parts of the evaporator section depended on the rotating position of the RRHP. Namely, vapor bubbles slowly swayed from the wind buffet to the wind trailing side at about 0.6 times/sec. But when the RRHP rotated to a quadrant of 1, bubble flow at the wind trailing side changed to intermittent slug flow. The heat flux was 7.7 kW/m^2, the boiling was not violent and large-sized vapor bubbles occupied the majority of the evaporator section compared to that of a rotational acceleration of 7 times . The flow pattern in the upper part of the evaporator section was annular flow and rivulet liquid film slowly flowed down to the liquid pool. When the RRHP rotated to quadrants 1 and 2, the liquid - vapor interface swung backward and forward according to the direction of rotation. This introduced a sharp liquid wave in the middle of the tube. The crest of this sharp and high wave easily broke into many droplets, which returned to the pool. The vapor bubbles swayed from the wind buffet to the wind trailing side when the RRHP rotated passed the angles of 90 and 270 degrees.

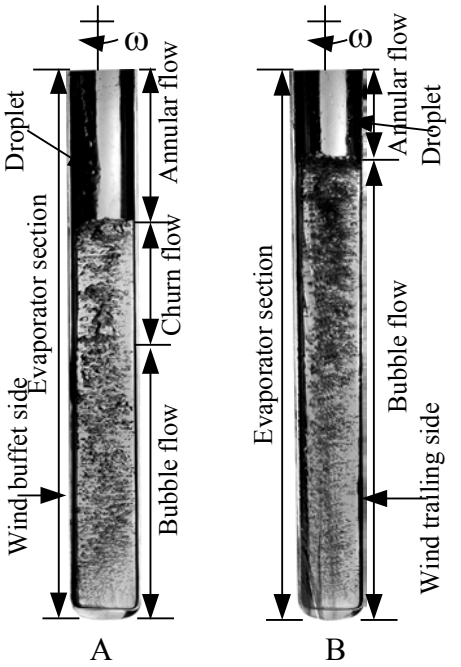


Figure	A	B
$\varpi^2 R$	1g	7g
Tv (^{o}C)	90	90
q (kW/m^2)	7.7	23.6

Figure 5 Internal flow patterns of RRHP at 90 degree

3.2.2 At high the rotational acceleration

Figure 5B shows the internal flow pattern of a RRHP at a rotational acceleration of 7 times that of gravitational acceleration. It can be observed that the flow pattern in the lower and middle parts of the evaporator was bubble flow while at the upper part of the evaporator the pattern was annular flow. At a heat flux of 23.6 kW/m^2, boiling was violent and small-sized vapor bubbles occupied the majority of the evaporator section and quickly swayed from the wind buffet to the wind trailing side at about 1.6 times/sec. At the upper part, although annular flow dominated, it could be observed that the liquid film from the condenser section was not smooth. Droplets fell directly onto the liquid pool because of the effect of rotational acceleration as shown in Figure 5B.

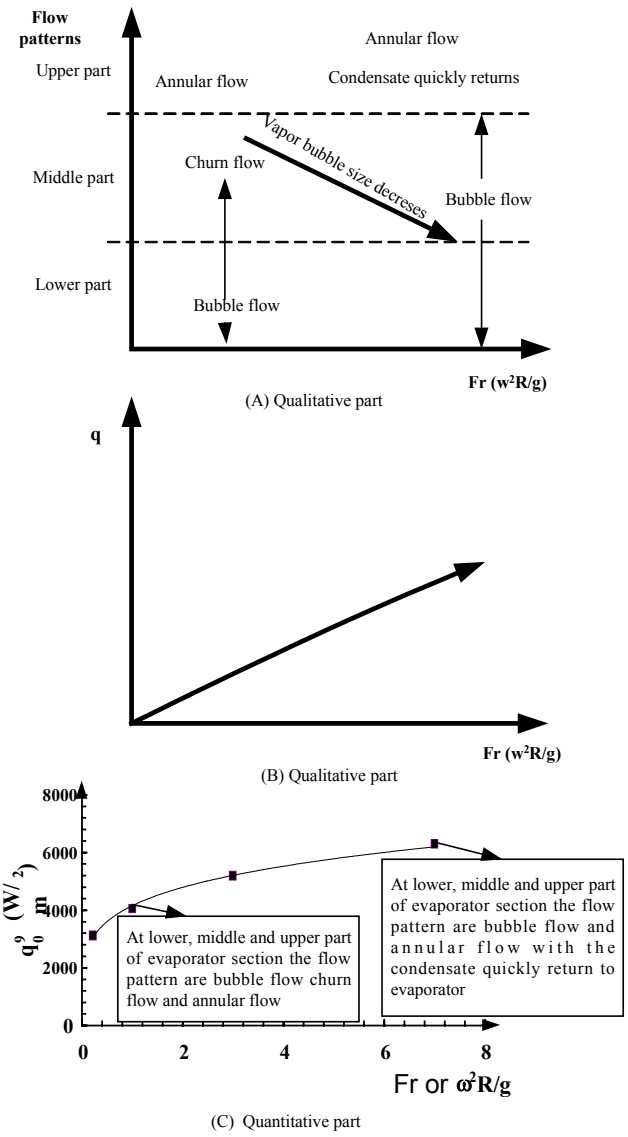


Figure 6 Comparison qualitative and quantitative part

The liquid - vapor interface was smooth when compared to the liquid - vapor interface of the rotational acceleration of 1 time. The liquid pool level of the RRHP at a rotational acceleration of 7 times that of gravitational acceleration was higher than that of a rotational acceleration of 1 time and covered about 17 % of the evaporator section. This is because at a rotational acceleration of 7 times that of gravitational acceleration, the amount of condensate that returned to the evaporator was higher than that of at 1 time, and it could return to the evaporator section at a quicker rate than that of the rotational acceleration of 1g.

Comparing these qualitative results with the quantitative research of Waowaew et al.[3], which is shown in the right hand third term of equation (1), it was found that the rotational acceleration affects the heat transfer of a RRHP. The g affects the vapor bubble size and the liquid return to the evaporator section as shown in Figure 6A-6C.

Figure 6A shows the effect of Froude number i.e. $\varpi^2 R / g$ or rotational acceleration on the flow patterns of a RRHP. The x-axis shows Froude numbers 1 and 7 and is related to the flow patterns shown in Figure 5. It can be seen that at these Froude numbers different flow patterns occur.

The y-axis shows the flow patterns; it is divided into the three regions of the evaporator section. At the Froude number of 1, at the upper part of the evaporator section, the flow pattern is annular flow. At the middle and lower parts the flow pattern is churn flow and bubble flow respectively. When the Froude number increases to 7, at the upper part of the evaporator section, the flow pattern is annular flow and at the middle and lower parts the flow is bubble with a decreased vapor bubble size as shown by the arrow line. This is because at a high Froude number or high initial force, there is high liquid density of the w orking fluid, this affects the mix of vapor bubbles and a quicker rate of condensate return to the evaporator section occurs. Figure 6B shows the connections of the flow patterns in Figure 6A to the heat flux corresponding to each flow pattern. As the Froude number increases, the heat flux increases too. This is because at a high Froude number, high liquid density of the working fluid, high liquid pressure and high boiling point affects supplies heat of a RRHP and one reason, to keeps the operating temperature of the RRHP.

The heat flux increase is connected to the vapor bubble size; as the vapor bubble size decreases the Bond number also decreases (see section 3.1) and when the length of the evaporator section is short, the vapor bubble size is smaller than that of an evaporator section of a longer length. Figure 6C shows the effect of Froude number on heat flux from the experimental results and the quantitative part. The x-axis shows Froude numbers of 0.2 to 7. The y-axis shows the experimental heat flux results of Waowaew et al. [3] as in equation (1), which is the power function form relationship of q and Fr. When comparing Figure 6B and 6C, it can be seen that the heat flux trend increased as the Froude number increased. An arrow line showing the heat flux increasing trend, as seen in Figure 6B, is a linear line representing the prediction of the vapor bubble size decrease and the quick return of the condensate to the evaporator section from an arrow line in Figure 6A.

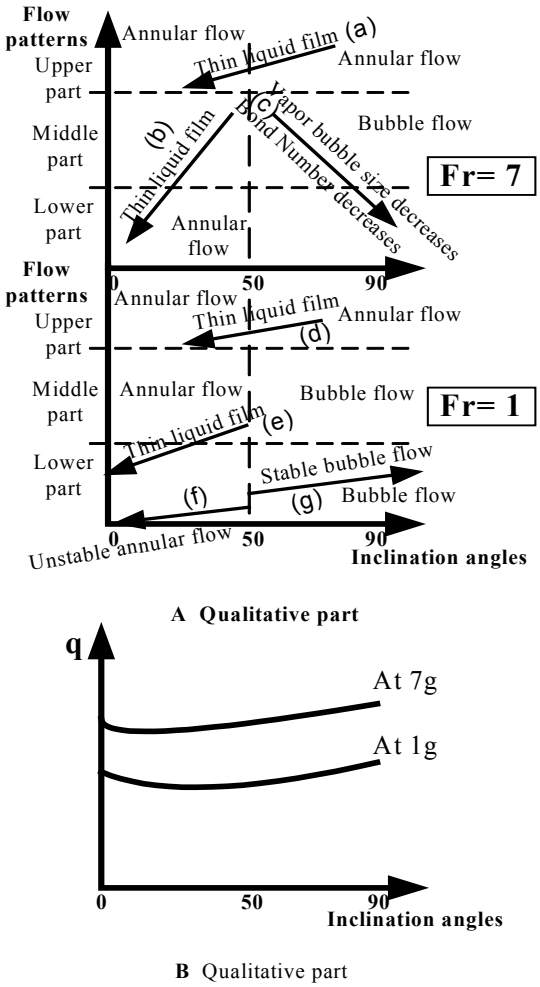


Figure 7 qualitative experimental results

The effect of the rotational acceleration on the internal flow patterns was: when the rotational acceleration of 1g changed to 7g, as shown in Figure 6A, the internal flow patterns of bubble flow, churn flow and annular flow changed to bubble flow and annular flow. The condensate quickly returned to the evaporator section. The effect of the rotational acceleration on the heat fluxes was: the heat flux increased when the rotational acceleration increased, as shown in Figure 6B-6C. It corresponds to the Froude number in the correlation of Waowaew et al.[3] as shown in equation (1). Namely, when the omega in Froude number in a correlation increases the heat flux increases too.

Figure 7 shows the conclusion of the qualitative experimental results obtained from section 3.1 and 3.2. Figure 7A shows the effect of the inclination angle on the flow patterns of the RRHP, which is an imbrication of Figure 4A and 6A at the rotational acceleration of 1g and 7g. This Figure is constructed to show the conclusion of the effect of the inclination angle and the rotational acceleration on the flow pattern of the RRHP. Figure 7B shows the connection of the flow patterns in Figure 7A to the heat flux corresponding to each flow pattern and inclination angle. The decreasing rate of thin liquid film line at the upper part of the evaporator at 7g (shown as arrow line a) was higher than that of 1g (shown as arrow line d). It was similar to the thin liquid film line at the inclination angle of 0 to 50 degrees (shown as arrow line b and e). This occurs because at Froude number 7 there is more inertia than a Froude number of 1, which directly affects the liquid film. The stable bubble flow arrow line (g line) is an indication that the inclination angle was approaching vertical position. The flow pattern was continuous bubble flow. The stable annular flow arrow line (f line) is an indication that the inclination angle was approaching horizontal position. The flow pattern was continuous annular flow because the liquid film continually swayed from the evaporator section to the condenser section, depending on the rotating position of the RRHP.

4. CONCLUSIONS

The effects of inclination angle, rotational acceleration and aspect ratios on the internal flow patterns of a RRHP at normal operating condition were experimentally investigated in this paper. When it is known the effect of each parameter has on the inside phenomena and internal flow patterns of a RRHP then it will be possible to correctly predict the condition by establishing a mathematical model. It was found from the experimental results that; the effects of inclination angle on internal flow patterns of a RRHP can be divided into 3 regions.

1. In the upper part of the evaporator section, the flow pattern is Annular flow with a decrease in the film thickness when the inclination angle decreases.

2. In the middle and lower parts, when the inclination angle increases from 50 to 90 degrees, the flow patterns is bubble flow with a decrease in vapor size i.e. Bond number is decreased.

3. In the middle and lower parts, when the inclination angle decreases from 50 to 0 degrees, the flow patterns is annular flow.

The effects of inclination angle on the heat flux is; at the rotational acceleration of 7g, the inclination angle of 50 degrees to 90 degrees, the heat flux changes from 19.2 to 23.6 kW/m^2. At the inclination angle of 0 degrees dryout occurs. The effect of the rotational acceleration on the internal flow patterns is; the internal flow patterns are bubble flow and annular flow. But at high rotational acceleration the condensate quickly

returns to the evaporator section and the liquid film is swept all time. The effect of the rotational acceleration on the heat flux is; at the rotational acceleration of 1g to 7g, the heat flux changes from 7.7 to 23.6 kW/m^2.

Moreover, all the experimental results support the correlation of Waoweaw et al.[3] as shown in equation (1) and the practical application of a RRHP.

5. NOMENCLATURE

Bo	Bond number = $d_i(g(\rho_l-\rho_v)/\sigma)^{0.5}$
E	electric voltage, Volt
I	electric current, Ampere
Fr	Froude number = $\varpi^2 R / g$
Q	heat transfer rate, W
Q_{lose}	conduction heat transfer rate of insulator, W
R	radial of rotation, m
ρ_l	liquid density of the working fluid, kg/m^3
ρ_v	vapor density of the working fluid, kg/m^3
σ	surface tension of the working fluid, N/m
ω	Angular velocity, rad/s

Acknowledgement

The research has been supported by the Royal Golden Jubilee Project of the Thailand Research Fund under the contract number PHD/0135/2543. The authors would like to thank for all supports.

References

1. Terndtoon, P., Chailanga, M., *Effect of Aspect ratios on Internal Flow Patterns of an Inclined Closed Two-Phase Thermosyphon at Normal Operating Condition.* Jour. Of Heat Transfer Engineering Taylor & Francis.

2. Maezawa, S., Yamaguchi, A., and Gi, K., (2002). *Condensation Heat Transfer on Radially Revolving Heat Pipe.* 12th International Heat Pipe Conference, Russia.

3. Waowaew, N., Terndtoon, P., S. Maezawa, S., Kamonpet, P. and W. Klongpanich, W., (2003). *Correlation to Predict Heat Transfer Characteristics of A Radially Rotating Heat Pipe at Vertical Position* J. Applied Thermal Engineering, Elsevier Science, Vol. 23, Issue 8, pp 1019-1032.

Study on the Heat Transfer Characteristics in a Copper-Water Variable Conductance Heat Pipe with Non-condensable Gas Reservoir

Ki-Ho Park*, Ki-Woo Lee*, Wook-Hyun Lee*, Kye-Jung Lee*, Jeong-Se Suh**

*Waste Heat Utilization Research Center, Korea Institute of Energy Research
71-2 Jang-dong, Yuseong-gu, Daejeon, 305-343 Korea
Phone : 82-42-860-3311, Fax : 82-42-860-3133, E-mail : ghpark@kier.re.kr

**Gyeongsang National University, Chinju, Kyongnam 660-701, Korea

Abstract

This paper is to research the heat transfer characteristic in a copper-water variable conductance heat pipes(VCHP) with a non-condensable gas and gas reservoir. The heat transfer characteristics in the VCHP have not yet been studied much researches. VCHP is used in many applications: thermal control of systems on satellites, semiconductor and telecommunication. VCHP has been able to apply for cooling of PCS base station system which has needed seriously variation of temperature in station system according to unseasonable weathers. The practical use of VCHP is a simple way to control the temperature of satellites. In this study, experimental investigations were performed to research the characteristics of variable conductance heat pipes with non-condensable gas reservoir and VCHP is fabricated, the heat transfer characteristic is evaluated. Distilled water was used as working fluid and nitrogen as non-condensable gas(NCG). When the quantity of non-condensable gas increases, the beginning operating temperature rises and it is seen a rise in wall temperature of all section of VCHP. As the quantity of working fluid increases, limitation power increases a little, but there is no difference in the wall temperature on evaporator section at the same input heat load. When the input heat load increases, it is seen the enlargement of the active portion of condenser section.

Key words: Variable conductance heat pipe, Heat pipe, Non-condensable gas, Working fluid

1. INTRODUCTION

The heat pipe, a sealed slender tube, transfers a large amount of heat by latent heat, which is poured the working fluid, is vaporized under low temperature in vacuum, operated with small temperature difference. Especially, because it is easy to attach fins on the evaporator and the condenser sections for the enlargement of the heat transfer surface area, it is effective to make the high efficiency of various cooling system and heat recovery technologies. The heat pipe is applied to very important technology for cooling system of advanced electronic equipment and semiconductor. A conventional heat pipe has severe variation of the operating vapor temperature in evaporator and condenser sections according to the heat load input. It is difficult to maintain constantly the operating temperature in a conventional heat pipe when thermal environment is varied severely. VCHP can be used in many applications: systems on satellites, semi-conductor and telecommunicati -on. VCHP has been able to apply for cooling of PCS base station system which has seriously variation of temperature in station system according to unseasonable weathers. A VCHP consists of container, working fluid and NCG, and has two heat transfer regions; evaporator and condenser. The condenser section is divided into active and inactive portion. An increase of heat load input causes an increasing vapor temperature and operating pressure. Hence, the length of the active portion of the condenser will be increased also. A VCHP is needed an optimal design, which can remove heat at varying heat rates and maintain constant temperature in evaporator and operating temperature. In this study, VCHP, which is based on the design theory with the noncondensable gas reservoir is designed, fabricated and has been performed to investigate the heat transfer performances according to the amount of NCG and the working fluid quantity.

2. THEORY

In order to control its operating temperature and conductance the commonly used methods are liquid-flow modulated, a vapor-flow modulated heat pipe and a gas loaded heat pipe. Figure 1

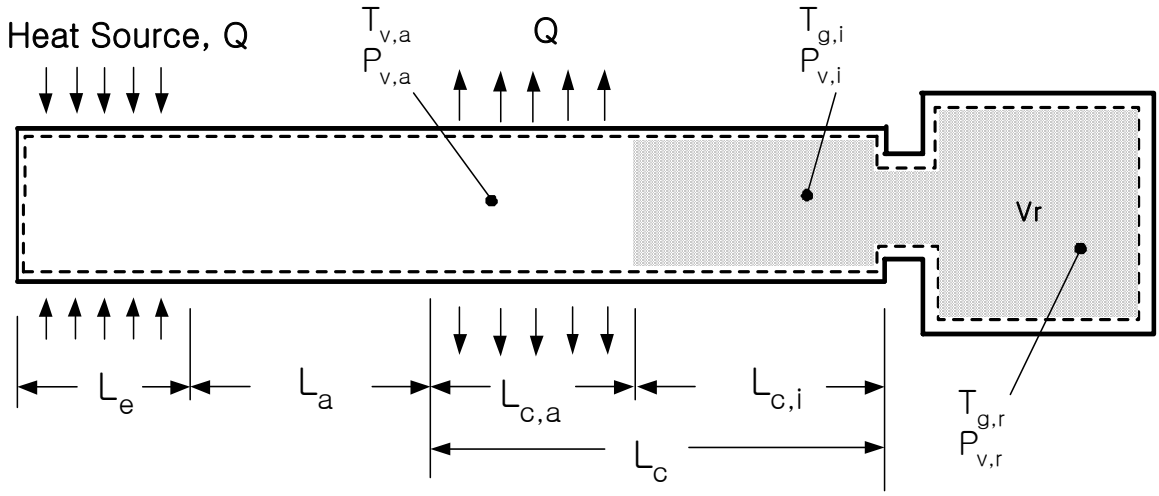


Fig. 1. Schematic diagram of variable conductance heat pipe with gas reservoir

shows a schematic of a gas-loaded heat pipe. In this figure, non-condensable gas in the right side of condenser section is in equilibrium the vapor pressure changed according to operating temperature of working fluid. When the heat load input increases, the temperature of working fluid increases and the vapor pressure rises. If the vapor pressure increases, the active length of the condenser section increases. Therefore, increasing the active length of the condenser section has the effect of the enlargement of the heat transfer surface area. As a result, lots of heat can be dissipated through the condenser section. On the contrary, when the heat load input decreases, the active length of the condenser section decreases. It causes a decreasing of the heat transfer rate. An interface area between the vapor and noncondensable gas shows the complex aspects. In this study we apply a flat front mode. In the VCHP the heat transfer rate dissipated through the condenser section can be expressed by equation(1).

$$Q = h_c C_p L_{c,a} (T_{v,a} - T_{s,c}) \quad (1)$$

The active length of the condenser section, Lc,a , is the decisive variable, determined the operating temperature by heat load input. To determine the active length of the condenser section, we apply the gas law to the non-condensable gas, which resides partly in the active portion of the condenser and partly in the gas reservoir.

$$m_g = P_{g,r} V_r/(R_g T_{g,r}) + P_{g,r} A_v (L_c - L_{c,a}) /(R_g T_{g,r}) \quad (2)$$

The first term of in the right side is the mass of the non-condensable gas in the gas reservoir, the second term is the mass of the non-condensable gas in the inactive portion of the condenser section. From Dalton's theory, *Pg,i*, *Pg,r* are expressed as follows:

$$P_{g,i} = P_{v,a} - P_{v,i}$$
$$P_{g,r} = P_{v,a} - P_{v,r} \quad (3)$$

Substitution of *Pg,r* and *Pg,i* from Equation (3) into Equation (2) followed by rearrangement results in the following expression.

$$L_{c,a} = L_c - m_g R_g T_{g,i} /((P_{v,a} - P_{v,i}) A_v) + V_r T_{r,i} (P_{v,a} - P_{v,i})/(A_v T_{g,r}(P_{v,a} - P_{v,I})) \quad (4)$$

3. EXPERIMENT

3.1 Experimental apparatus

Copper/water VCHP with non-condensable gas reservoir of diameter 6 mm is fabricated as shown in Table 1 and tested. The VCHP is tested

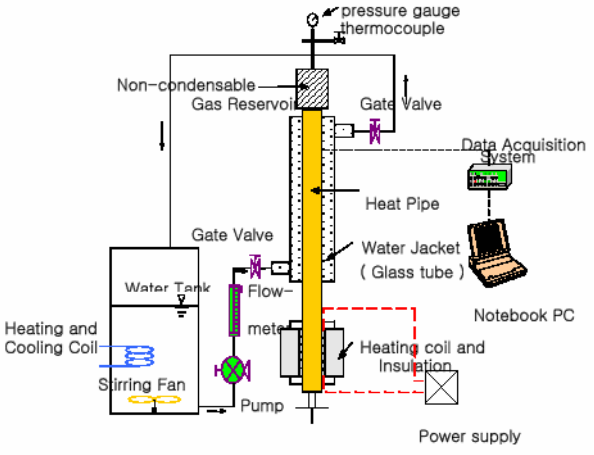


Fig. 2 Experimental apparatus

Table 1 Parameters of VCHP

Parameters	Specification
Container	
Material	Copper
Pipe diameter	6 mm(OD)
Total length	400 mm
Length of evaporator section	80 mm
Length of adiabatic section	60 mm
Length of condenser section	260 mm
Reservoir volume	3.4 x 10^{-6} m^3
Working fluid	Distilled water
Inclination angle	90°
Cooling water	15℃

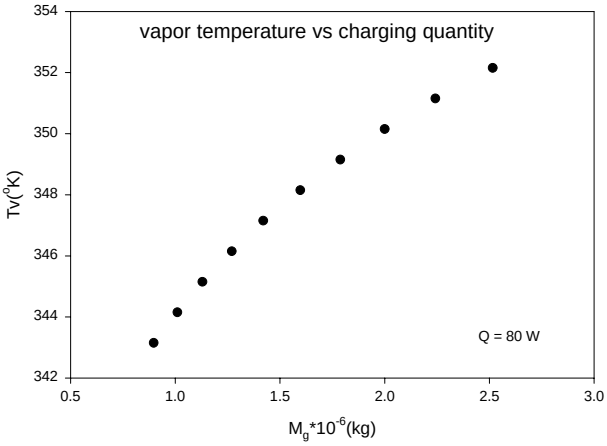


Fig. 3 Variation of vapor temperature with non-condensable gas quantity

vertically at horizon. Effective length of VCHP is 400 mm, evaporator section is 80 mm, adiabatic section is 60 mm, and condenser section is 260 mm. Copper/water VCHP, which are 6 mm outside diameter and 400 mm of effective length of VCHP, 260 mm of the condenser sectional length of heat pipe and 80 mm of the evaporator sectional length of pipe mm, 60 mm of adiabatic section and 3.4 x 10^{-6} m^3 of the non-condensable gas reservoir, is fabricated, the heat transfer characteristic is evaluated. Distilled water was used as working fluid and nitrogen as non-condensable gas(NCG), their amounts are determined by numerical results, and it is chosen because of low cost, non-toxity and high latent heat. The quantities of NCG are from 1.5 x 10^{-6} kg to 1.9 x 10^{-6} kg. Air inside pipe was removed by a vacuum pump to a pressure of 10^{-4} torr. Fig 2 is a schematic of experimental apparatus for a performance of VCHP. Experimental apparatus consists of a VCHP, a data acquisition unit, a constant temperature cooling water bath. Electricity is supplied to nichrome wire(4.5Ω /m), which is wrapped around evaporator section, by the variable voltage adjuster. It is once insulated with the cerak wool(k=0.075W/m℃) and then with urethane foam in order to minimize heat loss. The temperature of vicinity nichrome wire and the outside temperatures are measured to calculate heat loss. Once the adiabatic section is wrapped by insulation tape, and it is connected to the inclination angle adjuster made of insulation material of teflon. Water in constant temperature cooling water bath (heating capacity:750W, cooling capacity:250W) is supplied to the condenser section for sufficient cooling. For cooling, the condenser section is covered with a water jacket, which is a pyrex tube of 260mm length and 15mm diameter, and the tube is insulated with 10mm thick urethane. Heating rate, surface temperatures at each section, saturation temperature and inside pressure are measured to investigate the characteristic. In order to measure them, thermocouples are sticked to each section. In evaporation section three thermocouples are arranged at 20mm interval. Two thermocouples are also arranged at 20mm interval in adiabatic section, and seven thermocouples in condenser section are arranged at 30mm interval.

3.2 Experimental method

Experiment is performed at bottom heat mode and vertically at horizon. Heating rate, surface temperatures at each section, are measured to investigate the heat transfer characteristic and the variation of active portion of condenser section. The saturation temperature and the inside pressure at a boundry between adiabatic and condenser sections are measured to investigate the variation of the saturation vapor temperature. In order to measure them, thermocouples are sticked to each section, and data from these thermocouples are memorized in PC through the data acquisition system(DR230 Hybrid recorder, YOKOGAWA). Moreover, heat transfer rate at the condenser section is estimated by temperature difference between the inlet and outlet of cooling water.

Heat is loaded at interval 10W from 10W to estimate heat limitation for VCHP, and surface temperatures at evaporator and condenser section, temperatures at inlet and outlet of cooling water are measured to investigate the VCHP performance. Experiment is stopped at about 110℃ on the evaporator section, although temperature does not rise steeply, it is also stopped at dry-out condition regardless of temperature.

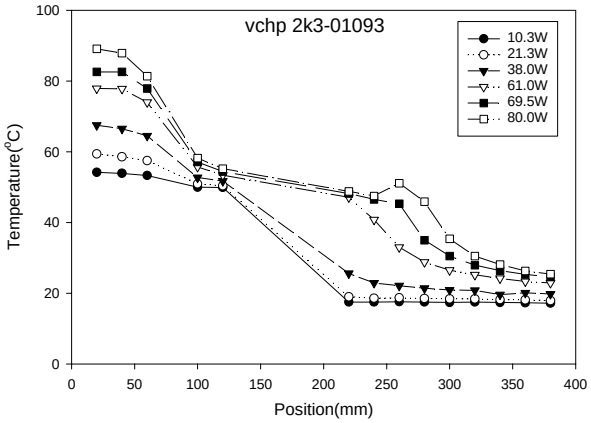


Fig. 4 Wall temperature distribution($1.5x10^{-6}$kg)

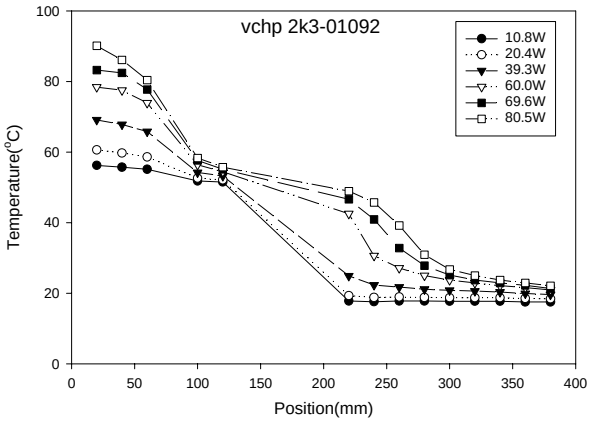


Fig. 5 Wall temperature distribution($1.7x10^{-6}$kg)

4. RESULTS AND DISCUSS

Figure 3 shows the predicted result of the variation of vapor temperature with the non-condensable gas quantity. In this figure, it can be seen that operating temperatures increases with increase of the mass of NCG. Inner vapor pressure

of VCHP increases with increase of the quantity of NCG. VCHP is considered to be operated when the operating vapor pressure is larger than the pressure of NCG. As the mass of NCG is large, the operating vapor temperature rises and inner

volume occupied inside of the condenser section is increased. Therefore, the active portion of heat transfer is increased with rising the operating temperature. Distribution of wall temperature at the mass of NCG, 1.5 x 10^{-6} kg, the working fluid

quantity, 2.5 cc, are shown in Fig. 4. When input heat load is 61W, wall temperature at

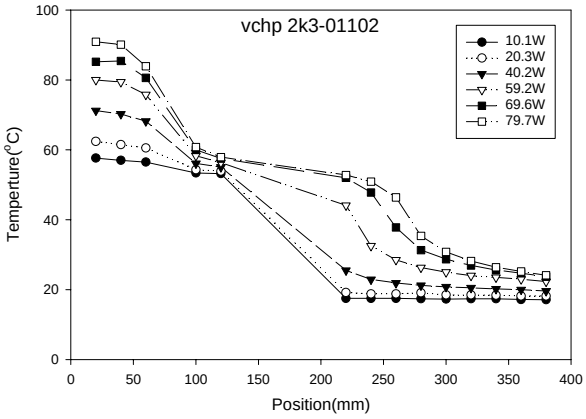


Fig. 6 Wall temperature distribution($1.9x10^{-6}$kg)

evaporator section is 77.7℃, adiabatic section is 55.7℃, when input heat load is 69.5W, wall temperature at evaporator section is 82.6℃, adiabatic section is 57.2℃, when input heat load 80W, wall temperature at evaporator 87.5℃, adiabatic section 58.2℃. When the input heat load changes from 60 W to 80W, wall surface temperature of evaporator section changes about 10 ℃. The temperature variation rate of wall temperature on evaporator section is found to be low from the increment temperature, ±5℃ at 70W±10W.

Distribution of wall temperature at the mass of NCG, 1.7 x 10^{-6} kg, the working fluid quantity, 2.5 cc, are shown in Fig. 5. When the input heat load is 60W, wall temperature at evaporator section is 78.3℃, adiabatic section is 56.3℃, when input heat load is 69.6W, wall temperature at evaporator section is 82.9℃, adiabatic section is 57.6℃, when input heat load 80W, wall temperature at evaporator 83.5℃. When the temperature of evaporator end section is rised, it is seen dry-out state. Although the difference of wall temperature is quite small, wall temperature of each section is a little higher than the case of Fig. 4. When input heat load is 10W, wall temperature of evaporator and adiabatic section is higher about 2-3℃ than these of Fig.4. As expected in the prediction, it can be seen that operating temperatures increases with increasing the mass of NCG. Inner vapor pressure of VCHP increases with increasing the quantity of NCG. VCHP is considered to be operated when the operating vapor pressure is larger than the pressure of NCG. As the mass of NCG is large, the operating vapor temperature rises and inner volume occupied inside of the condenser section is increased. Therefore, the active portion of heat transfer is decreased with rising the operating temperature. Figure 6 and Figure 7 show the distribution of wall temperature at the mass of NCG, 1.9 x 10^{-6} kg, the working

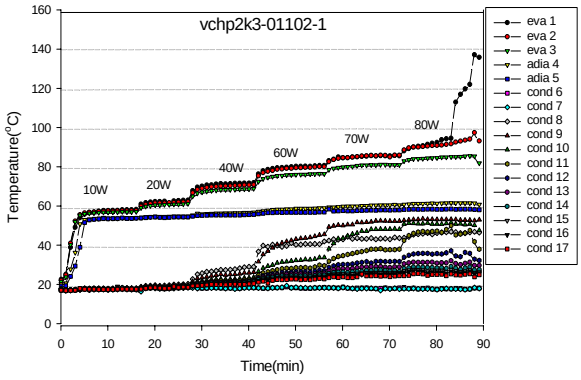


Fig. 7 Wall temperature distribution(2.5cc)

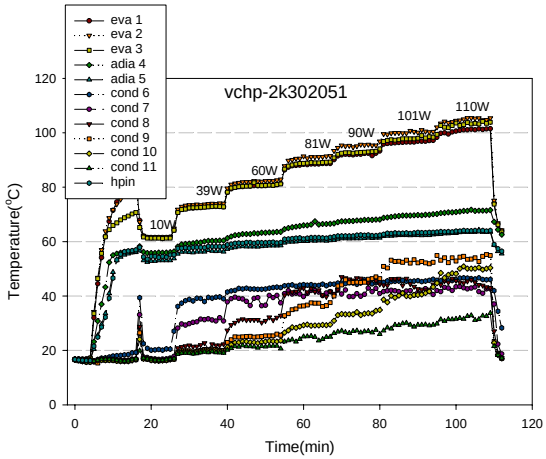


Fig. 8 Wall temperature distribution(2.8cc)

fluid quantity, 2.5 cc. When input heat load is 59.2W, the wall temperature at the evaporator section is 79.7℃, adiabatic section is 58.2℃, when input heat load is 69.6W, wall temperature at evaporator section is 85.3℃, adiabatic section is 58.2℃, when input heat load 79.7W, wall temperature at evaporator 89.8℃. When the temperature of evaporator end section is raised, it is seen dry-out state that interface between the vapor and noncondensable gas in the condenser section with increase of inner vapor pressure is enlarged, returning of working fluid to evaporator section is difficult. Comparing Figure 6 with Figure 4 and 5, when the input heat load is 10 W, the temperature of evaporator and adiabatic section is higher about 4℃ than these of case Fig.4, higher about 1℃ than these of case Fig.5.

From Fig. 7 it is found that the mass of NCG is concerned in the operating temperature and the movement of the inactive portion of condenser section. Distribution of wall temperature at the mass of NCG, 1.7 x 10^{-6} kg, the working fluid quantity, 2.8 cc, are shown in Fig. 8. When the input heat loads are 60W, 80.8W, wall temperatures at evaporator section are 82℃, 91.2℃, respectively. When the input heat load changes from 60 W to 80W, wall surface

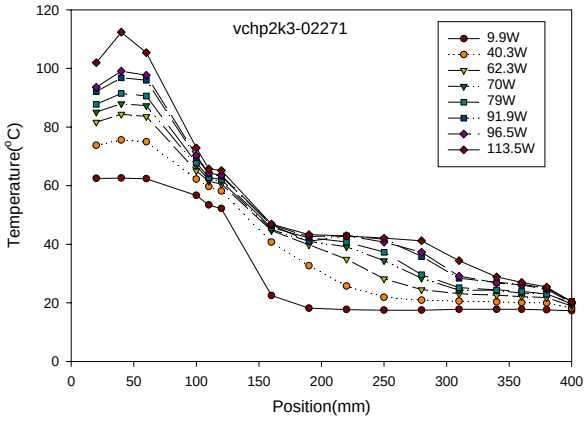


Fig. 9 Wall temperature distribution(3.0cc)

temperature of evaporator section changes about 9℃, it is not different from the results of Figure 4, 5, 6. But When the input heat load is 110W, it is seen that the state of dry-out isn't seen differently the result of the preceding and limitation power is high. The interface between the active and inactive portion of condense section is shown through wall surface temperature of condenser section. When the input heat load is 40W, wall surface temperature at 7 position of condenser section is 30℃, when the input heat load is 60W, wall surface temperature 40-45℃, In case of wall surface temperature at 9 position, when the input heat loads are 60W, 80.8W, 90W, wall surface temperatures of condenser section are 25℃,37.3℃,46.2℃, respectively. From this result , if the input heat load increases, it is seen that the operating vapor temperature rises and effective surface area of the condenser section is enlarged. As the operating vapor saturation pressure is high, the inactive portion of the condenser section moves to gas reservoir, consequently, increasing the active length of the condenser section has the effect of the enlargement of the heat transfer surface area. As a result, it is seen that the temperature of condenser section is increased.

Figure 9 shows the distribution of wall temperature at the mass of NCG, 1.7 x 10^{-6} kg, the working fluid quantity, 3.0cc. When the input heat loads is 62.3W, the wall temperature at the evaporator section is 81.7℃, the wall temperature of adiabatic section is 60.4℃. When the input heat load is 70W, the wall temperature at the evaporator section is 84.7℃, the wall temperature of adiabatic section is 62.4℃. When the input heat load is 79W, the wall temperature at the evaporator section is 88℃. When the input heat load is 91.9W, the wall temperature at the evaporator section is 92.1℃, the wall temperature of adiabatic section is 63.2℃. When the input heat

load is 96.5W, the wall temperatures at the evaporator section is 93.6℃. When the input heat loads 113.5W, the wall temperatures at the evaporator section 102-112℃, Experiment is stopped over 110 ℃. Comparing Figure 9 with Figure 5 and 6, when the input heat load is 10 W, the temperature of evaporator section is higher about 6℃ than that of case Fig.5, In this figure it is certainly seen the enlargement of active portion at wall temperature distribution of condenser section. When the input heat load is 40.3W, the wall temperature at 220mm position in condenser section is 25.7℃. When the input heat load is over 62.3W, the wall temperature distribution of condenser section shows 39.1-42.9℃. When the input heat load is 40.3W, the wall temperature of 250mm position condenser section is 21.9℃. When the input heat load is 62.3W, the wall temperature of condenser section is 28.2℃. When the input heat load are 70W, 91.9W, the wall temperatures of condenser section are 33℃, 41.7℃, respectively. From this result , if the input heat load increases, it is seen that the operating vapor temperature rises and effective surface area of the condenser section is enlarged. As the operating vapor saturation pressure is high, the inactive portion of the condenser section moves to gas reservoir, consequently, increasing the active length of the condenser section has the effect of the enlargement of the heat transfer surface area.

5. CONCLUSION

In this study, VCHP, which is based on the design theory with noncondensable gas reservoir is designed, fabricated and has been performed to investigate the heat transfer performances according to the amount of NCG and the working fluid quantity. The results are as follows:

(1) When the quantity of non-condensable gas increases, the beginning operating temperature rises and it is seen a rise in wall temperature of all section of VCHP.

(2) When the input heat load changes at 60W±10W, the wall surface temperature of evaporator section changes about ±4°C .

(3) As the quantity of working fluid increases, limitation power increases a little, but there is no difference in the wall temperature on evaporator section at the same input heat load.

(4) When the input heat load increases, it is seen the enlargement of the active portion of condenser section.

Acknowledgement

This work is supported by National Research Laboratory, Ministry of Science and Technology.

References

1. Chi, S.W., 1976, *Heat Pipe Theory and Practice*,Author, McGraw Hill , pp. 121-123.

2. Ioan Sauciuc, Aliakbar Akbarzadeh and Peter Johnson, 1996, Temperature Control Using Variable Conductance Closed Two- Phase Heat Pipe, Heat Mass Transfer, Vol. 23, No. 3, pp. 427-433.

3. P. F. Peterson, C. L. Tien, 1990, Mixed Double Diffusive Convection in Gas-Loaded Heat Pipes, Journal of Heat Transfer, Vol. 112, pp. 78-83.

4. Li Juxiang, Xu Tongming, 1992, A Study on the property of Heat and Mass Trans- fer of a gas-loaded Thermosyphon, 8th IHPC proceeding, pp. 323-327.

5. Byung Kyu Park, Geun Oh Kim, Moo Geun Kim, 2000, Transient Analysis of the Thermal Performance Characteristics of a Gas-Loaded Heat Pipe, Proceedings of the SAREK 2000 Winter Annual Conference, pp. 327-333.

6. D.E. Kim, Y.S. Park, J-S. Suh, K. W. Lee, 2001, Analysis of Thermal Performance of Variable Conductance Heat Pipe with a Axial Groove by considering the Diffusion Effect of Gas, SAREK 2001 Winter Proceedings, pp. 309-313.

7. J-S. Suh, 2001, Design Technology of Variable Conductance Heat Pipe and Its Application, 2001 The 2nd Waste Heat Utilization Workshop Proceedings, pp. 75-92.

8. D.E. Kim, Y.S. Park, J-S. Suh, K. W. Lee and K.H.Park, 2002, Thermal Analysis of Water-Copper Variable Conductance Heat Pipe with a screen mesh, KSME 2002 spring proceedings, pp. 1185-1190.

Analysis of Thermal Control Performance of Variable Conductance Heat Pipe with Axially Grooved Wick

Jeong-Se Suh*, Young-Sik Park*, Kyung-Taek Chung*, Ki-Woo Lee**, and Ki-Ho Park**

*School of mechanical and aerospace engineering and ReCAPT, GyeongSang Nat'l Univ., Jinju 660-701, Korea
Tel: +82-55-751-5312, FAX: +82-55-757-5622, E-mail: jssuh@gsnu.ac.kr

** Waste Heat Utilization Research Center, Korea Institute of Energy Research, Daejeon 305-343, Korea
Tel: +82-42-860-3166, FAX: +82-42-860-3133, E-mail: kwlee@kier.re.kr

Abstract

Heat pipe is a device that conveys efficiently thermal energy to heat sink taking advantage of phase change phenomena and operates with temperature difference of 3~5^{o}C between both of ends. Heat pipes with axially grooved wick have been utilized in many cooling applications to enhance heat transfer and achieve thermal control, and efficiently reduce the consumption of energy for thermal system. The operation temperature of a conventional heat pipe is passively determined by heat source and sink conditions. An increase in heat load causes the operation temperature of a heat pipe to excessively rise, and a reverse in the temperature gradient causes a reverse in the direction of heat transport. In practical applications, however, it is desirable to maintain portions of the pipe at a certain temperature range in spite of source or sink conditions. The variable conductance heat pipe(VCHP) has been proposed to achieve the required mode of operation of a heat pipe and control heat flow from thermal system. The present study has been conducted to analytically investigate the thermal performance of variable conductance heat pipe(VCHP) with axially grooved wick for thermal control of system. Numerical evaluation has been made for the thermal performance of VCHP, based on one-dimensional diffusion model that considers the diffusive expansion of inert gas due to the gradient of gas concentration.

Key words : Heat Pipe, Variable Conductance, Grooved, Heat Control, Water, Non-Condensable Gas

1. INTRODUCTION

The heat pipe of the various means of transmitting heat is, in many respects, the most satisfactory. Among the many outstanding advantages of using the heat pipe as a heat transmission device are: constructional simplicity, exceptional flexibility, accessibility to control, and ability to transport heat at high rate over considerable distance with extremely small temperature drop. Moreover, heat pipes require no external pumping power. The heat pipe is a conventional-scale device that conveys efficiently thermal energy to heat sink taking advantage of phase change phenomena and its size has generally about hydraulic radius of 0.01~0.1m. The heat pipe with grooves have been utilized in many cooling applications to enhance heat

transfer and achieve thermal control. To meet the demands of transferring increasingly larger heat fluxes, studies of the flow and heat transfer in heat pipe have been carried out to determine the capability of these systems.

In a variable conductance heat pipe, the gas reservoir is attached to the condenser end of the heat pipe. During its operation, the gas is swept by the vapor to the condenser end of the heat pipe and the gas reservoir. Presence of noncondensable gas in a port of the condenser prevents the vapor from condensing in that section. The noncondensable gas is shrunk by the expending of vapor of working fluid with increasing operation temperature, and the rate of increasing operation temperature of heat pipe is thus small by the heat transport capacity of heat pipe, compared with that of conventional heat pipe.

A survey of literatures reveals that Marcus[1] developed the model that analyzes the heat transport behavior of VCHP, and Chi[2] presented the modified model of VCHP in a steady-state operation. Bobco[3~5] has analyzed the thermal performance of VCHP from one-dimensional diffusion model, and the maximum heat transport capacity of VCHP. Kobayashi et al[6] and Sauciuc et al[7] studied analytically the thermal performance of thermosyphone with noncondensable gas reservoir. Peterson[8] studied the phenomena of convection and diffusion of vapor and inert gas in a reservoir.

Numerical analysis is made on the thermal performance of variable conductance heat pipe and investigate the thermal performance of variable conductance heat pipe(VCHP) with axially grooved wick for thermal control of system. Numerical evaluation has been made for the thermal performance of VCHP, based on one-dimensional diffusion model that considers the diffusive expansion of inert gas due to the gradient of gas concentration. Water is used as a working fluid and air as a non-condensable gas in the copper tube. As a result, the thermal performance of VCHP based on diffusion model has been compared with that of the conventional heat pipe, and the axial variation of pressure difference between vapor and liquid obtained. Additionally, it is found for the distribution of concentration of inert gas and temperature variation in the condenser region. The maximum heat transport capacity of variable conductance-heat pipe is provided by varying the operation temperature.

2. MODELING OF VARIABLE CONDUCTANCE HEAT PIPES

2.1 Physical Description and Basic Equations

The maximum heat transport capability of a variable conductance heat pipe is investigated numerically to predict the fluid-thermal behavior of variable conductance heat pipes. Figure 1 depicts the schematic shape and cross sectional diagram of variable conductance heat pipe considered in the present work. A variable conductance heat pipe is well known to effectively convey heat from evaporator region to condenser region with small variation of operating temperature. Working fluid in a variable conductance heat pipe vaporizes in the evaporator and condensates in the condenser. To efficiently analyze the characteristics of heat transport of variable conductance heat pipe, the following assumptions are introduced as: (1) Heat transfer processes in variable conductance heat pipe container and working fluid are considered to be one dimensional in the radial direction, such that axial heat conduction is neglected, (2) the working fluid flows only along the axial direction, (3) no part of the condenser is blocked by the liquid

working fluid, and (4) the liquid is distributed uniformly around the circumstance of heat pipe. For the steady-state operation of a variable conductance heat pipe, the conservation principle must hold over the cross section of the variable conductance heat pipe at any axial location for the continuity, momentum, and energy for the liquid and vapor. The Laplace-Young equation is additionally applied for the radius of curvature at the liquid-vapor interface.

The mass conservation over the cross section of variable conductance heat pipe is given by

$$\rho_v A_v \overline{w}_v = \rho_l A_l \overline{w}_l \qquad (1)$$

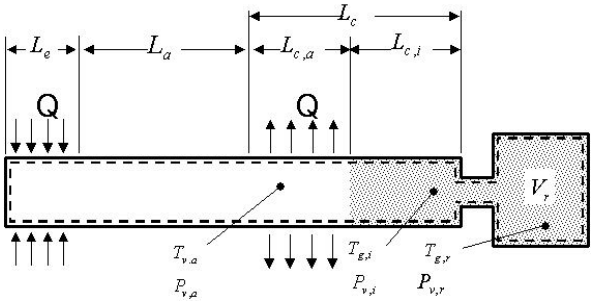


Fig.1 Schematic diagram of variable conductance heat pipe with gas reservoir.

where $\overline{w}_v$ and $\overline{w}_l$ are the mean vapor and liquid velocities in the axial direction, and $\dot{m}_l$ the mass flow rate of liquid.

The conservation of axial momentum equation for an incompressible vapor using the one-dimensional boundary-layer approximation is given by

$$\frac{d}{dx}(P_v + \rho_v g z \sin\phi + \rho_v \beta_v \overline{w}_v^2) = -f_v \frac{2\rho_v \overline{w}_v^2}{D_{h,v}} \qquad (2)$$

where β_v is the momentum flux coefficient, and f_v the friction coefficient. These coefficients for two-dimensional, laminar flow of channel can be taken from $(f\,\mathrm{Re})_v = 16$. The velocity of the liquid in the mesh wick is very slow in comparison to that of the vapor flow, so the interfacial shear for the vapor can be numerically obtained by assuming the liquid to be stationary[4].

The conservation of momentum equation for the liquid flow in the groove of variable conductance heat pipe is

$$\frac{d}{dx}(P_l + \rho_l g z \sin\phi) = f_l \frac{2\rho_l \overline{w}_l^2}{D_{h,l}} \qquad (3)$$

where f_l is the friction coefficient of the liquid flow. The inertia effects for the liquid flow are negligible in comparison to those due to viscous losses. The value of f_l can be taken from the previous results[9] that are numerically obtained from two-dimensional Stokes' equation considering the interfacial shear due to the frictional interaction. For the case of a channel flow with screen mesh wick, the equations related to friction coefficient of the liquid flow are given by a modified Blake-Kozeny equation:

$$(f\,\mathrm{Re})_l = \frac{244 r_h^2 (1-\varepsilon)^2}{d^2 \varepsilon^2} \qquad (4)$$

The conservation of energy equation for the liquid and vapor flows in a variable conductance heat pipe can be expressed in such a way that the mass flow rates of liquid and vapor varied along the axial direction by evaporation and condensation in the working fluid. The energy equation is as follows:

$$\frac{d}{dx}(\rho_l \overline{w}_l A_l) = \frac{1}{h_{fg}} \frac{dQ(x)}{dx} \qquad (5)$$

where $Q(z)$ denotes the local axial heat load function and h_{fg} the latent heat of the working fluid.

The interfacial radius of the meniscus curvature is related to the pressure difference between the

vapor and liquid, and can be taken in differential pattern from the Laplace-Young equation as follows:

$$\frac{dP_l}{dx} = \frac{dP_v}{dx} - \frac{d}{dx}\left(\frac{\sigma}{r}\right) \qquad (6)$$

where σ denotes the surface tension coefficient for the liquid.

For the above governing equations, the boundary condition for the liquid and vapor flows is

$$\overline{w}_l = \overline{w}_v = 0 \quad (x = 0 \text{ and } L_t) \qquad (7)$$

where L_t is the total length of variable conductance heat pipe. The boundary condition for the pressure of the liquid and vapor at the evaporator end cap is

$$P_v = P_{v0}, \; P_l = P_{v0} - \frac{\sigma}{r_0} \quad (x = 0) \qquad (8)$$

In the variable conductance heat pipe, the heat and mass balance equation as depicted in Fig. 2 can be expressed in the condenser port as follows:

$$\frac{d}{d}\left[k_p \pi (r_o^2 - r_i^2)\frac{dT_p}{dx}\right] + \frac{2\pi r_i k_e}{r_i - r_v}(T_{wv} - T_p) - 2\pi r_o h_{f,c}(T_p - T_s) = 0 \qquad (9)$$

$$\frac{dm_v}{dx} = -\frac{2\pi r_i k_e}{\lambda(r_i - r_v)}(T_{wv} - T_p) \qquad (10)$$

where T_{wv} is the wick temperature and depends on the mass fraction of working fluid χ_g and the partial pressure of working fluid P_v.

The relation between the mass flow rate and mass fraction of working fluid can be given by

$$\dot{m}_v = A\rho D\frac{d}{dx}(\ln \chi_g) \qquad (11)$$

The total heat transfer rate conveyed by the VCHP can be obtained in the following equation:

$$Q = \int_0^{L_c} 2\pi r_o h_{f,c}(T_p - T_s)dx \qquad (12)$$

2.2 Numerical Procedure

For the basic equations (1)-(12) in the variable conductance heat pipe, the governing equations (1), (2) and (3) are the function of *x* and the ordinary differential equations. The system of the governing equations was solved with the respective boundary conditions using the fourth-order Runge-Kutta and the shooting methods. The relative error for each of the governing equation was numerically less than 0.00001% with iterative calculation procedure.

For the evaporator and condenser of variable conductance heat pipe, the axial function of heat load is imposed as

$$Q(x) = \begin{cases} Q_{\max}(x/L_e), & 0 \le x < L_e \\ Q_{\max}, & L_e \le x < L_e + L_a \\ Q_{\max}(L_t - x)/L_c, & L_e + L_a \le x \le L_t \end{cases} \qquad (13)$$

where $Q_{\max}$ is the maximum heat transport capability of variable conductance heat pipe. The specification of variable conductance heat pipe mostly studied in the present work is listed in Table 1.

Table 1 Specification of variable conductance heat pipe used in this study

Description	Value
Number of groove	21EA
Total length	1.062m
Evaporator length	0.127m
Condenser length	0.30m
Radius of pipe	$8.8\text{x}10^{-3}$m
Radius of vapor core	$3.747\text{x}10^{-3}$m
Width of groove	$4.57\text{x}10^{-4}$m
Height of groove	$1.02\text{x}10^{-3}$m

3. RESULTS AND DISCUSSION

The results from this work are primarily presented for the variable conductance heat pipe using the working fluid of water in the operation temperature from 325K to 350K.

3.1 Characteristics of Maximum Heat Transport Capacity

The heat transfer and capillary limit in VCHP is expressed for operation temperature as shown in Fig. 2. As shown in this figure, the operating temperature of VCHP increases linearly with increasing heat transfer rate through the heat pipe. The heat transfer capacity of VCHP experiences the capillary limit over 44W and operating temperature 345K.

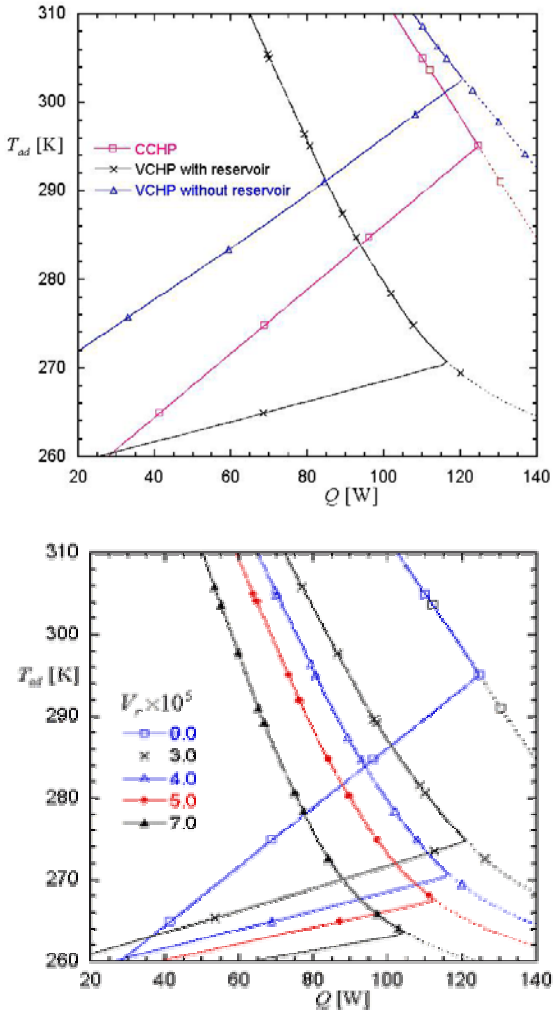


Fig. 2 Variation of operation temperature for heat flow in VCHP with gas reservoir.

3.2 Characteristics of gas mass fraction and temperature in the condenser port of VCHP

It is shown in Fig. 3 that the gas mass fraction varies with x increasing at condenser port of VCHP and the temperature of vapor-wick interface and pipe along the axial direction. It is also found out in this figure that the gas mass fraction increases in step above x=0.4m and maintains unit, whereas the temperature of vapor-wick interface and pipe decreases in step above x=0.4m and goes to the ambient temperature. It means that the non-condensable gas is pushed into the end cap of the condenser of VCHP, and thus the heat from evaporator does not convey to the end cap of the condenser of VCHP due to non-condensable gas occupied at the end cap of condenser.

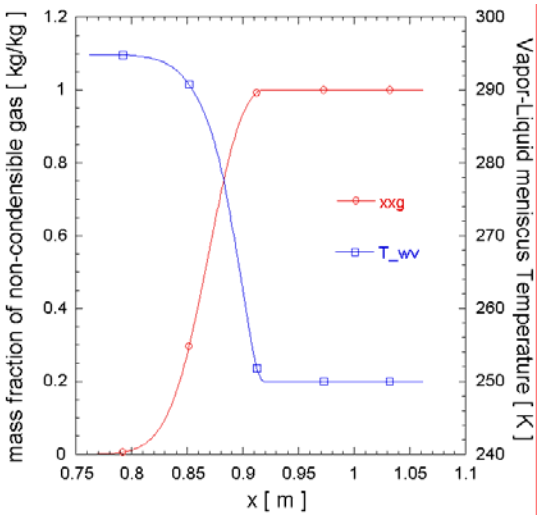


Fig. 3 Distribution of gas mass fraction with condenser length and Temperature of vapor-wick interface and pipe

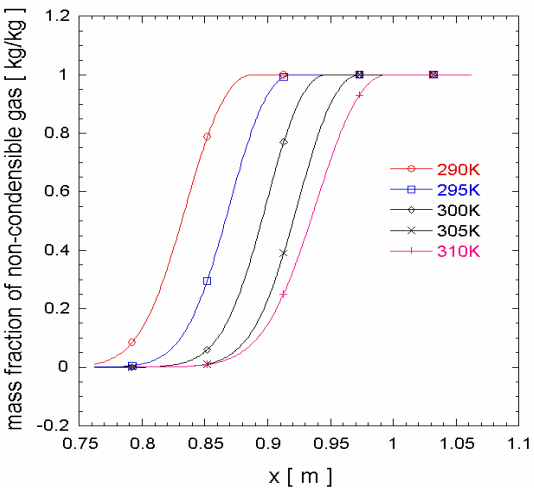


Fig. 4 Mass fraction of gas with operating temperature.

Figure 4 and 5 show the mass fraction of gas and the temperature of pipe with operating temperature, respectively. Mass fraction of gas and the temperature of pipe vary along axial direction of heat pipe, similar to those shown in Fig. 4. As the operating temperature increases, the position of stepwise variation of gas mass fraction and pipe temperature move toward the end cap of condenser port of heat pipe.

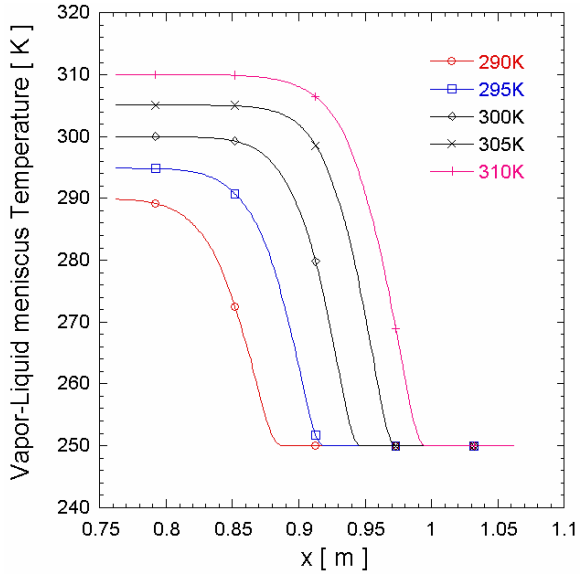


Fig. 5 Temperature of pipe with operating temperature.

4. CONCLUSIONS

In this work, the thermal performance has been investigated numerically for the variable conductance heat pipe(VCHP) with screen mesh wick for thermal control of system. Numerical evaluation has been based on one-dimensional diffusion model that considers the diffusive expansion of inert gas due to the gradient of gas concentration. Water is used as a working fluid in the copper tube and air as a non-condensable gas. As a result, the thermal performance of VCHP based on diffusion model has been presented for the maximum heat transport capacity of variable conductance-heat pipe by varying the operation temperature. Additionally, it is found for the distribution of concentration of inert gas and temperature variation in the condenser region.

Acknowledgements

This work is partially supported by Brain Korea 21 Projector, and ReCAPT.

References

1. Marcus, B.D., 1971, Theory and design of variable conductance heat pipe: Control techniques, 2nd rport by TRW Inc. to NASA, Contact No. NAS2-5503.

2. S. W. Chi, 1976, Heat Pipe Theory and Practice, McGraw-Hill, New York.

3. Bobco. R. P., 1987, Variable Conductance Heat Pipes: A First-Order Model, Journal of THERMOPHYSICS, Vol. 1, No. 1, pp 35-42.

4. Bobco. R. P., 1989, VCHP performance prediction: comparison of first-order and flat front models, Journal of THERMOPHYSICS, Vol. 3, No. 4, pp. 401-405.

5. Bobco. R. P., 1989, Variable Conductance Heat Pipe Performance Analysis, Journal of THERMOPHYSICS, Vol. 3, No. 1, pp. 33-41.

6. Yasunori Kobayashi, Akira Okumura, Toshihisa Matsue, 1991, Effect of Gravity and Non condensable Gas Levels on Condensation in

Variable Conductance Heat Pip Journal of THERMOPHYSICS, Vol. 5, Vo.1, pp 61-68.

7. Ioan Sauciuc, Aliakbar Akbarzadeh, 1996, Peter Johnson, Temperature Control Using Variable Conductance Closed Two-Phase Heat Pipe, Heat Mass Transfer, Vol. 23, No. 3, pp 427-433.

8. P. F. Peterson, C. L. Tien, 1990, Mixed Double-Diffusive Convection in Gas-Loaded Heat Pipes, Journal of Heat Transfer, Vol. 112, pp 78-83.

Performance of Heat Pipes for Solar Collector Using Binary Mixture Working Fluids

Jung, E.G.*, Chung, W.B.*, Boo, J.H.*, and Kwak, H.Y.**

*School of Aerospace and Mechanical Engineering, Hankuk Aviation University
200-1 Hwajeon, Deokyang-gu, Gyeonggi-do, 412-791, Korea
Phone: +82-2-300-0107, E-mail: jhboo@ hau.ac.kr
** Korea Institute of Energy Research, Daejeon, 305-343, Korea

Abstract

Heat pipes with binary mixture working fluid were fabricated and tested for applications where condenser temperatures to be in ranges of 0℃ to 130℃. The heat pipe container was copper tube of 8.0 mm O.D. and the capillary structure was woven-wire wick. The working fluid was ethanol-water mixtures with varying mole fraction. And the fill charge ratio was 20% by total heat pipe internal volume. The total length of the heat pipe was 1710 mm in which the evaporator section was 1570 mm, which was relatively long for solar collector applications. Cooling condition of the condenser section was cooled by convective coolant of which the inlet temperature was 10℃, 80℃ or 130℃. Heat pipe performance was examined with change of mixing ratio. Thermal load was adjusted by 20 W increment until the maximum wall temperature reached 150℃. Results show that for coolant temperatures 10℃ and 130℃, mixing ratio for best thermal performance was 0.8M+. For coolant temperatures 80℃, however, the optimum mixing ratio ranged from 0.3 to 0.5M+.

Key Words: Heat Pipe, Binary mixture, Ethanol-Water, Thermal resistance, Mole fraction.

1. INTRODUCTION

An evacuated solar collector using heat pipe is known to be suitable for medium temperature range (80 to 150℃) applications to secure industrial heat source. Heat pipe for the vacuum type solar collector should be able to endure sub-freezing temperature (below 0℃) in cold regions. It should also be able to operate normally at higher temperatures near or over 150℃. To meet the requirements of high performance in the above-mentioned temperature range, selection of proper working fluid is very important for fabrication processes.

Various experimental studies to enhance heat transfer performance of heat pipes for solar collector have been accomplished. Comparative study of a slab-wick, and a woven wire wick on the performance and optimum fill charge ratio of medium temperature heat pipes were conducted by Boo and Chung[1]. A study on an enlarged condenser surface to enhance heat transfer performance of heat pipes for similar application was examined by Boo et al[2].

Another way of enhancing performance of these heat pipes can be a proper selection of working fluid. Distilled water exhibits excellent heat transfer property up to 200℃. However, a critical aspect is that it freezes below 0℃. To solve this problem, various studies on the binary mixture have been carried out to make a working fluid which retains merit of water at higher temperature and does not freeze in lower temperature. A few previous studies have been performed to enhance the heat transfer performance using two-fluid mixture as working fluid (water and ethanol [3], water and methanol [4], water and ethylenglycol [5], and water and glycerin [6]). According to the literature, the case which uses water as a second fluid and ethanol as a first fluid have more excellent results. In these cases, the best performance was appeared in 0.3 to 0.5M+ (Mole fraction) [3~8].

Ethanol-water mixture was selected as working fluid in this study to enhance heat pipe performance for solar collector application. The heat pipe used woven-wire wick as a wick structure, and had an enlarged condenser section for wider heat transfer area. Experiment was conducted by increasing thermal load until any local wall temperature of the heat pipe reached 150℃.

2. EXPERIMENTAL APPARATUS AND MESURING METHOD

A schematic of the heat pipe used in this experiment was shown Fig. 1. Total length of copper tube container was 1710 mm, of which the inner diameter was 6 mm and outer diameter was 8 mm. The evaporator length of heat pipe was 1570 mm, adiabatic section length was 90 mm and condenser length was 90 mm. The woven-wire wick was inserted into the heat pipe as a capillary structure.

The end of the evaporator side of the heat pipe was welded. A needle valve was installed at the other end to supply working fluid of various mixing ratio and to evacuate. To enhance the heat transfer effect, a larger diameter tube (of 22 mm) was used at the condenser section than that for the evaporator section. The enlarged condenser section was inserted into a liquid–circulating cooler (cooling jacket) to which ten radial type fins were attached (Fig.2).

Working fluid of heat pipe was mixture of ethanol (99.9%) and water. Fill charge ratio was 20% of total heat pipe volume and the mixing ratio was denoted by mole fraction.

A data acquisition system was used to measure and record temperature data. A total of 9 chromel-alumel (K-type) thermocouples of AWG-28 were attached; four in the evaporator (T/C#1 : 50mm from pipe end, T/C#2 : 750mm, T/C#3 : 1300mm, T/C#4 : 1535mm) , one in the adiabatic section (T/C#5: 1595mm), two in the condenser (T/C#6 : 1620mm, T/C#7 : 1710mm), and one each at the inlet and outlet of the cooling jacket.

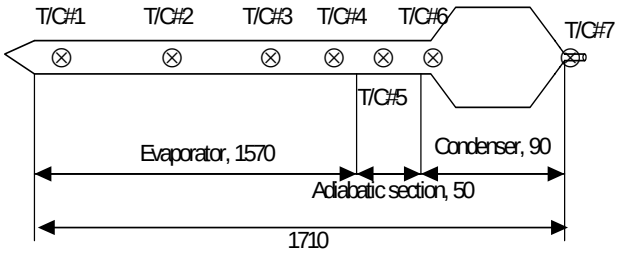


Fig. 1 Schematic of a heat pipe with enlarged condenser surface.

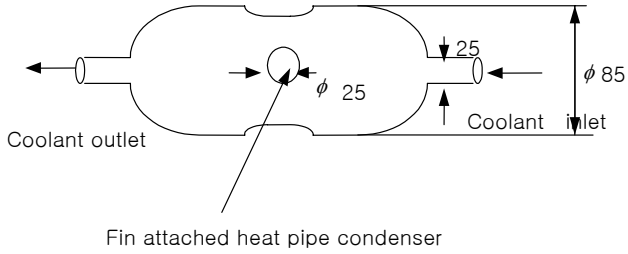


Fig. 2 Cooling jacket with fin attached heat pipe condenser.

The heat source in the evaporator was uniformly wound band heater of which the maximum heat generating capacity was 600W at 220V. The thermal load was controlled by a voltage regulator and its intensity was measured by a multimeter.

Evaporator and adiabatic section was wrapped by insulation material and ceramic fiber was used as insulation in the condenser section. Cooling jacket and a constant-temperature bath was used to supply fluid (Silicon oil) flow (0.6L/min) at a controlled temperature.

Coolant inlet temperatures was set to one of three temperatures 10℃, 80℃ or 130℃ to test heat pipe performance in a large temperature range. To preserve thermo-physical property of pure water and ethanol, supplied thermal load was adjusted by 20W increment until any local wall temperature of heat pipe reached maximum temperature of 150℃. For applications in solar collectors, the experimental setup in this study was constructed to align heat pipes at 45 degree tilt angle.

3. Test Procedure

Great care was taken to remove air and other non-condensable gases from the test heat pipe before charging a new mixture. A prescribed amount the mixture of the different mixing ratio was charged into tube. Once operation reached at a steady state in 30 to 40 min all the relevant test data were obtained through data acquisition system. After a test at each mole fraction, heat pipe was thoroughly cleaned.

Results of thermal performance analysis were summarized by thermal resistance against mole fraction or thermal load. Thermal resistance, R_{TH} , is defined as the difference of average temperatures in the evaporator and the condenser divided by input thermal load (equation 1).

$$R_{TH} = (T_{e,avg} - T_{c,avg}) / Q \qquad (1)$$

4. RESULTS AND DISCUSSION

The results focused on the effects of the mixture ratio on the thermal performance of heat pipes. In the figures and text below, mixing ratio is denoted by M+.

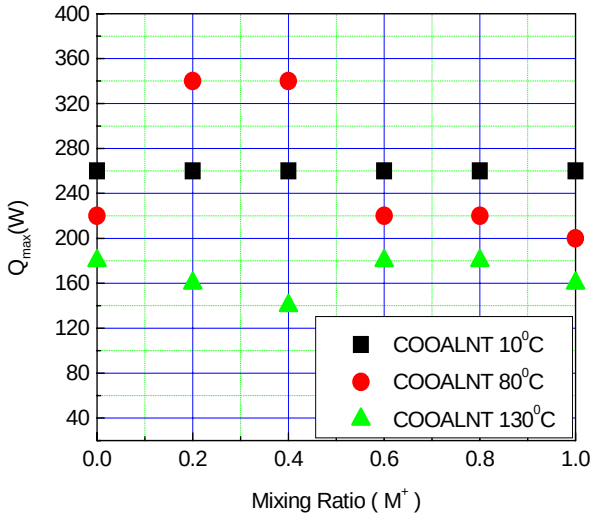


Fig. 3 Maximum thermal load against mixing ratio

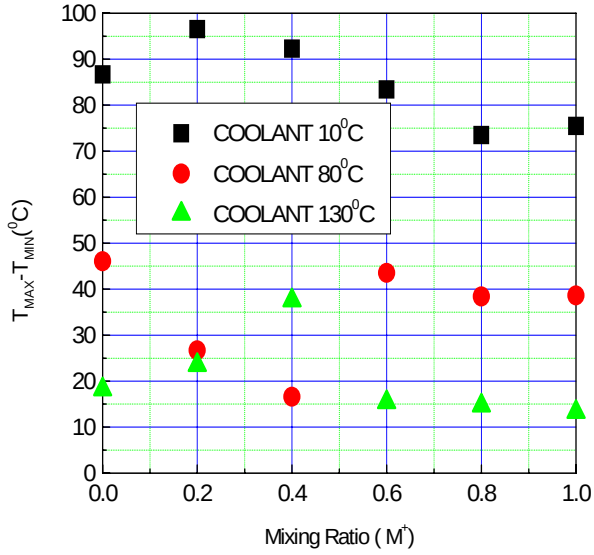


Fig. 4 Wall temperature difference against mixing ratio.

Fig. 3 shows maximum supplied heat load against mixing ratio. Q_{max} is identified when a local maximum temperature of heat pipe reached 150℃.

For coolant temperature of 10℃ almost no change was observed against mixing ratios. For coolant temperature of 130℃, Q_{max} exhibited the lowest value at around 0.4M+.

For coolant temperature of 80℃, Q_{max} was raised very high (340 W) at mole fractions of 0.2 to 0.4 M+. Q_{max} for other mole fraction showed 40 W lower than those for coolant temperature of 10℃, but 40 W higher than those for 130℃ cases.

Fig.4 represents difference between maximum and minimum wall temperatures against mixing ratio for each coolant temperature. The data were taken when the heat pipe was reached steady state without dryout. Temperature difference was largest for coolant temperature of 10℃. Except at the mixing ratio of 0.4M+, the temperature difference for coolant temperature of 80℃ was larger than for coolant temperature of 130℃. General tendency of temperature difference showed that it decreased as coolant temperature was raised.

For coolant temperature of 10℃, the temperature difference generally decreased with mixing ratio but a peak of 95℃ was observed at 0.2 M+, where the smallest value of 75℃ was observed at 0.8M+.

For coolant temperature of 80℃, the temperature difference decreased until 0.5M+, but increased abruptly near 0.5M+ and then decreased as the mixing ratio exceeded 0.6M+. Smallest temperature difference (16℃) was observed at 0.4 M+ and largest temperature difference (46℃) was observed at pure water (0.0M+).

For coolant temperature of 130℃, heat pipe temperature distribution was relatively even except at the maxing ratio 0.4M+, where the temperature difference was lager than those for other mixing ratios by more than 20℃. The temperature difference was smallest (12℃) at pure ethanol (1.0M+) and was largest (37℃) at 0.4M+.

Figs. 5 through 7 show adiabatic section wall temperature, T_a, against supplied heat flux. The adiabatic wall temperature is considered equal to the vapor temperature, as in many literatures. General tendency show that vapor temperature varied in proportionally with heat flux.

For coolant temperature of 10℃ (Fig.5), the adiabatic wall temperature showed linear increase for pure water (0.0M+), pure ethanol (1.0M+), and 0.8M+. For other mixing ratios, the adiabatic wall temperature showed almost same values for heat flux higher than 2000 W/m^2. Mixing ratio for the lowest adiabatic wall temperature was 0.8M+ and that for the highest adiabatic wall temperature was 0.4M+.

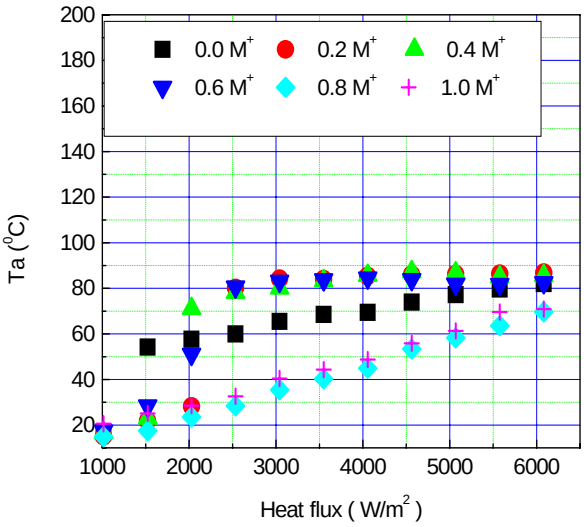


Fig. 5 Adiabatic wall temperature (vapor temperature) as a function of heat flux for coolant temperature of 10℃.

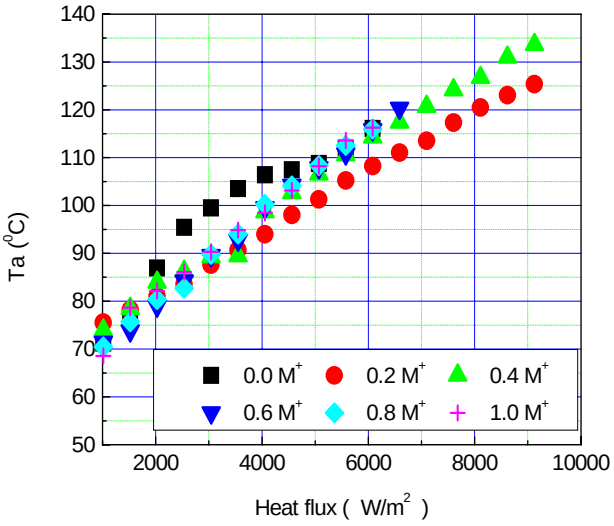


Fig. 6 Adiabatic wall temperature as a function of heat flux for coolant temperature of 80℃.

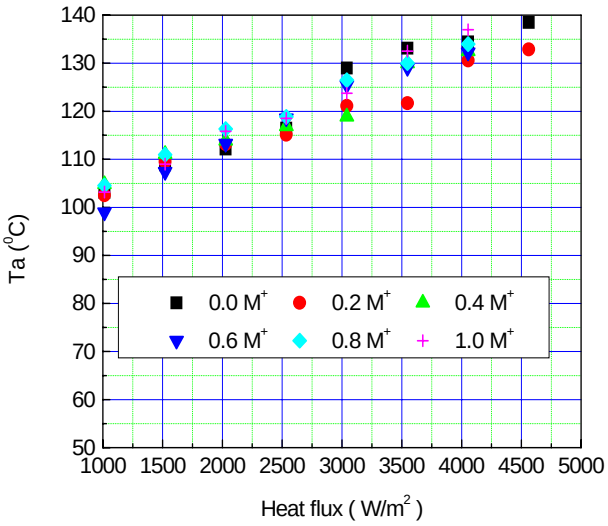


Fig. 7 Adiabatic wall temperature as a function of heat flux for coolant temperature of 130℃.

For coolant temperature of 80℃ (Fig.6), the adiabatic wall temperature was proportionally increased for all input heat flux. The lowest adiabatic temperature was achieved for 0.2M+ and the highest temperature was achieved for pure water. For coolant temperature of 130℃ (Fig.7), no peculiar statement can be made regarding vapor temperature except that it generally increased with heat flux.

Figs. 8 through 10 show thermal resistance against input heat flux for three different coolant temperatures. For coolant temperature of 10℃ (Fig.8), thermal resistance gradually decreased as input heat flux was increased. Pure ethanol showed the lowest thermal resistance until 2000 W/m^2 but increased abruptly at 2500 W/m^2 before it decreased again. Pure water exhibited the lowest thermal resistance from 2500 W/m^2 to 5000 W/m^2. When heat flux was 5800 W/m^2 and higher, the lowest thermal resistance was observed at 0.8M+. The highest thermal resistance was achieved at 0.6M+ for heat flux 2000 W/m^2 or lower. For heat flux higher than 2000 W/m^2, the highest thermal resistance occurred at 0.4M+.

For coolant temperature of 80℃ (Fig.9), Pure ethanol showed abruptly increasing thermal resistance at 4000 W/m^2 and showed the highest thermal resistance until about 5500 W/m^2. The lowest thermal resistance occurred at 0.4 to 0.6M+.

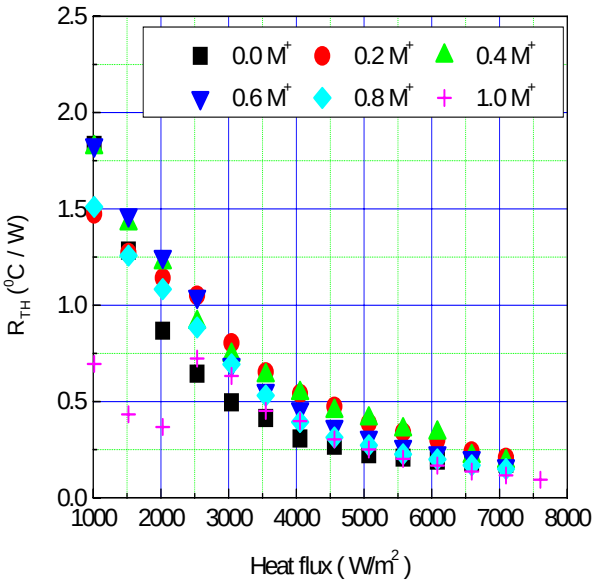


Fig. 8 Thermal resistance for the coolant temperature of 10℃ against heat flux.

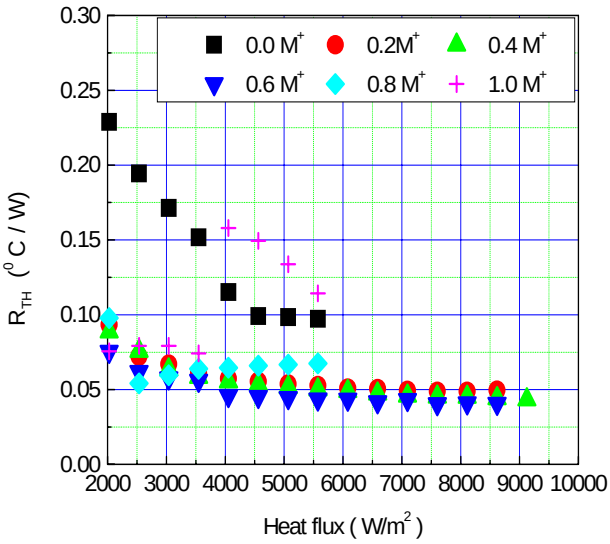


Fig. 9 Thermal resistance for the coolant temperature of 80℃ against heat flux.

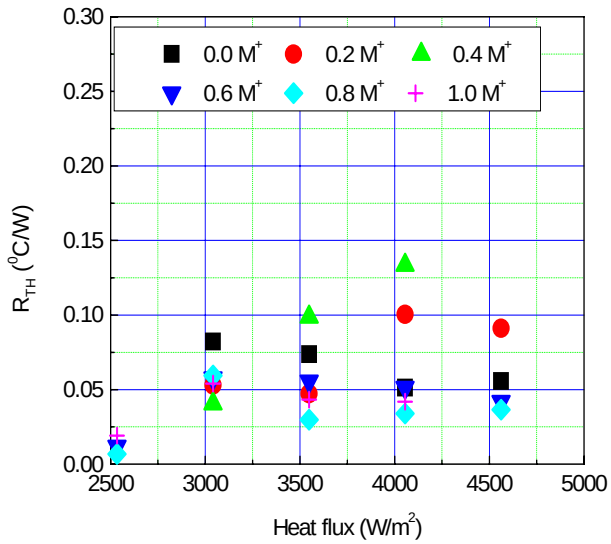


Fig. 10 Thermal resistance for the coolant temperature of 130℃ against heat flux.

For coolant temperature of 130℃ (Fig.10), thermal resistance distribution against input heat flux was irregular generally. Low thermal resistance was achieved at 0.8M+ and the highest resistance appeared for 0.4M+.

Figs.11 through 13 represent thermal resistance distribution against mixing ratio at various input thermal load.

For coolant temperature of 10℃ (Fig.11), thermal resistance was the lowest at mixing ratio of 0.8 M+ for every input thermal load. This corresponds to the best heat transfer performance.

For coolant temperature of 80℃ (Fig.12), the lowest thermal resistance was achieved at mixing ratio of 0.4M+ for all input thermal load. This result coincides with those in reference [3].

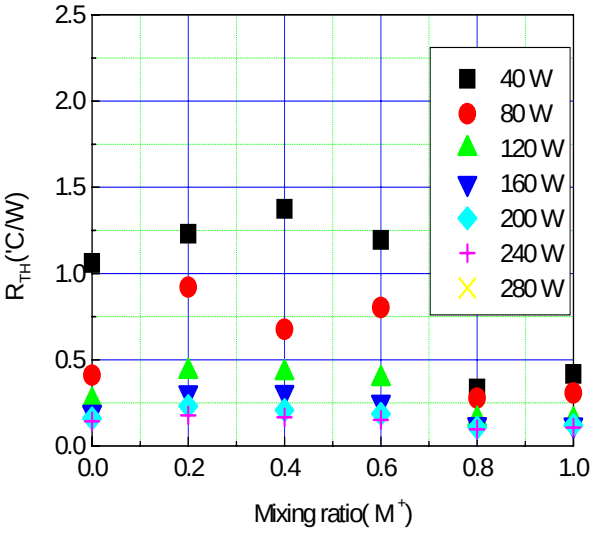


Fig. 11 Thermal resistance as a function of mixing ratio for coolant temperature of 10℃

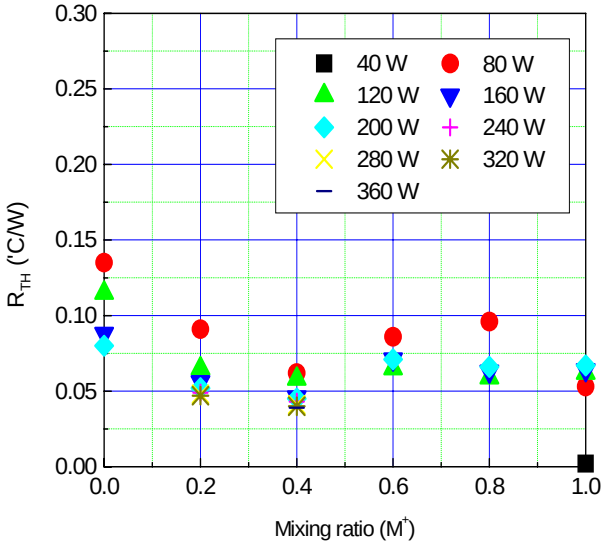


Fig. 12 Thermal resistance as a function of mixing ratio for coolant temperature of 80℃.

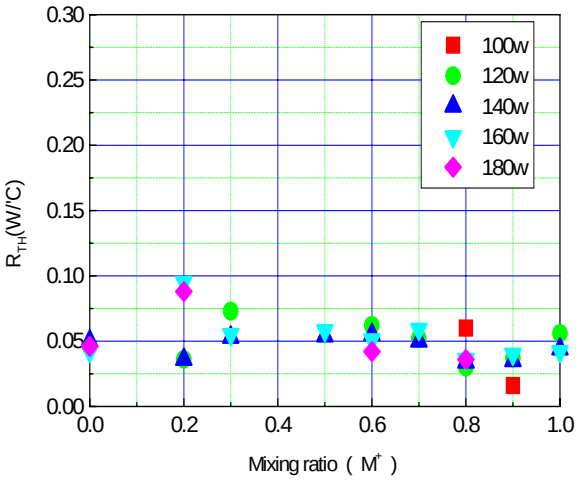


Fig. 13 Thermal resistance as a function of mixing ratio for coolant temperature of 130℃.

5. CONCLUSIONS

An effort was made to examine the thermal performance of a heat pipe using binary mixture as working fluid. The heat pipe had a woven-wire wick. Based on the experimental data, the following conclusions can be made:

For coolant temperature of 10℃, heat transfer performance for mixing ratio 0.8 M+ was superior to other mixing ratios from the viewpoints of heat transfer coefficient, thermal resistance, isothermal characteristic and low vapor temperature.

For coolant temperature of 80℃, heat transfer performance for mixing ratio of 0.4M+ was superior to other mixing ratios from the viewpoints of heat transfer coefficient, thermal resistance, and isothermal characteristics. However, mixing ratio 0.2M+ exhibited the lowest vapor temperature.

For coolant temperature of 130℃, heat transfer

performance for mixing ratio of 0.8 M+ was superior to other mixing ratios from the viewpoints of heat transfer coefficient, thermal resistance, isothermal characteristics and low vapor temperature.

Nomenclature

M_e Moles of ethanol, [mol]
M_w Moles of water, [mol]
M+ Mole fraction ($M_e / [M_w + M_e]$)
Q_{max} Maximum thermal load, [W]
T_a Adiabatic wall temperature, [℃]
R_{TH} Thermal Resistance, [℃/W]

References

1. Boo, J.H., and Chung, W.B., 1999, "An Experimental Study of a Slab-Wick Heat Pipe for Medium-high Condenser Temperature," the 11th International Heat Pipe Conference, Tokyo, No. A111-3.
2. Boo, J.H., Chung, W.B., and Kwak, H.Y., 2002, "Thermal Performance of Heat Pipes having Enlarged Condenser Section in an Elevated Operating Temperature Range," the 12th International Heat Pipe Conference, Moscow, No. H-1.
3. Peterson, G.P., 1994, *An Introduction to Heat Pipes*, John Wiley & Sons, pp.232-236.
4. Liu, F., Liu, J., Wang, K., and Guan, L., 1992, "The Visualization Studies on the Boiling Phenomena of Mixture Fluid in Thermosyphons," the 8th International Heat Pipe Conference, Beijing, No. A-P4.
5. Park, R.J., and Lee, Y., 1992, "Two-phase Closed Thermosyphons with Two-fluid Mixtures," the 8th International Heat Pipe Conference, Beijing, No. B-18.
6. Tien, C.L., and Rohani, A.R., 1992, "Theory of Two-Component Heat Pipes," Journal of Heat Transfer, November, pp.479-484
7. Qi, W., and Lang, Y., 1999, "Heat Transfer Characteristics of a Closed Two-Phase Thermosyphon Working with a Binary Mixture at Different Incline Angles," the 11th International Heat Pipe Conference, Tokyo, No. A5-2.
8. Pioro, L.S., Pioro, I.L., 1997, *Industrial Two-phase Thermosyphons,* Begell Bouse, pp.96-291.

A Study on the Heat Transfer Characteristics of Medium Temperature Heat Pipe

Y. S. Lee*, K. C. Chang*, J. R. Kim* and Y. S. Jang**

*Korea Institute of Energy and Research
+82-42-860-3161, +82-42-860-3133, yslee@kier.re.kr
**Kyung-Nam College of Inform and Technology

Abstract

The range of temperature of heat pipes that are generally used nowadays is between -150℃ and 300℃ and they belong to low-temperature heat pipes. Therefore there are many materials about the working fluid of these heat pipes. But more researches about working fluid are needed in the wide range of temperature with the extension of the use of heat pipes. Especially the researches and materials about the working fluid between 300℃ and 600℃ which can be used to operate a furnace heat recovery are much more needed.

If we see the working fluid of medium temperature heat pipes, we can tell the degree of mercurial content. But it is not so easy to use mercury in the experiment because of the danger of dealing with it. The purpose of this experiment is to compare and evaluate the characteristics of several working fluids which are used between 300℃ and 600℃ according to the variation of heating temperature and the inclinatory degree of heat pipes. Before making this experiment, I carried out an experiment "In which range of temperature Dowtherm A - that is largely used as medium temperature working fluid - has the highest efficiency?" according to the variation (300～600℃) of only heating temperature. And I will compare and evaluate which working fluid is more appropriate than other working fluids under the given condition in the next experiment.

Key words : medium temperature heat pipe, working fluid, heat transfer characteristics

1. INTRODUCTION

The performance of a heat pipe depends on the length of the evaporator, the kinds of working fluid according to the temperature range, and the inclined angle of the heat pipe. Among the factors, the working fluid selection according to the temperature range have the most relations with the performance as the working fluids adopted for the similar temperature range are different in characteristics and can result in huge gap in performance under certain temperature ranges. The current heat pipes are classified into the ultra low temperature, the normal temperature, and high temperature. The available temperature ranges are divided into below -150℃, -150 ～350℃ and over 350℃. The working fluids for the ultra low temperature heat pipe include hydrogen and neon, those for the normal temperature one distilled water and alcohol, and those for the high temperature cesium, lithium and other liquid metals. When the temperature ranges from 200℃～400℃, it's hardly possible to find a working fluid that is stable for operation. In addition, it's much harder to manufacture medium or high temperature heat pipes than low temperature ones since the former ones have high pressure inside and work at even higher temperature than the normal temperature, which increases the possibility of non-condensing gas. Thus it is highly demanding to select working fluids for the former ones as the technology has not been improved enough to maintain the purity of the filling medium and remove non-condensing gas taking place at the high temperature operation mode at the satisfactory level. The especially difficult spot is between the normal temperature and the high temperature, for which it's hard to find data concerning the working fluid of a heat pipe. More experiments should be conducted on the working fluid for more extensive temperature ranges since there has been increasingly expanding scope of heat pipe uses. In particular, the data on the working fluid for the medium temperature range that is used for a furnace is in the most need.

Currently they are using mercury for the working fluid for the temperature range, but mercury is hard to deal with.

In order to develop a high efficiency heat pipe

heat exchanger for heat recovery of the exhaust gas of medium temperature at 300℃～600℃ that is usually discharged from the industrial furnace, the basic experiments were conducted on a heat pipe, a heat exchanger was designed, and the results of numerical value analysis were compared and reviewed.

2. EXPERIMENTAL APPARATUS AND METHOD

2-1 Experimental Apparatus

The apparatus used for this study is shown in Fig. 1. The total length of heat pipe was 700mm, the length of evaporator was 300mm and the length of condenser was 300mm.

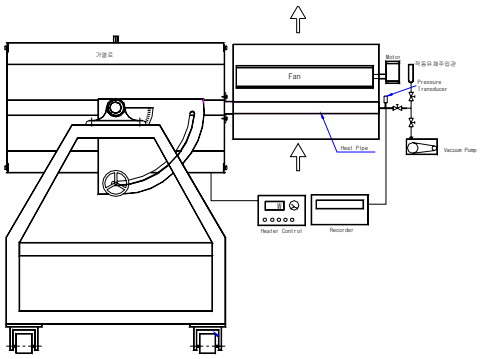


Fig. 1 Schematic diagram of experimental apparatus

Dowtherm A are used as the working fluid. All of the temperature measurements on heat pipe were 10 point K type thermocouple. Condenser wall temperature measurements were made by welded five of these thermocouples along the condenser surface. The evaporator section of heat pipe I electrically powered using a oven heater with a normal power of 6kW. All of the thermocouples were recorded using a data acquisition system and were calibrated to an accuracy of ±0.5℃ in constant temperature bath with a platinum resistance thermocouples.

Heat pipe consisted of 0.7m long, 28mm outside diameter and 25mm inside diameter SUS 316L. The working fluid as Dowtherm A was charged into the tube 10^{-3} torr vacuum pressure. The condenser section of the heat pipe was exposed the surrounding atmosphere at room temperature.

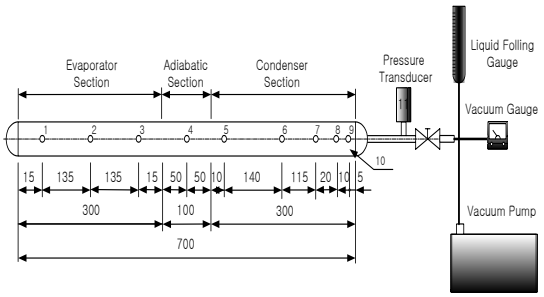


Fig. 2 Schematic diagram of heat pipes and position of thermocouple

2-2 Experimental Method

In the first series of experiments conducted, the effect of fill ratio on performance was determined. The heat pipe was filled with different fill ratio equal to 30%, 40% and 50% of evaporator volume. Heat input device is designed exploit the stainless steel pipe itself as the heat generator. Electrical power is passed through the pipe of evaporator section. An accurate variable transformer is used to control the amount of heat input. Heat pipe is well designed to be easily rotation from the horizontal to vertical and exact inclination angle can be read accurately. After adjusting the inclination angle, the heat input was continuously increased with small step size until the local temperature 500℃, 600℃, 700℃, and 1000℃.

3. RESULTS AND DISCUSSIONS

Fig. 3 describes the case in which the electric furnace was heated till the inside temperature reached 600℃ and maintained at the temperature when the heat pipe was put into the electric furnace.

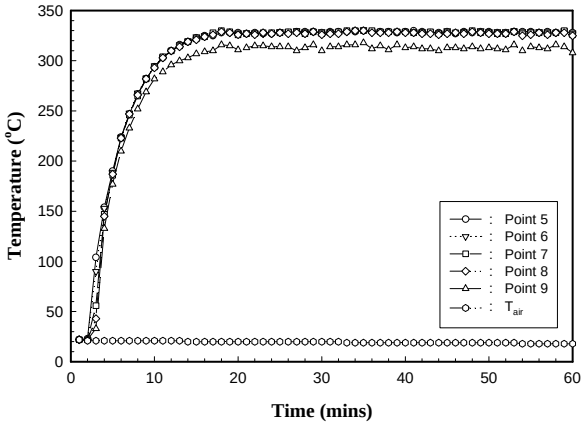


Fig. 3 Transient outer wall temperature in condenser during start-up(at Ta=500℃)

The angle of the heat pipe remained the same in the previous case at 10 degrees. From P5 to P9 the temperature of the condenser is shown while the flat part at the bottom presents the ambient temperature of the condenser. At the flat part the biggest temperature changes are observed at the evaporator in its outer wall temperature, which is indicated in the temperature of the heating zone. The graph shows that the temperature maintains in the almost similar distribution and that the heat pipe works normally at the exhaust heat of 500℃.

Therefore it is possible to use Dowtherm A as the working fluid at around 500℃. At Fig. 5, the furnace was heated until the ambient temperature reached 600℃ and maintained at the temperature when the heat pipe was inserted into the electric furnace. The angle of the heat pipe remained at 10 degrees.

As in the Fig. 3, the temperature was measured every 100mm at the condenser, which the results are revealed from P1 to P5 and resemble the similar trend observed in Fig. 4. The normal temperature changes began to be observed after 10 minutes, from which point the normal working also started.

At Fig. 4, the furnace was heated until the ambient temperature reached 600℃ and maintained at the temperature when the heat pipe was inserted into the electric furnace. The angle of the heat pipe remained at 10degrees.

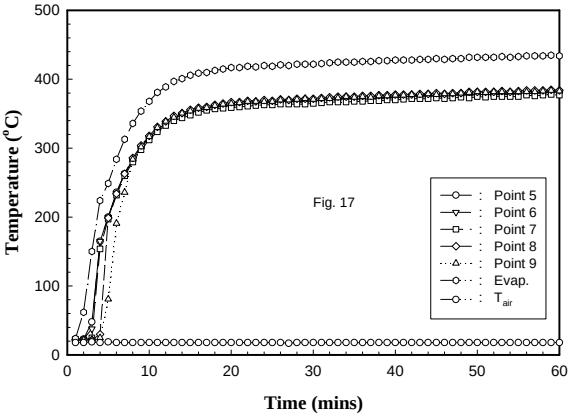


Fig. 4 Transient outer wall temperature during start-up(at Ta=600℃)

Fig. 5 presents the changes to the saturated pressure inside the heat pipe when the vapor temperature was increased to 150℃, 200℃, 250℃ and 300℃.

Fig. 6 shows the changes of the saturated pressure when the angle of inclination of the heat pipe was changed to 5, 30, 60 and 90 degree with the vapor temperature inside the heat pipe set at 250℃ and the charging rate of the working fluid set at 30%. The results tell that there are no influences from the changes of the angle of inclination.

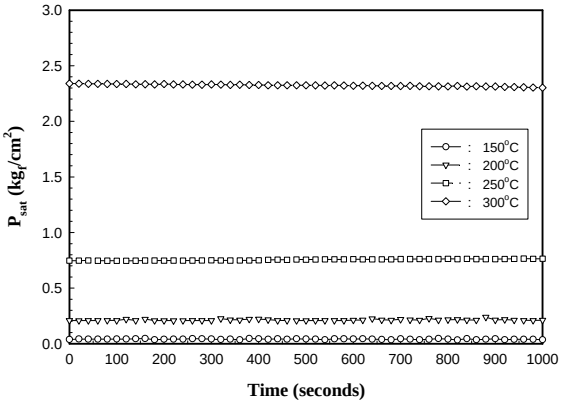


Fig. 5 Saturated pressure in heat pipe during start-up

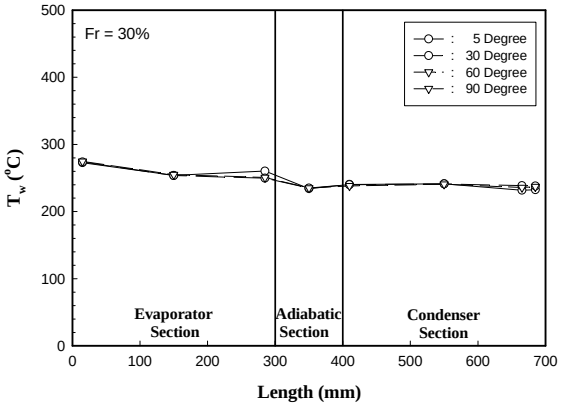


Fig. 6 Outer wall temperature depending on inclined set-up(at filling ratio 30%)

Fig. 7 presents the temperature distribution of the condenser of the heat pipe when the inside of the furnace was 800℃ in temperature. The abnormal signs started to show about 20 minutes after the measurement, when it was observed that the wall surface temperature of the condenser began to drop.

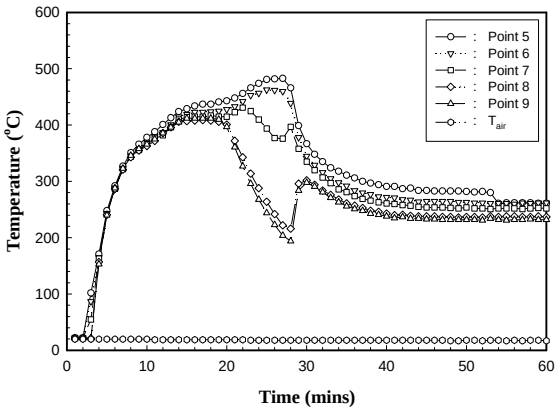


Fig. 7 Transient outer wall temperature during start-up(at Ta=800℃)

This was regarded as the working limits of the working fluid, which didn't seem to normal function any more. All these cases suggest that there happens to dry out when the ambient temperature is around 800℃ and the dry out leads to the remarkable deterioration in the performance of the heat pipe. That is, Dowtherm A means no operation at about 800℃ of ambient temperature. In this case the vapor temperature tends to be around 370℃, which seems to be the working limits of the working fluid.

Fig. 8 shows the temperature distribution when the vapor temperature was set at 250, 320, 370 and 400℃. The operation was normal when the vapor temperature was 370℃ or lower, and dry out took place as the temperature went up above 370℃.

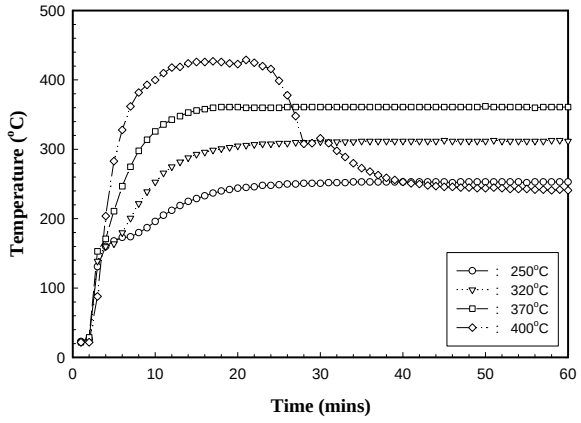


Fig. 8 Transient vapor temperature during start-up

Fig. 9 shows the thermal resistance of the part from the wall surface of the evaporator to that of the condenser according to the amount of working fluid and temperature changes. The lower was the temperature, the greater was the thermal resistance, which declined suddenly at 250℃. When the temperature was 250℃ or higher, the thermal resistance pattern was the same regardless of the amount of working fluid.

Fig. 10 presents the coefficient of heat transfer of the evaporator according to the changes of the vapor temperature. When the working fluid took up 40%, the temperature increased higher than the case of 30%. The temperature increase was slower than that of the condenser.

Fig. 11 presents the coefficient of heat transfer at the condenser when the working fluid was increased to 20%, 30% and 40%. As the vapor temperature went up higher, the coefficient of heat transfer grew bigger. The coefficient increased more when the working fluid was 40% than 30%. The coefficient went up almost 150℃ or higher when the temperature was 200℃ and the 40% of the working fluid was used, which proves that the working fluid works fine when the temperature is medium or high.

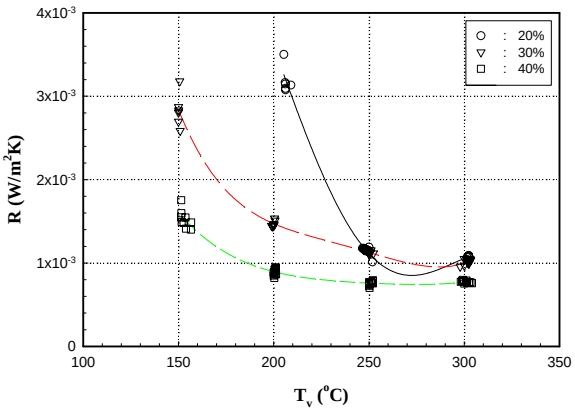


Fig. 9 Thermal resistance depending on vapor temperature and filling ratio

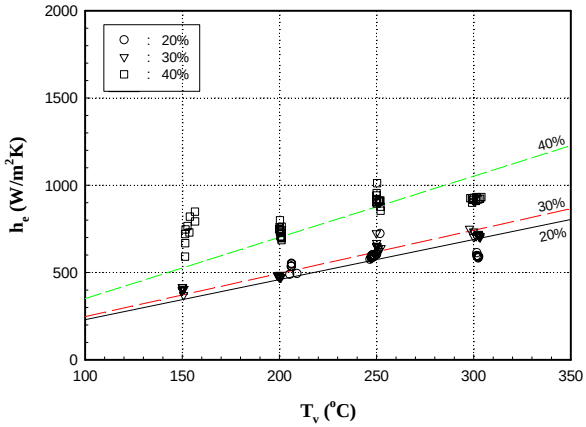


Fig. 10 Heat transfer coefficient in evaporator depending on vapor temperature and filling ratio

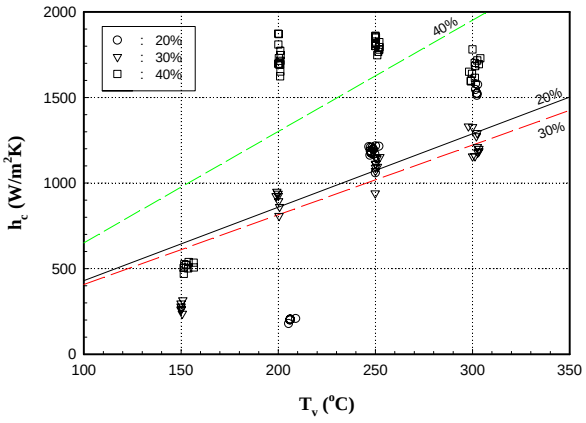


Fig. 11 Heat transfer coefficient in condenser depending on vapor temperature and filling ratio

4. CONCLUSIONS

The following conclusions were drawn from the results:

The medium temperature heat pipe was developed by using the Dowtherm A working fluid at the operational range of 150～420℃.

The higher was the saturated temperature, the higher was the wall temperature and heat conductivity of the heat pipe. The heat pipe was hardly working when the saturated temperature was 150℃ or lower.

When the condenser of the heat pipe was forced to cool and the saturated temperature of the working fluid was 300℃, the heat conductivity was about 630W. And it was further expected for heat conductivity to increase when a fin was attached to the exterior of the condenser.

References

1. H. J. Brommer, Theoretical and Experimental Investigation of Two-Component Heat Pipe. Institute of Kernenergetik, Stutgart, Federal Republic of Geomany. AiAA Paper No. 74-720.
2. J. M. Baum, M. N. Ivanovsky, Experimental Study of Heat and Mass Exchanger Phenomena in the Two-component Heat Pipe, Institute of Physics and Power Engineering. USSR Paper FB7.
3. C. L. TIEN , A. R. ROHANI, 1972, Theory of Two Component Heat Pipes, J. of Heat Transfer Nov. pp 479-484.
4. A. Faghri, 1986, Flow Analysis in Double-Walled Concentric Heat-Pipe Numerical Heat Pipe Vol. 10, pp583-593.
5. A. Faghri, S. Tomas, 1989, Performance Characteristics of a Concentric Annular Heat Pipe: Part1-Experimental Prediction and Analysis of the Capillary Limit. Tras. of the ASME. pp844-850.
6. A. Faghri, 1989, Performance Characteristics of a Concentric Annular Heat Pipe: Part2- Vapor Flow Analysis J. of Heat Transfer Vol.111, pp851-857.
7. Hideaki Imira, Masamichi Yoshida, 1998, The Extraction of Geothermal Energy by a Long Double Tube Therosyphon, Proceedings of 7th international Heat Pipe Conference, Edited L.L. Vasiliev, pp 349-359.

Transient and Start-up Behavior of a Double-Condenser Design LHP for Monitor of All Sky X-ray Image (MAXI)

Hiroki Nagai, Miki Muto*, Masahide Murakami*, Shiro Ueno, Masaru Matsuoka

Office of R&D, National Space Development Agency of Japan,
2-1-1 Sengen, Tsukuba, Ibaraki 305-8505 Japan
TEL: +81-29-868-4202, FAX: +81-29-868-5970, E-mail: nagai.hiroki@nasda.go.jp

*Institute of Engineering Mechanics and Systems, University of Tsukuba,
1-1-1 Tennoudai, Tsukuba, Ibaraki 305-8573 Japan

Abstract

A loop heat pipe (LHP) is used as the heat transport device to reject heat from the Monitor of All-sky X-ray Image (MAXI). Since this LHP was designed exclusively for the MAXI system, it is different from conventional LHPs in configuration, a double-condenser design. We experimentally investigated the effects of the particular design of this LHP on the heat transfer performance by using the LHP Ground Test Unit (GTU) on the ground. The steady heating experiment was carried out to investigate the steady state performance of LHP. When the two condensers were cooled at different temperatures under a steady heating condition, a quasi-periodic temperature oscillation was observed in the evaporator and accumulator area. We experimentally investigated the cause and the mechanism of the temperature oscillation.

Key words: LHP, MAXI, Double-condenser, Imbalance, Oscillation, Start-up

1. INTRODUCTION

The Monitor of All-sky X-ray Image (MAXI) is an X-ray all-sky monitor, which has been selected as a payload on JEM Exposed Facility. MAXI will scan the whole sky as the ISS orbits around the earth. MAXI is equipped with two kinds of X-ray slit cameras, a Gas Slit Camera (GSC) and a Solid-state Slit Camera (SSC). The detection sensitivity of them is the highest among those ever developed as all-sky monitors. MAXI is to perform the systematic survey of the X-ray variability to study the nature of the active celestial objects [1].

The SSC consists of 32 X-ray CCD chips. Each chip is cooled down to -60 °C by a Peltier device and the heat from the hot side of the Peltier device (camera body) is rejected from the two radiators. These radiators are placed on the top and front sides of the MAXI package. The Loop Heat Pipe is used to transport tens of watts of heat from the Peltier devices to the radiators. This model differs from conventional LHPs in the configuration that it has two-condensers connected in parallel to a common evaporator [2-4]. Each of the radiators has different radiation area and thus the different pipe length of the condenser. It is anticipated that the thermal condition of each condenser may be independent of each other because they point toward different directions. We experimentally investigated this effect on the heat transfer performance and the transient thermal behavior for case where there was some temperature difference between the two radiators. It should be added that the transient and start-up behavior from a low power state might be one of the technical concern for the LHP.

2. EXPERIMENTAL SETUP

The LHP Ground Test Unit (GTU) is schematically illustrated in Fig. 1. It consists of an evaporator, a hydro-accumulator, two condensers, two vapor lines, two liquid lines, and a liquid supply line. The LHP used in this study was procured from Swales Aerospace Corporation. A description of this unit provided by the vender is shown in Table 1. In this paper, the liquid lines between the junction and each condenser are called the liquid line-A and the liquid line-B. The line between the junction and the accumulator is called the liquid supply line. The vapor lines to each condenser branch off in the middle of the lines from the evaporator. They have flexible hose portions to facilitate bending. The LHP for the MAXI is actually used in a bent

Table 1 Main parameters of GTU

Vapor line ID	5mm
Liquid line, liquid supply line ID	2mm
Condenser ID	4mm
Accumulator ID	89mm
Accumulator length, Volume	89mm, 103.8cm^3
Length of vapor line (total, including flexible hoses)	2m
Length of liquid line (total, including flexible hoses)	1.1m
Length of Condenser-A	4.4m
Length of Condenser-B	3.2m
Working fluid	Propylene

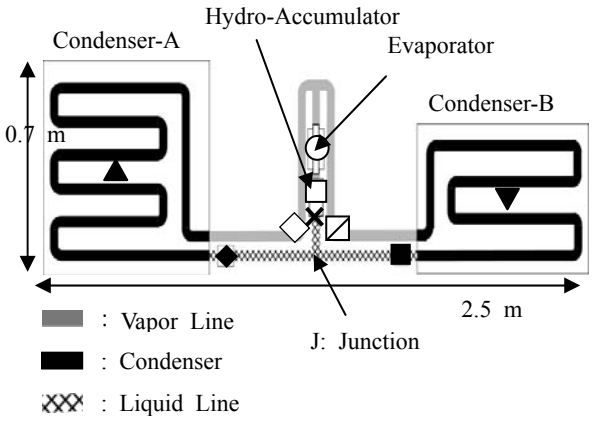


Figure 1 Schematic illustration of GTU. The location of thermocouples are; ○:Evaporator, ◇:Vapor Line-A, ▲:Condenser-A, ◆:Balancer-A,⊠:Vapor Line-B, ▼:Condenser-B, ■:Balancer-B, ×:Liquid Supply Line, □: Hydro-Accumulator.

configurations as the two radiators are set to face different directions (yaws and roll directions). The double-condenser design maximizes the available surface area for an active radiator while avoiding solar irradiation. In the present ground test, the GTU is set in a flat configuration on a horizontal table to minimize the gravity effect. The condensers are integrated into aluminum panel radiators. The flow balancers installed at the exit of each condenser are composed of fine porous flow passages. The working fluid is not ammonia but propylene in order to avoid freezing during the transfer period from the Exposed Pallet to the port, which takes 26.5 hours at maximum, under zero power conditions.

Thick copper plate cooled by forced flow of water supplied by two separate water chillers are bolted on each radiator and are used for heat sinks in the experiments. We call these plates the sink plates and designate the temperatures of the sink plates as T_{sink-A} and T_{sink-B}. Forty-six type-T thermocouples were used to measure the temperatures of the key portions of the GTU, the environment and cooling water. The locations of the representative thermocouples are also indicated in Fig.1.

3. RESULTS AND DISCUSSION

3-1 Steady State Performance

We conducted some tests to investigate the general performance of LHP for the case under an ambient temperature condition without sink plates. The heat transported from the evaporator to each condenser is released from the radiators by the natural convection of air at the temperature of 25℃. Figure 2 shows the result of the time variations of the temperatures at some key points as the heater power Q stepwise increases by every 10W from 40W up to 90W. Every temperature at each location of the loop reaches a steady-state value about three hours after the heater switched-on. From the uniformity of the steady temperatures throughout the loop except at the evaporator, it is found that this LHP has high thermal performance as a heat conductor. Figure 3 shows the steady temperature values at several locations as a function of Q. It is seen from Fig.3 as well as from Fig. 2 that the steady temperature of the whole GTU rises monotonously with Q. On the other hand, the temperature differences between the evaporator and two liquid lines decrease as the increase of Q up to 60W. It suggests that the GTU comes to operate with a high conductance as Q increases, and when Q = 60W, the GTU reaches a kind of constant conductance state. Figure 4 shows the temperature distribution along vapor and condenser lines for several values of the heater power Q under the ambient temperature condition. It is seen from Fig. 4 that the active vapor area expands in both condensers as the increase of Q up to 60W. The active vapor area here means the region where the temperature is almost the same as that at the evaporator and where the vapor exists. Over 70W, both condensers are occupied by the vapor, and the temperature of the whole GTU increases as the increase of Q. The constant conductance state above-mentioned is denoted as the operation when the whole areas of both condensers are active for vapor condensation. It is also observed from Fig. 4 that the length occupied with the vapor in the condenser-A is somewhat smaller than that in the condenser-B below 20W. This experimental result indicates

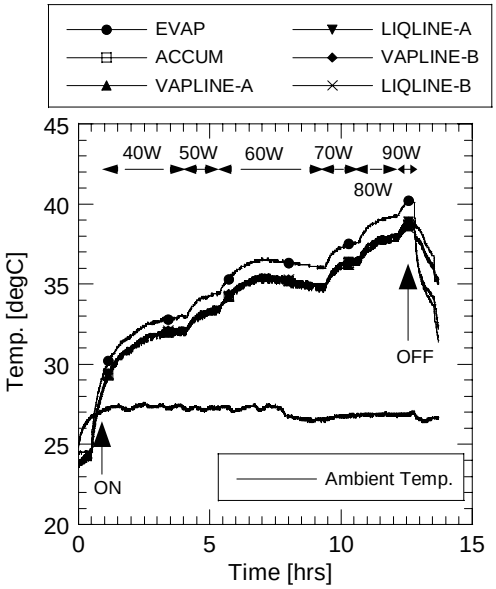


Figure 2 Time variations of temperatures at some key points as heater power Q stepwise increases by every 10W for 40W up to 90W.

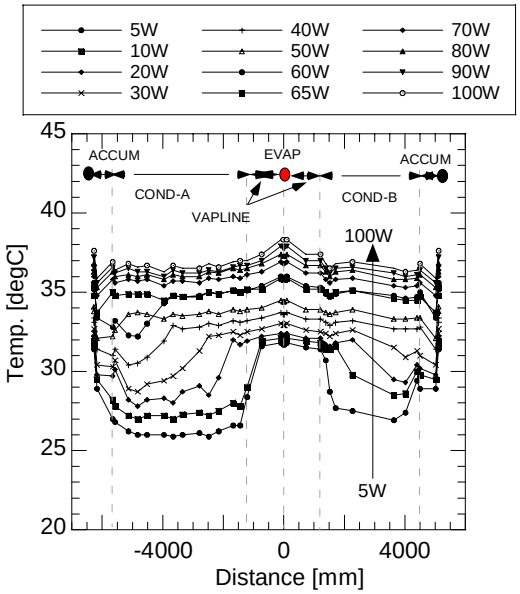


Figure 4 Temperature distributions along vapor and liquid lines for each heater power.

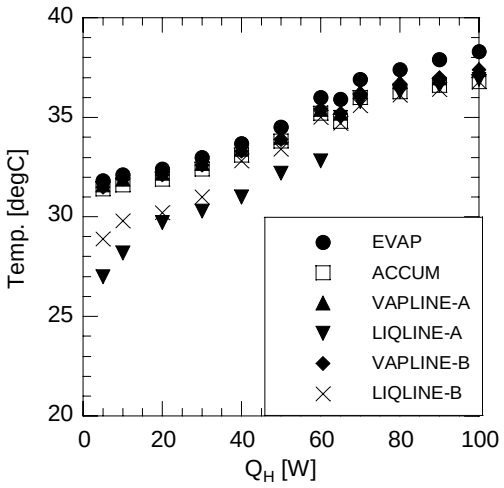


Figure 3 Steady temperatures at several locations as a function of Q.

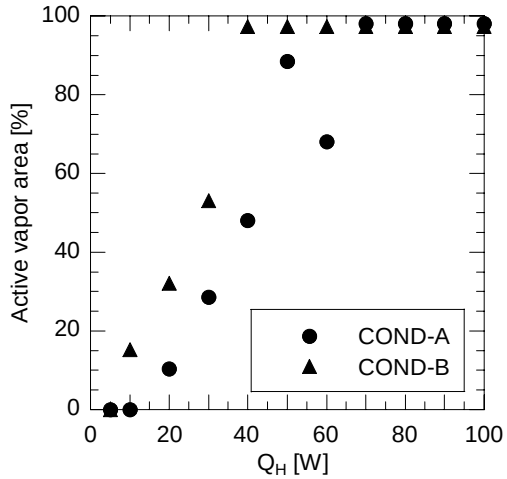


Figure 5 Active vapor areas in each condenser as a function of Q.

that the heat transported to each condenser is not always equal, especially in the case of lower input power. This may be caused by the working principle that the flow velocity of the working fluid in each condenser is adjusted to equalize the pressure drops through both condensers. In order to investigate the relation between the active vapor area and Q, we arranged the data into Figure 5, which shows the percentage of the active vapor area in each condenser as a function of Q. It is seen from this figure that active vapor area changes so that the lengths in two condensers should.

3-2 Imbalance Test

Figure 6 shows the time variations of temperatures at a number of key points where the condenser temperatures were unequal, 50℃ for T_{sink-A} and 5℃ for T_{sink-B}. In this case, it was anticipated that condenser-A stops the operation and condenser-B only rejects the heat because of the flow balancer is installed in the liquid lines. It, however, is of interest to note that a quasi-periodic temperature oscillation appeared in the evaporator and accumulator area with an amplitude of about 10℃ and a period of 60 minutes. The temperature of the liquid supply

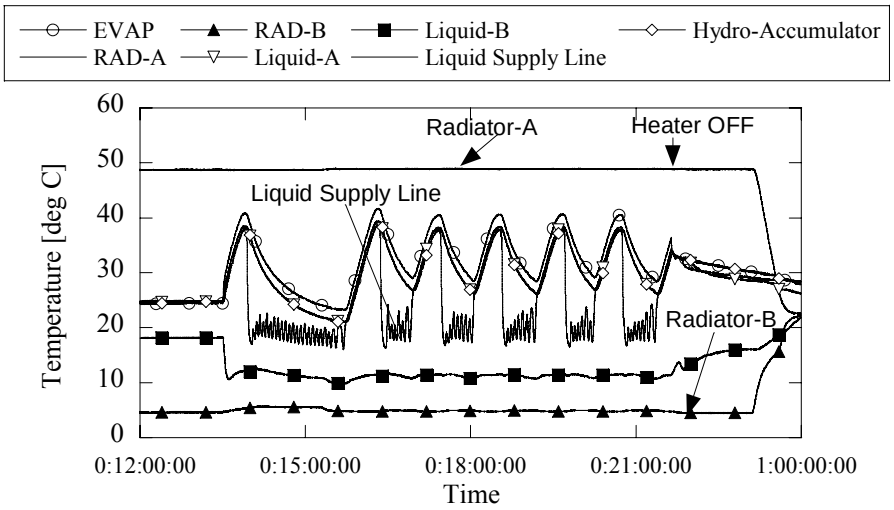


Figure 6. Time variations of the temperatures at several key points for case 1. T_{sink-A} and T_{sink-B} were set at 40℃ and 5℃, respectively, before the heater was switched on. Thermal oscillation is induced at Q=40W.

line also oscillates with an amplitude of 5℃ and a period of 3 minutes. This kind of temperature oscillation with such large amplitude and a period has not been reported for single-condenser LHPs. The distinctive feature of this phenomenon can be well understood if we look at the temperature variation at the liquid supply line. When the evaporator temperature rose, the temperature at the liquid supply line also rose as well as the temperature at the accumulator, and they were equal to one another. It suggests that saturated vapor occupied the liquid supply line and it was blocked with vapor bubbles. Subcooled liquid in the LHP was only existed in the condenser-B that was cooled to 5℃. Once the temperature at the liquid supply line dropped, the evaporator and accumulator temperatures gradually decreased. It indicates that the subcooled liquid from the condenser-B flowed into the accumulator through the liquid supply line, and gradually cooled down the evaporator and the accumulator. The main reason why the oscillation occurred is considered as follows. The temperature oscillation caused by oscillating mass flows between condensers. Mass flow oscillated between radiators depending on lower resistance path due to dried out of flow balancer. However, evaporator oscillates in temperature but does not shutdown.

Figure 7 shows the time variations of temperatures when T_{sink-B} was raised up to 25℃ for 90 minutes while Q was kept at 40W. This case may be considered as a simulation of the possible ISS orbital thermal environment for MAXI, in which the temperatures of one of the radiators become higher than that of the evaporator. It is seen that the temperature of the evaporator was kept almost constant even under such an abnormal radiator condition. The heat was rejected well from the condenser of lower temperature, condenser-A, when T_{sink-B} exceeded the temperature of the evaporator. Such a non-oscillating stable thermal behavior is assumed to continue because the balancer-B did not dry-out within 90 minutes. Judging from the above simulation result, we may conclude that it is almost impossible for a temperature oscillation to occur in actual cases because the temperatures of MAXI radiators change periodically only with a period of less than 2 hours.

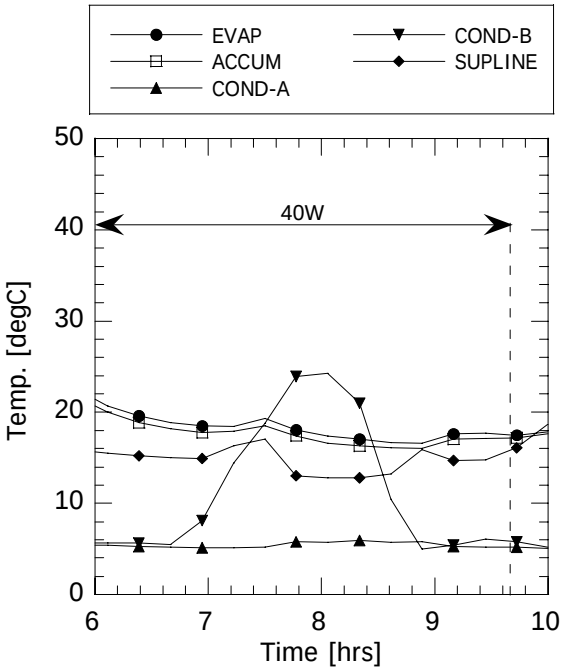


Figure 7 Time variations of the temperatures at several key points for case 3. T_{sink-B} was varied from 5℃ to 25℃ for 90 minutes from 6.7 hours to 8.2 hours while constant heating at 40W.

3-3 Start-up Test

Figure 8 is the result that the heater power Q=10W was first applied under the ambient temperature condition for 2 hours, and then Q was changed to 20W. It is indicated that the evaporator and the accumulator were heated to such a high temperature that the applied heater power was dissipated wholly to the surroundings by convection during the heating of Q=10W. When the heater power changed from 10W to 20W after a small temperature rise in the evaporator by a few degrees, the temperature of the evaporator and accumulator dropped rapidly. It is thus found that the required superheat between the evaporator and the accumulator was created when Q = 20W, and the LHP succeeded in the start-up at this moment.

The key to seriously influence the LHP start-up is the initial evaporator and accumulator condition. Generally, in the case where the LHP is used as the thermal control device, the temperature of the accumulator is controlled. If the accumulator is heated above the loop temperature, the liquid reserved in the accumulator goes out of there, and the loop gets flooded. Occupation of the liquid in the condenser prevents the heat input from being transported from in that section. Thus, the heat transported from the evaporator is smaller than that in the normal operation, and consequently the temperature of the evaporator

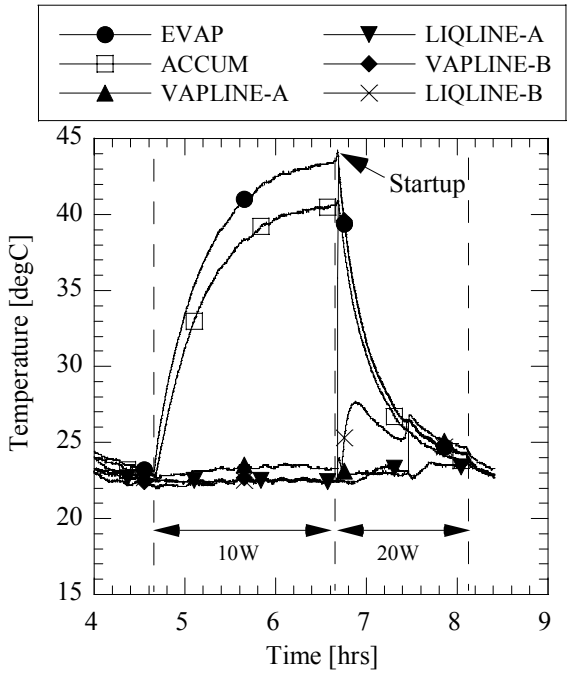


Figure 8. Start-up under temperature condition, where Q=10W was applied to evaporator. About 2 hours later, Q was changed to 20W.

becomes higher and the LHP stops. On the contrary, if the accumulator is cooled down, the surplus liquid is trapped in it, and the large portion of the condenser is filled with vapor. Thus, the evaporator soon cools down by releasing a lot of heat from the condenser.

In connection with the above, the following test was conducted, where only the accumulator was forced to cool by about 10℃ lower than the ambient temperature whereas the other portion of the LHP is exposed to the ambient thermal environment. Figure 9 shows the start-up where the heater power Q=40W was applied when the temperature of the accumulator reached 13℃ with cooling by the coolant and the other portions were at the room temperature of 25℃. As shown in the graph, the temperature of the evaporator overshot, and the heater was turned off because the temperature of the evaporator rose near the temperature margin of the device. In the normal operation at Q=40W, such a thermal behavior was not observed. Before testing, we were anticipated the start-up was more successful under the condition where the accumulator was cooled, but the most of the tests except at the relatively low power state resulted in start-up failures. The upper limits for the transported heat dropped by about 30W. It is supposed from this figure that when the heater power is applied, the vapor is not created in the evaporator because the temperature variation of the vapor line A and B was so gradually. This means the vapor passage were flooded with liquid at that time. Since the temperature variation at the accumulator was also very gradual, the evaporator core was filled with the liquid, and there were no vapor bubbles in it. By cooling the accumulator, the working fluid there is subcooled. Since the temperature of the subcooled liquid supplied in the evaporator core is considerably lower than the saturated temperature, more heater power is required for boiling. The temperature rise surpassing the quantity of subcooling is required for the incipient nucleate boiling. When the heater power is too large, the temperature of the evaporator exceeds the maximum temperature before the boiling is occurred. On the other hand, when the power is small, the evaporator is heated up gradually. Since the most liquid in the loop is trapped in the accumulator, the condenser is occupied with the vapor. Moreover, as the evaporator core is filled with liquid, the heat leak from the evaporator to the accumulator is small, and almost all the power is applied to the liquid in the vapor passage. Thus the start-up at low input power is easily achieved as compared with the start-up under the normal condition. As soon as

the nucleate boiling starts, the heat is transported to the condenser. However, a longer period, at fastest around an hour in the present case, is needed for the full start-up according to the amount of the power. Figure 10 shows the start-up under such a condition with an applied heater power of 10W. This figure indicates that the start-up was successful and no overshoot was observed. We tried the tests under the same condition at several times, and all the trials were successful. It is concluded that the upper limit of the transported heat under the situation where the only the accumulator is cooled down and the other portions of the LHP are at the room temperature is lower than that under the normal operation, and the greater care is needed for the start-up. The better way of the start-up is under this condition is that the heater power applied to the evaporator gradually is increased from lower power in order to prevent the temperature overshoot.

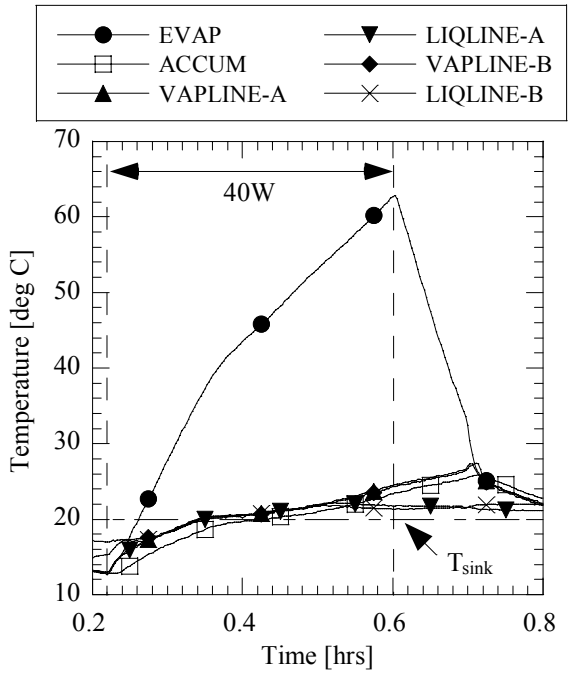


Figure 9. Start-up under the condition where only an accumulator cooled down to 13 ℃ whereas the other parts of LHP were exposed to ambient temperature condition.

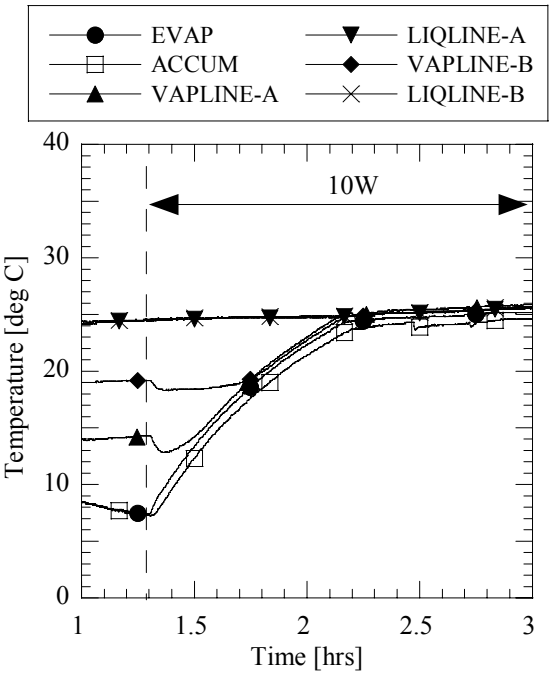


Figure 10. Successful start-up under the condition where only an accumulator cooled down to 10℃ whereas the other parts of LHP were exposed to ambient temperature condition.

4. CONCLUSION

To investigate the effects of the double-condenser design on the heat transfer performance, we conducted experiments using the LHP Ground Test Unit on the ground.

1. The thermal performance of the GTU was found to be satisfactory.
2. The heat is transported to each condenser so that the active vapor lengths in two condensers should become the same.
3. There were a few cases where a quasi-periodical temperature oscillation occurred in the evaporator and accumulator under unequal sink temperature condition.
4. When the accumulator was cooled down and the other portions of the LHP were at the room temperature, the temperature overshoot was apt to be occurred.

References

1. T. Mihara, M. Matsuoka, S. Ueno, H. Tsunemi and N. Kawai., 2001, “Monitor of All-sky X-ray Image (MAXI) on JEM-EF”, ISS Utilization Conference, AIAA Paper 2001-4973

2. Ku, J., 1999, “Operating Characteristics of Loop Heat Pipes”, SAE paper No. 1999-01-2007

3. Douglas, D., Ku, J. and Kaya, T., 1999, “Testing of the Geoscience Laser Altimeter System (GLAS) Prototype Loop Heat Pipe”, AIAA Paper 99-0473

4. Yu.F. Maidanik et al. “Some results of loop heat pipes development, tests and applications in engineering” Proc. Of the 5th Int. Heat Pipe Symposium, Melbourne, Australia, 17-29 Nov 1996, p-p 406-412

Miniature Loop Heat Pipes for CPU Cooling

V.M. Kiseev*, A.S. Nepomnyashy*, N.L. Gruzdova*, Kwang-Soo Kim**

*Ural State University, Department of Thermophysics and Surface Phenomena
Lenin av. 51, 620083, Ekaterinburg, Russia,
(3432) 616-775, (3432) 616-778 fax, Valery.Kiseev@usu.ru
**APACK, Inc., 59-6, Hwaam-dong, Yusung-ku, Daejon, 305-348, Korea,
+82-42-864-0815, +82-42-862-9815 fax, kskim@apack.net

Abstract

Extensive development Loop Heat Pipes (LHP) technology offers capabilities to play LHP an increasingly important role for instrument thermal control on some space and earth applications. However, heat transport systems on basis of miniature LHP (MLHP) are interesting in electronics packaging for high heat flux in zones of heat input and transport. The applications could include thermal management of a various electronic devices such as computer processors (CPU), where the heat dissipation requirement is expected to be in the range of 50 to 100 Watts. This paper presents some configurations of MLHP with flat plates of evaporators and examines the experimental data which are investigated for MLHP due to gravity. The heat transfer coefficient by phase exchange in the LHP capillary structures is investigated for different configurations of the vapor ducts, working fluids and capillary structures. Experimental tests verify that the Miniature LHP operate successfully by high heat flux in zones of heat input and transport and "loop heat pipe" heat transfer mechanism is better for these conditions than 'classical' heat pipe.

Key words: Loop Heat Pipe, Steady-state behavior, heat transfer coefficient, capillary structure, flat evaporator**.**

1. INTRODUCTION

Due to the extensive development efforts in ground tests and flight experiments over the last few years, the LHP have reached the state of technology readiness and commercialization. Theoretical studies are also being conducted to better understand the operational mechanism of the LHP. It is anticipated that the LHP will become a major player in the thermal management of space and terrestrial systems in the near future [1].

On the other hand, the LHP are excellent heat transfer devices for electronics packaging for high heat flux in zones of heat input and transport, when heat transport zone may connect heat source and heat sink by the flexible tubes at any orientation. It is important for a miniaturization of electronic components and for development of electronics as a whole [2,3].

This paper presents some configurations of MLHP with flat plates of evaporators and examines the experimental data which are investigated for MLHP due to gravity. The experiment effort was supplemented by extensive hardware development efforts, analytical modeling development and ground test verification. Extensive ground test verification has been performed by Ural State University(USU) during the past several years. Results that are presented include:

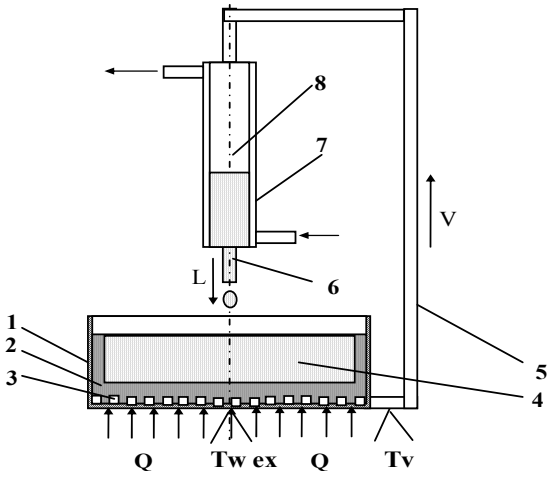
- The heat transfer coefficient by phase exchange in the LHP capillary structures as a function of heat input, of different configurations of the vapor ducts, of working fluids and of capillary structures.
- MLHP performance as a function of heat input/heat sink, of heat agent, of orientation and of accelerations.
- Power cycling and sink temperature cycling behavior.
- Temperature and pressure drop characteristics.

2. EXPEREMENTAL APPARATUS AND PROCEDURE

In fact, in electronics packaging for high heat flux in zones of heat input where the LHP capillary structure is a generator of vapor and capillary pump the heat transfer coefficient cannot be avoided. The external and internal heat transfer coefficient can be defined. The external heat transfer coefficient is defined by a good contact between electronic components and LHP evaporator wall and is not of interest of LHP performance. The internal heat transfer coefficient

is very important for LHP performance by high heat flux and defines the possibility to lead out of heat by using phase exchange in the LHP wick. In spite of a lot the theoretical and experimental studies in these conditions it is not a clear reply how to increase heat transfer coefficient by using capillary phenomena.

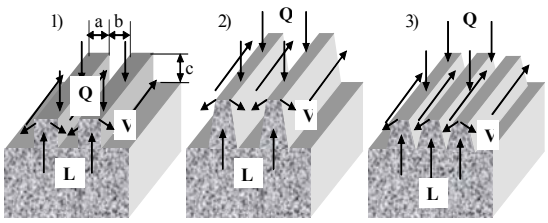
The effects of the phase exchange in the LHP wick were studied by using the open LHP system (external pressure about 10^5 Pa.). The schematic diagrams of experimental apparatus are shown in Fig. 1.



1 – LHP evaporator
2 – capillary structure (wick)
3 – vapor ducts (grooves)
4 – compensation chamber (cavity)
5 – vapor line
6 – liquid line
7 – condenser
8 – water cooler
9 – copper heater
Tw ex, Tw in, Tv – thermocouples

Fig. 1 Open LHP systems

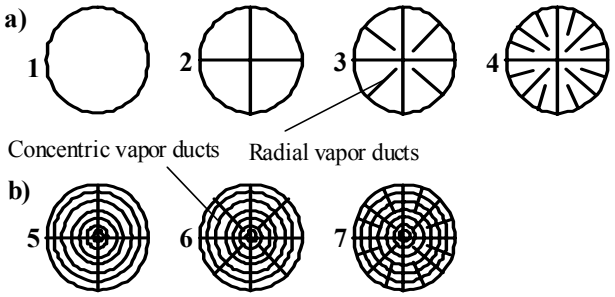
The configuration and the geometrical sizes of vapor ducts in the LHP open system (Fig. 1) were optimized. Fig. 2 and Fig. 3 give examined configurations of vapor ducts.



（1 – Rectangular vapor ducts, 2 – trapezoid vapor ducts, 3 – triangular vapor ducts）

Fig. 2 Geometry of concentric vapor ducts

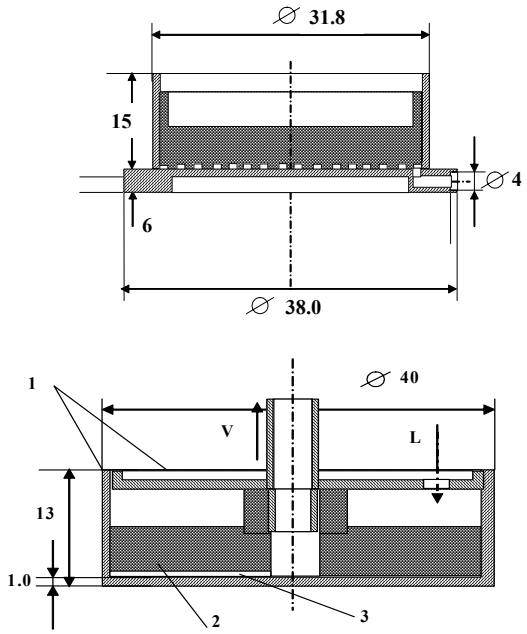
Metal wick development status including nickel and titanium with effective pumping in the range of 0.5 to 3 micron and permeability in the range 1 x 10^{-14} m^2 to 4 x 10^{-13} m^2 was based in this studying.



a) only radial vapor ducts
b) radial and concentric vapor ducts

Fig. 3 Configurations of vapor ducts (1 ~ 7)

The researching object (LHP or system of it's modeling) was located in thermostatic box where with a help of automatic regulation system the temperature of the environment was Tenv = 20±0.5 ^oC or Tenv = 50±0.5 ^oC. The methodic of the experiment was oriented on measuring of the temperature fields of researching objects with different heat agent, orientations and temperatures of the environment and heat sink. The heat input was controlled through variable transformers and measured with wattmeter. Heat input rate was given by a resistive electric heater and measured by a calorimetric plate. At the condenser heat out was taken by means of water in the water jacket which was installed in cooling section. Water flow rate and the inlet/outlet temperature were measured and heat transfer rates were calculated by calorimetric method. Temperature was measured with copper constantan thermocouples located at appropriate points on the tube wall and surrounding insulation at the evaporator, condenser and adiabatic sections in each. The precision of measurements of the heat flow rate was no higher than 5%, and the precision of measurements of temperatures was no higher than 0.5%. Before the beginning of the experiment was checked the connection between a wick and a case of evaporator by the air-bubble method. The experiments were realized for adverse 1g acceleration (evaporator above condenser "+H") and favorable 1g acceleration (condenser above evaporator "-H"). Fig. 4 shows the basic configuration and geometrical size MLHP flat plates of evaporators.



1 – case of evaporator, 2 – wick (capillary structure), 3 – vapor ducts

Fig. 4 The basic configuration and geometrical size MLHP flat plates of evaporators

3. EXPERIMENTAL RESULTS

At the first step of experiment was studied the influence of the wick (Table 1) thickness (**b)** (also see b in Fig. 2 as width of vapor grooves) on a heat transfer coefficient (**α**) with heat agent of water. This data are presented in Fig. 5, Fig. 6 and Fig. 7. The internal heat transfer coefficient **α** (W/m^2 K) is defined as

$$\alpha = \frac{q}{T_{win} - T_v}, \qquad q = \frac{Q_{tr}}{S_{inp}} \qquad (1)$$

where $\boldsymbol{q}$ is heat flux (W/m^2), $\boldsymbol{Q_{tr}}$ is heat transfer rates calculated by calorimetric method in condenser, $\boldsymbol{S_{inp}}$ is the square of the heat input surface, $\boldsymbol{T_{w\ in}}$ is temperature on the internal surface of a evaporator wall (the surface of the contact between a case wall and a wick) and $\boldsymbol{T_v}$ is temperature of vapor. As can be seen from this comparison the dependences **α = f(q)** have maximum that is evidence of a competing phenomena into capillary structure between liquid and vapor flow. Besides there is the increasing of heat transfer coefficient by the placing of concentric vapor grooves on the evaporator wall.

After optimization of the placing of the concentric vapor grooves that is determined practically of geometry of heat and mass input to surface of evaporation into capillary structure was made several series of experiments. The radial vapor ducts had only quadratic profile (1 x 1 mm) on a surface of the wick. The concentric vapor ducts had a different profile (Fig. 2).

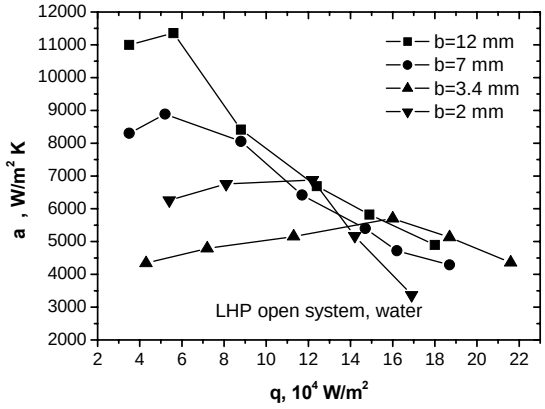


Fig. 5 Dependence the heat transfer coefficient **α** on the heat flux **q** for Titanium wick (No. 2, Table 1). Open LHP system by external pressure about 10^5 Pa. Conf. No. 6 (Fig.3), radial vapor grooves 1x1 mm and 13 concentric vapor c=0.5 mm, b=0.3 mm, a=0.7mm. The vapor grooves are located on the wick only

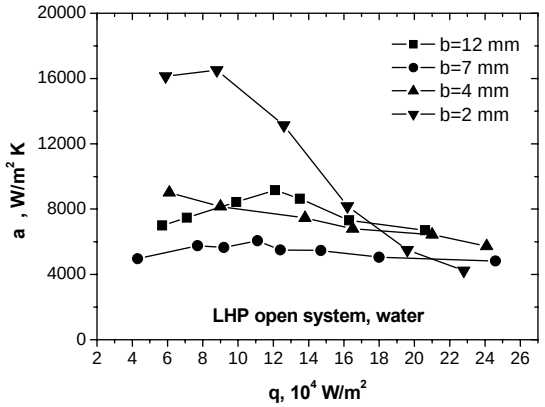


Fig. 6 Dependence the heat transfer coefficient **α** on the heat flux **q** for Titanium wick (No. 2, Table 1). Open LHP system by external pressure about 10^5 Pa. Conf. No. 6 (Fig.3), radial vapor grooves 1x1 mm on the wick and 13 concentric vapor grooves c=0.3 mm, b=0.3 mm, a=0.4 mm on the wall

Table 1. Main properties of metal wicks

No.	Wick material	Porosity ε, (%)	Effective pore radius R, 10^{-6} (m)	Permeability K, 10^{-14} (m^2)	Effective thermal conductivity λ, (W/m K)
1	Titanium (Ti)	55	4.1	33.9	1.29
2	Titanium (Ti)	50	3.6	28.3	1.77
3	Nickel (Ni)	65	0.65	2.2	8.04
4	Nickel chips of porous Ni	53	1.4	2.2	9.16

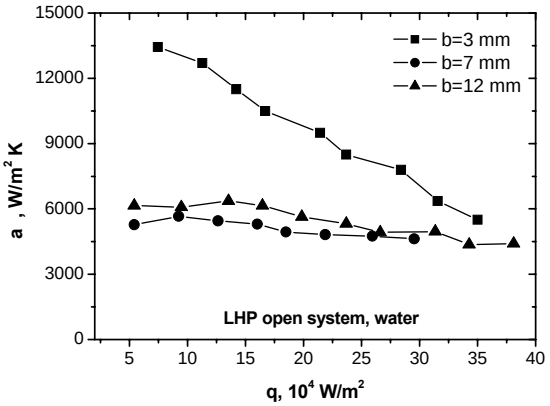


Fig. 7 Dependence the heat transfer coefficient **α** on the heat flux **q** for Titanium wick (No. 1, Table 1). Open LHP system by external pressure about 10^5 Pa. Conf. No. 6 (Fig. 3), radial vapor grooves 1x1 mm on the wick and 13 concentric vapor c=0.3 mm, b=0.3 mm, a=0.4 mm on the wall

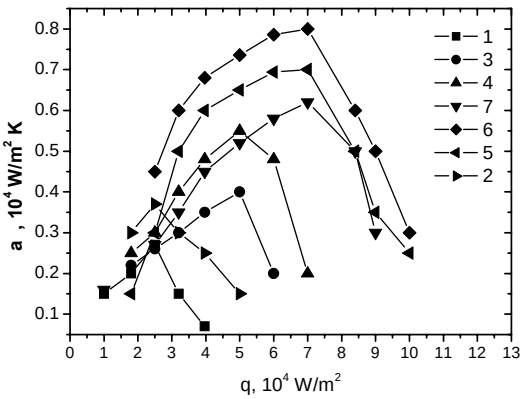


Fig. 8 Dependence the heat transfer coefficient **α** on the heat flux **q** for Nickel wick No. 3 (Table 1) 1 – No. 1 (Fig. 3), $\xi = 0$; 2 – No. 2 (Fig. 3), $\xi = 0.09$; 3 – No. 3 (Fig. 3), $\xi = 0.16$; 4 – No. 4 (Fig. 3), $\xi = 0.23$; 5 – No. 5 (Fig. 3), $\xi = 0.33$; 6 – No. 5 (Fig. 3), $\xi = 0.42$; 7 – No. 7 (Fig. 3), $\xi = 0.61$; Adverse 1g acceleration H = + 0.03 m; open LHP system. Heat agent: **acetone**

The next series of the experiments solved a problem of optimization vapor ducts configurations and sizes. The models of the capillary structure (No. 3, Table 1) had the optimal thickness δ = 6 mm. The vapor ducts (radial and concentric, Fig. 2) had quadratic profile (1 x 1 mm) on a surface of the wick and a different configuration. The effective diameter of the vapor duct D_{ef} and their total relative section ξ are defined as

$$D_{ef} = \frac{4S}{\Pi}, \qquad \xi = \frac{S_{vd}}{S_{inp}} \tag{2}$$

where S is the square of vapor duct section, Π is vapor duct perimeter; S_{vd} is the total square of the section of the vapor ducts on the surface of the contact between the wick and the wall of heat input. These data are presented in Fig. 8.

As can be seen from Fig. 8 the maximum heat transfer coefficient by the maximum of heat flux is achieved by $\xi = 0.4$ -0.45 (No. 5, Fig. 2) as for open LHP system and for close LHP system. Existence of an optimum in surface configuration of vapor grooves gives the evidence about the competition between hydraulic and thermal resistances in zone of vapor grooves.

By this study we didn't observe the visible influence of concentric vapor ducts profile on heat transfer process. Therefore we used triangular concentric vapor ducts surface as more technological. They were located on an internal surface of the wall of heat input.

After optimization of the coefficient ξ that is determined practically of geometry of heat and mass input to surface of evaporation into capillary structure was made several series of experiments. It solved a problem of optimization of a wick material and a heat agent in LHP directly. The LHP main specifications are presented in Table 2.

Table 2. Main specifications of LHP

Specifications	LHP1	LHP2
Total length, (mm)	350	450
Liquid/vapor line, (mm)	400 / 270	450 / 350
Evaporator length/diameter, (mm)	20 / 27	21 / 32
Condenser temperature	40 °C	45 °C
Condenser length/diameter, (mm)	85 / 9	85 / 9
Internal liquid/vapor line diameter, (mm)	2 x 0.5/ 2 x 0.5	1.6 x 0.3/ 3 x 0.5
Wick material (Table1, No)	Nickel No. 3	Titanium No. 1
Maximum total heat input, (W)	70 vertical (+90°)	160 vertical (-90°)
Maximum heat input flux, (W/m^2)	22 vertical (+90°)	30.5
Heat agent	Acetone	Water
Tw ex (Fig.1)	86 °C	150 °C
Thermal resistance, (K/W)	0.1-0.4	0.5 -0.8
Total mass of LHP, (g)	104	95

Fig. 9 shows the temperature of the LHP No.1 for the adverse 1g acceleration due to gravity (+90°). As can be seen from Fig. 8 the evaporator temperature increase rapidly by Q = 70 W and it is connected with heat transfer limitations.

Fig.10 gives the comparative analysis of the LHP No.1 operating characteristics for a different vector of acceleration. The favorable acceleration decreases the evaporator temperature up to 15-20% for different heat mode in these conditions.

The main thermophysical properties of heat agents are presented in Table 3.

The selection of LHP heat agents can be done on the base of a Heat Transfer Complex (HTC) $\frac{Hev \cdot \sigma_l}{\upsilon_v}$. The more this complex the better is heat agent for LHP. As can be seen from Table 3 the best heat agent for LHP by 60°C is ammonia.

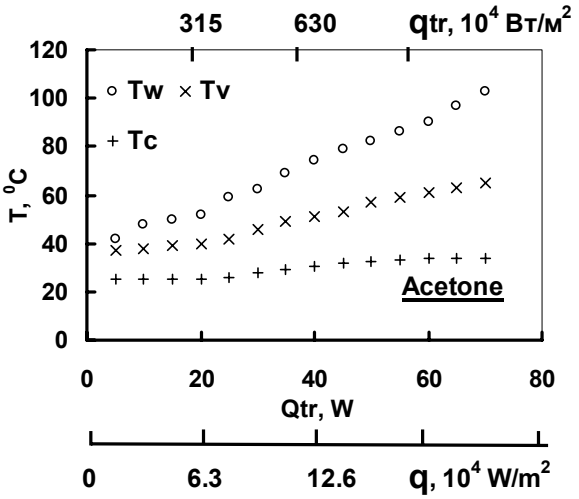


Fig. 9 Performance capabilities of LHP No.1 by an adverse 1g acceleration (+90°)

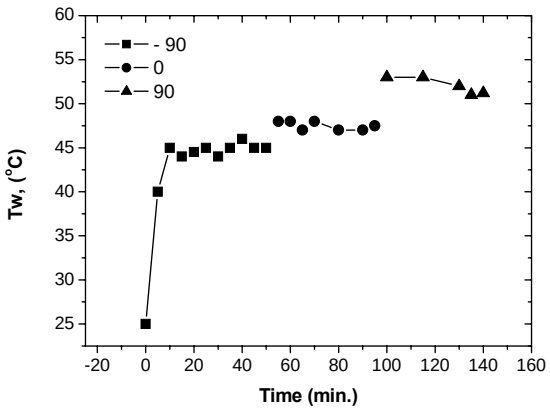


Fig. 10 LHP No.1 dynamic characteristics by the acceleration change (Q_{tr} = 25 W), heat agent-acetone

Fig. 11 gives the comparative analysis of the LHP No. 2 calculated pressure drop distribution for heat agent water and ammonia. The using ammonia appreciably decreases the vapor line pressure drop and improves the operating characteristics of LHP in these conditions.

Fig. 12 shows the temperature of the LHP No. 2 for the favorable 1g acceleration due to gravity (-90°). As can be seen from Fig. 12 the evaporator temperature increase rapidly by Q = 160 W and it is connected with heat transfer limitations.

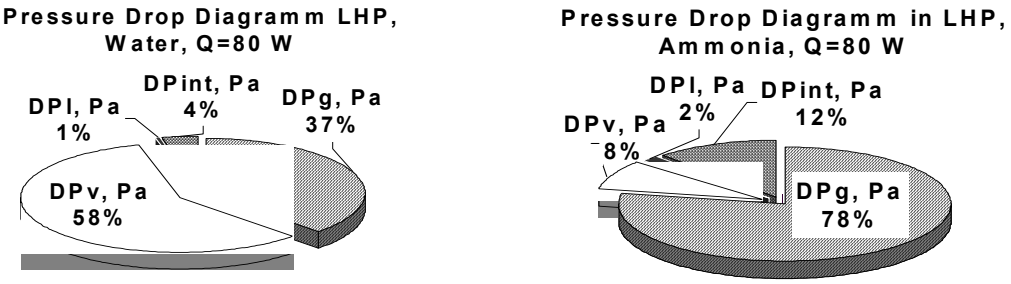


Fig. 11 Calculated pressure drop distribution of LHP No. 2 (Table 2): adverse 1g acceleration

Table 3. Main thermophysical properties of heat agents by 60 ^{o}C

Thermophysical properties	Water	Acetone	Ammonia
Hev Latent heat, (kJ/kg)	2359	517	1026
σ_l Surface tension, (10^{-3} N/m)	66.2	18.6	13.7
υ_v Vapor kinematic viscosity, (10^{-7} m^2/s)	800	38	6.2
HTC $\frac{Hev \cdot \sigma_l}{\upsilon_v}$, ($10^7$ W/m^2)	195.2	253.1	2267.1

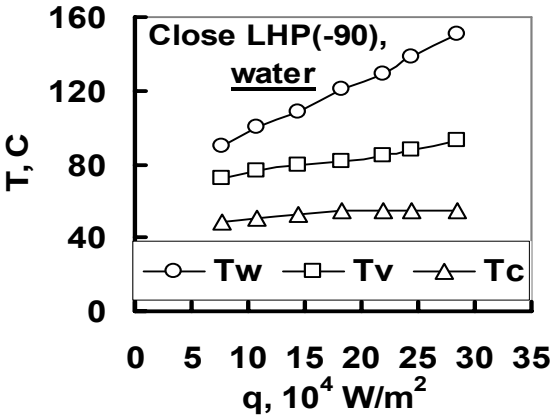


Fig. 12 Performance capabilities of LHP No. 2 by a favorable 1g acceleration (-90^{o})

4. CONCLUSIONS

The results obtained in heat transfer experiments in MLHP with flat plates of evaporators are summarized as follows:

(1) There is an optimal thickness of the fine porous wick (about 5-7 mm) for concrete conditions of MLHP operation.

(2) It is showed that for the intensification of heat transfer in zone of heat input of MLHP with flat plates of evaporators a special system of vapor ducts is necessary. There is the optimal surface square of vapor grooves not more than 0.4 – 0.5 from heat input square.

(3) The decreasing of the sizes and distance between concentric vapor ducts goes to intensification of heat transfer and the increase of heat transfer coefficient. The placement of concentric vapor grooves on an internal surface of the wall increase the heat transfer coefficient more than (10 – 30) %. Apparently, the decrease of distance between concentric vapor ducts decreases the distance of vapor exit from vapor pores to vapor grooves improves the vapor collection from pores and accordingly intensify heat transfer in fine porous structure.

(4) Experimental tests verify that the Miniature LHP operates successfully by high heat flux in zones of heat input and transport and “loop heat pipe” heat transfer mechanism is better for these conditions than ‘classical’ heat pipes. The best heat agent for LHP is heat agent with large Heat Transfer Complex by concrete conditions of LHP operation.

References

1. Faghri A. Heat pipe science and technology, Taylor & Francis, Washington, 1995, pp. 578-624.
2. Kiseev V., Belonogov A. Miniature heat transport systems with loop heat pipes, *Proc. of 4th Minsk Int. Seminar ‘Heat Pipes, Heat Pumps, Refrigerators”*, Minsk, Belarus, 2000, pp. 15-22.
3. Chernysheva M.A., Vershinin S.V., Maidanik Yu.F. Development and test results of loop heat pipes with a flat evaporator, *Proc. of 12th Int. Heat Pipe Conference*, Moscow, Russia, 2002, pp. 134-138.

Waste Heat Transportation by High-Speed Two-Phase Flow in a Closed Loop with a Vapor Accumulation Evaporator

Katsuhiko KADOGUCHI and Masakazu YAMAZAKI
Institute for Energy Utilization, National Institute of Advanced Industrial Science and Technology
16-1 Onogawa, Tsukuba, Ibaraki, 305-8569, Japan.
Tel. +81-29-861-8077, Fax +81-29-861-8208, e-mail : k.kadoguchi@aist.go.jp

Abstract

A heat transporting cycle already proposed by the authors was composed of the following processes: (A) accumulation of high-pressure vapor in an evaporator vessel, (B) discharge of the accumulated vapor from the evaporator followed by the condensation of a part of the vapor in the downstream condenser and the returning vapor-liquid two-phase flow from the condenser toward the evaporator, (C) return of the liquid to the evaporator through a check valve after the flow ceases. In the present study, the flow and downward heat transport characteristics of the device utilizing this method were investigated experimentally by a test loop of 3 m and 5 m in height. In the riser tube the high-speed upward returning two-phase flow with disturbance waves appeared. In some cases the operation ceased due to the blockage of this two-phase flow by a high condensate liquid column formed in the riser. A precise investigation showed that the flash evaporation rate in the evaporator during the period (B) must be large enough to avoid this blockage effect.

Key words : Intermittent Heat Transporting Device, Vapor Accumulation, High-Speed Two-Phase Flow, Operating Limit, Flash Evaporation.

1. INTRODUCTION

Recently the demand for the efficient recovery of the waste heat with small available energy is increasing to alleviate the global warming. For example, there are some heat sources in the urban area such as the outdoor unit of the air-conditioning system, the paved road and the walls of the buildings. They become one of the reasons causing the urban warming phenomenon, especially in the summertime in Japan. In addition, it is recently encouraged to build up and utilize the distributed energy systems for supplying electricity and cooling/heating thermal energy simultaneously to office buildings, apartment houses, etc. For the practical operation of this system, however, the heat of the exhaust gas from the electric generator (micro gas turbine, fuel cell, etc.) must be transported efficiently to the thermal energy utilization site.

For solving both problems, the efficient heat transport device must be indispensable. The distance of transportation needed for this device should be several meters at least. In such a case, much amount of the electric power is usually used for circulating the heat transport fluid, which leads to a large amount of the available energy loss considering the low temperature of the waste heat.

The authors originally proposed a unique method to avoid this available energy loss. By using this method, the power for circulating the heat transport fluid throughout the loop tube of several meters in length can be obtained from the heat source and the demand for electricity almost disappears. In addition, this method can be applied for the heat transportation regardless of the direction in case of the terrestrial usage.

There were some research works on the heat transport in the downward direction without additional power input, mainly the works on anti-gravity heat pipes [2-4]. Compared with them, the elements constructing the present system are simple, small in number and excellent in reliability of operation. (This comparison was described more precisely in [1].)

In the present paper the experimental results are shown and discussed on the flow and downward heat transport performances of a test loop utilizing the proposed method.

2. OPERATION CYCLE

The present heat transporting device is shown schematically in Fig.1. The operation is composed

Table 1 Description of operating process

Process	(1)	(2)	(3)	p_e	p_o	p_r	p_s
(A)	Closed	Open	Closed	↑	↓	↓	↓
(B)	Open	Closed	Closed	↓	↑↓	↑	↑
(C)	Open	Closed	Open	→	→	→	→

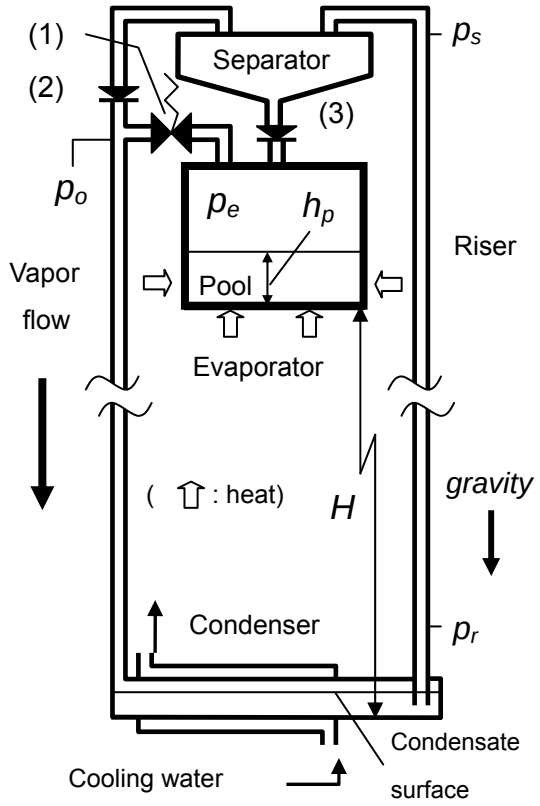


Fig.1 Simplified sketch of experimental setup

of three processes. These processes, designated by (A), (B) and (C) respectively, are described in Table 1. The present device is a closed loop system with an evaporator vessel at the position higher than a condenser. In the process (A), the evaporator is heated by the outside heat source of constant temperature, with a motor-operative valve (1) closed as shown in Table 1. Working liquid evaporates and the high-pressure vapor accumulates in the vessel, leading to the increase of p_e shown by an arrow in Table 1. This continues until the vapor temperature in the evaporator becomes close to, but slightly lower than, that of the outer heat source. At this time, the vapor is thermally saturated. On the other hand, the pressures in the loop p_o, p_r and p_s decrease due to the condensation of still vapor in the tube.

In the process (B) sudden discharge of the accumulated vapor occurs after opening the valve (1). The vapor flows into the downstream

Table 2 Experimental conditions

Liquid fill ratio: 26 % of evaporator volume			
Working fluid	H [m]	T_h [°C]	p_{eb} [kPa]
Water	3	103	120
		114	170
		120	220
	5	120	220
		124	250
		128	280
Methanol	3	64	120
		74	170
		83	210
	5	86	220
		90	250
		94	280

condenser. Downward heat transport is realized in this way. The condensate accumulated in the condenser is blown out into the riser tube by this vapor flow. In this period, the flash evaporation of the liquid occurs in the evaporator vessel due to depressurization. In the riser tube, the high-speed upward vapor-liquid two-phase flow appears. This process continues while p_e is higher than p_s.

In the process (C), the flow stops in the whole loop and the liquid and the vapor are stratified in the separator. Because the vapor pressure in the separator p_s is almost equal to p_e at this moment, the check valve (3) is opened automatically by the liquid accumulated on the bottom of the separator. Then the liquid returns to the evaporator. After this, the valve (1) is closed again, and the above cycle is repeated.

3. EXPERIMENT

The fundamental construction of the present experimental setup was the same as shown in Fig.1. The volumes of the evaporator and the separator were 0.0272 m^3 and 0.0081 m^3, respectively. The length and the inner diameter of the condenser was 0.8 m and 17 mm. The inner diameter of all the other tubes was 10 mm.

The experimental conditions were shown in Table 2. Water and methanol were used as two kinds of the working fluid. The cooling water temperature was kept at 15 °C at the inlet of the jacket. In the present experiment heat was supplied with T_h kept constant, the value of which was decided by taking into account the temperature of the waste heat from the distributed electric generator. In addition, the heater in the evaporator was turned on only during the period (A) described in the previous section.

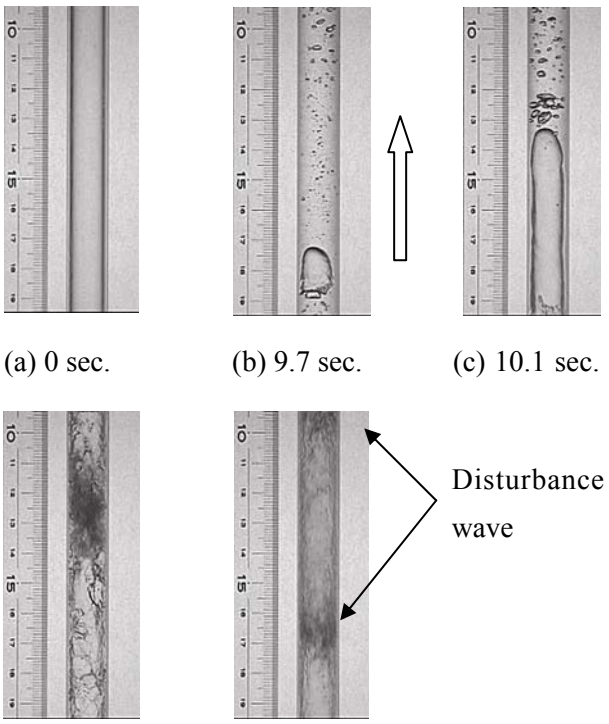


Fig.2 Flow pattern change in riser tube (methanol, H=3 m, T_h=74 °C)

4. RESULTS and DISCUSSION

4-1 Returning Two-Phase Flow Characteristics

Figure 2 shows the change of the two-phase flow pattern in the riser during the period (B). The pictures were taken at the position 1 m higher than the horizontal condenser. Just after opening the valve (1) in Fig.1, there was no liquid in the riser [Fig.2(a)]. Then the vertical tube was filled with liquid rising up from the condenser. Small droplets or cap bubbles sometimes appeared (b). After this liquid column remained in the tube for about 10 seconds, the upward vapor flow appeared in the core region (c). During penetrating the liquid column, the vapor lifted up a part of the liquid. This period ended within 2 seconds at most (d), and finally the high-speed upward annular flow appeared (e). In this final period a dark shade rose up intermittently with a very high speed, which should indicate the generation of the disturbance wave.

To examine this intermittent phenomenon in detail, the vapor and liquid flow rates in the riser were estimated by using the experimental data [5]. The velocity of the vapor discharging from the evaporator was obtained from the energy equation, assuming that the time-dependent unknown value was neglected. The next equation was obtained.

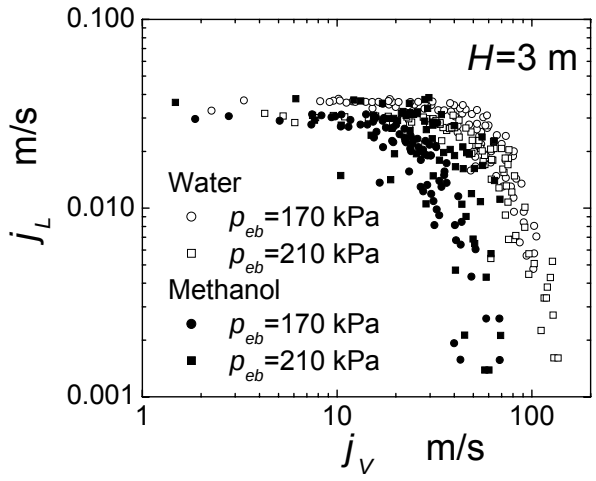


Fig.3 Calculated Volumetric flux

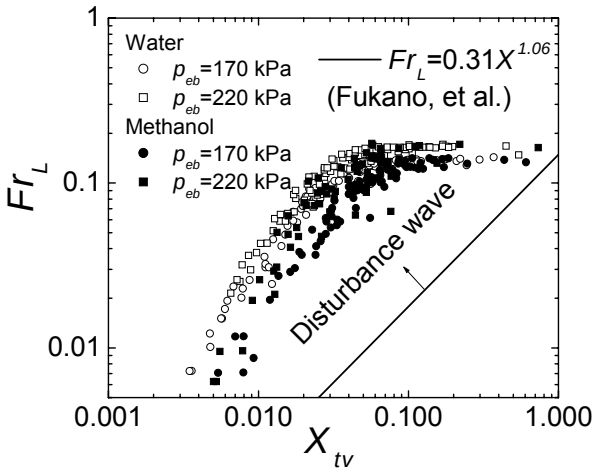


Fig.4 Comparison with correlation of Fukano

$$j_{V0} = c\sqrt{\frac{4(p_e - p_o)}{3\rho_V}} \qquad (1)$$

The relation between the volumetric flux of the upward liquid flow entering the riser j_L and the condensing heat transfer rate Q could be expressed by the next equation.

$$j_L = \frac{Q}{\rho_L A_r L} \qquad (2)$$

In addition, transient mass conservation was taken into account with the tube for downward vapor flow plus the condenser tube as a control volume. Finally, the next equation was obtained for the vapor flow.

$$j_V = j_{V0} - \frac{Q}{\rho_V A_r L} - \frac{l_d + l_c\left(\frac{d_c}{d}\right)^2}{\rho_V}\frac{d\rho_V}{dt} \qquad (3)$$

Figure 3 shows the examples of the changes of calculated j_V and j_L during the process (B) in four cases of the initial pressure in the evaporator p_{eb}. In this calculation, the experimental results of the instantaneous values of Q, p_e, and p_o were used and thermal properties were estimated as the saturated values. These results in Fig.3 were also compared in Fig.4 with the flow conditions under which the disturbance wave generates. The correlation of Fukano, et al. [6] for the thin liquid film flowing concurrently with the high speed gas flow was used for this comparison. The calculated flow conditions of vapor and liquid showed that the disturbance wave could occur in the present experiment, which was consistent with the result of the observation shown in Fig.2 (e).

4-2 Heat Transport Characteristics

Figure 5 shows the experimental results of the equivalent thermal conductivity k_{eq} defined by the following equation [1].

$$S = k_{eq} \frac{T_h - T_w}{H} (A_d + A_r) \qquad (4)$$

By using this definition, the present heat transport performance could be evaluated as the equivalent thermal conduction process in a virtual material with the thermal conductivity of k_{eq}. Compared with the thermal conductivity of metals like copper, the present method could transport heat in the downward direction more effectively with almost no additional power input.

4-3 Limit of Operation

Figure 6 shows the example of the change of pressures during the process (B) in case of the 4th successful cyclic operation by using methanol under the condition of p_{eb}=220 kPa. After the vapor began to discharge from the evaporator, p_o increased rapidly at first. It became close to p_e, and then decreased with p_e. The pressure p_r once increased due to the formation of a liquid column in the riser, then decreased because the vapor flow penetrated the column and the upward two-phase flow appeared as shown in Fig.2 (c)-(e). The vapor and liquid began to rush into the separator at t=40 sec. As a result p_s started to increase.

As the cyclic operation was repeated, however, the operation was stopped under some conditions. Fig.7 shows an example. This result was obtained under the same experimental conditions as shown in Fig.6. In this case the liquid column in the riser did not disappear and p_s did not increase, which suggested that the vapor flow rate at the exit of the condenser was not large enough to penetrate the liquid column. In addition, the comparison between Figs.6 and 7 showed that p_e in Fig.7 decreased more rapidly than in Fig.6. Based on this consideration, it was clear that the amount of vapor generated by flash evaporation in the evaporator decreased as the cyclic operation

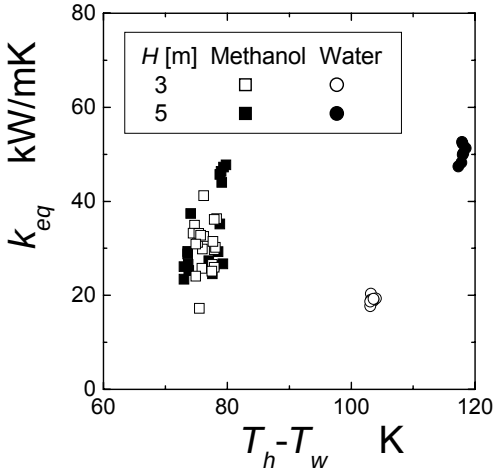


Fig.5 Equivalent thermal conductivity

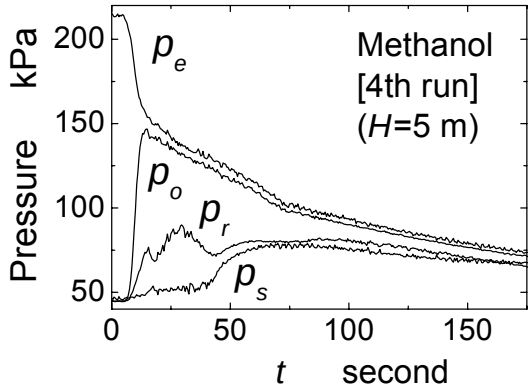


Fig.6 Change of *p* during vapor discharging period (successful operation)

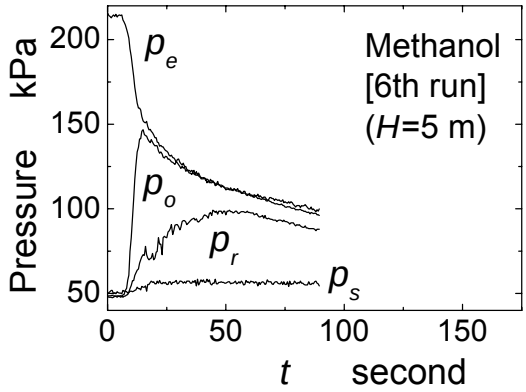


Fig.7 Change of *p* during vapor discharging period (operating limit)

proceeded. And this should be caused by the decrease of liquid in the evaporator pool due to the ineffective returning of the condensate from the separator to the evaporator through the check valve (3).

Based on the above-mentioned discussion, the changes of the height of the pool in the evaporator h_p and mass flow rate of vapor discharging from the evaporator m_{Vo} with time were evaluated by the following equations.

$$\frac{d[\rho_{Ve}(V_e - h_p A_e)]}{dt} = m_f - m_{Vo} \quad (5)$$

$$\frac{d(\rho_{Le} h_p A_e)}{dt} = -m_f \quad (6)$$

$$\frac{d[(C_{p\,Le}\rho_{Le} h_p A_e + B_h)T_h]}{dt} = -m_f L \quad (7)$$

Eqs.(5) and (6) were obtained by taking into account the transient mass conservation with the vapor space and the pool in the evaporator as two different control volumes, respectively. In Eq.(7), the transient conservation of thermal energy was considered with the pool plus the heating wall as a control volume.

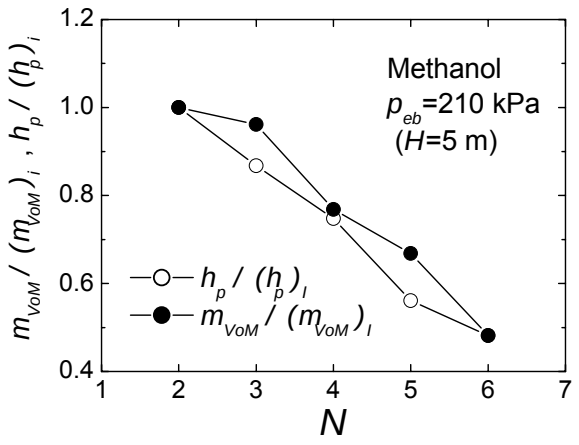


Fig.8 Estimation of the flash evaporation effect

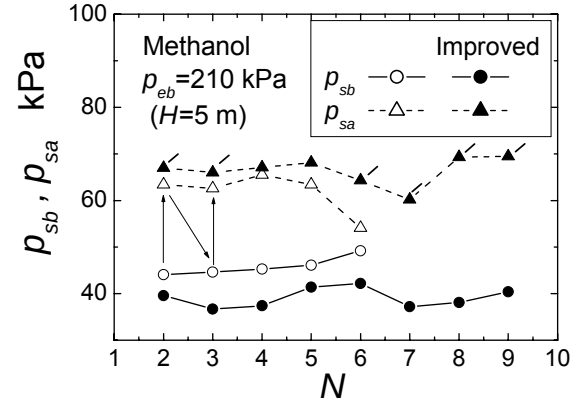


Fig.9 Improved performance of heat transportation

Figure 8 shows the results of calculation of h_p and m_{Vo} by using Eqs.(6)-(8). The values in this figure were taken at the time when p_r showed the maximum value during the process (B). Both h_p and m_{Vo} are shown as the ratio to the value in the 2nd cyclic operation. As the cyclic operation proceeded, both h_p and m_{V0} decreased, and in the 6th operation these values became less than half of the initial values.

In order for the condensate to return to the evaporator easily, the length of the tube above the check valve (3) was increased, resulting in the higher static pressure on the upstream side of the valve (3). Fig.9 shows the effect of this improvement on N. The measured values of p_s before and after the process (B) are shown. As the operation proceeded, p_s changed like the way shown by the arrows in this figure. The data with a short line on the right shoulder mean that the condensate returning from the separator to the evaporator was confirmed by the generation of the noise at the time when the condensate fell onto the liquid pool surface in the evaporator. This rearrangement of the piping was very much effective for the sustainable cyclic operation.

4-4 Heating Condition for Successful Operation

The operation of the present system depends strongly on the temperature of the heat source. Fig.10 shows the range of T_h for the successful operation. The arrows show the judgment that the operation could be repeated continuously under

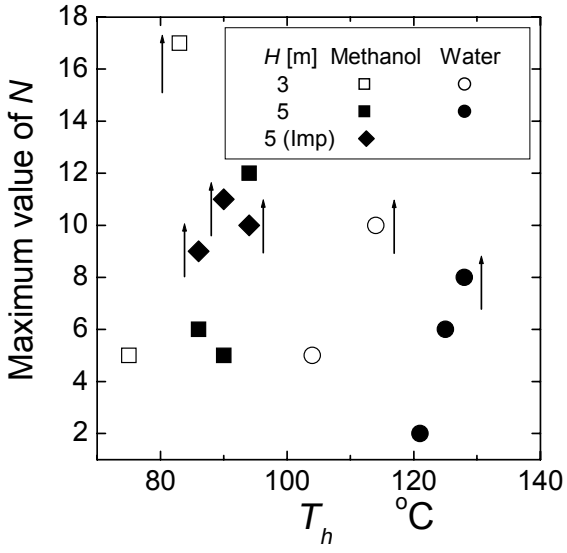


Fig.10 Maximum value of N

those heating conditions. The data shown by the symbols of diamond shape were obtained after the improvement mentioned in the previous section. Within the present experimental range, the system could work well when T_h was larger than 114 °C for H=3 m and 128 °C for H=5 m in case of the working fluid of water. In case of methanol, it could work well when $T_h > 83$ °C.

5. CONCLUSION

The characteristics of the downward heat transportation by using the proposed method were investigated experimentally. The results are summarized as follows.

1. The condensate could be returned upward by high-speed vapor-liquid two-phase flow accompanied by the generation of the disturbance wave.
2. Compared with heat conduction by metals like copper, the heat transport performance was improved significantly.
3. On the construction of the present system, attention must be paid to the operation of the check valve for returning the condensate from the separator to the evaporator.
4. The present system could operate successfully if the temperature of the heat source is selected appropriately.

Nomenclature

A : horizontal cross-sectional area, m^2
B_h : heat capacity of the heating wall contacting with the working liquid pool, J/K
C_p : specific heat, J/kgK
c : contraction coefficient
d : diameter of the tube, m
Fr_L : Froude number of liquid
H : elevation of the evaporator from the ground, m
h_p : depth of the pool in the evaporator, m
j : volumetric flux, m/s
k_{eq} : equivalent thermal conductivity, W/mK
L : latent heat of vaporization, J/kg
l : length of the tube, m
m_f : generation rate of vapor by flash evaporation in the evaporator, kg/s
m_{Vo} : mass flow rate of vapor discharging from the evaporator, kg/s
N : number of order of successive operation
p : pressure, kPa
Q : condensing heat transfer rate, W
S : total transferred heat averaged by the time needed for one whole operating cycle, W
T : temperature, °C
t : time, second
V : volume, m^3

Greek Letters

ρ : density, kg/m^3
X_{tv} : Martinelli parameter (turbulent vapor flow)

Subscript

a : value after the flow ceased
b : value just before opening the valve (1)
c : condenser
d : tube for the downward vapor flow
e : evaporator
h : heating wall
i : value of the 2nd (=initial) operation
L : liquid
M : time when p_r takes the maximum value
o : exit of the evaporator
r : position at the bottom of the riser tube
s : separator
V : vapor
w : cooling water in the condenser

Acknowledgement

The authors are grateful to Mr. Daisuke Okada (Staff Japan Co.) for the cooperation in the experiment.

References

1. Kadoguchi, K., et al., 2001, “Experimental Study on the Self-Operative Heat Transportation by Utilizing the Accumulated High-Pressure Vapor”, Proc. of the 5th World Conf. on Experimental Heat Transfer, Fluid Mechanics and Thermodynamics, Vo.3, pp. 2205-2211.
2. Imura, H. and Ipposhi, S., 1996, “Development of an Osmotic Heat Pipe”, Heat Pipe Technology-Theory, Applications and Prospects-, Pergamon Press, pp. 138-148.
3. Ogushi, T., Murakami, M. and Yamanaka, G., 1986, “Study of a Downward Heat Transport Device Using Vapor Pressure as the Liquid Pumping Force”, Trans. JSME (in Japanese), Vol.52, pp. 3348-3352.
4. Kawabata, K., Hashimoto, N. and Kamiya, Y., 1996, “Anti-Gravity Heat Pipe”, Heat Pipe Technology-Theory, Applications and Prospects-, Pergamon Press, pp. 168-175.
5. Kadoguchi, K. and Yamazaki, M., 2003, “Improvement of the Performance of a New Heat Transport Device Using the Intermittent Discharge of Accumulated Vapor”, Proc. of the 6th ASME-JSME Thermal Engineering Joint Conf.
6. Fukano, T., Itoh, A. and Ousaka, A., 1985, “Breakdown of a Liquid Flowing Concurrently with Gas in Horizontal Line”, Physicochemical Hydrodynamics, Vol.6, No.1/2, pp. 23-47.

Heat Transfer Characteristics in an Evaporator Section of a Looped Parallel Thermosyphon

Fumito Kaminaga, Chowdhury Feroz MD, Hideaki Watanabe, and Kunihito Matsumura
Department of Mechanical Engineering, Ibaraki University
4-12-1 Nakanarusawa, Hitachi, 316-8511, JAPAN
Tel: +81-294-38-5035 Fax: +81-294-38-5047
E-mail: kaminaga@mech.ibaraki.ac.jp

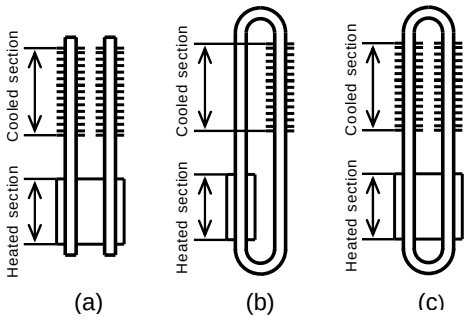
Abstract

A looped parallel closed thermosyphon is newly developed to resolve heat transfer defects of a conventional thermosyphon consisted of a single straight tube: low maximum heat transfer rate, non-uniform wall temperature of an evaporator section, and large deterioration effect of non-condensable gas on condensing heat transfer. It makes use of a fluid flow fluctuation by boiling in an evaporator section with a U-tube shape to improve the heat transfer characteristics. In the present study the maximum heat transfer rate and a wall temperature profile in the evaporator section are mainly examined in the looped parallel thermosyphon and they are also examined in a conventional thermosyphon to show how the new thermosyphon can improve the defects. The experiments and comparisons of two types of thermosyphon give the following findings: The wall temperatures are much more uniform in the new thermosyphon than those in a conventional one. The boiling heat transfer coefficients are similar in both types. The maximum heat transfer rate in the new type is much larger than that in the conventional one.

Key words: Thermosyphon, Loop, Maximum heat transfer rate, Wall temperature profile

1. INTRODUCTION

In order to release a large heat rate from electric or electronic devices such as a power transistor a multiple installation of a single tube type thermosyphon (STT) as shown in Fig.1a is commonly designed as a compact heat exchanger. But current rapid increase of the heat rate has made a conventional single tube type thermosyphon to have an insufficient performance to transmit the heat from the devices. Since the maximum heat transfer rate in the conventional thermosyphon is mainly determined by a countercurrent flow limitation between upward vapor flow and downward liquid film flow, the rate is not large enough. Other defects of the conventional thermosyphon consisted of a single tube are non-uniform wall temperature of an evaporator section and large deterioration effect of non-condensable gas on condensing heat transfer. At an upper part of an evaporator section boiling or film evaporation is fully developed, but at a lower part of it boiling is partially or does not occur. The wall temperature in an evaporator section, therefore, has a profile such as low at the upper part and high at the lower part. Non-condensable gas which gives large heat transfer deterioration is normally accumulated in an upper part of a condenser section since a top of thermosyphon tube is a dead end. Those defects can be resolved by giving a circulation of a working fluid in the thermosyphon using a loop type thermosyphon as shown in Fig.1b. But it has a half of heat transfer area in evaporator and condenser sections compared with the single type shown in Fig.1a. In order to make use of the total heat transfer area in the loop type thermosyphon a looped parallel thermosyphon (LPT) having a combination of two single type thermosyphons joined at top and bottom by two U-tubes is newly developed. It uses a fluid flow fluctuation by boiling in an evaporator section to improve the inside heat transfer characteristics.



(a) Single tube thermosyphon
(b) Looped thermosyphon
(c) Looped parallel thermosyphon

Fig.1 Thermosyphon arrangements

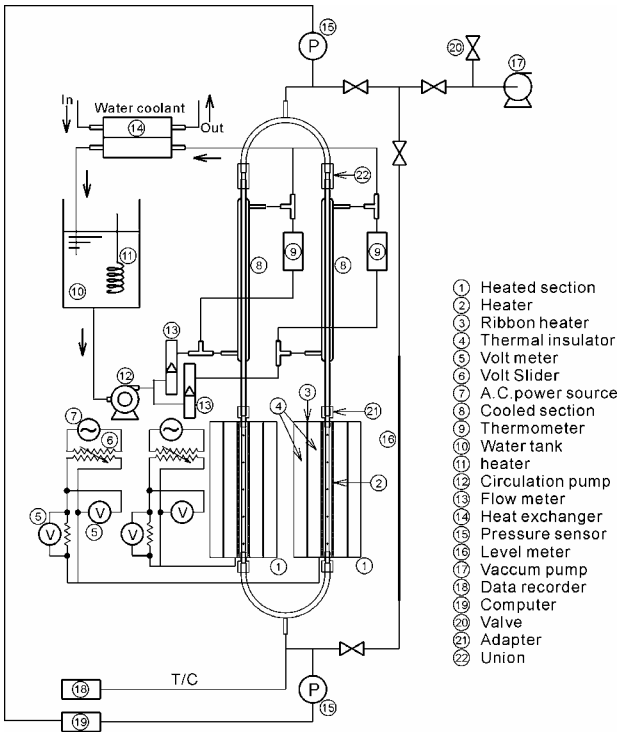


Fig.2 Experimental apparatus

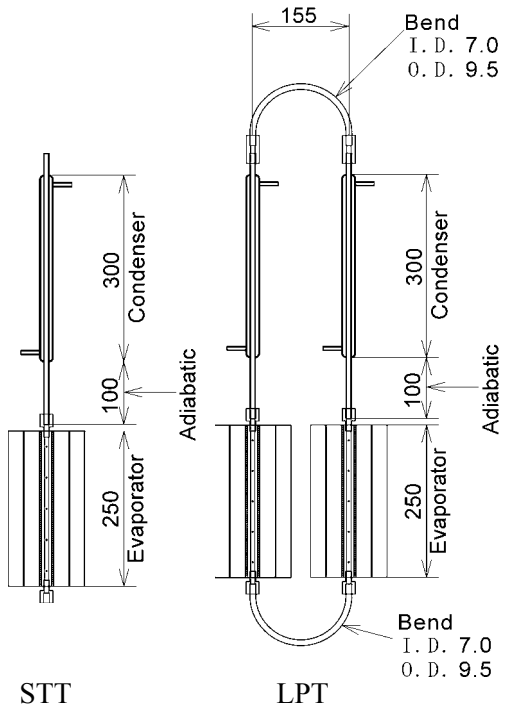


Fig.3 Dimensions of thermosyphons

In the present study the maximum heat transfer rate and wall temperature profile in an evaporator section are experimentally examined in the newly developed thermosyphon, LPT, and they are also examined in a conventional thermosyphon, STT, to show how the new thermosyphon can improve the heat transfer defects.

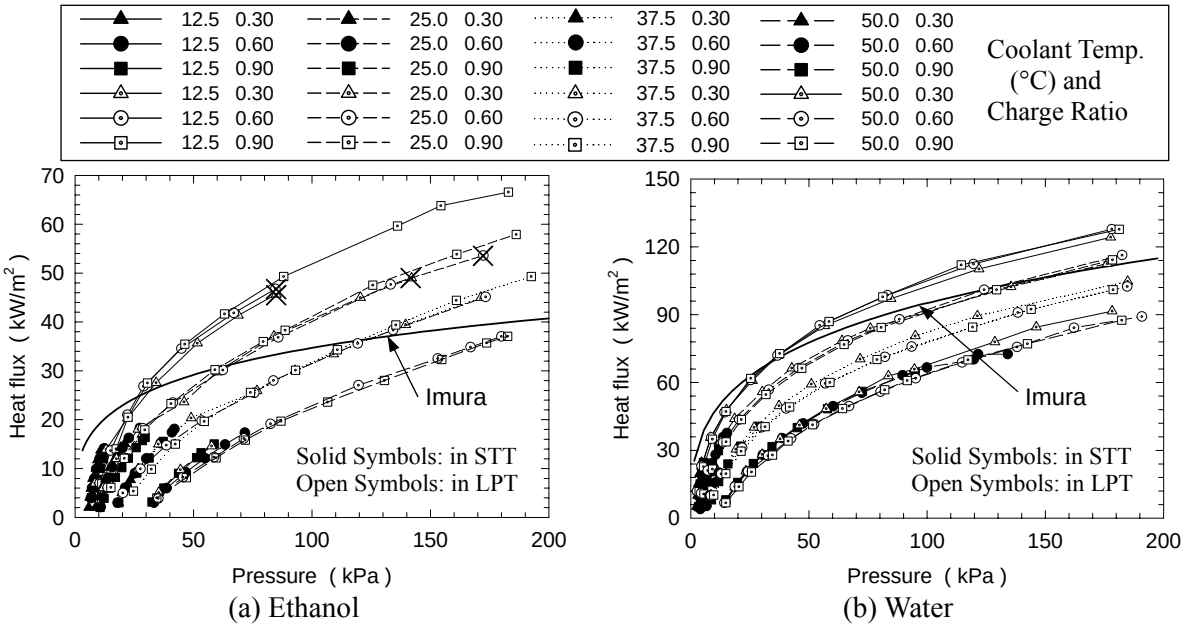
2. EXPERIMENTAL APPARATUS

The schematic diagram of the experimental apparatus is shown in Fig. 2. The test loop consists of three sections: evaporator, adiabatic, and condenser and is vertically oriented. Detailed dimensions of the LPT are shown in Fig. 3. This figure also indicates dimensions of a single tube thermosyphon made for comparing heat transfer performance. Two evaporator and two condenser sections are located at bottom and top of the loop, respectively. The evaporator section is made of a copper tube of 7 mm ID and 250 mm long and heated by a coiled sheath heater. The condenser section is made of a glass tube of 7.0 mm ID and 9.5 mm OD with a length of 300 mm surrounded by a glass tube jacket for flow visualization. The both tubes are connected by U-tubes with the same inside diameter at the top and the bottom. To measure wall temperatures on the evaporator section five calibrated chromel-alumel thermo-couples with a 0.5 mm diameter are embedded in longitudinal grooves made on each heated wall. The evaporator section is insulated by a rock wool insulator of 30 mm thick. The heater is also insulated by the same materials from the outside. A ribbon heater is placed around the insulator to compensate the heat loss from the heated section. The condenser section is cooled by a constant temperature water coolant circulating in an annular space between the glass tube and the jacket. To measure time variations of system pressure two pressure sensors are installed at the top and bottom ends of the U-tubes. A vacuum pump is equipped at the top of the loop to remove the resolved gas accumulated in the upper part of the condenser section before the experiment.

An input power to the heater in the evaporator section is increased stepwise. The measurements are made under a steady state condition at each input power. Water and ethanol are used as working fluids. The experimental parameters are a fill charge ratio and a coolant temperature. The range of the parameters are shown in Table 1.

Table 1 Experimental conditions and their ranges

Working Fluid	Charge Ratio, V^+	Coolant Temp., T_f (°C)
Water & Ethanol	0.3 0.6 0.9	12.5 25.0 37.5 50.0



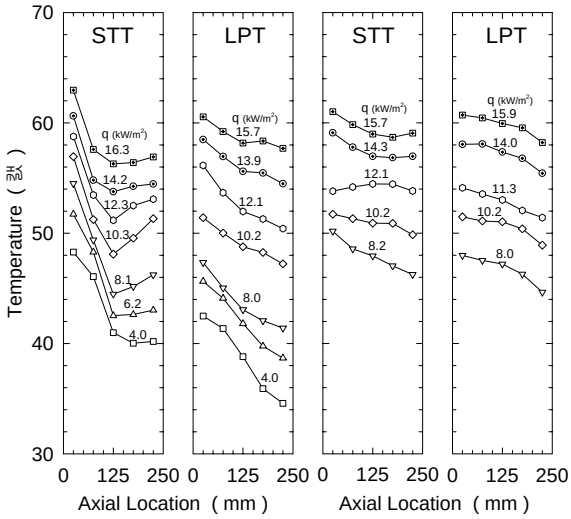
(a) Ethanol (b) Water

Fig.4 Relationship between heat flux and system pressure

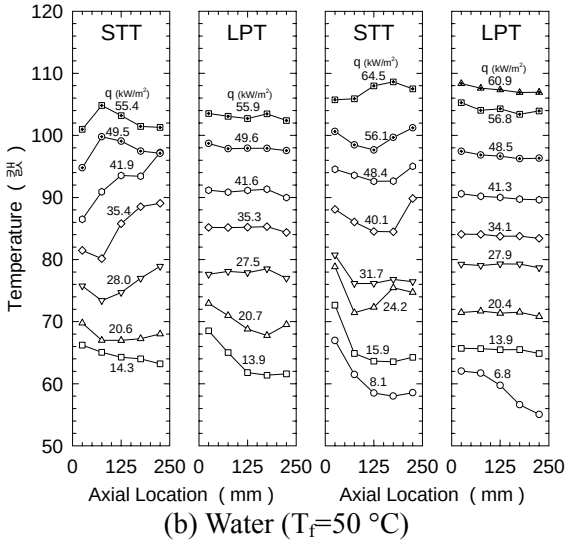
3. RESULTS AND DISCUSSIONS

3-1 System Pressure Characteristics

The relationship between heat flux and system pressure is shown in Fig.4. Figure 4a and 4b are the results of ethanol and water working fluid, respectively. In the figure the maximum heat flux variation to the pressure calculated by Imura's [1] correlation is plotted for comparison. The open symbols show the results of LPT and the solid symbols the results of STT. The figure indicates that the pressures has similar changes relating to the heat flux between STT and PLT and is not affected by the charge ratio but is primarily affected by the coolant temperature in the condenser section for both fluids. The cross marks in Fig.4a show the critical condition in PLT which is obtained at coolant temperatures of 12.5 and 25 °C and charge ratios of 30 and 60 %. The critical heat fluxes are almost 40 % larger than the Imura's correlation. On the other conditions for ethanol fluid in PLT the critical heat transfer does not occur since the permissible maximum system pressure is restricted to 200 kPa due to the glass made condenser section. The maximum heat fluxes in STT are around 70 % of the Imura's correlation on every condition. The critical condition is not obtained in the water working fluid tests in LPT, but the maximum heat fluxes obtained within the pressure limitation are all much larger than those obtained in STT.

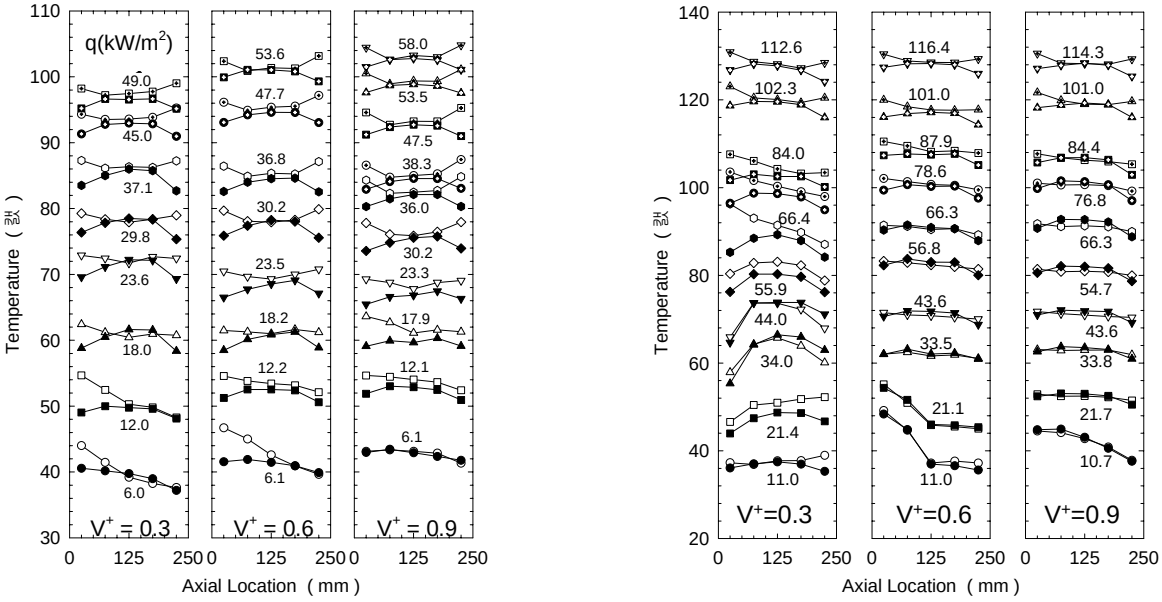


(a) Ethanol (T_f=25 °C)



(b) Water (T_f=50 °C)

Fig.5 Comparison of wall temperature profile



(a) Ethanol (T_f=25°C) (b) Water (T_f=25°C)

Fig.6 Wall temperature profiles in both sides of LPT

3-2 Temperature Profile and Pressure Fluctuation

Figure 5 shows measured axial wall temperature profiles from the bottom in the evaporator section for STT and LPT. The numbers indicate heat fluxes applied in the section. For the ethanol working fluid as shown in Fig5a the temperature at a lower part of the evaporator section shows a much larger value than that at a middle and higher part in the STT, on the other hand, in the LPT the temperature difference between lower and higher parts is smaller and becomes small with increasing heat flux. For the water as shown in Fig5b in STT the temperature profile is complex and a temperature difference along the elevation is large even at a high heat flux, but the difference in LPT is very small especially at a high heat flux.

Figure 6 shows the axial wall temperature profiles at both sides in LPT. The open and the solid symbols indicate the wall temperatures at the right and left sides, respectively. At a low charge ratio and a low heat flux the temperature difference in the axial direction is indicated, however, with increasing heat flux it becomes small and the influence of the charge ratio is disappeared. The temperature difference between two sides is much smaller for the water working fluid as shown in Fig.6b. This more uniform temperature profile must be realized by a large flow fluctuation occurred by vapor formation. The reason for the different temperature profiles, convex and concave, frequently shown especially in Fig.6a has not been cleared yet.

Figure 7 shows time variations of system pressure measured at the bottom of LPT on conditions selected from those in Fig.6. At the higher heat flux conditions the pressure indicates the larger fluctuation. This tendency is much clear with decreasing charge ratio.

Figure 8 show power spectrum densities of the pressure variations shown in Fig.7. The straight line means a characteristic frequency, f_U, of initial liquid in the U tube for each charge ratio. The dominant frequency in the PLT tube is smaller than the characteristic frequency at

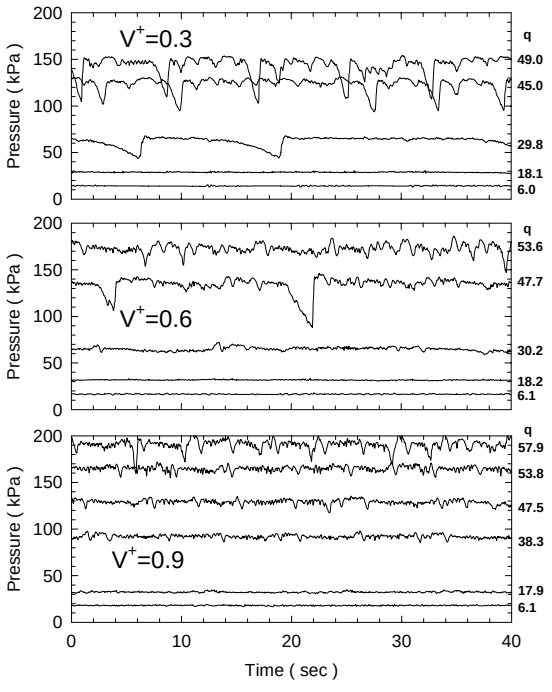


Fig.7a Time traces of system pressure (Ethanol, T_f=25°C)

V^+=0.3 both for ethanol and water, but with increasing charge ratio it slightly increases to the characteristic value and for the water as shown in Fig.8b it is closer to the value. This frequency close to the characteristic value must give a large fluctuation of the fluid. The large fluctuation is favorable to give uniform wall temperature profile in the evaporator section.

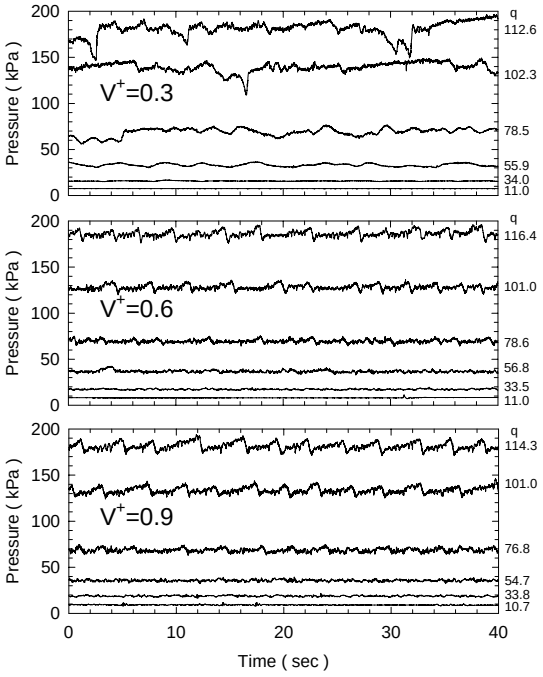
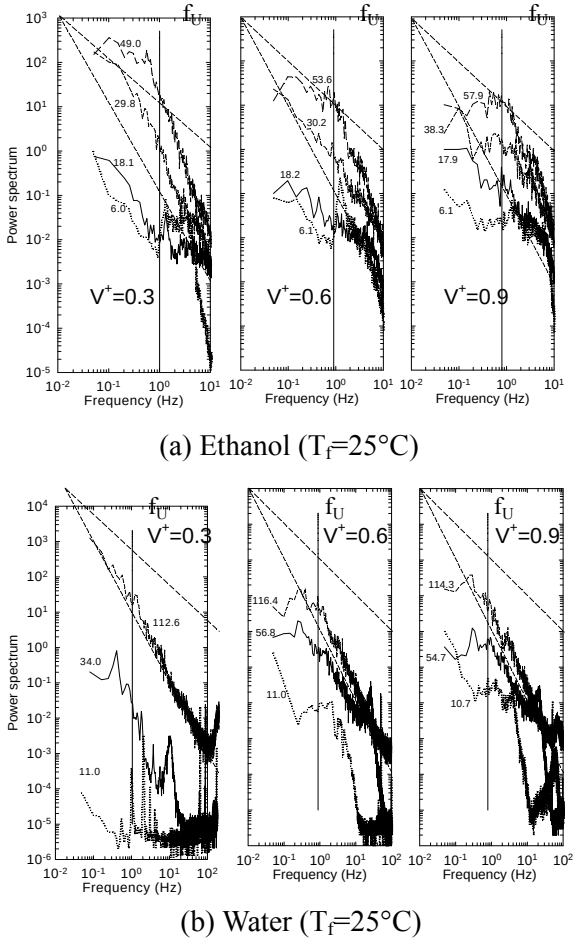


Fig.7b Time traces of system pressure (Water, T_f=25°C)



(a) Ethanol (T_f=25°C)

(b) Water (T_f=25°C)

Fig.8 Power spectrum density of system pressure fluctuation

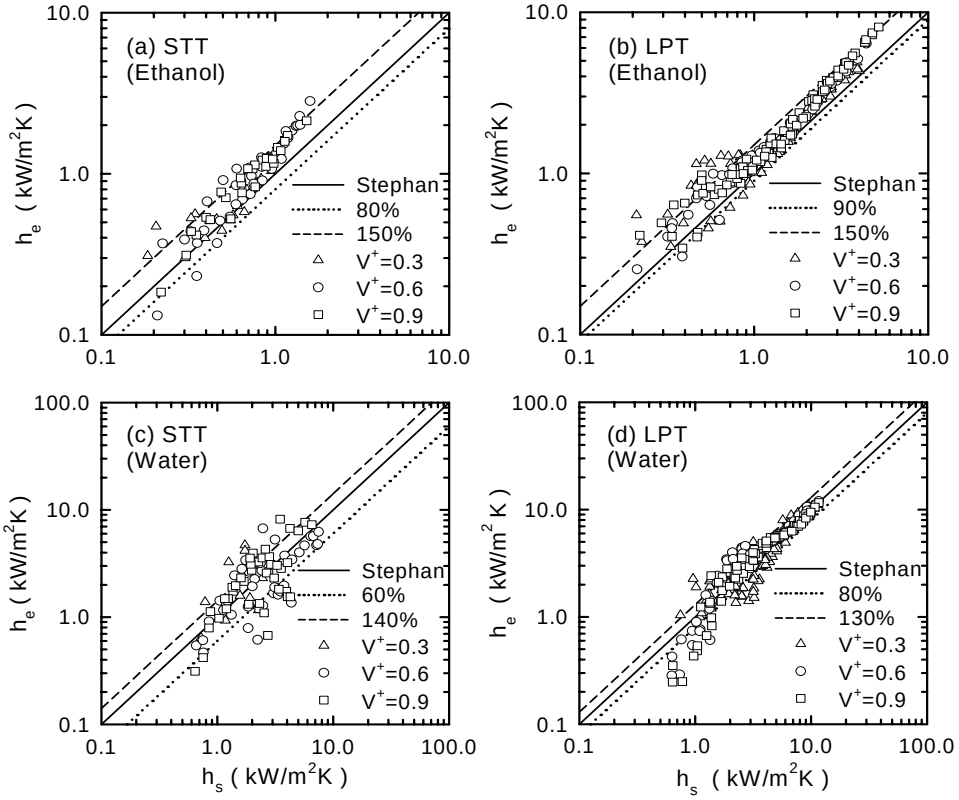


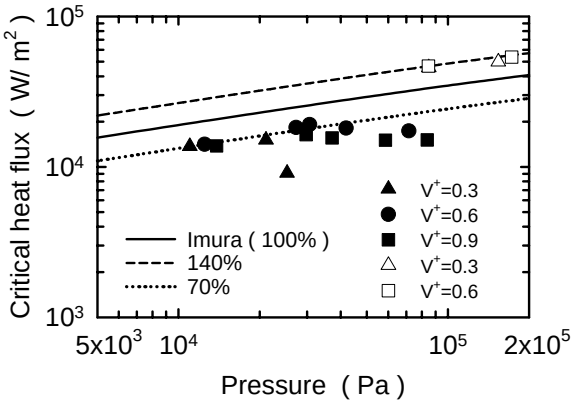
Fig.9 Comparison of measured heat transfer coefficient with one predicted by Stephan's correlation

3-3 Heat Transfer in Evaporator Section

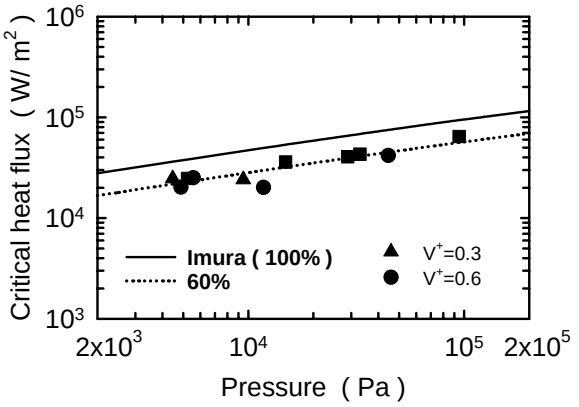
Figure 9 shows comparison of measured average heat transfer coefficients with values predicted by Stephan's nucleate boiling correlation[2] for STT and LPT. The data are scattered at low heat transfer coefficient, which means low heat flux, but with increasing it they are consistent with the correlation. For ethanol working fluid, the coefficients are by 50 % larger than those by correlation both for STT and LPT, and for water they are close to the correlation. The difference of the heat transfer coefficient in the heated section between STT and LPT is shown to be small and the effect of the charge ratio on it is negligibly small.

3-4 Critical Heat Flux

Figure 10 shows the relationship between critical heat flux and system pressure for STT and LPT. Imura's correlation [1] is also plotted in the figure with error levels. In the experiments the critical condition is defined for the wall temperature to be over 150 °C for STT and over 200 °C for LPT. In the STT the critical condition was encountered in all experimental conditions, but in the LPT only four conditions satisfied the critical condition and on the other conditions an increase of heat flux applied should be terminated since the system pressure is over a specified permissible value, 200 kPa. The critical heat fluxes for STT are by 30 to 40 % lower than that predicted by the correlation and the difference increases with increasing pressure, but the effect of the charge ratio is small on them. The critical heat fluxes for LPT are by 40 % larger than that by the correlation for ethanol working fluid and the amount of them is about five times larger based on an operation criterion or about twice on a correlation criterion than that in STT. The critical condition is not attained for the water working fluid in LPT, but the heat flux applied is much larger than the critical value for STT as shown in Fig.4. The maximum heat flux in LPT must be much larger than in STT.



(a) Ethanol (T_f=25°C)



(a) Water (T_f=25°C)

Fig.10 Critical heat flux
(Closed symbols: STT, Open symbols: LPT)

4. CONCLUSIONS

Experimental studies for the newly developed thermosyphon, LPT, give the following findings:
(1) The LPT can give much more uniform wall temperature in the evaporator section than that in the STT especially at a high heat flux.
(2) In the LPT a large pressure fluctuation is obtained. The magnitude of the fluctuation increases with increasing heat flux and charge ratio and this fluctuation makes the wall temperature uniform.
(3) The maximum heat flux in LPT is much larger than that in STT, but the difference of boiling heat transfer coefficient is small between STT and LPT.

Acknowledgments

This study is partially supported by Grant-in Aid for Scientific Research, No.14580540, of the Ministry of Education and the authors thank for financial assistance.

References

1. H. Imura, K. Sasaguchi, and H. Kozai, "Critical Heat Flux in a Closed Thermo-syphons," Int. J. Heat Mass Transfer, Vol.26, No.8 (1983) pp.1181-1188.
2. K. Stephan and M. Abdelsalem, "Heat-Transfer Correlations for Natural Convection Boiling," Int. J. Heat Mass Transfer, Vol.23, No.1 (1980) pp.73-87.

Heat Transfer Characteristics of Loop Thermosyphon Applied Heat Pump Dryer

W. Phaphuangwittayakul, P. Kamonpet, P. Terdtoon, W. Klongpanich, N.Vorayos and G.S.V. Raghavan*

Department of Mechanical Engineering, Faculty of Engineering, Chiang Mai University
Chiang Mai, 50200, Thailand.
*Department of Agric.& Biosystems Engineering, McGill University Montreal, Quebec, Canada. H9X 3V9
Tel. +66-53-944151E911 Fax. +66-53-226014, Email: phaphuang @ hotmail.com

Abstract

This paper studied the effect of loop thermosyphon (LTS) which was integrated with the heat pump dryer (HPD) for agricultural product. The evaporator and condenser sections of the LTS were equal to 0.45 m and adiabatic section of 1.2 m with 16 loops. The working fluid used was R-134a with filling ratio of 50% of evaporator section. The angle of the LTS used in the experiment was set at 20 degree to control direction of vapor and condensate of working fluid. A dryer of 100-kg capacity was modified to include a heat pump system. The system consisted of a condenser, evaporator, expansion valve and compressor. It operated with R-12 as working fluid. A special duct system was designed to suit the heat pump dryer. The performance of the system studied in this paper-included (i) Coefficient of Performance of the heat pump (COP_h), (ii) Coefficient of Performance of the refrigeration (COP_r), and (iii) Drying Efficiency (DE) and (iv) Effectiveness of LTS (Eff). Experiments were conducted using fresh longans and the data was analyzed to establish the effectiveness of the LTS in conjunction with the HPD. The condition of operation consisted of a recirculation air ratio of 50%, a by-pass air ratio of 10%, a hot air temperature of 70°C and an air flow rate of 2400 m^3/h. It was found from the experiment that the LTS can increase the COP_h, COP_r, DE from 2.37 to 3.10, 1.37 to 2.10, 89.32 to 92.84 %, respectively. The Effectiveness of LTS was found to be 0.14

Key words: Longan, Dryer, Heat pump dryer, Loop Thermosyphon

1. INTRODUCTION

Longan fruits are sphere in shape, 12.5 to 25 mm. in diameter, with dull brown skin, brittle, yellow-brown rind. It consists of dark-brown stone of approximately 10 mm. in diameter which is covered by white thick flesh. Longan blossoming starts in late December to late January, corresponding to the cool and dry winter months of the year. In Thailand, the longan is known as " Lumyai ". It is grown mainly in the upper north region such as, Chiang Mai, Lamphun, Chiang Rai, Payao, Nan, Lampang, Tak and Maehongson. This covers about 90 per cent of all planting area of the country. The longan varieties selected to grow all mainly E-dor, a small percentage of other varieties are considered at times [6].

Longan is an important economic fruit, which is enjoyed both by Thais and other nations. The export of longan amounts to 3,600 million Baht each year [7]. The structure of longan market has three sources of product consumption. These are fresh consumption in the country about 30%, export of fresh longan about 20%, processing as dried longan about 40% and processing as canned longan about 10%. Dried longan production is considerably larger with a value of about 1440 million Baht and tends to steadily increase.

Drying is one such method to preserve longan for a longan period. Furthermore, the volume and also the weight of longans are reduced to less cost for storage and transportation. In many applications of the drying in the tropical countries, the existing dehydration techniques involve solar and air drying methods. Solar drying is now considered inappropriate due to lacking of control in the drying condition, dependency on climatic condition and longer drying time. On the other hand, conventional hot air drying involves high drying temperatures. Drying at high temperatures may cause thermal injury to the fruits and inferior quality. Both methods have failed to effectively produce good quality product due primarily to the limitation of subjecting to drying air of less capacity to remove moisture. This limitation gave rise to the idea of developing a low relative humidity (LRH) dehydration system.

The Heat Pump is the system worthy of consideration. It can simultaneously raise the temperature and lower the humidity from that of the waste heat stream from dryer. The heat pumps has been known to be energy efficient when used in the drying process. Its ability to convert the latent heat of condensation into sensible heat at the hot condenser makes it unique in drying applications. A condenser of the heat pump system releases heat to the inlet air and increases its temperature. A heater could be used to keep the air temperature at specified value required for an agricultural product. After passing through the drying bed, the air will be drawn through an evaporator of the heat pump system. The moisture of the air will be removed keeping the humidity at a low value. The air can either be mixed with the fresh air or recirculated before passing it to the condenser again according to the required condition. By this method, higher quality of hot air can be achieved. This system will be named Heat-Pump Dryer (HPD). In order to increase performance of the HPD, a loop thermosyphon (LTS) is introduced into the system.

The LTS is a kind of heat pipe, which employs gravity to return the condensate back to the evaporator section by introducing the flow as one way circuit in a loop container. It can be divided into 3 sections: i) evaporator, ii) adiabatic and iii) condenser. The LTS is inexpensive, practical and no external power is required. Application of the LTS in the HPD can be done as the LTS is employed to transfer heat from hot air before entering the evaporator of the heat pump (pre-cooler) to the exit of the evaporator (pre-heater).

The mathematical simulation of fruit drying and heat pump assisted continuous dryer has study to investigate the effect on the performance of heat pump dryer. It was found that drying air temperature, recirculation air ratio (RAR), the fraction of evaporator by-pass air ratio (BAR), and specific airflow rate have affect the performance of HPD. The criteria were the coefficient of performance (COP), the moisture extraction rate (MER), dryer efficiency (DE) and the product throughput. About RAR, BAR, COP, MER and DE various authors have reported [1,2,4,5,8].

Chaitep et al [3] studied thermal effectiveness in air preheating by using a loop thermosyphon as a mean of energy saving in longan drying. Based on a thermal effectiveness of 0.337 from laboratory tests, they concluded that the pre-heater unit was suitable for industrial scale applications.

Phaphuangwittayakul et al [9] experimental studied loop thermosyphon as an energy saver in heat pump type dryer. The HPD was modified from conventional batch dryer with capacity 2000 kg. The heat pump system operated with R-12 as working fluid. The LTS designed employed copper tubes with 9.53-mm inner diameter with aluminum fin of 360 x 400 mm^2 heat transfer area. Forty-two loop of thermosyphon were employed with 20-degree inclination angle and 50 % filling ratio of evaporator section. They concluded that the LTS cloud increase performance and save energy consumption of the HPD.

Phaphuangwittayakul et al [10] studied the effect of by-pass air ratios and recirculation air ratios on by computer simulation program compared the specific energy consumption of HPD with and without the LTS. The designed LTS to be compared in numerical results was made of copper tube, with outside diameter of 4.8 cm, 8 loops. The evaporator and condenser section were 100 cm. Working fluid was R-123 with filling ratio of 50 % of evaporator section. They found from the calculation results that the optimum condition of 80% RAR and 80% BAR can provide the maximum energy saving of 46%.

It can be seen from previous researches that, the application of LTS in heat pump dryer for agricultural products is still been in needed. The objective of this researches that;

-To study the performance of the LTS

-To the effect of the LTS on the performance of the HPD.

2. MATERIALS AND METHOD

2.1 Heat Pump Dryer

Two HPDs, one without LTS and another with LTS were designed and built for a capacity of 100 kg of fresh longan. The heat pump unit uses refrigerant R-12 as working fluid while the loop thermosyphon employs R-134a.as working fluid. The specifications of the units are: 1.5 hp hermetic compressor, 1.75 hp condenser, 0.75 hp evaporator, about 100 kg of fresh longan was used

as raw product with 2400 m^3/h of air flow through the product. Temperature of the air was controlled at 70° C before its entry into the drying chamber. The air temperature, relative humidity and velocity are recorded at the point of entry into the evaporator section, at the exit, at the entry and exit of the condenser section and at the entrance of dryer chamber. Further air was recorded through the evaporator and condenser of the heat pump unit.

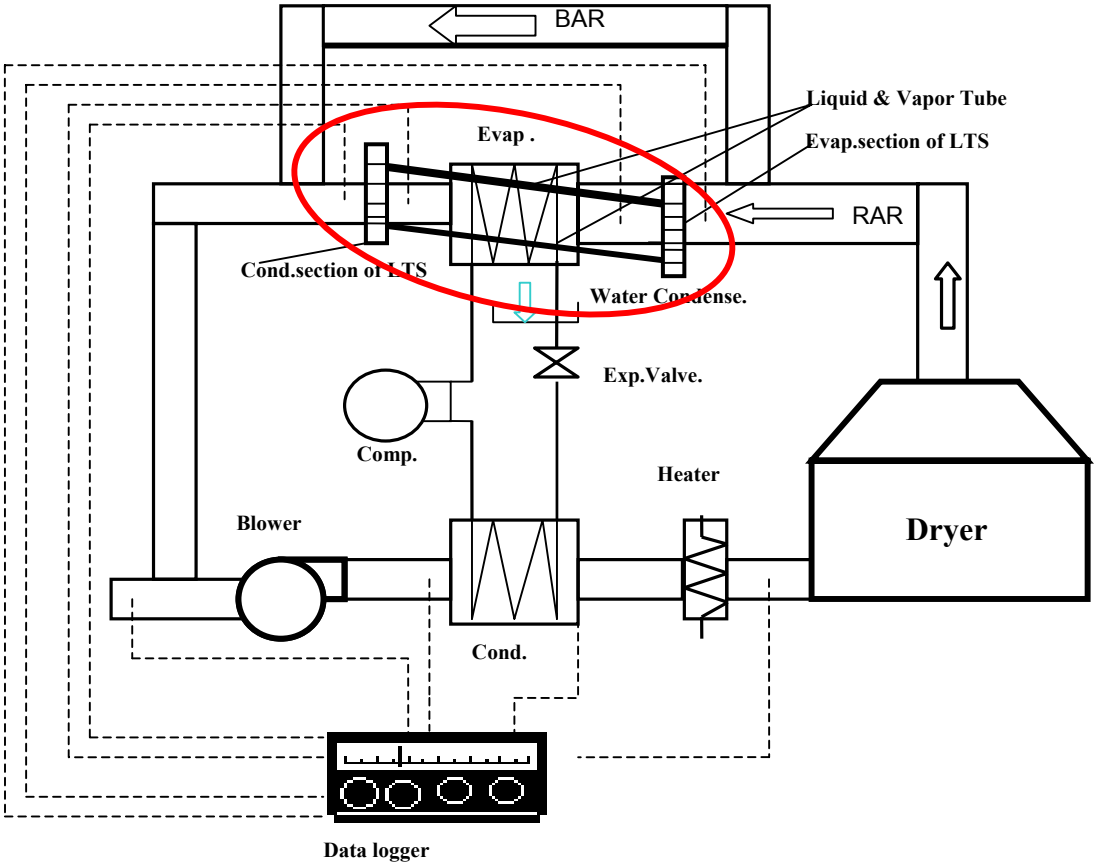


Figure 1. Schematic diagram of heat pump system with loop thermosyphon

2.2 Loop Thermosyphon (LTS)

The appropriate LTS was designed by computer program based on the lowest energy consumption condition of the HPD as established by Phaphuangwittayakul et al [10].

The construction of the LTS using copper tubes. The evaporator and condenser section tubing consisted of 9.53 mm. ID, 10 mm. OD, 12 fin/inch, 0.15 mm fin thickness, and 450x340 mm^2 heat transfer area with 16 loop circuits and electric heater of 6 kW was added to maintain the air temperature at desired point, the inclination angle of 12 degree, the filling ratio of 50% of evaporator section. The LTS is shown in Figure 2.

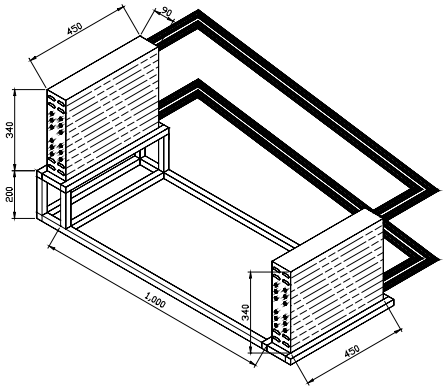


Figure 2. Loop thermosyphon

2.3 Installation of the LTS and testing procedure

After building the LTS unit, it was installed in the HPD appropriately and the schematic is shown in Figure 3. All sensors for the temperature, relative humidity and velocity were installed in the system to monitor the necessary data. Electric thermometer [TESTO model 454 with the accuracy $\pm 0.4\,^{\circ}\mathrm{C}$ and $\pm 2\,\%$of relative humidity (%RH)] was used to record temperature and relative humidity. In the addition, type-K thermocouples were also employed with the COMARK C8510 data logger to monitor the temperature a given point. The power consumption was measured using the DIGICON MG51 wattmeter with an accuracy $\pm 1\,\%$. The airflow was also recorded by using TSI model 8384-M flow meter with $\pm 3\,\%$ accuracy.

The experiment began by starting the heat pump, blower and the heater. The circulating air was heated when it passed through the condenser of further raised its temperature. After the exit from the dryer, the outlet air was passed through the evaporator of HPD. For the HPD with LTS mode the air passed through the evaporator section of LTS. This pre-cooled air was then directed into the evaporated section of HPD. The evaporator of HPD removed the moisture of air. The drier air was then directed through passed the condenser section of LTS where it was re-heated, its moisture was further reduced to some specific point and it was directed into the inlet section of the blower and the air was recirculated. All the necessary data were monitored to calculation of the heat transfer rate ($\dot{Q}$), the coefficient of performance of heat pump (COP_h), the coefficient of performance of refrigeration (COP_r), the drying efficiency (DE), number of transfer unit (NTU)and the effectiveness of the LTS (Eff) were made using the following equations.

$$\dot{Q} = \dot{m}_a C_p (T_o - T_i) \quad (1)$$

$$W_s = Qc\text{-}Qe \quad (2)$$

$$COP_h = \dot{Q}_C / W_s \quad (3)$$

$$COP_r = \dot{Q}_e / W_s \quad (4)$$

$$DE = \frac{(\omega_o - \omega_i)}{(\omega_{sat} - \omega_i)} \quad (5)$$

$$NTU = \frac{AU}{\dot{m} Cp} \quad (6)$$

$$Eff. = \frac{(T_{h,in} - T_{h,out})}{(T_{h,in} - T_{c,in})} \quad (7)$$

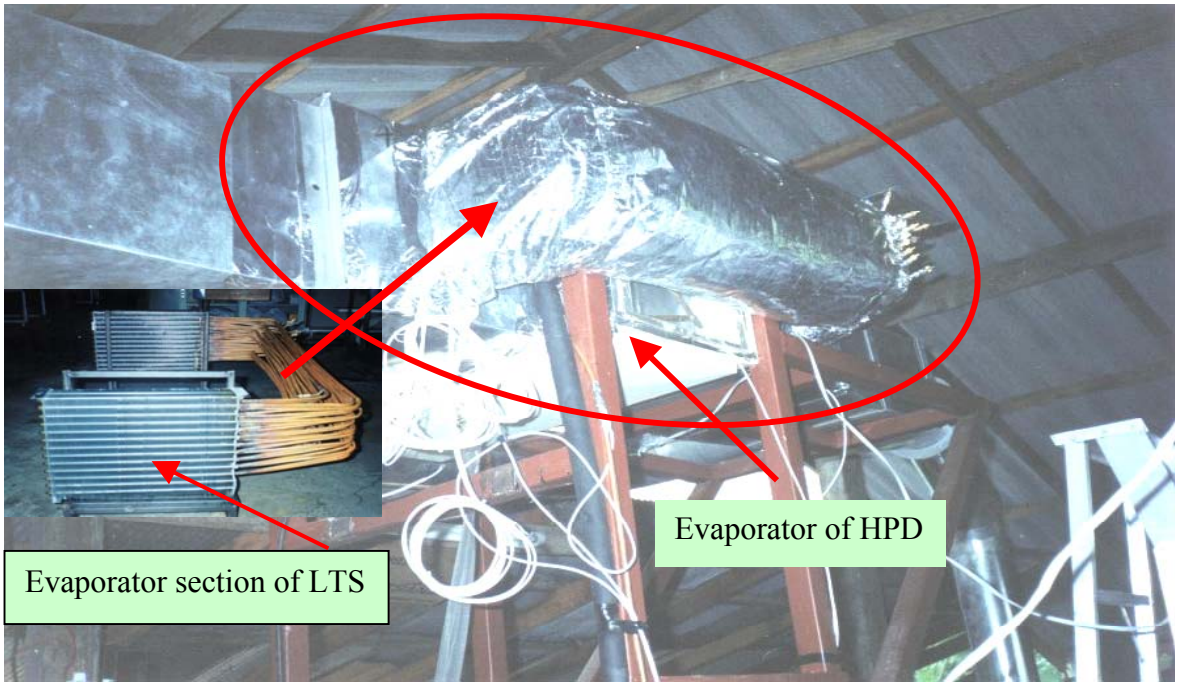


Figure 3. Installation of LTS with HPD

3. RESULTS AND DISCUSSION

The experimental results were compare between two modes, HPD with and without LTS. The two HPD were operated at the highest performance condition of RAR 50%, BAR 10%, air temperature 70 °C and air flow rate 2400 cubic meter per hour, during operation the position of tray of products (bottom and top) must be changed every 4 h period of drying time. The results of the experiment consist of drying curve, coefficient of performance of heat pump (COP_h), coefficient of performance of refrigeration (COP_r), drying efficiency (DE), NTU and effectiveness of LTS (Eff).

3.1 Drying Curve

Figure 4 shows the drying curve, the average value of moisture content with drying time every 4 hours and change the position of tray, which input fresh longan between bottom and top together.
The moisture contents (MC) of the two HPD were compared.

The MC of HPD with and without LTS considerably reduce when the drying time increases (from 89% to 27% (wb) for the HPD without LTS and 89% to 26% (wb) for the HPD with LTS). It can be considered that rate of decreasing of MC of the HPD with LTS is higher than that of the HPD without LTS. The drying time of HPD with LTS is less than the HPD without LTS about one hour. This is corresponding with results from experimental result of Phaphuangwittayakul et al [9].

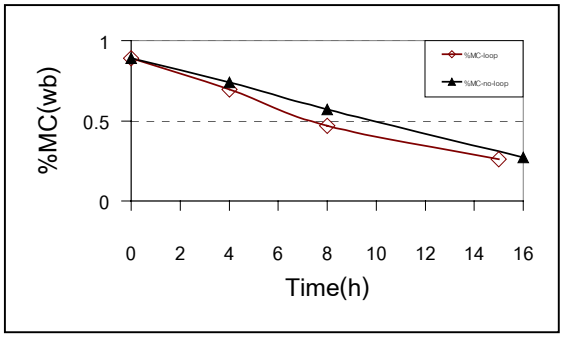


Figure 4. Moisture content and time

It can be concluded that the LTS can better reduce the moisture content rate of fresh longan in HPD than the conventional HPD and the drying time is also reduced about one hour.

3.2 Coefficient of Performance of Heat Pump (COP_h)

Table 1 shows the value of COP_h of the HPD with and without LTS at the highest performance. It is found from the results that the average value of COP_h of the HPD with LTS is 3.10, which is higher than the COP_h of HPD without LTS of 2.37. This result is corresponding to the system of the LTS as an energy saver in HPD of Phaphuangwittayakul et al [9].

It can be stated that LTS can increase the performance of heat pump of HPD about 30.80 % (from 2.37 to 3.10.)

Table 1 Experimental results.

Type of HPD	COP_h	COP_r	DE(%)	Eff
Without LTS	2.37	1.37	89.32	-
With LTS	3.10	2.10	92.84	0.14

3.3 Coefficient of Performance of Refrigeration (COP_r)

Table 1 shows the value of COP_r of the HPD with and without LTS at the highest performance. It is found from the results that the average value of COP_r of the HPD with LTS is 2.10, which is higher than the COP_r of HPD without LTS of 1.37. This result is corresponding to the system of the LTS as an energy saver in HPD of Phaphuangwittayakul et al [9].

It can be stated that LTS can increase the performance of refrigeration of HPD about 53.28 % (from 1.37 to 2.10.)

3.4 Drying Efficiency (DE)

Table 1 shows the value of DE of the HPD with and without LTS at the highest performance. It is found from the results that the average value of DE of the HPD with LTS is 92.84 %, which is higher than the DE of HPD without LTS of 89.32%. This result is corresponding to the system of the LTS as an energy saver in HPD of Phaphuangwittayakul et al [9].

It can be stated that LTS can increase the efficiency of HPD about 3.52 % (from 89.32% to 92.84%).

3.5 Number of Transfer Unit (NTU_h) of LTS

Figure 5. shows the results of NTU_h and the Effectiveness of LTS .When the NTU_h increases from 0.2 to 0.9. The effectiveness of the LTS increase from 0.13 to 0.45. When compare this result with the result of drying rice of 500 kg by using the LTS as an energy saver in HPD of Phaphuangwittayakul et al [9], It can be seen that the results are in good corresponding.

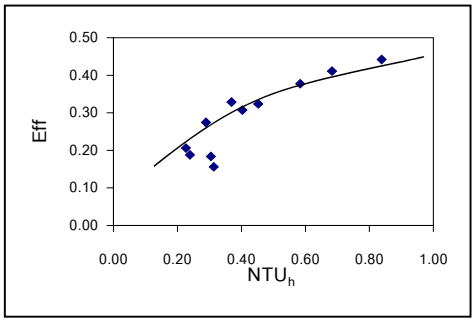


Figure 5. Effectiveness of LTS and NTU_h

4. CONCLUSION

The LTS affects the HPD by increasing the performance of HPD and the average drying time as follow;

The LTS can increase the COP_h as 30.8 % (from 2.37 to 3.10)

The LTS can increase the COP_r as 53.28 % (from 1.37 to 2.10)

The LTS can increase the DE as 3.52 % (from 89.32 to 92.84%.)

The effectiveness of LTS used in this research was 0.14

Nomenclature

W_s	power of compressor (kW)
Q_e, Q_c	heat transfer rate at evaporator and condenser (kJ/h)
T	temperature (°C or K)
RH	relative humidity (decimal)
DE	drying efficiency (%)
MC	moisture content of crops (% wb.)
COP_h	coefficient of performance of heat pump (decimal)
COP_r	coefficient of performance of refrigeration (decimal)
ω	humidity ratio (kg_{water}/kg dry air)
Eff.	effectiveness of loop thermosyphon
$\dot{m}$	mass flow rate of working air (kg/s)
$\dot{Q}$	heat transfer rate (kW)
RAR	recirculation air ratio (decimal)
BAR	by-pass air ratio (air is not enter evaporator of HPD, decimal)
HPD	heat pump dryer
LTS	loop thermosyphon
NTU	number of transfer unit
wb	wet basis (%,decimal)

Subscripts

a	air
c	condenser
e	evaporator
s	shaft

Acknowledgement

The authors would like to express their sincere thank to the Ministry of Science and Technology of Thailand has been supported this research.

Reference

1.Achariyaviriya, A. Soponronnarit,S. and Tiansuwan, J. (2000). Mathematical Simulation of Longan Fruit Drying, The Kasetsart Journal natural Sciences, April-June, Volume 34 Number 2, pp290-300

2. Clements, S., Jai, X. and Jolly, P. (1993). Experimental verification of a heat pump assisted continuous drying simulation model, International Journal of Energy Research Vol. 17, pp19-28.

3. Chaitep, S., Terdtoon, P., Tantakom, P. and Phaphuangwittayakul, W. (1999). Looped Thermosyphon as An Energy Saving in Longan Dryer, International 11th Heat Pipe Conference, Musashinoshi Tokyo, Japan, pp250-255.

4. Jolly, P. Jia, X and Clements, S (1990), Heat Pump Assisted Continuous Drying Part1:Simulation model, International Journal of Energy Research, Vol. 14, pp757-770.

5. Jai, X., Jolly, P. and Clement, S. (1990). Heat pump assisted continuous drying Part2: Simulation results, International of Energy Research Vol. 14, pp771- 782.

6. Klongpanich, W. (1991). Longan Drying in Thailand, A thesis submitted for Doctor of Philosophy at the University of Reading, pp241.

7. Office of Agricultural Economics, Ministry of Agriculture and Cooperatives report. (2002), Thailand.

8. Prasertsan, S., Saen-saby, P., Ngamsritrakul,P., and Prateepchaikul,G. (1996), Heat Pump Dryer PART 1: Simulation of the models, International Journal of Energy Research. Vol.20, pp1067-1079.

9. Phaphuangwittayakul, W.Terdtoon, P. Tantakom, P. Vorayos, N and Fulford, D. (2000). Looped Thermosyphon as an Energy Saver in Heat-Pump Dryer, International 6th Heat Pipe Symposium,Chiang Mai, Thailand, pp192-201.

10. Phaphuangwittayakul, W.Terdtoon, P. Khamonpet, P. Vorayos, N. Klongpanich,W. and Fulford, D. (2002). Effect of By-Pass Air Ratio and Recirculation Air Ratio on Heat Transfer Characteristics of Heat-Pump Type Dryer with Looped Thermosyphon as an Energy Saver, International 12th Heat Pipe Conference, Moscow, Russia, pp525-530.

Startup and Operating of a Loop Heat Pipe at Different Evaporator Orientations

Jianfeng Cao, Zengqi Hou

Chinese Academy of Space Technology
Box 9628, Ext. 5, Beijing, 100086, P. R. China
Tel: 8610-68378475, Fax :8610-68378449, E-mail:wxfcjf@sina.com

Abstract

To eliminate the suspicion that loop heat pipe is affected by evaporator orientation, a loop heat pipe was tested at different evaporator orientations. Operating characteristics at different anti-gravity (evaporator above condenser) height, -1m, 0, +1m, were compared. Startup tests were taken at six evaporator orientations: at zero anti-gravity height, evaporator was above, below, and horizontal with compensation chamber, and at 1m anti-gravity height, evaporator was above, below, and horizontal with compensation chamber. These tests indicated that the loop heat pipe could operate stably at different status, and anti-gravity could affect LHP's startup, if evaporator is above compensation chamber at the same time, startup would be very difficult.

Key words: loop heat pipe startup

1. INTRODUCTION

Loop heat pipe (LHP) is a high-effective heat pipe, developed in the end of last century. It can transport 10 ~1000 Watts to several meters away along smooth and somewhat flexible pipe, even if heat source is 2 ~ 3 meters above cold place. Now, loop heat pipe has been used as the heat- dissipating device for aerospace, airplane or terrestrial heat generating equipments. In thermal control technology of man-made satellites, its advantages are very distinct. It liberates the arrangement of heat generating equipments, enable them to be mounted at any expected place in the satellite. Use loop heat pipe as the primary heat transport device,

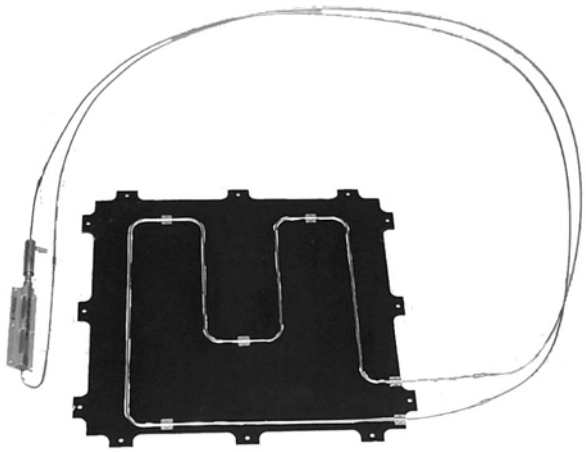


Fig.1 Loop heat pipe

Tab.1 main parameter of LHP

evaporator	envelope material: SS size：Φ13mm*130mm
	saddle material: aluminum alloy bottom size: 38mm*120mm
	wick material: sintered nickel powder pore dimeter: <1.5μm
compensation chamber	material: SS size: Φ15mm*50mm
condenser	material: aluminum alloy size: 430mm*400mm*2.5mm
Vapor/liquid line	material: SS cross-section size: Φ3mm*0.5mm length: 1.7m
agent	ammonia

deployable radiator can be made very simple and very efficient.

In a recent Chinese earth-observing satellite, a loop heat pipe, fabricated by Chinese Academy of Space Technology, was applied. In the pressurized cabin of the satellite, there is a gyroscope, which generates about 30W waste heat. Several electric fans were distributed in the cabin to force filled gas cycling, however, there are many devices nearby that gas flow and surface radiation is blocked. In order to improve the cooling condition, LHP's evaporator, with a Aluminum alloy saddle soldered below, is mounted onto the gyroscope's top face, and its condenser is located on the top of a colder device about 1m away. There is enough open space above the condenser, most of waste heat is moved off by forced gas flow. Flexible vapor line and liquid line zigzag among some

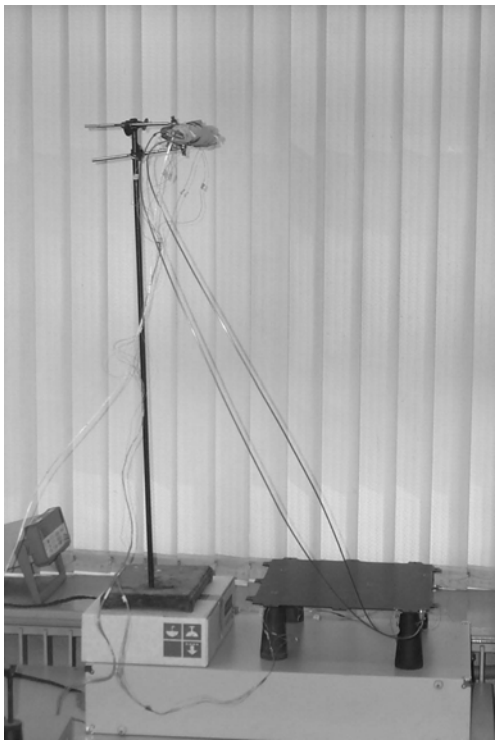


Fig.2 Loop heat pipe in testing

equipments, linking the evaporator to the condenser. Figure 1 is the picture of the LHP and table 1 lists its main parameters.

Loop heat pipe's anti-gravity operating performance makes its placing position not need so strict as normal longitudinal-grooved heat pipe in terrestrial tests. But whether can it smoothly startup and operate at any evaporator orientations? Are there any differences between different orientations? Consequently, in satellite's terrestrial experiments, should we worry about the orientation of loop heat pipe? These questions need to answer by experiment. This paper describes the experiment process and result.

2. EXPEREMENT SET-UP

A film electric heater was bonded under evaporator saddle, providing steady heat load. The condenser was fixed at horizontal position. Airflow forced by a nearby electric fan blew to the condenser. Air flow's temperature, the same as room's temperature, was 27 ± 0.5℃. The flexibility of vapor and liquid lines made the evaporator could turn and move up and down.

3. STEADY-STATE OPERATING

During steady-state experiment, the evaporator is kept in horizontal state, that is, in the same level with the compensation chamber. Three status were compared: (1) h=0(h, anti-gravity height, the height of evaporator above condenser), (2) h=1m, (3) h=-1m. after the loop heat pipe start up at h=0, 30W heat load, for each status, heat load to evaporator cycled once as following sequence: 30W→20W→10W→5W→10W→20W→30W→40W→50W→100W→50W→40W→30W, then changed into next status. The whole steady-state experiment lasted 15 hours; the loop heat pipe was operating very stably. Fig. 3 shows the evaporator saddle's and vapor line's temperature.

As fig.3, except h=-1m and heat load is 40W and 50W, both evaporator temperature and vapor temperature are linear with heat load. moreover, the three lines representing vapor temperature are nearly the same. This implies that the loop heat pipe was operating at constant conductance mode during the whole experiment. In different anti-gravity height, the scopes of evaporator temperature are not so the same, when h=1m, is 0.33℃/W, h=0, is 0.30℃/W, h=-1m, is 0.26℃/W. this difference might be due to the move of evaporating interface in evaporator porous wick.

4. STARTUP AT LOW HEAT LOAD

In real application of LHP, the thermal capacity of heat-generating equipment or evaporator saddle may conduct low heat load onto evaporator when LHP starts up. Several authors have proved that low heat load is less advantageous to LHP's startup than high heat load[1]. So we chiefly studied the startup at low heat load.

Six status were compared: h=0, E is horizontal with CC, E above CC, E below CC; and h=1m, E horizontal with CC, E above CC, E below CC(here E is the evaporator, CC is the compensation chamber.). heat load at startup was 5W. For each status, before heat was loaded, the LHP was kept at that status at least one hour, in order to make vapor and liquid distribution into equilibrium.

Showed in fig. 5, as h=0, the LHP could start up smoothly, while as h=1m, if E above CC, the LHP was difficult to startup, however, if E is below CC or E horizontal with CC, though LHP could startup, the vapor temperature was higher than h=0. It can be explained as: if evaporator is above condenser, part of liquid in the compensation chamber or in the core of porous wick may drop into external pipe lines, so there is much vapor in the core when heat is loaded. The vapor's existence not only reduces the area that liquid flow into the wick and blocks liquid flow, but enhances the leak heat to core vapor through wick. More leak heat makes the temperature of vapor in core or compensation chamber increase, and the loop finally reaches a higher temperature level. Fig 5b and 5d show steadily fluctuate, which may be relate to the movement of bubbles in the core.

Startup failure in fig. 5f can be explained as fig. 4. If E above CC, most liquid in CC and wick core will drops to the bottom of CC, when anti-gravity height is zero or not so high(as the case of fig.5e), the capillary force in the gap between penetrated tube and inner wall of wick can hold enough liquid in the core, however, when anti-gravity height is much higher, this capillary force cannot hold liquid in core, the liquid originally in the core drops into external pipe lines, startup is difficult because liquid is absence in the core.

5. CONCLUSION

The loop heat pipe can operate stably while anti-gravity height is –1m, 0, or +1m. If the condenser is cooled with the same temperature air flow as surrounding, loop heat pipe operates at constant-conductance mode.

The status of evaporator above condenser is disadvantageous to LHP's startup. Especially, when the height between them is high and evaporator is above compensation chamber, LHP is difficult to startup. In terrestrial test and application, this status should be avoided.

Two more phenomena were observed and worthy of our farther study, one is that evaporator thermal conductance related to anti-gravity height, the other is that temperature was fluctuant regu-

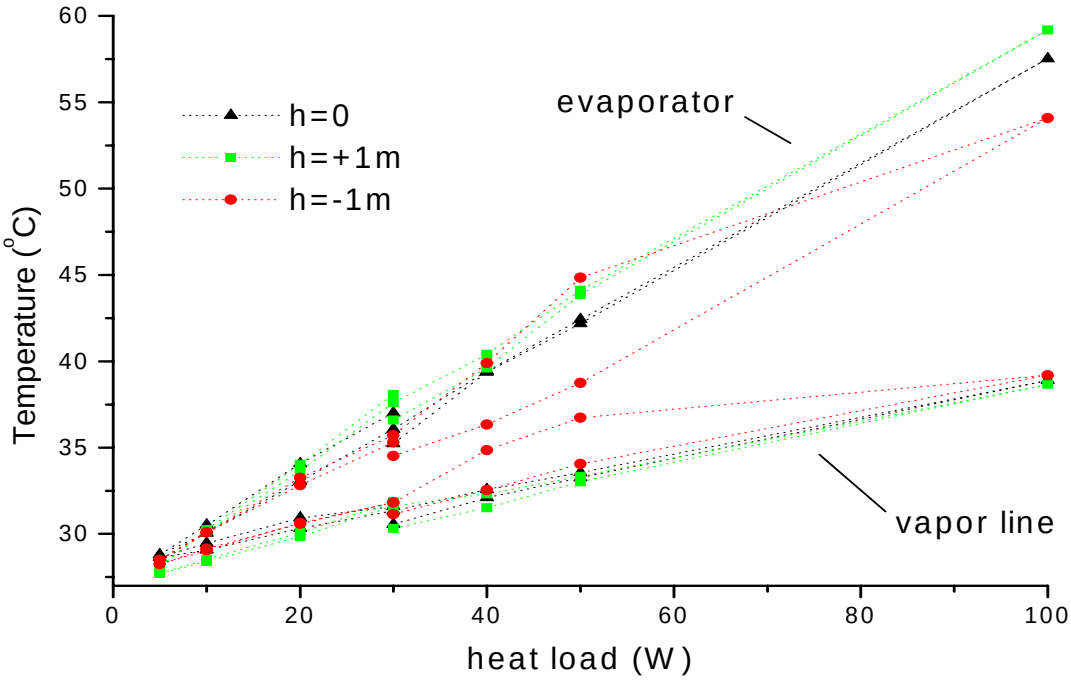


Fig. 3 steady-state operating performance

larly after LHP started up in anti-gravity status.

References

1. Maidanik Y.F., Solodovnik N., Fershtater Y., 1995, "Investigation of dynamic and stationary characteristics of a loop heat pipe", Proc., 9th IHPC

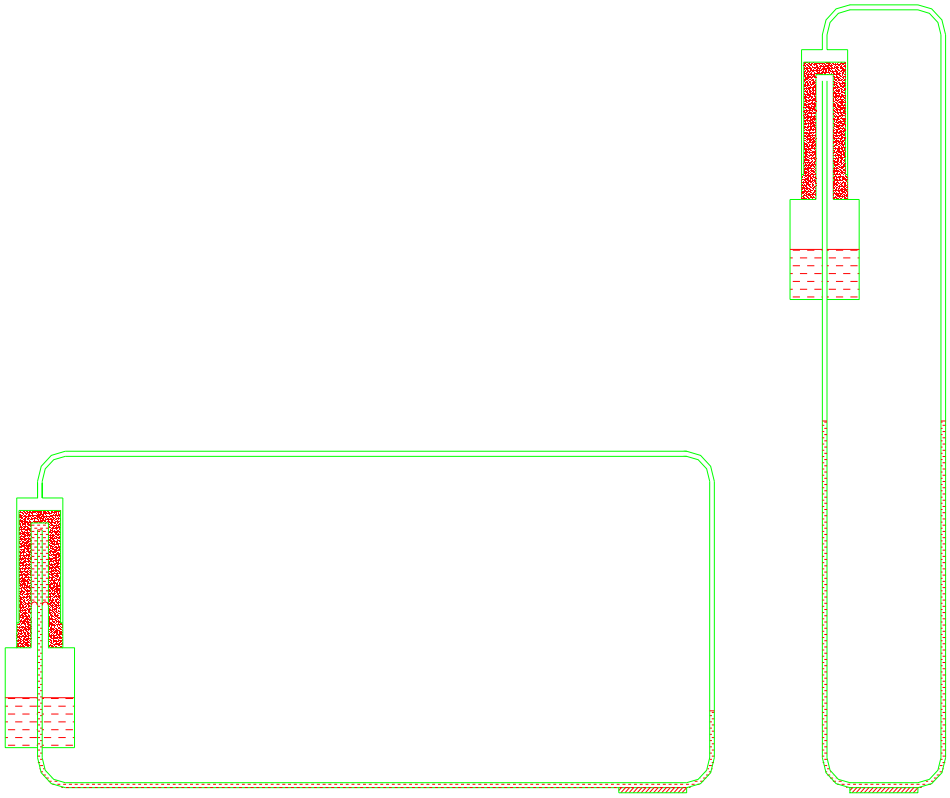
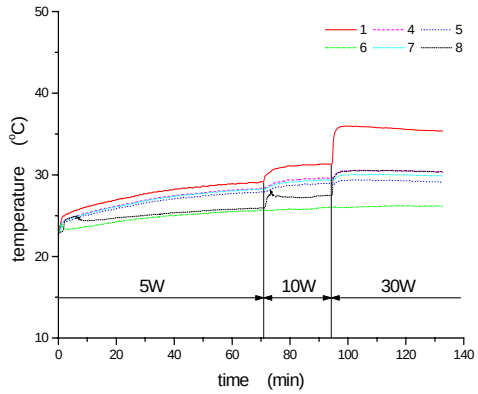
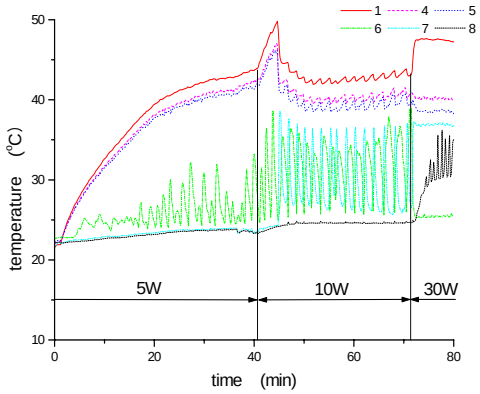


Fig.4 vapor/liquid distribution at low and high anti-gravity height before startup

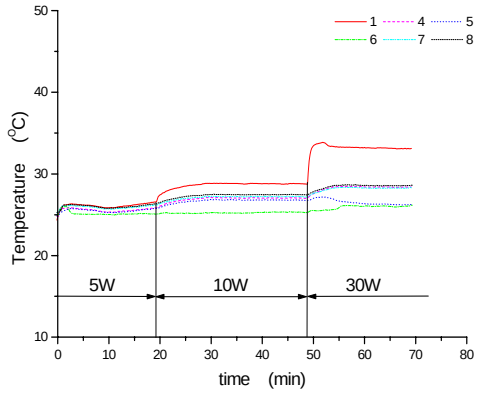


a. h=0

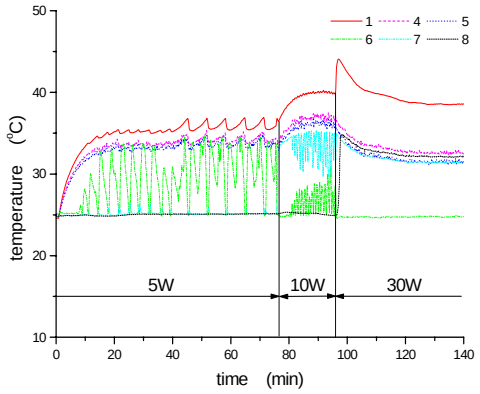


b. h=1m

Ⅰ E horizontal with CC

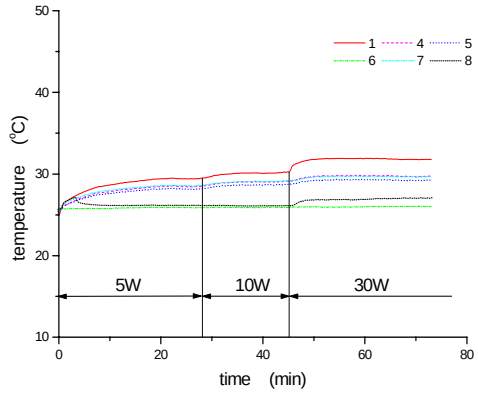


c. h=0

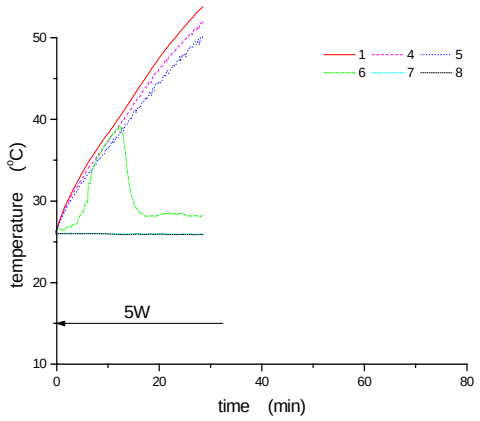


d. h=1m

Ⅱ E below CC



e. h=0



f. h=1m

Ⅲ E above CC

Fig. 5 startup at low heat load in different evaporator orientations

1 evaporator saddle 4 vapor line inlet 5 compensation chamber

6 liquid line outlet 7 vapor line outlet 8 condenser line near its inlet

An Experimental study on the Operational Characteristics of Closed Loop Type Thermosyphon for Solar Hot Water Heater

Myeong Cheol Kang*, Yong Heack Kang*, Won Gee Chun**

*Korea Institute of Energy Research(KIER), 71-2, Jang-Dong, Yusong-Ku, Taejon, 305-343, Korea
**Department of Neclear and Energy Engineering, Cheju National University, Cheju, 690-756, Korea
Tel.: 042-860-3568; Fax: 042-860-3739: E-mail: mckang21@kier.re.kr

Abstract

In the present study, the natural circulation and the closed loop type thermosyphon system have been investigated theoretically and experimentally. Therefore, the natural circulation type and the closed loop type thermosyphon systems are widely used for solar domestic hot water systems(SDHWS). The closed loop type thermosyphon system, which hires the concept of a wickless heat pipe, is a circulation device for transferring heat produced at the collector. The working fluid runs through a closed circulation loop carrying heat from the collector to the storage tank. In this paper, the operational characteristics of various working fluids are examined with the whole performance of the system. The working fluids experimented in the present study are ethanol, water, and a binary mixture of ethanol and water(ethanol/water). Various amounts of working fluid were tested where the working fluid occupies 30, 40, 50, 60 or 70% of the loop volume. In case of a small fill charge ratio, such as 30% and 40%, dry-out phenomena were observed. While for the large fill charge ratio, in the case of 70%, stagnation phenomena were occurred. The performance data obtained from the indoor experimentation was applied for the outdoor test under solar radiation. The efficiency of the closed loop type thermosyphon system was 46% with high solar radiation and 43% with low solar radiation.

Key words: closed loop type thermosyphon, solar domestic hot water system(SDHWS)

1. INTRODUCTION

A variety of solar energy system have been developed and practiced using SDHWS(solar domestic hot water system). The thermosyphon SDHWS and closed loop type thermosyphon system deem most attractive in solar water heating applications. But thermosyphon SDHWS have limited operation in low temperatures and freezing destriction of working fluid in winter. The best solution for freezing destriction is to use of the 2-phase closed loop type thermosyphon.

The 2-phase closed thermosyphon is a circulation device that the heat produced at the evaporator area is transferred into the condenser area in the loop by working fluid. Heat responsibility is very fast through phase change of working fluid. High heat transfer rate has obtained by low temperature in the closed loop type thermosyphon. The advantage of the system is

high heat transfer rate. A phase change of the working fluid occurs at the evaporator section and the vapor is transported to the condenser by the density gradient.

The system of 2-phase closed thermosyphon uses heat-pipe. The construction of the 2-phase closed thermosyphon is simpler, lower collector area and system weight than the traditional thermosyphon SDHWS. Also, the operation is not constricted relatively.

An experimental study of the heat transfer performance at inclined two-phase closed thermosyphon has been studied by K. Negishi and T. Sawada(1983). Water and ethanol have been used as the working fluid. The experimental parameters were the amount of working fluid and the inclination angle. They obtained the overall heat transfer coefficients and the thermal characteristics.

C. Casarosa and E. Latrofa(1983) studied the experiment on a two-phase thermosyphon using water as the working fluid and observed Geyser Effect. The heat transfer coefficient at the thermosyphon evaporator has been measured.

Experimentation of the thermosyphon with a binary mixture studied by H. Y. Kwak and C. B. Kim(1995). The operating characteristics of a two-phase thermosyphon with a stable water /ethanol mixture was experimentally investigated and carried out for start-up, steady state, inclination and heat transfer limitation.

In the present study, a two-phase closed thermosyphon using heat-pipe was developed and investigated.

In this study, the closed loop type thermosyphon does not used heat-pipe, but similar to operating principle. The closed loop type thermosyphon geometry and experimental apparatus is showed on Fig. 1. Water, ethanol and water/ ethanol mixture have been used as the working fluid. An experiment on the closed loop type thermosyphon has been carried out for operation characteristics of working fluid rate and outdoor test was implemented.

2. EXPERIMENTAL APPARATUS

To determine the characteristics of closed loop type thermosyphon, the indoor tests consist of loop type thermosyphon, storage tank, vacuum pump(rotary pump), plate heater, voltage regulator and power supply, hot water tank, chiller and data acqusition. A schematic diagram of the experimental set-up is shown on Fig. 1. The thermosyphon is a copper tube whose diameter is 9.52mm and total length is 20mm. The heat exchanger of spiral type in storage tank was connected thermosyphon.

To supply thermal power in the thermosyphon into the irradiation conditions, a plate heater controlled by a voltage gauge and voltage regulator is used. A vacuum pump with a rate of 10^{-3} Torr was used to remove air in inner space of thermosyphon. After evacuating air, the working fluid was injected into the thermosyphon.

The thermocouples are installed at the thermosyphon for temperature measurement. Fig. 1. shows the location of the thermocouples in thermosyphon system.

3. EXPERIMENTAL PROCEDURE

Remaining closed loop type thermosyphon under vacuum condition continuously is very important, so evacuating air should be removed by vacuum pump. To evacuate and fill-charge working fluid in inner space of the thermosyphon, the three-way valve should be installed. A kind of filling working fluid is water(H2O), ethanol(C2H5OH) and binary mixture of water and ethanol. The amount of working fluid was

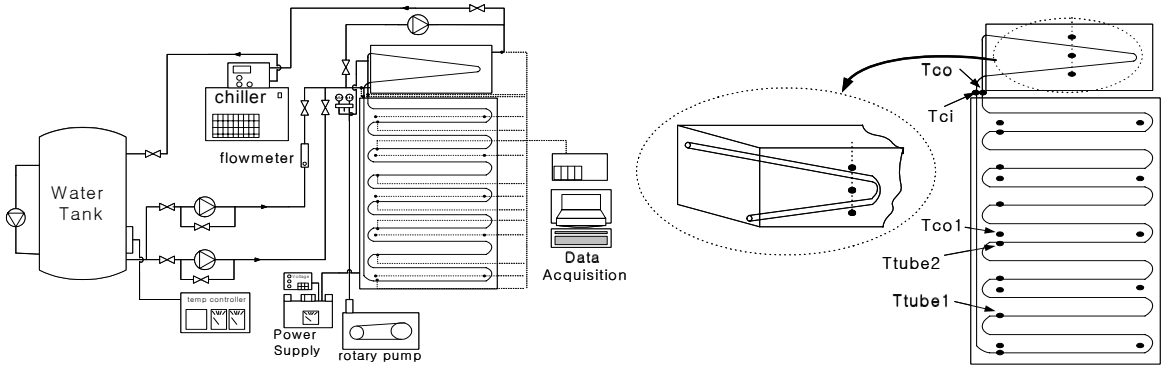


Fig. 1 Schematic diagram of the experimental setup and location of the thermocouple

varied 30, 40, 50, 60, or 70% of loop volume in thermosyphon, respectively.

Before starting experimental measurements, we filled the cooling water in tank. The mean temperature of cooling water was kept at 25℃. The thermal power was varied from 220 W/㎡ to 880 W/㎡, corresponding to irradiation conditions.

4. RESULT AND DISCUSSION

4.1. Characteristics for working fluid ratio

The experimentation of operating characteristics in thermosyphon was implemented in order to decide the working fluid and working fluid ratio. After filling the working fluid and supplying thermal power, the temperature distributions on the thermosyphon and the water of tank were measured.

Fig. 2. shows the temperature distribution for fill-charge ethanol(30%). When thermal power of 440 W/㎡ is supplied, outlet temperature of thermosyphon is higher than plate and tube temperature in thermosyphon. This phenomenon is dry-out because the amount of working fluid is small. Furthermore, when the amount of working fluid is 40%, dry-out occurred. But when a working fluid ratio is 50%, 60% and 70%, system temperature is steady.

When working fluid is water, a small amount of working fluid(30%, 40%) occurred dry-out at the supplied thermal power of 660W/㎡ and 880 W/㎡, respectively

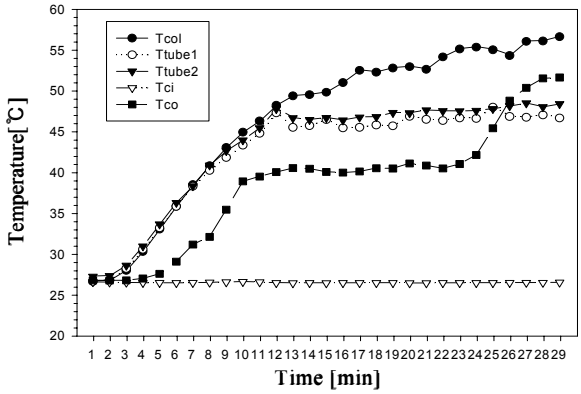


Fig. 2 Temperature variation of the system: ethanol(30%)

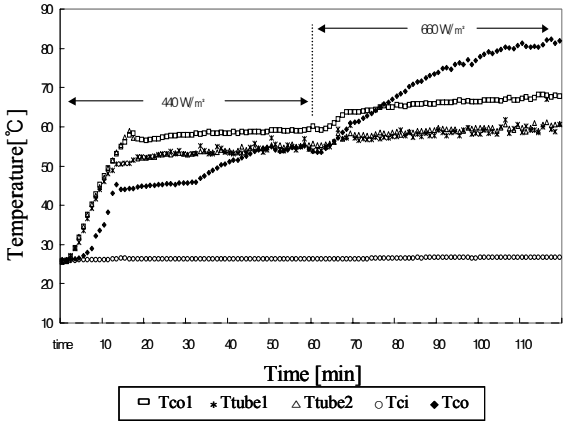


Fig. 3 Temperature variation of the system: water(30%)

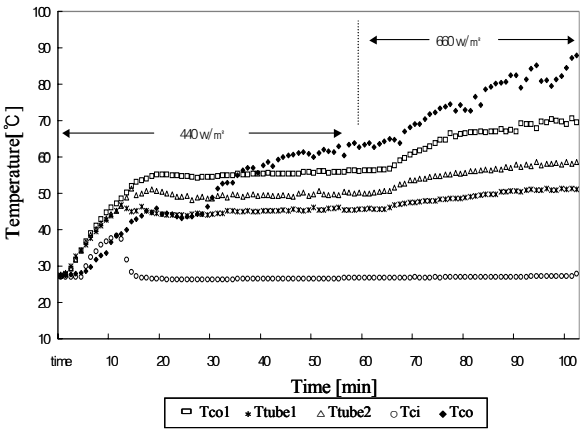


Fig. 4 Temperature variation of the system: ethanol+water(30%)

Fig. 3. showed temperature distribution on the thermosyphon at the fill ratio of 30%. Fig. 4. showed temperature distribution on the thermosyphon at a fill ratio of 30% water and ethanol mixture. Fig. 5. showed the thermal storage capacity and efficiency when the amount of working fluid is 50, 60 and 70%. Fig. 6. showed the thermal storage capacity and efficiency when the amount of working fluid is 50%, 60% and 70% at water. Fig. 7. showed the thermal storage capacity and efficiency when the amount of working fluid is 50, 60 and 70% at mixture of water and ethanol.

At a fill ratio of 70% water, ethanol, and mixture a stagnation phenomenon began to appear at the inlet thermosyphon, respectively.

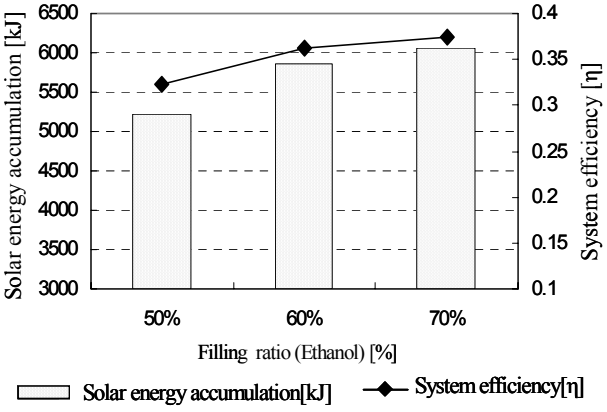


Fig. 5 Solar energy accumulation & system efficiency : Ethanol(50%, 60%, 70%)

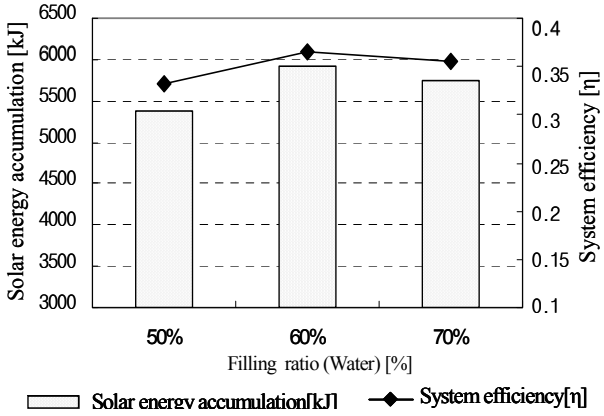


Fig. 6 Solar energy accumulation & system efficiency : Water(50%, 60%, 70%)

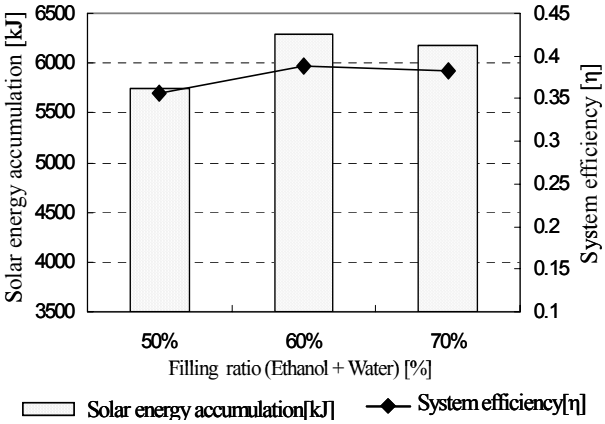


Fig. 7 Solar energy accumulation & system efficiency : ethanol+water(50%, 60%, 70%)

4.2 Comparison efficiency for working fluids

In order to select a working fluid, water, ethanol and mixture of water and ethanol are used as the working fluid. The amount of working fluid was 60% of loop volume in thermosyphon.

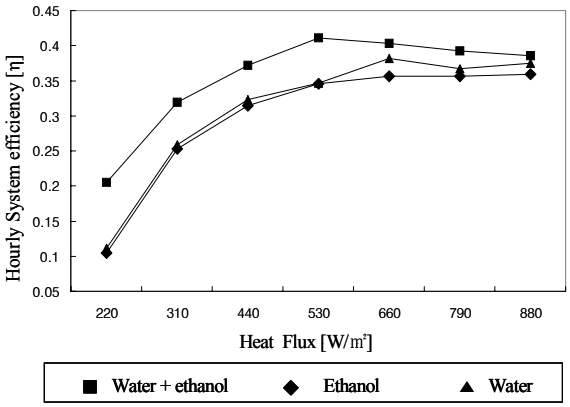


Fig. 8 Comparison of the efficiency(60%)

Experimentations have been carried out for operating characteristics of working fluid which can increase the thermal power.

Fig. 8. showed the comparison of the storage efficiency. The efficiency of mixture is higher than those of water and ethanol.

4.3. Outdoor(field) test

To investigate performance of the system, the outdoor test was implemented. Fig. 9 showed the thermal performance characteristics of thermo-syphon system in case of high irradiation and high initial water temperature(HRHT). In this case, the system efficiency is 46%. Fig. 10 showed the temperature variation of the system in case of high irradiation and low initial water temperature (HRLT). In case of the HRLT, the system efficiency is 47%.

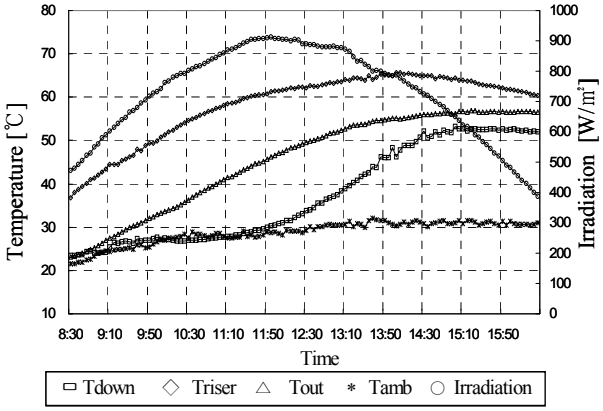


Fig. 9. Temperature variations of the system(HRHT)

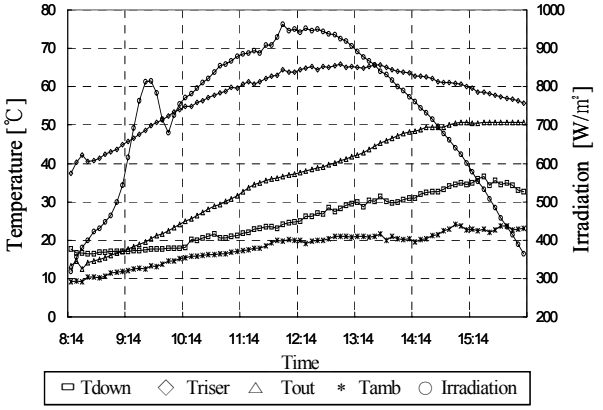


Fig. 10. Temperature variations of the system(HRLT)

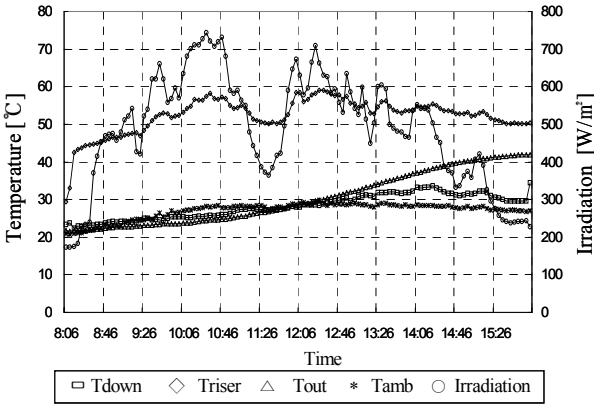


Fig. 11. Temperature variations of the system(LRHT)

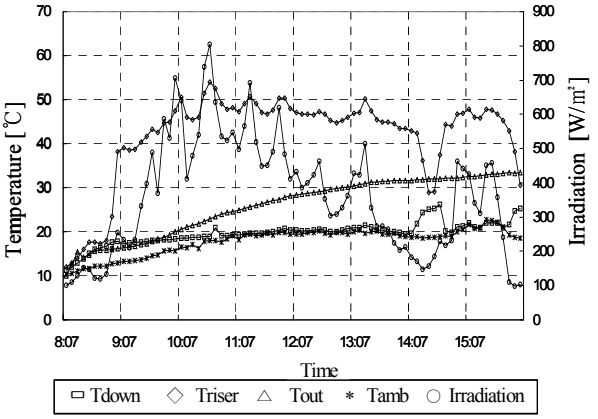


Fig. 12. Temperature variations of the system(LRLT)

Fig. 11 is the temperature variation of the system in case of low irradiation and high initial water temperature (LRHT) and Fig. 12 is in case of low irradiation and low initial water temperature (LRLT). And system efficiency is 43% and 37% with low irradiation and low initial water temperature (LRHT) and LRLT, respectively.

5. CONCLUSION

The work presented here is to determine the working fluid and rate of working fluid through experimental of operating characteristics. The conclusion of the study can be summarized as follows:

(i) When an amount of working fluid is 30%

and 40%, dry-out phenomenon began to appear at evaporator in thermosyphon. In order to avoid dry-out phenomenon, it is necessary to fill ratio between 50% and 70%. However, when an amount of working fluid is 70%, a stagnation phenomenon began to appear from the inlet thermosyphon.

(ii) An experimentation has been carried out for operating characteristics of working fluid increasing the thermal power. We obtain the comparison of the storage efficiency. The efficiency of mixture is higher than those of water and ethanol.

(iii) The performance data obtained from the indoor experimentation was applied for the outdoor test under solar radiation. The system efficiency of the closed loop type thermosyphon was 46% (HRHT), 47%(HRLT), 43%(LRHT) and 37% (LRLT), respectively.

Nomenclature

Tamb	ambient temperature
Tci	collector intlet temperature
Tcol	forth plate temperature
Tco	collector outlet temperature
Tdown	collector inlet temperature
Tout	outlet temperature
Triser	collector outlet temperature
Ttube1	second tube temperature from bottom
Ttube2	fourth tube temperature from bottom

References

1. Casarosa C. and Latrofa E. 1983, The geyser effect in a two-phase thermosyphon, Journal of the Heat Mass Transfer, Vol. 26, No. 6, pp. 933-941.

2. Kanji Negishi and Teruo Sawada, 1983, Heat transfer performance of an inclined two-phase closed thermosyphon, Journal of Heat Mass Transfer, Vol. 26, No. 8, pp. 1207-1213.

3. R. S. Soin, S. Raghuraman and V. Murali, 1987, Two-phase water heater: Model and long term performance, Solar Energy, Vol. 38, No. 2, pp. 105-112.

4. T. Y. Bong, K. C. Ng and H. Bao, 1993, Thermal performance of a flat-plate heat pipe collector arry, Solar Energy, Vol. 50, No. 6, pp. 491-498.

5. H. Y. Kwak and J. B. Kim, 1995, A study on operating characteristics of the two-phase closed thermosyphon with a binary mixture, The korea energy engineering, Vol. 4, No. 1, pp. 95-102.

6. Zbyslaw Pluta and Wlodzimiera Pomierny, 1995, The theoretical and expermental investigation of the phase-change solar thermosyphon, Renewable Energy, Vol. 6, No. 3, pp. 317-321.

7. W. G. Chun, Y. H. Kang, H. Y. Kwak and Y. S. Lee, 1999, An experimental study of the utilization of hest pipes for solar water hesters, Vol. 19, pp. 807-817.

Thermosyphon Kit for Conversion of Electrical Bakery Ovens to Gas

Marcia B. H. Mantelli, André Lopes, Geraldo J. M. Martins,
Rafael Zimmerman and Rovanir Baungartner

Department of Mechanical Engineering
Federal University of Santa Catarina
Campus Universitário Trindade, Florianopolis, SC, Brazil
88040-900 Phone: + 55 48 234 21 61 Ext. 214, Fax: + 55 48 3317615
marcia@emc.ufsc.br, marcia@labsolar.ufsc.br

Henrique G. de Landa

CENPES, Petrobras
Cidade Universitária Q. 7, Ilha do Fundão
21949-900 Rio de Janeiro, RJ, Brazil

Abstract

Electrical driven bakery ovens are cost ineffective due to two main reasons: the electricity fare is high and the quality of the product is poor, causing the waste of a high amount of bread, inadequate for selling. A Kit, designed to convert bakery ovens from electrical into gas is presented in this paper. The Kit consists of twenty thermosyphons displayed in two rows of ten, vertically aligned, closed to the lateral walls of the oven. A combustion chamber is installed under the rear face of the baking chamber. Twenty burners are specially designed for this application and installed under each thermosyphon evaporator. The heat is generated by gas burning (GLP or Natural) in the combustion chamber. These ovens present several advantages when compared to the electrical conventional ones: uniform temperature distribution inside the baking chamber; no contact between the combustion gases and the bread; short temperature recovering time after operational door openings, easy control of the cooking temperature, reduced operation cost and short time of investment recovering. The higher heating ramp time is a disadvantage, but new developments are proposed to solve this problem in the near future.

Key words: thermosyphon, heat pipes, bakery ovens, baking chamber, combustion chamber.

1. INTRODUCTION

The Brazilian Government has to deal with the serious energy crisis that the country faces. Several energy conservation programs have been created, including the stamping of bakery ovens, which are ranked according to its energy use efficiency. In this frame, bakery oven factories are looking for simple technological solutions to improve the thermal performance of the equipment that they manufacture.

Thermosyphons are efficient devices designed to transfer high heat rates from large distances when subjected to small temperature differences (see Peterson [1]). They are basically composed by a sealed metal tube, which is evacuated and where a certain amount of working fluid is inserted. There are three main regions in a thermosyphon: evaporator, adiabatic section and condenser. Saturated liquid and vapor operates in a closed cycle inside the tube.

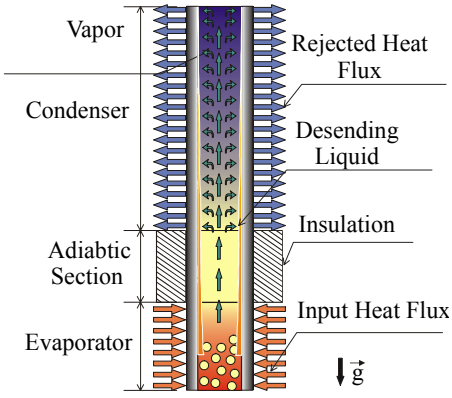


Figure 1. Schematic of the thermal performance of a thermosyphon.

Figure 1 shows a schematic of the thermosyphon thermal performance. The heat imposed to the evaporator, always located at a lower position, evaporates the liquid accumulated in a small pool. The formed vapor migrates to the condenser by pressure unbalance. Heat is removed

from the condenser and the condensed liquid returns to the evaporator by the action of gravity.

1-1 The Ordinary Baking Oven

According to Mantelli et al. [2], the ordinary bakery ovens are usually driven by GLP or electricity. Wood is still used in a minor scale. The gas represents a lower operational cost but the electrical ovens are considered safe and easy to operate. Both models, specially the electrical ones, present thermal inefficiencies. In this case, the generated heat is concentrated in about 10% of the volume of the baking chamber, being inefficiently distributed by means of a 1 HP ventilator, causing super and under-heated areas, which affect the quality of the baked bread.

On the other hand, the GLP ovens reject combustion gases at high temperatures, resulting in energy losses. In addition to this, the combustion takes place in a lower region of the baking chamber and the hot gases, resulted from the gas burn, heat the baking chamber. Besides, to guaranty a reasonable temperature distribution, a ventilator, similar to the one employed to the electrical oven, is used.

1-2 The Bread Baking Process

According to Kupka and Mantelli [3], despite of the equipment to be employed (gas or electrical) the baking process involves two basic steps. First, the already grown bread dough at room temperature is inserted in the pre heated oven. The dough temperature increases to up to 100 ^{o}C, when the dough water starts to be vaporized. Then, in a second phase, the temperature of the dough is kept in an almost constant level, while the water is eliminated through the external surface of the bread. Hasatani et al. [4], [5] made an experimental analysis of the behavior of two bread doughs with the same compositions but with different weights and submitted to three different temperature levels: 150 ºC, 200 ºC and 250 ºC. The initial dough weights were 1560 g and 50 g. The bread baking was monitored by a weighing scale so that it was possible to relate the temperature level to the dough weight. These authors concluded that the vapor flux, from the bread to the environment, reaches its maximum at the point when the dough presents a uniform temperature. The bread hard cover starts to be formed when the heating phase is finished. Independently of the dough weight, the bread baking temperature is kept at around 100 ºC.

2. THE THERMOSYPHON KIT

A common electrical bakery oven bought from the market was adapted with thermosyphons, in order to be able to work both with gas and electricity.

The thermosyphons used in the Kit were specially developed for this application (Mantelli et al. [6]). To allow the action of the gravity in the return of the condensed fluid to the evaporator, the thermosyphon should be positioned in a vertical (or close to) position. On the other side, to facilitate the heat transfer from the burners, the thermosyphon evaporator should not be vertical; in fact, the more tilted the evaporator in relation to the condenser, the better.

As described by Mantelli et al. [7], the following configuration was selected. The selected tube is made of stainless steel (a good material for food manipulation) and presents an external diameter of 1,905 cm. The condenser is 1 m long, while the evaporator is 30 cm long with an inclination of 45^{o}. The water was selected as the working fluid, due to its good thermal properties and for the reason of being harmless in the case of accidental fluid release to the baking chamber. The filling ratio (ratio of the liquid volume to the evaporator volume) was chosen to be 80%. Figure 2 shows a drawing of the thermosyphon developed.

As concluded by Mantelli et al. [6], each thermosyphon should transfer at least 400 W of heat power to work properly. Around 20 thermosyphons were aligned, in two lines of ten, along each of the lateral walls of the oven.

Geometrically, the oven can be described as composed by two main compartments: the upper, representing the baking chamber and the lower, representing the combustion chamber, where the burners are installed. Figure 3 shows those compartments before the thermosyphon installation. The thermosyphons are positioned to lead through both compartments. The combustion heat generated by the burners is transferred to the baking chamber by means of the thermosyphons, in order that only the heat is transferred, not the combustion gases, which can be harmful to the health. In Figure 3 one can also see the ventilator in the central region of the baking chamber, which is a part of the original oven. The tubes located close to the ventilator are actually the electrical resistors.

Figure 4 shows a schematic of the Kit installed in the bakery oven, without the trays. In this figure one can observe the vertical long condenser located close to the baking chamber lateral walls and the inclined evaporator, in the combustion

chamber. It is important to note that the Kit can be installed in the oven with no major modifications, within the space available between the trays and the chamber walls.

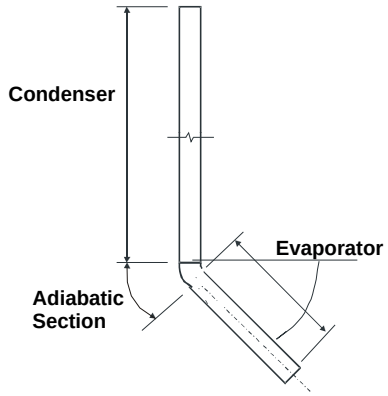


Figure 2. Schematic of the thermosyphon developed for the Kit.



Figure 3. Photo showing the combustion and the baking compartments.

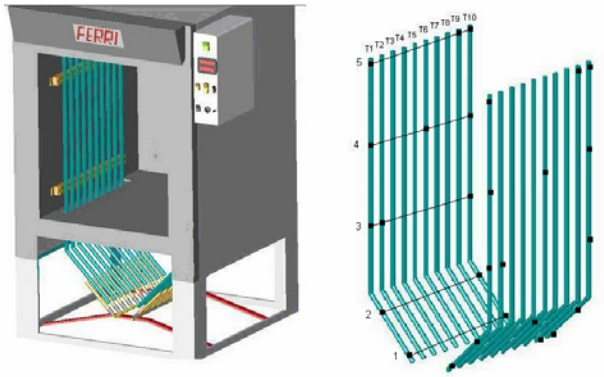


Figure 4. Kit installed in the baking chamber.

3. THE EXPERIMENTAL WORK

After the installation of the Kit, the oven assisted by thermosyphons was monitored by means of several Type K fiber glass recovered thermocouples, installed in different points along the walls, the tubes, the baking chamber environment, the combustion chamber, etc. The temperature reading errors of the thermocouples were ± 1 ^{o}C. Figure 5 presents the temperature reading points used to monitor the temperature distribution inside the baking chamber, while in the right side of Figure 4, the thermocouple positions over the thermosyphons are shown.

The gas and energy consumption need to be measured for the reason that the energy conservation is one of the objectives of the present work. The gas consumption was measured through its volume and weight, using a mass flow rate gage of ± 0,1 dm^3 of uncertainty and the weight was measured by means of a analogical scale of ± 10 g of uncertainty. The measurements were repeated each 15 minutes during the experiments. The electrical energy consumption was obtained through a electrical power meter, with an uncertainty of ±5 W.

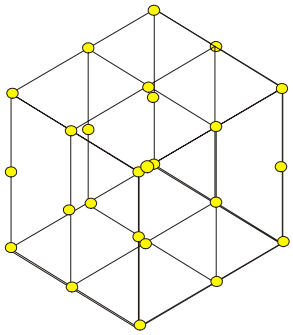


Figure 5. Lay out of the baking chamber temperature reading positions.

4. EXPERIMENTAL RESULTS

In all the tests performed, the measurements were done in transient conditions, which are the actual conditions in which real ovens work.

The temperature distribution of the baking chamber was measured for the electrical and the thermosyphon assisted ovens. Figure 6 shows a comparison between the temperature distribution for the thermosyphon assisted oven (left) and the electrical one (right).

The temperature distribution of the central regions of the baking chamber can be observed in Figure 7. The two left pictures refer to the mean planes between the front and the rear walls (upper) and between the two vertical lateral walls (lower) for the electrical oven, while the two right pictures refer to the thermosyphon assisted gas oven. In fact, these pictures represent the region where the bread is actually cooked.

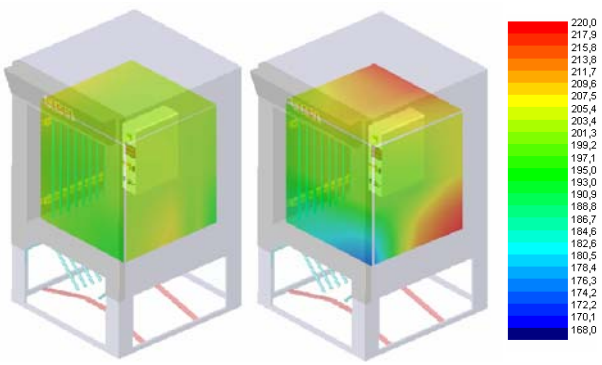


Figure 6. Baking chamber temperature distribution for themosyphon assisted oven (left) and electrical oven (right).

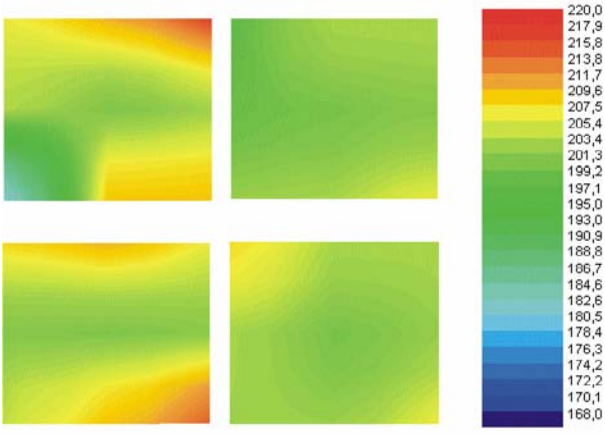


Figure 7. Temperature distribution for mean vertical planes of the baking chamber.

From Figures 6 and 7 one can see clearly that the thermossifon assisted oven presents a very uniform temperature distribution and no waste of the product is observed.

Figure 8 shows the bread obtained using the thermosyphon assisted oven (upper picture) and electrical oven (lower picture). One can note that the quality of the bread produced using the electrical oven vary very much along a single tray. This can not be observed form the thermosyphon assisted oven.

Figure 9 presents the time evolution of the temperatures for some locations along the thermosyphon assisted oven. The temperature of the combustion chamber reaches much higher levels than the temperature of the baking chamber, showing that a considerable amount of the energy being produced by the gas burn has not been used for baking. This happens due to problems in the design of the combustion chamber. As expected, the rear wall, which is in fact the division wall between the combustion and the baking chamber, and that therefore is in contact with the combustion hot gases, also presents high temperature levels. On the other hand, the released gases temperature is not very high, indicating that recoverable energy is not being wasted to the atmosphere.

To compare the performance of the electrical and thermosyphon assisted ovens in normal operation and to simulate the normal operation of a bakery, ten full runs of bread were baked in a row (five with the electrical and five with the thermosyphon assisted oven). The temperature readings for a thermocouple located in the center of the baking chamber is plotted against time for both tests in Figure 10. A complete baking cycle is composed by a heating ramp, where the baking chamber temperature is elevated from the room to the baking temperature, around 200 ^{o}C. At this time, the oven is opened to insert the dough full trays and a sharp temperature drop can be observed. Then the bread heats up and the baking chamber temperature also increase but in a lower rate than when it is empty. When the bread is ready, the oven is opened again to remove the baked bread and the temperature drops again. The door is then closed and the cycle starts again, but from the second cycle on, the initial temperature level is higher.

In Figure 10, one can observe that the electrical oven took around half the time to proceed with the five baking cycles, showing that heating ramps (rate of heating from the room to the baking temperature) for the first and subsequent runs are much steeper then for the thermosyphon assisted oven. For these ovens, the electrical resistances dissipates heat inside the baking chamber, so that 100% of the energy produced is delivered to the air to be heated and the heat losses happen just through the baking chamber external walls. Actually, it is desirable to warm up quickly the oven from the room temperature or after the bread is removed from the chamber. Therefore, the heating ramp can be considered one disadvantage of the thermosyphon assisted oven. However, the dough should have been kept at baking temperatures (around 200 ^{o}C) for some time to allow the dough to undergo all the chemical reactions that they need to grow and to form the hard cover. Actually, high heat fluxes cause poor temperature distribution, and poor quality of the bread. Furthermore, the electrical oven temperatures are difficult to control, as it can be observed by the different values of the temperature peaks observed in Figure 10 for the oven warm up, before the insertion of the dough to be baked.

5. ECONOMIC ANALYSIS

An economic analysis was performed for the operation of both the electrical and thermosyphon assisted ovens. The cost of the bread depends on the number of consecutive baking runs. Table 1 shows the costs, in the Brazilian currency (1 Real ≅ 3 US$), involved for one baking run, for the electrical and thermosyphon assisted oven. The price of the KWh of electricity was considered R$ 0,288. The price of the GLP was R$ 30,00 for 13 Kg of gas. Each baking run was considered to produce 240 breads. The gas power was estimated by the multiplication of the inferior heat power (45217.44 kJ/Kg) and the gas weight.

The waste of the product by over or under-baking represents an important increase in the cost of the bread production. The baking runs using electrical oven, performed in the Laboratory, following the procedures recommended by the oven manufacturer, showed that more then 10% of the breads were inadequate for selling.

In contrast, the cost of the Kit, including stainless steel tubes, burners, gas feeding tabulation, charging and cleaning materials, etc, is around R$ 1600,00. Considering all these costs, an analysis was performed for the kit investment recovering time. In other words, a study was done to find out how many months were necessary to return the capital invested in the Kit, considering the cost savings in energy and in the lack of bread waste.



Figure 8. Photos showing the quality of bread for electrical ovens (upper) and thermosyphon assisted ovens (lower).

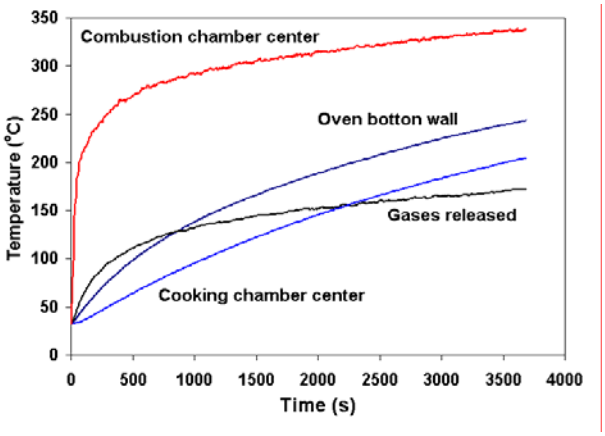


Figure 9. Temperature as a function of time for several points in the thermosyphon assited oven.

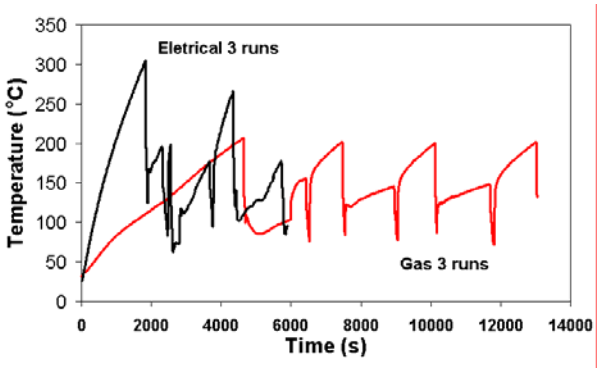


Figure 10. Baking chamber center temperature cycles for five baking in a row for the electrical and thermosyphon assisted ovens.

Figure 11 shows two curves of the investment returning time as a function of the number of baking runs per day. One curve considers no product losses while the other considers 10 % of losses. As already noted, the returning time decreases sharply as the number of baking run by day increases. Also, the losses parameter is very important. Considering ten runs a day, which is a typical number for a medium size bakery, if no losses are considered, the money invested can be recovered in about 18 months. If 10% of losses are considered, the recovering time is about 10 months.

6. CONCLUSIONS

A kit to convert electricity driven ovens to Natural or GLP gas was developed at LABSOLAR/NCTS. The project was proposed in the frame of the energy crisis that Brazil faces and has three main objectives: to substitute electricity by gas, to improve the efficiency in the energy use and to improve the quality of the bread.

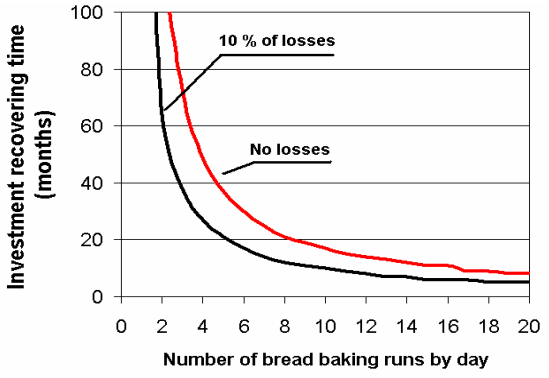


Figure 11. Investment recovering time as a function of the number of baking runs per day.

Table 1. Energy costs.

Electric Oven	
Ventilator power (mean value)	0.892 kWh
Thermal resistances	13.285 kWh
Overall consumption	14.18 kWh
Cost per hour	R$ 4.083
Cost per baking run	R$ 3.062
Cost per baking bread	R$ 0.0128
Thermosyphon gas assisted oven	
Volumetric mean consumption of gas	0.401 m^3/h
Mass mean consumption of gas	0.85 kg/h
Mean burner power	10.68 kW
Efective burner power (60 % of burner power)	6.41 kW
Ventilator cost per hour	R$ 0.257
Gas cost per hour	R$ 1.962
Overall cost per baking run	R$ 3.032
Overall cost per baked bread	R$ 0.0126

The kit is composed by thermosyphons installed close to the lateral vertical walls and was mounted inside a usual commercial oven. The modified oven can work both with electricity and gas. The temperature distribution inside the baking chamber is much more uniform for the gas then for the electrical oven. As a result, 100% of the bread produced presented the same quality all over the trays.

However, the heating time of the electrical oven is larger than that for the gas driven oven. In reality, the product waste causes larger economical losses then the energy waste.

The fact that the combustion chamber temperature is very high means that this chamber is not well designed. Actually, its volume is larger than the volume of the baking chamber. The heating ramp is of the same order of magnitude of the conventional gas ovens. Certainly the combustion chamber should be redesigned in the future to enable the energy conservation using the thermosyphon technology. It is important to note that even with this temporary adverse condition, the investment returning time is short. This time certainly will decrease much more after the combustion chamber improvement and after the implementation of an industrial series production of the Kit.

The thermosyphon assisted ovens still present other advantages when compared to the electrical conventional ones. In opposite to the conventional gas ovens, there is no contact between the combustion gases and the bread. Also, the temperature recovering time during operational doors openings is shorter, given that the thermosyphon temperature increases and the device works as a thermal capacitor, which deliver more heat when the doors are shut again. Furthermore, the thermosyphon technology allows easy control of the baking temperature.

Acknowledgement

The authors acknowledge the CENPES/Petrobras for financing this project and CNPq for providing the scholarship for the students.

References

1. Peterson, G.P., 1994, “An Introduction to heat pipes. Modeling, Testing and Applications”, Wiley Interscience, New York - USA.
2. Mantelli, M. B. H., Lopes, A. A., Teixeira, A., Reis, F., Martins, G., J. M., Zimmermann, R., Baungaertner, R., 2003, “Desenvolvimento de um Kit para Fornos Elétricos de Cocção Utilizando Termossifões com Gás Natural” - (in Portuguese), Final Report, UFSC, Brazil.
3. Kupka, A. S. and Mantelli, M. B. H., “Análise de um Forno de Cocção de Pães Assistido por Termossifões de Duas Fases - (in Portuguese)”, 2001, Master Engineering Dissertation, UFSC, Brazil.
4. Hasatani, M., Arai, N., Harui, H., and Itaya, Y., 1992, “ Effect of the Drying on Heat Transfer of Bread During Baking in Oven”, Drying Technology, Vol. 10, nº 3, pp. 623-639.
5. Hasatani, M., Arai, N., Katsuyama, H., Harui, H., Itaya, Y., Fushida, N., and Tatsukawa, N., 1991, “Heat and Mass Transfers in Bread During Baking in an Electric Oven”, IDS'91, pp. 385-393.
6. Mantelli, M. B. H., Colle, S., Moraes, D. U. C., and Carvalho, R. D. M.,1999, “Study of Two-Phase Closed Thermosyphons for Bakeries Oven Applications”, 33rd National Heat Transfer Conference, Albuquerque, New Mexico, EUA.
7. Nisgoski, A., Silva, A. K., Mantelli, M. B. H. and Landa, H. G., 2002, “Theoretical and Experimental Study of Two-Phase Vertical and Loop Thermosyphons”, Proceedings of the 12th International Heat Pipe Conference, Moscow, Russia, pp. 279-284.

Development of Heat Pipe Heating Roller in Laser Printer

Kwang Soo Kim*, Hung Bae Kim*, Kyung Woo Lee**

* R&D Center, APACK, Inc., 59-6, Hwaam-dong, Yusung-ku, Daejon, 305-348, Korea
Phone : +81-42-864-0815, Email : kskim@apack.net
** R&D Team of Digital Printing Division, Samsung Electronics Co., 416, Maetan-3 dong, Paldal-gu, Suwon, Gyeonggi-do, 442-742, Korea
Phone : +81-31-200-4173, Email : doshisha@samsung.co.kr

Abstract

In laser printer system, heating roller (HR) is essentially needed because of the fixing of printed toner on the paper. Halogen lamp which now used in laser printer requires a long time for the preheating heating roller. Instant-on-fuser, so called "Heat Pipe Heating Roller (HPHR)" is developed through this study adopted heat pipe. Comparing with halogen lamp type fuser, new instant-on-fuser is innovative product of which printing quality was improved dramatically. In order to develop HPHR, experimental and numerical study is performed. New printing system doesn't need halogen lamp any more, and warm-up time was reduced to zero second. Instant-Printing and high thermal capacity enabled high printing quality and low power loss. The first print out time (FPOT) which is one of the important specifications 12 seconds in HPHR system comparing with 42 seconds in halogen system. And the temperature uniformity along the length is less than 3 ℃ in HPHR System, but larger than 8℃ in halogen lamp system.

I. INTRODUCTION

Laser Beam Printer (hereinafter the "LBP") has seen speedy changes in its environment, which include shift towards high-speed and color printing. This change requires higher printing speed, higher image quality and lower power consumption. Transfer of image to printing paper requires low power consumption, but fixing of toner on printing paper requires high energy consumption. Especially, fuser is known to consume over 80% of power consumed by LBP.[1],[2] For this reason, LBP makers accelerate development of fuser since it is a core part of electronic products using toner to print image. Present halogen lamp type fuser needs preheating time, i.e., warm-up time. Therefore, user has to accept time loss from waiting for warm-up time. Especially, unnecessary power consumption must be accepted while printer is idle, since preheating is necessary.

Instant-on-fuser developed through this study is an innovative product. It adopts heat pipe boasting excellence in both heat conductivity and heat capacity, minimizes the deviation of surface temperature of heating roller, which is a core part of fuser, and provides superior fixity than halogen lamp type fuser. Therefore, it can substitute for halogen lamp type fuser and realize "warm-up time zero". Finally, instant-on-fuser provides speedy printing, excellent heat capacity, excellent performance in re-printing and lower power consumption.

Fig. 1 shows the principle of toner fixing of currently used halogen lamp type LBP. Fig. 2 shows instant-on-fuser type heating roller (Heat Pipe Heating Roller) which applies heat pipe and coil heater developed through this study. Generally, Fixing technology means following; Heating roller in the upper section, which is controlled by temperature sensor, i.e., fuser, and pressure roller in the lower section engage and rotate. The paper having images transferred from drum passes between fuser and pressure roller. Then, images are fixed on the paper.

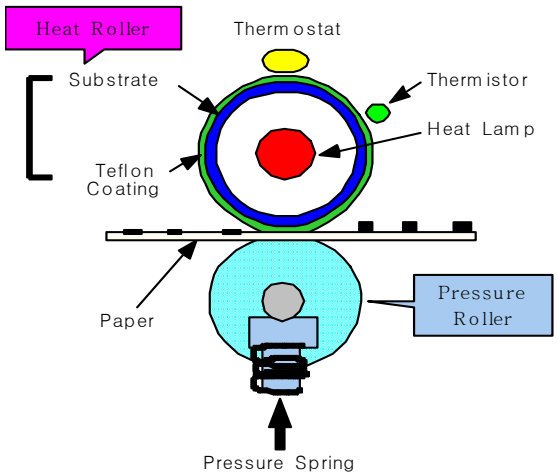


Fig. 1 Conventional fuser with halogen lamp

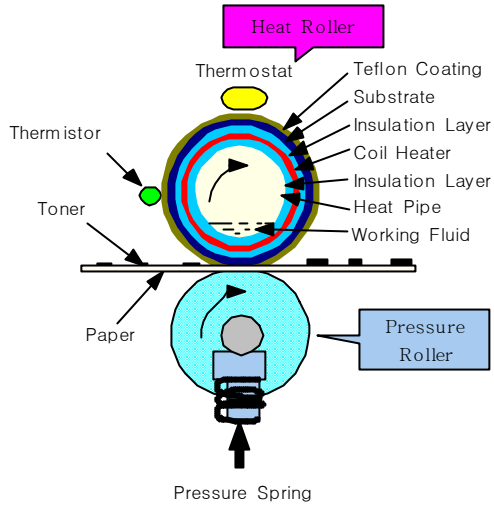


Fig. 2 Instant-on-fuser with heat pipe

2. EXPERIMENTAL AND NUMERICAL STUDY

2.1 Experiment equipment and method

Fig. 3 shows a configuration of equipment for experimenting instant-on-fuser.

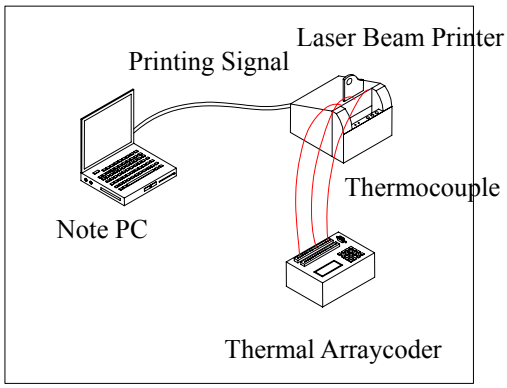


Fig. 3 Experimental schematic

Following devices were used for experiment.
- Printer : 12ppm Mono Laser Printer
- Temperature measure
  : Thermal Array Recorder (Graphtec)
- Data processor : Note PC
- Current measure : WT-2000 / yokogawa
- Flicker measurer: HARMONICS-1000

HPHR was mounted to the fuser frame with thermocouple attached. The surface temperature of fuser was measured and analyzed while LBP was processing printing. Fig. 4 shows the developed HPHR, and attachment of thermocouple to fuser frame for measuring the surface temperature of HPHR.

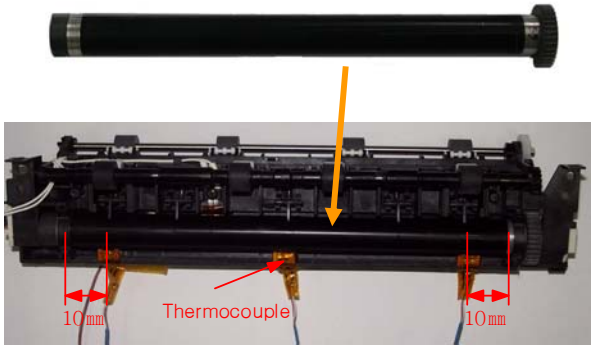


Fig. 4 Fuser frame with heating roller and thermocouple attached

As shown in Fig. 4, the surface temperature of HPHR was measured on the location 10mm away from both ends of fuser teflon coating, and on the center. The time for first paper to exit out of exit sensor after LBP received printing command, i.e., FPOT (First Print Out Time) was measured. The evenness of longitudinal temperature of fuser was measured and analyzed while LBP was printing.

2.2 Numerical analysis

This study carried out a numerical analysis using Fluent Code, so as to predict the thermal transfer mechanism of fuser applying heat pipe. Fig. 5 shows thermal transfer analysis model. Fig. 6 shows prediction of difference between temperature rise over time and surface temperature of fuser. As shown in Fig. 5, calculation area was set to axis symmetry analysis model in order to find radial temperature distribution. The boundary conditions were set to the external conditions of aluminum pipe (h_{air}=20W/㎡K, Tair=20℃) which constitutes the substrate of fuser roller, and heat input (Q=1.1 kW). Initial condition was that calculation for whole area started at normal temperature 20℃. As shown in Fig. 6, it takes about eight 8 seconds from normal temperature to fixing temperature

(≒185℃), meaning that instant-on -fuser can be achieved. Also, deviation in the longitudinal surface temperature of fuser showed evenness within 3℃ because of coil heater winding method and heat pipe. Especially, the fixing roller developed through this study cools down slowly because of heat pipe boasting excellent heat capacity, when printing stops under suspended issue of print commands. (Cooling Rate: 0.7℃/sec)

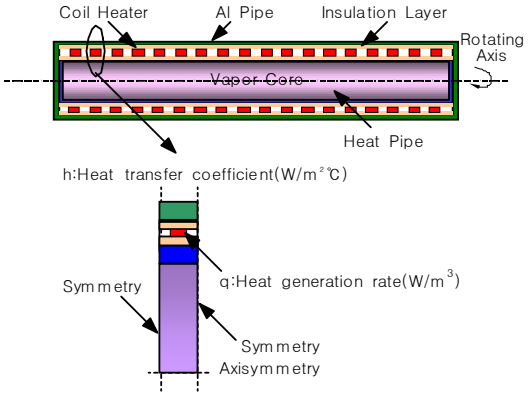


Fig. 5 Thermal transfer analysis model

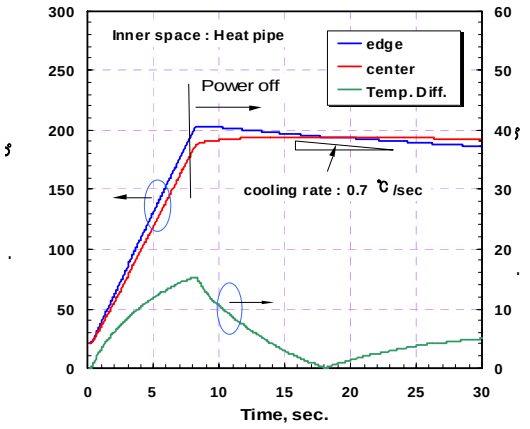
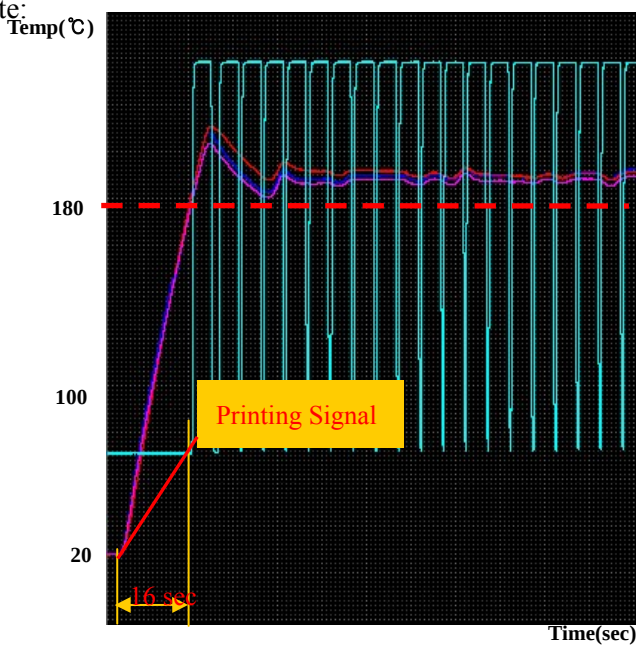


Fig. 6 Temperature rise and deviation in the surface temperature of fixing roller

3. RESULTS AND OBSERVATIONS

3.1 Temperature rise and evenness in the surface temperature of fuser roller

Instant-on-fuser applying heat pipe was mounted to the LBP with 12ppm. The longitudinal surface temperature of fuser roller and rising time from fixing temperature were measured. The measurement results are shown in Fig. 7. Fig. 8 shows current values under changing power, FPOT and relation with rising time. As shown in Fig. 7, HPHR does not supply power to fuser while LBP switch is ON. When printing command is issued, HPHR receives it and performs printing process by reaching from normal temperature to fixing Temperature speedily without warm-up. If printing command is not issued, power is not supplied to fuser. Therefore, power consumption for stand-by is reduced remarkably. In other words, low power consumption is realized.



Power = 1.1 kW(220V)	Rising Time	Rising Rate
25℃ → 135℃	11 sec	↓
25℃ → 145℃	12 sec	↓
25℃ → 185℃	16 sec	10 ℃/sec

Fig. 7 Surface temperature and rising time of instant-on-fuser during printing

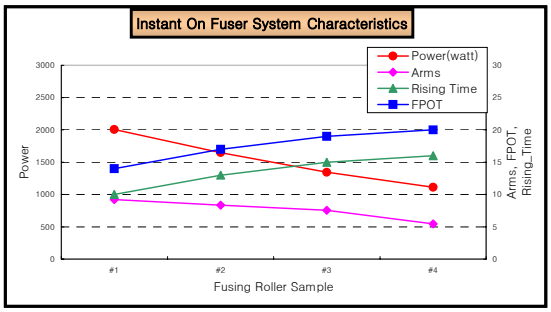


Fig. 8 Performance characteristics of fixing system by power

As shown in Fig. 8, this study measured the rising time from normal temperature to fixing temperature, including FPOT under changing power, and resulted changes in current values. If only rising time is considered, the higher is necessary power value, the FPOT is more excellent. However, printer set, i.e, system exceeds the capacity of power line that is specified in the standards of electric safety. Also,

applying power exceeding a specified level causes flicker. Therefore, this study selected current/power values enabling instant fusing while satisfying maximum power value and flicker both of which are prior problems to be solved in getting certification of safety standards. Based on this, this study mapped S/W and H/W. As results, this study found an optimal condition (1114 W, 5.4 Arms) satisfying the requirements of excellent fixity and FPOT in current printer system (12 ppm). Also, since heat pipe was applied, deviation in the surface temperature of fuser was minimized (within 3℃) and fixing quality in printing achieved remarkable improvement. Because of excellent heat capacity of heat pipe, reprinting speed got speedier and higher fixity was realized.

3.2 Comparison of cooling speed based on fixing method

The graph below compares cooling curves of HPHR and halogen lamp type fuser after power off.

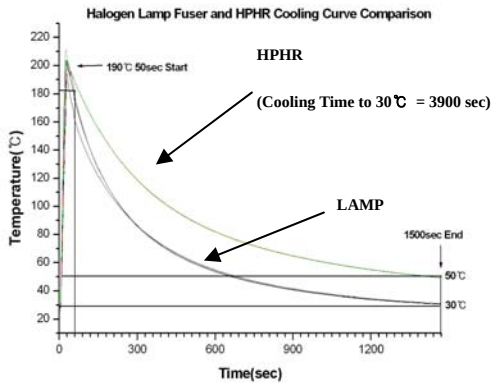


Fig. 9 Comparison of cooling curves based on fixing methods

Fig. 9 shows cooling time (natural non-power cooling) of each fixing method under LBP set status. Set based on instant-on-fuser applying heat pipe cools down to 44℃ during 1,500 seconds. In case of halogen lamp fuser, set cools down to 30℃. This is because of heat pipe's unique heat capacity. It takes about 3,900 seconds to cool down the set based on instant-on-fuser applying heat pipe to the same temperature as the cooling temperature of halogen lamp type fuser based set.

3.3 Comparative view on the power consumption /flicker based on fixing method

Power consumption and flicker value are important criteria for classification LBP, and very important for electric safety standards. Flicker value was calculated by setting current consumption for printing and frequency of power-on as variables. Higher flicker value means that printer consumes higher power than other electronic devices. In reality, when flicker value gets much higher, light may flicker at the time of LBP power-on. It is general to measure power consumption for one hour from the second sheet of paper printout after first sheet of paper printout. Regarding flicker value, current value for ten minutes after printout of second sheet of paper is measured. <Table 1> shows power consumption and flicker value measured by using the set applying respectively halogen lamp type fuser and HPHR type instant-on-fuser.

<Table 1> Comparison of flicker and Power consumption based on fixing method

	Halogen Lamp Fuser	HPHR Fuser
Power consumption	273 W-hr	238 W-hr
Flicker	0.74	0.63

As shown in <Table 1>, power consumed per hour by HPHR type instant-on-fuser is about 40 W lower than halogen lamp type fuser. Flicker value under HPHR type instant-on-fuser is about 15% lower than halogen lamp type fuser. This proves that HPHR type instant-on-fuser has excellent performance of keeping temperature while printing due to its superior heat capacity. Replacing halogen lamp with HPHR will reduce power consumption by about 13 ~ 15% in the long run.

4. CONCLUSION

This study reached following conclusions by developing HPHR type instant-on-fuser system.

(1) When print command is issued, LBP receives print signal and reaches 185℃, which is needed for fixing, from normal temperature within about 16 seconds without warm-up. Then, it could print first sheet of paper within a short time.

(2) The deviation in the longitudinal surface temperature of fuser was minimized within about 3℃ while printing, so as to maximize fixing quality in the direction of paper width.

(3) If LBP is ON or if print command is not issued after printing, power is not supplied to fuser, leading to remarkable reduction of power consumption for stand-by. Therefore, low power consumption is realized.

(4) Since the system has superior ability to keep temperature during printing, the current/power consumed by printing process is reduced by about 15%.

Conclusively, this study realized instant-on-

fuser system satisfying the requirements like low power consumption and temperature evenness.

References

[1] Hitoshi Nagato, Koichi Ishii, Yukio Tsuda, Takahito Kabai, Yuzo Koike, *"省電力定着方式"*, Japan Hardcopy'94, pp.57-60, 1994.
[2] Yasumasa Ohtsuka, Kouichi Okuda, Youji Tomoyuki, Akira Kuroda, *"オンデマンド定着技術の検討"*, Japan Hardcopy'94, pp.61-64, 1994.
[3] Amir Fagri, *"Heat Pipe Science and Technology"*, Taylor & Francis, 1995.
[4] Kim, K. S, Kim, W. T., Song, K. S., LEE, K. B., *"Experimental Study on the Cooling Characteristics of Thermosyphon for the High Power Electric Component"*, The Society of Air Condition and Refrigerating Engineers of Korea, Vol. 10, pp.137-146, 1998.
[5] Koichi Mashiko, Masataka Mochizuki, Yuji Sato, *"Advanced Cooling System Combined with Heat Sink and Heat Pipe for Cooling PC",* 11th IHPC, Vol. 2, pp.75-79, 1999.
[6] Mochizuki, M., Mashiko, K., Nguyen, T., Saito, Y., Goto, K. *"Cooling CPU Using Hinge Heat Pipe",* Heat Pipe Technology, Pergamon, pp.218-229, 1997.
[7] Kim, K. S., Moon, S. H. and Choi, C. G., *"Cooling Characteristics of Miniature Heat Pipes with Woven-Wired Wick*", 11th Int. Heat Pipe Conf., Tokyo, Japan, Vol. 1, pp.20-25, 1999.
[8] Kim, K. S., Won, M. H., Baek, B. J., *"Numerical Study Study of Surface Temperatrue Uniformity on the Electrically Induced Heating Roll"*, 15th Energy Saving Tech. Workshop, pp.375-385, 2000.

Overview Latest Technologies Using Heat Pipe and Vapor Chamber for Cooling of High Heat Generation Notebook Computer

Masataka Mochizuki, Thang Nguyen, Koichi Mashiko, Yuji Saito, Tien Nguyen,
Xiao Ping Wu, and Vijit Wuttijumnong

Fujikura Ltd.
1-5-1, Kiba, Koto-Ku,
Tokyo 135, Japan
Tel. 81-3-5606-1174
Fax. 81-3-5606-1514
Email: mmotizuk@fujikura.co.jp

Abstract

The trend of the processor performance and heat dissipation increased significant every year. In the year 2000, the clock speed of processor used in notebook is marginal 1GHz and heat dissipation marginal 20 W, but in the current year 2003 the processor's clock speed is higher than 2 GHz and heat dissipation higher than 50 W and approaching 100 W by year 2004. Heat dissipation increased but in contrary the size of the processor reduced and thus the heat flux is critically high. The heat flux is about 10-15 W/cm^2 in the year 2000 and could reach over 100 W/cm^2 by year 2004. The purpose of this paper is to provide overview of various cooling solutions using heat pipe and vapor chamber for cooling high power processors in a confined space of the notebook.

Key words : Heat pipe, vapor chamber, heat spreader, remote heat exchanger, heat sink, heat transfer.

1. INTRODUCTION

Higher performance processor will have larger heat generation. This creates a challenge in providing thermal solution in a confined space in the notebook since high performance processor and additional features such as more Cache, more DRAM, larger HDD, PCMCIA, CD/DVD ROM and the like take up spaces and higher total power dissipation in notebook. It is a challenge to provide the thermal solution without compromising the notebook's size and weight.

The processor's die surface where most heat generated is usually small approximates 10 mm x 10 mm. For effective cooling the heat must spread to a larger surface area and away from the processor, as there are usually restricted space available in the vicinity of the processor. Heat must be transferred to a remote location where there is space available for cooling, for example in the corners or on the sides of the notebook. The best known device for effective heat transfer with lowest thermal resistance is heat pipe and vapor chamber. Basically, heat pipe and vapor chamber is a 2-phase heat transfer device. It is an evacuated and sealed container in which contains a small quantity of working fluid. One end of the container is heated, causing the liquid to vaporize and the vapor to move to the cold end and condensed. Since the latent heat of evaporation is large, considerate quantities of heat can be transported with a very small temperature difference from end to end. Thus it is a device of very high thermal conductance. Its equivalent thermal conductivity can be several hundred times than that of a solid copper of the same dimensions. Heat pipe and vapor chamber emerged as the most appropriate technology and cost effective thermal solution due to its excellent heat transfer capability, high efficiency and its structure simplicity. It has many advantages compared to other cooling devices such as fans, thermo-electric module, liquid pump loop device are that it has simple structures, no moving parts and does not use electricity. Selection of the working fluid is based on the operating temperature of the application. In computer application, the operating temperatures are normally between 50 -

100 °C. At this temperature range water is the best working fluid. In this paper, we will review various latest technologies of using heat pipes and vapor chambers for cooling of high performance notebook computer.

2. COOLING SOLUTIONS

A basic formulation to calculate the thermal resistance required for the cooling solution as follows :

Rja = Rjc + Rca = (Tj-Ta-Tsys)/Q

Where,

Q = Heat dissipation [W]

Rja = Thermal resistance from the CPU die to ambient [°C/W].

Rjc = Thermal resistance from the CPU die to CPU case surface [°C/W].

Rca = Thermal resistance from CPU case surface to ambient [°C/W].

Ta = Ambient temperature [°C].

Tj = Junction temperature inside die [°C].

Tsys = Temperature rise of the system inside of notebook [°C].

The Rjc is approximate 0.33 °C/W and is predetermined by the chip manufacturers. The thermal solution provider can control only the Rca. This thermal resistance consisted of thermal interface material and the cooling solution. Fig.1 showed the required thermal resistance Rjc and Rca vs. heat dissipation, assuming the maximum CPU's junction temperature of 100 °C, an outside ambient of 35 °C and system temperature rise of 10 °C,

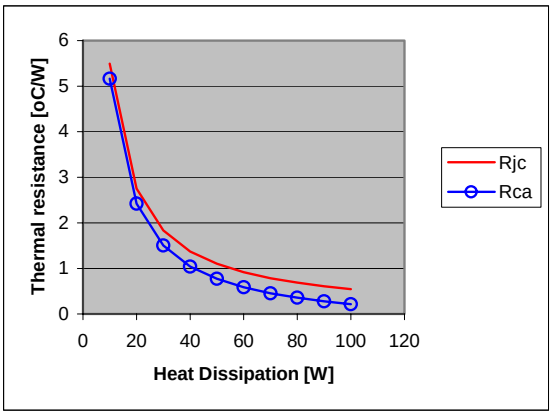
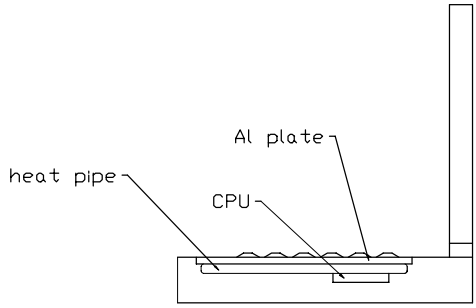


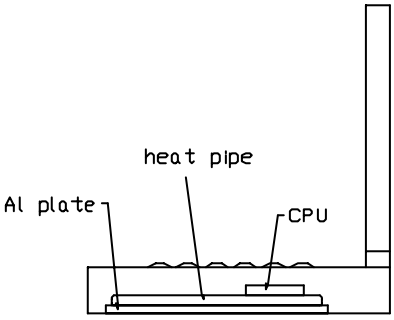
Fig.1 – Rjc and Rca vs. Heat input

(1) Example 1 - Heat pipe with spreader plate

In the previous couple of years the heat dissipation from the processor was less than 10W. The common method of cooling was using heat pipe to transfer heat from the processor to a heat spreader plate, usually made of aluminum, under the keyboard or on the chassis of the notebook as shown in Fig. 2 (a) and (b), respectively.



2(a) Heat Spreader Plate Under Keyboard



2(b) Heat Spreader Plate On Chassis

An example of this system consisted of a rectangular heat spreader plate made of aluminum, placed on the chassis of the notebook. The dimensions of the plate are approximately 0.6 mm thick, length 190 mm and width 100 mm. The heat pipe was a 3 mm round that was pressed into elliptic cross section of dimensions approximately 2 mm x 3.6 mm x 200 mm (height x width x length) to accommodate for the height constraint in the notebook. Heat pipe was mechanically attached to the heat spreader plate by used of rivets. The heating and cooling sections of the heat pipe is approximately 30 mm and 170 mm respectively. Test results of this system is shown in fig.8. The Rca is about 8 °C/W. If based on the constraints of Tj =100 °C; Ta = 35 °C and Tsys = 10 °C, then this system can dissipated 7W.

(2) Example 2 - Hinged heat pipe system

For the hinged heat pipe system, the heat from the processor is transferred onto the aluminum heat spreader plate located at the back screen of the display as shown in fig. 3. Basically this system consisted of 2 off 4mm heat pipes and a copper made hinge connector of size approx. length 25 mm, width 7mm and height 17mm. The primary heat pipe is fixed to a heating block that contact to the heat source, transferring heat to the secondary heat pipe via a hinge connector that

joined the two heat pipes together. The second heat pipe is used to transfer heat onto the aluminum heat spreader plate which size approx. 170 x 250x 0.4 mm. The purpose of the connector is to enabling heat transfer from first to second heat pipe and to allow the second heat pipe to rotate when opening and closing notebook's lid. The results is shown in fig.8. Rca achieved about 5 ^{o}C/W. Using the same constraints as described in above this system can dissipated 11 W.

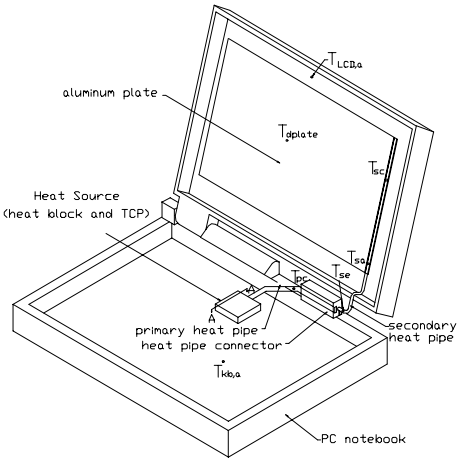


Fig.3 – Hinged heat pipe system

(3) Example 3 – Hybrid system

The hybrid system consisted of heat pipes, diecast plate, fins and fans as shown in fig. 4. The 3 heat pipes used to spread heat on the aluminum die cast plate. Aluminum fins attached to the heat pipe and radial fans were used to blow air directly through fins. As shown in fig.8. The Rca of this system was about 1.8 ^{o}C/W, capable to dissipate 30W.

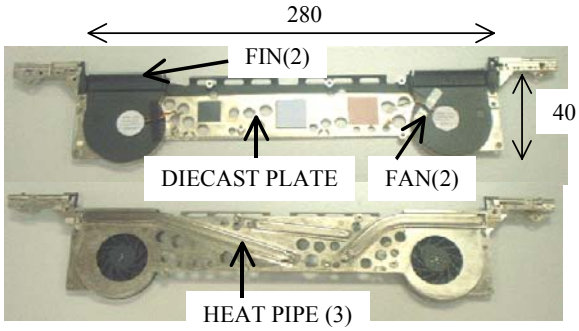


Fig.4 – Hybrid system

(4) Example 4 – Remote Heat exchanger (RHE)

Basically the remote heat exchanger consisted of heat pipe, fin and fan as shown in fig. 5(a) and 5(b). Prototype in fig. 5(a) has 1 heat pipe and 1fin heat exchanger, whereas prototype in fig. 5(b) has 2 heat pipes and 2 fin heat exchanger. The fans in both cases are similar in size (approx. 45mm x 10mm) and in performance, approx. air flow 0.15 m^3/min at 0 Pa and 90 Pa at 0 m^3/min. The Rca approx. 1.4 and 1.1 ^{o}C/W respectively as shown in fig. 8.
This corresponding to heat dissipation of 40W and 50W respectively.

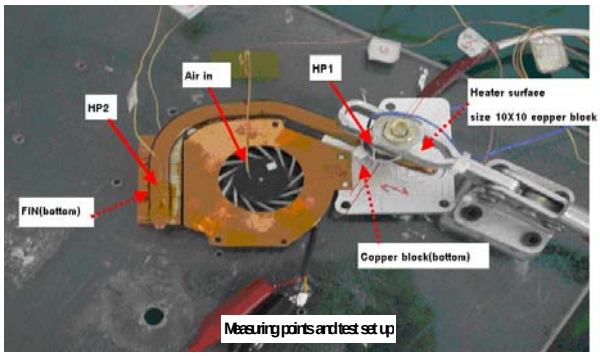


Fig. 5(a) – RHE type 1

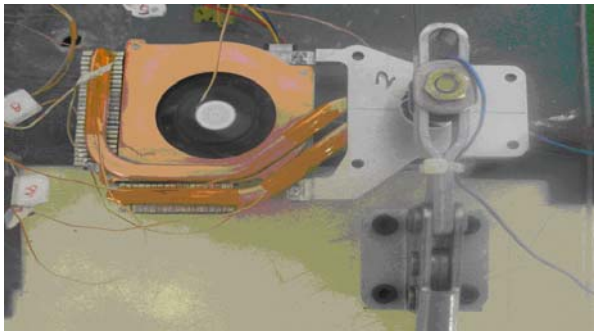


Fig. 5(b) – RHE type 2

(5) Example 5 – Vapor chamber solution

The principle of operation of vapor chamber is similar to heat pipe which is a 2-phase heat transfer device. Heat pipe is made from round pipe and after can be bent and flatten to required shape. Vapor chamber body is made from stamping or cold forging or machining so the shape is fixed and so can not be bent or flatten. Examples given in fig. 6 shows photos of various vapor chamber shapes and sizes.

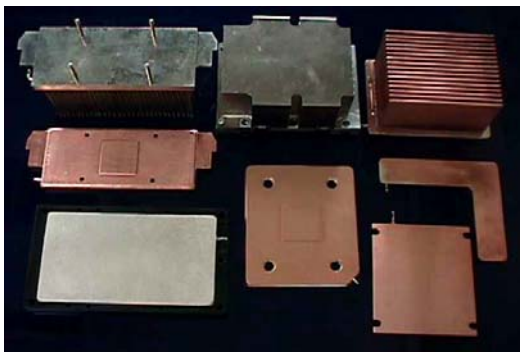


Fig.6 – Photos of vapor chambers

An example of vapor chamber solution is shown in fig. 7. The Rca of this system is about 0.6 ^{o}C/W as shown in fig. 8. As have mentioned if the constraints Tj =100 ^{o}C; Ta = 35 ^{o}C and Tsys = 10 ^{o}C, then this system can dissipated more than 90W.

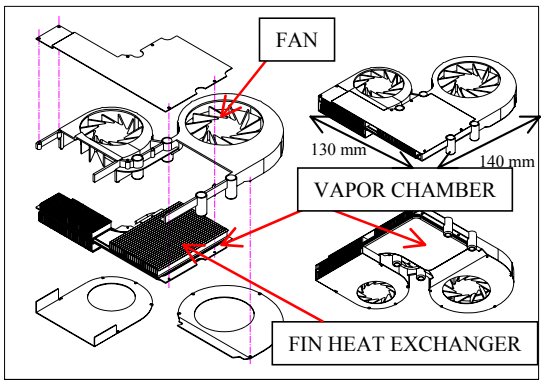


Fig.7 – Vapor chamber solution

Vapor chamber performance is more superior than heat pipe. The advantages of vapor chamber solution compared to heat pipe solution are as follows :

- Heat flow 2-dimensional compared to 1 dimensional flow as in heat pipe. This gives vapor chamber higher heat transfer and lower thermal resistance.
- Higher heat flux capability.
- Vapor chamber body has uniform temperature distribution, large body surface area so excellent for heat dissipation.
- Vapor chamber can be directly contact with CPU, eliminating conducting and contacting resistance of the "heat block" which heat pipe attached to.
- Fins can be attached direct to vapor chamber, having higher surface of contact so thus can reduce contact resistance and increase fin efficiency.

A summary of the Rca and heat dissipation capability for various thermal solution is shown in table 1.

3. CONCLUSION

As the processor's die surface where most heat generated is usually small, and heat dissipation is large required large space for cooling. The most effective way to spread the heat at minimal temperature gradient are to use heat pipe or vapor chamber. They help to reduce spreading resistance and thus improve overall performance of the cooling system. At the high heat dissipation and high heat flux vapor chamber is more suitable for superior performance.

References

[1] T. Nguyen, M. Mochizuki, K. Mashiko, Y. Saito and I. Sauciuc, "*Advance Cooling System Using Miniature Heat Pipes In Mobile PC*", Itherm '98, May 27-30, Seattle, WA, USA.

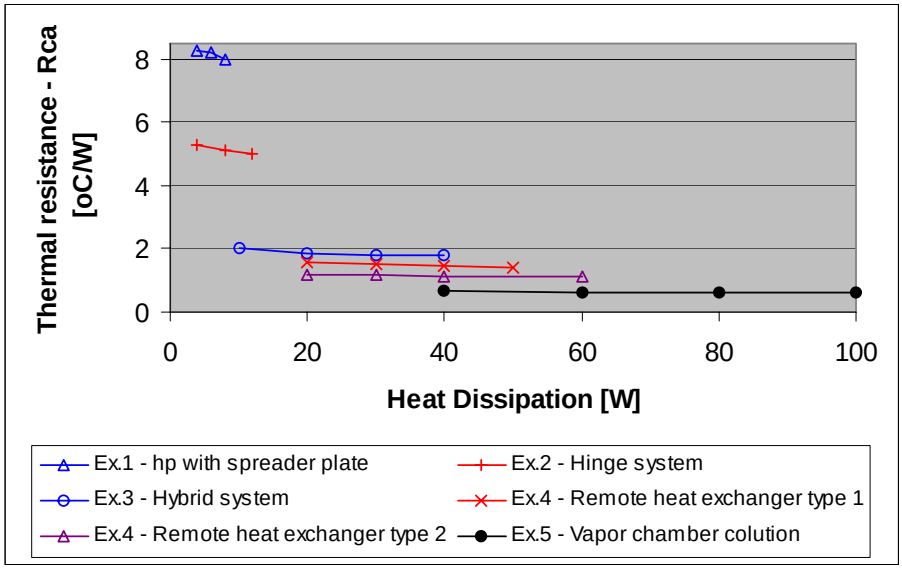


Fig. 8 – Thermal resistance Rca vs. heat input for various thermal solution

Table 1- Summary of thermal solution

No.	Solution	Rca [oC/W]	Q [W]
1	Heat pipe with speader plate	8	7
2	Hinged heat pipe	5	11
3	Hybrid	1.8	30
4a	Remote heat exchanger type 1	1.4	40
4b	Remote heat exchanger type 2	1.1	50
5	Vapor chamber	0.6	100

The Experimental Study on the Improvement of Enthalpy Effectiveness of HPHE with Water Spray on Condenser Section

Jin-Kwan Hong* ,Sang-Gon Choi**, Kwun-Ok Yang*** , Yun-Sik Byun***
*Department of Building Equipment & System Eng., Kyungwon Univ.,Sungnam City 461-701, Korea
**Department of Building Equipment & System Eng., Graduate school of Kyungwon Univ.
***Yupoong Co. Ltd, Pyungtaek City 459-040, Korea

Abstract

Experimental study for performance improvement of heat pipe heat exchanger(HPHE) was carried out. The Performance test was conducted by varying tilt angle, air velocity, fin type and number of rows in the case of with and without water spray in condenser section of HPHE.

Experimental results show that the enthalpy effectiveness of HPHE in the case of water spray is increased with maximum 20% comparing with the case of without water spray in condenser section. The experimental results will be useful in a variety of applications, especially in design and manufacturing of a high-effectiveness energy recovery systems, as alternatives of rotor type heat exchangers, which have cross contamination problem in Building Air Conditioning,

Key words: Enthalpy effectiveness, Water spray, Heat Pipe Heat Exchanger, Integral fin, Aero fin

1. INTRODUCTION

For improvement of indoor air quality (IAQ) in the building air conditioning system, it is common that air conditioning system supplies fresh outdoor air whose volume is equivalent to 20~30% of its total air volume for the inside of the building and simultaneously exhausts inside air to the outdoor as much as air volume supplied. As a matter of fact, outdoor air load forms significant portions of the cooling and heating loads in living space because it is necessary that fresh outdoor air should be supplied so as to improve IAQ. It seems that the energy saving effect will be economically considerable if Heat Recovery Technology is adopted to reduce outdoor air load in the system.

The purpose of this study is to fabricate Heat-Pipe Heat Exchanger (HPHE) to which the Heat Pipe[1] designed to be suitable to low temperature range was applied and install it on the Air Handling Unit for waste heat recovery so as to reduce outdoor air load resulting from the intake of fresh outdoor air in both summer and winter.

Especially in summer conditions, this study attempted to maximize the heat recovery effect in evaporation section by carrying out water spray on condenser section. So, we also tried to measure enthalpy effectiveness with installing HPHE on the experimental Air Handling Unit (AHU) and investigate the changes in enthalpy effectiveness with water spray on condenser section. Also, we investigate the changes in temperature effectiveness without water spray on condenser section in winter. Temperature and enthalpy effectiveness are defined by following equations as heat recovery performance parameter.

$$\eta_t = \frac{t_{fa} - t_{oa}}{t_{ra} - t_{oa}} \ldots\ldots (1)$$

$$\eta_h = \frac{h_{oa} - h_{fa}}{h_{oa} - h_{ra}} \ldots\ldots (2)$$

Where, t_{fa} : Fresh Air Temperature,
t_{oa} : Out door Air Temperature,
t_{ra} : Return Air Temperature ,
h_{fa} : Fresh Air Enthalpy,
h_{oa} : Out door Air Enthalpy,
h_{ra} : Return Air Enthalpy

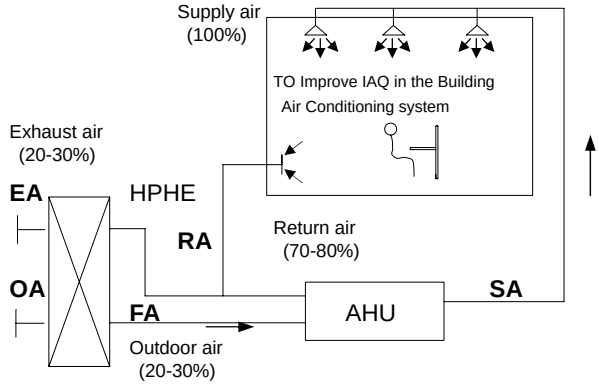


Fig 1. Heat recovery system in the building air conditioning system

2. EXPERIMENTAL APPARATUS & PROCEDURE

2.1 Experimental Apparatus

Experimental apparatus used in this study

includes AHU that controls both temperature and relative humidity of air, data acquisition system that transmits data on temperature and relative humidity by measuring point into computer, HPHE , and water spray system that sprays water on HPHE.

Table 1 Specifications of AHU for Experiment

	Specification
Size	4300W×1450H×1350T
Fan	Max. flowrate : 125CMM 2HP, #3DS
Cooling capacity	25,000 kcal/h
Heating capacity	30kW (Electric heater)

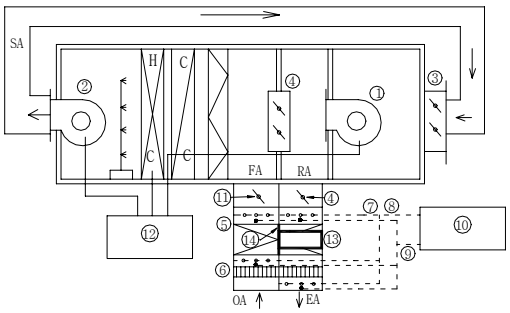
2.1.1 AHU for Experiment

Fig. 2 shows components of experimental apparatus. AHU can precisely control the air volume and velocity through the attached inverters to both air-supply and air-exhaust fan, and has electric heating and cooling coil to control temperature and relative humidity.

2.1.2 The Manufacturing of HPHE

We manufactured HPHE with adopting heat pipe that fin is attached to the outside of heat pipe so as to improve its heat transfer performance.

Fig.3 presents cross sections of heat pipe used in manufacturing HPHE.[1]. We set the dimensions of heat pipe and the inflow of working fluid[2] as same conditions under which water spray experiment on single heat pipe was previously carried out[3]. Manufactured heat pipe has a total length of 1,080mm. Fin is attached to the point of 1,000mm to make the length of heat transfer section amount to 1,000mm. Sections of 40mm from both extremes of heat pipe are used as assembly parts into which the case of heat exchanger is inserted.



①Return Air Fan
②Supply Air Fan
③Return Air Damper
④Exhaust Air damper
⑤HPHE
⑥Honey Comb
⑦~⑨ Thermocouple
⑩ Data Acquisition System
⑪ Out Air Damper
⑫ Control Panel
⑬ Water Spray System

Fig.2 Schematic diagram of experimental apparatus

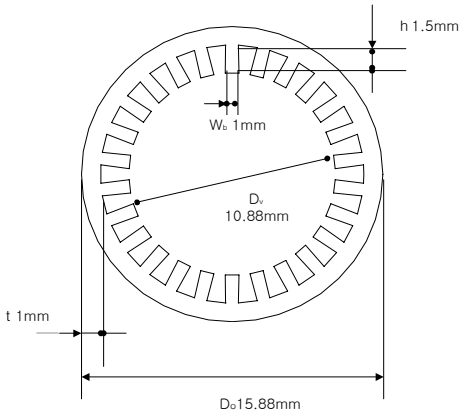
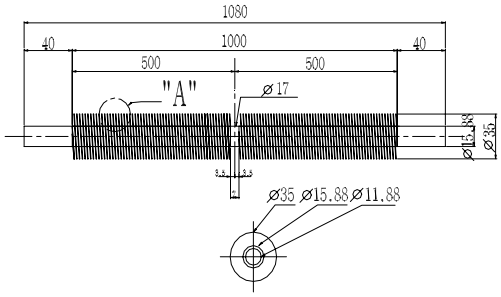
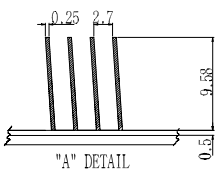


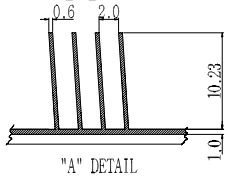
Fig.3 Cross sections of heat pipe



a) Schematic dimensions heat pipe



b) Cross section of Aero fin



c) Cross section of Integral fin

Fig. 4 Schematic drawing of heat pipe

Fig.4 includes drawings showing the outside and cross-section of the heat pipe attached to HPHE. Manufactured HPHEs have two types: "general type" that aero fin is attached to the outside of heat pipe. "Integral type" that the extruded fin is manufactured as a single body with heat pipe. Two types of HPHE were used in performance experiments in summer and winter. Table 2 presented below shows dimension of each type of heat exchanger used in heat transfer performance tests, which includes 1-, 2-, 3-, and 4-row heat exchanger of general type that aero fin is attached to heat pipe and 6-row heat exchanger of integral type in which heat pipe is manufactured as a single body with the fin.

Considering the constraints, we carried out experiments from 1- to 10-row heat exchanger of general type through combination of 1-, 2- and 4-row, and only a 6-rows heat exchanger of integral fin type.

Table 2 Specifications of HPHE

Rows		Specification
HPHE (General type attached aero fin)	1	1180W×510H×125T
	2	1180W×510H×165T
	3	1180W×510H×200T
	4	1180W×510H×245T
	5	1180W×510H×370T
	6	1180W×510H×410T
	7	1180W×510H×445T
	8	1180W×510H×570T
	9	1180W×510H×610T
	10	1180W×510H×735T
HPHE (6 rows) (Integral type attached integral fin)		1180W×510H×315T

Water spray system installed on condenser section of HPHE is made up of water tank for water spray (shown in Fig. 5) and water supply apparatus (shown in Fig. 6). In water tank for water spray, 8mm acryl board is used as its floor plate and side plates are made of 5mm acryl boards. It is designed to make one side leaning downward higher lest the water spill over even when the tilt angle of water tank reaches to 5°deg . It is also designed to maintain constant water spray volume, that is to say, 1 lpm per 1 row, by arranging total 18 holes that has a size of 1.3 mm in a row at intervals of 23mm. To spray water with precise volume, water levels are marked on the side of water tank so that water could keep constant levels. 1-, 2-, 3-, and 4-row water tank were respectively manufactured in accordance with the rows of HPHE, and then installed on the upper side of the condenser section of HPHE.

In addition, 6-row water tank was specially manufactured for water spray on the 6-row HPHE of integral type. Water distribution apparatus as shown in Fig. 6 is installed on each water tank.

To distribute constant water volume, flow control valve was equipped on each distribution pipe. To keep in as constant level as possible the pressure within the pipe while water flows from supply pipe to distribution branch pipe, vent pipe is installed on the upper side of water supply head.

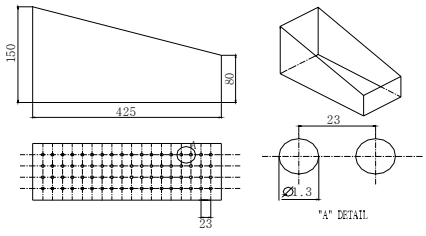


Fig. 5 Detailed drawing of water spray tank

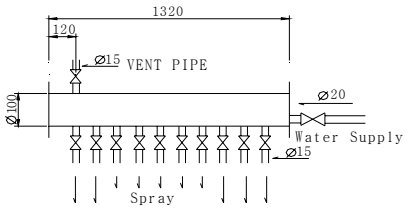


Fig. 6 Water spray piping system

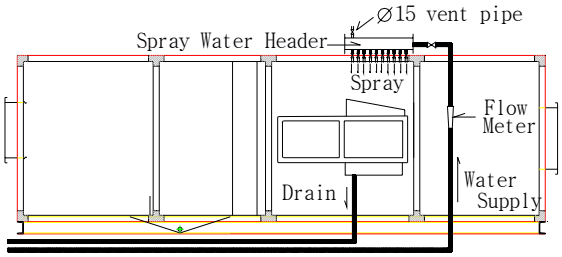


Fig. 7 Schematic diagram of water spray system

2.2 Experimental Method & Test

2.2.1 Winter test

Winter experiment was carried out in the period from December to January to meet the condition of intense cold, and we made the outdoor air at that period supplied for the AHU for experiment. Experiment was carried out from 8 pm to 4 am when actual temperature of outdoor decreased relatively low and All Air System was adopted as an air conditioning method in this experiment.

For general type HPHE, performance tests ranging from 1- to 10-row were accomplished, and each result by row was measured during the 30-minute experiment after 30-minute stabilizing period elapsed. Performance test on each row of HPHE was carried out under the same condition (i.e. 5° deg of tilt angle) that water spray characteristics experiment[3] on single heat pipe was and horizontal condition of 0° deg of tilt angle. Indoor temperature condition was set on the basis of single default one of 20°C(temperature) and 50%(relative humidity) and heat transfer was made brought about through AHU under the state that the outlet conditions of air exhaust side of heat exchanger was kept stable.

In winter, test were carried out under the general condition without water spray because the condenser section of heat exchanger applied heat to the supplied outdoor air. In this case, performance was tested on the basis of temperature effectiveness because only was sensible heat transfer occurred.

To test performance of heat exchangers, we carried out a series of tests with changing air velocity within AHU into 1m/s, 1.5m/s, 2m/s, 2.5m/s, and 3m/s in order. Inverters were installed on both extremes of air-supply and air-exhaust fan

so as to control air velocity. To measure air velocity, 16 measuring points were selected, all points located within the cross section of duct at the point of 150mm from the downstream of honeycomb in air-supply inlet and air-exhaust outlet. We calculated the air volume in duct through face air velocity calculated by averaging air velocity measured at each point.

We selected three measuring points on both front and rear sides of HPHE installed on both air-supply inlet and air-exhaust outlet, and thus measured temperature at total 12 points with installing T-type thermocouple diagonally on rectangular duct. Averaged measurement value at each point was used as reference temperature.

Measuring relative humidity was carried out with GHD-30(R.T). Before it was installed on each measuring point, we adjusted it to measure relative humidity within the error range of 3%RH under the same humidity condition that was measured by Assmann psychrometer.

2.2.2 Summer test

In summer, test were carried out with directly supplying outdoor air for AHU from 1 pm to 4 pm during the August. In summer, performance test was accomplished under the condition that water sprayed on the condenser section of HPHE. Considering domestic weather condition having a rainy season, we carried out under the raining condition with or without spraying water on the condenser section of HPHE. Other conditions such as rows of heat exchanger, tilt angle, and indoor temperature were set as same under which winter tests were carried out.

In summer conditions, we adopted enthalpy effectiveness as a standard for performance test because the relative humidity of air passing through HPHE was varied with water spray in summer conditions other than in winter conditions. To do this, we installed total 4 humidity sensors on both inlet and outlet of heat exchangers located in air-supply and air-exhaust duct.

Measuring points for temperature was selected at the same points as in winter conditions, and enthalpy was calculated by averaging temperature measured at each point by temperature sensor and by using relative humidity measured by humidity sensor.

3. EXPERIMENTAL RESULTS & DISCUSSIONS

We tested the performance of heat exchangers with changing the row of HPHE, tilt angle, and air velocity in summer and winter conditions.

Fig. 8 presents the temperature effectiveness calculated by row of heat exchanger under the winter condition that tilt angle of general HPHE is set as 0° deg and air velocity passing through it changes.

Fig. 8 shows that temperature effectiveness as a whole decreases in winter as air velocity passing through heat exchanger increases. In 10-row heat exchanger, temperature effectiveness is shown as 73%, its highest point, at 1m/s of air velocity, and then decreases by 12% into 61% at 3m/s. It shows that temperature effectiveness as a whole decreases by 5~7% every time the air velocity passing through heat exchanger increases by 1m/s.

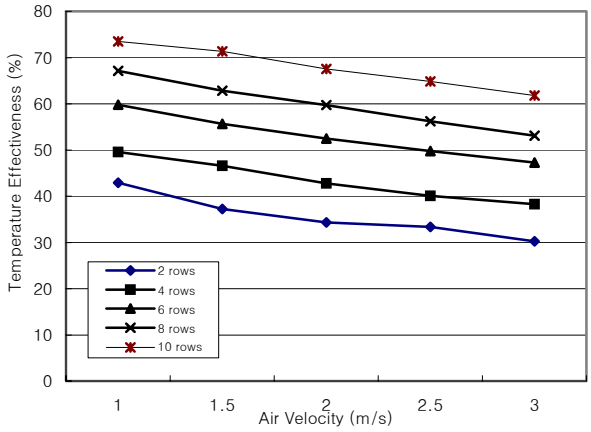


Fig. 8 Effectiveness w.r.t air velocity for values of rows at 0°deg tilt angle in winter

It is presumed to result from that fact that when the air velocity passing through heat exchanger increases, by-pass factors increase because the exposed time of the surface of fin installed on the heat pipe of heat exchanger to the air passing through it decreases.

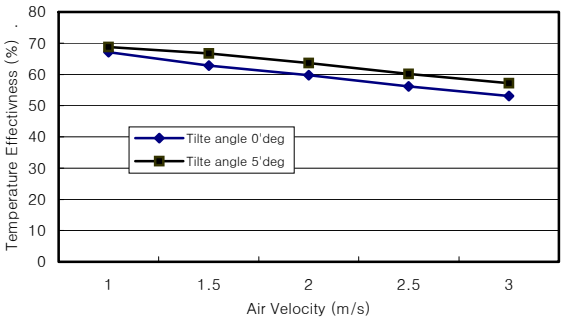


Fig. 9 Effectiveness w.r.t air velocity for values of tilt angle in winter

In Fig. 9, we can see that performance of heat exchanger is improved up to by 5% under the winter conditions that tilt angle of general 8-row HPHE is set as 5° deg and air velocity passing

through it is changed compared to the tilt angle of 0° deg. As mentioned earlier, it is thought to result from the fact that the performance of general HPHE is improved because the returning of working fluid to evaporator section of single heat pipe is carried out in a more smooth way in 5° deg of tilt angle than in 0° deg. It also shows that keeping its tilt angle at 5° deg helps to improve performance of heat exchanger when we apply HPHE to winter conditions[1].

Fig. 10 presents the enthalpy effectiveness calculated by row of heat exchanger under the summer conditions that tilt angle of general HPHE is set as 5° deg and air velocity passing through it changes while water spray is carried out on condenser section. As shown in Fig 10, enthalpy effectiveness in summer conditions presents different tendency from in winter ones.

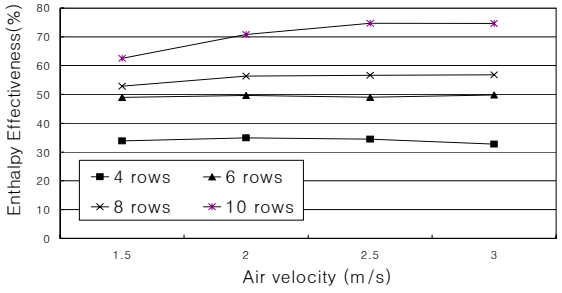


Fig. 10 Effectiveness w.r.t air velocity for values of rows at 5°dig tilt angle in summer

We can see that enthalpy effectiveness is much more increased in 2.5～3m/s than in 1.5m/s in case of over 6-row heat exchangers. It is assumed to result from the fact that much more heat can be eliminated from the installed condenser section because water evaporation in condenser section increases through water spray on condenser section as air velocity increases. In 6- and 8-row heat exchanger, it is shown that the increase of enthalpy effectiveness is successively diminished as air velocity begins to increase from 2m/s. In 10-row heat exchanger, it starts to be successively diminished around 75% level successively as air velocity starts to increase from 2.5m/s. It demonstrates that improvement of its performance through the increase of water evaporation by changing rows of heat exchanger has some limitations. We can validate this result from the fact that enthalpy effectiveness increases up to at 2.5m/s of air velocity and begins to decrease at 3m/s in 4-row heat exchanger. This result also enables us to foresee that when we continue to increase air velocity, the more air velocity increases, the more effectiveness decreases as shown in winter conditions.

Fig. 11 presents enthalpy effectiveness by row of heat exchanger under the summer condition that tilt angle of general HPHE is set as 0° deg and air velocity passing through it changes while water spray is carried out on condenser section. Different from in 0° deg of tilt angle, it is shown that effectiveness increases in a relatively stable, linear way as air velocity changes in 8- and 10-row heat exchanger.

In case of 10-row heat exchanger is installed with 0° deg of tilt angle, its enthalpy effectiveness amounts to it highest point at 69%. In this case, working fluid returning from condenser section more decreases than in 5° deg of tilt angle because tilt angle has an influence on single heat pipe within heat exchanger. It relatively reduces the exhausted heat resulting from water evaporation due to water spray on condenser section.

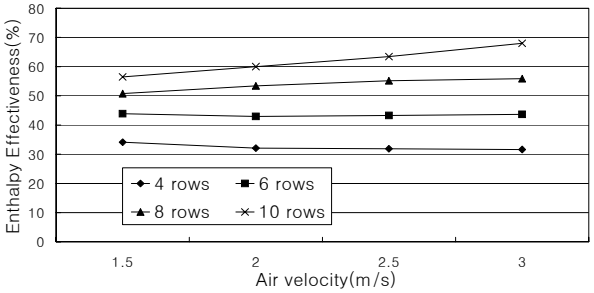


Fig.11 Effectiveness w.r.t air velocity for values of rows at 0°deg tilt angle in summer

But continual increase of enthalpy effectiveness in condenser section is due to increase of velocity that is helpful to spray water evaporation in condenser section. Thus, the increase of enthalpy effectiveness in a linear form is thought to be a phenomenon, which can be observed in a transient stage.

Fig. 12 presents enthalpy effectivenesses in general 6-row heat exchanger calculated by changes in air velocity passing through it under the wet (i.e. outdoor air is in the state of raining) and normal conditions with or without water spray.

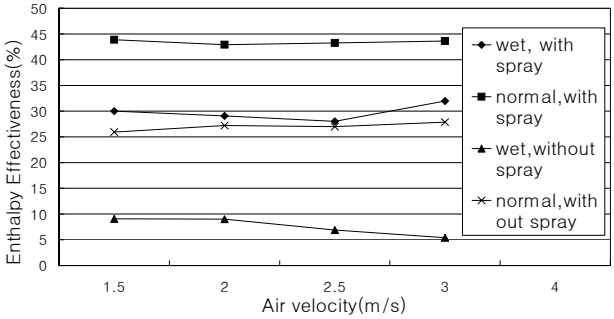


Fig. 12 Effectiveness w.r.t air velocity for values of condition at 0°deg tilt angle

in summer(6 rows)

In Fig 12, we can see the influences which water spray has on performance improvement of heat exchanger. In normal conditions, enthalpy effectiveness with water spray is higher than without it by 16~19%. In wet conditions, the former is also higher than the latter by 20～25%. Thus, we can see that, irrespective of outdoor air conditions, water spray can improve the performance of HPHE. This result corresponds to that of performance test carried out on single heat pipe under the condition of water spray on its condenser section.[3][4]

Fig. 13 shows enthalpy effectiveness by case and includes 4 cases: case A is under the condition that tilt angle of 6-row integral type HPHE is set as 0° deg without water spray on the condenser section of heat pipe; case B is under the condition that tilt angle of 6-row integral type HPHE is set as 0° deg with water spray; case C is under the condition that tilt angle of 6-row general type HPHE is set as 0° deg without water spray; and case D is under the condition that tilt angle of 6-row general type HPHE is set as 0° deg with water spray. It shows that performance of heat exchanger is more improved with water spray than without it, irrespective of the types of HPHE (general or integral).

Fig. 14 presents enthalpy effectiveness by case and includes 2 cases: case A is under the condition that tilt angle of 6-row integral type HPHE is set as 5° deg without water spray on the condenser section of heat pipe; and case B is under the condition that tilt angle of 6-row integral type HPHE is set as 5° deg with water spray. Also in integral type HPHE to which integral fin is attached, water spray improves its performance as in general type one to which aero fin is attached. In integral type, enthalpy effectiveness increases by 9%~19% because of the evaporative cooling in condenser section due to water spray.

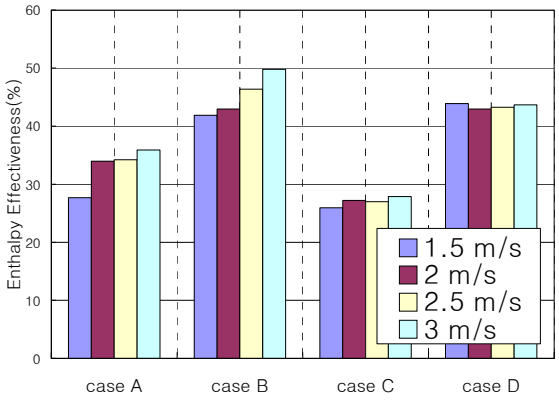


Fig. 13 Effectiveness w.r.t air velocity for values of condition at 0°deg tilt angle in summer (6 rows)

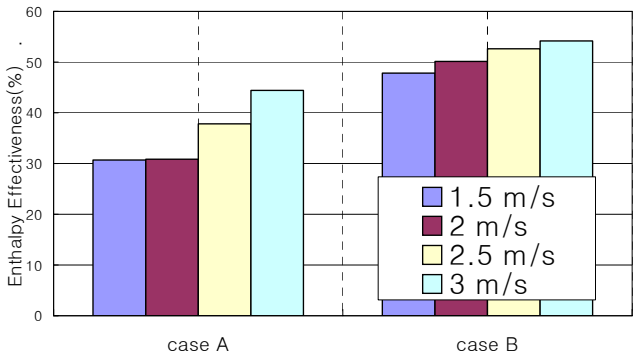


Fig. 14 Effectiveness w.r.t air velocity for values of condition at 5°deg tilt angle in summer (6 rows)

Fig 12 also presents such test result as shows relatively higher enthalpy effectiveness with water spray than without it. It suggests that the performance of HPHE can be improved through water spray, irrespective of kinds of the attached fins to the outdoor of single heat pipe.

4. CONCLUSIONS

In this study, the performance test under the summer conditions was carried out on 6-row HPHE with 0° deg and 5° deg of its tilt angles (i.e. its evaporation section has a tilt to downward from the horizontal line by 0° deg and 5° deg), and under the winter conditions, performance test by row was carried out on general type HPHE whose rows ranging from 1 to 10 with 0° deg and 5° deg of their tilt angles. The conclusions in this study can be summed up as follows:

1. The temperature effectiveness of HPHE amounts to its highest point at 73% in winter conditions, while its enthalpy effectiveness amounts to its peak point at 75% in summer conditions. This result shows superior performance of HPHE.
2. The effectiveness of HPHE is shown higher in maintaining its tilt angle at around 5° deg than at 0° deg, irrespective of the kinds of attached fins to it and whether or not water spray is carried out.
3. In summer conditions, it is shown that the heat transfer performance of HPHE can be improved through water spray because of evaporative cooling effect in condenser section of heat pipe, under both wet (i.e. raining) and normal (i.e. fine) conditions.
4. According to the test result on single heat pipe to which integral fin is attached, it is shown that, in case of 6-row HPHE, integral type is superior to general one in improving performance,

because it can reduce the contact resistance against fin and it can increase effectiveness by 6% as well.

5. According to above conclusions, installing an HPHE with having a tilt angle by 5° deg and applying integral type to it in both summer and winter conditions help to improve its heat recovery performance. Especially in summer conditions, water spray on condenser section can remarkably improve the performance of HPHE up to by 20%. We expect that these results can be applied to design of heat exchanger.

Acknowledgements

The authors wishes to acknowledge the financial support of the Korea Small and Medium Business Administration made in the technology innovation program year of 1999

Reference

1) J. K. Hong, S. G. Choi, D. S. Kim, W. B. Chung, Y. S. Bun, K. O. Yang, 2001, "The Experimental Study on the Performance Improvement of Aluminum Grooved Heat Pipe due to increased number of Grooves", Korean Journal of Air-conditioning and Refrigeration Engineering,13(6),pp474-481.(in Korean)

2) Chi, S.W.,1976, "*Heat Pipe Theory and Practice*", A Source book, Hemisphere Publishing Co.

3) J. K. Hong, D. S. Kim, 2000, "The Experimental Study on the Working Characteristic of Heat Pipe with Water Spray System in Condenser Section" , Proceedings of the SAREK 2000 Summer Annual Conference, pp. 462-469.(in Korean)

4) S. G. Choi, 2001, "The Experimental Study on the Performance Evaluation of Heat Pipe Heat Exchanger", Kyungwon Univ. Master Thesis.(in Korean)

Perspective Thermo Control System for a Spacecraft Having Onboard Equipment with Increased Heat Release

V. Dvirnyi, V. Dorokhov, V. Bartenev, A. Loganov

Reshetnov's NPO PM;

662971, Zheleznogorsk sity, Lenin st., 52.

Tel/Fax: (39197) 24302

E-mail: dvirnyi@npopm.ru

Abstract

In the report are discussed a possibility and conditions of application in the communication satellite of the two-phase thermal control system with the mechanical pump. The choice of the heat-carrier is reasonable and the settlement evaluation of some hydraulic and thermal performances of a system for large heat release is indicated. The ability of maintenance of a necessary thermal mode of a set of low-power gears with the heat-carrier a freon 152 is shown. The advantage of the active two-phase thermal control system on a comparison with a liquid system, used now on the russian satellite, is shown.

Key words: two-phase thermal control system, communication satellite.

1. INTRODUCTION

Till recently Reshetnov's NPO PM has counted on the use of active liquid systems while developing the Thermal Control Systems. Such systems have shown sufficient efficiency and reliability when total heat release of radio equipment is within the limits of 4 kW. There has been no failure case of TCS during flight time since all the time of space operation. The mechanical pumps have shown a value of more than 180 thousand hours operating time during the resource tests and they have been working until now. In the70-s the experiments on loop heat pipes have begun. As a result the three «Horizont»-type communication satellites provided with experimental two-phase loops were launched.

Total view of experimental loop pipe is in fig.1.

NPO PM has an experience of development and operation of two-phase loops with the mechanical pump. In 1987 year the simulator of TCS was developed for realization of electronic equipment ground tests. Structure of the indicated system includes the thermal control system with the pump (pump is shown in fig. 2) and automatic control system. The maximum value of removed thermal power is 2850 W, heat-carrier - Freon 113. The system was used for its designed purpose for a long time and is in working order now.

Now we have a new tendency to increase a power of radio equipment on the communication satellites by sharp magnification of repeater quantity. Simultaneously there is a reduction of device power consumption (up to 140-180 W for the most high-power device), which complicates the application of capillary pumps.

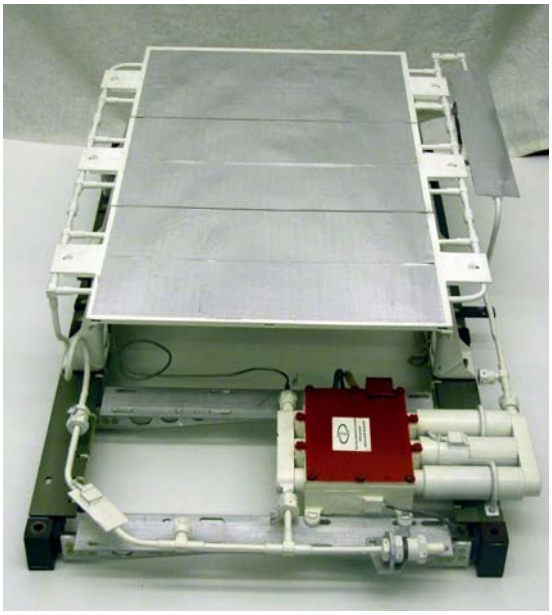


Figure 1



Figure 2.

On the other hand, the efficiency of active liquid TCS is considerably reduced when magnification of heat release is more than 8 kW. It results in the necessity of considerable increase of radiator - emitter sizes (more than 22 м^2). Besides, it becomes more difficult to provide a reliable work of the mechanical pump during15 years when its power consumption is restricted. The mass of such pump will appreciably increase as well. The sharp increase of pump load is caused by the fact that the significant rise of thermal capacity forces to increase a flow rate of working liquid proportionally. In this case, the pump power consumption will increase approximately in 10 times when devices heat release increase in 4 times.

Evaporation heat involving in heat exchange process will allow first of all to reduce a size of the radiator - emitter. So when it is considered that the heat radiation occurs at t = 40°C (313K) from the radiator panels with two-phase coolant, then the area of panels equaled to 18 м^2 is required. A single-phase liquid TCS has nonuniform temperature distribution in liquid and actual average temperature of radiator panels is considerably below 40°C. The large amount of heat, which is constant along the full length of pipelines, releases when a vapor condensation takes place in radiators – emitters. The temperature constancy of liquid-vapor mixture in pipeline can be provided with a pressure regulation.

There is a possibility to reduce a minimal necessary working fluid rate at least in 1,5 times in a system with the two-phase heat-carrier in comparison with the single-phase carrier, though the actual reduction of pump power can be a little less. It is due to the liquid heat-carrier used in a new system, which has the greater density, and the additional resistance introduced by a vapor component of mixture.

In this papier a possibility of two-phase TCS having the mechanical pump are explained giving an example of system having a heat release of 8 KW. The device thermal capacity, removed by this TCS, is 15, 45 and 135 W. Total number of heat-generating devices and units is more than 100 pieces.

2. TWO-PHASE COOLANT TCS OPERATIONAL CONDITIONS

2.1 Choice of a heat-coolant

As the new satellites should operate during a long period of time, the choice of the heat-carrier counts for a great deal. Ammonia is not suitable for such system. This is dictated by high operating pressure of ammonia (about 2 MPa). The tightness of pipeline system for the term of 15 years, as its maintenance at such high pressure requires large material and money costs. Besides the vapor of new heat-carrier should have rather high density to ensure a low pressure loss. The high vapor density is also required in order to provide better heat transfer maintenance. As a result of the multidisciplinary analysis the heat-carrier Freon 152A was selected. It has much lower operating pressure in comparison with ammonia and sufficiently high vapor density at operating temperatures (35 to 40°C). Such combination of coolant characteristics allows receiving rather low value of pressure loss when a liquid-vapor mixture flows on the pipeline and also more security of a two-phase thermal control system.

The calculations show at Freon-152a rate 100 cm^3/sec a calculated heat rate required for total evaporation at t = 40°C (313K) amounts to 22,3 kW.

Mixture composition (fraction of vapor mass) in two-phase TCS has an fundamental importance. Due to a vapor volume, exceeds volume of fluid considerably, the stream of liquid-vapor mixture can have different effectiveness depending on the fraction of vapor mass. Obviously, when the relative fraction of vapor mass is close to 1, the cooling action of stream will be insufficient.

The most actual problem of this kind TCS application can be called as «problem of the last device ». As a relative mass of vapor fraction is increased during liquid-vapor mixture moving from the pump through cooled devices, there is a risk, that the flow condition will not ensure the removal of this device heat capacity the «last» device. In the present work it is evaluated a

possibility to provide thermal control maintenance number of devices, when the liquid-vapor mixture passes through them sequentially.

For this purpose it is considered a flow condition of the two-phase heat-carrier (Freon 152a) at volume liquid flow 100 cm^3/sec and inner pipeline diameter of 16 mm.

2.2 Two-phase TCS performance

The fraction of vapor mass X^m is one of the major characteristics of two-phase flow (It is offered by the authors of this paper):

$$X^m = \frac{\dot{m}''}{\dot{m}_\Sigma} = \frac{\dot{m}''}{\dot{m}'' + \dot{m}'} \qquad (1)$$

Where $\dot{m}''$ - vapor mass flow rate, kg/sec;

$\dot{m}'$ - liquid mass flow rate, kg/sec;

$\dot{m}_\Sigma$ - total mass flow rate of TCS, kg/sec.

It is easy to express a ratio the phase volumes with x^m, i.e., volume of vapor phase of liquid-vapor mixture (LVM) vapor phase is:

$$\dot{V}'' = x^m \dot{V}_\Sigma \frac{\rho'}{\rho''} \qquad (2)$$

where $\dot{V}''$ - volume flow of vapor phase;

$\dot{V}_\Sigma$ - total volume of liquid;

ρ' - density of liquid phase;

ρ'' - density of saturated vapor in vapor phase.

Taking into account the relationship between operating pressure, viscosities and Freon-152a surface tension force [1], we suppose a LVM has an annular flow within a sufficient large range of X^m. This flow condition leads to separation of the stream, i.e. the liquid phase is adjacent to the pipeline walls, the vapor phase predominates in a center. This flow condition is suitable to cool the devices, when the liquid phase continuity condition is provided on the pipeline walls. For estimating the stability of a ring-type mode with increasing x^m a liquid and vapor fractions flow velocity distribution on a pipe radius was obtained. The dependence of vapor and liquid fractions flow on pipe radius was determined by [2]:

$$v_x = v_{max}\left(1 - \frac{r}{r_0}\right)^n \qquad (3)$$

where n is determined by the results of Nikuradze and Mebius' tests [1] depending on the value of number of Reynolds Re.

r_0 – inner pipe radius;

r – a distance from pipe centerline up to a point, in which it is possible to determine a flow velocity;

$$\mathrm{Re} = \frac{d\bar{v}}{\nu} \qquad (4)$$

d – inner pipe diameter;

$\bar{v}$ - mean flow velocity inside a pipe;

ν - kinematics viscosity.

For a numerical analysis of the flow inside the pipe the following assumptions were also taken:

1) the liquid flow structure near the pipe walls at $x_m<0.4$ is described by an equation (3);

2) v_{max} is determined in view of the liquid velocity increased near the vapor pipe;

3) a liquid velocity increases considerably due to a vapor ejection in the close vicinity to a vapor pipe;

4) vapor and liquid velocities are identical on a calculated boundary of liquid and vapor phases;

5) a mean velocity of each phase is determined by a flow velocity distribution liquid and vapor fractions on a calculated boundary of phases.

Calculation with the above assumptions gave the following results:

1) the calculated mean vapor velocity increases (full polyline in fig. 3) in the range of x^m values from 0 up to 0,6;

2) when x^m beyond 0.7, the curve has a critical point. It's most probably, that after this point there should follow a separation of liquid from walls and change of ring-type flow mode to a dispersed one.

Example of calculated flow velocity distribution liquid and vapor fractions inside a pipe at different fractions of vapor mass is shown in fig.4

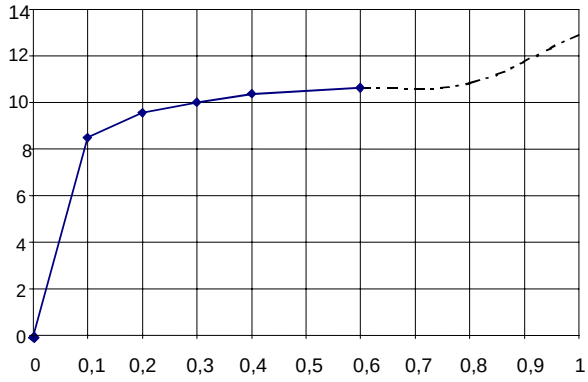


Figure 3. Plot of mean vapor velocity vs x_m.

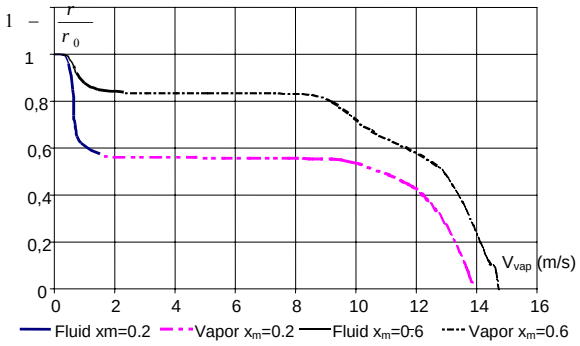


Figure 4. Flow velocity distribution on a pipe radius

2.3 Efficiency of the developed TCS in comparison with liquid one

The dependence of removed heat power value on fraction of vapor mass (performance of the evaporator) is shown in fig. 5. (The Freon-152a evaporation heat is 260,5 kJ/kg at T = 313K [3]).

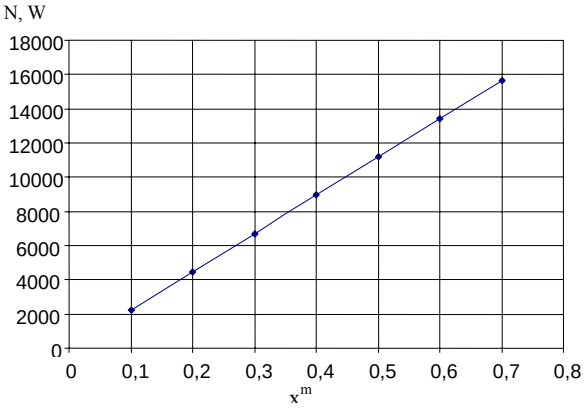


Figure 5. Plot of removed heat power total value against x^m , at volume liquid flow of 100 cm^3/sec.

The plot shows that at indicated flow rate value within the limits of a ring-type flow mode the maximum allowable heat load in the pipeline is no more than 14 kW without risk of overheating of devices. Analysis shows that the liquid Freon-152a flow rate can be reduced up to 80 cm^3/sec at the maximum value of removed power of 8 kW. In liquid TCS removal of the same thermal power value needs iso-octane volume flow of 130 cm^3/sec.

2.4 Conclusions

The thermal control system with the two-phase heat-carrier Freon-152a at removed heat power value of 8 kW allows considerably reducing area (from 22.1 up to 18 m^2) of panels for the radiators - emitters on telecommunications satellite. And liquid coolant flow rate is also considerably reduced. Thus, dimensions of radiator panels and mass reduction can be obtained at least without increase in mass and power consumption of the mechanical pump.

References

1. V.V. Kaffarov, 1962, The Fundamentals of masse transfer , Publishing house "Higher School", Moscow, pp. 142-144
2. .P. Ginsburg, 1970, The theory of a resistance and heat transfer , Publishing house of Leningrad Univercity, pp. 101-103
3. N.B. Vargaftik, 1963, The directory on thermal to properties of gases and liquids, Publishing house "Higher School", Moscow, pp. 209-213

The Application of Heat Pipe Embedded Panel for the Transponder of Communication and Broadcasting Satellite(CBS) Payload System

Jong-Heung Park*, Jang-Sup Choi*, Seong-Pal Lee*, Hyung Je Woo**
* Communications Satellite Development Center
Electronic and Telecommunications Research Institute (ETRI), Daejeon, Korea
** Satellite Payload Development Section/Space Development & Research Center
Korea Aerospace Industries(KAI), Daejeon, Korea
Email**:** jpark@etri.re.kr, chaos@etri.re.kr, spallee@etri.re.kr, hjwoo@koreaaero.com

Abstract

ETRI has developed the transponder for the communications and broadcasting satellite(CBS) payload system to provide the satellite services in Korea. In space product, the heat pipe embedded sandwich panels are generally used to integrate and assemble the communication equipment and to provide the thermal path to the space with appropriate mechanical structure. This paper describes the design and layout of heat pipe in the honeycomb sandwich structure, the manufacturing of the heat pipe embedded panel, the tests for the operations and the results of test. The actual applications to the communication transponder in the CBS program are also presented.

Key words: Heat Pipe, Heat Pipe Embedded Panel, Space Application.

1. INTRODUCTION

ETRI has developed the Ku band and Ka band payload system for the communications and broadcasting satellite(CBS) to provide the satellite services in Korea. The payload systems consist of the transponder and the antenna subsystem[1]. The antenna subsystem transmits and receives the signals between the satellite and the ground station. The transponder subsystem takes the signals from the antenna, frequency converts, amplifies, and then sends the signals to the antenna. The transponder is composed of many RF equipment, named receivers, filters, amplifiers and multi-plexers. Some of those equipment dissipate a lot of heat to the panel or neighboring structure. Since the performance of these equipment is reliable only within the typical temperature ranges, the thermal control of the transponder is very important parameters to develop the payload system.

In the space product, the heat pipe embedded panel is generally used to integrate and assemble the communication equipment and to provide the thermal path to the space with appropriate mechanical structure[2]. This paper describes the design and layout of heat pipe in the honeycomb sandwich structure, the thermal analysis, the manufacturing and heat pipe embedding in the panel, the tests for the proper operations, and the comparisons of test with the analysis. The actual applications to the communication transponder in the CBS program are also presented.

2. DEVELOPMENT OF HEAT PIPE EMBEDDED HONEYCOMB SANDWICH PANEL

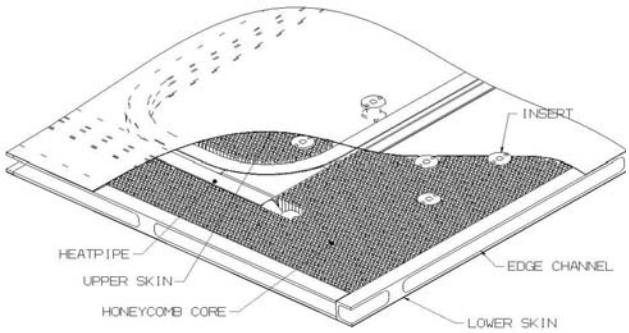


Figure 1. Heat Pipe Embedded Honeycomb Sandwich Panel.

2-1 Design

As shown in Figure 1, the heat pipe embedded honeycomb sandwich structure panel is typically used for the space structure. According to the heat pipes embedded in the panel, the transponder electronic equipment can be controlled within the operating temperature range approximately –40 ^{o}C to 80 ^{o}C. In this temperature range, the electronic components are working with a high reliability.

Transponder panel layout is designed by the following rationales:

- All transponder equipment are placed on one panel
- Equipment layout constraints on minimal RF loss and thermal considerations,
- High heat dissipative equipment mounted on heat pipes embedded in the panel
- Panel size (1.3m x 1.3m) determined based on radiation cooling surface and area required for test fixture,
- Easy accessibility during Assembly, Integration and Test operation.

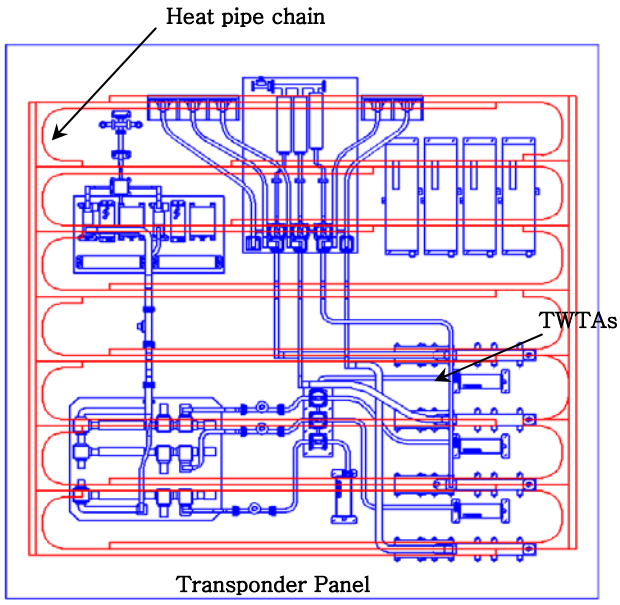


Figure 2. Heat Pipe Layout

Based on these rationales, the transponder panel layout is designed as shown in Figure 2. All heat pipe are thermally connected as a chain and have redundant thermal path to prevent any abnormal operation throughout the life. Especially, the high heat dissipation equipment such as TWTA(Traveling Wave Tube Amplifier), high power loads, are placed on the heat pipe chain respectively due to the high heat dissipations. Three types of heat pipe(I, J, U type) are selected for layout.

Thermal analysis was performed to predict the temperatures under the space environment and test environment. The heat dissipations from the RF equipment were derived at the worst case condition. Figure 3 shows the network of thermal resistance of the face sheet, the heat pipe, the honeycomb core, and the boundaries. The SINDA(Systems Improved Numerical Differencing Analyzer) code was used to calculate the temperature.

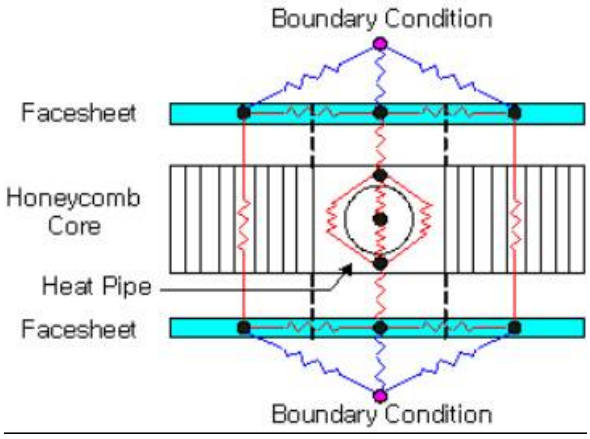
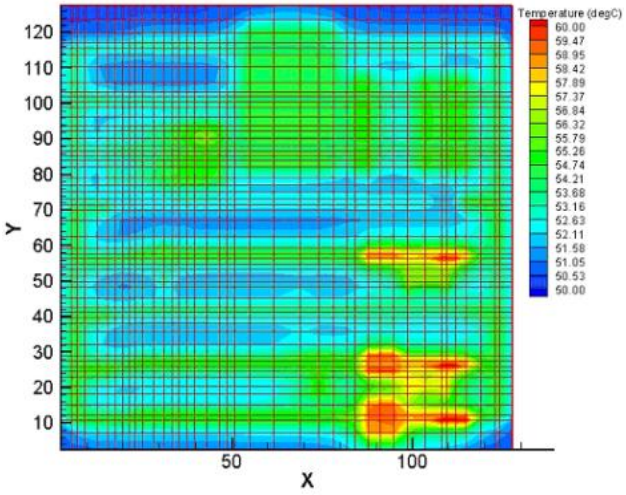
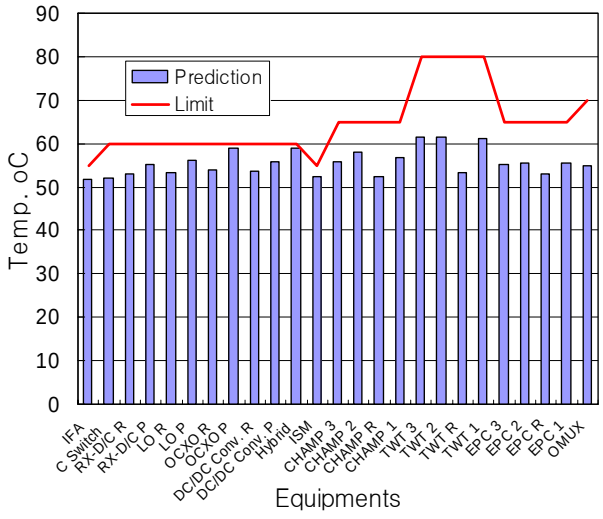


Figure 3. Model for Thermal Analysis



(a) Temperature Profile on the Panel



(b) Equipment Temperature for Hot Case

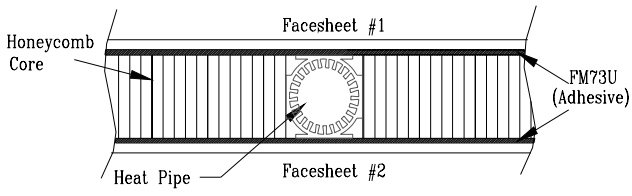
Figure 4. Thermal Analysis

Figure 4 shows the temperature contours and the temperature of each equipment at the one of the hot case operation. As shown in Figure 4(a), the hot spot appears in the TWTA interface which dissipates the highest heat, 78Watt. Considering the temperature distributions, the heat seems to

be well spread over the whole panel. The redline in Figure 4(b) means the limit of temperature to guarantee the reliable operation of equipment. It is understood that all predicted temperatures are below the limit, consequently, the thermal design is well performed and optimized.

2-2 Manufacturing

The panel including the heat pipes was manufactured in the domestic company with the space qualified material and process. The heat pipes are tested and evaluated with the designated qualified process such as “heat pipe burst pressure test” prior to the delivery to panel[3].



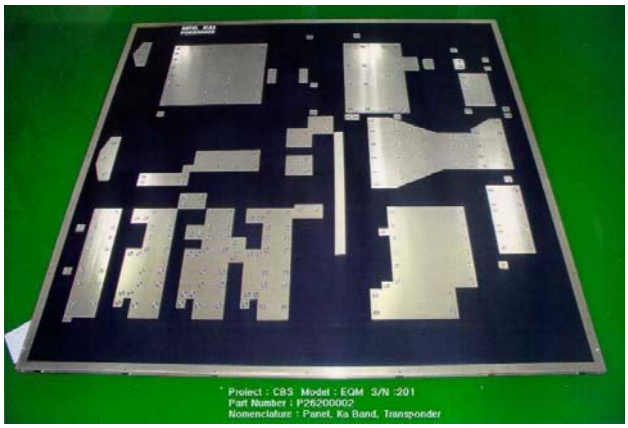


Figure 5. Photo for the bare panel

The heat pipes used are a groove type with the aluminum (Al 6063-T6) and the ammonia as a working fluid. The materials are Al6061-T6 for the face skin and Al5056 for the honeycomb core. The zero gravity heat transport is at least 4,500 Watt-incjes over an operation temperature range –25 ^{o}C to 80 ^{o}C. This capacity was verified throught the flight acceptance test. The film adhesive are used between the core, heat pipe and face sheet. The final thickness of panel is 14.7mm. Figure 5 shows the photo of panel manufactured. The inserts for equipment mounting were embedded and the thermal painting with mask has also been processed.

2-3 Test and Evaluation

In addition to the mechanical test and bonding investigation[4], the thermal test also performed for the panel to verify the correct heat pipe operations. Figure 6 shows the test method to verify the heat pipe operation. Total 16 thermocouples were attached on both end of the panel. The heating plate is placed along the centerline of the panel. While maintaining the panel horizontally, the heating plate was heated up to 100^{o}C, then the temperatures at 16 points was measured simultaneously. Since this test was performed at ambient condition, the influences of convection to the air could not be removed completely. However, it was found that the temperatures of 16 points were uniformly distributed with an accuracy of ±1.2^{o}C difference.

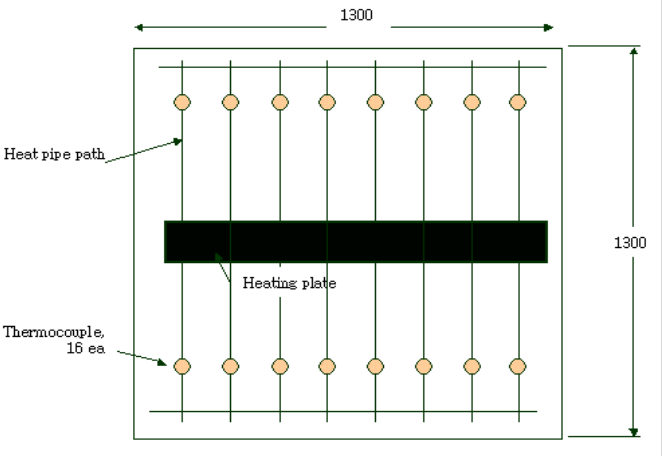


Figure 6 Thermal Test Configurations

2-4 Applications

This panel was delivered to transponder assembly. All transponder RF equipment and fixings were mounted on the panel. Figure 7 shows the photo of Ka-band transponder after the assembly.

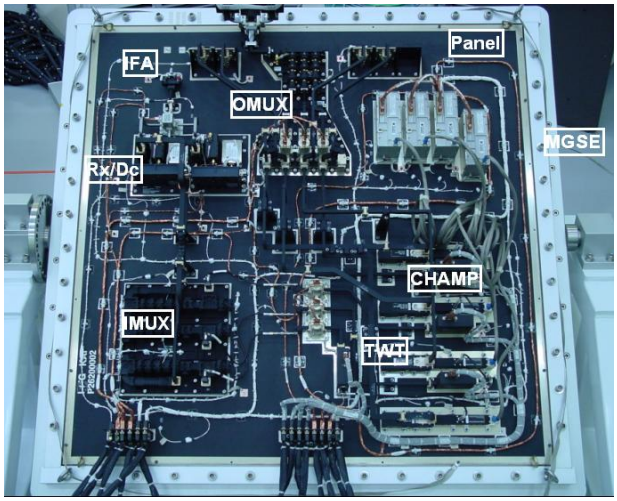


Figure 7. Photo of Transponder

This transponder went through the functional and environmental test including vibration and thermal cycling. Figure 8 shows the thermal test configuration inside the thermal chamber. Total 35 thermocouples were attached on every equipment and panels. In addition to these thermocouples, the flight thermistors were also monitored through the transponder control station. During the thermal cycling, there was no unexpected thermal behaviors or abnormal operation, which means the heat pipes inside the panel were working very well.



Figure 8. Transponder Thermal Cycling Test

The comparisons of the test results with the analysis were presented in Figure 9. In this case the TWTA 1, 2 and 3 are turned-on simultaneously, consequently, the temperatures on these equipment is higher than that of TWTA-R. Considering the temperature of non-heat dissipating equipment(IFA, ISM), the maximum difference is about 5°C, which means the heat pipe is working well.

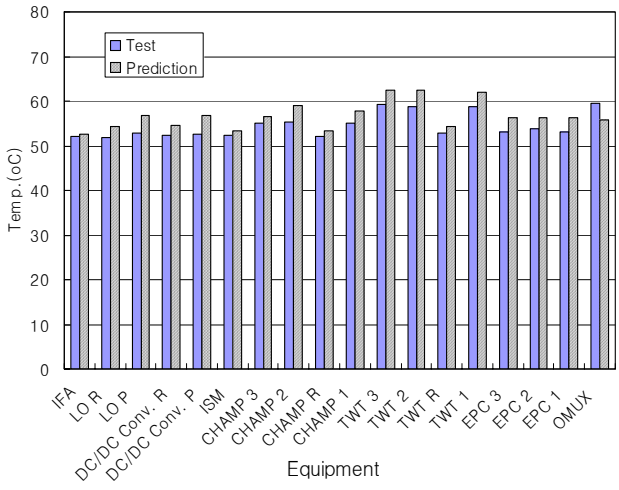


Figure 9 Test vs. Prediction

As shown in figure, the overall predicted temperatures are slightly higher than those of test except the equipment named "OMUX". This seems to be caused by the worst case analysis and radiation that was not considered in the analysis. For "OMUX" case, the electrical loss, equivalent to the heat, seems to be greater than estimated. Due to the simplifications of the thermal modeling compared to the hardware, there are some discrepancies between the analysis and the measured temperatures. However, the differences are within ±3°C max, which is compliant to the requirement ±5°C .

3. CONCLUSIONS

The design, manufacturing, and test of the heat pipe embedded honeycomb sandwich panel for the communication satellite transponder panel have been introduced. The design and manufacturing process are confirmed by a serious of qualified tests. In addition to the panel test itself, the application to the communication satellite transponder and environmental test results were also presented. By this comparison, it is possible to conclude that the heat pipes embedded inside the sandwich-panel were operating very well to provide the thermal path between cold and hot spot. Since all the processes to build this panel are followed by the international space regulations, the whole processes are qualified and to be used as a flight hardware in the near future.

References

1. S. P. Lee, T. J., Chung, J. H. Park, I. B. Yom, J. W. Eun, W. S. Choi, J. M. Kim, "Satellite Communication Payload System Development Technology", Proc. of APSCC 2002 Conference, 6~8, Nov., 2002, pp.1065-1075
2. J. H. Park, "A Study on the Thermal Performance of Heat Pipe for Optimum Placement of Satellite Equipment," ETRI Journal, Vol. 19, No. 2, 1997
3. J. S. Choi, J. H. Park, S. P. Lee, H. J. Woo, "Heat Pipe Embedded Panel Development for the CBS Transponder", Proc. of the KSAS Spring Annual Meeting, 2003, pp. 598-601
4. H. S. Seo, J. S. Choi, H. J. Woo, J. H. Park, "Estimation of Structural Reliability for the CBS Ku-band Transponder Panel using Environmental Vibration Test", Proc. of the KSAS Spring Annual Meeting, 2003, pp. 686-689

HEAT PIPES APPLIED IN SPACECRAFT

Miao Jianyin Shao Xingguo Li Tinghan Cao Jianfeng Mi Min Lv Wei Yang Huning
Chinese Aerospace of Science and Technology Corporation
P.O.Box 9628-5, Beijing, China 100086.
Tel:(+86)-10-68378475, Fax:(+86)-10-68378449, E-Mail: Jymiao@263.net

ABSTRACT

Heat pipes applied in China aerospace field are introduced. Two typical aluminum-ammonia axially grooved heat pipes used in the satellite thermal control system are mentioned. Further more the corresponding test subject and test apparatus are introduced briefly. Other kinds of heat pipes developed based on their correlative application background are summarized, such as loop heat pipe, flexible heat pipe, miniature heat pipe, Gas-controlled heat pipe, cryogenic heat pipe, etc. Applications of heat pipes in spacecrafts are also introduced in this paper.

Keywords: heat pipe spacecraft application

1 INTRODUCTION

In 1976, aluminum-ammonia axially grooved heat pipes were successfully used in the satellite thermal control system for the first time in China. This had greatly improved thermal design technology. Now, as an important means of thermal control, heat pipes and their applications are developing continuously. In details, heat pipes have run to many styles including eighteen sorts of aluminum-ammonia axially grooved heat pipe, flexible heat pipe, capillary pumped loop, loop heat pipe, single-grooved heat pipe, miniature heat pipe, Gas-controlled heat pipe, cryogenic heat pipe, etc. Further more, the aluminum-ammonia axially grooved heat pipes have been widely used in the thermal control system of spacecrafts, and the detailed technique criterions about heat pipe design, manufacture and application in the spin stabilized satellite and the three axis stabilized satellite have already been published. Heat pipes and LHP also have come into use in the thermal management system and the deployable radiator of large-scale spacecraft project.

2 ALUMINUM-AMMONIA AXIALLY GROOVED HEAT PIPES

2.1 Characteristics of Two Typical Aluminum -ammonia Axially Grooved Heat Pipes

From 1976, the aluminum-ammonia axially grooved heat pipes used in spacecraft of China have been improved continuously, and now CASC can provide a series of heat pipes with properties of reliability and stability to meet different needs. Equipment.1 shows the details of aluminum-ammonia axially grooved heat pipes.

Equipment.1 Characteristics of Heat Pipes

Type of heat pipe	RG-O1-30×ϕ15	RG-G2-25 × 25
Material	6063	6063
Working fluid	Ammonia	Ammonia
weight（kg/m）	0.36	0.70
Q_{max} （20℃）W·m	135	78×2
ΔT（℃）	≤1	≤1
h_e(W/ m² ℃)	>8000	>6000
h_c(W/ m² ℃)	>10000	>9000
Leak rate ($Pa·m^3/s$)	2×10^{-8}	2×10^{-8}
Operating temperature range （℃）	-60~60	-60~60
Operating life	8 years	8 years
Application methods	Surface installation	Pre-buried

Fig.1 to Fig.4 showed the cross section and the picture of rectangle grooves.

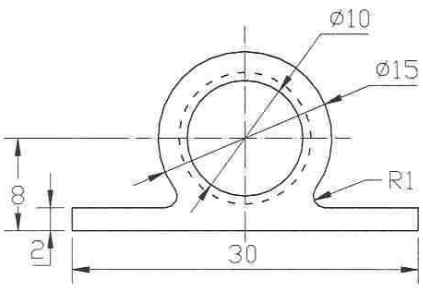


Fig.1 RG-O1-30×ϕ15

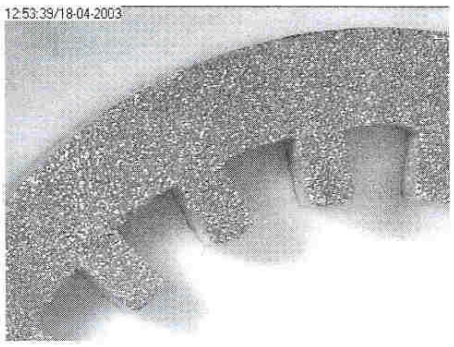


Fig.2 Grooves of RG-O1-30×ϕ15

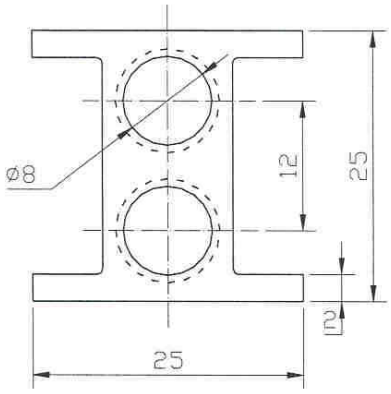


Fig.3 RG-G2-25×25



Fig.4 Grooves of RG-G2-25×25

2.2 The main test items of heat pipes

There are specified criterions on the performance testing and checking to make sure the heat pipes be available for use in spacecraft.

1) Leak rate

The leak rate of the aluminum-ammonia heat pipe used in aerospace must not be more than 2×10^{-8} Pa·m^3/s. Above this, the leak rate of the body and the injector should not be more than 1×10^{-8} Pa·m^3/s.

2) Criterion of High Temperature Test

When the heatpipe is produced, there should be a temperature holding test according to its application method so as to see if the material and jointing intension can meet the needs. The temperature test condition are showed in Equipment 2.

Equipment.2 Criterion of High Temperature Test

Installing mode	Temperature of adiabatic part(℃)	Time to be hold(h)
Surface installation	60±3	1
Pre-buried	95±3	1

3） Isothermal Test

The temperature difference between adiabatic zone and condensation zone should not be more than 1 ℃.

4） Maximal Heat Transport Capacity

The maximal heat transport capacity test should be carried out for newly developed heat pipe and provide reference for application.

5）Temperature Cycle Test

Heatpipe should undergo the temperature cycle specified in Equipment3 for 100 times. After this the isothermal performance should still be qualified. This test applies to the newly developed heatpipes.

Equipment.3 Criterion of Cycle Test

High temperature (℃)	≥60
Time to be sustained (Min)	≥30
Low temperature (℃)	≤-60
Time to be sustained (Min)	≥30
Rate of temperature changing (℃/ Min)	≥20

6） Uncondensable Gas Test

In the long-term communication satellite (15 years)and large power, heat pipe should work at rather high temperature（about 50℃）for long. The uncondensable gas produced by the heat pipe itself after working for a long period of time is the main reason which results in the disabling of the heat pipe. CASC plan to take such approaches to test the uncondensable gas as showed below.

a) Aging at High Temperature

Keeping heat pipes at 80±3℃for 144 hours. That is to speedup the likely chemical reaction process between the pipe material (6063) and the wording fluid (ammonia) or the decomposition of the working fluid, thus the uncondensable gas is given off to be gotten rid of in advance.

b) Uncondensable Gas Test

After aging in high temperature, under the working temperature -20℃, testing the length of the gas column which not more than 20mm/m is qualified.

However, on the other hand, the aging test stated above would decrease the lifetime of the heat pipe to some extent, which is the shortcoming of this way of testing the uncondensable gas. There'll still be a lot of work to do in future work to find a better testing method and to keep the long lifetime of heat pipes.

2.3 Main Apparatuses in Heat Pipe Manufacturing and Performance Testing

Below are the pictures and brief introduction of the main apparatuses in the heat pipe manufacture.

Heat pipe Filling Equipment

The filling equipment has the functions of heating or cooling the ammonia chamber, measuring the height of liquid ammonia and alarming automatically. Minimum filling matter is 0.01g and the filling precision is±3.5%.

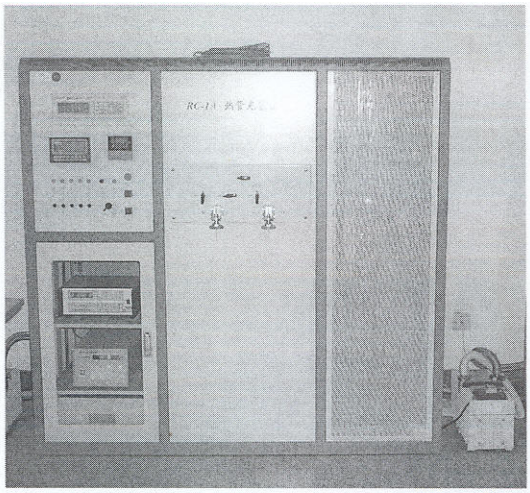


Fig.5 Heat Pipes Filling Equipment

Welding Equipment

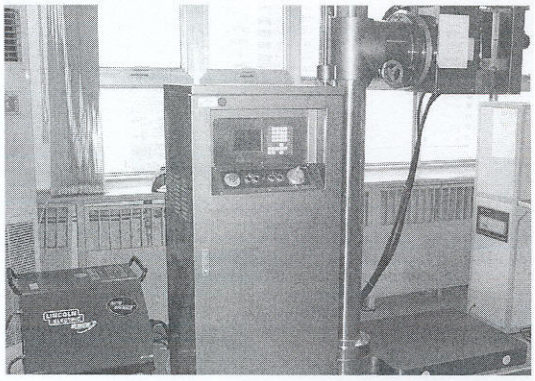


Fig.6 Welding Equipment for Injector

The welding equipment can automatically weld the injector of heat pipe. After welding, the heat pipe leak rate is not more than1×10^{-8} Pa·m^3/s after being heated to 95±3℃ for an hour. This is an important method to assure the long lifetime of heat pipes.

Isothermal Performance Testing Equipment

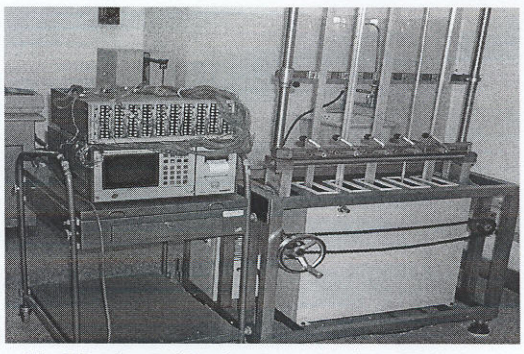


Fig.7 Isothermal Performance Testing Equipment

The testing equipment applies to all heat pipes

with different section shape and size and outline. The hot end of the heat pipe is heated by warm water. The temperature is measured and collected by computer. There could be 5 heat pipes at one time and the inclining angle of the support is adjustable.

Lifetime Testing Equipment

There're two purposes of lifetime testing:

1) To get the real lifetime of the aluminum-ammonia grooved heat pipe made under present technology level.

2) To get the law of the performance deterioration after working for a long time and the reason that resulting this so as to take relative approaches in the manufacture process and to prolong the lifetime of heat pipes.

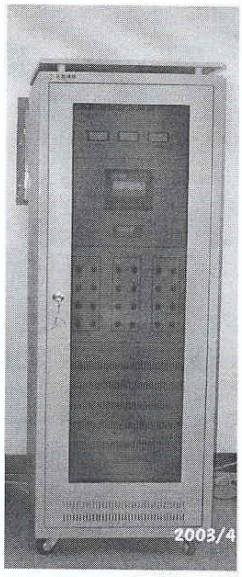


Fig.8 Lifetime Testing Equipment

This test had begun since 2002 and up till now has continued about 8000 hours. There're 24 heat pipes attended the test. The working temperature is about 45℃。

3 Development of Other Kinds of Heat pipes

3.1 Loop Heat Pipe (LHP)

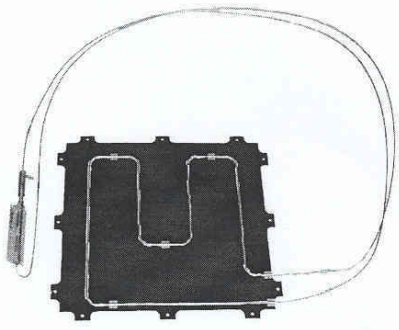


Fig. 9 Loop Heat Pipe

Since 1998, on the basis of CPL, the heat pipe department of CASC began to do the research on LHP. We have past the concept research, theoretical model and engineering model stages. Now flying test is in plan (launching in 2003). The typical performances of LHP are as showed in Equipment.4 and Equipment.5.

Equipment.4 Parameters of LHP

Working fluid	Ammonia
Capillary structure	Nickel power(sintered)
The effective capillary radius	0.8~0.9μm
Permeability(m^2)	5×10^{-14}~1×10^{-13}
Diameter of evaporator (mm)	13
Length of evaporator (mm)	130

Equipment. 5 Performance of LHP

Operating temperature range (℃)	-60～+60
Heat transport capacity at 60℃ (W)	>100
Distance of heat transport (m)	>8
Height against gravity (m)	>2
Heat resistance of evaporation (K/W)	<0.2
Heat resistance of condensation (K/W)	0.02~0.1
Total heat resistance (K/W)	0.2~0.3
weight (kg)	0.5~1.5

3.2 Flexible Heat Pipes

The flexible heat pipes research was firstly begun in 2000. Its overall length is 650mm with

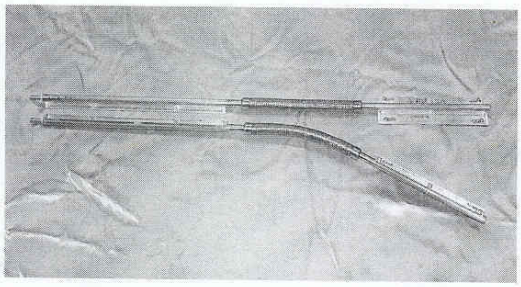


Fig.10 Sample of Flexible Heat Pipes

the minimum bending radius of 70mm. The main parameters are showed in Equipment.6 and Equipment.7.

Equipment.6 Parameters of Flexible Heat Pipes

Material of rigid part	Stainless steel tube with inner whorl
Material of flexible part	Corrugation tube (stainless steel)
Capillary core	Fiberboard of stainless steel covered by mesh
Working fluid	Ammonia
Length（mm）	650
Diameter of rigid part (mm)	9
Diameter of flexible part (mm)	8

Equipment.7 Performance of Flexible Heat Pipes

Operating temperature range（℃）	-20～+40
Heat transport capacity (straight)（W）	>30
Heat transport capacity (bend angle : 90°)（W）	>30
Heat resistance（℃/W）	< 0.3
Leak rate（$Pa \cdot m^3/s$）	$< 1 \times 10^{-8}$

The data showed above comes from reference [1]. In 2002, after passed the pressure test, bending test and mechanical tests, the flexible heat pipe was successfully used for the heat dissipation of gyro electronics in the satellite.

3.3 Gas-controlled Heat Pipes



Fig.11 Sample of Gas-controlled Heat Pipes

Equipment.8 Performance of Gas-controlled Heat Pipes

Material of heat pipes	6063
Working fluid	Ammonia
Control gas	Nitrogen
Total length（mm）	900
Length of condensation part（mm）	130
Inner diameter of gas storage chamber（mm）	15
Length of gas storage chamber（mm）	220
Operating temperature range（℃）	-10～+50
The maximal heat transport capacity（W）	60
Rate of heat transport changing	1/10
Temperature change of heat pipe (heat load changed from 2.7W to 30.4W)（℃）	<2.6

3.4 Miniature Heat Pipes

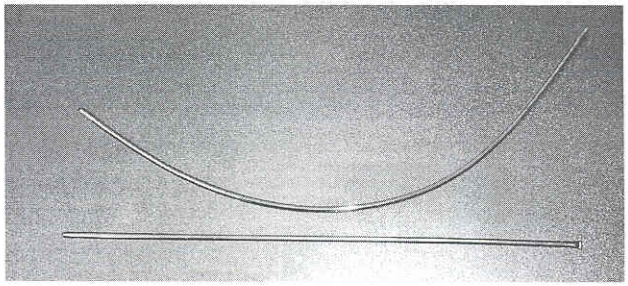


Fig.12 Sample of Mini-heat Pipes

Equipment.9 Parameters of Mini-heat Pipes

Material of heat pipes	Copper tube
Working fluid	ethanol
Outer diameter（mm）	3
Inner diameter（mm）	1.8
Capillary structure	Rectangle groove (0.2 × 0.2mm) covered with two layer copper mesh(200M)
Number of grooves	20
length（mm）	250
weight（kg/m）	0.035
Operating temperature range（℃）	20～100
The maximal heat transport capacity（W·m）	1.5
h_e（W/m^2 ℃）	>1000
h_c（W/m^2 ℃）	>1000

3.5 Cryogenic Heat Pipes

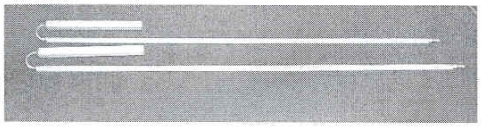


Fig.13 Samples of Cryogenic Heat Pipes

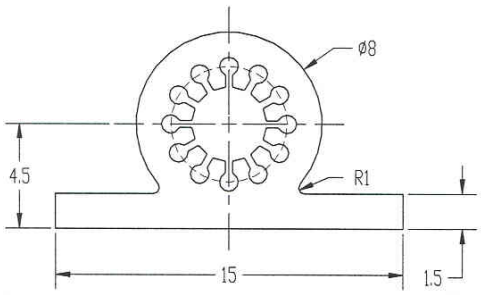


Fig.14 Section Shape of Cryogenic Heat Pipes

Cryogenic heat pipes is the key technology in the joining between the space infrared explorer and refrigerator and in the isothermalization of radiating refrigerator. Fig.13 is the sample of the present cryogenic heat pipe, and fig.14 shows the section shape. The heat pipe body is made of 6063, the gas-store room is made of 3003. The working fluid is nitrogen of high purity of 99.9993%. The operating temperature range is 80～110K with the theoretical maximal heat transfer capacity of 4.5Wm at 100K. All tests on the heat pipe are in preparation at present. And the maximal heat transfer capacity had been tested in December, 2002 (filled with ammonia). The testing results show that the maximal heat transfer capacity is 32W·m（20℃）, which improved by 50% comparing with the rectangular-grooved aluminum-ammonia heat pipe of the same tube diameter. Furthermore, the instability phenomenon such as temperature vibrating doesn't appear as reference [2] stated.

3.6 High Heat Transport Capacity Heat Pipes

To meet the demands of the large spacecraft, especially the communication series satellites, for heat pipes with large heat transfer capacity, CASC began to make research on the single grooved heat pipe ever since 1998[3]. Fig.15 and Fig.16 show the section of the single grooved heat pipe. Testing results showed the heat transfer capacity of this kind of heat pipes improved greatly. The maximal capacity reached at 1032Wm（at 37℃） when the diameter of the vapor tube is 15mm and that of the liquid tube is 7mm, while the value of the usual heat pipe with the diameter of 15mm is 248 W·m（at 20℃）. However it was also showed that, under the maximal capacity, the temperature of the heat pipe fluctuates badly and the temperature difference was rather large. Now there is not yet a valid method to solve the above problem which placed an obstacle in the application of the single grooved heat pipe. The research work on this kind of heat pipe has stopped at present.

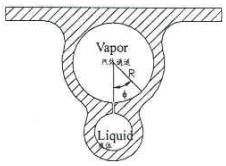


Fig.15 Cross Section of Single-Grooved Heat Pipes

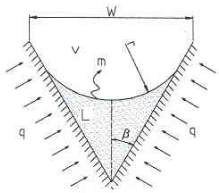


Fig.16 V Shape Groove and Liquid Film

Ω-shape axial grooved heat pipes had gained the attention of many heat pipe research organizations these recent years. Lavochkin Association (Russia) had carried on detailed investigation on it and had

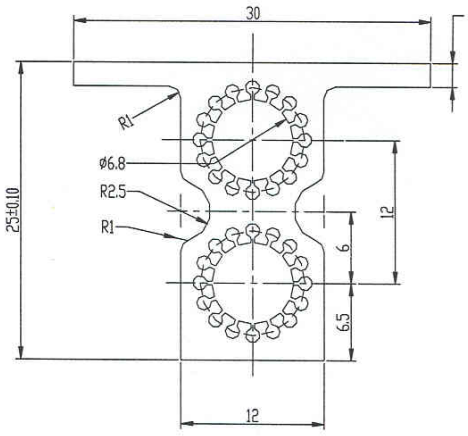


Fig.17 Section of Ω-Shape Grooves

come to serial products [4]. ALCATEL SPACE Industries (France) also worked on this type of

heat pipes. Now the Heat Pipe Department of CASC has taken the Ω-shape axial grooved heat pipes as this year's research project, Fig.17 is one of the types under research.

4 Applications of Heat Pipes in Spacecraft

From the first time that heat pipes were used in thermal control system of GEOS-Ii in 1968, applications of heat pipes in spacecraft have been recognized in the world. Since 1976, Aluminum-ammonia axially grooved heat pipes developed by heat pipe department of CASC have been applied in about 45 different satellites and 4 test airships. No failures on orbit have been reported.

1n 1997 a Telstar (DFH-3) were launched successfully in China, and there were thirteen aluminum-ammonia axially grooved heat pipes used in the thermal system. Eight of them were used as pre-buried heat pipes, and the others were used as surface-installed heat pipes. The flight data indicates that these heat pipes have been working in the orbit successfully. For the large scale communication satellite (DFH-4), the heat load is up to 9000W. Then heat pipe network (pre-buried heat pipes and surface- installed heat pipes were used together to form heat transport network) has to be used in the thermal control of the controlled board.

The FY-2 launched in June, 2000 is a spin-stabilized satellite with 100r/m rotate speed. The control board vertical to the spin axis was pre-buried with eight aluminum-ammonia axially grooved heat pipes. Showed as Fig.18, the control board is an aluminum honeycomb (Diameter,2m). Heat pipes were pre-buried in the side where the apparatus installed (Fig.19). Considering the influence of the spin (100r/m) on the heat pipes, the radius of evaporation part must larger than the radius of condensation part, and this can be achieved though some offset to the control board center. The maximal heat transport capacity of each heat pipes is 64W·m at 20℃. The ground test showed us that the maximal temperature difference in the control board was less than 3℃ when the heat load of each apparatus was 0~25W. The orbit data showed that the maximal temperature between apparatus was less than 4℃。

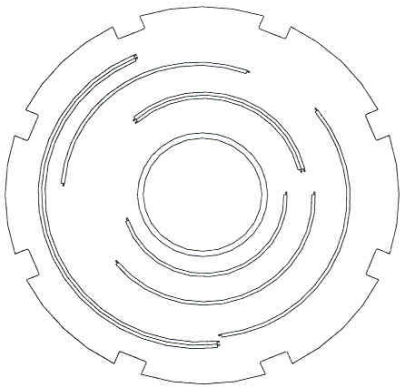


Fig.18 Position of Pre-buried Heat Pipes in the Control Board

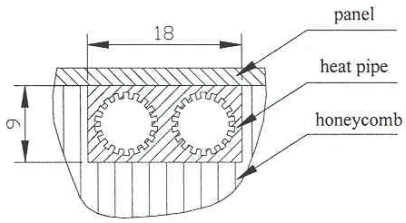


Fig.19 Heat pipes pre-buried in the Honeycomb

In October 2002, the flexible heat pipe was used in satellite for the first time in China. The experimental results and the telemetric data showed the application was successful.

5 Conclusion

Two typical aluminum-ammonia axially grooved heat pipes applied in China aerospace field are introduced in this paper. The test subject and test apparatus about heat pipes are introduced briefly too. Developing of other kinds of heat pipes are summarized, such as loop heat pipe, flexible heat pipe, miniature heat pipe, gas-controlled heat pipe, cryogenic heat pipe, etc. Applications of aluminum-ammonia axially grooved heat pipes in

China satellites are presented.

Reference

[1]Cao Jianfeng, Shao Xingguo, Liu Zijun. "Design and Tests of Flexible Heat Pipes". 12th International Heat Pipe Conference, May 19-24,2002, Moscow.

[2]C.Hoa, B.D.emolder, A.Alexandre. "Roadmap for Developing Heat Pipes for ALCATEL SPACE's Satellites". 12th International Heat Pipe Conference, May 19-24,2002, Moscow.

[3] Jianyin Miao, Xingguo Shao, Tinghan Li. "Experimental Study on Single-Groove Heat Pipe". 12th International Heat Pipe Conference, May 19-24,2002, Moscow.

[4]V.Barantsevich, O.Golovin K.Goncharov, A.Orlov. "Investigation Performance of Axial Grooved Heat Pipes with High Thermal Capacity". 12th International Heat Pipe Conference, May 19-24,2002, Moscow.

Thermosyphon as an Energy Saver in Aeroponic System: A Case of Mathematical Modeling

N. Srihajong, S. Ruamrungsri, P. Terdtoon, P. Kamonpet, and T. Ohyama*

Department of Mechanical Engineering, Faculty of Engineering
Chiang Mai University 50200, Thailand
Tel: +66 53 94 4151 Fax: +66 53 22 6014 Email: Narong_sri@hotmail.com
*Faculty of Horticulture, Niigata University, Japan

Abstract

This project presents an establishment of a mathematical model explaining the operation mode of and aeroponic system for agricultural products. It consists of the greenhouse for temperature control with evaporative cooling and the refrigeration unit for temperature control of nutrient. High energy of reduce the temperature is needed due to high the heating load of greenhouse and refrigeration systems. The purpose is to study the rate of energy consumption and the feasibility to employ heat pipe as an energy saver. Application of thermosyphon (T.S) is remove heat from the wall of greenhouse before entering into the greenhouse. So, the cooling load of evaporative cooling is decreased, and remove heat from the nutrient that move out of the chamber of an aeroponic system. When the evaporator receives heat from the nutrient, the working fluid evaporates into vapor and flows to condense at the condenser section. The outlet temperature of nutrient from evaporator section is, therefore, decreased. A computer program that can simulate the heat transfer performance of the thermosyphon of aeroponic systems was created and was used to simulate the established program with the in-situ data and to find out the most appropriate design for the normally available aeroponic system. The results of simulation were obtained. It can be seen from the simulation when thermosyphon is installed, that the heating load of greenhouse decreases of 14.23 kW, 36.45%. Also the energy efficiency ratio(EER) of refrigeration unit increase of 2.0 Btu/h/W, 14.28%.

Key words: Aeroponic system, Energy saver, Thermosyphon

1 INTRODUCTION

At present, Thailand is an agricultural country and trying to be one of the newly industrialized countries. The agricultural industry is an important factor to increase an income of agriculturist and country. In case of the agricultural productivity process, the media-free planting system is widely accepted that it can efficiently increase the production rate.

The media-free planting systems have two types, hydroponic and aeroponic systems [6]. The aeroponic is a media-free planting system whereby the roots of the plants are completely or partially exposed to the air. The plants are anchored in holes, atop a panel of polystyrene foam. From a sealed trough below, a fine-mist of soluble nutrient is sprayed and it adhered to the roots. Most of systems that are applied to control the greenhouse and nutrient temperature are evaporative cooling and refrigerant system, [2,3]. The greenhouse is covered with polyethylene film. This system is based on air suction from greenhouse by using exhausted fan. But in this system, the fan and evaporative cooling must always work so the electrical energy consumption is high as a result.

For the nutrient passes through the chamber, its temperature will unavoidably increase due to the thermal mass of the plant. In order to maintain the temperature of nutrient at its specified level, an additional refrigeration system is needed. This leads to higher energy consumption in the system, resulting in the higher investment cost and also the operating cost for all agriculturalists. Thus, there should be a device that can reduce the energy of evaporative cooling of greenhouse and refrigeration system. The thermosyphon is chosen as the device to save the energy in the system.

The application of thermosyphon in aeroponic system can be shown as schematic diagram in Figure 2. Namely, the heat pipe is applied to remove heat from the nutrient exiting the chamber by the thermosyphon at its evaporator section. The outlet temperature of nutrient from evaporator section is, therefore, decreased. And

the heat pipe can be also used to remove heat from the wall of greenhouse before moving into the greenhouse. The cooling load of evaporative cooling is decreased. The aeroponic system with an integrated heat pipe employed to reduce the energy consumption has more advantage than the general type i.e. lower consumption of electrical energy. This is because there is heat rejection from the nutrient i.e. the working fluid is used to remove heat from the evaporator section up to condenser section. This kind of energy reduction method employs no external mechanical energy. Therefore, if the investigation is seriously worked, it will results in energy saving in agricultural industry and also decreasing budget of agriculturists

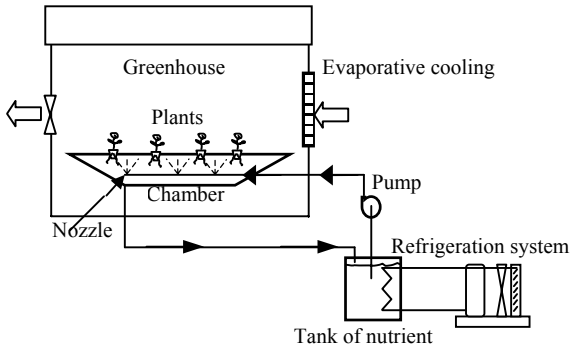


Figure 1 Conventional of aeroponic system.

2.MATHEMATIC MODELING

Figure 1 shows the diagram of the aeroponic without thermosyphon, in which the air is sucked passed evaporative cooling, inside of the greenhouse and the air is sucked by fan. And the nutrient passed refrigeration system, pump, chamber and returning nutrient to refrigeration system.

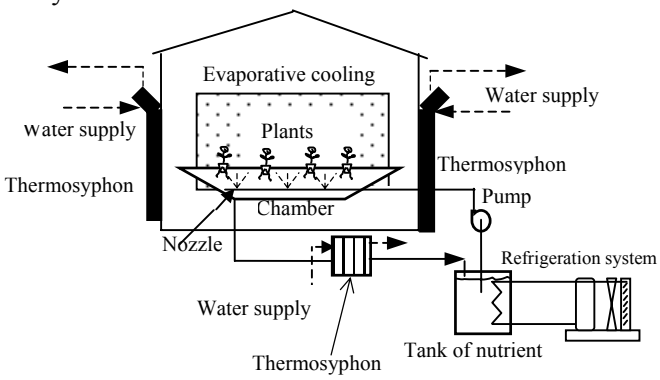


Figure 2 Aeroponic system with thermosyphon.

Figure 2 shows the aeroponic with thermosyphons, in which the thermosysphon is applied to remove heat from the wall of greenhouse so that reduce the energy of evaporative cooling system and remove heat from the nutrient so that reduce the energy of refrigeration system. We will establish program, which simulate these two systems and find out the most appropriate design.

2.1 Numerical formulation

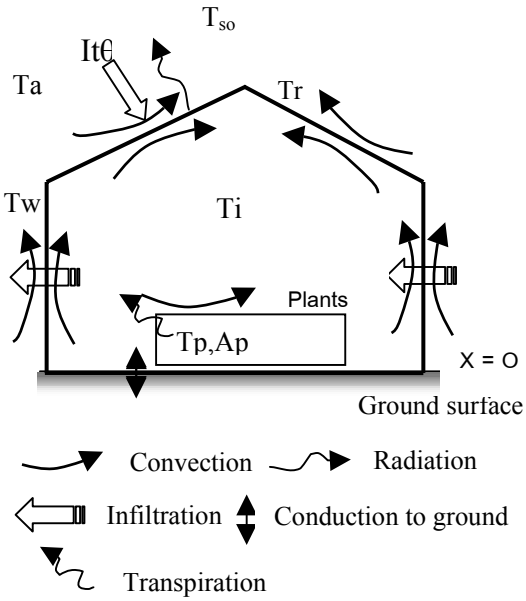


Figure 3 Schematic diagram of greenhouse.

Figure 3 shows the thermal energy balance of the greenhouse. The heating load of greenhouse from solar radiation passes through wall and roof of greenhouse from which it absorbs heat and the remaining solar radiation will pass into the greenhouse. The temperature different, which varies by time, heat convection, radiation, can be determined by using the following equations [4];

$$Q_{gh} = \begin{bmatrix} \sum Q_{wall} + \sum Q_{roof} - Q_{inf/\,vent.} - Q_{evap} \\ -Q_g - Q_{plant} - Q_{chamber} \end{bmatrix} + \tau_g \alpha_a \left(\sum It\theta_w A_w + \sum It\theta_r A_r \right) \quad (1)$$

where Q_{wall} is the heating load of wall which is given by

$$Q_{wall} = \rho_w C_w V_w \frac{dT_w}{dt} = \begin{bmatrix} (\alpha It\theta_w) + h_{cwo}(T_a - T_w) \\ -h_{rwo}(T_{so} - T_w) + h_{cwi}(T_i - T_w) \end{bmatrix} A_w \quad (2)$$

Q_{roof} is the heating load of roof which is given by

$$Q_{roof} = \rho_r C_r V_r \frac{dTr}{dt} = \begin{bmatrix} (\alpha It\theta_r) + h_{cro}(T_a - T_r) \\ -h_{rro}(T_{so} - T_r) + h_{cri}(T_i - T_r) \end{bmatrix} A_r \quad (3)$$

$Q_{inf/vent}$ is the infiltration/ventilation of greenhouse which is given by

$$Q_{inf\,il\,/\,vent.} = 0.5 V_i N (T_i - T_a) \quad (4)$$

Q_{evap} is the heating load of evaporative cooling

$$Q_{evap} = \rho_a C_{pa} V_r (T_a - T_i) + \rho_a V_r \left[w_a (h_{ga} - h_{gi}) - w_i (h_{gi} - h_{gw}) \right] \quad (5)$$

Q_g is the heat transfer of ground which is given by

$$Q_g = \left[\frac{K_g A_g}{L} \right] (T_i - T_g) \quad (6)$$

Q_{plant} is the heat transfer of plants which is given by

$$Q_{plant} = \left[\frac{\rho_a cp_a (e_{s,Tp} - e)}{\gamma (r_s + r_{a,H_2o})} + \frac{\rho_a (T_p - T_i)}{r_{a,H}} \right] A_p \quad (7)$$

and Q_{ch} is the heat transfer of chamber which is given by

$$Q_{ch} = Q_{convect} + Q_{plant} + Q_{It\theta_in} = h_C A_C (T_c - T_i) + Q_{plant} + \left[(aIt\theta_{out} + bIt\theta_{out}^2) A_C \right] \quad (8)$$

For the refrigeration system the evaporator, compressor and condenser model can be derived. The details are as follow;

The condenser model can be developed by the principle of energy conservation [5]. It is given by

$$Q_c = Q_e + P_C \quad (9)$$

The evaporator model can be derived from equations of heat transfer by the principle of mass and conservation [5].

$$Q_e = b_1 + b_2 T_{er} + b_3 T_{cr} + b_4 T_{er}^2 + b_5 T_{cr}^2 + b_6 T_{er} T_{cr} + b_7 T_{er}^2 T_{cr} + b_8 T_{er} T_{cr}^2 + b_9 T_{er}^2 T_{cr}^2 \quad (10)$$

The compressor model is given by

$$P_c = a_1 + a_2 T_{er} + a_3 T_{cr} + a_4 T_{er}^2 + a_5 T_{cr}^2 + a_6 T_{er} T_{cr} + a_7 T_{er}^2 T_{cr} + a_8 T_{er} T_{cr}^2 + a_9 T_{er}^2 T_{cr}^2 \quad (11)$$

The coefficient of performance (COP) of refrigeration system is refrigeration capacity (W) per compressor power (W), it can be written as

$$COP = \frac{Q_e}{P_c} \quad (12)$$

and the energy efficiency ratio (EER) of refrigeration system is theoretically refrigeration capacity per hour (BTU/h) per compressor power (W).

$$EER = \frac{3.6 Q_e}{1.055 P_c} \quad (13)$$

For the heat transfer of thermosyphons was computed by according to the principle to the total internal thermal resistance of the T.S.

The diagrams showing the calculated daily heating load and temperature of the greenhouse and refrigeration system were present in Figure 4. The input data are as follows: day, month, Ti_set, length of chamber, number of plants.

2.2 The conditions of program simulation

The mathematical model has been solved with the help of a computer program based on Matlab software version R12. The conditions of simulation program are as follow;

- The size of greenhouse of 12x4x4 meter.
- The greenhouse temperatures of 25 ^oC, 30 ^oC and 35 ^oC.
- The nutrient solution temperatures of 20 ^oC, 25 ^oC and 30 ^oC.
- The chamber length of 3 meter.
- The 1.5 Hp hermetic compressor and operates with 12500 Btu/h evaporator.

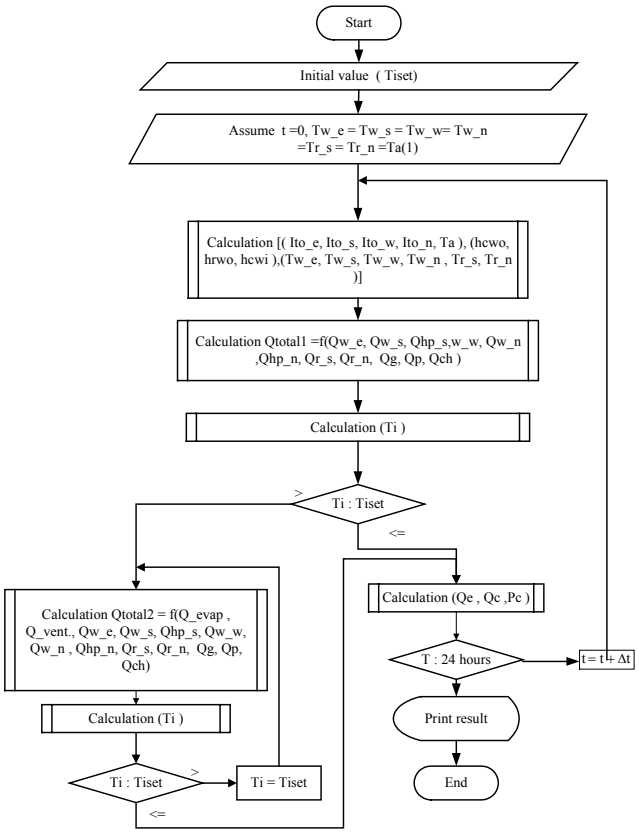


Figure 4 Schematic diagram of greenhouse.

The conditions of simulation program normally used in Thailand. Plants can be well grown in these conditions.

3. RESULTS AND DISCUSSION

3.1 Daily heating load of greenhouse

Figure 5 shows the daily heating load of greenhouse without themosyphon from 0.00 h to 24.00 h. Daily heating load of greenhouse is taken for days of the months of April because April is the hottest month in Thailand. The controlled temperatures of greenhouse (Ti_set) are 25, 30 and 35 ^{o}C, respectively. It can be seen that at Ti_set of 25 ^{o}C and from 0.00 h to 6.00 h, the heating load is low and at 6.00 h to 12.00 h the heating load gradually increases. After that the heating load gradually decreases and it is constant from 18.00 h to 24.00 h. The maximum heating load of greenhouse is 39.23 kW. For at Ti_set 30 and 35 ^{o}C, the heating loads are lower than at Ti_set 25 ^{o}C. The maximum heating loads are 37.12 kW and 34.64 kW, respectively. Because this research is new research that can not be compared with other research, but it will tendency for further research.

It can be concluded that at Ti_set 25 ^{o}C the maximum heating load is 39.23 kW and when Ti_set increases the heating load decreases.

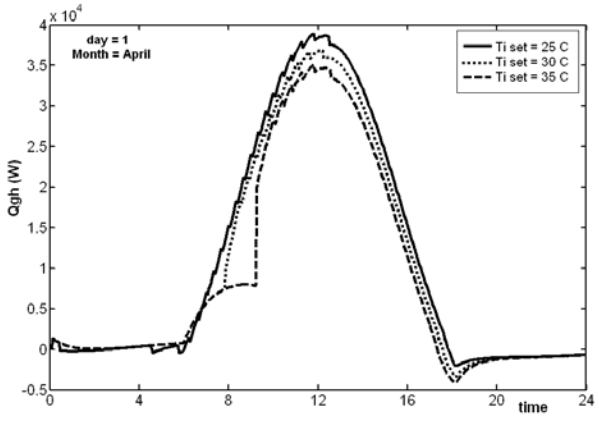


Figure 5 The daily heating load of greenhouse without themosyphon from 0.00 h to 24.00 h, Day =1, Month = April.

3.2 Daily heating load of refrigeration unit

Figure 6 shows the daily heating load of refrigeration unit without thermosyphon at the Ti_set of greenhouse is 35 ^{o}C. The controlled temperature of nutrient,(Tw_set) are 20, 25 and 30 ^{o}C, respectively. It can be seen that at the Tw_set of 20 ^{o}C the Qe, Qc and Pc of the refrigeration system are highest, 156 kW-h, 198 kW-h and 42 kW-h, respectively. Due to high the nutrient temperature passes through the chamber also the refrigeration system use high energy into the temperature reduce is needed. And when the Tw_set increases the heating load of the refrigeration system gradually decreased. Then at Tw_set is 25 ^{o}C, it is optimum Tw_set. Because this Tw_set, the refrigeration system will use low energy. These findings agree with the results of Jie et al.(2001). It was seen that, most of grow plants is temperature between 20 to 25 ^{o}C.

It can be concluded that at Tw_set of 20 ^{o}C the heating load higher than the Tw_set of 25 and 30 ^{o}C.

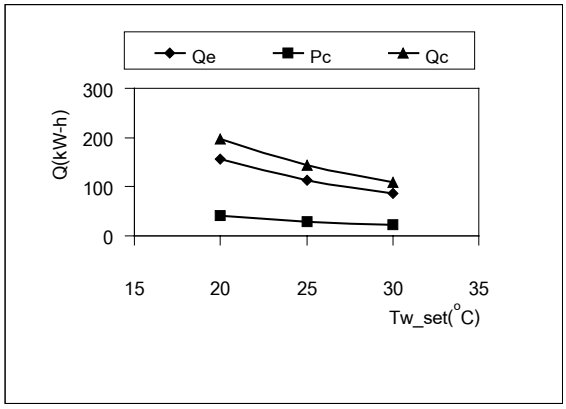


Figure 6 Nutrient temperature, (Tw set) with daily heating load of refrigeration system, Day =1, Month = April and Ti_set of 35 ^{o}C.

3.3 Thermosyphon design

The thermosyphon designs has two parts, energy server of greenhouse and of the nutrient passes though chamber before into the nutrient tank. The optimum condition of heat transfer rate of the thermosyphon is achieved by cost for construction, E by C. At Ti_set of 25 ^{o}C, the heating load of greenhouse is the highest and Tw_set of refrigeration system of 25 ^{o}C is the optimum point of refrigeration system. It is condition to design thermosyphon. It was found from the simulation program that thermosyphon will be installed at south and north walls of greenhouse with the diameter 25.4 mm OD. 61 tube will be installed at the south wall and 30 tube at the north wall. The length of evaporator and condenser sections are 1500, 200, 300 mm, respectively which made of copper tube, will be used working fluid is R-134a. Its filling ratio is 50% of the evaporator. And the thermosyphon design for nutrient before passing into the tank

was 15.7 mm OD in size with, 35 tube. The length of evaporator and condenser sections of 200, 100, 200 mm, respectively. Copper tube will be employed with R134a as working with filling ratio of 50%.

3.4 Energy saving by thermosyphon installation

Figure 7 shows the saving of heating load at the wall of greenhouse with and without thermosyphon from 0.00 h to 24.00 h, with Ti_set of 25 ^{o}C. It can be seen that, at the south wall of greenhouse, thermosyphon can decrease the heating load from 550 W/m^2 to 300 W/m^2. Figure 8 shows heating load of greenhouse with and without thermosyphon. It can be seen that the heating load decrease from 39.23 kW to 25.1 kW which means the heating load of greenhouse can be reduced as 14.3 kW, or 36.45 %.

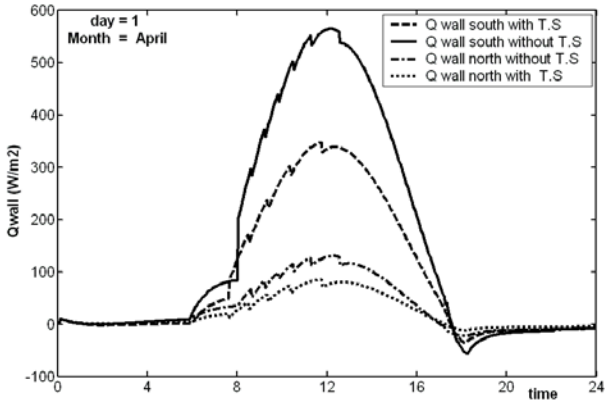


Figure 7 the heating load at the wall of greenhouse with and without thermosyphon from 0.00 h to 24.00 h, Day =1, Month = April.

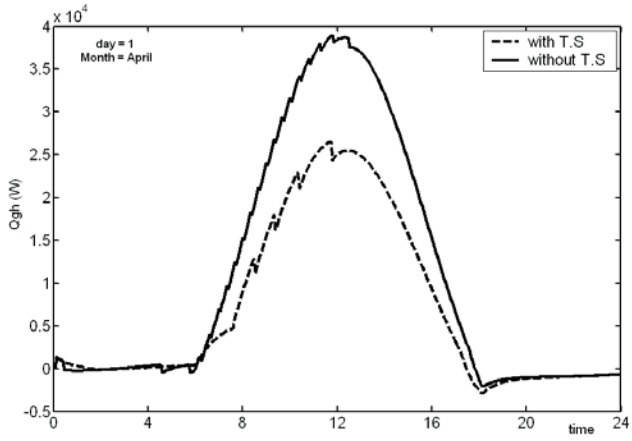


Figure 8 the heating load of greenhouse with and without thermosyphon from 0.00 h to 24.00 h, Day =1, Month = April.

Figure 9 and 10 show the coefficient of performance (COP) and Energy efficiency ratio (EER) of refrigeration system at any time with the Tw_set of 20 ^{o}C and Ti_set of 35 ^{o}C. It can be seen that at 8.00 h to 24.00 h the coefficient of performance and energy efficiency ratio of refrigeration system with thermosyphons are much higher than the one without thermosyphon about 0.5, or 12.5% and 2.0 (Btu/h)/W, or 14.28%, respectively.

It can be seen that, the greenhouse with thermosyphon can reduce heating load of 36.45%, and the COP and EER of refrigeration system increase of 12.5%, 14.28%, respectively.

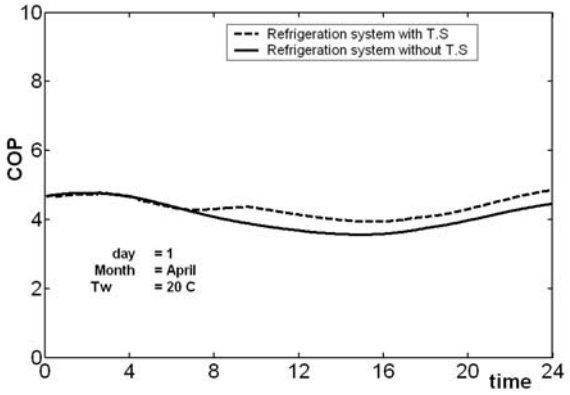


Figure 9 the coefficient of performance (COP) of refrigeration system from 0.00 h to 24.00 h, Day =1, Month = April, Tw_set of 20 ^{o}C and Ti_set of 35 ^{o}C.

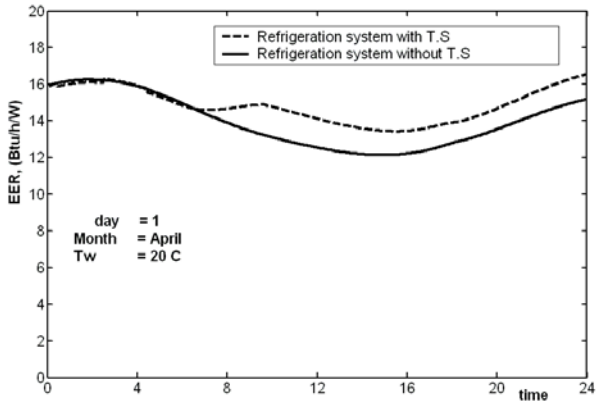


Figure 10 the energy efficiency ratio (EER) of refrigeration system from 0.00 h to 24.00 h , Day =1, Month = April , Tw_set of 20 ^{o}C and Ti_set of 35 ^{o}C.

4. CONCLUSTIONS

The optimization of the thermosyphon for aeroponic system in this research has been found as follows;

- Ti_set is 25 ^{o}C, with the maximum heating load of 39.23 kW.
- The themosyphon can save energy of greenhouse from 39.23 kW to 25.1 kW or 36.45%.
- The thermosyphon can increase the COP of refrigeration system about 0.5 or 12.5%.
- The thermosyphon can increase the EER of refrigeration system about 2.0 (Btu/h)/W or 14.28%.

Acknowledgements

This research was conducted under the Royal Golden Jubilee Scholarships of Thailand Research Fund (Contract No. 1.M.CM/45/A.1). The authors would like to express their sincere appreciation for all of the support provided.

Nomenclature

A area, (m^2)
a_1 to a_9 constant values.
b_1 to b_9 constant values.
C_p specific heat, (J/kg ^{o}C)
COP coefficient of performance of refrigeration system.
EER energy efficiency ratio of refrigeration system (BTU/h)/W
h heat transfer coefficient, (W/m^2 ^{o}C)
h_g enthalpy of saturated water vapor, (kJ/kg)
$It\theta$ solar radiation, (W/m^2)
K_g thermal conductivity of soil, (W/m^{o}C)
L length, (m)
$e_{s,Tp}$ saturated vapor pressure of air at the leaf temperature, (mmbar)
e water vapor pressure of free air, (mbar)
m mass flow rate, (kg/h)
P power consumption in the compress, (kW)
$Q_{inf/vent}$ sensible and latent heat infiltration, (W)
Q heat loss, (W)
rs stomatal resistance, (s/m)
r_{a,H_2O}, $r_{a,H}$ boundary layer resistance (reciprocals of conductance) to movement of water vapor and heat, (s/m)
rs stomatal resistance, (s/m)
T temperature, (^{o}C)
V_a volumetric airflow rate, (m^3/h)
w humidity ratio, (kg_w/kg_a)

Greek letters
ρ density, (kg/m^3)
α_a absorptivity of air in the greenhouse
τ_g transmissivity of cover
γ psychometric constant, (Pa/^{o}C)

Subscripts
1 inlet
2 outlet
a air or ambient air
c convection
ch chamber
e east and evaporator
cr condenser of refrigeration system
er evaporator of refrigeration system
g ground or floor of greenhouse
i,o inside and outside
M mass
n, s north and south
p plants
r roof
t temperature
w wall and west
gw saturated water vapor at thermodynamic

References

1. Jain, D., Taiwari, G.N., *Modeling and optimal design of ground air collector for heating in controlledenvironment greenhouse.* Energy Conversion &Management, Vol.44, 2003, pp. 1357-1372.
2. Jie, H., L.S.Kong., *Growth and photosynthetic responses of three aeroponically grown iettuce cutivars (Lactuca sativa L.) to different rootzone temperatures and growth irradiances under tropical aerial conditions.* Journal of the Korean Society for Horticultural Science, Vol. 152, 2001, pp. 387 – 389.
3. Lim,M., Lee, S. K., *Pilot scale culutivation cultivars of iceberg lettuce (Lactuca sativa L) using aeroponic system through root-zone cooling*. Singapore Journal of Priimary Industries, Vol. 24, 1996, pp. 11-17.
4. Prasomsub, J., Thepa, S., *Feasibility of Evaporative Cooling Application in Flower's Geenhouse*. Mater of science, Energy Technology, KMITT University, Thailand, 1998.
5. Stoecker, W.F., Jones, J.W., *Refrigeration and Air conditioning.* 2nd Edition. New York, McGraw-hill, 1982, pp. 281-293.
6. Yang, W.M.,Chung, S.J. and Kim, Y.D., *Comparative studies of the Physioecological and morphological adaptation of greenhouse tomato grown using aeroponics and nutrient film technique.III. Characteristics of physioecological adaptations.* Korean Society for Horticultural Science, 1989.

Numerical Simulation for the Thermal Design of 1U-2Way Server

Myong-Hee Won*, Woo-Seok Moon **, Byung-Joon Baek***, and Bock-Choon Pak****

* APACK, Inc., 59-6, Hwaam-dong, Yusung-ku, Daejon, 305-348, KOREA
Tel. +82-42-864-0815, Fax. +82-42-862-9815, mhwon@apack.net
** Graduate School, Dept. of Precision Mech. Eng., Chonbuk National University
*** Automobile Hi-Technology Research Center, Engineering Research Institute, Chonbuk National University
**** Division of Mechanical Engineering, Chonbuk National University

Abstract

In this study, the new heat pipe heat sink module are developed for the cooling of AMD Opteron Processor installed in 1U-2Way server, and the thermal performance is compared with that of heat sink type cooler in common use. The numerical simulation is performed by using the ICEPAK 4.0, computer code used exclusively for the heat and flow predictions in electronic package and compared with some experimental results for the validation of calculation. The higher temperature of CPU located far from the fan for common heat sink type cooler can be reduced remarkably by using heat pipe connecting CPUs and there is little difference between the two CPUs in the temperature. Temperature of RAMs, however, is not affected by the existence of heat pipe. In case of heat pipe heat sink module, location of fan could be moved toward the RAMs to cool down without much increase in CPU temperature. Relatively uniform temperature distribution in RAM surface was also obtained in this case.

Key words: CPU, cooling, heat pipe, heat sink

1. INTRODUCTION

Increased miniaturization of microelectronic components and chip clock speed has caused the heat dissipation to increase drastically. The temperature due to this increased heat dissipation can significantly affect on the component reliability. Also, a demand on the system performance and reliability has increased the needs for a better thermal management on electronic equipment.

Recent developments in the area of IT like internet require that PC need to be capable of processing more data with a high speed. To meet this requirement, high-performance devices built in PC have been developed. Especially, CPU shows competitive release of more speedy products and shift toward being more compact and thinner. This leads to higher heat density and increased heat dissipation, making CPU temperature rise and causing the shortened life, malfunction and failure of CPU. Cooling of CPU has been taken seriously. Pentium 4 CPU and Athlon XP, released by Intel and AMD respectively, have high heat dissipation, requiring excellent cooling performance. For example, 2GHz Pentium 4 processor made in 0.18㎛ manufacturing process has TDP(Thermal Design Performance) 75.8 W, requiring cooling performance 0.47 °C/W (@40 °C). 2GHz Pentium-IV Processor made in 0.13㎛ manufacturing process has a little lower TDP 52W and requires cooling performance 0.53 °C/W (@40°C). However, cooling is still a serious problem. AMD CPU has the same serious cooling problem [1].

With appearance of high-performance CPU requiring high cooling performance, cooling methods have shown many changes. Conventional CPU cooling used normally extruded aluminum heat sink showing superiority in terms of unit price, weight and performance. As CPU heat dissipation has been on the gradual incline and computer has shifted toward being compact, heat sink has limited cooling performance in the insufficient space. Therefore application of heat super-conductive heat pipe is considered seriously. Water cooler has been developed energetically to cause no acoustic noise [2].

Heat sink with high performance to price is still preferred by PC makers and enjoys dominance, but it uses fan with high revolution speed to solve the problem of limited cooling capacity, making acoustic noise attract attention [3].

In this study, the new Heat Pipe Cooling

Module (Fin Stack Type) and the Heat Pipe Heat Sink are developed for the cooling of AMD Athlon 64 Processor installed in 1U 4way server, and the thermal performance is compared with that of Heat Sink Type Cooler in common use. The numerical simulation is performed by using the ICEPAK 4.0, computer code used exclusively for the heat and flow predictions in electronic package and compared with some experimental results for the validation of calculation.

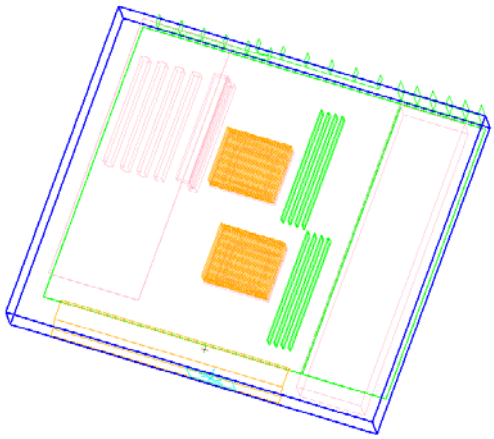
2. NUMERICAL MODEL

The numerical simulation is performed by using the ICEPAK 4.0, computer code used exclusively for the heat and flow predictions in electronic package and compared with some experimental results for the validation of calculation. Two types of cooling modules shown in Fig.1 are used as computational model. Fig.1 (a) shows the heat sink type cooler in general use and Fig,1 (b) illustrates the newly proposed "heat pipe heat sink" module. The typical heat sinks are attached on CPU with 90W/each heat generation rate (Fig.1). Heat sinks (base, fin), two CPUs, 8 RAMs, main and sub. board, CPU socket, PCI slot, dummy board and CPU substrate are installed in 434x375x41mm^3 case. Heat sink consists of 50 fins with 0.3mm thickness. Base and fins are made of copper. The thermal properties and materials used for simulation are shown in following table.

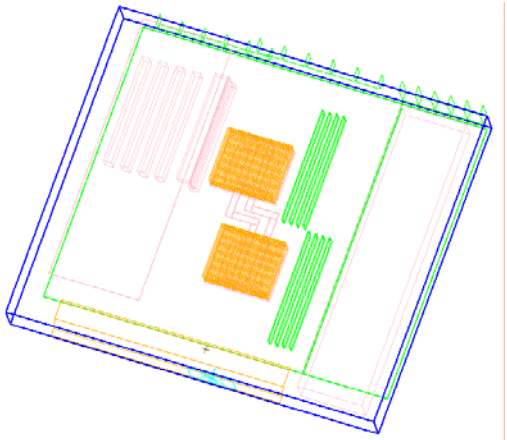
Fig.2 is fan characteristic curve which the numerical calculation is used.

Table 1 Materials and thermal properties

Material	Desnsity (kg/m^3)	Specific heat (J/kg-K)	Thermal Conductivity (W/m-K)	Components
Air@300K	1.1614	1005	0.0261	-
Copper	8940.6	385	390.88	heat sink (base, fin)
Epoxy-glass fiber	1900.0	795.0	0.17	main & sub board, RAM dummy board, CPU substrate
Mylar (Polyester)	1309.3	1182.8	0.16	CPU socket PCI slot
Aluminum 2024-T6	2770.0	875.0	177	cable duct
Ceramic @373K	3970.0	910.0	15	CPU die
Heat Pipe	-	-	30000	heat pipe



(a) heat sink type



(b) HPHS type (heat pipe heat sink module)

Fig.1 Configuration of numerical model

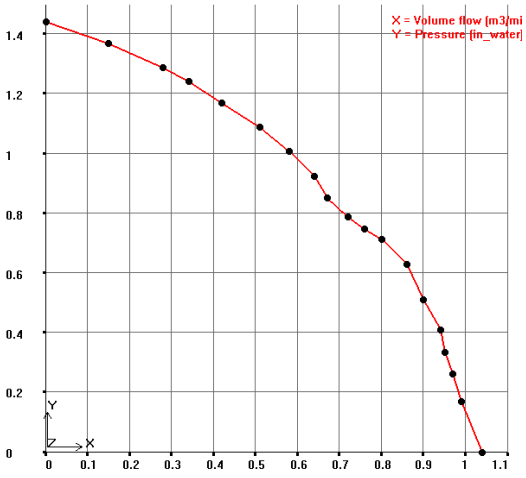


Fig.2 Fan characteristic curve

2-1 Heat generation of each component

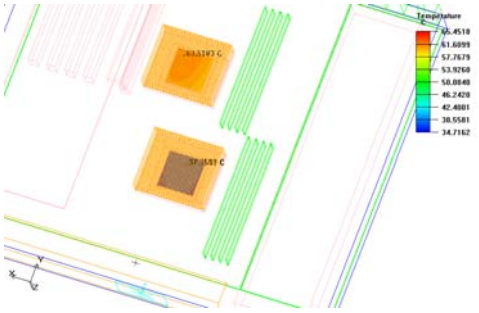
Heat generation of CPU1, CPU2 is 90W/each, and that of RAM is 10W/each. It was assumed that all the component except CPUs and RAMs are dummy, which have no heat generation, but exert only the flow resistance.

2-2 FAR (Free Area Ratio) of rear vent

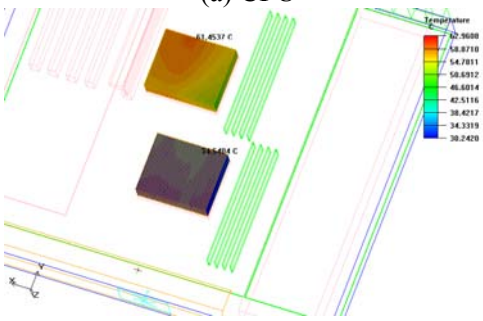
The rear side of 1U server is composed generally of many ports which are connected to different device. It has also many hole so that an inside air is flowed out. The pressure drop happens when the fluid flows through the hole. We must find the value of FAR to perform the numerical calculation about rear part. The FAR is the ratio of the area through which the fluid can flow unobstructed to the total planar area of the obstruction. The rear vent of 1U server is composed of 3 areas and each FAR value is the 0.71, 0.73 and 0.66.

3. RESULT AND DISCUSSION

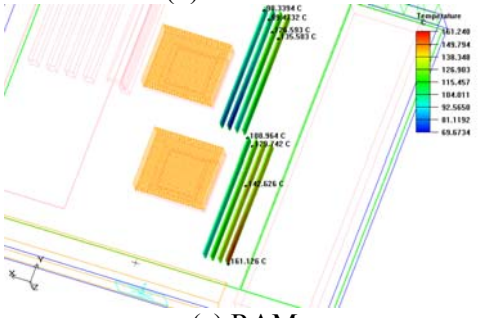
The cooling performance of common "heat sink type" cooler on the AMD Athlon 64 processor was simulated and compared with that of newly proposed "Heat Pipe Heat Sink" module.



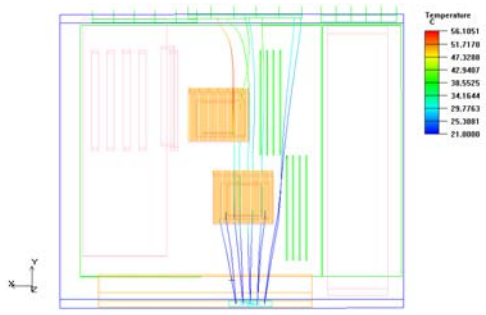
(a) CPU



(b) Heat Sink



(c) RAM



(d) Flow pattern of air

Fig.3 Contour of surface temperature and flow pattern of air

Fig.3 shows the contours of surface temperature and flow pattern of air induced by the cooling fan for heat sink type cooler. The surface temperature of CPU1 near the fan shows uniform and about 26℃ lower temperature than that of rear side of CPU2. There exists no big difference between surface temperature of heat sink and CPU in Fig.3 (b). The surface temperature of RAM surface (Fig.3 (c)) varies from 98.3℃ to 161℃, which represents the influences of air flow as shown in Fig.2 (d). The RAM1 located at dead zone of air flow at the bottom right shows the elevated temperature.

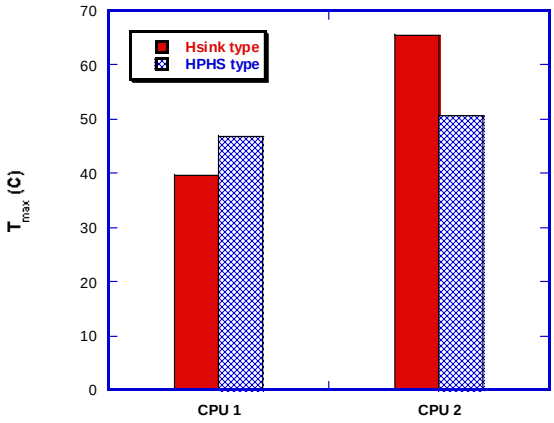


Fig. 4 Maximum temperature of CPUs

Fig.4 shows the effect of heat pipe on the maximum temperature of CPU. The maximum temperature of CPU2 with heat sink shows higher temperature of 66℃ than that of CPU1 of 40℃(ΔT=26℃), due to the fact that the cooling air from inlet is heated through the movement of heat sink of front CPU1. This temperature differences might be decreased by using the heat spreading frames connecting both CPUs and spreads heat from CPU2 to CPU1, which is easy to cool down by direct inlet flow through the fan. Two heat pipes (7.4mm width, 4mm thickness) are

used as a heat spreading frames with high thermal conductivity in this study. As a result, the temperature of CPU2 (rear) reduced remarkably and the temperature of both becomes similar each other.

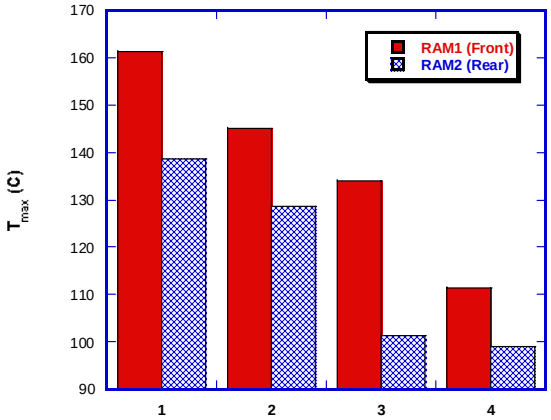


Fig.5 Maximum temperature of RAM for heat sink type

Fig.5 represents surface temperature RAM1 (front) and RAM2 (rear) for heat sink type. Most of the air from the inlet passes through CPU and RAM2, therefore temperature of RAM2 is relatively higher than that of RAM1, especially 3rd and 4th row. The RAM1 located at dead zone of the row at the bottom right shows the elevated temperature compared with the temperature of RMA2.

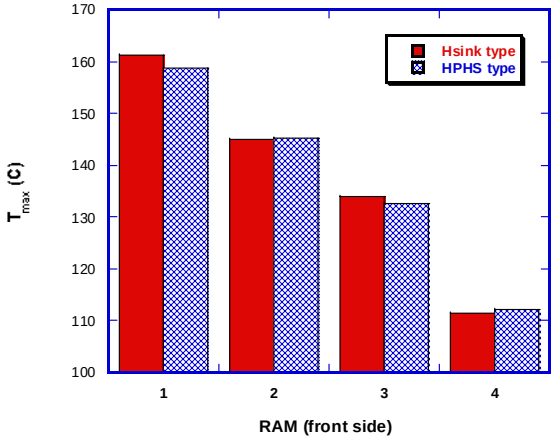


Fig.6 Maximum temperature of RAM1

Fig.6 represents the effect of heat frames on the temperature of rear side of RAM. The temperature of RAM near the CPU is relatively low due to the less flow resistance. It is not surprising that the heat pipe located between CPU1 and CPU2 do not make any considerable effect on the RAM temperature.

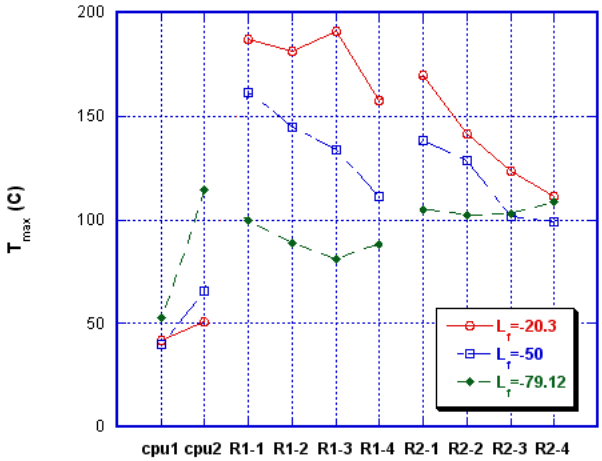


Fig.7 Effects of fan locations on the maximum temperature for heat sink type

Fig.7 shows the effect of fan location on the maximum temperature for heat sink type cooler. L_f represents the location of fan from the orgin of the system. When L_f =-50mm, the fan locates in front of the CPU1 and locates in front of the CPU2 at L_f =-20mm, respectively. Most of the inlet air flows over the CPUs at L_f =-20mm, therefore the temperature of each CPU is low and represents very small temperatrue difference ΔT=9.5℃. The temperatures of the RAM1 maintain high due to the stganation region of the flow and decreases steeply as the flow rate increases through the RAM behind CPU1. In case of L_f = -50mm, most of the flow directed to RAM2 and temperature differences of CPUs increase to ΔT=27.1℃ and RAM near the CPU maintains lower temperature than that of outside. As L_f moves to -79mm, temperature differences of CPUs increases remarkably to ΔT=61.7℃, however, RAM temperature reduces significantly and shows relatively uniform distribution.

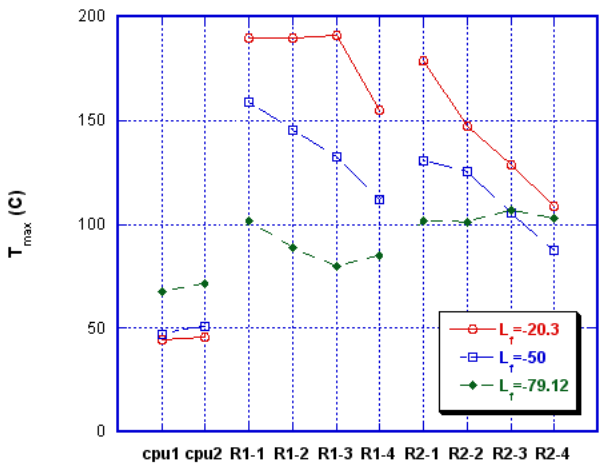


Fig.8 Effects of fan locations on the maximum temperature for heat pipe heat sink type

Fig.8 illustrates the effect of fan location on the maximum temperature for heat pipe heat sink type cooler. Temperature of CPU2 increases slightly from that of CPU1 due to heat spreading effect of heat pipe. As L_f moves from -20mm to -79mm, temperature differences of CPU is not so significant as shown in Fig.7, however, the RAM temperature decreases remarkably and mainain relatively uniform distribution. As a result, the location of fan could be adjusted to direct the inlet air flow toward the RAMs.

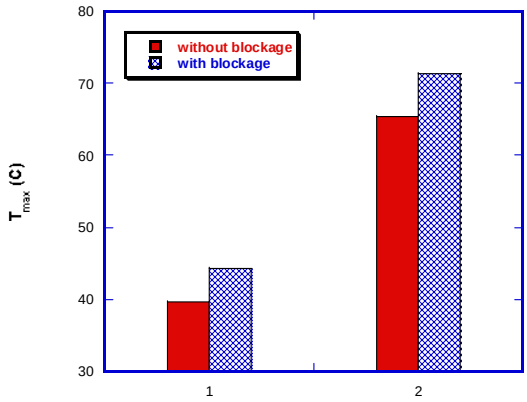


Fig.9 Effects of flow resistance on the maximum temperature of CPUs

Fig.9 shows the effect of flow resistance on the maximum temperature of CPU. The two blockages simulating cable duct, cables and several dummies were adapted as a flow resistance in front of the CPU1. 97mm x 50mm x 22mm dummy block is placed in front of the CPU1. It was shown that temperature rise grows to 6°C in CPU2 compared to 4.6°C in CPU1 due to the existence of blockage.

4. CONCLUSIONS

The numerical simulation was performed by using the ICEPAK 4.0, computer code used exclusively for the heat and flow predictions in electronic package. The cooling performance of common "Heat Sink Type" cooler and newly proposed "Heat Pipe Heat Sink" module was compared and can be summarized as follows.

1) The higher temperature of CPU located far from the fan for common heat sink type cooler can be reduced remarkably by using heat pipe connecting both CPUs and there is little difference between the two CPUs in the temperature. Temperature of RAMs, however, is not affected by the existence of heat pipe.

2) In case of heat pipe heat sink module, location of fan could be moved toward the RAMs to cool down without much increase in CPU temperature. Relatively uniform temperature distribution in RAM surface was also obtained in this case.

3) Only one fan (30cfm) was sufficient to cool the entire system by using heat pipe and choosing optimum fan locations in this study.

References

1. Frank P. Incropera, David P. Dewit, 1996, *Fundamentals of Heat and Mass Transfer, 4th Edn.*, John Wiely & Sons, Inc.

2. W. M. Kays, M. E. Crawford, 1983, *Conventional Heat and Mass Transfer*, McGraw-Hill

3. Krarus, A. D., Bar-Cohen, A., 1983, *Thermal Analysis and Control of the Electronic Equipment*, McGraw-Hill

4. Calvin C. Silverstein, 1992, *Design and Technology of Heat Pipes for Cooling and Heat Exchanger*, Hemisphere Publishing Corporation

5. Amir Faghri, 1995, Heat Pipe Science and Technology, Taylor & Francis

6. Koich Mashiko, Masataka Mochizuki, Yuji Saito, 1999, "Advanced Cooling System Combined with Heat Sink and Heat Pipe for Cooling PC," 11th IHPC vol.2, pp.75-79

Development and Application of Evacuated Tube Solar Collectors with Heat Pipe in Korea

H. Y. Kwak, J. H. Boo*, W. B. Chung*

New and Renewable Energy Research Department, Korea Institute of Energy Research(KIER),
hykwak@kier.re.kr
* Hankuk Aviation University

Abstract

This article introduces development and application of a evacuated tube solar collector (ETSC) with heat pipe in Korea. The ESTC for medium temperature uses anti-freezing heat pipe with woven-wire wick, titanium selective coating and glass-to-copper direct sealing, and "dry connection" between condenser of heat pipes and a manifold.
A field test was performed for the ETSC system that installed in beer works in Gwang-ju city. The system for process heat is consist of 2-ton buffer storage tank and collector modules (with 91.44㎡ collector area) and controller.
As the test results, the ETSC system satisfactorily operated even unfavorable condition unlike flat plate solar collectors. In a clear day, the ETSC system produced approximately 4.2 ton heated water of 85 C per day and showed 46% of mean system efficiency.

Key words: evacuated tube solar collector (ETSC), glass-to-copper direct sealing, heat pipe

1. INTRODUCTION

Solar energy is a quantitatively unlimited, clean and non-pollutant renewable energy resources. It has a great potential for industrial and commercial usages. For example, solar hot water system for domestic use has been very popular in many counties.
In Korea, the industries consume 47.7% of the total national energy, and the manufacturing sector uses 91.5% out of it.
The main energy resources available in Korea are oils, coals, and gases. There have been continuous efforts among the industries to reduce such energy consumptions by research and development technology for energy savings, yet the technology has limited to a level of satisfaction. In some advanced countries, research and development programs in solar energy applicable to the industrial uses are very active, and some systems are in the commercial market. It is, therefore, our purpose to develop the solar thermal systems that can provide necessary thermal energy for the industrial process heat. First, it is necessary to review the heat process of each industrial sector, which demands large amount of energy. Then, we need to identify the potential for energy savings assisted by a solar energy system for each sector, and modify the system(s) to maximize the efficiency. The refined and advanced solar systems may save a lot of energy used in the industries of high-energy demand. In addition, the information on these new technologies should be available to the policy makers and researchers to apply to many different areas.
Since the solar energy technology in the medium and high temperature applications can contribute to the clean environment by reducing the use of fossil fuel, and can also provide high-energy savings, this is very important research project. Recently, the Korean government has recognized such facts and classified this area as one of the very important subjects by putting it in a long-term research strategy.
For the medium temperature solar systems Korea Institute of Energy Research(KIER) with cooperation of APACK Ltd. have successfully developed a new type of ETSC with heat pipe, and have put into practical application in Korea.
As heat pipe technology is applied to evacuated tubes and heat transfer fluid of the collector does not have to pass through evacuated tubes, therefore the heat pipe ETSC has many advantages;
- Resistance to freeze
- Fast Start-up
- Low heat losses
- Resistance to high pressure
- Resistance to thermal shock

2. RESEARCH AND DEVELOPMENT

We have started R&D on the ETSC since 1998. These works mainly include manufacturing technology of ETSC and configuration design of collector modules. Achievements of R&D are

satisfactory and have been used for ETSC production.

2-1. Characteristics of ETSC

The advantages of the ETSC are as follows;
1) As vacuum techniques are applied, heat loss from absorber of solar collectors can be reduced, which means increased collector efficiency,
2) It adopted heat pipes that operate constantly in medium temperature ranges, and has quick thermal response and good thermal transportation,
3) Compared to concentrating collectors, it is more practical in Korea, as it utilizes diffuse radiation as well as directs one,
4) As the collector slope does not have a great impact on its performance, it can be applied onto building walls as an architectural element.
The new ETSC developed by KIER has larger dimensions with an outer diameter 102mm and a length of evaporator 1800mm as shown in Fig. 1.
The key technologies of ESTC are glass/copper tube housekeeper sealing, heat pipes, "dry connection" heat exchanger between condenser of heat pipe and a manifold, Tinox coating, and getter and others.

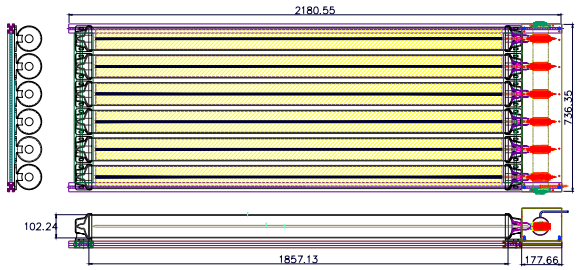


Fig. 1. Outline of ESTC Module

2-2 Glass-to-copper tube housekeeper sealing technology

KIER has developed a direct sealing method for vacuum sealing a heat pipe to a glass tube in an evacuated tube solar collector. It was known that the direct sealing method was represented by the sealing method, which was known as housekeeper or kruh seals(1,2). The direct seals of glass to copper tube are based either on the fact that the stresses developed in the glass are minimized by the deformation (elastic or plastic) of the metal or on the fact that the developed stresses are only compression (3).
It was known that for constructing the direct sealing having the glass inside and outside the metal, the thin edge of the copper tube is heated red hot in a flame and glass tube is pushed over the feather edge(1). Also, many tools have been developed to improve this complex process. However the principle know-how for process has never been revealed.

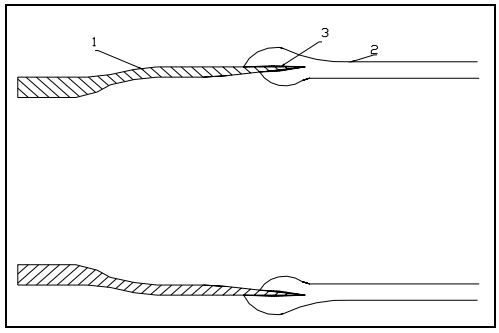


Fig. 2. Glass/copper tube housekeeper sea1

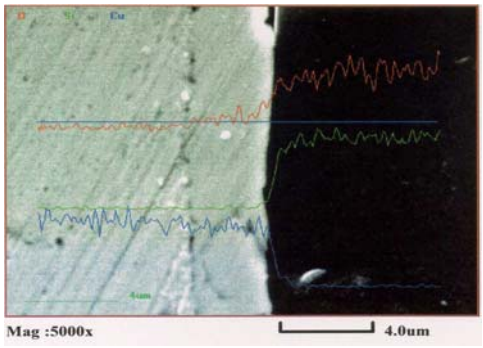


Fig. 3. SEM and EDS line on the cross section of glass/copper sealing interface

Fig. 2. shows a diagram where copper edge manufactured by drawing method is sealed to glass. The tip of copper tube was drawn with a thinner one than original thickness so that the tip thickness is ranging from 0.01mm to 0.07mm. The end of glass tube sealed to copper was preheated by using welding machine, which had both glass and copper tube holder of a high speed and jam and stretching function of copper toward glass tube, and was to be sufficiently softened above glass softening temperature.
For high temperature copper selective oxidation deficient environment, the end of copper tube, which was coated in borate slurry, was laid under helical type-coil induced by high frequency induction (HF) and was covered with a glass cap.
Fig. 3. shows the cross section of glass/copper tube sealing interface. The thickness of the newly formed interface layer was about 3?m, and this layer has an ability to endure the thermal stress as mentioned below. An EDS line profile of Cu shows this layer has major Cu composition. For Si element, no Si trace was found clearly on the section. But it is thought that this interface comprises of chemical reacting layer of major Cu2O and glass, considering an oxygen trace on interface

2-3 Heat Pipes for ETSC

For heat pipes with ethanol as a working fluid operating in a relatively high condenser temperature range of 80 to 150℃, an adequate wick geometry must be provided to ensure an operation against unfavorable condition.
A special working condition of an elevated condenser temperature may arise in such case as a solar collector for a medium-high temperature range. For this case, a heat pipe must be designed properly so that it may transfer a certain amount of heat to the abnormally hot condenser from the evaporator of which the relative temperature potential is not so high.
Among many wick structure candidates for this application, only screen wicks were considered. a slab wick was considered based on the promising performance and tested at the previous studies(4, 5).In addition, a woven-wire wick was selected and tested as one of the alternative wick structure candidates. A woven-wire wick is known to exhibit an improved capillary limit and retain a resilient force to keep itself tightly attached to the inner wall of the container. Another advantage of the woven-wire wick is the convenience in fabrication and low cost.
The total length of the heat pipe used in the experiment was 1.8m and the outer diameter of the condenser was varied with short axial length. The maximum outer diameter was 19mm and was reduced linearly to 15mm at the end of condenser. In Fig. 4, shows a heat sink structure that was dipped into the heat transferring fluid in the ETSC. Ten radial fins were soldered around the heat sink. The pipe material was copper and working fluid was ethanol. Several different kinds of heat pipes having enlarged condenser were fabricated: a slab wick heat pipe, a single layer and a double layer of woven-wire wick heat pipe and a thermosyphon.



Fig. 4. Photos of condenser of heat pipe and heat sink



(a) Slab wick



(b) Woven-wire wick

Fig. 5. Photos of wick structures

The inner part of the slab was made of 6 layers of 20 mesh stainless steel wire screen, and the outer part was made 2 layers of 200 mesh wire screen. Two layers of 200 mesh screen were also used as circumferential wick of heat pipe to distribute the working fluid over the inner surface of the pipe wall(See Fig. 5(a)). The woven -wire wick was made of 24 bundles of wires, and each bundle had ten copper wires(See Fig. 5(b)).

3. APPLICATION FOR INDUSTRIAL PROCESS HEAT

The ESTC can be used not only for low temperature industrial processes, such as washing industry of food utensils and dying industry, but also for medium temperature applications in food processing, fiber and paper industry etc. In addition it can be applied for heating and cooling in various building types.
For the field test for solar system of industrial process heat, a number of evacuated tubes are installed in OB beer company located in Gwang-ju city, Korea. Solar heating system for Industrial process heat normally uses forced circulation. The system includes ETSC modules, 2 ton buffer storage tank, plate type heat exchanger, pump, controller and monitoring device, etc shown in Fig. 6. ETSC modules absorb solar radiation and heat up the heat transfer fluid within the manifold. By a constant difference of temperatures between the outlet temperature of ETSC and the bottom temperature of the buffer storage tank, the pumps in solar loop and storage tank operate simultaneous. A collected heat transferred to the load through the storage tank when the storage

upper side temperature at 85℃.

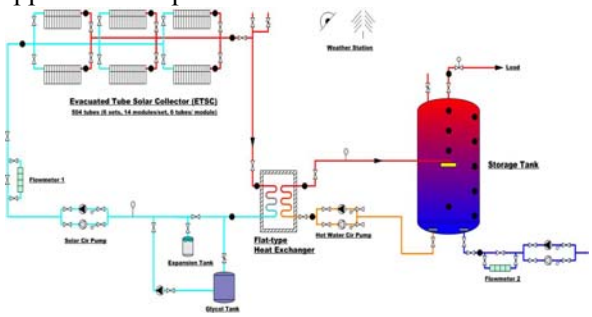


Fig. 6. Schematic diagram of ETSC for industrial process heat

Fig. 7. and Fig. 8 show daily operation of ETSC system. Typical solar collector system(like as Flat Plate collector) decrease its thermal performance when the collector loop circulation temperature has above 80℃ and insolation falls below 400W/㎡.

In contrast, the ETSC system satisfactorily operated even unfavorable test condition.

The concave section in Fig. 7. is due to dumping of process heat source to the load and newly incoming fluid from the outside. per day with 46% mean efficiency

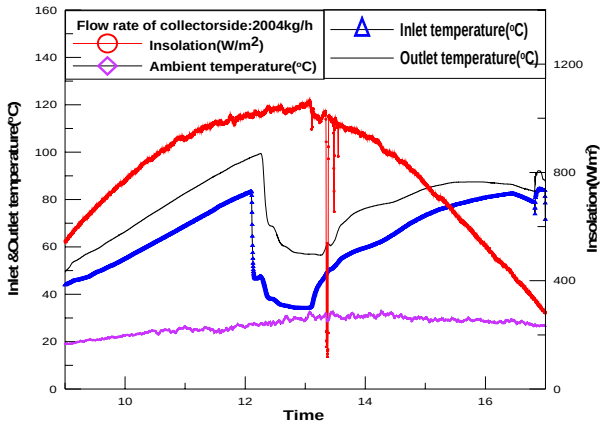


Fig. 7. Daily behavior of ETSC system

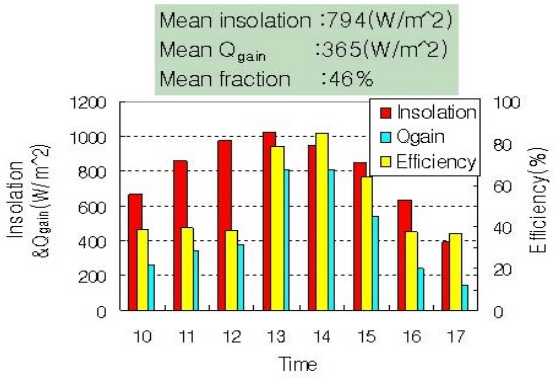


Fig. 8. Daily thermal performance of ETSC system



Fig. 9. Photos of ETSC system for field test

4. CONCLUSION

As heat pipe technology is applied to evacuated tube solar collector, the ETSC with heat pipe has many advantages such as resistance to freeze, fast start-up, low heat losses and resistance to thermal shock. The ETSC with heat pipe developed by KIER with cooperation of APACK, Ltd. adopts some sophisticated manufacturing technology and the new way of dry connection, therefore thermal performance as well as reliability and durability of collectors are obviously increased. The ETSC system installed in beer works to supply its process heat and field test has been performed since May, 2003

The system satisfactorily operated. Even the system undergoes unfavorable condition (circulation temperature at 85℃ , insolation below 400W/㎡) . And it produced 4.2 ton heated water per day, and showed 46% mean system efficiency in a clear day.

References

1. A. Roth, “Vacuum Sealing Techniques" (American Society Classics, 1993), p 169-188, p752-753.
2. W. Kohl, Vacuum, 11(1961), p53.
3. H. Rawson, "Glasses and their applications" (Bell & Bain Limited, 1991), p69-74.
4. Boo, J.H., Chung, W.B. and Kwak, H.Y., "Heat Transfer Performance of a Heat Pipe for Solar Collectors", KSME Fall Annual Conference, 2000, pp. 117-122.
5. Chung, W.B., Boo, J.H., Kwak, H.Y. and Chun, M.S., "Comparative Study of Heat Pipes Having a Woven-wire wick and Slab wick for an elevated Condenser Temperature range", KSME Fall Annual Conference, 2001, pp. 163-186.

Fundamental Investigations on Heat Transfer Characteristics of Heat Sinks with a Vapor Chamber

Yasushi Koito*, Kazuki Motomatsu*, Hideaki Imura*,
Masataka Mochizuki**, and Yuji Saito**
* Dept. of Mechanical Engineering and Materials Science,
Faculty of Engineering, Kumamoto University,
2-39-1, Kurokami, Kumamoto 860-8555, JAPAN
Tel & Fax: +81-96-342-3760, E-mail: koito@gpo.kumamoto-u.ac.jp
** Fujikura Ltd., 1-5-1, Kiba, Koto-ku, Tokyo 135-8512, JAPAN

Abstract

A novel heat spreader called "Vapor Chamber" has been developed to achieve efficient cooling of microprocessor units (MPUs) equipped in personal computers, servers and workstations. By fitting the vapor chamber between the top of the MPUs and the bottom of the heat sink, which is much larger than the former, the heat generated from the MPUs is spread uniformly to the heat sink. This paper describes the fundamental experiments on the heat transfer characteristics of the heat sink with the vapor chamber. In the experiments, the heat sink is placed in a wind tunnel and air-cooled by a blower, supplying the heat fluxes by a heater to a part of the bottom of the vapor chamber fitted on the bottom of the heat sink. The temperature at the top of the heater, the temperatures at the bottom of the heat sink and the wind temperatures at the inlet and outlet of the heat sink are measured, and the thermal resistances of the vapor chamber and the heat sink are calculated respectively. The experiments are performed by changing the wind velocity in the wind tunnel, the wind temperature at the inlet of the heat sink, the inclination of the heat sink with the vapor chamber and the heat flux, and the effects of these operating conditions on the thermal resistances of the vapor chamber and the heat sink are discussed.

Key words: Heat Transfer, Vapor Chamber, Heat Spreader, Heat Sink, Experiment.

1. INTRODUCTION

Recently, as the performance of microprocessor units (MPUs) equipped in personal computers, servers and workstations progresses quickly, the necessity of developing advanced cooling systems for the MPUs becomes stronger because of the higher heat generation from the MPUs. Generally, the MPUs are cooled by a heat sink with a fan. However, because the heat fluxes generated from the MPUs are considerably large and the sizes of the MPUs are much smaller than those of the heat sink, the temperature gradients in the heat sink are comparatively large, resulting in the larger thermal resistances and the lower cooling efficiency. Therefore, the effective heat spreaders are needed to spread the heat generated from the MPUs to the heat sink uniformly.

In response to this, a plate-type heat pipe called "Vapor Chamber" has been developed. By fitting the vapor chamber between the top of the MPUs and the bottom of the heat sink, which is much larger than the former, the heat generated from the MPUs is spread uniformly to the heat sink. In addition, the thickness of the vapor chamber is less than 5 mm and its weight is lighter compared to the conventional heat spreaders made of aluminum plates, copper plates and so on.

Several researches have been already conducted experimentally on the heat transfer characteristics of the heat sink with the vapor chamber. Mochizuki *et al*. developed the trapezoidal vapor chamber in which the top is larger than the bottom, and found the effective inner structures of the vapor chamber [1]. Wuttijumnong *et al*. examined the effect of the amount of the working fluid in the vapor chamber on the heat transfer characteristics of the heat sink with the vapor chamber [2]. Mashiko *et al*. showed that the total thermal resistance of the heat sink with the vapor chamber is smaller than that of the heat sink without the vapor chamber when the ratio of the bottom area of the heat sink to the top area of the MPUs is greater than 5 [3]. Nguyen *et al*. concluded experimentally that the performance of the heat sink with the vapor chamber is approximately 25% and 45% better than that of the heat sink

with the conventional heat spreaders made of copper plates and aluminum plates respectively [4].

However, no experimental investigations have been conducted on the thermal resistances of the vapor chamber and the heat sink, which are important factors to improve the performance of the heat sink with the vapor chamber. In the present study, therefore, the temperature distributions in the heat sink with the vapor chamber are measured, and the thermal resistances of the vapor chamber and the heat sink are calculated respectively. The effects of the operating conditions on the thermal resistances are discussed.

2. VAPOR CHAMBER

A photograph of the heat sink with the vapor chamber is shown in Fig. 1, and Fig. 2 shows the details of the vapor chamber. The vapor chamber is a two-phase closed flat chamber made of copper. Water is enclosed as the working fluid, and sinter sheets and sinter columns made of small copper particles (particle size: 100 ~ 200 mesh, porosity: 40%) are used as the wick in the vapor chamber. The sinter sheets are 0.5 mm in thickness and are attached to the internal surface of the vapor chamber. Eleven sinter columns are set in the vapor chamber to ensure the circulation of the working fluid.

The vapor chamber is fitted between the top of the heat source and the bottom of the heat sink, which is much larger than the former (see Fig. 3). Inside the vapor chamber, the working fluid receives the heat from the heat source and evaporates. The generated vapor spreads and flows to the upper internal surface, where it condenses, and the condensate returns to the lower internal surface through the wick to continue the circulation of the working fluid. Consequently, the heat generated from the heat source is spread uniformly to the heat sink.



Fig. 1 Photograph of the heat sink with the vapor chamber

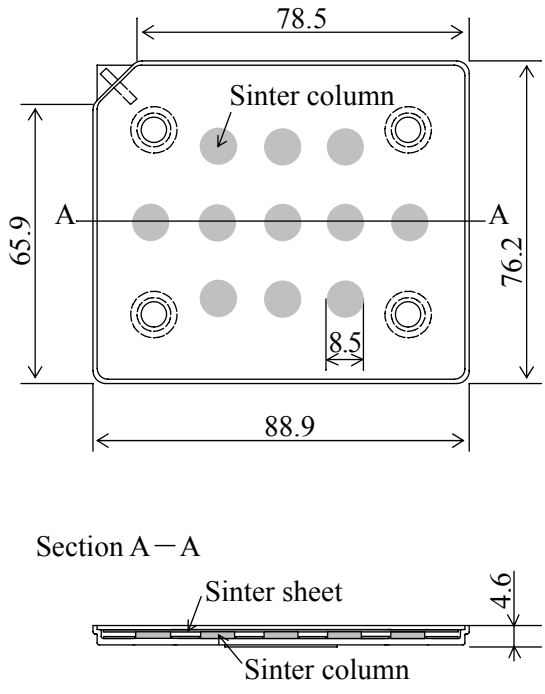


Fig. 2 Details of the vapor chamber

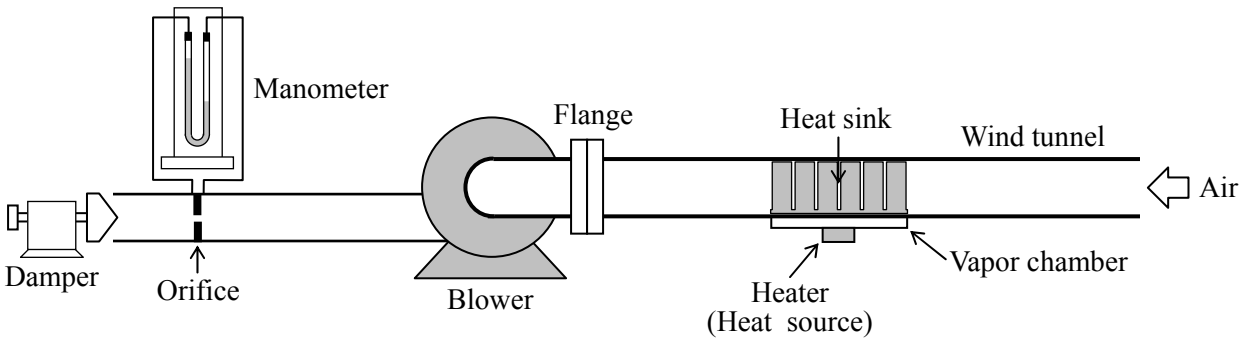


Fig. 3 Schematic diagram of the experimental apparatus

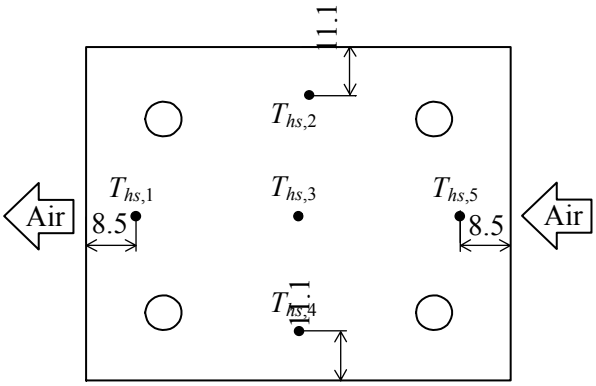


Fig. 4 Measuring points of the temperatures at the bottom of the heat sink

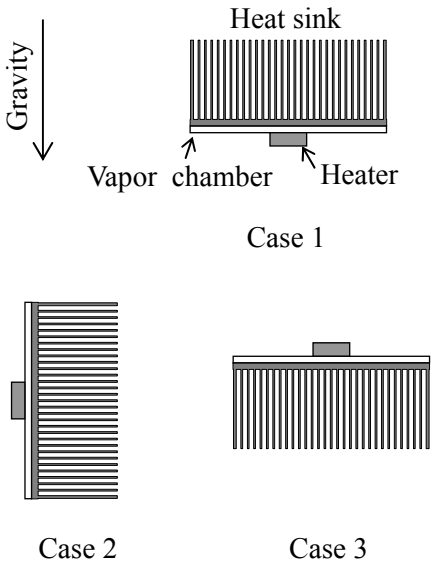


Fig. 5 Inclination of the heat sink with the vapor chamber

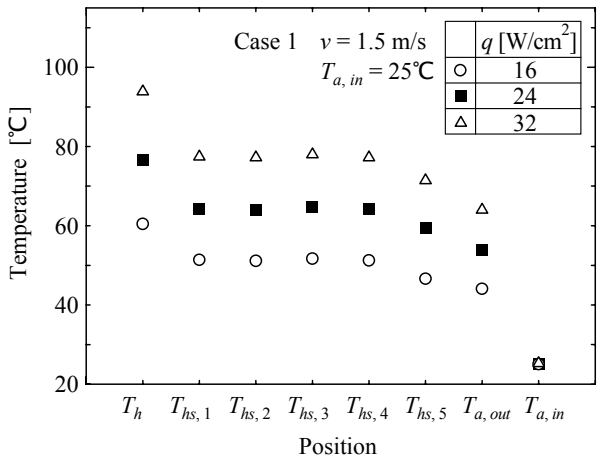


Fig. 6 Temperature distributions of the bottom of the heat sink

3. EXPERIMENTAL APPARATUS and PROCEDURE

The experimental apparatus shown in Fig. 3 consists of a wind tunnel, a heat sink with a vapor chamber, a heater used as a heat source, a blower, a damper and an orifice with a manometer. The wind tunnel is 890 mm long and its cross section is rectangle (height: 31.0 mm, width: 78.0 mm). The heat sink is placed at the center of the wind tunnel in contact with the internal surface of the wind tunnel so as not to cause the airflow deviation along the gap between the heat sink and the wind tunnel. The vapor chamber is fitted between the top of the heater and the bottom of the heat sink. The bottom area of the heat sink, which is equal to the top and bottom areas of the vapor chamber, is 11.3 times as large as the top area of the heater (24.5 mm square). The flange is used to incline the wind tunnel and the heat sink with the vapor chamber (see Fig. 5) for the purpose of investigating the effect of the inclination on the heat transfer characteristics of the heat sink with the vapor chamber.

In the experiments, the heat fluxes are supplied by a heater to a part of the bottom of the vapor chamber fitted on the bottom of the heat sink, and the heat sink is air-cooled by a blower. The wind velocity is controlled by a damper. Temperature distributions of the heat sink with the vapor chamber in a steady state are measured by K-type thermocouples. The temperature of the heater, T_h , is measured by a thermocouple fixed in a small groove made on the top of the heater. The temperatures at the bottom of the heat sink, $T_{hs,1}$ ~ $T_{hs,5}$, are measured by five thermocouples at each location shown in Fig. 4. Five small holes are made at the bottom of the heat sink and the thermocouples are inserted there. The wind temperatures at the inlet and outlet of the heat sink, $T_{a,in}$, $T_{a,out}$, are measured by two thermocouples at each location. The wind velocity is measured by an orifice with a manometer.

The experiments are performed by changing the apparent wind velocity in the wind tunnel, v (1.0, 1.5, 2.0 m/s), which is 0.73 of the pore velocity in the heat sink, the wind temperature at the inlet of the heat sink, $T_{a,in}$ (20, 25, 30 °C), the inclination of the heat sink with the vapor chamber (Case 1, Case 2, Case 3 shown in Fig. 5) and the heat flux supplied by the heater to a part of the bottom of the vapor chamber, q (0 W/cm^2 ~ critical heat flux). The heat flux when T_h becomes 100 °C is regarded as the critical one.

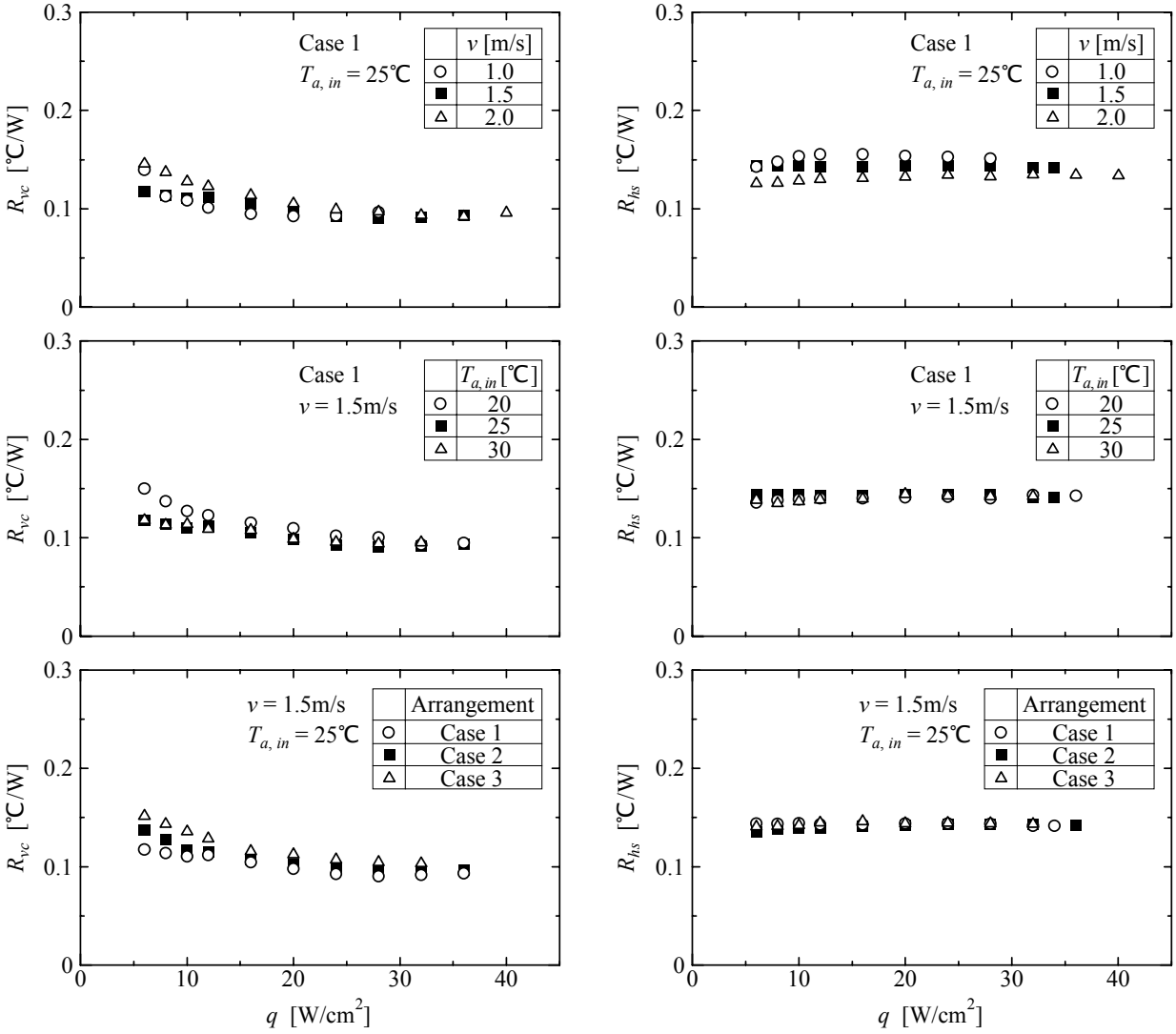


Fig. 7 Relation between the thermal resistances and the heat fluxes supplied to the vapor chamber

4. EXPERIMENTAL RESULTS and DISCUSSION

The temperature distributions of the bottom of the heat sink, $T_{hs,1}$ ~ $T_{hs,5}$, are shown in Fig. 6 with the temperature of the heater, T_h, and the wind temperatures at the inlet and outlet of the heat sink, $T_{a,in}$, $T_{a,out}$. Although $T_{hs,5}$, which is located near the wind inlet of the heat sink, is slightly lower than $T_{hs,1}$ ~ $T_{hs,4}$, the temperatures at the bottom of the heat sink, $T_{hs,1}$ ~ $T_{hs,5}$, are almost the same, implying that the heat supplied from the heater to a part of the bottom of the vapor chamber is spread uniformly to the heat sink.

The thermal resistances of the vapor chamber, R_{vc}, and the heat sink, R_{hs}, are defined respectively by,

$$R_{vc} = \frac{T_h - T_{hs,m}}{qA} \tag{1}$$

$$R_{hs} = \frac{\Delta T_{hs}}{qA} \tag{2}$$

where $T_{hs,m}$ is the arithmetic mean temperature at the bottom of the heat sink, A the top area of the heater (24.5 mm square) and ΔT_{hs} the logarithmic mean temperature difference between $T_{hs,m}$ and the wind temperatures $T_{a,in}$, $T_{a,out}$ expressed as,

$$\Delta T_{hs} = \frac{T_{a,out} - T_{a,in}}{\ln\{(T_{hs,m} - T_{a,in})/(T_{hs,m} - T_{a,out})\}} \tag{3}$$

Figure 7 shows the effects of the apparent

wind velocity in the wind tunnel, v, the wind temperature at the inlet of the heat sink, $T_{a,in}$, the inclination of the heat sink with the vapor chamber, Case 1, Case 2, Case 3 shown in Fig. 5, on the relation between the thermal resistances, R_{vc}, R_{hs}, and the heat fluxes supplied by the heater, q. Irrespective of the experimental conditions, R_{hs} is substantially independent of q, while R_{vc} increases as q decreases because effective evaporation does not occur in the vapor chamber for the case of small q. It is also found that R_{vc} is not affected by the inclination of the heat sink with the vapor chamber. This is because the sinter columns set in the vapor chamber ensure the circulation of the working fluid.

5. CONCLUSIONS

Experimental investigations have been conducted on the heat transfer characteristics of the heat sink with the novel heat spreader called "Vapor Chamber". The heat sink is placed in a wind tunnel and air-cooled by a blower, supplying the heat fluxes by a heater to a part of the bottom of the vapor chamber fitted on the bottom of the heat sink. The temperature at the bottom of the heat sink is found to be almost uniform, implying that the heat supplied from the heater to a part of the bottom of the vapor chamber is spread uniformly to the heat sink. It is also shown that the thermal resistances of the vapor chamber and the heat sink are hardly affected by the wind velocity in the wind tunnel, the wind temperature at the inlet of the heat sink and the inclination of the heat sink with the vapor chamber.

References

1. M. Mochizuki, K. Mashiko, K. Goto, Y. Saito, M. Nagata, K. Eguchi, T. Nguyen, P. Ho, "Cactus-type Heat Pipe for Cooling CPU", Proc. 5th Int. Heat Pipe Symposium, 1996, pp. 194-198
2. V. Wuttijumnong, M. Mochizuki, K. Mashiko, I. Sauciuc, T. Nguyen, "The Optimum Working Fluids Ratio for Vapor Chamber", Proc. 6th Int. Heat Pipe Symposium, 2000, pp. 159-163
3. K. Mashiko, M. Mochizuki, Y. Saito, T. Nguyen, R. Boggs, I. Sauciuc, "Advanced Cooling System Combined with Heat Sink and Heat Pipe for Cooling PC", Proc. 11th Int. Heat Pipe Conf., 1999, pp. 464-468
4. T. Nguyen, M. Mochizuki, K. Mashiko, Y. Saito, "Use of Heat Pipe / Heat Sink for Thermal Management of High Performance CPUs", Proc. 16th IEEE SEMI-THERM Symposium, 2000, pp. 76-79

Research and Development of Heat Pipe Heat-sink For CDMA Base Station Power Module

Jun Zhuang*, Hanzhong Tao**, Hong Zhang**
*Nanjing HETE Energy Conservation & Environmental Protection Co. Ltd.
Zhong Shan Science & Technology Development Zone, Dachang District Nanjing, Jiangsu Province, 210048 P.R.CHINA
Tel: +86-25-8399616, Fax: +86-25-8399580
Email: jzhang@heatpipe.com.cn
**Institute of Heat Pipe Technology Nanjing University of Technology
No. 5 XinMoFan Road, Nanjing, 210009, P.R.CHINA
Tel & Fax +86-25-6637973
Email: hzhang01@jlonline.com

Abstract

This article presents the research and development of a heat pipe heat-sink for CDMA base station power module, in which the temperature rise and distribution of temperature field were calculated with FEM (finite element method) analysis software at given ambient temperature and heat dissipation requirement conditions. A type of screen wick has been selected, for which the osmotic capacity of the wick and the capillarity limit of the heat pipe have been calculated and measured. The heat sink was subjected to temperature impact test (at –40℃~100℃) and salt fog corrosion test, for determination and comparison of performance. The performance is lowered by less than 2% after the tests as compared with that before the tests; therefore it can meet the application requirements.

Key words: heat pipe heat sink, CDMA, permeability

1. INTRODUCTION

With the rapid development of telecommunication technology, the power of electronic modules used in base stations is daily increasing, and more heat is produced accordingly. The traditional extrusion formed aluminum heat sink can no longer meet the requirements for normal heat dissipation. A heat sink for base station is usually mounted outdoor on the roof of a high building, so it is required to be small in volume, light in weight, and able to withstand the impact from temperature variations in different seasons and long-term corrosion from atmosphere. A heat-sink should have a heat dissipating capacity of over 100W under natural convection condition, to ensure its reliable operation with low maintenance demand.

2. STRUCTURE DESIGN

A heat-sink is as shown in Fig. 1: it consists of six heat pipes of φ10×1×850mm and 25 aluminum

fins. The evaporating and condensing segments of the heat pipe are at an angle of 90°. The heat produced in the power module is transferred via the base board to the evaporating segment of the heat pipe, and then by the heat pipe to the condensing segment, where it dissipates to the atmosphere via the fins. The heat flow route is as shown in Fig. 2.



Fig.1. Photo of heat- sink

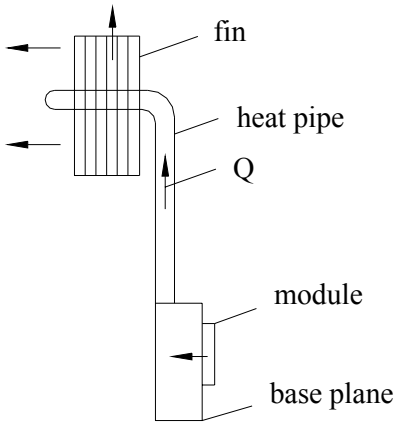


Fig.2 heat flow route

3. NUMERICAL ANALYSIS

On the basis of original design requirements, we used the FEM analysis software to simulate and calculate the heat dissipating power of the heat-sink at different ambient temperature conditions and the maximum temperature rise of the hot module, as shown in Fig. 3. The relevant data are as given in Tables 1 and 2:

Table .1 Parameters of modules

Heat producing block dimensions	300 mm×300 mm×20 mm
Heat flow density	1500 W/m^2
Heat pipe equivalent thermal conductivity	50000 W/(m • K)
Fin material	Aluminum
Number of fins	32
Fin dimensions	300 mm×218 mm×1 mm

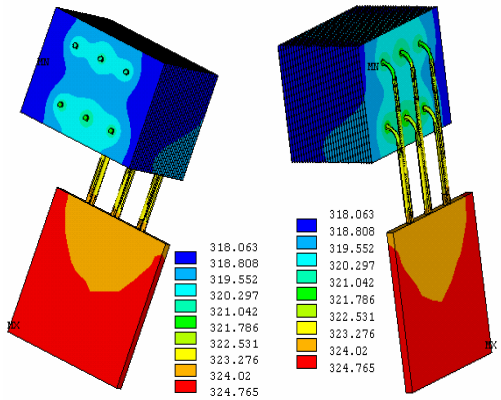


Table 2 Calculation results

Ambient temperature K	heat transfer coefficient W/(m^2 • K)	temperature of block / K
303	5	314.584
313	5	324.756
333	5	344.765

Fig. 3 Temperature field with an ambient temperature of 40℃ and a convection heat exchange coefficient of 5

4. CALCULATION AND ETERMINATION OF WICK PERMEABILITY

The permeability testing device is as shown in Fig. 4 [1]:

The permeability can be calculated using the following formula:

$$K = \frac{\mu_l \dot{m} l}{\rho^2 g h A_w} \quad (1)$$

For a multi-layer wick, the permeability can also be obtained using formulas:

$$K = \frac{d^2 \varepsilon^3}{122(1-\varepsilon)^2} \quad (2)$$

$$\varepsilon = 1 - \frac{1.05\pi N d}{4} \quad (3)$$

where: N : mesh;

d : wire diameter

the error of the calculated and measures values are listed in Table 3.

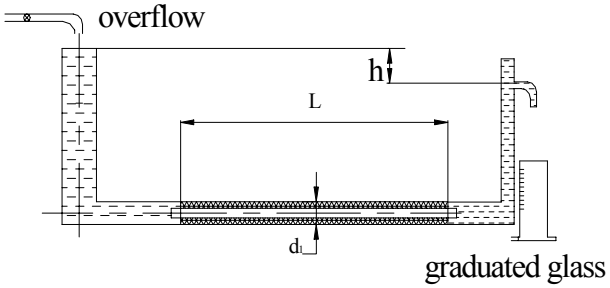


Table 3

	permeability K
Calculated value	1.08×10^{-10}m^2
Measured value	1.37×10^{-10}m^2
Error	21%

Fig. 4 Test set of the permeability

5. CALCULATION AND ETERMINATION OF CAPILLARITY RADIUS

The effective capillarity radius can be calculated using the following formula:

$$r_c = \frac{2\sigma}{\rho g h} \quad (5)$$

where: r_c : effective capillarity radius

σ : liquid surface tension

ρ : liquid density

Table 4

	Calculated value	Measured value
r_c/m	$r_c = \frac{1}{2N}$	$r_c = \frac{d+w}{2}$
	4.23×10^{-5}	5.7×10^{-5}

g : gravitational acceleration

h : liquid lifting height

For a multi-layer screen wick, effective capillarity radius can be calculated using the following formula[2]:

$$r_c = \frac{d+w}{2} = \frac{1}{2N} \quad (4)$$

where: d : wire diameter;

w : wire spacing;

N : mesh

The results of calculation and measurement are shown in Table 4.

The test setup for performance of a single heat pipe is as shown in Fig. 5, where the evaporating and condensing segments of the heat pipe are respectively heated or cooled by constant temperature water from a constant temperature water bath. It can measure the power transferred by heat pipe at different steam temperature.

The correlation of single heat pipe power and heat resistance is as shown in Fig. 6.

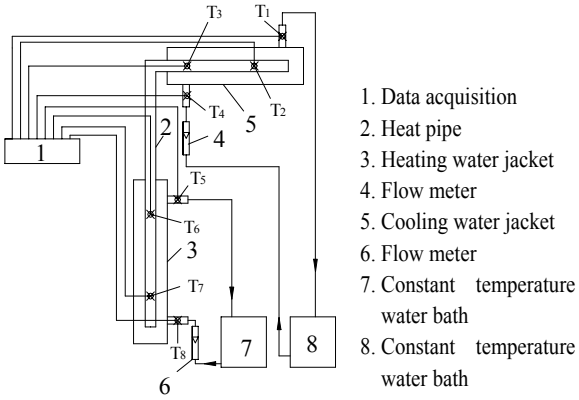


Fig.5 The test setup for heat pipe

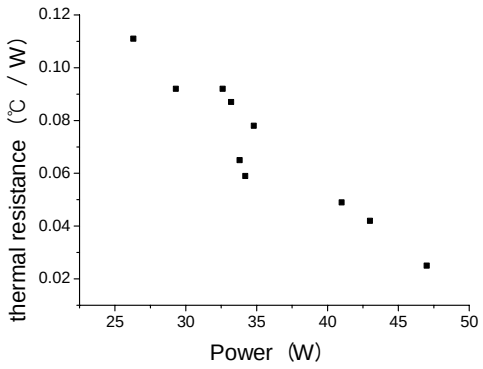


Fig.6 Thermal resistance of heat pipe

The heat-sink performance is tested in a room with constant temperature. The room is equipped to simulate different ambient temperature. The simulated ambient temperature for testing is respectively 30℃, 40℃, 50℃ and 60℃. The test setup is as shown in Fig. 7.

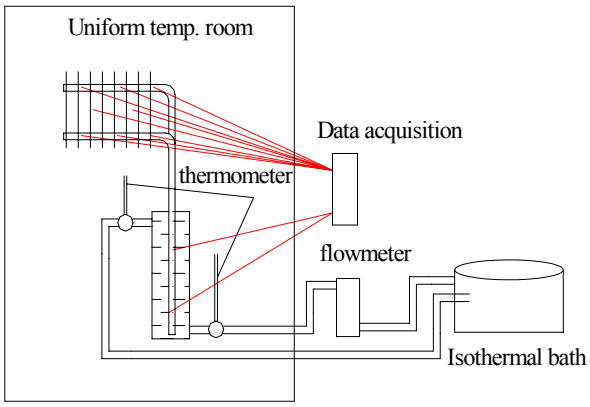


Fig.7 Scheme of experimental apparatus

At the heat pipe evaporating segment of the heat-sink, hot water from a constant temperature water bath simulates the heating amount of the power module. The heat dissipating segment of the heat-sink operates on natural convection. To test the withstanding ability of heat-sink to severe environment, the heat-sink is subjected to tests on salt fog corrosion, alternative temperature variation, vibration and impact in ISO salt fog test box, TSR-63 high-low temperature (－40℃~100℃) impact test table, CP-100 impact test table and V-860 electromagnetic vibration test table. The results measured before and after the tests are shown in Table 5:

Table. 5

	Before tests				After tests			
temp. $\overline{t_\infty}$ ℃	33	41.3	50	59.6	31	41	51.7	59.3
power, W	246	204	113	95	241	201	111	94
deterioration $\overline{t^h}$ %					2.0	1.5	1.8	1.05

6. CONCLUSION

We have successfully developed a heat-sink for use on CDMA base station power modules, and the results of analysis using FEM software well agree with the performance tests in actual

application conditions. Tests on heat-sink to withstand severe operation environment show that its operation performance can remain unchanged in such conditions, therefore it meets the design requirements.

Reference

1. Ogushi, T. Sakurai, Y. Composite Wick Heat Pipes, 4th International Heat Pipe Conference, 1981,651

2. Chi,s.W. Heat Pipe Theory And Practice, McGraw-hill 11(1976)

A Compact Cooling System with Triple Technologies

Jemmy Sutanto Bintoro*, Aliakbar Akbarzadeh**, Masataka Mochizuki***, and Thang Nguyen***

*Georgia Institute of Technology
Woodruff School of Mechanical Engineering, 801 Ferst Drive N.W., Atlanta-Georgia, 30332, U.S.A
Tel: 1 404 509 5355, Fax: 1 404 249 7728, Email: jemmy.sutanto@me.gatech.edu
**RMIT University
Bundoora East Campus, P.O Box 71, Bundoora Victoria, 3083, Australia
Tel: 61 3 9925 6079, Fax: 61 3 9925 6108, Email: akbar@rmit.edu
***Fujikura Ltd.
1-5-1, KIBA, KOTO-KU, Tokyo 135-8512, JAPAN
Tel: 81 3 5606 1174, Fax: 81 3 5606 1514, Email: mmotizuki@fujikura.co.jp

Abstract

This paper present a new cooling system that adopted triple technologies: heat pipe, impingement jet, and mini channel heat exchanger. The system had capability of removing maximum heat of 200 W from a single microchip, D = 12 mm, it is equivalent to the heat flux of 177 W/cm^2. The system maintained the maximum chip-surface temperature of less than 95 ºC and the chip temperature variation of less than 2.5 ºC. At ambient, 30 ºC, the surface temperature of heat exchanger is less than 65 ºC.

Key words: Heat pipe, Impingement jet cooling, Mini channel heat exchanger (MCHE)

1. INTRODUCTION

Computer development on the recent decades has been very fast. It is always accompanied with the increase of heat dissipation and miniaturization of computer chips. The traditional method in removing heat by relying on the natural/forced convection by using fins and fan are no longer adequate for the recent developed computer chip [1]. Intel projects a heat flux level of 100 W/cm^2 that has to be removed for the next millennium microprocessor [1,3]. This paper present a new cooling system that adopted triple technologies: Heat pipe, impingement jet, and micro channel heat exchanger. The overall cooling system reflects the Heat pipe technique; with the heating section where the heat from electronic chip is absorbed and the cooling section where the heat is rejected to the ambient. Since early 1990, impingement jet has been known for cooling of turbine blades and laser weapons in the US army, it has the capability of removing heat at ultra heat flux level (> 150 W/cm^2) [2,4]. This technique was adopted in the system to remove the heat from a single computer chip with the diameter of 12 mm. The technique of mini channel heat exchanger was used to remove the heat finally to the ambient. The designed system was completely closed and compact; it was completely portable for any demonstration purpose. The system simulated a real practical application of electronic cooling. This paper focuses in reporting the experimental results of the system that shows the cooling capacity at different fluid flow rate.

2. NOMENCLATURE

$\dot{Q}$ = Rate of heat transfer (W)
ρ = Density of the fluid (kg/m^3)
$\dot{V}$ = Volume flow rate of the fluid (m^3)
$\dot{m}$ = Mass flow rate of the fluid (kg/s)
C_p = Specific heat at constant pressure (J/Kg.K)
T = Static temperature of the fluid (ºC)
ΔT = Temperature difference (ºC)
LMTD = Log Mean Temperature Difference (ºC)
P = Static Pressure of the fluid (Pa, kPa)
Re = Reynold number
Nu = Nusselt number
h = Convective h.t coefficient (W/m^2.ºC)
k = Conduction h.t coefficient (W/m^2.ºC)
μ = Dynamic viscosity of the fluid (N.s/m^2)
ν = Kinematic viscosity of the fluid (m^2/s)
d = Diameter of the nozzle (m, mm)
D = Diameter of the computer chip (m, mm)
U = Average velocity (m/s)
r = Radius (m, mm)
L = Characteristic length of computer chip (m, mm)
COP = Coefficient of Performance
Pr = Prandtl number
V = Voltage (V)
I = Current (A)

3. PRINCIPAL IDEA OF THE SYSTEM

The system used the principal of triple technologies: Heat pipe, Impingement fluid jet, and mini channel heat exchanger. The application is more likely for cooling system inside a desktop and a central computer even though the ultimate aim of this project if for laptop computer application. The overall schematic of the system is shown in the figure 1 below. The technology of liquid impingement method was used to remove the heat from a computer chip, D = 12 mm (A_c = 1.13 cm^2). In this system, deionized water was used as the liquid for jet-impingement. The maximum heat dissipated from the chip is 200 W with the total heat flux of 177 W/cm^2. The technology of mini channel heat exchanger was used to remove heat from the water (Fluid) to the environment/ambient. 6 (Six) micro Channel tubes with the diameter of 0.05 inch = 1.27 mm were embedded within the aluminum heat exchanger. This mini channel was designed for working in the single-phase condition. Fans were attached on the heat exchanger to increase the convection heat transfer. The technology of Heat pipe was applied as the working principal of the overall system. The overall set up of the system was similar to the Heat pipe, with some vapor generated in the heating section (evaporator). The system also had a micro pump with a power input of maximum 7.2 W. The temperature – entropy diagram of the system under isentropic condition is shown in the figure 2 below.

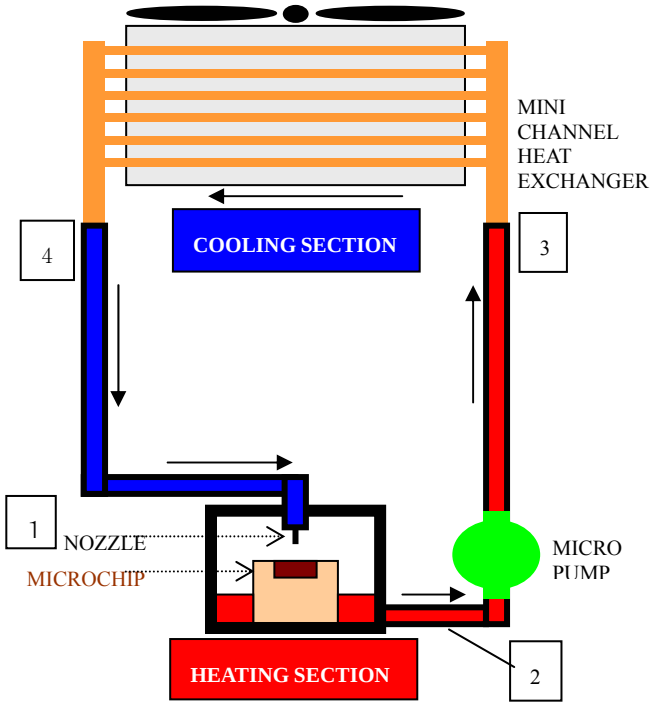


Figure 1 Schematic diagram of the cooling system for computer-chip

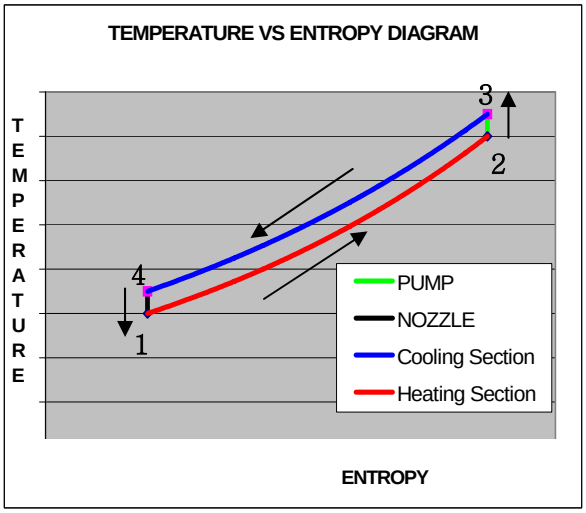


Figure 2 Temperature Vs Entropy diagram of the cooling system under isentropic condition

4. DESIGN PARAMETERS

Since this report was sponsored by companies, Fujikura Ltd and Panasonic, there were a lot of parameters assigned in the design of the system. The parameters are: the system has to maintain the micro-chip temperature to be less than 95 ºC at any time, The maximum temperature variation over the chip surface diameter is 3 ºC, the maximum surface temperature of the mini channel heat exchanger is 65 ºC, The system has to be able to operate at its maximum capacity in the ambient temperature of 45 ºC.

5. DESIGN OF THE SYSTEM

There were two important designs for this cooling system: design of the impingement water jet and mini channel heat exchanger.

Impingement Water Jet

It is assumed that the power dissipated from the computer chip is equal to the power absorbed by the impingement water jet, since it can be expressed as:

$$\dot{Q} = \dot{m} . C_p . (T_o - T_N) \quad \text{.....equation 1}$$

Based on the Newton heat transfer equation, the heat dissipated from the computer chip can be expressed by the following equation:

$$\dot{Q} = \bar{h} . C_p . LMTD$$

$$\dot{Q} = \bar{h} . C_p . \frac{(T_c - T_O) - (T_c - T_N)}{\ln((T_c - T_O)/(T_c - T_N))} \quad \text{.eqtn 2}$$

For the design the T_c, chip surface temperature, is designed to be 85 ºC that is 10 ºC less than the parameter. The T_N, fluid temperature in the nozzle outlet, is assigned to be 50 ºC that is 15 ºC less than the maximum surface temperature of mini channel heat exchanger. There is no valid equation for "h" but there were some correlations developed in the literatures. The correlation used in the design of the system is coming from (Womac, 1993) after some modification to make it suitable for circular chip instead of square one.

$$\frac{\overline{Nu_D}}{Pr^{0.4}} = 0.489\,Re_d^{0.5}.\frac{d}{D} + 0.8135\,Re_L^{0.532}.\frac{1}{D.(D-d)}.(D^2 - 1.144\,d^2)$$

.....equation 3

$$Re_d = \frac{\rho . U_N . d}{\mu} \quad ;$$

$$Re_L = \frac{\rho . U_N . 0.5\,(D-d)}{\mu} \quad ;$$

$$\overline{h_D} = \frac{\overline{Nu_D} . k}{D} \quad \text{.....} \quad \text{.....equation 4}$$

After some manipulations of equation 1 to 4, the two unknowns, T_O and $\bar{h}_D$, are determined and some other important data. Finally, in order to remove heat of 200 Watts from a single chip with 12 mm diameter and the nozzle diameter of 0.5 mm, the followings are required:

$\dot{m}$	=	4.7215 gr/s
$\bar{h}_D$	=	59,646 W/m ^{2}.K
Nu_D	=	1,085
Nu_d	=	45.186
$Nu_d/Pr^{\wedge}(1/3)$	=	32.612
$\dot{V}$	=	289.1 ml/min
U_N	=	24.52 m/s
Re_d	=	28,627
ΔP_N	=	295 kPa

Mini Channel Heat Exchanger (MCHE)

Mini Channel was used in the cooling section to enhance the convective heat transfer inside the water (fluid) flow and at the same time giving a compact design. Circular shape mini channel was developed. The thermal balance of the mini channel heat exchanger is shown in the figure 3 below. The designed temperature of the fluid entering the MCHE was assigned to be 70 ºC, which is 5 ºC smaller than the designed temperature of the water leaving the heating section. The assigned ambient temperature was 40 ºC, with the force fan velocity of 10 m/s. The thermal resistance of the MCME was simplified by the negligence of the conduction resistance of the heat exchanger fins and the micro channel tubes, as shown in figure 4. By simple energy balance of equation 1, the fluid temperature leaving the MCME can be found as T_{OUT} = 59.871 ºC. In the design, it was initially assumed that the total length of the micro channel was 1 m, with the circular diameter of 1.27 mm. Under this condition, the flow velocity was fully turbulent, since a uniform velocity profile was assumed.

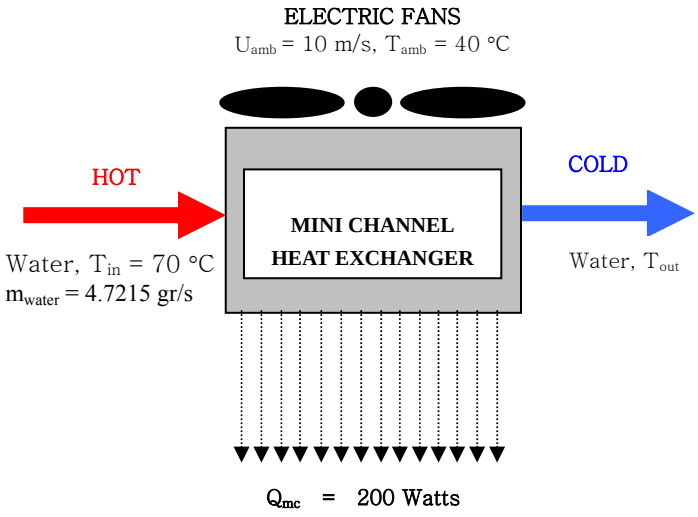
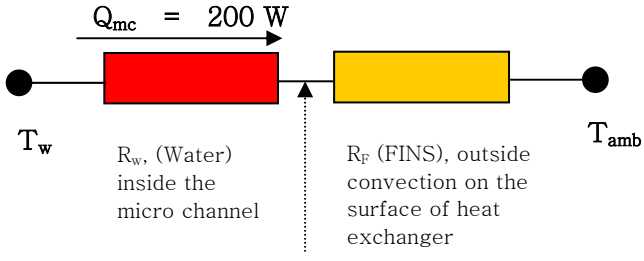


Figure 3 Thermal balance of the mini channel heat exchanger (MCHE)



Negligible resistances of the heat exchanger fins and mini channel tubing

Figure 4 Thermal resistance of the heat transfer process at MCHE

The internal resistance of the mini channel can be determined by the following equation:

$$\overline{h_D} = \frac{\overline{Nu_D} \cdot k}{D} \qquad R_W = \frac{1}{\overline{h} \cdot A_{channel}}$$

.....equation 5

Where "D" is the diameter of the channel

For the turbulent flow inside the tube, the Nusselt number can be approximated by: (Incropera, p.460)

$$\overline{Nu_D} = 0.023 \cdot Re_D^{4/5} \cdot Pr^{0.3}$$ .....equation 6

The total thermal resistance is shown as follows:

$$R_{TOTAL} = R_W + R_{FIN} = R_W + \frac{1}{\overline{h}_{OUT} \cdot A_{HE}}$$

The Nusselt number for the outside force convection is determined by: (Incropera, p.460)

$$\overline{Nu_L} = 0.664 \cdot Re_L^{1/2} \cdot Pr^{1/3}$$ .....equation 7

After some manipulations the following results was determined, for the channel diameter of 1.27 mm and the length of 1 m, it is required to have fins extended surface with the area of 0.265 m^2 at the ambient air velocity of 10 m/s.

6. TESTING RIG

The testing rig was built is a compact and small scale. It was completely portable and had the capability to remove 200 W of heat. The schematic figure of the testing rig setup is shown in the figure 5 below, with the following descriptions:

Main components (dark blue labels)

1. Impingement Water Jet Cooling System

Main Transducers (light blue labels)

1. T-type digital thermometer reading; 2. T-type digital thermometer reading; 3. K type digital thermometer; 4. DC Power Supply; 5. Power regulator; 6. Digital Multi Meter; 7. Digital Multi Meter

Instrumentations system (green labels)

1 - 12. T-type thermocouple; 13. Three K – type thermocouples; 14. Power cable of the heating element

Figure 6 shows the close up outlook of the compact cooling system; the brief specifications of the system are as follows:

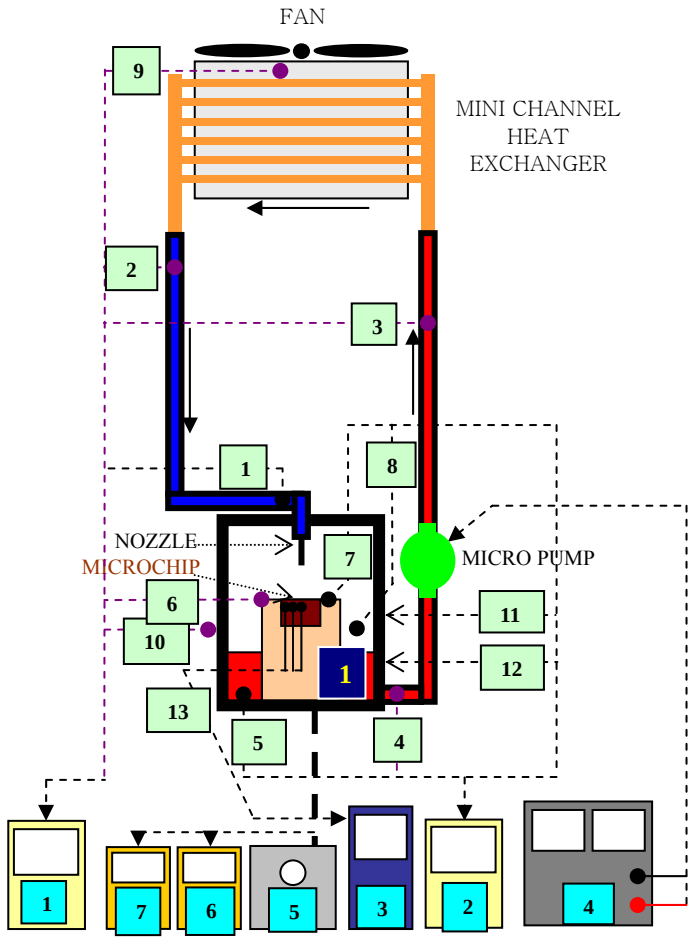


Figure 5 The schematic of second/final testing rig setup, showing instruments and main components

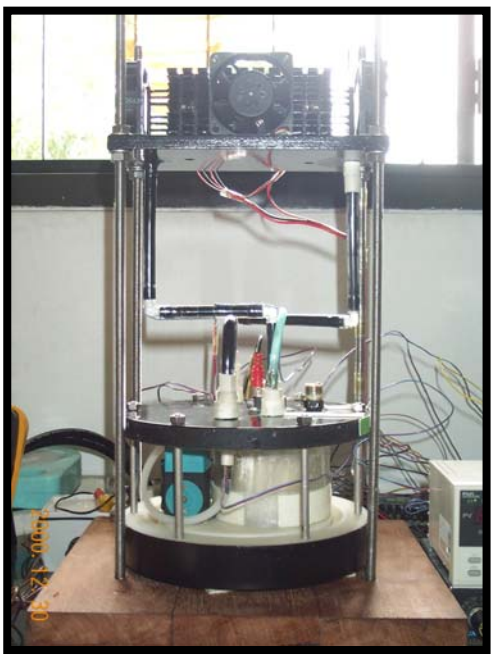


Figure 6 The close up outlook of the cooling system

Maximum cooling capacity = 200 Watts
Micro Chip diameter = 12 mm
Maximum chip temperature = 95 C
Max surface temp of Heat Exchanger = 65 C
Max power consumptions = 7.2 Watts
Overall setup dimensions = 500 mm x 200 mm x 200 mm
Overall setup weight = 1690 grams

7. RESULTS AND DISCUSSION

The variation of the chip surface temperature with the power dissipation is shown in the figure 7. It shows that the increase on the power dissipation from the computer chip, which also means the increase in the system cooling capacity, leads to the increase on the chip surface temperature. The increase seems to be linearly varied with the power dissipation.

The variation of the heat transfer coefficient, over Reynold number at the nozzle diameter of 0.5 mm is shown in the figure 8. It shows that as the Reynold number increases, the heat transfer coefficient of the heating section increases. The figure shows a lot of data points; they are basically the average of the data taken from most of the experimental tests. It can be approximated that there is a linear increasing relation between the heat transfer coefficient and the Reynold number.

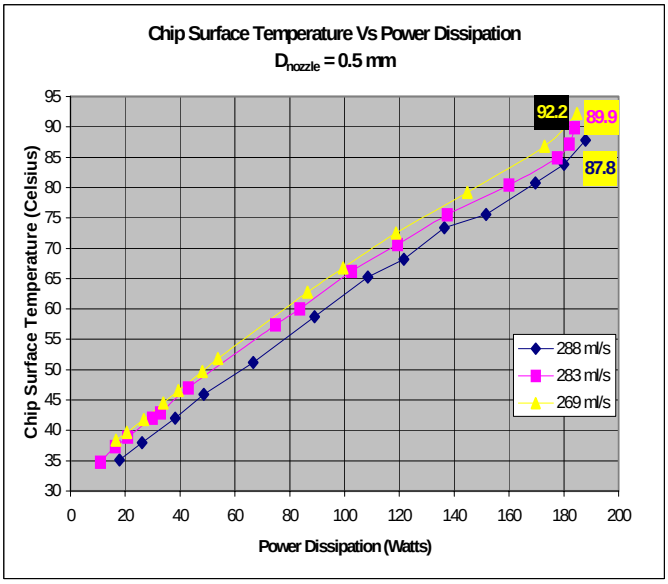


Figure 7 The variation of chip surface temperature at different power dissipation from the computer chip

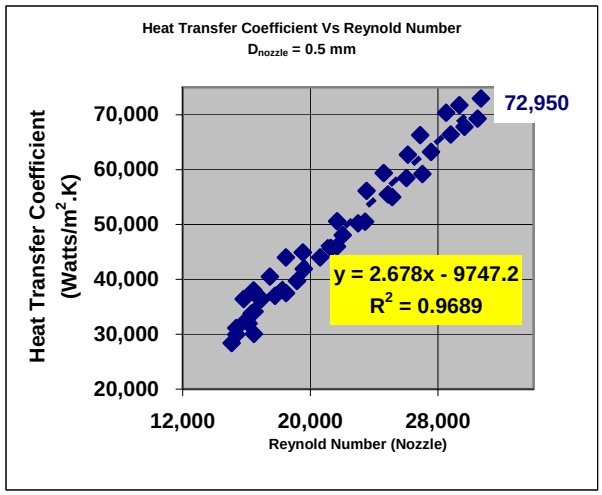


Figure 8 The variation of the Heat Transfer Coefficient with Reynold number at nozzle diameter of 0.5 mm

Figure 9 shows the convective heat transfer performance between the operation using the nozzle diameter of 0.5 mm and 0.8 mm. It shows that the "Nu" increases at higher Reynold number, both in d_{nozzle} = 0.5 mm and 0.8 mm. The figure also shows that the "Nu" of system at d_{nozzle} = 0.8 mm is higher than d_{nozzle} at 0.5 mm at a particular Reynold number. For example at the Reynold number of roughly 21,750, the Nusselt number at d_{nozzle} = 0.8 mm is 80.5, meanwhile at d_{nozzle} = 0.5 mm, it is 39.4. This was mostly due to the fact that the "Cooling Section/Micro Channel Heat Exchanger" performed better at the bigger diameter = 0.8 mm. Contribution of the value of "D" in the equation of "Nu" increases the value of "Nu", at bigger diameter.

Figure 10 shows the comparison of the inlet temperature of the mini channel at different nozzle geometries. It seemed that the inlet temperature at bigger nozzle geometries (d_{nozzle} = 0.8 mm) is less than the ones that d_{nozzle} = 0.5 mm. The differences on these values are increasing with the increasing in the power dissipation. In fact the graph shows that the differences are only distinguished on high power dissipation. At low power dissipation (< 60 Watts), there is almost no difference in these values. For example at the power dissipation of roughly 188 Watts, the inlet temperature of the mini channels at the d_{nozzle} = 0.8 mm was about 59.6 °C. Meanwhile at the d_{nozzle} = 0.5 mm the inlet temperature was about 64 °C, since there is a significant difference of 4.4 °C.

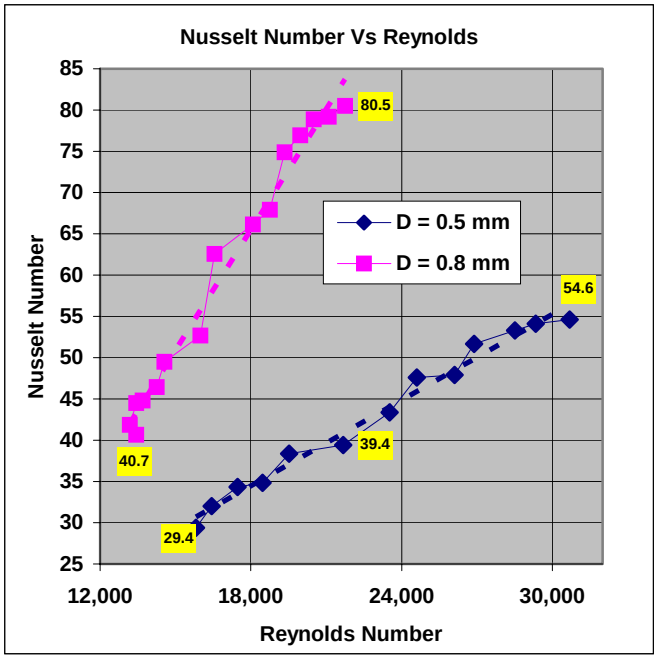


Figure 9 Variation of Nusselt number at different nozzle diameter

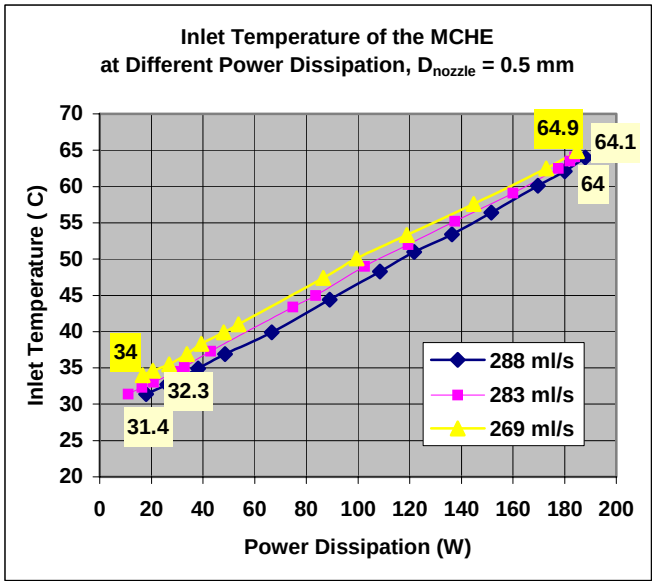


Figure 10 Variation of the inlet temperature of the Mini Channel Heat Exchanger at different power dissipation

Figure 11 shows the comparison of the value "Nu / Pr^(1/3)" gathered from the experiment with the existing correlations "Womac et al (1993)" and "Martin et al (1977)". It shows that at the nozzle diameter of 0.5 mm, the experimental values of "Nu / Pr^(1/3)" some what agree and lie between the correlation made by Martin (1977) and Womac (1993) on the Reynold number range between 22,000 – 31,000.

It is shown in the figure that for higher "Reynold number" the experimental results go closer to the correlation made by Martin (1977). The experimental values are somewhere intersecting with the correlation made by Womac at the value of "Nu / Pr^(1/3)" of 30. The same comparison also discussed for different nozzle diameter, which is at d_{nozzle} = 0.8 mm.

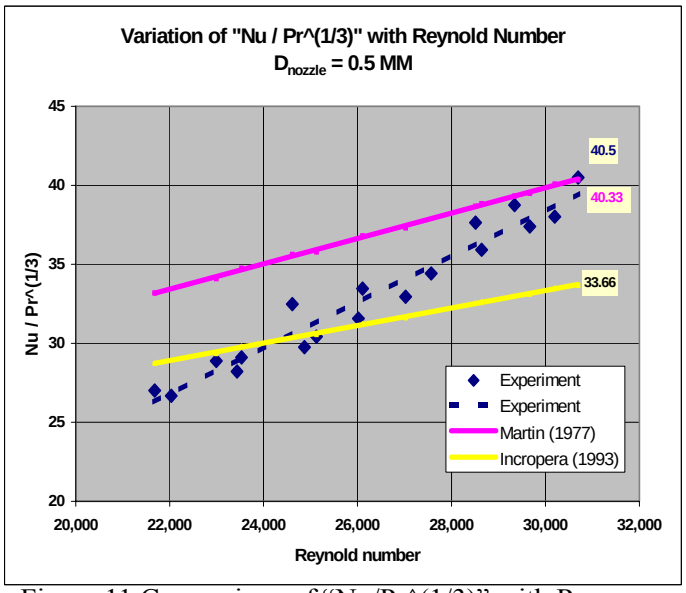


Figure 11 Comparison of "Nu/Pr^(1/3)" with Re at d_{nozzle} = 0.5 mm with other literature correlations

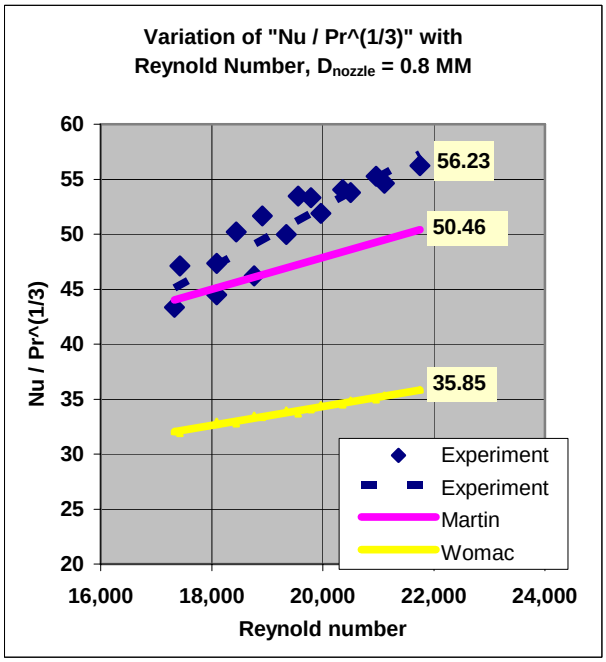


Figure 12 Comparison of "Nu/Pr^(1/3)" with Re at d_{nozzle} = 0.8 mm with other literature correlations

Figure 12 below shows the comparison of the experimental values of "Nu/Pr^(1/3)" with the correlations made by Martin and Womac at the range of Re number, from 17,000 to 22,000. It shows that the experimental values of

"Nu/Pr^(1/3)" are greater than other correlations. It is clearly shown in the graph that they lay above other correlations. This graph also support the previous statement that the experimental system has better "convective heat transfer" performance on the d_{nozzle} = 0.8 mm than d_{nozzle} = 0.5 mm. It is shown in the figure that for lower "Reynold number" the experimental results go closer to the correlation made by Martin (1977). At higher Reynold number, the experimental results are always greater than any correlation, for example at the Re = 21,800 the experiment has "Nu/Pr^(1/3) = 56.23, meanwhile the Martin correlations has 50.46, and Womac correlation has 35.83.

Acknowledgements

Thanks for Fujikura Ltd and Panasonic Japan for the support in this project

References

[1] D.C. Wadsworth, Issam Mudawar, 1990, "Cooling of a Multichip Electronic Module by Means of Confined Two Dimensional Jets of Dielectric Liquid", Journal of Heat Transfer, Transactions of ASME, vol. 112, pp 891 – 897

[2] D.C. Wadsworth, Issam Mudawar, 1992, "Enhancement of Single-Phase Heat Transfer and Critical Heat Flux From an Ultra-High-Flux Simulated Microelectronic Heat Source to a Rectangular Impinging Jet of Dielectric Liquid", Journal of Heat Transfer, Transactions of ASME, vol. 114, pp 764 – 768

[3] D.H. Wolf, R. Viskanta, F.P Incropera, 1990, "Local Convective Heat Transfer From a Heated Surface to a Planar Jet of Water With a Nonuniform Velocity Profile", Journal of Heat Transfer, Transactions of ASME, vol. 112, pp 898 – 905

[4] D. J. Womac, S. Ramadhyani, F. P. Incropera, 1993, "Correlating Equations for Impingement Cooling of Small Heat Sources With Single Circular Liquid Jets", Journal of Heat Transfer, Transactions of ASME, vol. 115, pp 106-115

[5] Frank P. Incropera and David P. DeWitt, 1996, *Fundamentals of Heat and Mass Transfer*, John Wiley & Sons, New York 4th edition, pp 387 – 392,

[6] Martin, H., 1977, "Heat and Mass Transfer between Impinging Gas Jets and Solid Surfaces," in J.P Hartnett and T.F. Irvine, Jr., Eds., Advances in Heat Transfer, Vol. 13, Academic Press, New York

A Generalized Mathematical Model to Account for the Effect of Liquid-vapor Interfacial Shear Stress of a Heat Pipe with a Grooved Wick Structure: Modified Shah Method

Joung Ki Seo*, Sung Jin Kim, Kyu Hyung Do

Department of Mechanical Engineering
Korea Advanced Institute of Science and Technology
Taejon, 305-701, Korea
Tel : +82-42-869-3043, Fax : +82-42-869-3043,
E-mail Address: hagis@.kaist.ac.kr

Abstract

Liquid flow passage of a heat pipe with a grooved wick structure is not enclosed but open to vapor core region where vapor flows in the direction opposite to the liquid flow. These counter-flows of liquid and vapor cause an additional shear stress at liquid-vapor interface. The effect of the interfacial shear stress on the flow characteristics, such as liquid pressure drop and velocity distribution becomes more significant as the outer diameter of the heat pipe reduces. However, it is difficult to obtain the flow the characteristics of liquid flow in a groove due to the geometric complexity of groove walls and the liquid-vapor interfacial shear stress, which in turn requires heavy reliance on extensive CFD simulations or expensive experiments. In order to eliminate this difficulty, a new method based on the one proposed by Shah is explained to determine the flow characteristics for an open channel with an arbitrary cross section where the counter-current flow exists at the liquid-vapor interface. In order to check the validity of the modified Shah method, numerical results based on the modified Shah method are compared with those presented by numerical and analytical results from previous investigations and excellent agreements are obtained.

Key words: Heat pipe, Liquid-vapor interfacial shear stress, Open channel

1. INTRODUCTION

Miniature heat pipes with a small outer diameter (O.D. hereafter) of 3mm or 4mm have been widely used in cooling microprocessors in notebook and desktop PC applications due to their powerful heat transfer capability and small size. As the power density of critical electronic components is increased, the need for a heat pipe with a higher heat transport rate and a lower thermal resistance is greater than ever in the development of future electronic equipment. In order to cope with this practical demand, it is necessary to enhance the thermal performance of a miniature heat pipe, by optimizing the wick structure of a heat pipe.

It is well-known that the liquid pressure drop along the wick structure is a dominant one among the other pressure drops of the working fluid and the precise estimation of the liquid pressure drop is very important in developing an analysis model for fluid flow in a heat pipe. For a heat pipe with a grooved wick structure, the liquid flow passage of is not enclosed but open to vapor core region where vapor flows in the direction opposite to the liquid flow. These counter-flows of liquid and vapor cause an additional shear stress at liquid-vapor interface. The effect of the interfacial shear stress on the flow characteristics, such as liquid pressure drop and velocity distribution becomes more significant as the outer diameter of the heat pipe reduces. Therefore, a model for dealing with the effect of the counter-flows has been critical issue in developing mathematical models for heat pipes with grooved wick structure. However, it is difficult to obtain the flow the characteristics of liquid flow in a grooved wick structure due to the geometric complexity of groove walls and the liquid-vapor interfacial shear stress, which in turn requires heavy reliance on extensive numerical simulations or expensive experiments.

Ayyaswamy et al. [1] used the Galerkin boundary method to solve the Poisson equation to determine the fluid velocity distribution and Poiseuille number for the liquid flow in triangular grooves with circular interface and zero interfacial

shear stress. Hufschmidt et al. [2] solved the momentum equation for the laminar flow of liquid in rectangular grooves with a flat liquid-vapor interface and a uniform shear stress imposed at the liquid-vapor interface. However, these analytic results were obtained using unrealistic boundary conditions at the liquid-vapor interface in a heat pipe.

Ma et al. [3] determined the Poiseuille number for the liquid flow in triangular grooves with liquid-vapor interfacial shear stress by transforming momentum equation into Laplace equation. In their approach, an experimentally determined coefficient was required since the liquid-vapor interfacial velocity is unknown function of vapor velocity. Peterson and Ma [4] conducted an analytical and experimental investigation on the countercurrent liquid-vapor interactions and the liquid friction factor for triangular grooves using the Nachtsheim-Swigert iteration scheme. The agreement between the experimental data and the numerical model was within 10%.

Suh et al. [5] investigated numerically the effect of liquid-vapor interfacial shear stress on the liquid flow in trapezoidal and sinusoidal grooves. Thomas et al. [6] studied fully-developed laminar flow in trapezoidal grooves with shear stress at the liquid-vapor interface using finite difference method and validated their numerical results by comparing existing analytical solutions for the liquid flow in triangular and rectangular grooves. However, no correlations of liquid pressure drop with groove geometry were provided in [6], the numerical results of Thomas et al. were hard to be applied in developing mathematical models for heat pipes.

In order to overcome the limitations due to unrealistic boundary condition in analytic approaches and computational difficulties in numerical approaches, we suggest a powerful analytic method called a modified Shah method. The main objective of the present study is to develop a new mathematical method by which one can estimate the pressure drop and velocity distribution of liquid flow in a groove with an arbitrary cross section where the counter-current flow exists at the liquid-vapor interface.

2. MATHEMATICAL FORMULATION

2.1 Liquid pressure drop in grooves

By modeling the grooved wick structure as a porous medium, the liquid pressure gradient can be expressed by

$$\frac{dP_l}{dx} = -\frac{\mu_l u_D}{K} \tag{1}$$

which is known as Darcy's law. Using the relationship between the Darcian velocity (u_D) and the averaged pore velocity (u_p), $u_D / u_p = \varepsilon$, and the mass flow rate in the wick structure, $\dot{m}_l = \rho_l A_p u_p N$, Eq. (1) yields

$$\frac{dP_l}{dx} = -\frac{\mu_l \varepsilon u_p}{K} = -\frac{\mu_l \varepsilon \dot{m}_l}{\rho_l A_p N K} \tag{2}$$

where the permeability of a groove with an arbitrary cross-section, K, can be written as [7]

$$K = \frac{D_{h,p}^2 \varepsilon}{2 f \mathrm{Re}_{h,p}} \tag{3}$$

The counter-flows of liquid and vapor cause an additional shear stress at the liquid-vapor interface, which makes the analysis of the liquid flow difficult. The effect of the counter-flows on the interfacial shear stress can be accounted for by introducing a correction factor, α, when substituting Eq. (3) into Eq. (2), which results in the following equation [8]:

$$\frac{dP_l}{dx} = -\frac{2\mu_l f \mathrm{Re}_{h,p} \dot{m}_l}{\rho_l A_p N D_{h,p}^2} \alpha + \rho_l g \sin\beta \tag{4}$$

where the last term is included for a pressure drop due to gravity. In Eq. (4), the Poiseuille number, $f\mathrm{Re}_{h,p}$, the correction factor, α, the actual liquid flow area, A_p, and the mass flow rate of liquid, $\dot{m}_l$ need to be expressed in terms of the geometric variables and thermo-physical properties of the liquid in order to quantitatively evaluate the liquid pressure gradient.

Note that $f\mathrm{Re}_{h,p}$ in Eq. (4) is the Poiseuille number for an open channel without liquid-vapor interfacial shear stress and α is the ratio of an actual liquid pressure gradient with the counter-flow effect included to an ideal liquid pressure gradient with zero interfacial shear stress. This ratio can be expressed as

$$\alpha = 1 + F\,\psi \tag{5}$$

where

$$\psi = \frac{D_{h,p}\tau_{v,i}}{\mu_l u_p} = \frac{D_{h,p} r_v}{2\mu_l u_p}\left(\frac{dP_v}{dx}\right)$$

F is a function of the geometric variables, and the contact angle and ψ is the non-dimensional shear stress at the interface.

2.2 Modified Shah method

Velocity field and pressure distributions for closed channels with a circular or rectangular cross section can be derived easily by using an analytic method. Also, Shah [9] developed a simple but accurate numerical method to determine the flow characteristics for a closed channel with an arbitrary and constant cross section. However, it is difficult to obtain analytically the flow characteristics such as the liquid pressure drop and the velocity distribution for an open channel with an arbitrary cross section, which in turn requires heavy reliance on extensive CFD simulations or expensive experiments.

To eliminate these difficulties, in the present study, a new method based on the one proposed by Shah[9] is suggested to determine the flow characteristics for an open channel with an arbitrary cross section where the counter-current flow exists across the open interface.

The governing equation and boundary conditions for fully-developed liquid flow along an open channel with an arbitrary and constant cross section, and the counter-current flow at the open interface (shown in Fig. 1) can be expressed by

$$\nabla^2 u_l = \frac{1}{r}\frac{\partial}{\partial r}\left(r\frac{\partial u_l}{\partial r}\right)+\frac{1}{r^2}\frac{\partial^2 u_l}{\partial \theta^2}=\frac{1}{\mu_l}\frac{dP_l}{dz}=C_1 \quad (6)$$

$$\text{B.C.s} \qquad u_l = 0 \qquad \text{on } \Gamma_{wall}$$
$$\tau_l = -\tau_v \qquad \text{on } \Gamma_{interface}$$

By applying the following transformation in Eq. (7), as Shah [9] suggested, the governing equation

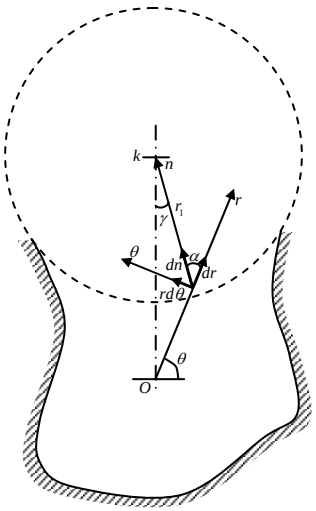


Fig. 1. Schematic view of a channel with an open and arbitrary cross-section

and the boundary condition can be reduced to Eq. (8)

$$-\frac{u_l}{C_1} = u_l^{\,*} - \frac{r^2}{4} \quad (7)$$

$$\nabla^2 u_l^{\,*} = 0 \quad (8)$$

$$\text{B.C.s} \qquad u_l^{\,*} = \frac{r_i^2}{4} \qquad \text{on } \Gamma_{wall}$$
$$\mu_l\left(\frac{\partial u_l}{\partial n}\right) = -\mu_v\left(\frac{\partial u_v}{\partial n}\right) \qquad \text{on } \Gamma_{interface}$$

where n represents the normal direction to the liquid-vapor interface.

Assuming that the vapor velocity at the interface equals zero, the liquid velocity gradient term in the above boundary condition becomes

$$\left(\frac{\partial u_l}{\partial n}\right) = -\frac{\mu_v}{\mu_l}\left(\frac{\partial u_v}{\partial n}\right) = \frac{f\,\mathrm{Re}_{h,v}}{2D_{h,v}}\frac{\mu_v}{\mu_l}\overline{u}_v \quad (9)$$

In the meantime, Eq. (8) has a series solution in the form of

$$u_l^{\,*} = a_0 + \sum_{j=1}^{N} r^j\left(a_j\cos(j\theta)+b_j\sin(j\theta)\right) \quad (10)$$

or

$$-\frac{u_l(r,\theta)}{C_1} = -\frac{r^2}{4} + a_0 + \sum_{j=1}^{N} r^j\left[a_j\cos(j\theta)+b_j\sin(j\theta)\right] \quad (11)$$

Differential form of Eq. (11) becomes

$$-\frac{1}{C_1}\frac{\partial u_l(r,\theta)}{\partial n} = -\frac{r}{2}\left(\frac{\partial r}{\partial n}\right) + \sum_{j=1}^{N} jr^{j-1}\left[\cos(j\theta)\left(\frac{\partial r}{\partial n}\right)-r\sin(j\theta)\left(\frac{\partial \theta}{\partial n}\right)\right]a_j + \sum_{j=1}^{N} jr^{j-1}\left[\sin(j\theta)\left(\frac{\partial r}{\partial n}\right)+r\cos(j\theta)\left(\frac{\partial \theta}{\partial n}\right)\right]b_j \quad (12)$$

From Eq. (10), u_l^* can be evaluated as long as we determine the $2N+1$ unknown coefficients a_0, a_j, and b_j. This can be done by applying boundary conditions at the wall and the liquid-vapor interface. Along the wall, n points are selected to conform to the geometry of the open channel and a no slip condition is applied to generate n boundary conditions for Eq. (11). Similarly, m points are selected along the liquid-vapor interface

where the continuous shear stress condition is applied to generate *m* boundary conditions for Eq. (12). Since *n*+*m*=2*N*+1, these 2*N*+1 equations generated from Eqs. (11) and (12) can be solved using linear algebra. Also, two gradient terms in Eq. (12) can be derived from a geometric relationship by assuming a circular interface as:

$$\frac{dr}{dn} = \sin\theta \cdot \cos\gamma \mp \cos\theta \cdot \sin\gamma \tag{13}$$

$$\frac{d\theta}{dn} = \frac{1}{r}\left(\cos\theta \cdot \cos\gamma \pm \sin\theta \cdot \sin\gamma\right) \tag{14}$$

where

$$\cos\gamma = \frac{k^2 + r_1^2 - r^2}{2kr_1}$$

$$\sin\gamma = \sqrt{1 - \left(\frac{k^2 + r_1^2 - r^2}{2kr_1}\right)^2}$$

To evaluate the ratio of the actual liquid pressure drop with the counter flow effect included to the ideal liquid pressure drop with no vapor flow effect, as in Eq. (5), iterative calculations are needed and the entire calculation procedure can be summarized as follows (A primed variable denotes that it is affected by non-zero vapor flow):

1) Generate 2*N*+1 equations and solve these equations for, a_0, a_j and b_j in Eqs. (9), (11), and (12) for a no vapor flow case.
2) Calculate $-\overline{u}_l / C_1$.
3) Assume the averaged vapor velocity $\overline{u}_v$ and the averaged liquid velocity $\overline{u}_l' = \overline{u}_l$ and take C_1 as C_1'.
4) Solve the equations for, a_0, a_j and b_j in Eqs. (9), (11), and (12).
5) Recalculate C_1' based on a_0, a_j and b_j and replace $C_{1,old}'$ with $C_{1,new}'$.
6) Repeat 3) to 5) until $C_{1,old}' \approx C_{1,new}'$.
7) Calculate the pressure drop ratio along the open channel relative to the closed channel with an arbitrary cross section from following equation.

$$\left(\frac{dP}{dz}\right)_l' \Big/ \left(\frac{dP}{dz}\right)_l = \frac{\overline{u}_l'}{\overline{u}_l} \frac{\int_{A_c} f(r,\theta) dA_c}{\int_{A_c} f'(r,\theta) dA_c} = (1+\alpha) \tag{15}$$

3. NUMERICAL RESULTS

In order to check the validity of the modified Shah method, numerical results based on modified Shah method are compared with those presented by Ayyaswami et al. [1] and Hufschmidt et al. [2]. In comparison to numerical results by Ayyaswami et al, the maximum error for the Poiseuille number is 0.2% as shown in Fig. 2. Also, in comparison to analytic results by Hufschmidt et al., the maximum errors for the Poiseuille number and *F* are 0.02% and 2%, respectively, as shown in Fig. 3.

In addition, velocity distribution obtained from Hufschmidt et al. [2] for rectangular groove with the flat interface where the counter-current flow exists is compared with the results of modified Shah method and shown in Fig. 4. Non-dimensional velocity distributions show very close agreement with each other, which confirms the validity of the modified Shah method.

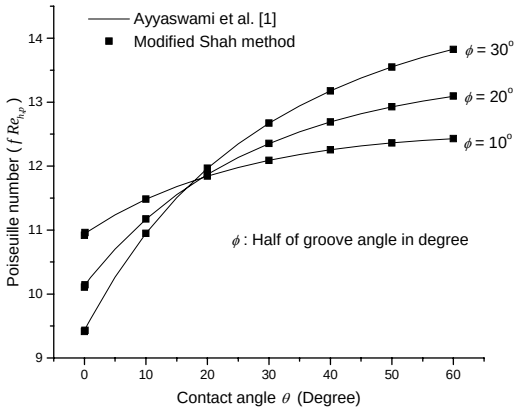


Fig. 2 Comparison of numerical results for Poiseuille number

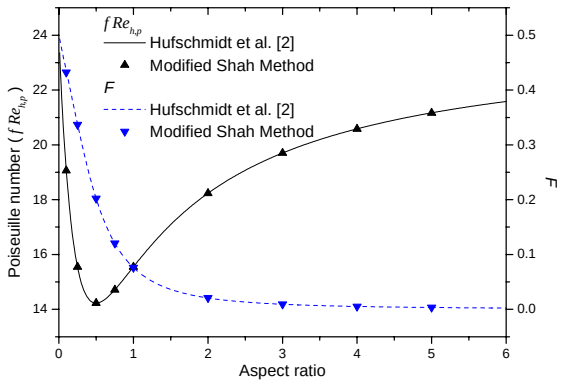
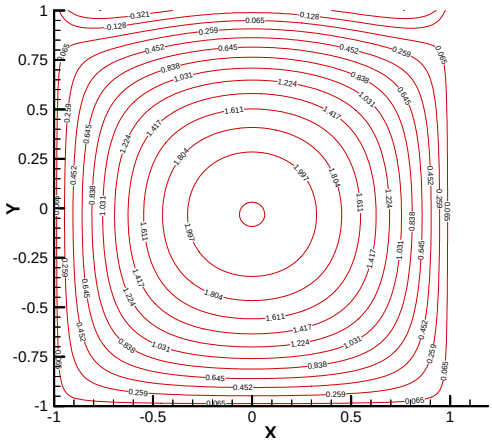
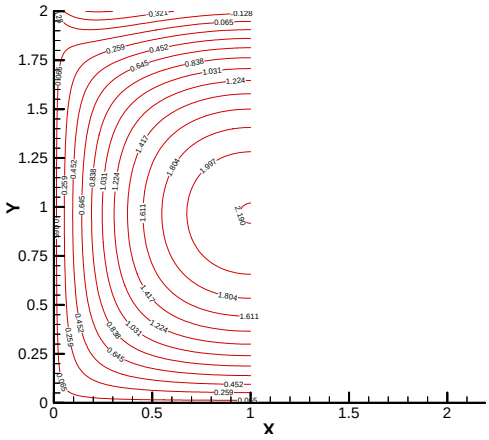


Fig. 3 Comparison of results for Poiseuille number and *F*



(a) Modified Shah method



(b) Analytic solution, Hufschmidt et al.[11]
(Symmetric with respect to x=1)

Fig. 4. Non-dimensional velocity distribution

4. Conclusion

A one-dimensional mathematical model for a liquid pressure drop in a groove with an arbitrary cross section has been developed including the effects of shear stress at the liquid-vapor interface. In particular, a novel method called a modified Shah method is suggested and validated; this method is accounts for the effect of the liquid-vapor interfacial shear stress. The analytical results based on the modified Shah method are compared with those of previous investigations and excellent agreement is achieved.

Acknowledgement

This work was supported by Center for Electronic Packaging Materials of Korea Science and Engineering Foundation

References

1. P. S. Ayyaswami, I. Catton, D. K. Edwards, 1974, "Capillary flow in triangular grooves," J. Appl. Mech. Vol. 41, pp. 332-336.
2. E. Hufschmidt, E. Burck, G. Di Cola, H. Hoffman, 1975, "The shearing effect of vapor flow on laminar liquid flow in capillaries of heat pipes," NASA TT-F-16601, pp. 1-21.
3. H. Ma, G. Peterson, X. Lu, 1994, "The influence of vapor-liquid interactions on the liquid pressure drop in triangular microgrooves," Int. J. Heat Mass Transfer, Vol. 37, pp. 2211-2219.
4. G. Peterson, H. Ma, 1996, "Analysis of countercurrent liquid-vapor interactions and the effect on the liquid friction factor," Exp. Thermal Fluid Sci., Vol. 12, pp. 13-24.
5. J. S. Suh, R. Greif, C. P. Grigoropoulos, 2001, "Friction in micro-channel flows of a liquid and vapor in trapezoidal and sinusoidal grooves," Int. J. Heat Mass Transfer, Vol 44, pp. 3103-3109.
6. S. K. Thomas, R. C. Lykins, K. L. Yerkes, 2001, "Fully developed laminar flow in trapezoidal grooves with shear stress at the liquid-vapor interface," Int. J. Heat Mass Transfer, Vol. 44, pp. 3397-3412.
7. A. Faghri, 1995, *Heat Pipe Science and Technology*, Taylor & Francis, pp. 124-125.
8. S. J. Kim, J. K. Seo, K. H. Do, 2003, "Analytical and experimental investigation on the operational characteristics and the thermal optimization of a miniature heat pipe with a grooved wick structure," Int. J. Heat Mass Transfer, Vol. 46, pp. 2051-2063.
9. R. K. Shah, Laminar Flow Friction and Forced Convection Heat Transfer in Ducts of Arbitrary Geometry, Int. J. Heat Mass Transfer 18 (1975) 849-862.

Theoretical Analysis of Two-phase Heat Spreaders with ifferent Cross-section Micro Grooves

F. Lefèvre*, R. Revellin, M. Lallemand

Centre de Thermique de Lyon, UMR CNRS 5008
Institut National des Sciences Appliquées
20 avenue Albert Einstein
69621 VILLEURBANNE Cedex - France
Tel: (33) 4 72 43 82 51 ; Fax: (33) 4 72 43 60 10
e-mail: lefevre@genserver.insa-lyon.fr

Abstract

In this paper, we present a capillary two-phase flow model of flat spreaders with micro grooves of different cross-sections. This model permits to calculate the maximum heat transfer capabilities and the optimal liquid charge of the spreader. The spreader is divided into several control volumes for which the conservation equations of mass, momentum and energy are written for liquid and vapour phases and the Laplace-Young equation for the curvature radius at the liquid-vapour interface. The resulting set of first order, non linear, coupled ordinary differential equations are solved numerically with a fourth order Runge-Kutta method. This model is able to take into account different operating configurations. We present the results obtained for trapezoidal and rectangular micro grooves cross-sections. For the particular case of rectangular grooves, we have developed a model, including the longitudinal curvature radius, which permits to take into account the meniscus movement from the top to the bottom of the groove in the evaporator section. We find a good agreement between our model and the experimental results of Hopkins for any vapour saturation temperatures.

Key words: Micro Heat Pipes, Heat Spreader, Capillary Flow

1. INTRODUCTION

Micro heat pipes are commonly used to act as an efficient heat spreader, to eliminate hot spots and to reduce temperature gradients of electronic components. The more simple heat spreader consists in a row of tubes of triangular cross section, whose corners are used as a wick structure to return the liquid from the condenser to the evaporator. This type of micro heat pipes has been theoretically and experimentally studied by several authors ([1], [2]).

The heat spreaders that we consider in this paper are long axial grooved heat pipes with a singular flat vapour channel. This type of spreaders permits to dissipate more heat power than the row of triangular micro heat pipes, because of a lower vapour pressure drop. They have been experimentally and theoretically studied by Hopkins [3] for rectangular and trapezoidal grooves. A one dimensional model

describing the fluid flow in the miniature grooved heat pipe was presented for trapezoidal grooves, but only a closed-form solution was given for the case of rectangular grooves. In this paper, we propose a capillary flow model, based on the conservation equations too, which permits to cope with the limiting case of rectangular grooves. This model has been applied to different configurations of the spreader (i.e. different location of the evaporator and condenser sections), including the one of Hopkins [3] for the validation.

2. THE CAPILLARY ONE DIMENSIONAL TWO-PHASE FLOW MODEL

In this part, we present a capillary two-phase flow model for flat heat spreaders. This model permits to calculate the maximum heat transfer capabilities and the optimal liquid charge of the spreaders.

2.1 The experimental design

The heat spreaders under investigation are long axial grooved heat pipes with a singular flat vapour channel as shown in figure 1. The groove cross sections are either trapezoidal or rectangular.

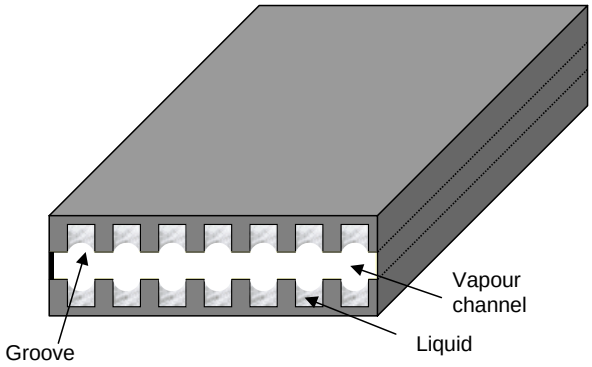


Figure 1: Schematic of the flat heat spreader

Two different operating configurations are studied in this paper. In the first case (figure 2), the electronic component to be cold is placed in the middle of the upper face with a condenser occupying the entire lower face. With this operating configuration, called configuration A, it is necessary to have vertical grooves at each spreader tip in order to connect the upper and lower faces.

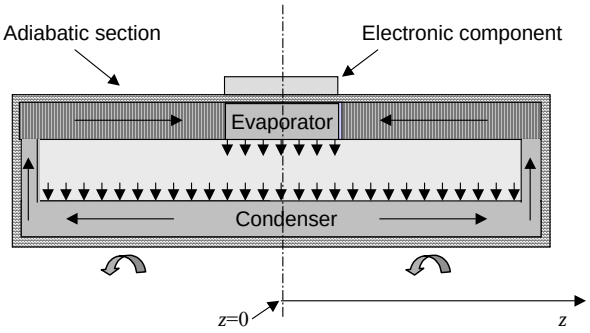


Figure 2: Schematic of the flat heat spreader, configuration A

In the second configuration, called configuration B (figure 3), the evaporator and the condenser are placed on both the lower and upper sides, each one at an extremity of the spreader.

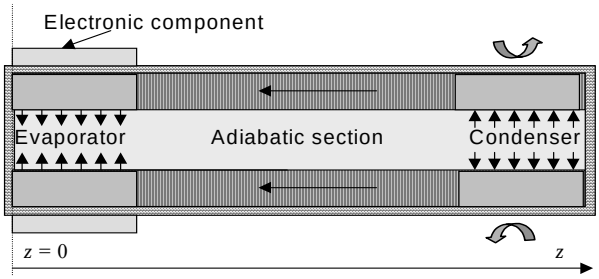


Figure 3: Schematic of the flat heat spreader, configuration B

2.2 The model equations

Our capillary two-phase flow model is similar to the one developed by Longtin [1] for triangular micro heat pipes, but it takes into account both the evaporator and condenser regions. The evaporator and the condenser sections are covering all the width of the spreader, which permits to study only one groove in configurations A and B. For the particular case of configuration A, as the electronic component is located in the middle of the groove, only one half of the groove is considered.

Our model is a one dimensional steady state model, which considers only axial variations

along a groove. The spreader is divided into several control volumes for which the conservation equations are written for the liquid and vapour phases. For the liquid phase, the equations are written in both the upper and lower sides. Subscript 1 is relative to the upper side and subscript 2 to the lower side. For the mass balance, we obtain:

$$\frac{d\left(A_{l1}u_{l1}\right)}{dz}dz = A_{i1}v_{il1}dz \tag{1}$$

$$\frac{d\left(A_{l2}u_{l2}\right)}{dz}dz = A_{i2}v_{il2}dz \tag{2}$$

$$\frac{d\left(A_{v}u_{v}\right)}{dz}dz = -\frac{\rho_l}{\rho_v}\left(A_{i1}v_{il1} + A_{i2}v_{il2}\right)dz \tag{3}$$

where subscript l and v are relative to the liquid and the vapour respectively. The axial coordinate z is represented in figures 2 and 3, u is the velocity, ρ the density, A the cross section and A_i is the liquid-vapour interfacial area per unit length. The radial velocity of condensation or evaporation v_{il}, is calculated from the energy balance:

$$v_{il} = -\frac{\dot{q}}{\rho_l A_i \Delta h_v} \tag{4}$$

where $\dot{q}$ is the heat power per unit length of condensation or evaporation, which is assumed to be uniform in the condenser and evaporator sections and equal to zero in the adiabatic section. Δh_v is the latent heat of vaporisation.

Three additional equations are obtained from the momentum equation:

$$\rho_l \frac{d\left(A_{l1}u_{l1}^{\ 2}\right)}{dz}dz = -\frac{d\left(A_{l1}P_{l1}\right)}{dz}dz + \left|\tau_{i1}\right|A_{i1}dz - \left|\tau_{lw1}\right|A_{lw1}dz - \rho_l A_{l1} g \sin\theta dz \tag{5}$$

$$\rho_l \frac{d\left(A_{l2}u_{l2}^{\ 2}\right)}{dz}dz = -\frac{d\left(A_{l2}P_{l2}\right)}{dz}dz \pm \left|\tau_{i2}\right|A_{i2}dz - \left|\tau_{lw2}\right|A_{lw2}dz - \rho_l A_{l2} g \sin\theta dz \tag{6}$$

$$\rho_v \frac{d\left(A_{v}u_{v}^{\ 2}\right)}{dz}dz = -\frac{d\left(A_{v}P_{v}\right)}{dz}dz - \left|\tau_{i1}\right|A_{i1}dz - \left|\tau_{i2}\right|A_{i2}dz - \left|\tau_{vw}\right|A_{vw}dz - \rho_v A_v g \sin\theta dz \tag{7}$$

P is the pressure, τ_{lw} and τ_{vw} the liquid-wall and vapour-wall shear stresses and θ is the tilt angle. τ_i is the interfacial shear stress, depending on the operating configuration for equation (6). Indeed, in configuration B, the liquid and the vapour in the lower face are countercurrent whereas in configuration A, they have the same direction.

In equations (1) to (7), A_l, A_v, A_{vw}, A_{lw}, and A_i depend on the groove geometry, the contact angle and the radius of curvature. The radius of curvature r, is obtained by deriving the Laplace-Young equation with respect to z for the upper and the lower faces:

$$\frac{dP_{l1}}{dz} = \frac{dP_v}{dz} - \frac{d}{dz}\left(\frac{\sigma}{r_1}\right) \tag{8}$$

$$\frac{dP_{l2}}{dz} = \frac{dP_v}{dz} - \frac{d}{dz}\left(\frac{\sigma}{r_2}\right) \tag{9}$$

where σ is the surface tension. Thus, we obtain a set of 10 equations, including 8 coupled differential equations.

2.3 Boundary conditions

The resulting set of first order, non linear, coupled ordinary differential equations are solved numerically with a fourth order Runge-Kutta method using the following boundary conditions:

$$u_{l1}\big|_{z=0} = u_{l2}\big|_{z=0} = u_v\big|_{z=0} = 0$$

$$P_v\big|_{z=0} = P_{sat}$$

$$P_{l1}\big|_{z=0} = P_{sat} - \frac{\sigma}{r_1\big|_{z=0}} \tag{10}$$

$$P_{l2}\big|_{z=0} = P_{sat} - \frac{\sigma}{r_2\big|_{z=0}}$$

P_{sat} is the saturation vapour pressure. To determine the boundary conditions for the meniscus radius r, we suppose that, at the end of the evaporator (configuration B) or at its centre (configuration A), the groove is empty, which corresponds to a blocking limit (figure 4(a)). At the beginning of the evaporator, the meniscus is considered at the bottom of the groove, which corresponds to the drying limit and to a minimum value of the meniscus radius, r_{min} (figure 4 (c)). In order to find the maximum heat transfer capability

of the spreader, a shooting method is used on variable $\dot{q}$. To calculate this maximum, we search $\dot{q}$, so that, at the end of the condenser section, the value of r is infinite. With these boundary conditions, the value of r_1 and r_2 at z=0 depends on the operating configuration: in both configurations r_1 is equal to r_{min}, r_2 is equal to r_{min} in configuration B and is infinite in configuration A. The value of r_{min} depends on the groove geometry and of the contact angle β_0. This latter angle depends of the wall and fluid properties.

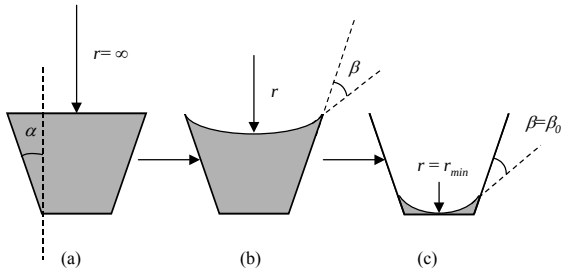


Figure 4: Schematic liquid-vapour meniscus variation from the condenser to the evaporator

2.4 Model for rectangular grooves

As we can see in figure 4 for a trapezoidal groove, the change in the meniscus radius from the condenser to the evaporator, which creates the capillary pressure, happens in two stages. At the beginning of the condenser, the meniscus stays on the top of the groove with a contact angle β varying until it reaches the value β_0. Then, the meniscus goes down in the groove with $\beta=\beta_0$ until the bottom of the groove. During this stage, the meniscus receeds in the groove ans its radius decreases, which creates the pressure gradient. For rectangular grooves, the meniscus radius remains equal to r_{min} from the top to the bottom of the groove.

Thus, we have introduced the longitudinal curvature radius in the capillary flow model in order to have a pressure gradient from the top to the bottom of the groove. If δ is the thickness of the liquid in the groove, the longitudinal radius of curvature can be written as follows:

$$r_l(z)=\frac{\left(1+\left(\frac{d\delta}{dz}\right)^2\right)^{\frac{3}{2}}}{\frac{d^2\delta}{dz^2}} \tag{11}$$

Let us intoduce δ' the derivative of δ with respect to z:

$$\frac{d\delta}{dz}=\delta' \tag{12}$$

Introducing eq.(12) in eq.(11) leads to a first order differential equation:

$$\frac{d\delta'}{dz}=\frac{\left(1+\delta'^2\right)^{\frac{3}{2}}}{r_l(z)} \tag{13}$$

where $r_l(z)$ is obtained from the Young – Laplace equation:

$$r_l(z)=\frac{1}{\frac{P_v-P_l}{\sigma}-\frac{1}{r}} \tag{14}$$

Introducing equations (12) to (14) in our model permits to cope with the particular case of rectangular grooves. At z=0, δ' is equal to zero and a shooting method is used in order to obtain an infinite value for $r_l(z)$ when the meniscus reaches the top of the groove.

3. RESULTS AND DISCUSSION

In this part, we present the results obtained for rectangular channels with the same geometrical parameters for the flat heat spreader than those of the experimental spreader of Hopkins [3] (figure 5). The total length of the spreader is equal to 120 mm.

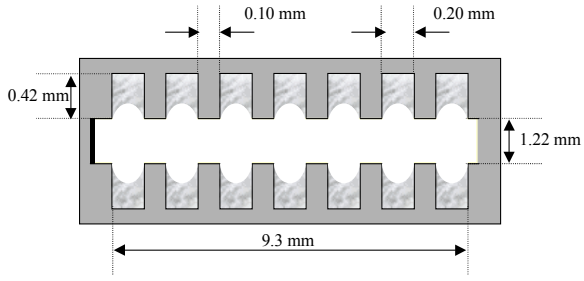


Figure 5: Schematic cross section of the experimental flat heat spreader

3.1 Validation with experimental data [3]

The experimental results obtained by Hopkins are those of configuration B with an evaporator length of 15.6 mm, an adiabatic length of 70 mm and a condenser length of 34.4 mm. The flat spreader, made in copper is filled with water. These experimental results are compared with our numerical model in figure 6 for different saturation temperatures.

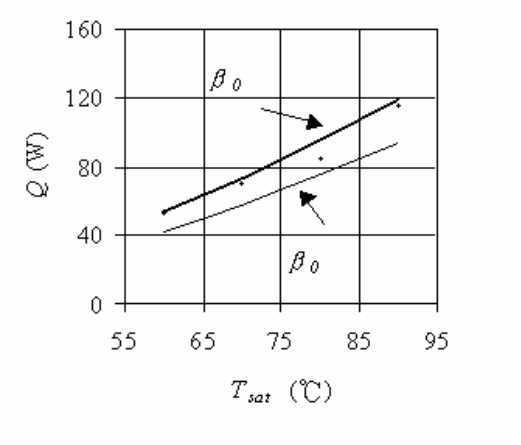


Figure 6: Maximum heat transfer Q versus the saturation temperature (+ Hopkins (1999), — β_0=60°, - β_0=50°)

We have considered two values of the contact angle (β_0=50° and β_0=60°), corresponding approximatively to experimental measurements given in [4] and [5] for the copper/water couple. As we can see, the maximum heat powers Q, calculated and measured, are very close, which validates our model. Nevertheless, it is important to notice that the calculated results are very sensitive to the parameter β_0. Afterwards, β_0 will be set to a value of 50°.

In figure 7, we present the results obtained for the liquid and the vapour pressures and the meniscus radius versus the axial coordinate for T_{sat} equal to 70°C. The curvature radius varies from a value of 1.56×10^{-4} m to a value of 0.1 m, which corresponds to a numerical infinite value. By integrating the area of the liquid and the vapour all along the length, we can calculate the optimal fill charge of the heat spreader. In this case, we find an optimal mass of 590 mg. The pressure drop is 3 times more important for the liquid than for the vapour.

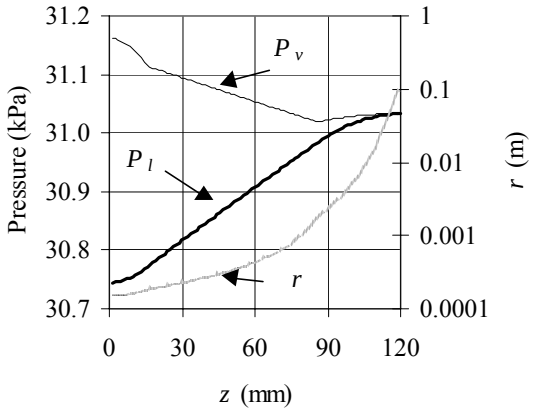


Figure 7: Liquid and vapour pressures and meniscus radius (β_0=50°, T_{sat}=70°C)

3.2 Comparison between trapezoidal and rectangular grooves

In this part, we compare the performance of the spreader in configuration B for trapezoidal and rectangular grooves. The geometrical parameters are the ones given in figure 5, excepted the distance between two grooves and the groove width. These last parameters are chosen in order to have the same groove number and the same groove cross-section for both cases. For example, the dimensions are given for α = 5° in figure 8.

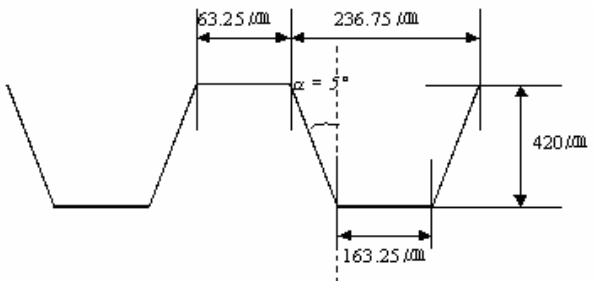


Figure 8: Trapezoidal cross-section for α = 5°

The maximum heat power and the corresponding minimum radius is shown in figure 9 versus the angle of the groove _ figure 4. As we can see, the perfomance of the heat spreader decrease with an increase of . Paradoxically,

r_{min} decreases when increases, which means that the capillary pressure is more important for the trapezoidal grooves than for the rectangular ones.

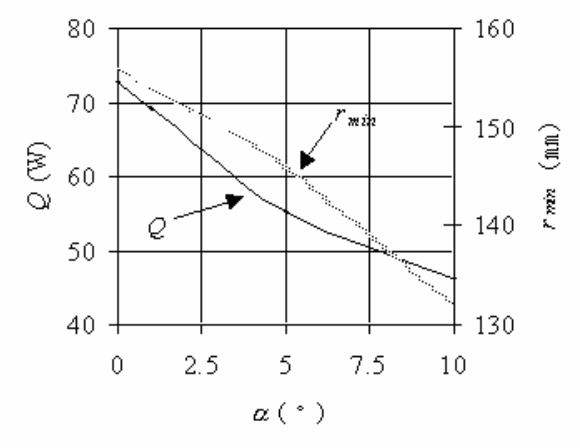


Figure 9: Maximum power and minimum meniscus radius (T_{sat}=70°C)

The reason why the performance are worst for the trapezoidal grooves can be explained from figure 10, which presents the thickness of the liquid in the middle of the groove versus z. At z = 0 mm the groove is empty and at z = 120 mm it is full of liquid. As we can see at the beginning of the evaporator, for the rectangular grooves, the grooves are filled on a shorter distance than for the trapezoidal ones. This is the reason why we have introduced the longitudinal curvature radius in our model in the case of the rectangular grooves. In the evaporator section, the liquid pressure drop is more important in the trapezoidal grooves because the liquid area is lower, which explains the bad performances with this geometry.

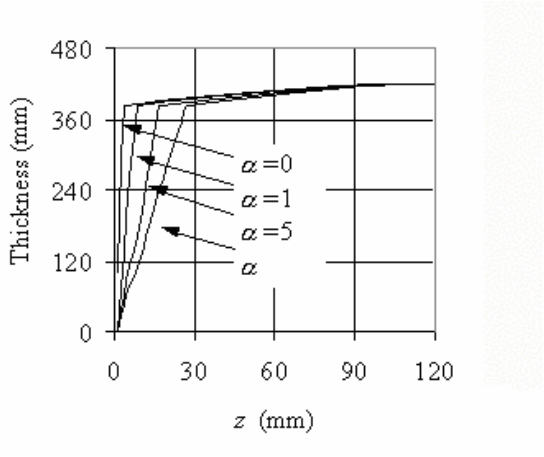


Figure 10: Thickness of the liquid in a groove versus z for different values of

3.3 Comparison between configurations A and B

In this part, we present the results obtained with the configuration A with an evaporator length equal to 31.2 mm, which represents the same evaporating area than in configuration B.

In figure 11, the maximum heat power versus T_{sat} is shown for configurations A and B. Configuration A permits to obtain better performances than configuration B with a maximum heat power nearly four times greater. Indeed, the distance covered by both the vapour and the liquid is much smaller in configuration A, which involves lower pressure drops for the same dissipated heat power.

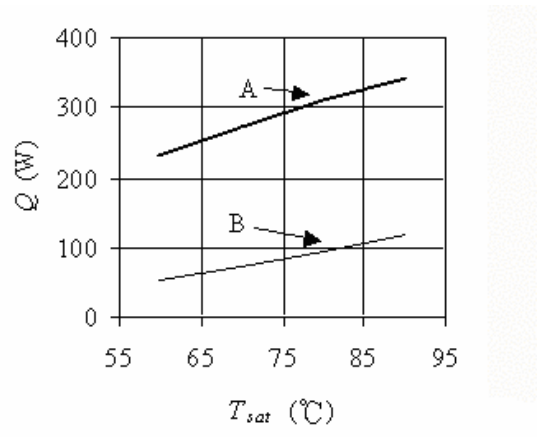


Figure 11: Maximum heat power for the spreader in configuration A and B versus T_{sat}

In figure 12, the liquid and vapour pressure are given versus z for T_{sat} equal to 70°C. Only one

half of the spreader is represented because of the configuration symmetry.

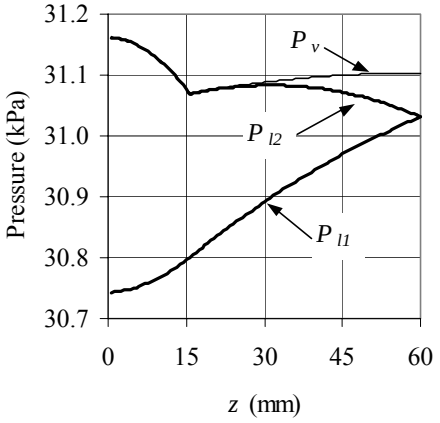


Figure 12: Liquid and vapour pressure, T_{sat}=70°C

In the lower side of the spreader (side 2), the pressure difference between the vapour and the liquid is null from z = 0 mm to z = 30 mm, which means that the meniscus radius remains infinite in this section (figure 13).

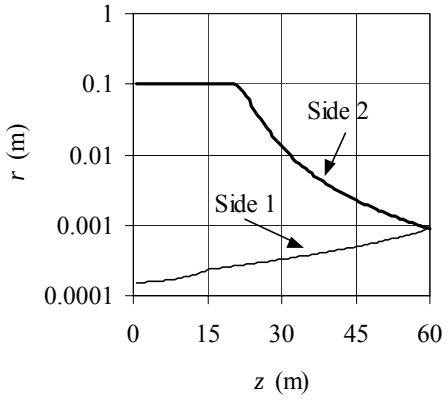


Figure 13: Meniscus radius in sides 1 and 2

In fact, as the liquid velocity is very low at the beginning of the condenser section, the pressure drop is lower in the liquid than in the vapour. So, we have imposed an infinite value for r, while the pressure drop is lower in the liquid than in the vapour. At z = 60 mm, the pressure in side 1 is equal to the one in side 2, because the rise of the liquid from side 2 to side 1 is not taken into account in our model. Indeed, the pressure drop at the extremity is negligible compared to the pressure drop in the entire groove, even if the liquid has to flow against the gravity.

4. CONCLUSION

In this paper, we have presented a capillary flow model, which permits to calculate the capabilities of a heat spreader with long axial capillary grooves. Rectangular and trapezoidal grooves have been investigated for different configurations. For a same cross section area rectangular grooves have better performances than trapezoidal ones. The performances of the heat spreader can be improved by the choice of the operating configurations, i.e. the location of the evaporator and condenser sections.

References

[1] Longtin J.P., Badran B., Gerner F.M., 1994, "A one dimensional model of a micro heat pipe during steady-state operation", J. Heat Transfer, Vol. 166, pp.709-715

[2] Le Berre M, Launay S., Sartre V., Lallemand M., 2003, "Fabrication and experimental investigation of silicon micro heat pipes for cooling electronics", J. Micromechanics and microengineering, Vol.13, pp .1-6

[3] Hopkins R., Faghri A., Khrustalev, D., 1999, "Flat miniature heat pipes with micro capillary grooves", J. Heat Transfer, Vol. 121, pp. 102-109

[4] Peterson G.P., Babin B.R., 1989, "Analytical and experimental investigation of miniature heat pipes – phase II", Final Report WRDC-TR-89-2067

[5] Nagai N., Takeuchi M., Kimura T., Kanashima T., 1998, "Attemps for measuring contact angles on superheated walls", 11th IHTC, Kyongyu, Korea, Vol. 4, pp. 137-141

Heat Transfer Characteristics in Flat Plate Micro Heat Pipe

Masafumi KATSUTA*, Yuji HOMMA*, Naoto HOSOYA*, Tomoya SHINDO*,
Junji SOTANI**, Yuichi KIMURA** and Yoshio NAKAMURA**
*Waseda University, 3-4-1 Ohkubo,Shinjuku-ku,Tokyo,Japan 169-8555
Tel/Fax:03-5286-3251
e-mail:katsuta@waseda.jp
**Furukawa Electric, 5-1-9 Higashihachiman,Hiratsuka-shi,Kanagawa,Japan 254-0016

Abstract

Because of the rapid increase in the clock speed in high performance CPU and the integration density in a multi-function SOC (System on Chip), a new concept of cooling device will be required in the near future. Considering this situation, a recently developed flat-type micro heat pipe (μHP) attracts attention, because of the easy installation in PC and the assurance of the sufficient contact area. In this research, an experimental study is made to investigate the heat transfer characteristics of such a heat transfer device in detail and finally, a prediction method of maximum heat transfer capacity is proposed.

We use three different length micro heat pipes, namely those of 118mm, 200mm and 250mm in length. By adjusting the capacity of a cooling fan, the vapor temperature at the adiabatic part is kept constant. In this study, the length of micro heat pipe, the vapor temperature at the adiabatic part, inclination and rotation angles are taken as experimental parameters. At the point just before the dry-out which is defined as a point at which thermal resistance begins to rise, the heat load to micro heat pipe is estimated to be the maximum heat transfer capacity of a micro heat pipe.

As a result, the maximum heat transfer capacity increases with decreasing the micro heat pipe length. Also increasing the inclination angle and vapor temperature, results in increase in maximum heat transfer capacity of the heat pipe. Based on these experimental trends, a pressure balance equation (capillary force limit) is proposed to predict the maximum heat transfer capacity analytically. The comparison between experimental and analytical results are made and it is confirmed that 200mm and 250mm μHP to some extent show successful agreement.

Key words: Flat Type Micro Heat Pipe, Maximum Heat Transfer Capacity, Heat Transfer Coefficient, Capillary Force Limit.

1. INTRODUCTION

The technical development of an advanced computing system has been directly in connection with an available cooling solution for its reliable operation. Because of the rapid increase in the clock speed in high performance CPU and the integration density in multi-function Soc.(System on Chip), a new cooling device will be required in the near future. With these situations, micro heat pipes have been used as the thermal controlling device of the laptop size PC. As a candidate a of micro heat pipe, various kinds of new heat pipe concepts such as SEMOS heat pipe (Self-Exciting Mode Oscillating-Flow heat pipe), oscillating heat pipe, PHP (Pulsating heat pipe) and CPL (Capillary heat pipe) have been proposed and extensively studied (in detail).[1)-5)] Soon, these new heat transport device will be put into commercial use. Recently, however, the newly developed flat type micro heat pipe (μHP) attracts attention, because of easy installation in PC and assurance of the sufficient contact area.[6),7)]

Therefore, this study attempts to provide the heat transfer characteristics of flat type micro heat pipe based on the experimental work. Finally a prediction method of maximum heat transfer capacity taking account of the capillary force limit is proposed as the most interesting and crucial characteristic for application.

2. EXPERIMENTAL EQUIPMENT AND PROCEDURE

Fig. 1 illustrates a schematic diagram of experimental setup for thermal performance test. This apparatus consists of the main test section, an electrical power supplier and the data acquisition

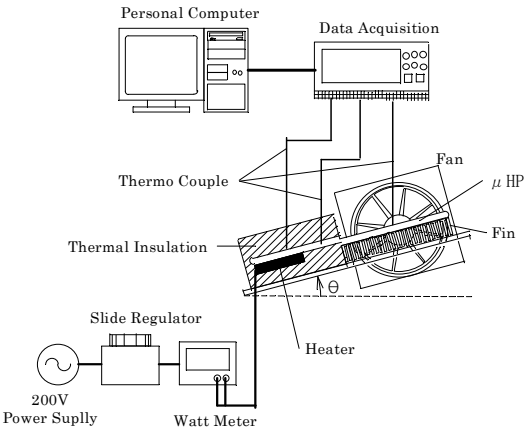


Fig.1 Schematic diagram of experimental apparatus

system with PC. A flat plate heat pipe is placed on the variable inclined plate and electrical power is applied to the cartridge heater embedded in the heater block. On the other hand, the forced convection cooling using fan and plate fin is adopted for the heat sink (condensation) part. Throughout the performance test, the evaporator and condensation parts are thermally insulated to prevent heat loss. The surface temperature of micro heat pipe is measured by 7 thermocouples. We use three different micro heat pipes, namely 118mm, 200mm and 250mm in length. The width and thickness of these micro heat pipes are the same, 9mm and 1mm respectively. The evaporator length is fixed at 40mm. Contrary to this, the length of the condensation part is different depending on the total length of micro heat pipe, 100mm for a 200 and a 250mm micro heat pipes, 68mm for a 118mm micro heat pipe. Internal wick is made of copper knitted fine wire and pure water is used as working fluid.

By adjusting the capacity of a cooling fan, the vapor temperature at the adiabatic part is kept constant. At this constant vapor temperature, the experimental run is performed. All experimental data are measured after vapor temperature at adiabatic part reaches to steady state.

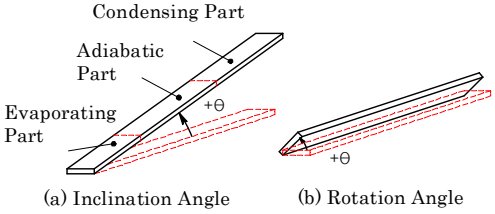


Fig. 2 Angle of Heat Pipe

In this study, the length of a micro heat pipe, the vapor temperature at the adiabatic part and inclination and rotation angle are taken as experimental parameters as shown Table 1. The definitions of inclination and rotation angles are shown in Fig.2.

2.1 Data reduction

The thermal resistance is calculated as follows:

Thermal resistance(total) $$R_{e-c} = \frac{T_{eave} - T_{cave}}{Q} \quad (1)$$

Thermal resistance (evaporator)

$$R_{e-sat} = \frac{T_{eave} - T_{sat}}{Q} \quad (2)$$

Thermal resistance(condenser)

$$R_{c-sat} = \frac{T_{sat} - T_{cave}}{Q} \quad (3)$$

The relation of the thermal resistance against heat load is shown in Fig.3. From this figure, the dry-out, which is defined as a point that thermal resistance begins to rise, is estimated. At the point just before the dry-out (as the typical example from Fig.3, the maximum heat transfer capacity is estimated as 6.5W), the heat load of the micro heat pipe is considered to be the maximum heat transfer capacity of the micro heat pipe.

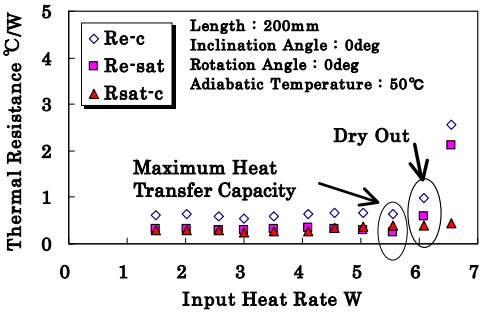


Fig. 3 Typical example of thermal resistance

3. EXPERIMENTAL RESULTS AND DISCUSSION

3.1 Heat transfer characteristics

The temperature distribution on the surface of the micro heat pipe is shown in Fig. 4. As the heat load increases, the temperature at the evaporator part increases. On the other hand, the temperature at condensation part decreases with the increasing heat load and especially sharp temperature drop happens at the condensation edge. This trend shows that the actual operation region of the heat pipe is gradually restricted from the condensation part.

Table 1 Specifications of heat pipe and experimental conditions

Length of heat pipe	mm	118(112),150(144),200(194),250(244)
Volume fraction of working fluid	vol%	30
Thickness of heat pipe	mm	1
Adiabatic temperature	℃	40,50,60
Inclination angle	deg	-90,-45,-30,-15,0,15,30,45,90
Rotation angle	deg	0,45,90

Moreover, an average heat transfer coefficient is calculated in order to discuss the above-mentioned effects and tendency.

The effects of the inclination angle on the average evaporation and condensation heat transfer coefficient as function of heat flux are represented in Fig.5. Regardless of the inclination angle, the evaporative heat transfer coefficient increases with increasing heat flux, whereas the heat transfer coefficient at the condensation part has almost a constant value. The possible reason is as follows: the interface area of the liquid film and vapor generated in the wick becomes large with decreasing working liquid thickness. In addition, the effects of the inclination angle on both of the heat transfer coefficients are small.

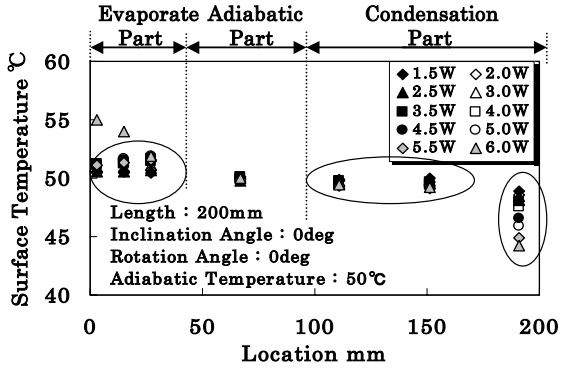
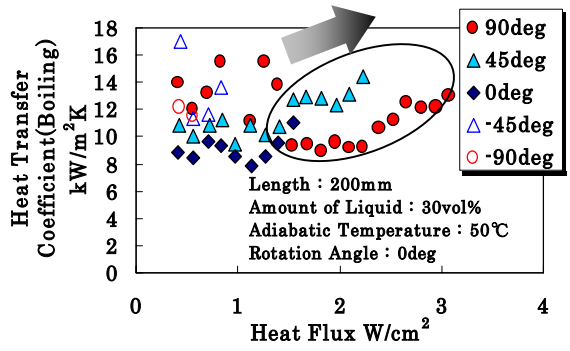
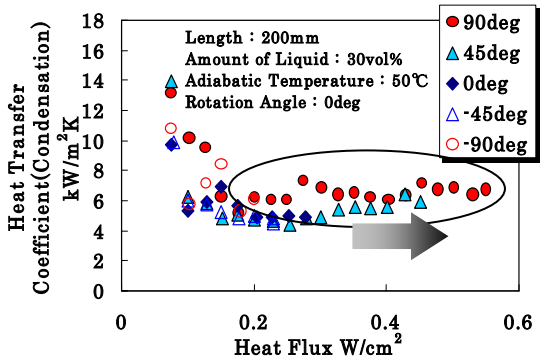


Fig.4 Surface temperature distribution



(a)



(b)

Fig.5 Effect of inclination angle on heat transfer coefficient

Variation of heat transfer coefficient as the function of heat flux with respect to the vapor temperature at the adiabatic part is represented in Fig. 6. These figures show that the heat transfer coefficient at the evaporator part increases as the vapor temperature at adiabatic part increases. The effects of heat flux have the same trend as that we have in Fig. 5.

3.2 The prediction of maximum heat transfer capacity

Judging from experimental results, it is decided that the traditional model for a normal heat pipe, namely capillary force limit is still applicable to the flat plate micro heat pipe. To propose the simulation model, following assumptions are used:

1. Cross sectional dimensions

Most of dimensions are the same as that of the test sample, however, since the width of the inner wick can not be directly measured, we estimate it by using a X-ray photograph. In addition to this, 4 angles are assumed to be the right angle and a wick is placed at the center of heat pipe cross section (Fig. 7).

2. Wick model

Fig. 7 shows an idealized cross sectional view of used wick. On the other hand, Fig .8 illustrates the cross section replacing the uniformly distributed small hales having the same void fraction as that of base cross section shown in Fig. 7.

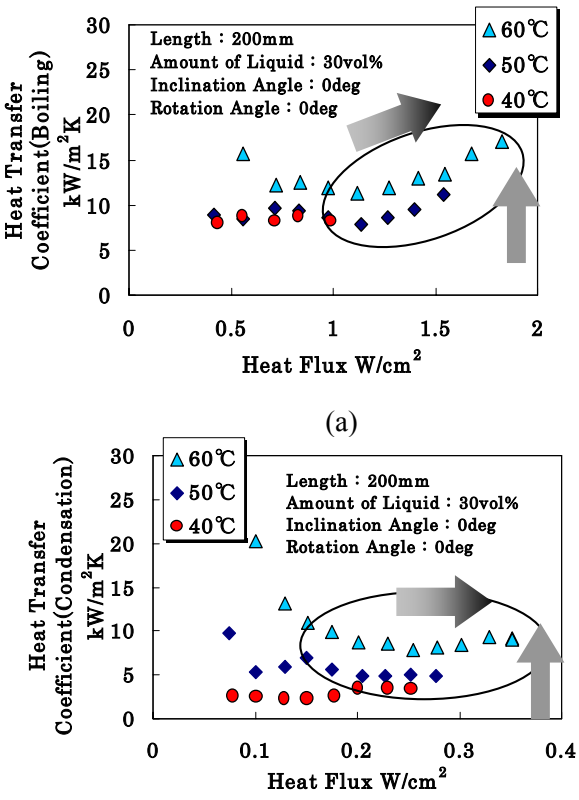


Fig.6 Effect of adiabatic temperature on heat transfer coefficient

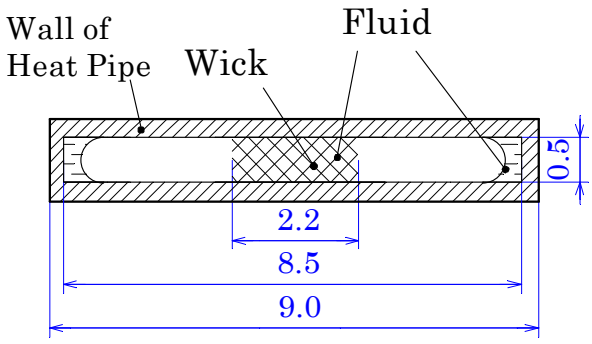


Fig. 7 Ideal cross sectional view of flat plate micro heat pipe

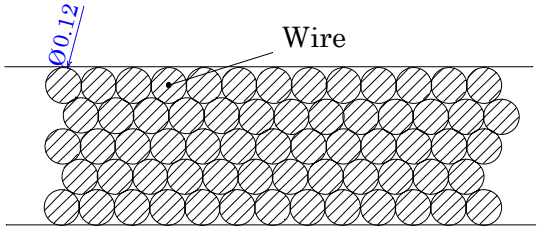


Fig. 8 Cross section of model wick having equivalent void as that of ideal wick

As mentioned earlier, the basic pressure balance equations for a normal circular heat pipe is used. To apply this basic model to a flat plate micro heat pipe, capillary force generated by grooves should be considered as additional term Eq.(3). From Fig. 8, the pore number, radius and permeability are calculated as Table 2.

$$\Delta P_{wc,\max} + \Delta P_{gvc,\max} \geq \Delta P_{wl} + \Delta P_{gvl} + \Delta P_v + \Delta P_b + \Delta P_e + \Delta P_{con} \quad (1)$$

$$\Delta P_{wc,\max} = \frac{2\sigma}{r_{wc}} \quad (2)$$

$$\Delta P_{gvc,\max} = \frac{2\sigma}{r_{gvc}} \quad (3)$$

$$\Delta P_{wl} = \frac{\mu_l Q L_{eff}}{K_w A_w \rho_l \lambda} \quad (4)$$

$$\Delta P_{gvl} = \frac{\mu_l Q L_{eff}}{K_{gv} A_{gv} \rho_l \lambda} \quad (5)$$

$$\Delta P_v = \frac{12 \mu_V Q L_{eff}}{h^3 w_V \rho_V \lambda} \quad (6)$$

$$\Delta P_b = \rho_l g\left(h\cos\theta - L\sin\theta\right) \quad (7)$$

$$\Delta P_e = \frac{\sqrt{2\pi R T_{V,e}}}{\alpha_C\left(1-(1/2)\left(RT_{V,e}/\lambda\right)\right)} \times \frac{Q}{\lambda(\omega_V + h)L_e} \quad (8)$$

$$\Delta P_{con} = \frac{\sqrt{2\pi R T_{V,c}}}{\alpha_C\left(1-(1/2)\left(RT_{V,c}/\lambda\right)\right)} \times \frac{Q}{\lambda(\omega_V + h)L_c} \quad (9)$$

Table 2 Pore number and radius (N=48)

Pore number N	Pore radius r_{wc} [m]	Permeability K_w [m^2]
48	5.02×10^{-5}	1.08×10^{-10}

In Figs. 9 and 10, experimental data of the maximum heat transfer capacity as function of inclination angle and vapor temperature at adiabatic part with heat pipe length as a parameter are compared with calculated data using capillary force limit (Eq.(1)). The maximum heat transport

capacity data tends to increase as the inclination angle increases. This is because of the effect of gravity which works as driving force in addition to capillary force in the case of a positive inclination angle and vice versa. On the other hand, the maximum heat transfer capacity increases, as the vapor temperature at adiabatic part rises, since the improved thermal properties of working fluid is in favor of the generated capillary force. Additionally, the shortest micro heat pipe has the highest heat transfer capacity at all experimental conditions. That is the result of decreasing the pressure loss in both liquid and vapor phase as the length of micro heat pipe decreases. Based on these experimental trends, we propose a following pressure balance equation (the capillary force limit) to predict the maximum heat transport capacity analytically.

$$\Delta P_{wc,\max} + \Delta P_{gvc,\max} \geq \Delta P_{wl} + \Delta P_{gvl} + \Delta P_v + \Delta P_b + \Delta P_e + \Delta P_{con} \quad (1)$$

The micro heat pipe using in this study is so thin that we assume the liquid is transported not only through a wick structure but also through both groove like sides of a micro heat pipe. It is necessary to add terms of the capillary force and heat loss of grooves in the pressure balance equation. Moreover a wick structure is idealized and, as a result, it is estimated that a pore radius is $r_{wc}=5.02\times10^{-5}$ and a permeability is $K_w=1.08\times10^{-10}$. Although there is difference between predictive and experimental values of maximum heat transfer for the case of 118mm micro heat pipe, in the case of 200mm and 250mm, the prediction and experiment show a reasonable agreement. Since the adiabatic length of 118mm micro heat pipe is small, it is necessary to define a new value for effective length of 118mm.

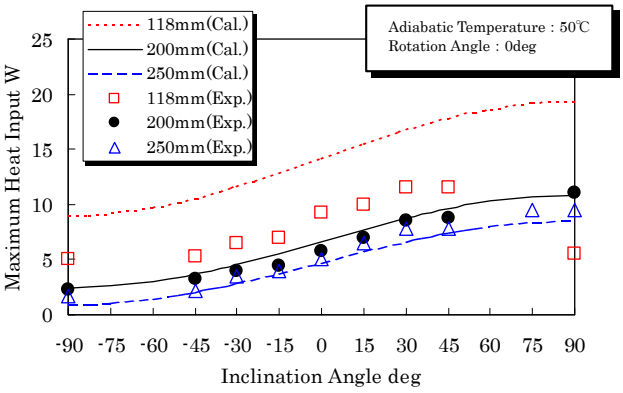


Fig.9 Maximum Heat Transfer capacity (effect of inclination angle)

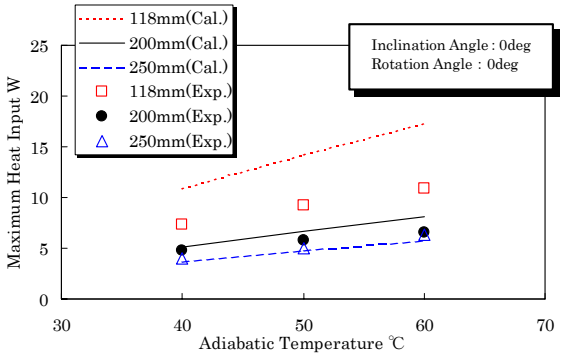


Fig.9 Maximum Heat Transfer capacity (Effect of adiabatic temperature)

4. CONCLUSION

[1] The influence of the length, the angle the and vapor temperature at an adiabatic part on the performance limit are taken into consideration. As a result, it is shown that by decreasing the micro heat pipe length, the maximum heat transfer capacity increases. Also increasing the inclination angle and the vapor temperature, results in increase in maximum heat transfer capacity of the heat pipe.

[2] The tendency of the average heat transfer coefficient of a flat micro heat pipe is taken into consideration. As a result, the behavior of working fluid is predicted. Also the predictive calculation based on the pressure balance equation is carried out and it is confirmed that 200mm and 250mm μHP to some extent show good predictive results.

Nomenclature

μ_v	: vapor viscosity	[kg/ms]
μ_l	: liquid viscosity	[kg/ms]
ρ_v	: vapor density	[kg/m^3]
ρ_l	: liquid density	[kg/m^3]
σ	: surface tension	[N/m]
λ	: latent heat of evaporation	[J/Kg]
r_{wc}	: effective pore radius(wick)	[m]
A_w	: cross sectional area of wick	[m^2]
r_{gvc}	: effective pore radius(groove)	[m]
A_{gv}	: cross sectional area of groove	[m^2]
K_w	: permeability of wick	[m^2]
L_{eff}	: effective length	[m]
K_{gv}	: permeability of groove	[m^2]
Q	: heat load	[W]
h	: thickness of vapor channel	[m]
θ	: inclination angle	[deg]
w_v	: width of vapor channel	[m]
L	: length of heat pipe	[m]
g	: acceleration of gravity	[m/s^2]
α_c	: evaporation and condensation factor	
R	: gas constant	[J/KgK]
T_v	: working temperature	[K]
L_c	: length of condenser section	[m]

Symbols for pressure drop

$\Delta P_{wc,\max}$: *wick capillary force*
ΔP_{wl} : *liquid flow pressure drop* (*wick*)
ΔP_{v} : *vapor flow pressure drop*
ΔP_{b} : *pressure drop by body force*

ΔP_{e} : *pressure drop due to evaporation*
ΔP_{con} : *pressure drop due to condensatin*
$\Delta P_{gvc,\max}$: *groove capillary force*
ΔP_{gvl} : *liquid flow pressure drop* (*groove*)

References

1) S. khandekar, M.Groll, P.Charoensawan and P.Terdtoon Pulsating Heat Pipe: Thermo-uidic Characteristics and Comparative Study with Single Phase Thermosyphon, Heat Transfer 2002, Grenoble, P.308
2) M. Hosoda, S. Nishio, R.Shirakashi, Study of Meandering Closed-Loop Heat –Transport Device (Vapor-plug Propagation Phenomena), JSME International Journal, Series B, Vol.42, No.4, PP737-744,1999
3) N. Nishio, S. Nagata, S. Baba and R.Shirakashi, Thermal Performance of SEMOS Heat Pipes, Heat Transfer 2002, Greoble, p.311
4) Y. Miyazaki and F. Polasek, Operating Limit of Oscillating Heat pipe, Heat Transfer 2002, Grenoble P.312
5)M. Katsuta, T Arai, N.Hosoya and K. Tanaka, design of Capillary Pumped Loop to be boarded on the Artificial Satellite(Users) .and Development of its Analytical Model, Heat Transfer 2002, Grenoble, P.305
6) K. Nanba et.al., Furukawa Electric Review, Furukawa Electric, Vol.101, (1998) P.22.
7) J. Niekawa et.al.,Micro heat pipe and an in troduction of a heat dissipation technology,Nik kei Kogyo Shinbun Ltd., (1999),32-39.

Operating Performance of Micro Heat Pipe for Thin Electronic Packaging

Seok Hwan Moon, Gunn Hwang, Sang Choon Ko, Youn Tae Kim
Microsystem Team, Human Information Department,
Electronics and Telecommunications Research Institute,
161 Kajong-Dong, Yusong-Gu, Taejon 305-350, KOREA
Email : {shmoon, hwangun, scko, ytkim}@etri.re.kr

Abstract

A high-density and slim-type packaging technology in a notebook PC or a handheld PC has been developed as the importance of portability is increased more and more recently. The heat dissipation generated in small-sized electronic units should be made effectively for operating stability during life-time. In the present study, micro heat pipe(MHP) and flat plate micro heat pipe(FPMHP) with the polygonal cross section have been manufactured and investigated for operating characteristics and heat transfer limits. One of the distinguished characteristics for the MHPs does not have additional wick. For a small-sized heat pipe like as the one in the present study, a high precision technology is needed in the manufacturing process. The developed MHPs have triangular or rectangular cross-section. The FPMHP has modified rectangular cross-section together with the prior two shapes. The containers for the MHP and FPMHP were obtained by drawing and extrusion process, respectively. Therefore the enhancement for productivity could be achieved. From the test results, it was seen that the triangular MHP can dissipate 7W of a thermal load and the modified FPMHP 14.19W.

Key words : Electronic cooling, Thin packaging, Micro heat pipe, Heat transfer limit

1. INTRODUCTION

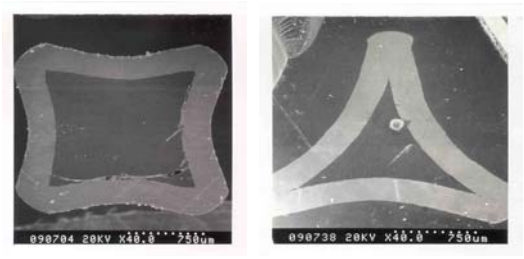
The major trends of mobile information technology have been the miniaturization together with enhancing the performance of personal mobile information device, such as handheld personal computer, PDA(Personal Digital Assistant), and notebook PC. The power consumption and the heat generation per unit area have been increased with the advents of high advanced system. An importance of thermal management in the mobile device will be growing more and more for reliability and life-time assurance of the component in such a highly integrated and compacted packaging system within thin space only available. It will be difficult to apply the traditional cooling technique, e.g. heat sink, heat pipe, fan, and etc., to such an ultra-slim type mobile device. It may be possible for a heat pipe with the diameter of 3 mm or more to be pressed to less than 2 mm thickness used in the system. But it is still remained a problem that the maximum pressed thickness of the pipe is constrained by the available cross sectional area of the pressed pipe, which is related with the performance of the heat pipe.[1] Considering the technical trend for miniaturized packaging of components which requires a very limited space installed in a system, it is inevitable to apply a micro cooling device. There are many merits for MHP compared with other micro cooling device. The major technique to develop the MHP is a micro scaled design and manufacturing technology. And it is important to create the effective capillary structure for achieving high thermal performance. There have been few papers dealt with experimental results since Cotter[2] proposed the first paper about MHP technology in 1984. We still have various research areas about MHP applicable to such ultra-slim type electronic device. In this present study, MHPs and FPMHPs with an equivalent diameter from 1 mm to 2 mm and polygonal cross section were designed and manufactured. The object of this study is to analyze the thermal performance and the characteristics of the MHPs and the FPMHPs. These results can be used as the basic useful data to design a cooling module applicable to the high heat generation component in a compact slim type mobile system, such as sub-notebook PC, mobile phone, PDA, handheld PC, and etc.

2. EXPERIMENTS

2-1. Experimental Apparatus

The MHP is smaller than the miniature heat pipe with 3 mm diameter and larger than micro heat pipe with micron sized diameter. The dimension of the MHP is the critical minimum size producible by current mechanical technique and the manufacturing process is simple with good productivity. These micro structures of the MHP may be manufactured with etching technology,[3] but this approach has disadvantages in the view of productivity and manufacturing cost.

The developed MHP was manufactured with drawing process and has many advantages especially for productivity. The Fig. 1 shows the cross section of the MHPs which was manufactured with the drawing process. This MHPs need no wick to be attached at the inner wall of the miniaturized heat pipe, but uses the polygonal corners made with structural plastic deformation of its own as the wick



(a) (b)

Fig. 1 Cross section of micro heat pipes

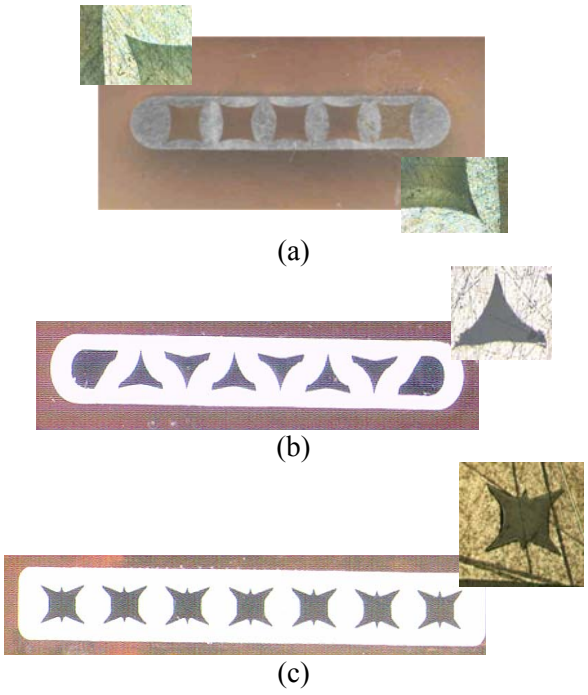
The liquid condensed at the condenser of the MHP is returned to the evaporator along the polygonal corners. It is important for a MHP to have sharp corners for securing a small capillary radius of the meniscus. The rectangular MHP (Figure 1a) has advantages for heat transfer performance, with larger inner space for vapor flowing and one more corners for liquid path than the triangular MHP (Figure 1b). Although the rectangular MHP has the above advantages, the capillary radius at the corners of the triangular MHP is smaller than that of the rectangular MHP. The specification of the developed MHPs is described briefly in table 1.

Figure 2 shows the cross sections of the FPMHPs. The FPMHPs were made by extrusion process with high productivity and economic cost for manufacturing. The edges of them have very sharp corners.

Table 1 Experimental specification of the micro heat pipes

	Triangular MHP	Rectangular MHP
Total length	50mm/100mm	
Evaporator length	10mm/20mm	
Adiabatic section length	15mm/30mm	
Condenser length	25mm/50mm	
Number of corner	3	4
Working fluid	Pure water	
Fill ratio of working fluid	20%	
Test inclination angle	Horizontal	
Container material	Copper	
Container manufacturing method	Drawing	

The performance of the modified rectangular FPMHP in Fig. 2(c) is better than those of the rectangular type in Fig. 2(a) and the triangular type in Fig. 2(b) as described in next section. The merit of the triangular type in Fig. 2(b) is that it can be designed with very compact structure. Fig. 2(c) shows the modified rectangular FPMHP and this type was developed from the rectangular type to get sharper corners and larger inner space for increasing vapor flowing. The specification of the FPMHPs is shown in Table 2.



(a)

(b)

(c)

Fig. 2 Cross section of the flat plate micro heat pipes

Table 2 Experimental specification of the flat plate micro heat pipes

Type of FPMHP	Thickness	Width	Total length
Rectangular type	2mm	12mm	50mm
Triangular type	1.5mm	12mm	50mm
Modified rectangular type	1.5mm	14mm	50mm

2-2. Experimental Setup and Procedure

The performance testing apparatus of the micro heat pipe was composed of MHP or FPMHP, vacuum chamber unit, constant temperature bath to cool the MHP, data logger system, and DC power supplying unit as shown in Figure 3. The evaporator was heated by the thermal wire with Ni-Cr and DC power supplying unit. The thermal wire with 0.36mm (electric resistance per unit length:10Ω/m) of diameter was wound on the heating element attached at the wall of evaporator by the identical interval of 0.5 mm in order to supply the thermal load constantly. Thermal grease (thermal conductivity: 0.74W/m°C) was filled between the pipe wall and the heating element in order to reduce the contact thermal resistance. At the condenser, the water jacket was installed to cool the MHP with water cooling method. Thermal grease was filled between the pipe wall and the water jacket too.

The vacuum chamber (10^{-2} torr ~ 10^{-3}torr) made of acryl was used to minimize the heat loss to the environment as shown in Figure 3. This chamber has a cylinder shape body for tilting test. To measure the temperatures on the wall of the MHP, K-type thermocouples (Φ 0.08mm) were attached at 2 points of the MHP evaporator wall, 1 point of the adiabatic section, and 2 points of the condenser by soldering method. The locations of the thermocouple are shown as X in Fig. 3. The measured temperatures are recorded by data logger system.

The MHP and FPMHP were made of oxygen free copper and aluminum respectively and the wall thickness of the oxygen free copper was 0.27~0.28mm. The stilled water with high surface tension and large latent heat between 30°C and 160°C was used as the working fluid. The filling ratio of the working fluid was 20% to the internal volume of the MHP and FPMHP. It was appeared that the heat could not be transferred to the end of the condenser by the liquid blocking for the MHP with the equivalent diameter of 1 mm ~ 2 mm. The temperature at the end of condenser was lowered to the amount of 5°C ~ 20°C by the liquid blocking and the heat transfer rate of the MHP was decreased.

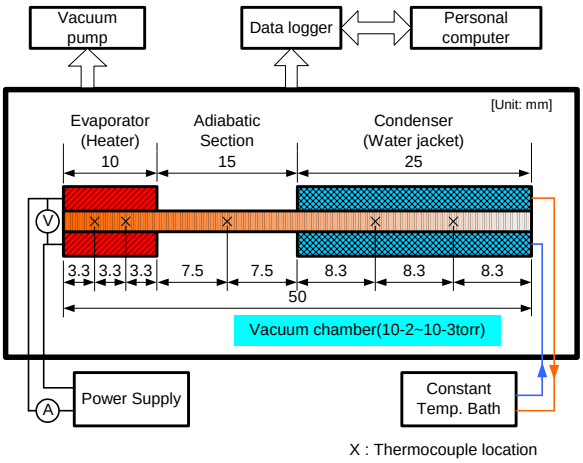


Fig. 3 Experimental apparatus

The experiment was performed to analyze the thermal performance of the developed MHP and FPMHP. The thermal load was supplied to a MHP and FPMHP was increased stepwise by 0.5W from 0.5W. The test was completed when the wall temperature of the evaporator was rapidly increased due to dryout. When the wall temperature of the MHP was recorded when it reached the steady state after the wall temperature begins to rise as the input power was supplied at each step of the thermal load. The wall temperatures of each evaporator, adiabatic section and condenser were averaged in the each zone. The MHP under the test was installed in the chamber under the vacuum condition of 10^{-2} torr ~ 10^{-3} torr with vacuum pump during the test.

3. RESULTS AND DISCUSSION

3-1. Micro heat pipe

Figure 4 presents the test results for optimizing an amount of the working fluid in case of the triangular MHP. In general, the optimized amount of the working fluid in the heat pipe could be determined when the maximum heat transfer rate and the minimum thermal resistance is being achieved simultaneously in that amount. As shown in Figure 4, it is seen that the optimized amount of the working fluid for the triangular MHP is about 20% to the internal volume. The thermal resistance can be calculated by (1),

$$R = \frac{T_e - T_c}{Q} \qquad (1)$$

where T_e and T_c are wall temperatures at the evaporator and the condenser of the MHP respectively, and Q(W) is a thermal load at the evaporator.

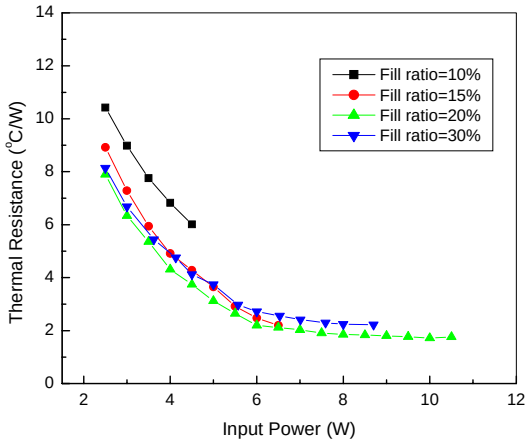


Fig. 4 Optimum filling ratio of working fluid for the triangular MHP

Figure 5 presents the comparison between the triangular and the rectangular MHP for the thermal performance. The tested MHP has a fill ratio of 20% to the internal volume of the MHP. The operating temperature was not constant but was increased with increasing of the thermal load simultaneously. The heat dissipating at the condenser was accomplished by circulating of 20°C water which was controlled to a constant temperature using the constant temperature bath. As shown in Fig. 5, the heat transfer limit of the triangular MHP was 1.6times larger than that of the rectangular MHP. The heat transfer limits were 4.5W and 7W for the triangular and the rectangular MHP, respectively. This result is due that the sharpness in the corners for the rectangular MHP was not achieved compared to that for the triangular MHP, and the capillary pressure which is needed for returning condensed liquid to the evaporator can not be obtained sufficiently.

Because the rectangular MHP has more a corner than the triangular MHP, the rectangular MHP may has an advantage in thermal performance. However, due that a radius of curvature in the corner is not small sufficiently for retaining capillary pressure, the performance of the rectangular MHP can't be superior to that of the triangular MHP. Among the operating limits in the heat pipe, the performance of the MHP is very largely restricted by the capillary limit.[4]

The factor which affects very largely on the capillary limit is the radius of curvature in corners. The radius of curvature (r) is a function of a corner aperture angle (ϕ), a contact angle (α), and a location of the meniscus contact point in the corner (χ) as shown in (2).[5] Except the two factors of α, χ which is fixed as a heat pipe kinds and operating conditions, ϕ is the most important factor to the radius of curvature. The smaller a corner aperture angle is, the smaller a radius of curvature is. Then high capillary pumping pressure and high maximum heat transfer limit can be obtained.

$$r = f(\phi, \alpha, \chi) \qquad (2)$$

Namely, because the corner aperture angle of 60~70 degree in the rectangular MHP of the present study is larger than that of 30~40 degree in the analytical result of Zaghdoudi et al(1997)[5], the small radius of curvature can not be obtained.

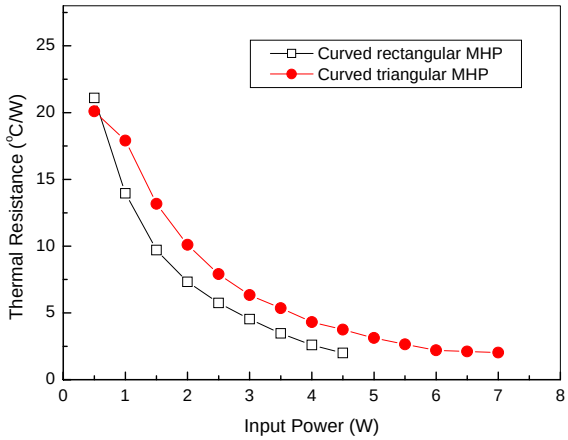


Fig. 5 Comparison of thermal performance between triangular and rectangular MHP.

Figure 6 presents the test results to investigate the effect of the total pipe length on the thermal performance of the triangular MHP. The total pipe length of 50mm and 100mm were considered. As shown in Figure 6, the thermal performance of the triangular MHP was considerably affected by the total pipe length and the thermal performance was enhanced as the total pipe length was increased. If the total pipe length was reduced from 100mm to 50mm the thermal performance was enhanced about 92%.

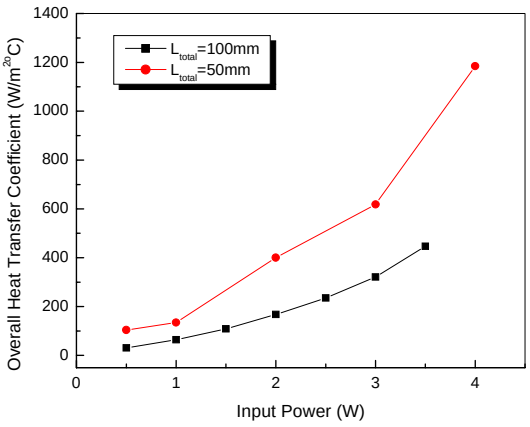


Fig. 6 The effect of total pipe length on the thermal performance of the MHP

Figure 7 presents the experimental results of the present study and Moon et al(1999)[6] for the heat transfer limit. The MHP which was tested in the study of Moon et al(1999) had a triangular cross-section and a stainless steel as container material. The pure water was used as the working fluid. As shown in Figure 7, the heat transfer limit of the present study is 1.7~2.1 times larger than that of Moon et al. over the operating temperature of 60~80°C. This result means that

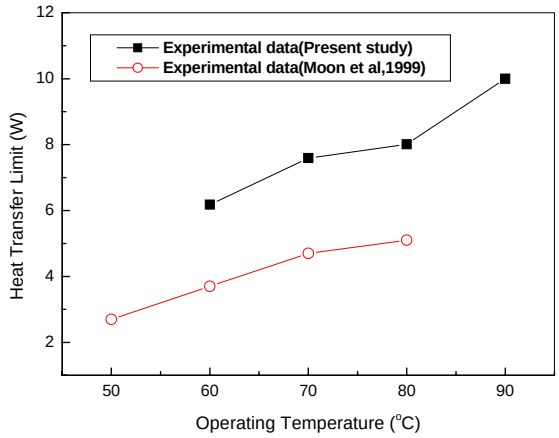


Fig. 7 Comparison of heat transfer limit between the present study and Moon et al.(1999)

the large capillary limit in the present study was obtained compared to that of Moon et al.. High productivity and simple manufacturing process were considered and enhanced performance was obtained compared to that of Moon et al. for the future applications.

3-2. Flat Plate Micro Heat Pipe

Figure 8 shows the experimental results for the temperature distributions along the axial length in case of the rectangular FPMHP. As shown in Figure 8, the temperature at the condenser followed instantly the one at the evaporator as soon as the thermal load was supplied to the evaporator. This means that the manufactured FPMHP has the constant temperature characteristics which is among the common heat pipe properties. The temperature difference between the evaporator and the condenser for the rectangular FPMHP was 2.2~11.9°C. The test results was not presented in this document, but the temperature difference between the evaporator and the condenser for the triangular and the modified rectangular FPMHP were 2.7~12.25°C and 2.3~9.65°C respectively.

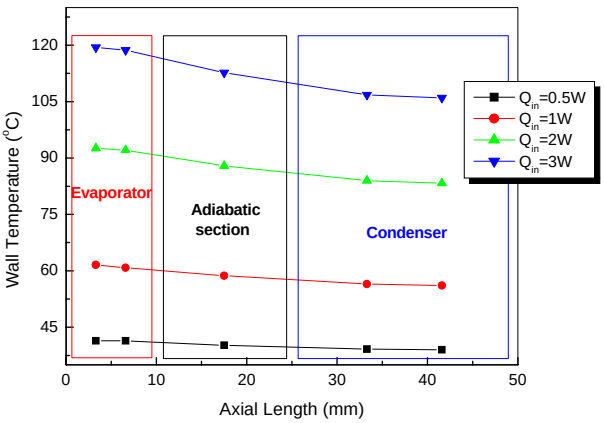


Fig. 8 The temperature distributions along the axial length for the rectangular FPMHP.

Figure 9 presents the experimental results of the thermal performance for the FPMHPs shown in Figure 2. The test was performed below 120°C of the temperature at the evaporator. As shown in Figure 9, the limiting power for the modified rectangular FPMHP was higher than that of other two FPMHPs. Although the modified rectangular FPMHP has a small space for vapor flow, showed the superior thermal performance compared to the rectangular FPMHP relatively. This is due that the large capillary force for returning the condensed liquid to the evaporator could be created in case of the modified rectangular FPMHP. In the meantime, the triangular FPMHP showed the small limiting power compared with the rectangular FPMHP. The limiting power for the triangular FPMHP, the rectangular FPMHP and the modified rectangular FPMHP were 8W, 13.66W and 14.19W respectively.

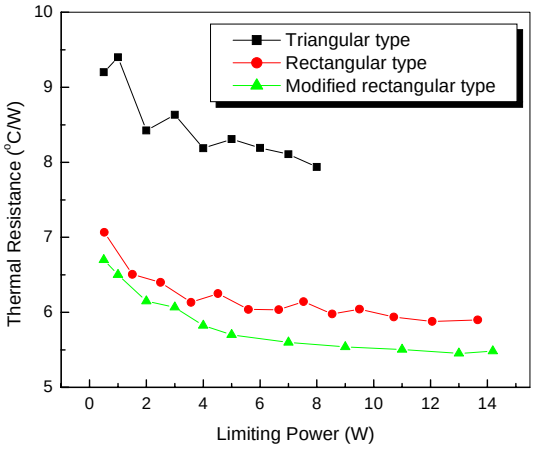


Fig. 9 Comparison of thermal performance between the developed FPMHPs

4. CONCLUSION

The MHPs and FPMHPs suitable for a slim-sized electronic device were developed through this study. The container for the MHP with the equivalent diameter of about 1~1.5mm and the FPMHP with the thickness of 1.5~2mm could be obtained through a common extrusion and drawing process respectively, therefore it is possible for those to achieve enhancing productivity. The corner structure for the sufficient capillary force in the MHPs and FPMHPS manufactured through above process could be created too. The developed MHPs showed the good isothermal property over from evaporator to condenser, and the temperature difference between evaporator and condenser was about 4~6°C. The developed FPMHPs showed the good isothermal property too. It was seen that the developed triangular MHP and the modified rectangular FPMHP could transport about 7W and 14.19W of the thermal loads respectively. Because the MHP and the FPMHP could be manufactured with a simple process, the lowest cost could be achieved. Moreover, due to a small size and thin thickness of those, it is considered that those could be provided as a cooling solution suitable for a portable electronic device in the future.

References

[1] Moon, S. H., Yun, H. G., Hwang, G., Choy, T. G., "Operation Performance of Miniature Heat Pipe with Composite Wire Wick", IMAPS 2001, pp. 207-211, 2001.

[2] Cotter, T.P., "Principles and Prospects for Micro Heat Pipes", Proceedings of the 5th Int. Heat Pipe Conference, 1984.

[3] Gerner, F. M., "Flow Limitation in Micro Heat Pipes", AFSOR Final Report, No. F49620-88-6-0053, Wright-Patterson, AFB, Dayton, OH., 1989.

[4] Hopkins, R., Faghri, A., Khrustalev, D., "Flat Miniature Heat Pipe with Micro Capillary Grooves", Transaction of the ASME, Vol. 121, pp. 102-109, 1999.

[5] Zaghdoudi, M. C., Sartre, V., Lallemand, M., "Theoretical Investigation of Micro Heat Pipes Performance", 10th Int. Heat Pipe Conf., Germany, Sep. 21-25, F-9, 1997.

[6] Moon, S. H., et al., "An Experimental Study on The Performance Limitation of a Micro Heat Pipe with Triangular Cross-Section", 11th Int. Heat Pipe Conf., Japan, Sep. 12-16, A1-4, 1999.

Mathematical Model for Predicting the Transport Phenomena of the Evaporating Meniscus Region in a Capillary Channel

Kyoungwoo Park
School of Mechanical Engineering, Hanyang University
17 Haengdang-dong, Sungdong-gu, Seoul 133-791, KOREA,
Tel. : +82-2-2290-1639, Fax : +82-2-2291-4070, kwoopark@hanyang.ac.kr

and Kwan-Soo Lee
School of Mechanical Engineering, Hanyang University
17 Haengdang-dong, Sungdong-gu, Seoul 133-791, KOREA,
Tel. : +82-2-2290-0426, Fax : +82-2-2295-9021, ksleehy@hanyang.ac.kr

Abstract

The transport phenomena during evaporation in the extended meniscus region of a micro capillary channel are investigated numerically. For this purpose, a mathematical model is developed in which different physical approaches are made to derive the governing equations for the meniscus and thin film regions, respectively. In this model, variation of the vapor pressure and the disjoining pressure effect are included and various friction forces acting on the channel and fluids are also considered. The results show that the local heat transfer coefficient has an extremely large value in the thin film region in spite of its small scale of heat transfer area. The heat transfer rate, however, is larger for the meniscus than for the thin film region. The length of the extended meniscus region is mainly affected by the heat flux, the channel height and the dispersion constant.

Key words: Micro-capillary channel, Evaporation, Extended meniscus region, Phase change, Control volume

1. INTRODUCTION

The size of electronic devices is miniaturized by the advancement of packaging technology so that the generated heat per unit area is increased dramatically. According to this trend, the control of heat generated in micro-scale electronic devices has been issued in the research area of heat transfer. A capillary pumped loop (CPL) system using a phase-change technique to enhance the heat transfer rate has drawn great attention to the fields of chip-level cooling in micro-scale devices. The evaporator, which is the key component of CPL system, is divided into the meniscus, thin film, and adsorbed regions during the evaporating process of the working fluid.

Much attention has been paid to the predicting the evaporating transport phenomena in the thin film region of the evaporator by numerically and experimentally [1-4]. Longtin et al. [5] proposed a mathematical model using the control volume method to predict the fluid-thermal characteristics of the micro heat pipe having a triangular cross section. They neglected the effect of disjoining pressure and the liquid and vapor phases were assumed to flow in a counter-flow manner. They concluded that the radius of curvature increases linearly along the flow direction. Sartre et al. [6] presented a three-dimensional model for predicting the heat transfer characteristics in the extended meniscus region of a micro heat pipe array. This model adopted a similar mathematical concept suggested by Longtin et al. and considered the heat conduction effect at the substrate. They reported that both the apparent contact angle and the heat transfer rate increase with increasing wall superheat. Their results, however, are limited to those of the thin film region only. Peles and Harber [7] developed a one-dimensional model that accounts for the boiling two-phase flow and heat transfer phenomena in a triangular micro channel. They assumed that the vapor pressure was constant and they did not take into account the friction forces both at the liquid-vapor interface and at the solid wall. As mentioned earlier, many studies have assumed a constant vapor pressure and they have not considered the simultaneous effects of the disjoining pressure and the variation in vapor pressure in obtaining the mathematical model in the extended meniscus region.

In this work, a comprehensive mathematical

model is presented to describe the two-phase transport phenomena of the extended meniscus region in a micro capillary channel. The effects of the vapor and disjoining pressures are included in this model. The governing equations are obtained by applying different physical approaches to the meniscus and thin film regions. The effects of the applied heat flux and the inlet liquid velocity on the transport phenomena are investigated. The emphasis is also focused on the effects of the dispersion constant, the channel height, and the heat flux on the location of dry-out point.

2. MATHEMATICAL MODELING

A working fluid in a micro capillary channel evaporates due to the applied heat, resulting in the thinner liquid film thickness and an increase in the radius of curvature at the liquid-vapor interface. The schematic configuration of the phase change phenomenon in a micro capillary channel in a micro evaporator is schematically shown in Fig. 1. Heat is applied to both the bottom and top walls of the channel. Only the lower half of a micro channel is considered due to the geometric symmetry. The basic assumptions are found in Ref.[4].

The behavior of the liquid-vapor interface is governed by the pressure difference in the liquid and vapor phases. The pressure difference can be expressed by the augmented Young-Laplace equation, which is given by the summation of the capillary pressure and the disjoining pressure:

$$P_v - P_l = P_d + P_c = -\frac{\bar{A}}{\delta^3} + \sigma K \qquad (1)$$

where δ is the liquid film thickness, $\bar{A}$ the dispersion constant ($=-2.87\times10^{-21}$ J, water), and σ the surface tension. The mean curvature at the liquid-vapor interface (K) can be given as the sum of the axial and vertical curvatures

$$K = K_x + K_y = \frac{d^2\delta}{dx^2}\left[1+\left(\frac{d\delta}{dx}\right)^2\right]^{-1.5} + \frac{1}{(H/2-\delta)}\left[1+\left(\frac{d\delta}{dx}\right)^2\right]^{-0.5} \qquad (2)$$

Substituting Eq. (2) into Eq. (1) and assuming the constant surface tension, the variation of the film thickness can be obtained as

$$\frac{d^2\delta}{dx^2} + \frac{1}{(H/2-\delta)}\left[1+\left(\frac{d\delta}{dx}\right)^2\right] - \frac{1}{\sigma}\left(P_v - P_l + \frac{\bar{A}}{\delta^3}\right)\left[1+\left(\frac{d\delta}{dx}\right)^2\right]^{1.5} = 0 \qquad (3)$$

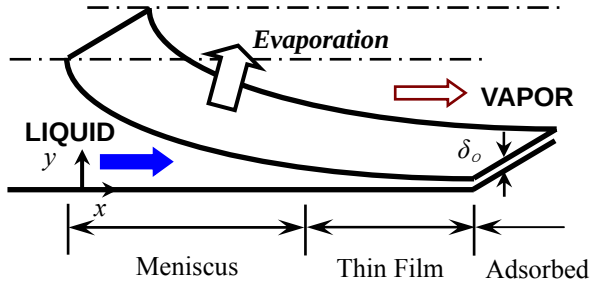


Fig. 1 Schematic diagram of evaporator and its coordinate system

The profile of the liquid film thickness can be computed using the liquid and vapor pressures as shown in Eq. (3). Therefore, the flow and thermal analyses should be performed in the extended meniscus region.

2-1 Liquid phase

Meniscus region **:** The theory of momentum over the control volume per unit width (see Fig. 2) is applied for obtaining the mathematical model for the meniscus region. The momentum equation can be written as

$$\left(\rho_l u_l^2 + P_l\right)\frac{d\delta}{dx} + 2\rho_l \delta u_l \frac{du_l}{dx} + \frac{\delta dP_l}{dx} = \tau_{l,i} - \tau_{l,w} \qquad (4)$$

where u and τ represent the velocity and shear stress, respectively. In Eq. (4), the shear stresses at the wall and at the liquid-vapor interface are given by [8]

$$\tau_{l,w} = 0.5\rho u_l^2 f, \quad \tau_{l,i} = 0.5\rho_v u_v^2 f - \rho_v u_v v_{v,i}, \quad f = k/\mathrm{Re}_{D_h} \qquad (5)$$

In the friction coefficient (f), k depends on the geometric configuration. The value of 24 is used in this study for the infinite parallel-plate [9]. In addition, the Reynolds number is defined based on

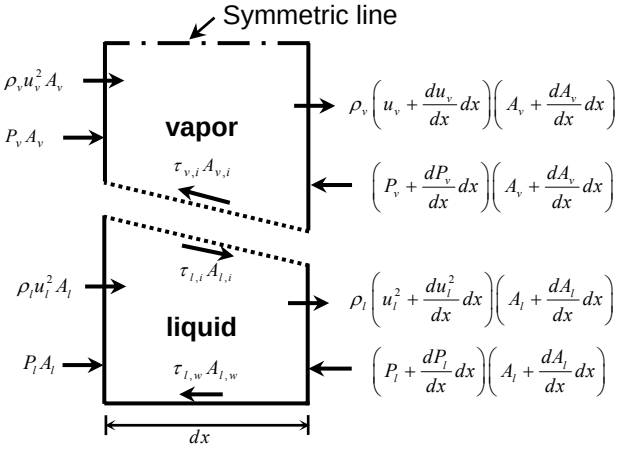


Fig. 2 Momentum equation for liquid and vapor phases in the meniscus region

the hydraulic diameter, D_h which varies along the flow direction and sets to δ (i.e., $D_h \approx \delta$).

The velocity of the liquid phase, u_l can be obtained from the mass conservation equation. The evaporative mass flow rate through the liquid-vapor interface, $\dot{m}_{ev}$ is given by

$$\dot{m}_{ev} = \rho_l A_{l,i} v_{l,i} = \rho_v A_{v,i} v_{v,i} \tag{6}$$

where $v_{l,i}$ and $v_{v,i}$ are the *y*-directional velocities of the liquid and vapor phases, respectively, at the liquid-vapor interface. $A_{l,i}$ and $A_{v,i}$ denote the liquid- and vapor-side areas, respectively.

Applying the mass conservation theory to the control volume, as shown in Fig. 2, we can obtain the equation

$$u_l \frac{d\delta}{dx} + \delta \frac{du_l}{dx} + v_{l,i} = 0 \quad . \tag{7}$$

The evaporative velocity($v_{l,i}$) can be obtained using the relationship between heat flux and evaporative mass flow rate which is defined as

$$\dot{m}_{ev} = \frac{\int_x^{x+dx} q'' dx}{h_{fg}} = \frac{q'' A_w}{h_{fg}} \tag{8}$$

where h_{fg} is the latent heat of vaporization.

Combining Eq. (6) with (8), the evaporative velocity for the liquid phase can be calculated as

$$v_{l,i} = \frac{q'' A_w}{\rho_l A_{l,i} h_{fg}} \quad . \tag{9}$$

Thin film region : The Navier-Stokes equation in the thin film region can be approximated by the lubrication theory. Using the boundary conditions for a shear stress at the liquid-vapor interface ($y = \delta$) and a no-slip at the liquid-solid interface ($y = 0$), the equation for the liquid pressure can be obtained as

$$\frac{dP_l}{dx} = \frac{3}{2\delta}\left(\delta - \frac{H}{2}\right)\frac{dP_v}{dx} - \frac{3\nu_l}{\delta^3}\dot{m}_l \tag{10}$$

where $\dot{m}_l$ represents the liquid mass flow rate per unit width.

2-2 Vapor phase

Meniscus region: For the vapor phase, the following governing equations are obtained using the momentum and the mass conservation equations for streamwise direction as in the liquid phase (see Fig. 2).

$$\begin{aligned} -\left(\rho_v u_v^2 + P_v\right)\frac{d\delta}{dx} + 2\rho_v\left(\frac{H}{2} - \delta\right)u_v \frac{du_v}{dx} \\ + \left(\frac{H}{2} - \delta\right)\frac{dP_v}{dx} = -\tau_{v,i} \end{aligned} \tag{11}$$

$$-u_v \frac{d\delta}{dx} + \left(\frac{H}{2} - \delta\right)\frac{du_v}{dx} - v_{v,i} = 0 \tag{12}$$

where the vapor-side shear stress at the liquid-vapor interface($\tau_{v,i}$) has the same magnitude but the opposite direction, compared to the liquid-side shear stress which is defined in Eq. (5).

Combining Eq. (6) with Eq. (8), we can obtain the evaporative velocity of the vapor phase.

$$v_{v,i} = \frac{q'' A_w}{\rho_v A_{v,i} h_{fg}} \tag{13}$$

Thin film region: The pressure variation of the vapor phase can be obtained using a form of the momentum equation similar to the one used for the liquid phase and the boundary conditions (i.e., shear stress at $y = \delta$ and symmetric condition at $y = H/2$):

$$\frac{dP_v}{dx} = \left\{ \dot{m}_v + \frac{dP_l}{dx}\left(-\frac{\delta^2 H}{4\mu_l} + \frac{\delta^3}{2\mu_l}\right)\rho_v \right\} \Big/ A \tag{14}$$

where $\dot{m}_v$ is the mass flow rate for the vapor per unit width and *A* is

$$\begin{aligned} A = &-\frac{H^3}{24\nu_v} + \frac{\rho_v \delta H^2}{4\mu_l} + \frac{\delta H^2}{4\nu_v} - \frac{\rho_v H \delta^2}{\mu_l} \\ &- \frac{H\delta^2}{2\nu_v} + \frac{\delta^3}{3\nu_v} + \frac{\rho_v \delta^3}{\mu_l}. \end{aligned} \tag{15}$$

3. NUMERICAL PROCEDURE

The flow and heat transfer characteristics of the extended meniscus region of a micro capillary channel are governed by the liquid film thickness, velocities and pressures for liquid and vapor phases. The governing equations in the meniscus region(i.e., Eqs. (3), (4), (7), (11) and (12)) are expressed as second-order and non-linear ordinary differential equations. Therefore, the following inlet conditions are needed to solve them.

$$\begin{aligned} &\delta_0 = H/2.5, \quad \left.\frac{d\delta}{dx}\right|_0 = specific, \quad u_{v,0} = 0, \\ &u_{l,0} = specific, \quad P_{v,0} = P_{v,sat}(T_{v,0}), \\ &P_{l,0} = P_{v,0} - \frac{\sigma}{\left(H/2 - \delta_0\right)} - \frac{\bar{A}}{\delta_0^3} \end{aligned} \tag{16}$$

To prevent the singularity in Eq. (3), the inlet film thickness of $\delta_o = H/2.5$ is used. The gradient of the film thickness at the inlet is set to a large negative value. The inlet pressure of the vapor phase is set to a pressure at a saturation temperature of 383 K, and the experimental data of Khrustalev and Faghri [10] was used to obtain the inlet velocity of the liquid phase. Computation

starts with the meniscus region. In the meniscus region, the flow and thermal characteristics are investigated by solving the governing equation with the inlet conditions, using the 6th order Runge-Kutta method. The pressures for the liquid and vapor phases are obtained by using the finite difference method. In this calculation, the *x*-location where the disjoining pressure is greater than or equal to the capillary pressure is treated as the starting point of the thin film region (or junction of the meniscus and thin film regions). Thus, the values corresponding to all variables (δ, u_v, u_l, P_v, P_l) at this point are used as the inlet conditions for the thin film region. With conditions calculated and the governing equations (i.e., Eqs. (3), (10) and (14)), the transport phenomena for the thin film region are examined until the value of the thin film thickness is equal to 10^{-9} m which is the value of film thickness in the adsorbed region [11].

4. RESULTS AND DISCUSSION

A new mathematical formula employing different analytical approaches for the meniscus and thin film regions are presented in order to examine the transport phenomena in the extended meniscus region. Based on the developed model, the two-phase flow and thermal phenomena are investigated. Water is used as the working fluid at a saturation temperature of 383 K.

4-1 Flow and thermal characteristics

The typical profile of the liquid film thickness (δ) in the extended meniscus region is shown in Fig. 3. The channel height is 150 μm, the inlet velocity of liquid phase is 0.027 m/s, and the heat flux is 1.0 MW/m^2. It can be seen from Fig. 3 that the liquid film decreases exponentially as the working fluid flows toward the adsorbed region.

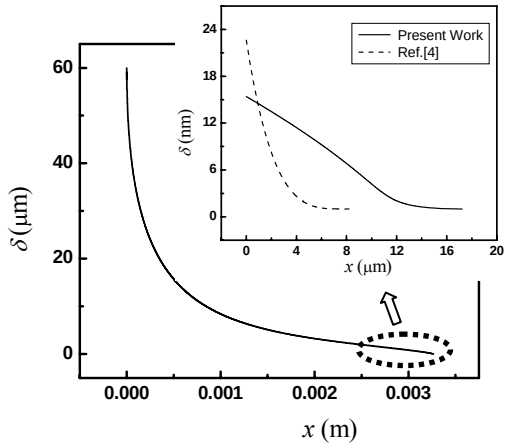


Fig. 3 Liquid film thickness for extended meniscus region and thin film region

This profile is attributed to the fact that the evaporative mass flux due to the applied heat is much larger in the thin film than in the meniscus region.

The inset in Fig. 3 shows the enlarged film thickness near the thin film region. The dotted line is the work of Park et al. [4]. They analyzed only the thin film region . The location of x = 0 mm in the inset indicates x = 3.264 mm in the extended meniscus region (i.e., the junction of the meniscus and thin film regions). The length of the thin film region (L_{thin}) is 17.5 μm that corresponds to about 0.5% of the extended meniscus region and the liquid film thickness at the inlet of thin film region (δ_j) is estimated to be 16.2 nm. Park et al. predicted that L_{thin} = 8.2μm and δ_j = 23.4 nm. The discrepancy between our results and those of Park et al. may be due to the mathematical model and the boundary conditions at $\delta = \delta_j$.

The flow field in the extended meniscus region occurs as a result of the pressure difference of the liquid and vapor phases as shown in Eq. (3). Figure 4 shows the pressure drop of the liquid and vapor phases along the flow direction. Both the liquid and vapor pressures decrease as the fluid flows toward the adsorbed region. This indicates that the liquid and vapor phases flow in the same direction. This result is different from that obtained by Longtin et al. [5] in which the liquid and vapor phases flow in the opposite direction. The figure also shows that the liquid pressure drop is several hundred times greater than the vapor pressure drop. Therefore, it can be concluded that the shear stress at the liquid-vapor interface is mainly due to the liquid pressure drop and the flow characteristic in the evaporator is strongly influenced by the liquid rather than by the vapor pressure.

Table 1 shows the local heat transfer coefficients for several *x*-locations. The local heat transfer coefficient is defined as $h(x) \approx k_l / \delta(x)$. The local heat transfer coefficient in the meniscus

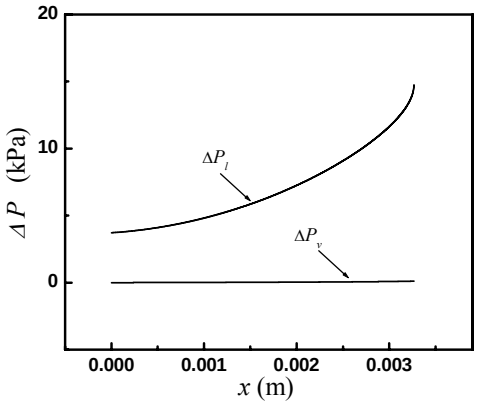


Fig.4 Pressure drop of the liquid and vapor phases

Table 1 Local heat transfer coefficients for various locations

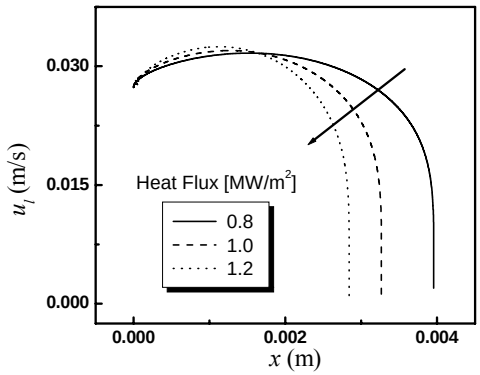
x	1	2	3	3.2641*	3.2665
h	7.1	18.2	70.6	2673	57944

* : starting point of the thin film region

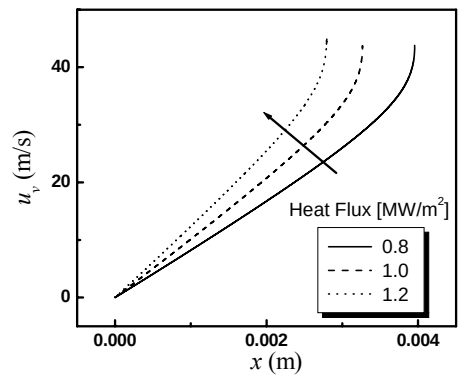
region is small, while that in the thin film region is extremely large. The abrupt increase of *h(x)* in the thin film region is due to the reduced thermal resistance by the thinner liquid film thickness. The average heat transfer coefficients for the meniscus and thin film regions are 31.4 and 14293, respectively. The heat transfer rate, however, is larger for the meniscus than for the thin film region because of the very short length of the thin film region.

4-2 Effect of heat flux and inlet liquid velocity

Figure 5 represents the predicted liquid and vapor velocities under the various heat flux conditions. For a constant heat flux, the liquid velocity gradually increases and has a maximum value at the location of 40% of the extended meniscus region as shown in Fig. 5(a). Thereafter, the liquid velocity decreases and finally



(a) Liquid velocity



(b) Vapor velocity

Fig. 5 Liquid and vapor velocities with heat flux

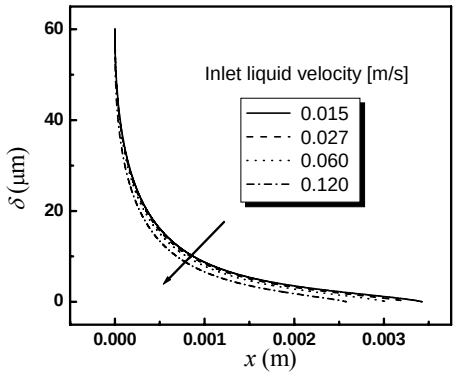


Fig. 6 Film thickness with inlet liquid velocity

approaches zero. The profile of the liquid velocity is similar for all heat flux conditions. Figure 5(b) presents the effect of the heat flux on the vapor velocity. The vapor velocity increases linearly along the flow direction and increases sharply near the thin film region. It should be noted that the evaporative mass flux in the thin film region is dramatically increased due to high heat transfer, as shown in Table 1. The maximum vapor velocity does not change even though the heat flux increases. Comparing Fig. 5(a) with Fig. 5(b), the vapor velocity is much larger than the liquid velocity for the same x-location and a constant heat flux, as expected. Notice that the vapor velocity is about one thousand times as fast as the liquid velocity under a given heat flux.

Figure 6 shows the profile of the liquid film thickness for various inlet liquid velocities. The film thickness and length of the extended meniscus region decrease with increasing inlet liquid velocity. This is mainly due to the increased pressure difference between the liquid and vapor phases with increasing inlet liquid velocity. However, the influence of the inlet liquid velocity on the profile of the film thickness is less significant.

4-3 Dry-out point

The most important factor in designing the micro evaporator is to predict the location where the dry-out phenomenon occurs.

Another interesting result predicted from the present model is shown in Fig.7, which gives the length of the extended meniscus region for various heat fluxes (q''), channel heights (H), and dispersion constants ($\bar{A}$). The length of the extended meniscus region decreases exponentially with increasing heat flux. This is due to the decreased liquid film thickness caused by the increased evaporative mass flux at the liquid-vapor interface as the heat flux increases. For $q'' < 5$ MW/m^2, L decreases dramatically, but for $q'' > 5$ MW/m^2, L does not change. This implies

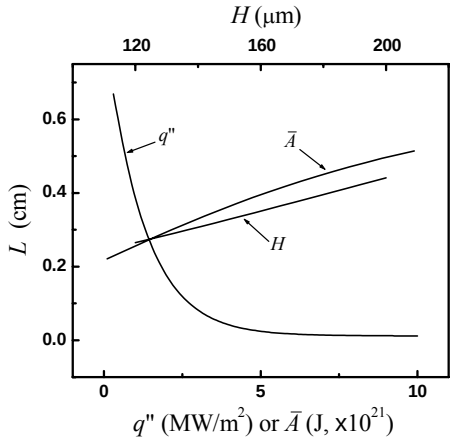


Fig. 7 Effect of heat flux, channel height, and dispersion constant on the length of the extended meniscus region

that the variation of the heat flux has a negligible effect on the length of the extended meniscus region if the heat flux is greater than 5 MW/m^2. In addition, when $q'' > 5$ MW/m^2, the value of L is about 0.2 mm. The liquid film thickness increases with channel height because of the attenuated pressure gradient of liquid phase. The thicker film thickness causes the evaporative mass flux at the liquid-vapor interface to decrease and L increases linearly. The length of the extended meniscus region increases linearly with the dispersion constant. The reason for this is that for a larger dispersion constant, the extended meniscus region is extended farther down the channel because the attractive force strongly acts on the region between the liquid and the solid wall. Therefore, it can be concluded that the surface treatment plays an important role in designing the micro evaporator because the dispersion constant is strongly related to the surface roughness.

5. CONCLUSIONS

In this study, a mathematical model describing the two-phase flow and thermal characteristics of the extended meniscus region in a micro capillary channel is successfully developed. Based on the developed model, the transport phenomena are investigated and the effects of various parameters on the flow and heat transfer performance were also discussed.

The results show that the profile of the liquid film thickness decreased exponentially and the vapor and liquid phases flow in a parallel-flow manner. The local heat transfer coefficient has a very large value in the thin film region. The heat transfer rate, however, is larger for the meniscus than for the thin film region. The influence of inlet liquid velocity on the profile of the liquid film thickness is less significant. The maximum liquid velocity occurs at approximately 40 % of the extended meniscus region and the variation of the heat flux has a negligible effect on it. With increasing heat flux, the length of the extended meniscus region decreases exponentially. However, the length of the extended meniscus region linearly increases with the dispersion constant and the channel height.

Acknowledgements

This research was supported by The Center of Innovative Design Optimization Technology (iDOT), Korea Science and Engineering Foundation.

References

1. B.V. Derjaguin, B.V., S.V. Nerpin, N.V. Churaev, Effect of film transfer upon evaporating liquids from capillaries, RILEM Bull. 29 (1) (1965) 93-98.
2. X. Xu, V.P. Carey, Film Evaporation from a Micro-Grooved Surface-An Approximate Heat Transfer Model and its Comparison with Experimental Data, AIAA J. of Thermo- physics and Heat Transfer, 4 (4) (1990) 512-520.
3. J.M. Ha, G.P. Peterson, The Interline Heat Transfer of Evaporating Thin Film Along a Micro Grooved Surface", ASME J. Heat Transfer, 118 (1996) 747-755.
4. K. Park, K.J. Noh, K.S. Lee, Transport phenomena in the thin film region of a micro-channel, Int. J. of Heat and Mass Transfer, 46(12)(2003), 2183-2188.
5. J. P. Longtin, B. Badran, F. M. Gerner, A one-dimensional model of a micro heat pipe during steady-state operation, ASME J. of Heat Transfer 116 (1994) 709-715.
6. V. Sartre, M. Zaghdoudi, M. Lallemand, Effect of interfacial phenomena on evaporative heat transfer in micro heat pipes, Int. J. Therm. Sci. 39 (2000) 498-504.
7. Y.P. Peles, S. Haber, A steady state, one dimensional model for boiling two phase flow in triangular micro-channel, Int. J. of Multiphase Flow 26 (2000) 1095-1115.
8. F. Blangetti, M. K. Naushahi, Influence of mass transfer on the momentum transfer in condensation and evaporation phenomena, Int. J. of Heat and Mass Transfer 23 (1980) 1694-1695.
9. A. Bejan, Convection Heat Transfer, 2nd ed., John Wiley & Sons, Inc., 1995, pp. 102-104.
10. D. Khrustalev, A. Faghri, Thick-film phenomenon in high-heat-flux evaporation from cylindrical pores, ASME J. of Heat Transfer 119 (1997) 272-278.
11. J.H. Lay, V.K. Dhir, 1995, Shape of a vapor stem during nucleate boiling of saturated liquids, ASME J. of Heat Transfer 117 (1995) 394-401.

Fabrication of Film Type Heat Pipe

Shung-Wen Kang*, Meng-Chang Tsai*, Yu-Hsing Lin**
*Department of Mechanical and Electro-Mechanical Engineering, Tamkang University
151 Ying-Chuan Rd.,Tamsui, 25137, Taiwan, R.O.C
Tel：886-2-26215656 Ext. 2613；Fax：886-2-26209745, swkang@mail.tku.edu.tw
**Department of Mechanical Engineering, St. John's & St. Mary's Institute of Technology

Abstract

This paper describes the development of Film Type Heat Pipe (FTHP), the size of the undergone research is composed of a single-layer copper net using 65mm×40mm×0.31mm whereas the size of a double-layer copper net using 65mm×40mm×0.51mm. Using the vacuum diffusion welding and soldering to make copper foil plate (0.055mm), copper net (0.1mm) and copper tube (diameter 1.5mm) for bonding together. And then it is vacuumed and filled it with different amount of water and methanol. Using the electronic heat plate device (1.27mm×1.27mm), the testing method was carried out. The voltage is adjusted at one side with 3V (1.08W) to 8V (7.76W), in order to increase the heat constantly using the power supply. And on the other side the cooling effect is made with the help of water container (22℃). Applying Temp Scanner and T type thermocouple for measuring the temperature.

The more or less quantity of methanol used is better than water because the boiling point is low and it works on the low power input. When the power input is 7.76W, the single-layer copper net is filled with 70% methanol as compared to unfilled the evaporator temperature is low with 49.7℃. FTHP is made of copper net and easily get folded, hence the fluid will leak from the folds, and meanwhile it doesn't have a good contact with electronic heat plate. In the future it can be considered to increase the tenacity of the film to minimize the folds.

Key words：copper foil plate、copper net、vacuum diffusion welding

1. INTRODUCTION

3M (1990)(1)released an article named "Technology description and applied data of Fluorinert™ liquid radiator" (3M Industrial Chemical Products Division). Such radiator is classified as a kind of Fluorinert – multi-membrane sealed component (FLHS: Fluorinert Liquid Heat Sink) cooling with single phase and easy to be installed. Regarding the standard exterior size of FLHS, the thickness approximates to 3.2 mm and the width of four sealed edges approximates to 5.1 mm. Chen Sung-Po (2001)(2)focuses on the discussion of the influence, from capillary structure, on the netting heat pipes and delivers a reference for interior capillary structure concerning the design of heat pipes. The heat pipe's function of conducting heat is significantly corresponding with capillary structure; the capillary structure chiefly supplies the fluid circulation with capillary thrust and fluid channels.

Industry-Academic cooperation for patent (2001)(3)introduces another type of heat pipe. Please refer to Figure 1 and Figure 2 for the 3-D Diagram. It's a heat pipe made of membrane on the top and bottom, which is tightly connected along the sealed edge. The top membrane and bottom membrane connected at many points will lead to protruding surface. When such pipe is heated, the protruding surface of the top membrane and bottom one will be swollen so as to contact with the heat source closely. We can make use of these characteristics to enhance heat-conducting efficiency and improve heat dissipation of the heat pipe. Accordingly,

condensed work fluid (i.e. the phase change of work fluid, like fluid or vapor) will be reversed to the heat source of the pipe through the capillarity generated by sequential grooves, and, as a result, the conversion efficiency of thermal energy can be improved.

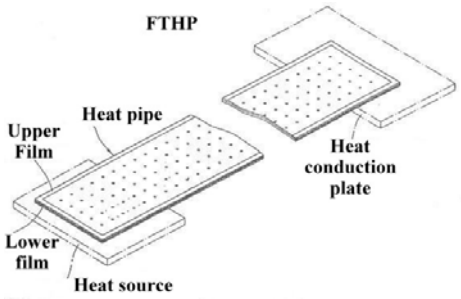


Fig.1. Schematic view of 3-D FTHP-1 〔3〕

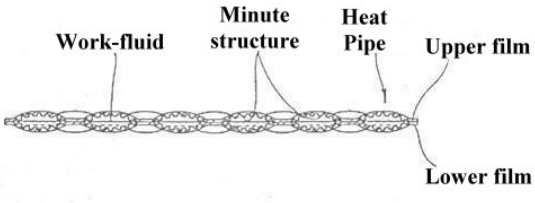


Fig.2. Schematic view of 3-D FTHP-2 〔3〕

2. DESIGN and FABRICATION

Graphite mold shown in Figure 3 was used to fix copper foil plate and copper net to form 65×40×0.055 mm film type heat pipes. Specifications of copper foil plate and copper net is shown in Figure4. Figure 5 shows the constitution of the foil plate, net and tube.



Fig.3. Upper and lower graphite mold

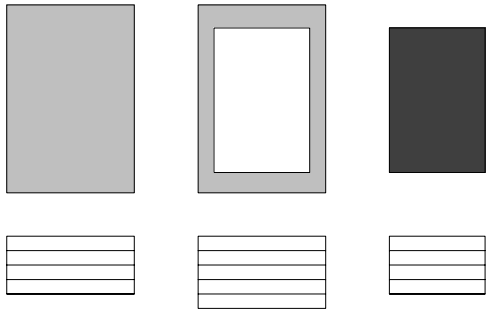


Fig.4. Specifications of Cu foil plate and Cu net

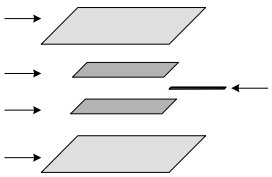


Fig.5. Constitution of Cu foil plate, net and tube

The joint is performed by using the vacuum diffusion welder and bonding parameters as referred by Figure 6. It can be distinguished into the single-layer copper net and double-layer copper net; bonding semi-finished material is sh own in Figure 7. Then, we will fix the foresaid copper tube on proper position of these two sets of semi-finished material. Next, we inject tin paste (Sn Ag 96.5/3.5) into four sides of one semi-finished material and inject more tin paste into the joint of the copper tube to seal the wrinkles thoroughly and avoid leakage. The copper foil plate, copper net and copper tube, injected with tin paste and disjointed, are jointed by Hot Plate afterwards. The copper foil plate surrounding the heat pipe will be connected when Hot Plate warms up to 230℃.

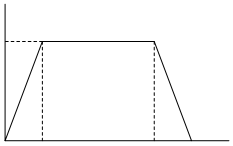


Fig.6. Cu foil plate and Cu net bonding parameter

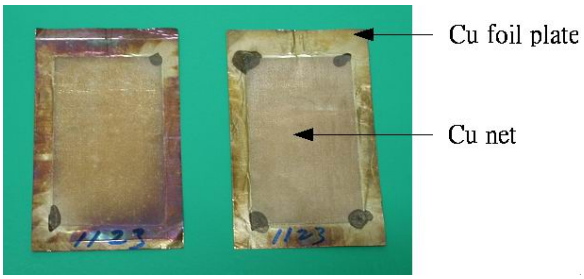


Fig.7. Finished bonding of Cu foil plate and net

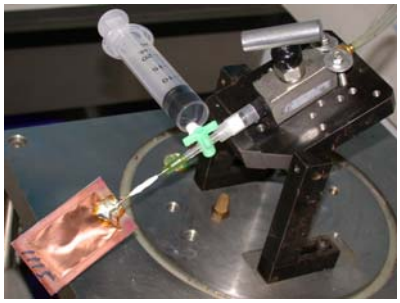


Fig.8. Air extracting and fluid filling

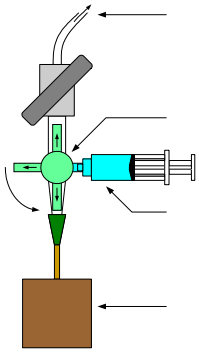


Fig.9. Air extracting and filling – 2 (4)

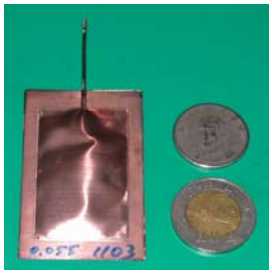


Fig.10. Finished bonding of FTHP

Refer to Figure 8 for air extracting and filling; Figure 9 for sketch (4); and Figure 10 for finished bonding of FTHP filled, sealed, jointed by tin paste and welding tin.

Diffusion welding needs smoother interface and cleaner surface while the roughness of the contact should not be larger. Hence the joint is harder to acquire and so high-intensity joint is obtained. Leakage of the interface always appears when the saturation pressure of work fluid is higher and the diffusion welding is not properly jointed.

Tin paste, used in the later part of the fabrication, may acquire an optimum level of joint intensity where unexceptionally high saturation pressure is endurable. However, the welding tin paste has excellent mobility, so the interface is not well controlled, causing some diversities of volume among the heat pipes.

Sort of diversities of volume among individual heat pipe lead to uncertain ratio of the fillin g volume and affect the contrast during the test. Be sure to keep the air from permeating into the heat pipe when the opening is sealed, lest the he at conductivity should lower down.

3. TEST

The method of operation of FTHP is shown schematically in Fig. 11. The test platform, as shown in Figure 12, consists of power supply, powerful sponge, cooling sink, t emp scanner, PC, thermocouple, stainless clip, meter, and thermal compound, etc. The test approach is referred below.

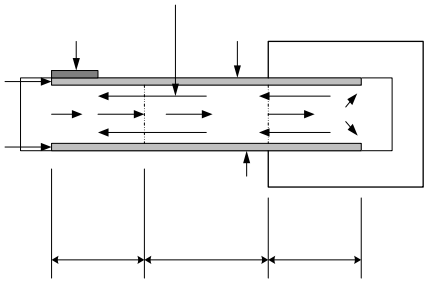


Fig.11 Film Type Heat Pipe operation

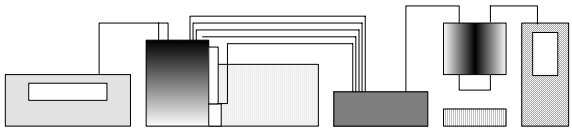


Fig.12. Schematic view of test platform apparatus

(1) Fix electronic heat plate device, and three thermocouple in the front (evaporator), middle (adiabatic) and back (condenser) of the heat pipe by applying thermal compound, Teflon heat-resistant tap.

(2) Fasten Thermocouple 4 on the test platform near the heat pipe to measure the environmental temperature, and fasten thermocouple 5 in cooling sink to measure the temperature therein.

(3) Switch on the Temp Scanner, computer and launch the screen of Chart View for basic configuration including a temperature retrieve of a point every 3 seconds (so there will be 600 points for 30 minutes). Then observe the real-time temperature alteration from the digital window of this software.

(4) Turn on the power supply. This experiment is performed from 3 voltages, and the voltage is adjusted every 5 minutes.

(5) Activate the meter and begin to count time, measure and observe.

(6) Pay attention to the raise of the temperature and restrain it from rising up to over 170℃ lest the electronic heat plate device should be burned out.

(7) Use EXCEL to collect the data acquired and to figure out and draw relation graphs of "Time–Temperature" and "Power–Thermal resistance".

(8) The last minute of the interval of 5 minutes is deemed a steady state; therefore, there will be 20 points within a steady state. Besides, let P = I × V, where P symbolizes Power (Watt), I symbolizes Electric Current (Ampere), and V, Voltage.

(9) To avoid a burned out electronic heat plate device, it's mandatory to use stainless clip to stop a gap between the electronic heat plate device and the heat pipe (hinder the loading of the electronic heat plate device from overweighed), while the heat pipe would be pressed. Thus, working fluid will be resulted in a phase change of vapor restraining the heating area of the heat pipe from propping up, which, consequently, affects this heat pipe in making and moving.

4. DISCUSSIONS

1. From Figure 13: the temperature of the double-layer copper net is lower than that of the single-layer regarding non-filling in the structure of the heat pipe, then we can conclude that the double-layer is superior to in heat conductivity.

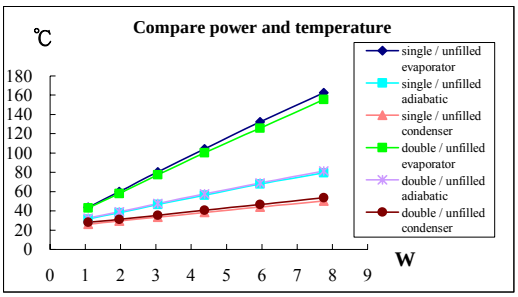


Fig.13. Compare power and temperature – test 1

2. From Figure 14: when there's no clear difference of filling volume, the temperature of the double-layer copper net is still lower than that of the single-layer; so different structure also affects the heat conductivity.

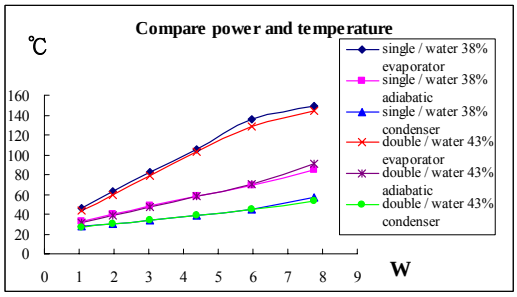


Fig.14. Compare power and temperature – test 2

3. From Figure 15: when the filling volume of the single-layer copper net is more than that of the double-layer copper net by 9%, the temperature of the single-layer copper net is lower than the double-layer copper net. From this we can speculate that the volume of the work fluid will replace structural difference and affect overall heat conductivity.

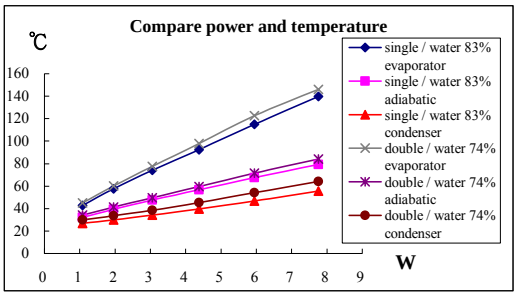


Fig.15. Compare power and temperature – test 3

4. From Figure 16: the heat pipe with more filling volume features better heat conductivity, under the same structure and work fluid, and the making and moving of the phase change turns clearer. Under 7.76W, the temperature of the single-layer copper net with 70% of methanol rises slowly while the temperature on the other end is higher. That is because the vapor generated in the exterior of the heating end carries heat to the other end (cooling end) and leads to the decline of the temperature in the heating end.

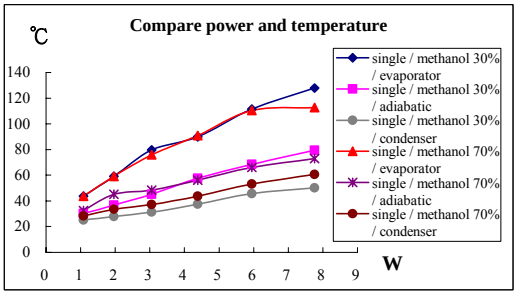


Fig.16. Compare power and temperature – test 4

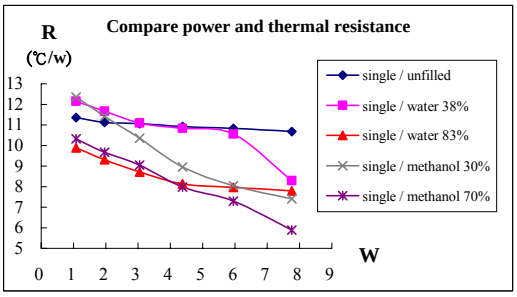


Fig.17. Compare power and thermal resistance – single layer Cu net

5. Figure 17: shows that the thermal resistance of water declines dully under higher voltages but methanol has a larger drop. Under the same structure of the single-layer copper net, the thermal resistance of methanol is lower than that of water, regardless of the volume of work fluid.

6. From Figure 18: the double-layer copper net with work fluid of water, the volume resistance of the heat pipe with fewer filling volume changes later, and the thermal resistance of which is lower where under 7.76W.

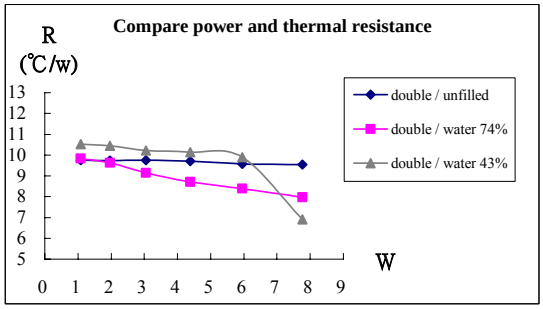


Fig.18. Compare power and thermal resistance – double layer Cu net

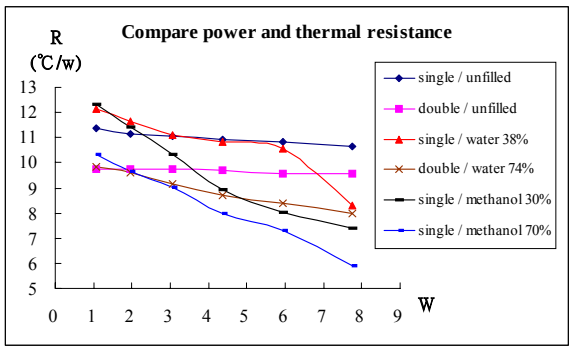


Fig.19 Compare power and thermal resistance

7. We can draw some conclusions from Figure 19: (1) The thermal resistance value hardly changes for unfilled heat pipe because the pipe is a well-mixed material; a well-mixed material has immobile heat conductivity. (2) The thermal resistance value changes later for the work fluid of water with fewer filling volume. (3) The thermal resistance value changes earlier for the work fluid of water with more filling volume or for the work fluid of methanol.

5. CONCLUSIONS

1. FTHP is always swollen after the heating test, the saturated vapor pressure in the interior is elevated correspondingly which, adversely, retards the boiling. Eventually, the phase change is available only in higher temperature.

2. It is essential to maintain a specific space for the heat pipe. After the air inside is evacuated, the pipe appears flat on account that the interior pressure fails to arrange a specific space. When work fluid reaches to boiling and the phase changes, vapor pressure should prop up the outer copper foil plate in advance so as the vapor of work fluid could flow to the condenser. Under such circumstances, some vapor pressure must be wasted to enhance the heating temperature for such making and moving. But the rising temperature violates the rule of heat conducting efficiency by lowering down the temperature and, furthermore, restrains work fluid from reversing.

3. The double-layer copper net, from the experimental test, is superior to the single-layer copper net in heat conductivity.

4. Significant diversity of the work fluid volume will replace structural difference and affect overall heat conductivity.

5. Methanol, in this experimental test, performs better efficiency than water regardless of filling volume; moreover, methanol has distinct making and moving at lesser watts because of lower boiling point. In case the power is set at 7.76W, the heating end of the single-layer copper net with 70% of the heat pipe filled with methanol features lower temperature, less than that of the unfilled single-layer copper net by 49.7℃ approximately.

Acknowledgement

This work was supported by the National Science Council of Taiwan, Republic of China under contract No. NSC 91-2622-E-032-003-CC3.

References

(1) 3M Industrial Chemical Products Division. "Fluorinert™ Liquid Heat Sink", St. Paul, Minnesota. 1990.

(2) Chen Sung-Po, "Determination of Penetration Ratio Regarding Heat Conductivity of Small-Sized Metal Netting Heat Pipe", Master thesis, Graduate Institute of Mechanical Engineering, NTUST, Taiwan, 2001.

(3) Ko Yao-Lin, "Soft Swellable, Flexible Membrane Pipe", Taiwan, Republic of China,Patent, Patent No. 452117, 2001.

(4) Ko Ming-Han, "Fabrication of Metallic Micro Heat Pipe Heat Spreader", Master Thesis, Graduate Institute of Mechanical Engineering, Tamkang University, Taiwan, 2002.

(5) Hou Tung-Fu, "Fabrication of Micro Loop Heat Pipes", Master Thesis, Graduate Institute of Mechanical Engineering, Taiwan, Tamkang University, 2002.

Thermal Performance of a Grooved Flat-Strip Heat Pipe with Multiple Heat Source Locations

Park, Soo Yong and Boo, Joon Hong
School of Aerospace and Mechanical Engineering
Hankuk Aviation University
200-1, Hwajon-dong, Deokyang-gu, Koyang-city, Kyonggi-do,
412-791, KOREA
+82-2-300-0107, +82-2-3158-2131, jhboo@hau.ac.kr

Abstract

A series of experiments was conducted to examine characteristics of a grooved flat-strip heat pipe having multiple heat sources. The dimensions of the heat pipe were 150(L)×20(W)×5(H) mm of which the thickness may fall into a miniature heat pipe. The inner grooves of the heat pipe have the aspect ratio of 1 to 2.5(0.42×1.05 mm) whose pitch was 0.84 mm. Four block heaters (10×20 mm) were placed in the evaporator section of the heat pipe at intervals of 20 mm.

Six different heating modes were tested in which maximum of two heaters work simultaneously. The maximum input heat load was 160W and the maximum surface heat flux of 80 W/cm^2 was achieved while the operating temperature was kept below 100℃. In the nearest heating mode (from the condenser location), the heat pipe exhibited more stable temperature distribution than the far heating mode where the heaters is located furthest from the condenser.

Key words: flat-strip heat pipe, rectangular grooves, multiple heat sources

1. INTRODUCTION

Due to increase of power density and heat dissipation requirement of various electronic products, development of a higher efficiency thermal spreader emerges as a challenging problem. There is no question in that heat pipe can be a strong candidate to solve problems of this kind. Especially, flat heat pipes have advantages in electronics application because it can be attached on the component surface with moderate or high heat fluxes [1].

In recent years, researches for high performance miniature heat pipe were performed where one of high aspect ratio grooves, a sintered power wick, or a special design wick was adopted [2-4]. Cheng et al. conducted theoretical analysis of flat miniature heat pipes (FMHP) with high aspect ratio. The FMHP was fabricated by ultra-deep LIGA process. In their study, the maximum heat transfer rate reached 391W at a working temperature of 100℃ [5]. Lin et al. fabricated and tested high performance miniature heat pipes using capillary structures made of a folded copper sheet fin and achieved 140W/㎠ heat flux using concentrated heating modes [6]. Maziuk et al. presented software for flat miniature heat-pipe parameters prediction and numerical modeling. The study compared the result of numerical analysis with the experimental data for the FMHP with a copper sintered powder wick structure with water [7].

Heat pipes with sintered metal wick or specially designed insertions may exhibit higher performance than simple rectangular groove heat pipe. However heat pipes with rectangular miniature grooves have advantage of easiness in fabrication and low manufacturing cost. The need of a study on heat pipe with multiple heat sources has been raised considering electronic applications in which several heat generating chips and processors packaged closely each other are desired to be cooled with a single heat pipe. For this reason there have been a few previous studies on multiple heat source problems in heat pipe.

Faghri and Buchko performed an experimental and numerical study of low temperature heat pipe with multiple heat sources [8]. They suggested a mathematical model to predict the performance of the heat pipe and performed an experiment using 1 m long copper-water heat pipe with four heaters. Park conducted the optimization of the heat source distribution in satellite equipment, in both numerical and experimental way, for a copper-

water heat pipe with two heat sources [9].

The objective of this study is to understand the heat transfer characteristics of the grooved flat heat pipe subject to four different heat source locations. It is considered that two of the heat sources may work simultaneously. In this experimental study, input thermal loads and inclination angles were varied. The temperature distribution, thermal resistance of the heat pipe, and heat transfer coefficient of the evaporator and condenser section were the major concerns.

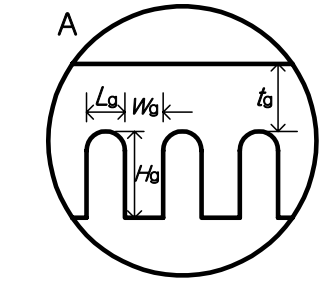
2. EXPERIMENTAL SETUP AND PROCEDURE

The dimension of the heat pipe in this study were 150(L)×20(W)×5(H) mm respectively. There were sixty grooves machined at the inner surfaces of the heat pipe.

The width and the depth of the groove were 0.42mm and 1.05mm and the end shape of the groove has a half circle due to a matching method. The pitch of the grooves was 0.84mm. A cross section of the heat pipe and grooves are shown in Fig. 1.

Fig. 2 shows thermocouple locations on the heat pipe. There were fifteen K-type thermocouples on the upper surface of the heat pipe with 10mm spacing. Four electric heater blocks (20(W) × 10(L) × 10(H) mm) were attached on bottom side of the heat pipe. The spacing of the heaters was 20mm each. Each heater had a maximum heating capacity of 300W and was controlled individually.

A cooling block (copper, 20(W)×30(L)× 10(H) mm) was attached to the condenser surface of the heat pipe. The coolant of the



H_g = 1.05 mm
L_g = 0.42 mm
W_g= 0.42 mm
t_g = 0.66mm

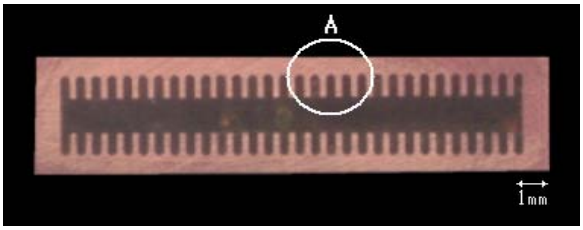


Fig. 1 Cross-section of the flat-strip heat pipe and groove shape

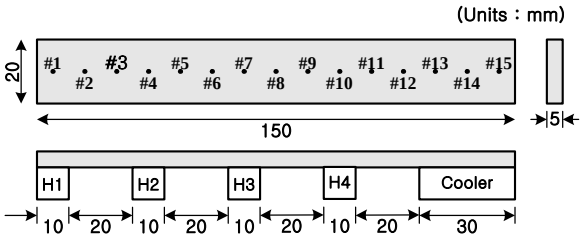


Fig. 2 Heat pipe dimensions and thermocouple locations

cooling block was water and the inlet temperature of the coolant was kept at 30℃ by a constant temperature circulation bath. Four thermocouples (No. is #1, #4, #7, and #10) were located in the evaporator and three thermocouples (No. is #13, #14, and #15) were installed in the condenser section to measure the temperature.

The working fluid was water and the charge amount was calculated based on the volume of all the grooves. The charge amount of working fluid in this study was 3.98 cc which corresponded to 100% charge ratio.

In every heating mode the heat pipe was tested at horizontal position and at adverse tilt angle of -5°. Six different heating modes were tested and they were shown in Fig. 3. In H1&H3 heating mode, heaters 1 and 3 operated simultaneously. And heater 1 and heater 4 operated simultaneously in H1&H4 heating mode. The thermal loads were regulated from 20 W to 160W, either gradually or with a step change. The maximum operating temperature was maintained below 100℃ considering applications involving electronic components.

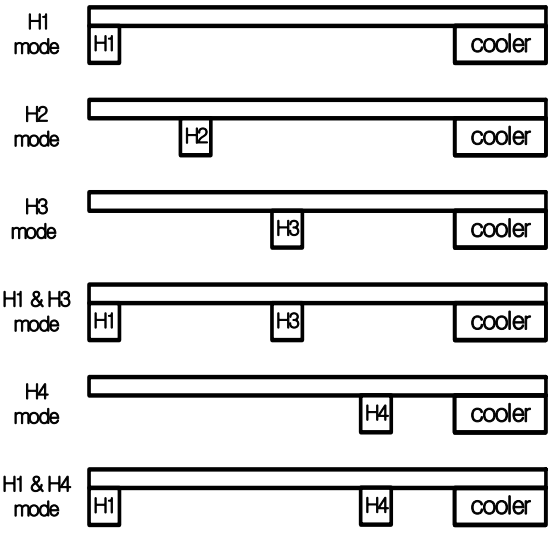
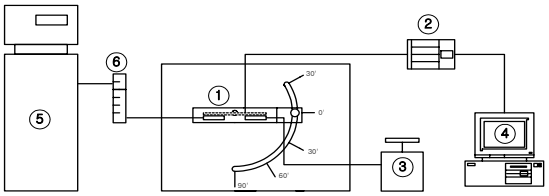


Fig. 3 Tested heating modes



1: Heat pipe
2: Recorder
3: Power supply
4: IBM PC
5: Circulation bath
6: Flow meter

Fig. 4 Experimental Setup

The schematic of the experimental setup is shown in Fig. 4. A test bed was designed so that it can regulate inclination angle of the heat pipe. All the thermocouples were connected with a data acquisition system, and a desktop PC saved a whole set of temperature data in every 5 seconds. The volume flow rate of the coolant for the cooling block was measured by a rotameter and was adjusted to 0.2 liters/min.

As a performance measure of a heat pipe the thermal resistance was calculated for every case tested. The thermal resistance of a heat pipe is defined as,

$$R_{HP} = \frac{T_e - T_{c.m}}{Q_{input}} \tag{1}$$

where T_e and $T_{c.m}$ is a wall temperature of the heating region and a mean temperature of the condenser region, respectively. Q_{input} is a input thermal load at the evaporator.

To estimate the heat transfer coefficients of the evaporator and condenser, the following two equations can be used.

$$h_e = \frac{Q_{input}}{A_e(T_e - T_{a.m})} \tag{2}$$

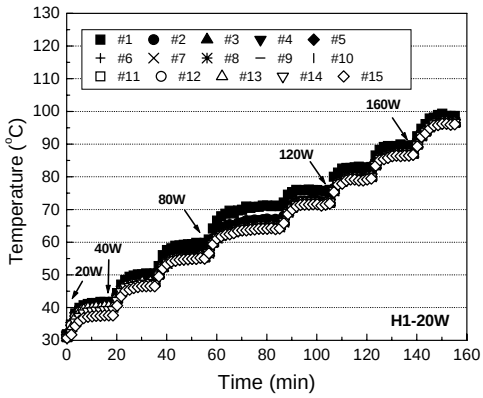
$$h_c = \frac{Q_{input}}{A_c(T_{a.m} - T_{c.m})} \tag{3}$$

where A_e and A_c are the surface area of the evaporator and condenser section, respectively, and $T_{a.m}$ is the mean temperature of the adiabatic section, which is regarded as an operating (or vapor) temperature of the heat pipe. For the tested heat pipe in this study, A_e was 2㎠ and A_c was 6㎠.

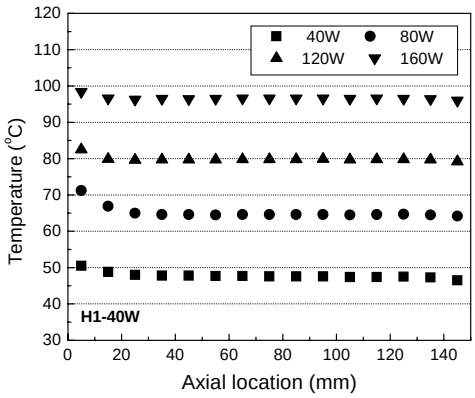
3. RESULTS AND DISCUSSION

3-1 Temperature distributions

Figs. 5 (a) and (b) shows the temperature variation and distribution as a function of thermal loads for the heat pipe in horizontal position which is heated by the H1 heater in Fig. 3. The maximum input thermal load of the heat pipe was about 160W while the operating temperature was limited to 100℃. The dry-out of the heat pipe was not observed for the maximum heat load although a sudden increase of temperature of T/C #1 was notice at 80W. Fig. 5 (b) shows the temperature distribution at H1 heating mode. The largest temperature difference across the heat pipe length of 7℃ was observed at 80W. At horizontal position, no distinct variation of the temperature distribution was observed in the H1 heating mode. Even for a step heating of 160W, the temperature distribution and increase were stable while the operating temperature was kept below 100℃ and the average temperature difference across the whole length of a heat pipe was about 2.5℃.

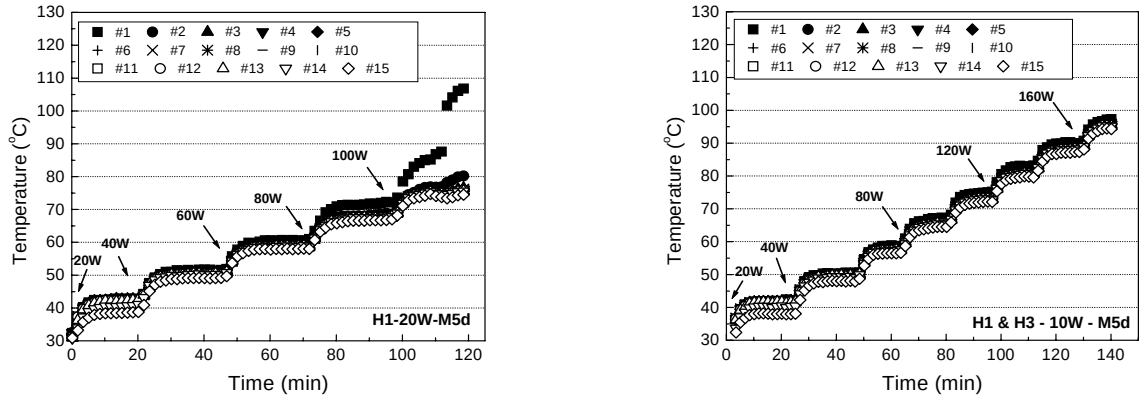


(a) Temperature variations against heat input and time



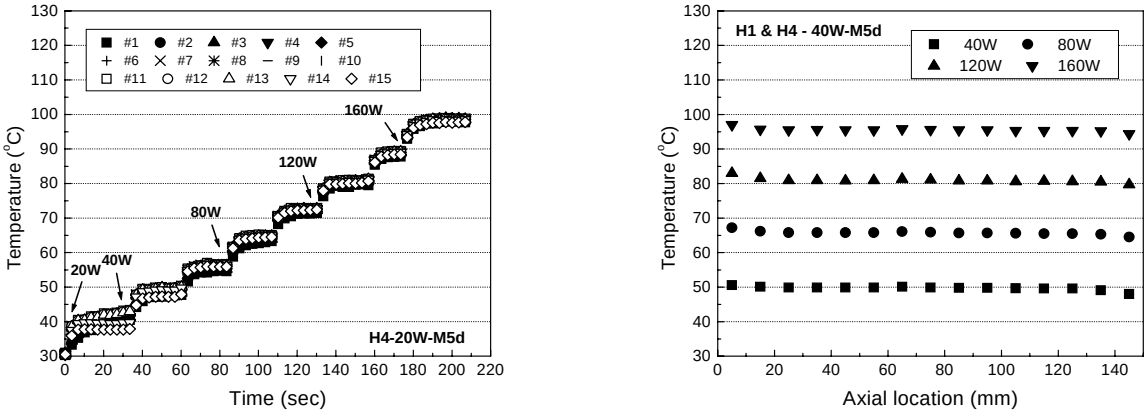
(b) Axial temperature distribution

Fig. 5 Surface temperature variations for H1 heating mode (horizontal position)



(a) H1 heating mode (b) H1 & H3 heating mode

Fig. 6 Comparison of surface temperature variations with adverse tilt (-5 deg.) for H1 and H1&H3 heating mode



(a) H4 heating mode (b) H1 & H4 heating mode

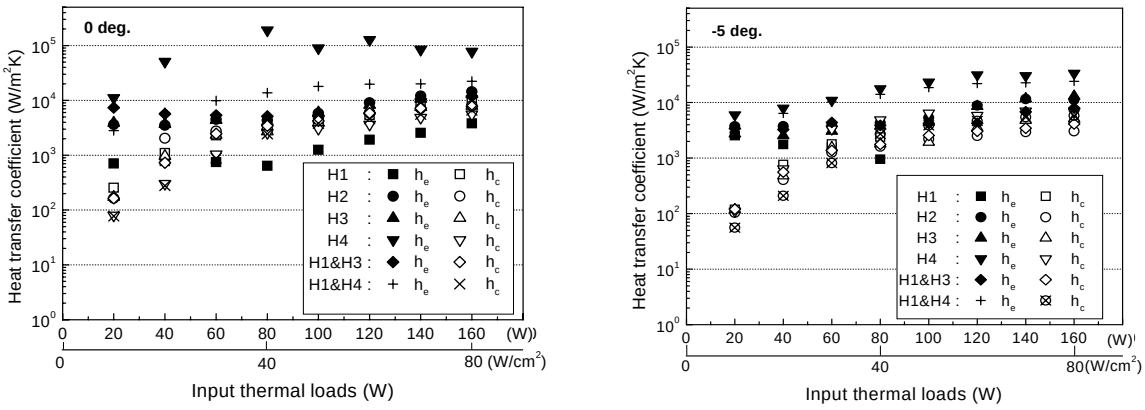
Fig. 7 Surface temperature variations for H1 and H1&H4 heating modes with adverse tilt (-5 deg.)

Fig. 6 shows the surface temperature variation of the heat pipe as input heating mode for the adverse tilt angle of –5 deg. Fig. 6 (a) represents H1 heating mode and (b) is H1&H3 heating mode. In H1 heating mode, the maximum heat load was 80W because a dry-out occurred at 100W. In H1&H3 heating mode, the dry-out was not observed and the maximum heat load was reached 160W. Before a dry-out occurred in H1 heating mode, the surface temperature was a little higher and the difference of them across the whole length was larger than those in H1&H3 heating mode at 80W. It is considered that the dispersed heating extended the limitation of the operation and improved the temperature distribution.

Fig. 7 (a) shows the temperature variation of the heat pipe for the H4 heating mode with the adverse tile angle. In the H4 heating mode, the least temperature difference were observed of which the average value was 1.8℃. In the adverse tilt angle, the upper part of the heated location worked as a shorter heat pipe in bottom heating mode. And the lower part of the heated location worked as a shorter heat pipe in adverse tilt, thus caused an increase of operation (capillary) limit. Fig. 7 (b) represents for H1&H4 heating mode in the adverse tilt angle of 5 degrees. For the dispersed heating of two locations, temperature distribution became relatively more stable than that of H1 heating mode in Fig. 5 (b).

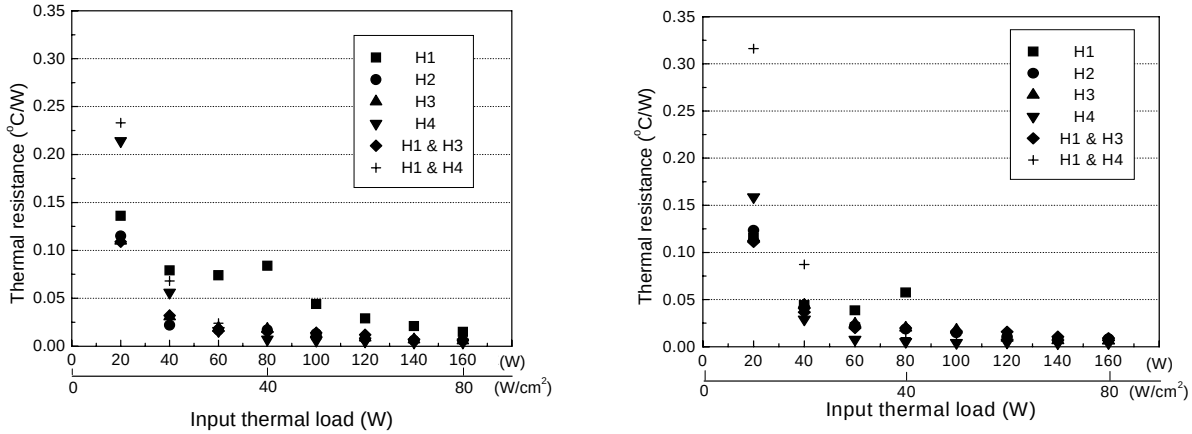
3-2 Thermal performances

The heat transfer coefficients of the heat pipe are shown in Fig. 8 as a function of input thermal load and heating mode. Fig. 8 (a) presents the values at the horizontal position of the heat pipe with respect to the input thermal load. The heat transfer coefficient at the evaporator section ranged from $10^3 \sim 10^5$ W/m^{2}K. The heat transfer coefficient of the evaporator exhibited the highest value for the H4 heating mode, which was up to about 100,000 W/m^{2}K. The lowest heat transfer coefficient occurred for the H1 heating mode. The H1&H4 heating mode has second highest value, which was about 10,000 W/m^{2}K. Fig. 8 (b) shows the values for the –5 adverse tilt angle. As the horizontal state, H1 and H1&H4 heating



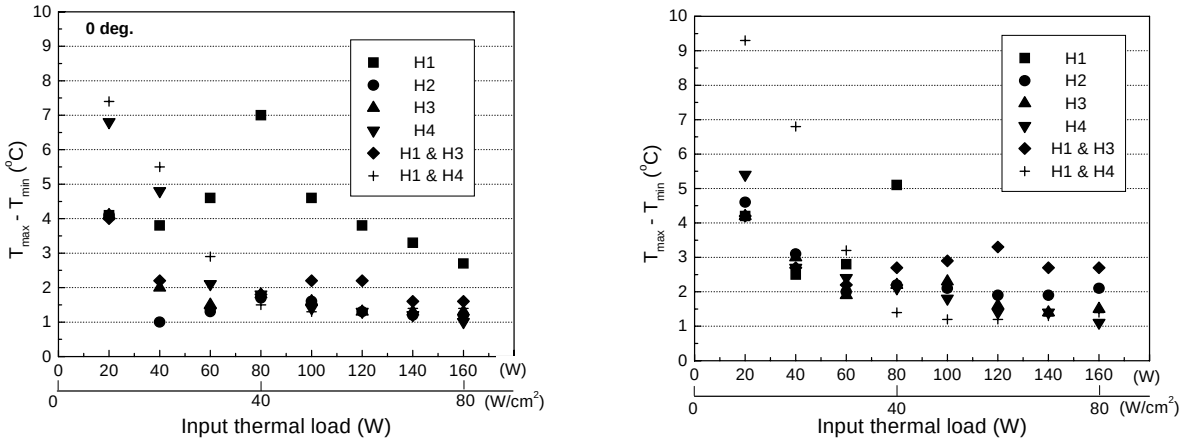
(a) Horizontal position (b) –5 degree

Fig. 8 Variation of the heat transfer coefficients as a function of heating mode and thermal load



(a) Horizontal position (b) –5 degree

Fig. 9 Variation of the thermal resistances as a function of heating mode and thermal load



((a) Horizontal position (b) –5 degree

Fig. 10 Variation of the temperature difference as a function of heating mode and thermal load

mode have the highest heat transfer coefficient. No significant difference was observed in the condenser section between the two heating modes.

Fig. 9 shows the variation of the thermal resistance as a function of the heating mode and input thermal load. In most cases, the highest thermal resistance was observed at H1 heating mode. The value increased to 80W. Thermal resistance showed decreasing tendency up to the maximum thermal load of 160W. In normal operation state of the heat pipe, the most of the

thermal resistances were lower than 0.02 ℃/W. However, the heat pipe in H1 heating mode exhibited relatively large values. Fig. 9 (b) shows the thermal performance at the adverse tilt angle of -5 degrees. The thermal resistances showed similar patterns and the values were only a little higher than the horizontal position in (a). Exceptionally for H1 mode, the values were lower.

Fig. 10 shows the maximum temperature differences on the heat pipe wall as a function of heating mode and input thermal load. In the horizontal position, the differences were about 2℃ or less except H1 heating mode while the heat pipe was in normal operation. For the adverse tilt angle of -5 degree, the temperature differences were less than 3℃ in most cases. Both horizontal position and adverse tilt exhibited the lowest thermal resistance for H1&H4 heating mode. And the next lowest temperature differences were observed in H4 heating mode.

4. CONCLUSIONS

A flat miniature heat pipe of 5mm thickness with axial grooves was manufactured and tested to examine the performance when heat source locations are changed. Through an analysis of experimental data the following conclusion can be stated;

(1) The maximum heat transfer rates of the tested heat pipe changed only slightly with a tilt angle (0 deg. and –5 deg.). The maximum thermal load achieved 160W, which corresponds to the heat flux of 80W/cm^2.

(2) The most stable and effective heating mode was H4 mode. It is considered that the result was due to the shortest effective length of heat pipe. For adverse tilt angle, the higher part of the heated section operated as a shorter heat pipe in bottom heating mode. And the lower part of the heated location worked as a shorter heat pipe in adverse tilt, thus caused an increase of operation (capillary) limit.

(3) Multiple heat source modes improve the thermal performance of the heat pipe in the bottom heating mode. When the heat sources are dispersed in a certain interval, the operation limit has been improved.

Nomenclatures

A_c	condenser section area (m^2)
A_e	evaporator section area (m^2)
h_c	heat transfer coefficient of condenser (W/m^{2}K)
h_e	heat transfer coefficient of evaporator (W/m^{2}K)
H_g	height of the groove (mm)
L_g	width of the grooves gap (mm)
R_{HP}	thermal resistance (℃/W)
$T_{c,m}$	mean temperature of condenser section (℃)
$T_{a,m}$	mean temperature of adiabatic section (℃)
T_e	temperature of evaporator section (℃)
Q_{input}	input thermal load (W)
W_g	width of the groove (mm)

References

1. Faghri, A., 1995, *Heat Pipe Science and Technology*, Taylor & Francis, pp. 625-631

2. Park, S. Y. and Boo, J. H., 2001, "Experiment Study of a Flat-Strip Heat Pipe with a Combined Wick of Axial Groove and Screen Mesh," Proceedings of the KSME Spring Annual Meeting, Heat Engineering Division, pp.741-745

3. Chen, Y. M. et al., 2001, " Thermal Performance of Sintered Miniature Heat Pipes," J. of Heat and Mass Transfer, Vol.37, pp.611-616

4. Moon, S. H., Kim, C. J., Kim, B. H., Hong, S. E., Lee, J. S., 1999, An Experimental Study on the Performance Limitation of A Micro Heat Pipe with Triangular cross-section, 11th IHPC.

5. Cheng, Y. 2002, "High Performance Flat Miniature Heat Pipes Fabricated by UD-LIGA Process," Microsystem Technologies, Vol.9, pp.23-24

6. Lin, L. et al., 2002, "High Performance Miniature Heat Pipe," International Journal of Heat and Mass Transfer, Vol.45, pp.3131-3142

7. Maziuk, V. et al., 2001, "Miniature Heat-Pipe Thermal Performance Prediction Tool-Software Development," Applied Thermal Engineering, Vol.21, pp.559-571

8. Faghri, A. and Buchko, M., 1991, *Experimental and Numerical Analysis of Low-Temperature Heat Pipes with Multiple Heat Sources*, Journal of Heat Transfer, Vol.113, pp.728-734

9. Park, J. H., 1997, *A Study on Thermal Performance of Heat Pipe for Optimum Placement of Satellite Equipment*, ETRI Journal, Vol. 19, No. 2, pp.59-70

The Effects of Various Transverse Accelerations and Their Induced Body Forces on the Cooling Performance of Micro Heat Pipes

Masafumi Katsuta, Ahmad Jalilvand, Yuji Homma
Waseda University, 3-4-1 Ookubo, Shinjuku-ku, Tokyo 169-8555, Fax & Tel: +81-3-52863251, E-mail: jalilvand@fuji.waseda.jp

Abstract

The idea of using micro heat pipes for thermal control of computer and electronic components of spacecrafts, has necessitates the better understanding of the thermal behavior of this type of heat pipes under acceleration. The objective of present study has been derived from the fact that normally no aircraft can maintain its stability without rotating (rolling) around its axis while it is revolving in the air. Rotational acceleration along with revolving motion of the aircraft about an axis in the air will result in new direction and magnitude for the acceleration applied to the liquid in heat pipe; therefore, under these transverse accelerations, different capillary limits will be anticipated. In this study, a kinematic analysis is carried out to determine the direction and magnitude of acceleration applied to a flat plate heat pipe used for cooling a special device in an aircraft. Assuming the heat pipe is properly primed and operating normally in a zero gravity environment, the most damaging accelerations will be those occurring along the longitudinal axis since these are most likely to deprime the liquid channel. Therefore, the component of acceleration, which is along the longitudinal axis of heat pipe, is determined. Then, an analytical investigation based on capillary limit of heat pipe is carried out to determine the maximum heat transport capacity of micro heat pipe under pure longitudinal acceleration. In addition, the special way of installing heat pipes to minimize the damaging effects of acceleration is determined. As a result, both revolving and rotating speed of the airplane affect the maximum heat transport capacity of flat plate micro heat pipe.

Key words: Micro heat pipe, longitudinal acceleration, Maximum heat transport capacity

1. INTRODUCTION

Thermal control is a crucial aspect for insuring the normal performance of modern electronic devices; therefore the heat generated in these devices must be dissipated in order to maintain operating temperature in normal range. The importance of heat dissipation is much more vital for electronic devices, which are used in fighter aircrafts and spacecrafts. Micro heat pipes as a cooling strategy for compact electronic equipment present a promising alternative to traditional cooling schemes and offer the possibility of high local heat removal rates and high level of temperature uniformity across individual electronic components. Considering the acceleration field on the performance of micro heat pipes used in spacecrafts and shuttles, and also the knowledge of the capability of micro heat pipes to remove the delivered heat in such conditions, are very significant for electronic package designers. During a maneuver, the micro heat pipes experience different types of accelerations. Normally no aircraft can maintain its stability without rotating (rolling) around its axis while it is revolving in the air. Rotational acceleration along with revolving motion of the aircraft about an axis in the air will result in new directions and magnitudes for the acceleration applied to the liquid in the grooves and wick structures, but the most damaging accelerations will be those occurring along the longitudinal axis of the micro heat pipes since these are most likely to deprime the liquid channel. Consequently, when an aircraft is revolving in the air, capillary limit of the heat pipe will be affected significantly with revolving speed. The purpose of this study is to investigate the operations of micro heat pipes under pure longitudinal acceleration.

Only a limited number of investigations were found which focused on revolving heat pipes, Chen and Lou [1] and Chen and Tu [2] investigated the heat transfer performance of inclined revolving heat pipes. The test results of Keiyou and Maezawa [3] indicated that the optimum fill ratio for revolving heat pipes was approximately 10% by volume, however, Curtila and Chataing [4] concluded that the fill ratio must be between 25 and 30%. A majority of the investigations concerned with revolving heat pipes attempted to predict the heat transfer coefficient theoretically. Nusselt types of

analyses were used to compute the liquid film thickness and several dimensionless semi-empirical expressions were developed. Among these, the prediction of Keiyou and Maezawa [3] best fits the accumulated experimental data. Bontemps et al. performed a kinematic analysis of revolving heat pipes and reached several qualitative conclusions [5]. In this investigation [5], the momentum equations are solved based on Nusselt`s theory and an expression of power input under high rotational speeds is obtained as a function of the speed of revolution, the inclination angle, the temperature difference, the geometry and working fluid properties. The resulting equation indicates that the heat flux is proportional to the square root of the rotational speed.

In this study, the operation of a micro heat pipe that is installed in an aircraft is investigated. As a first step a kinematic analysis is conducted to determine the acceleration applied to a micro heat pipe. This acceleration is due to revolution and rotation of the aircraft. In the next step, the component of acceleration, which is in the direction of longitudinal axis of heat pipe, is determined, because this component has the most damaging effects. Then, an analytical study based on capillary limit is performed to observe the effects of longitudinal body force on the operation of micro heat pipes. Finally, the special way of installing a micro heat pipe in an aircraft to minimize the damaging effects of acceleration is determined.

2. FLAT PLATE MICRO HEAT PIPE

In this study, a flat plate micro heat pipe is considered as a sample. Fig 1. Shows a schematic view of a flat plate heat pipe. As it is seen in Fig. 2, condensed liquid in the condenser returns to evaporator by the capillary mechanism. Capillary force is produced by wick structure at the center of heat pipe and two grooves at the two sharp edges (Fig. 2). In flat plate heat pipes, the stable working fluid circulation is achieved through the capillary pressure head developed by the wick structure and sharp edges. Therefore, to apply the basic model to a flat plate micro heat pipe, capillary force generated by grooves should be considered as additional term. The maximum heat transfer attainable in a heat pipe is achieved under conditions such that the capillary pressure head is greater than or equal to the sum of pressure losses along the vapor-liquid path. In order for the heat pipe to operate properly, the following pressure balance must be satisfied:

$$\Delta P_{wc,\max} + \Delta P_{gvc,\max} \geq \Delta P_{wl} + \Delta P_{gvl} + \Delta P_v + \Delta P_b + \Delta P_e + \Delta P_{con} \quad (1)$$

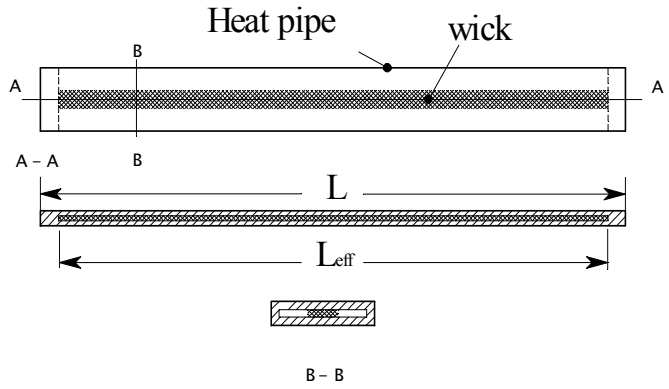


Fig 1 Schematic view of a flat type micro heat pipe

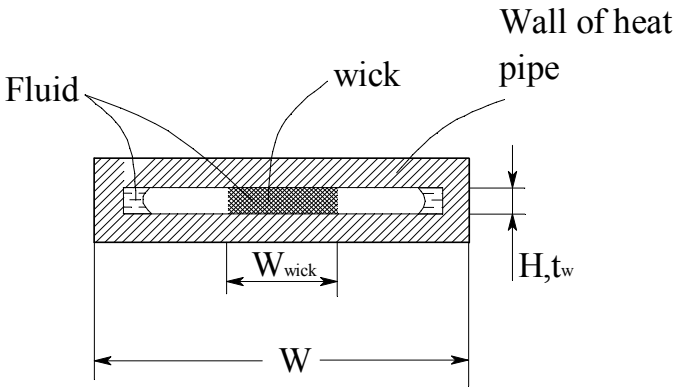


Fig. 2 Cross sectional view of a flat plate micro heat pipe

In equation (1), the terms on the left hand side are driving pressure produced by wick structure and grooves respectively. The first two terms on the right-hand side of equation (1) are liquid pressure drops in wick structure and grooves. The next two terms are pressure drops in vapor phase and pressure drop due to body forces, respectively. The last two terms are pressure drops, which occurs during phase change of working fluid in heat pipe. In this study, the pressure drop due to phase change is neglected.

3. METHOD OF ANALYSIS

In this work, a mathematical model is used to determine the acceleration applied to a flat plate micro heat pipe, which is installed in an aircraft. The acceleration, which is applied to a heat pipe, is the result of revolving an aircraft about an axis

in the air and rotating about aircraft's main axis. Then, the maximum heat transport capacity of a flat plate micro heat pipe, based on capillary limit and different revolving and rotating speed of aircraft is obtained. As a last step, the optimum configuration of a micro heat pipe to minimize the damaging effects of acceleration is determined.

3-1 DETERMINATION OF ACCELERATION

Fig.3 illustrates the position of an aircraft in the air with corresponding angular velocities. It is assumed that the aircraft is revolving with a constant angular velocity (ω_1) in a plane, parallel to the earth surface. Therefore, an acceleration (a_r) toward the center of revolution is generated. Since ω_1 doesn't change with time, no tangential acceleration (a_t) will exist along the aircraft's path. Furthermore, it is assumed that the aircraft rotates around its axis with a constant angular velocity (ω_2) while it is revolving. Although the angular velocity changes with time, both at the beginning of rolling (rotating) and at the end of rolling, we consider ω_2 constant, because these changes happen in short periods of time. The aircraft never continues rolling after reaching to a definite angle.

We consider the inertial reference frame (x_1, y_1, z_1) at the point, which axis of revolution passes through the air; and system (x_2, y_2, z_2) at the intersection point of aircraft's main axis with the wing's axis.

The acceleration vector at point P moving with liquid in a micro heat pipe, with respect to the inertial reference (x_1, y_1, z_1) is [7]:

$$\vec{A}_P = \vec{A}_{O_2/O_1} + \vec{A}_{P/O_2} \qquad (2)$$

Where:

$$\vec{A}_{P/O_2} = \vec{A}_{P'} + \vec{A}_{P/aircraft} + \vec{A}_{coriolis} \qquad (3)$$

In the above equations, P is a point moving with a liquid particle in micro heat pipe and P' is a fix point, which happens to coincide with P at the instant considered. In micro heat pipes, the liquid velocity in the grooves and wick structure is very small, therefore it is assumed that the liquid particle has no relative acceleration and no relative velocity with respect to airplane. On the other hand, it is assumed that P is immobilized on aircraft with no acceleration. With this assumption, the effects of coriolis acceleration are neglected. Therefore, the last two terms of Equation (3) is neglected.

Another force that is applied to the system is gravity force ($\vec{F}_g$) that is supposed to be important in small transverse accelerations.

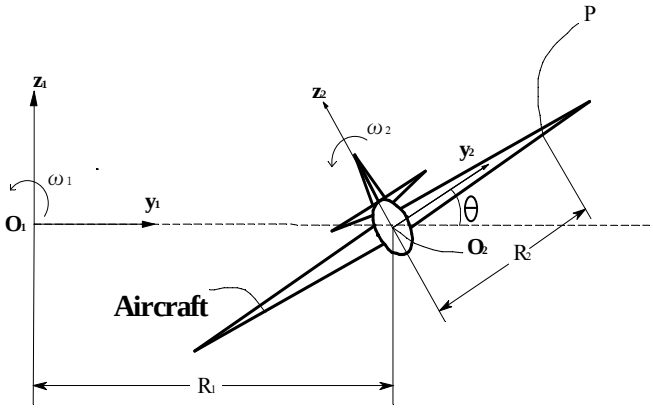


Fig.3 Position of the aircraft in the air (backward view)

With these assumptions, the absolute acceleration that is experienced by liquid particles in a micro heat pipe, can be expressed as:

(4)

$$\vec{A}_p = \vec{\omega}_1 \times (\vec{\omega}_1 \times \vec{R}_1) + \vec{\omega}_2 \times (\vec{\omega}_2 \times \vec{R}_2) + \vec{F}_g$$

By using proper transformation, we express the acceleration of point P in terms of (x_2, y_2, z_2):

(5)

$$\vec{A}_P = (-R_1\omega_1^2 \cos\theta - R_2\omega_2^2 - g\sin\theta)\hat{e}_{y_2} + (R_1\omega_1^2 \sin\theta - g\cos\theta)\hat{e}_{z_2}$$

We assume that α, β, γ are the angles, which are made by the longitudinal axis of micro heat pipe with respect to x_2, y_2, z_2 respectively (Fig. 4). The acceleration component that is along the longitudinal axis of micro heat pipe is the most

damaging component, therefore the dot product of acceleration vector which is defined by equation (5) and the unit vector along the longitudinal axis of heat pipe is performed to determine the acceleration component that is along micro heat pipe:

(6)

$$\vec{A}_{p_{critical}} = \begin{bmatrix} (-R_1\omega_1^2\cos\theta - R_2\omega_2^2 - g\sin\theta)\hat{e}_{y_2} \\ +(R_1\omega_1^2\sin\theta - g\cos\theta)\hat{e}_{z_2} \end{bmatrix} \bullet (\cos\alpha\hat{e}_{x_2} + \cos\beta\hat{e}_{y_2} + \cos\gamma\hat{e}_{z_2})$$

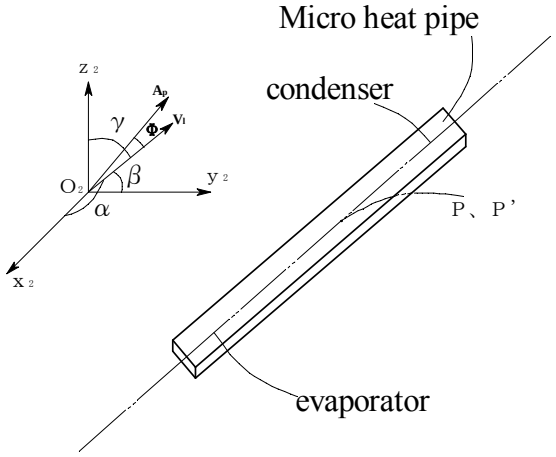


Fig. 4 The direction of micro heat pipe in the space with respect to x_2, y_2, z_2

For the special case that is considered in this study, the acceleration vector is in z_2y_2 plane. Also, it is assumed that the direction of longitudinal axis of heat pipe is from evaporator toward condenser.

3-2 MAXIMUM HEAT TRANSPORT CAPACITY

To predict the maximum heat transport capacity of a flat plate micro heat pipe, the pressure balance equation is used (Eq. 1). Each term in Eq. 1 is obtained as follow:

$$\Delta P_{wc,\max} = \frac{2\sigma}{r_{wc}} \quad (7)$$

$$\Delta P_{gvc,\max} = \frac{2\sigma}{r_{gvc}} \quad (8)$$

$$\Delta P_{wl} = \frac{\mu_l Q L_{eff}}{K_w A_w \rho_l \lambda} \quad (9)$$

$$\Delta P_{gvl} = \frac{\mu_l Q L_{eff}}{K_{gv} A_{gv} \rho_l \lambda} \quad (10)$$

$$\Delta P_v = \frac{12\mu_v Q L_{eff}}{h^3 w_V \rho_V \lambda} \quad (11)$$

$$\Delta P_b = \rho_l \vec{A}_{p_{critical}} L \quad (12)$$

In this study, ϕ is considered as the angle between acceleration vector ($\vec{A}_p$) and the leading vector of longitudinal axis of heat pipe ($\vec{V}_l$). From Fig. 4 it is seen that when $0^\circ \le \phi \le 90^\circ$, the acceleration assists the liquid to return from condenser to evaporator. When $90^\circ \le \phi \le 180^\circ$, the acceleration hinders the liquid to return from condenser to evaporator. It is obvious that installing the micro heat pipe in a way that the leading vector of its longitudinal axis is along the acceleration vector with same direction is the best position. In this paper, it is assumed that leading vector of heat pipe make equal angles with x_2, y_2 and z_2. Some of the properties of flat plate micro heat pipe that are taking into consideration in this paper are listed in Table 1. For more details about the properties of heat pipe, wick structure, working fluid and …, refer to [6].

Table 1. Specifications of flat plate micro heat pipe

Length of Heat Pipe	200	mm
Adiabatic Temperature	50	$^\circ C$
Volume fraction of working fluid	30	Vol %
Thickness of heat pipe	1	mm
Permeability (Wick)	1.08×10^{-10}	m^2
Permeability (Groove)	1.04575×10^{-8}	m^2
Capillary radius (Wick)	5.01513×10^{-5}	m
Capillary radius (Groove)	5.0×10^{-4}	m

4. RESULTS AND DISCUSSION

Fig. 5 shows the maximum heat transport capacity of a flat plate heat pipe, which is installed in an aircraft to dissipate heat from an electronic or a computer device. When the aircraft is revolving in the air with constant angular velocity ω_1 and at the same time rotating about its own main axis with angular velocity ω_2, the heat transport capacity of the flat plate heat pipe is affected significantly. In this study, it is assumed that the micro heat pipe is installed in the aircraft in a way that the acceleration which is caused by ω_1 and ω_2 hinders the liquid to return from condenser to evaporator. In this way, the most critical case is taking into consideration. As it is seen in Fig. 5, increasing both ω_1 and ω_2 decreases Q (the maximum heat transport capacity of a flat plate micro heat pipe). Consequently, the temperature of the heating zone increases and can results in partial or total failure of a heat-generating device that could be an electronic or a computer device.

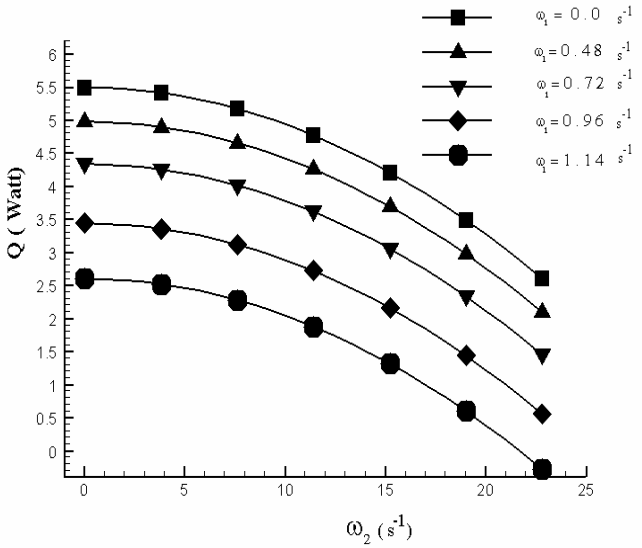


Fig.5- Maximum heat transport capacity of a flat plate micro heat pipe with respect to revolving and rotating angular velocity (ω_1, ω_2).

($R_1 = 10.$ m, $R_2 = 3.$ m and $\theta = 30.^\circ$)

In reference [6], the operation of flat plate heat pipe under different inclination angles is investigated experimentally; therefore, To verify the results of this paper, the computer code is run for $\omega_1 = \omega_2 = 0.0$, in this way, the flat plate micro heat pipe, which is installed in the aircraft, is only under gravitational acceleration (g). The results are shown in Fig. 6.

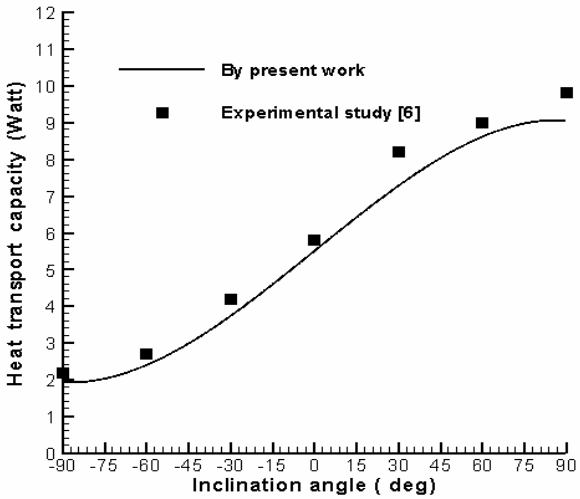


Fig.6- Maximum heat transfer capacity (Inclination Angle)

As it is seen in Fig. 6, there is a good agreement between the experimental study and the results of this paper.

5. CONCLUSION

In this study, the effects of transverse accelerations on the operation of a flat plate heat pipe are investigated. During maneuver or combat of an aircraft, the flat plate heat pipe, which is installed in the aircraft to dissipate heat from an electronic or a computer device, is under different transverse accelerations. Moreover, transverse accelerations and their induced body forces are mainly caused by rotation and revolution of an aircraft in the air; consequently, the operation of a flat plate heat pipe is strongly affected by revolving and rotating speed of an aircraft and will cause total or partial failure of the operation of a micro heat pipe.

The results of this paper can be useful for electronic package designers who wish to design an effective method for cooling computer or electronic components to be installed in spacecrafts or space shuttles. By installing a micro heat pipe in a special way in an aircraft (which has been investigated in this paper), the damaging effect of transverse body forces is minimized. Another interesting field of study, which needs more investigation, is the operation

of a micro heat pipe in zero gravity environments.

Nomenclature

μ_v : Vapor viscosity $[kg/ms]$

μ_l : Liquid viscosity $[kg/ms]$

ρ_v : Vapor density $[kg/m^3]$

ρ_l : Liquid density $[kg/m^3]$

σ : Surface tension $[N/m]$

λ : Latent heat of vaporization $[N/m]$

r_{wc} : Effective pore radius (wick) $[m]$

A_w : Cross sectional area (wick) $[m^2]$

r_{gvc} : Effective pore radius (groove) $[m]$

A_{gv} : Cross sectional area (groove) $[m^2]$

K_w : Permeability of Wick $[m^2]$

L_{eff} : Effective length $[m]$

K_{gv} : Permeability of groove $[m^2]$

Q : Heat Load $[W]$

h : Thickness of vapor channel $[m]$

W_v : Width of vapor channel $[m]$

W_{Wick} : Width of Wick structure $[m]$

W : Width of flat plate heat pipe $[m]$

H : Internal thickness of heat pipe $[m]$

t_w : Thickness of wick structure $[m]$

L : Length of heat pipe $[m]$

g : Gravitational acceleration $[m/s^2]$

ω_1 : Revolving angular velocity $[s^{-1}]$

ω_2 : Rotational angular velocity $[s^{-1}]$

R_1 : Radius of revolution $[m]$

R_2 : Radius of rotation $[m]$

$\vec{A}$: Acceleration vector $[m/s^2]$

V_l : Leading vector of heat pipe

x_2, y_2, z_2 : Rotational coordinate system

α : Angle between V_l and x_2 [Rad]

β : Angle between V_l and y_2 [Rad]

γ : Angle between V_l and Z_2 [Rad]

ϕ : Angle between V_l and $\vec{A}$ [Rad]

x_1, y_1, z_1 : Inertial coordinate system

θ : Angle between y_2 and horizontal direction [Rad]

$\Delta P_{wc,\max}$: Capillary force (Wick) $[N/m^2]$

$\Delta P_{gvc,\max}$: Capillary force (Groove) $[N/m^2]$

ΔP_{wl} : Liquid flow pressure drop (Wick) $[N/m^2]$

ΔP_{gvl} : Liquid flow pressure drop (Groove) $[N/m^2]$

ΔP_v : Vapor flow pressure drop $[N/m^2]$

ΔP_b :Pressure drop due to body force $[N/m^2]$

ΔP_{con} : Pressure drop due to condensation $[N/m^2]$

ΔP_e :Pressure drop due to evaporation $[N/m^2]$

References

1) Chen, J. and Lou, Y.S., "Investigation of the Evaporation Heat Transfer in the Rotating Heat Pipe", Proc. 7th Int. Heat Pipe Conf., Minsk, USSR, May 1990, pp. 21-25

2) Chen, J. and Tu, C., "Condenser Heat Transfer in Inclined Rotating Heat Pipe", Proc. 6th Int. Heat Pipe Conf., Grenoble, France, May 1987, pp. 25-29

3) Keiyou, G. and Maezawa, S., "Heat Transfer Characteristics of Parallel Rotating Heat Pipe" Proc. 7th Int. Heat Pipe Conf., Minsk, USSR, May 1990, pp. 21-25

4) Curtila, R. and Chataing, T., "Experimental Study of a Revolving Heat Pipe", Proc. 5th Int. Heat Pipe Conf., Tsukuba Science City, Japan, May 1984, pp. 14-18, 268-273

5) Bontemps, A., Goubier, C., Marquet, C. and Solecki, J.C., "Theoretical Analysis of a Revolving Heat Pipe", Proc. 5th Int. Heat Pipe Conf., Tsukuba Science City, Japan, May 1984, pp. 14-18, 274-279

6) Masafumi Katsuta, Yuji Homma, Naoto Hosoya, Tomoya Shindo, Junji Sotani, Yuichi Kimura and Yoshio Nakamura, " Heat Transfer Characteristics in Flat Plate Micro Heat Pipe", 7th International Heat Pipe Symposium, Korea.

7) Meriam, J. L., Dynamics, John Wiley & Sons, 1975.

Mathematical Modeling and Thermal Optimization of a Micro Heat Pipe with Curved Triangular Grooves

Kyu Hyung Do, Sung Jin Kim, and Jung Ki Seo

Department of Mechanical Engineering
Korea Advanced Institute of Science and Technology, Taejon, 305-701, Korea
Tel.: +82-42-869-3083, Fax: +82-42-869-8207, E-mail Address: doggu@kaist.ac.kr

Abstract

In the present study, the heat transfer and fluid flow characteristics in a micro heat pipe with curved triangular grooves are investigated using both numerical and experimental methods. In the numerical part, a one-dimensional mathematical model for the micro heat pipe with curved triangular grooves is developed and solved to obtain the maximum heat transport rate, the capillary radius distribution, the liquid, and the vapor pressure distributions along the axial direction of the micro heat pipe under the steady-state condition. In particular, the modified Shah method is used to calculate the pressure drop induced by the liquid-vapor interfacial shear stress. Experimental investigations are conducted to validate the numerical model. In these experiments, the micro heat pipe with 0.56 mm in hydraulic diameter and 50 mm in length is tested and the surface temperatures at the wall of the micro heat pipe with curved triangular grooves are measured by thermocouples, as the operating temperature varies from 40^{o}C to 70^{o}C with an increment of 10^{o}C. The experimental results for the maximum heat transport rate agree well with those of the numerical investigations. Finally, thermal optimization of the micro heat pipe with curved triangular grooves is performed using the numerical model.

Key words: Micro Heat Pipe, Curved Triangular Groove, Thermal Optimization

1. INTRODUCTION

Miniature heat pipes are widely used for cooling electronic equipments with high heat generation due to its compact size and their powerful heat transfer capability[1]. However, as the size of electronic equipments such as notebook PC and PDA (Personal Digital Assistants) decreases, the electronic equipments require more compact cooling devices to provide reliable system operation. Therefore, many researchers have been investigated using analytical, numerical, and experimental methods to characterize the thermal performance of a micro heat pipe since Cotter[2] introduced the concept of a micro heat pipe. In the early stage of this research, Babin et al.[3] developed a simple model and conducted experiments for the maximum heat transport rate of a micro heat pipe with a curved rectangular cross section. In their model, it is assumed that liquid-vapor interfacial velocity was zero, which is not appropriate assumption for the liquid pressure drop and leads to disagreement with experimental results. In order to solve these problems, Khrustalev and Faghri[4] obtained numerically the liquid-vapor interfacial shear stress using FEM in their mathematical model for calculating the maximum heat transfer rate of a polygonal micro heat pipe with having *N* triangular corners. However, the capillary pumping pressure and the liquid pressure drop were not accurately predicted because the curved triangular groove was modeled as the triangular groove in their model. Also, Longtin et al.[5] developed a one-dimensional model to predict the fluid-thermal behavior of a polygonal micro heat pipe with having *N* triangular corners. However, they assumed that Poiseuille number ($f_l \operatorname{Re}_{D_{h,v}}$ = 14.7) for the vapor flow was constant along the axial direction to calculate the liquid-vapor interfacial shear stress. Because the geometric shape of vapor core region changes along the axial direction of a micro heat pipe, the assumption for a constant Poisueille number for the vapor flow may not be appropriate and hence, liquid-vapor interfacial shear stress may not be predicted precisely.

In this paper, a one-dimensional mathematical model for the micro heat pipe with curved triangular grooves is presented. Especially, in order to calculate the pressure drop induced by the liquid-vapor interfacial shear stress of curved triangular grooves easily, we use a modified Shah

method suggested by Kim et al.[1]. In order to validate the mathematical model presented by this work, experiments are conducted to obtain the maximum heat transport rate of the micro heat pipe with curved triangular grooves and experimental results are compared with the maximum heat transport rate obtained by the mathematical model. In addition, the results of the maximum heat transport rate obtained by the mathematical model are compared with experimental results presented by Babin et al.[3]. Finally, the thermal optimization of geometry for a micro heat pipe with the curved triangular grooves is conducted using the mathematical model under the fixed filling rate of working fluid.

2. MATHEMATICAL MODELING

During the steady state operation, heat pipes operating at normal temperature are mostly terminated by the capillary limitation.

The capillary pressure P_c can be expressed by the well-known Laplace-Young equation.

$$P_c = P_{vx} - P_{lx} = \sigma\left(\frac{1}{R_{1x}} + \frac{1}{R_{2x}}\right) \tag{1}$$

where R_{1x} and R_{2x} are the principal capillary radii of the meniscus. Since R_{2x} is much larger than R_{1x}, it is quite reasonable to assume that $R_{1x} \approx R_c(x)$ and $R_{2x} \approx \infty$. The differential form of Eq. (1) then becomes

$$\frac{dP_{vx}}{dx} - \frac{dP_{lx}}{dx} = -\frac{\sigma}{R_c(x)}\frac{dR_c(x)}{dx} \tag{2}$$

In order to solve the governing equation, Eq. (2), we need a precise model for the pressure gradient by the vapor flow dP_{vx}/dx and the pressure gradient by the liquid flow dP_{lx}/dx.

2-1 Model for the pressure drop of the vapor flow

For a two-dimensional incompressible vapor flow with evaporation and condensation at the liquid-vapor interface, Faghri[6] developed an analytical model for the vapor pressure distributions at each section using the continuity and momentum equations. Faghri analytically obtained the vapor pressure distributions of a circular heat pipe when evaporation and condensation are uniformly occurred along the circumferential direction at the evaporator section and the condenser section, respectively. However, we can not use the equations for the vapor pressure distributions given by Faghri in this paper because the micro heat pipe has non-circular cross-section. Therefore, the vapor pressure distributions presented by Faghri are modified as follows:

$0 \le x \le L_e$,

$$P_e = \rho_v\left(-8\left|\frac{\mathrm{Re}_{r,e}}{2}\right| - \frac{16}{3}\left|\frac{\mathrm{Re}_{r,e}}{2}\right|^2\right)\left(\frac{4x\nu_v}{D_{h,v}^2}\right)^2 + P_{in,e} \tag{3}$$

$L_e \le x \le L_e + L_a$,

$$P_a = \rho_v \overline{w}_a\left(-\frac{32(x-L_e)\nu_v}{D_{h,v}^2}\right) + P_{in,a} \tag{4}$$

$L_e + L_a \le x \le L_e + L_a + L_{eff,c}$,

$$P_c = 8\rho_v \overline{w}_{v,a}^2\left(1 - \frac{2}{3}\left|\frac{\mathrm{Re}_{r,c}}{2}\right|\right)\left(\left|\frac{\mathrm{Re}_{r,c}}{2}\right|\right)\left(\frac{4(x-L_e-L_a)\nu_v}{\overline{w}_{v,a}D_{h,v}^2}\right)^2$$
$$-8\rho_v \overline{w}_{v,a}^2\left(1 - \frac{2}{3}\left|\frac{\mathrm{Re}_{r,c}}{2}\right|\right)\left(\frac{4(x-L_e-L_a)\nu_v}{\overline{w}_{v,a}D_{h,v}^2}\right) + P_{in,c} \tag{5}$$

where

$$\mathrm{Re}_{r,e} = \frac{\dot{Q}_e D_{h,v}}{NPe_l L_e h_{fg}\mu_v}, \quad \mathrm{Re}_{r,c} = \frac{\dot{Q}_c}{\pi L_{eff,c} h_{fg}\mu_v}, \quad \overline{w}_a = \frac{4\dot{Q}_e}{\rho_v \pi D_{h,v}^2 h_{fg}}$$

The radial Reynolds numbers, $\mathrm{Re}_{r,e}$ and $\mathrm{Re}_{r,c}$ can be obtained from the mass balance of each section. In particular, the radial Reynolds number is revised at the evaporator section in order to consider the effect of the non-uniform evaporation along the circumferential direction. In order to model the vapor pressure gradient, we use a differential form of Eq. (3) to Eq. (5) in the present study.

2-2 Model for the pressure drop of the liquid flow

When the liquid-vapor interfacial shear stress is zero, the pressure drop of the liquid flow passage is identical to that of an open channel flow, which is not affected by the liquid-vapor interfacial shear stress. However, the liquid flow passage of a micro heat pipe is open to the vapor core region where vapor flows in the direction opposite to the liquid flow. These counter-flows of liquid and vapor cause an additional shear stress at the liquid-vapor interface. The effect of the counter-flows on the interfacial shear stress can be accounted for by introducing a correction factor, α. Therefore, the pressure gradient by the liquid flow is expressed by

$$\frac{dP_l}{dx} = -\frac{\mu_l \varepsilon \dot{m}_{lx}}{\rho_l A_{lx} NK}(1+\alpha) + \rho_l g \sin\beta \tag{6}$$

where the permeability of a groove with an arbitrary cross-section, *K*, can be written as [7]

$$K = \frac{D_{h,l}^2 \varepsilon}{2 f_l \mathrm{Re}_{D_{h,l}}} \tag{7}$$

The last term is included for a pressure drop due to gravity in Eq. (6). In Eq. (7), $f_l \mathrm{Re}_{D_{h,l}}$ is the Poiseuille number for an open curved triangular channel without the liquid-vapor interfacial shear stress and in Eq. (6), the compensation factor, α, is the non-dimensional additional pressure drop due to the liquid-vapor interfacial shear stress. In order to calculate the Poiseuille number and α, a modified Shah method presented by Kim et al.[1] is used in this study. Also using the modified Shah method, the Poiseuille number and α are obtained and correlations for the Poiseuille number, $f_l \mathrm{Re}_{D_{h,l}}$ and α of the curved triangular grooves are presented. Generally speaking, the Poisueuille number is only a function of the geometric shape of the flow passage for laminar flow. α is a function of the geometric shape and the non-dimensional shear stress at the liquid-vapor interface as in [8].

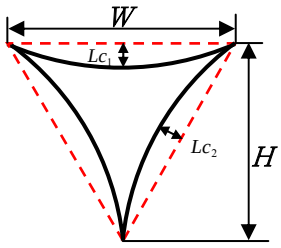


Fig. 1. Cross sectional view of a curved triangular groove

Figure 1 illustrates the geometric shape of the curved triangular grooves which are analyzed in the present study. The non-dimensional shear stress at the interface and geometric parameters are as follows:

$$\psi = \frac{D_{h,l}\tau_v}{\mu_l \bar{u}_l}, \quad Ar = \frac{H}{W}, \quad Cr_1 = \frac{Lc_1}{W}, \quad Cr_2 = \frac{Lc_2}{W} \tag{8}$$

Correlations for the Poiseuille number and α of curved triangular grooves are expressed by

$$f_l \mathrm{Re}_{D_{h,l}} = \left(y_0(Cr_1) + \frac{a(Cr_1)}{Ar} + \frac{b(Cr_1)}{Ar^2} + \frac{c(Cr_1)}{Ar^3} \right) \cdot d(Cr_2) \tag{9}$$

where,

$$y_0(Cr_1) = 11.60 + 1.725Cr_1 - 1.942Cr_1^2,$$
$$a(Cr_1) = 2.921 - 2.845Cr_1 - 21.47Cr_1^2,$$
$$b(Cr_1) = -1.002 - 3.806Cr_1 + 9.084Cr_1^2,$$
$$c(Cr_1) = 0.1 + 0.5347Cr_1 + 2.478Cr_1^2 - 45.68Cr_1^3,$$
$$d(Cr_2) = 1 - 2.086Cr_2 - 10.75Cr_2^2$$

$$\alpha = \psi \cdot f(Ar) \cdot g(Cr_1) \cdot h(Cr_2) \tag{10}$$

where,

$$f(Ar) = \frac{1}{5.339 + 5.483Ar},$$

$$g(Cr_1) = 1 - 0.9140Cr_1 + 2.114Cr_1^2,$$
$$h(Cr_2) = 1 + 1.253Cr_2 + 19.91Cr_2^2$$

In comparison to the Poiseuille number and α based on the modified Shah method and those obtained by correlations, the maximum errors for the Poiseuille number and α are within 5%.

By combining Eqs. (2), (6), and the vapor pressure gradient equation presented by Faghri[6], and ordinary differential equation can be established as

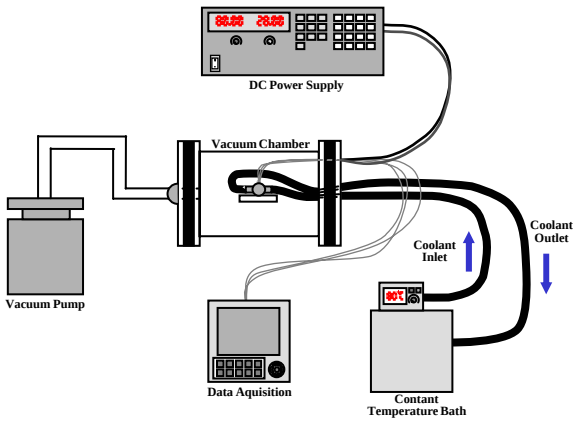
$$\frac{dR_x}{dx} = \frac{R_x^2}{\sigma}\left[\left(\frac{\mu_l Q_x f_l \mathrm{Re}_{D_{h,l}}}{N D_{h,l}^2 A_{lx} \rho_l h_{fg}} (1+\alpha) + \rho_l \sin\beta \right) - \frac{dP_{vx}}{dx} \right] \tag{11}$$

Eq. (11) becomes an ordinary differential equation of $R_x(x)$ and can be solved numerically using the 4th order Runge-Kutta method. Note that all the thermo-physical properties are assumed to be constant and evaluated at the working temperature of the micro heat pipe. In order to calculate the Poiseuille number and α of curved triangular grooves, correlations of Eq. (9) and Eq. (10) are used.

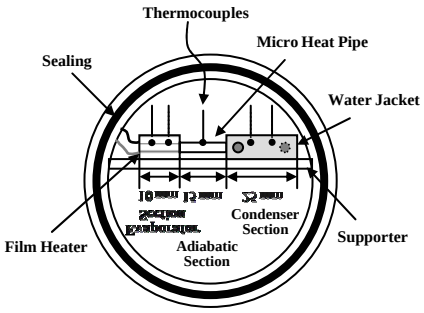
In solving Eq. (11), an initial value of $R_x(x)$ at x =0 and a convergence criterion are necessary. If a heat pipe is to transport a maximum amount of heat, a minimum capillary radius should be formed at the beginning of the evaporator section and a maximum capillary radius at the point where the liquid block starts at the condenser section[9]. In the present study, the initial value of $R_x(x)$ at x =0 is assumed to be $50\mu m$ and the flooding condition is used by means of the convergence criterion.

3. EXPERIMENT

In order to verify the proposed mathematical model, experiments for measuring the maximum heat transport rate are conducted and the experimental data are compared with the numerical results obtained from the model.



(a) Schematic diagram of the experimental facility



(b) Schematic diagram of the vacuum chamber

Fig. 2. Experimental apparatus

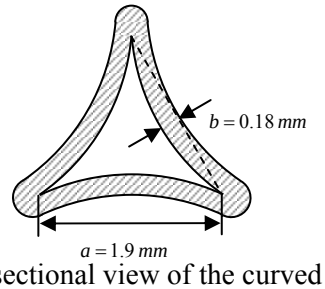


Fig. 3. Cross sectional view of the curved triangular micro heat pipe

An experimental facility consists of a vacuum chamber, a DC power supply, a constant temperature bath, a data acquisition system, and a vacuum pump as shown in Fig. 2(a). The vacuum chamber is made of Acryl and evacuated by the vacuum pump. The micro heat pipe in the vacuum chamber is composed of the evaporator section (10 *mm*), the adiabatic section (15 *mm*), and the condenser section (25 *mm*) as shown in Fig. 2(b). Figure 3 illustrates the cross-sectional view of the micro heat pipe tested in the present study. Because the cross sectional shape of the micro heat pipe is non-circular, in order to provide uniform heat flux to the micro heat pipe, a circular film heater with a 10 *mm* length is mounted at the evaporator section and the space between the film heater and the micro heat pipe outer wall is filled with thermal grease. In order to dissipate heat loaded at the evaporator section, a water jacket is mounted at the condenser section. The coolant temperature is controlled by the constant temperature bath to adjust the amount of heat dissipated. The micro heat pipe is made of copper and charged with distilled, deionized water in the amount of 20% of its void volume. According to Stepanov et al.[10], the contact angle is 33^{o} for copper-water.

To reduce any heat losses through convection, the experiments are conducted in a vacuum of $>10^{-2}$ Torr. Measuring the outer surface temperature, thermocouples with 30 gages are used. Five thermocouples are attached to the outer surface of the micro heat pipe using thermal epoxy: two on the outer surface of the evaporator section, one on the outer surface of the adiabatic section, and two on the outer surface of the condenser section.

Because the vacuum chamber is evacuated, heat loss by conduction is negligible. Therefore, the maximum heat transport rate is regarded as the heat input rate, of which the thermal conductance reaches a constant value at the specified working temperature. The experimental procedure can be summarized as follows:

1) When the desired vacuum has been obtained, warm up the micro heat pipe by supplying the power to the film heater until the temperature at the adiabatic section reaches a specified working temperature.
2) Once the working temperature is obtained, increase the heat load and adjust the coolant temperature to maintain the working temperature.
3) Record all the temperatures of the experimental apparatus, the heat input rate, and the coolant temperature.
4) Repeat step 2) and 3) until the thermal conductance which is defined in Eq. (12) reaches a nearly constant value.

$$TC = \frac{\dot{Q}_{input}}{\overline{T}_e - \overline{T}_c} \tag{12}$$

5) Repeat from step 1) to step 4) changing the operating temperatures.

The working temperatures are chosen to be 40^{o}C, 50^{o}C, 60^{o}C, and 70^{o}C, which are in a typical temperature range for electronic equipment cooling applications of heat pipes. To verify the reliability of the experimental results, the experimental procedure for the micro heat pipe is repeated three times per the specified working temperature.

4. RESULTS AND DISCUSSION

4-1 Comparison of the numerical results with the experimental results

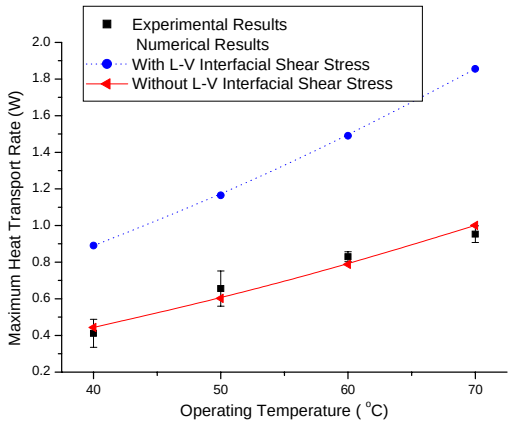
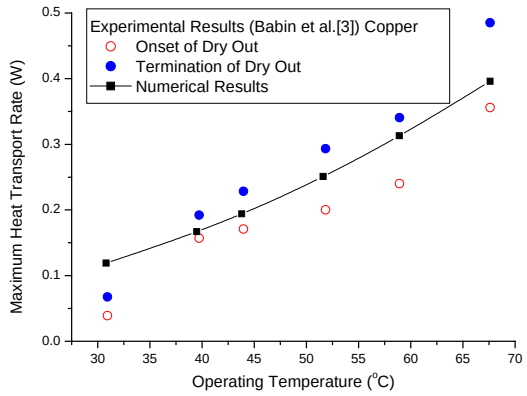
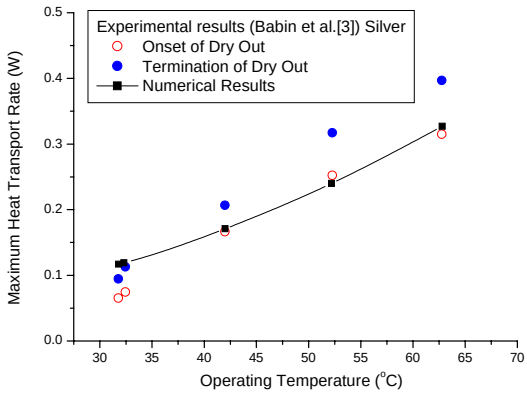


Fig. 4. Comparison of the numerical results with the experimental data for the maximum heat transport rate

In Fig. 4, the numerical results are compared with the experimental data for the maximum heat transport rate of the micro heat pipe with curved triangular groove. For experimental data reduction, we consider the precision error from the repeatability of the experimental data. The bias error is neglected because the bias error is relatively small compared to the precision error. The uncertainty evaluation is performed in accordance with a 95% confidence interval. When the experimental data for the maximum heat transport rate are compared with the numerical results, the maximum error is 8.5% as shown in Fig. 4. The close agreement between the numerical results and experimental data represent the validity of the proposed model in the working temperature range of 40°C to 70°C. If the effect of the liquid-vapor interfacial shear stress is not included (i.e. α =0) in the proposed model, the maximum error is 99% compared with experimental data as shown in Fig. 4. This result implies that the model for the liquid-vapor interfacial shear stress is very important in accurate prediction of the maximum heat transport rate of the micro heat pipe.



(a) Copper-water micro heat pipe



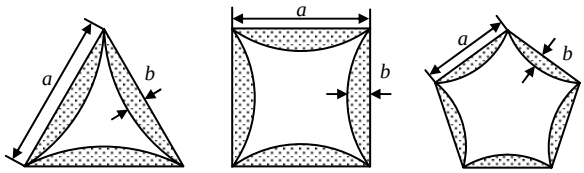
(b) Silver-water micro heat pipe

Fig. 5 Comparison of the numerical results with the experimental data for the maximum heat transport rate

In addition, the results of the maximum heat transport rate based on the mathematical model are compared with experimental results presented by Babin et al.[3]. Babin et al. performed experiments of micro heat pipes made of copper-water and silver-water. As shown in Fig. 5(a) and 5(b), the agreement between the experimental results of the onset of dryout and the present numerical prediction is good. Also, figure 5(b) shows that the mathematical model presented in this study is applicable to micro heat pipes with the different contact angle. The contact angle used in the present study is 38° for sliver-water from the results of Stepanov et al.[10].

4-2 Thermal optimization for geometry

During steady-state operation of the micro heat pipe, the capillary pumping pressure, the driving force must be larger than the sum of other pressure drops. Therefore, to enhance the maximum heat transport rate of the micro heat pipe, the capillary pumping pressure should be increased or the other pressure drops decreased.



(a) Curved triangle (b) Curved rectangle (c) Curved pentagon

Fig. 6 Various cross-sectional shapes of the micro heat pipe

Table 1. Specifications of the micro heat pipe with curved triangular grooves

Material		Working fluid		Working temp.		
Copper		Pure Water		60°C		
Cross section	$(b/a)_{max}$	PF (%)	Contact angle (°)	Length (*mm*)		
				Evaporator section	Adiabatic section	Condenser section
Curved triangle	0.133	20	33	20	10	20
Curved rectangle	0.2					
Curved pentagon	0.254					

Figure 6 shows various cross sections of the micro heat pipe. In the present study, an optimization of the groove geometry to enhance the maximum heat transport rate is performed. Geometric parameters and other relevant specifications of the micro heat pipe with curved triangular grooves are summarized in Table 1. The effects of the optimization parameter, *b*/*a* on the maximum heat transport rate are evaluated using the proposed model and shown in Fig. 7. As shown in Fig. 7, there exists optimal shape parameter, *b*/*a* in the micro heat pipe with N curved triangular grooves (N=3,4,5). The phenomenon can be explained as follows: shape parameter, *b*/*a* has two competing effects on the

maximum heat transport rate under the fixed filling rate of working fluid. The first one is the promotion of the maximum heat transport rate because the capillary pumping pressure is increased as the shape parameter is increased. The second effect is the restraint of the maximum heat transport rate because mass flow rate of working fluid is decreased as the shape parameter is increased. Therefore, there exist optimal shape parameters in micro heat pipes with various cross sectional geometry under the fixed filling rate of working fluid.

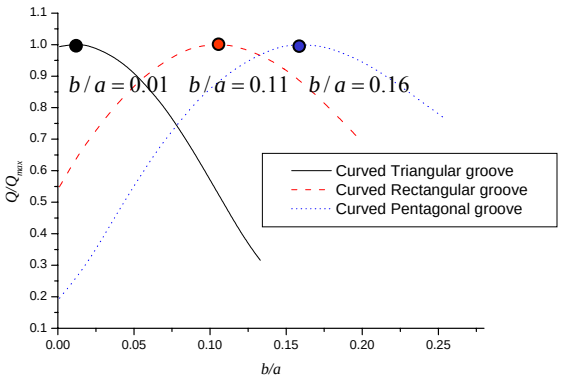


Fig. 7 Shape parameter, (b/a) vs. the non-dimensional maximum heat transport rate, (Q/Q_{max})

5. CONCLUSION

A one-dimensional mathematical model for the micro heat pipe with curved triangular grooves is presented. Especially, in order to calculate the pressure drop induced by the liquid-vapor interfacial shear stress of curved triangular grooves easily, we use a modified Shah method suggested by Kim et al. In order to validate the mathematical model presented by this work, we experimentally obtain the maximum heat transport rate of the micro heat pipe with curved triangular grooves. The experimental results are compared with the maximum heat transport rate obtained by the mathematical model. The maximum error is within 8.5%, which is a good agreement. In addition, the results of the maximum heat transport rate based on the mathematical model are compared with experimental results presented by Babin et al.. The agreement between the experimental results and results of the present numerical prediction is good. Finally, the thermal optimization of a micro heat pipe with the curved triangular grooves is conducted using the mathematical model under the fixed filling rate of working fluid.

Acknowledgement

This work was supported by Center for Electronic Packaging Materials of Korea Science and Engineering Foundation.

Nomenclature

A	area, m^2
Ar	aspect ratio, H/W
b/a	shape parameter
Cr	curvature ratio
Lc	length of curvature, m
D	diameter, m
f	skin friction coefficient
h_{fg}	latent heat of vaporization, J/kg
K	permeability, m^2
L	length, m
N	total number of groove
P	pressure, Pa or wetted perimeter, m
Pe	perimeter, m
PF	filling rate of working fluid, %
Q	heat rate, W
R	radius, m
Re	Reynolds number
T	temperature, ^oC
TC	thermal conductance, $W/^oC$
u	velocity, m/s
$\overline{w}$	averaged vapor velocity, m/s
x	distance from the evaporator section end cap, m

Greek Symbols

α	non-dimensional additional pressure drop
β	tilt angle, degree
μ	viscosity, kg/m-s
ν	kinematic viscosity, m^2/s
ρ	density, kg/m^3
σ	surface tension coefficient, N/m
τ	shear stress, N/m^2
ψ	non-dimensional shear stress at the interface

Subscripts

a	adiabatic section
c	condenser section or capillary
e	evaporator section
eff	effective
h	hydraulic
i	liquid-vapor interface
in	Inlet
l	liquid
max	maximum
v	vapor
w	wall
x	distance from beginning of the evaporator section

Superscripts

–	average

References

1. S. J. Kim, J. K. Seo, and K. H. Do, Analytical and Experimental Investigation on the Operational Characteristics and the Thermal Optimization of a Miniature Heat Pipe with a Grooved Wick Structure, Int. J. Heat Mass Transfer 46 (2003) 2051-2063
2. T. P. Cotter, Principles, and Prospects for Micro Heat Pipes, Proceedings of the 5th International Heat Pipe Conference, Tsukuba, Japan, 1984, pp. 328-335.
3. B. R. Babin, G. P. Peterson, and D. Wu, Analysis and Testing of a Micro Heat Pipe During Steady-State Operation, Proceedings of ASME/AIChE National Heat Transfer Conference, Philadelphia, Pennsylvania, 1989, 89-HT-17.
4. D. Khrustalev, A. Faghri, Thermal Analysis of a Micro Heat Pipe, J. Heat Transfer 116 (1994) 189-198.
5. J. P. Longtin, B. Badran, and F. M. Gerner, A One-Dimensional Model of a Micro Heat Pipe During Steady-State Operation, J. Heat Transfer 116 (1994) 709-715.
6. A. Faghri, Performance Characteristics of a Concentric Annular Heat Pipe Part II Vapor Flow Analysis, J. Heat Transfer 111 (1989) 851-857.
7. A. Faghri, Heat Pipe Science and Technology, Taylor & Francis, Washington, 1995, pp. 124-125.
8. E. Hufschmidt, E. Burck, G. Di Cola, and H. Hoffman, The Shearing Effect of Vapor Flow on Laminar Liquid Flow in Capillaries of Heat Pipes, NASA TT-F-16601, 1975, pp. 1-21.
9. R. Hopkins, A. Faghri, and D. Khrustalev, Flat Miniature Heat Pipes with Micro Capillary Grooves, J. Heat Transfer 121 (1999) 102-109.
10. V. G. Stepanov, L. D. Volyak, and Y. V. Tarlakov, Wetting Contact Angles for Some Systems, J. Engineering Physics 32 (1977) 1000-1003.

Forced Convective Flows in Microchannels for Cooling Electronic Devices

Jung-Yeul Jung*, Ho-Young Kwak*, Sarng Woo Karng** and Yoon Pyo Lee**
*Mechanical Engineering Department, Chung-Ang University, Seoul, 156-756 Korea
Telephone Number; +82-2-820-5280, Fax Number; +82-2-826-7464 and, E-mail; kwakhy@cau.ac.kr
**Thermal/Flow Control Research Center, Korea Institute of Science and Technology,
P.O. Box 131, Cheongryang, Seoul, Korea

Abstract

Convective flow in microchannels turns out to be very effective for cooling electric devices. To investigate the convective phenomena in microchannels, polysilicon heater and micro-sensors were fabricated at the front side of the chip. In this study, forced convective heat transfer coefficients and friction factor for flow of water in microchannels with rectangular cross section were measured. A double side polished wafer whose specification is (100) orientation, P-type and 525 μm (±5μm) thickness was used in this experiment. Five microchannels connecting two reservoirs on one side of the wafer and a localized heater and seven polysilicon temperature sensors along the selected channels on the other side of it were fabricated. A pyrex-7740 glass wafer was anodically bonded to the silicon substrate to cover the fluid reservoirs and microchannels. The temperature sensors were calibrated prior to the measurement. The flow rate or pressure drop in microchannels was dependent on the thermal boundary thickness crucially. Finite volume method simulation for the Navier-Stocks equation was also performed for the flow geometry concerned.

Key words: forced convection, heat transfer, microchannel, micro temperature sensor, pressure drop

1. INTRODUCTION

Recently many investigators have studied on microchannel fluid flow and heat transfer characteristics. Understanding of fluid flow characteristics and heat transfer mechanism in microchannels turns out to be very important for application in the thermal control of electronic devices[1,2]. Also the flow of liquids and gases in microchannels are known to be a fundamental building block for microfluidic systems which have many applications in biomedical engineering[3]. In the past ten years or so, gas and liquid flow behavior and heat transfer characteristics in various microchannels[4,5] and minichannels[6,7,8] have been studied extensively. In fact, a considerable heat flux of the order of 10^7 W/m^2 has been removed by means of the forced convective flow of water in microchannels with maintaining the surface temperature below 71 ℃[1]. Microfluidic systems now also find many applications including chemical analysis, biological sensors, drug delivery and sequencing or synthesis of nuclear acids and others[3].

After Tuckerman's[9] initiative work on the fluid flow and heat transfer characteristics in microchannels, many researchers tried to measure the friction factor[4,7,8] and convective heat transfer coefficients in microchannels and minichannels[6,10,11]. Harley and Bau[12] measured friction factor in a rectangular channel having dimension of 50 μm width and 100 μm height, and in a trapezoidal channel having dimension of 33 μm height and 63 μm / 111 μm width with working fluids of n-propanol and fluorocarbon. Pfahler et al.[5] measured the friction factor in a rectangular channel having rather small hydraulic diameter of 5.84 and 8.89 μm with n-propanol. Shortly after these works, Choi et al. [13] reported the friction factors and convective heat transfer coefficients in microtubes by using N_2 gas. Recently flow characteristics of water in microtubes[14] and trapezoidal microchannels [15] were also investigated.

From these measurements the friction flow constant $C = f \mathrm{Re}_{D_h}$ was found to be lower than that obtained from the theoretical prediction for channels with rectangular cross sections[16]. However, the friction flow constant values obtained for the trapezoidal cross section were much higher than those from the theoretical values. It has also been found that the measured heat transfer coefficients in microchannels were departed considerably from the experimental results obtained for the macroscopic size channels. Unfortunately, less extensive work has been done for measurements

of the convective heat transfer coefficients in the microchannels. Also more works are needed to unveil additional information for the behavior of fluid flow in microchannels.

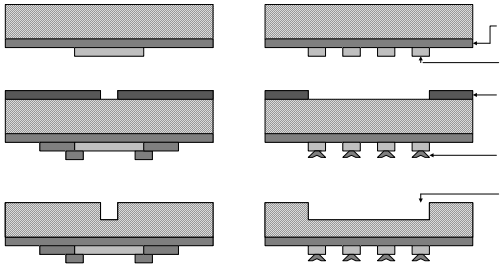
In this study, the friction flow constant and the convective heat transfer coefficients in microchannels with rectangular cross section were measured. For the microchannels tested, the friction flow constants measured are close to the theoretical value of 57.0. The measured Nusselt number in the laminar regime tested could be correlated by the following type of Peng and Peterson's relationship[8],

$$\mathrm{Nu} = 8.16\times10^{-3}\left(\frac{D_h}{W_c}\right)^{0.48}\left(\frac{H}{W}\right)^{0.0054}\mathrm{Re}_{D_h}^{\ 1.05}\,\mathrm{Pr}^{1/3}.$$

2. DEVICE DESIGN AND FABRICATION

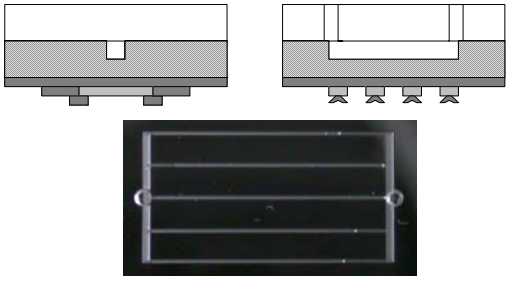
A double side polished silicon wafer(p-type <100> single crystal with 525±5 μm thickness) was used to fabricate an integrated microsystem consisting of five microchannels on one side and a localized heater and seven polysilicon temperature sensors along the selected channel on the other side. The die size of the device is 10 mm×20 mm. The fabrication began with thermal growth of a 0.5 μm oxide layer on the front side of the silicon wafer. An 0.540 μm polysilicon film was deposited on the top of the oxide layer and patterned to serve as the heater and the temperature sensors. The length of the temperature sensors was fabricated to be the same as the width of the flow channel. On the back side of the wafer, an oxide layer was also formed and patterned to serve as an etch mask for plasma etching which produced 100 μm deep flow channel with rectangular cross section. Major fabrication steps described above are shown schematically in Fig. 1. After these processes being completed, a pyrex-7740 glass wafer having two holes for inlet and outlet port of liquid was anodically bonded to the back side of the silicon substrate to cover the fluid manifolds and microchannels. The fabricated microchannels were 100 μm-width, 100 μm-depth and 15 mm-length. The width and length of the manifold are 500 μm by 9 mm with the depth of 100 μm. Schematic and enlarged pictures of the completed device are shown in Fig. 2.

The micro polysilicon sensors were used for measuring wall temperature along the channel. Precision of polysilicon sensors were validated with theoretical and experimental study[17,18].



(a) End view (b) Side view

Fig.1 Schematic of major steps to fabricate microchannels, heaters, and sensors



(a) End view (b) Side view

(c) Enlarged top view of the device

Fig. 2 Schematic of fabricated microchannels

3. EXPERIMENTAL APPARATUS

A schematic of experimental apparatus is shown in Fig. 3. The apparatus consist of a) a working fluid handling system, b) a microchannel test chip, and c) a data acquisition system. The working fluid handling system includes a high pressure gas source, a pressurized fluid reservoir, a micro filter, a pressure gauge, and a volumetric graduate. Deionized water was used as working fluids. The working fluid was supplied by a high pressure argon gas and the driving pressure was adjusted by a pressure regulator. The liquid was freely discharged from the outlet manifold so that the pressure at outlet is atmosphere. The test device was packaged on a PCB with metal pattern designed for I/O connector. Current to the heater in the test chip was supplied by a DC voltage source. The voltage values from the two T-type thermocouples to measure the liquid temperatures at inlet and outlet ports, and resistance values from the polysilicon sensors to measure the wall surface temperatures along the channel were monitored by a multimeter(HP 34401A). All data at selected driving pressures to the microchannel and/or at selected powers to the heater were obtained at steady state conditions. Deionized water at approximately 21~24℃ was fed into the input manifold through the inlet hole at the driving pressures up to 0.2 MPa.

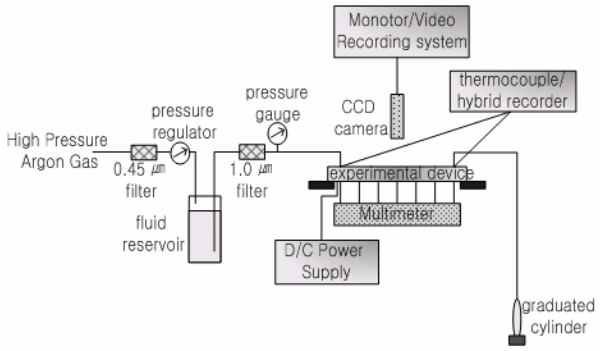


Fig.3 Schematic of the experimental apparatus

4. NUMERICAL ANALYSIS

Numerical simulation was performed for one of five channels in the device.

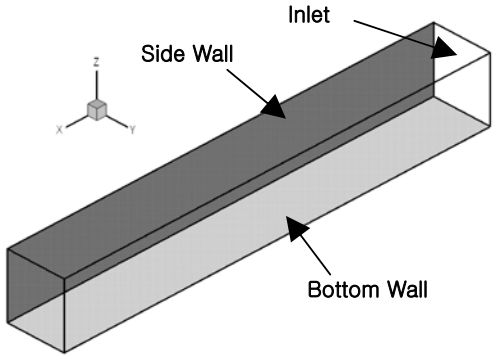


Fig. 4 Computational domain for a microchannel (100 μm× 100 μm×15mm)

Figure 4 shows the numerical calculation region. The following assumptions were used to set up the governing equations to investigate the liquid flow and heat transfer characteristics in microchannels.

(1) incompressible liquid flow
(2) steady fluid flow and heat transfer
(3) laminar flow
(4) constant properties except liquid viscosity

Variations of liquid properties except viscosity are small within the temperature range tested and these properties can be assumed to be constant. However, the variation of water viscosity depending on temperature is so significant that viscosity cannot be assumed to be constant. A relation between viscosity and temperature for water may be obtained from the following equation[19],

$$\eta = -24.71 + 4209/T + 0.04527T - 0.3376\times10^{4}T^{2} \quad (1)$$

where η in cP and T in Kelvin.

Based on the above assumptions, the governing equations used to simulate the fluid flow and heat transfer in microchannel are as follows.

$$\nabla\cdot\vec{u} = 0\,; \text{ (Continuity Eq.)} \quad (2)$$

$$\rho(u\cdot\nabla\vec{u}) = -\frac{\partial P}{\partial x} + \nabla\cdot(\mu\nabla\vec{u})\,; \text{ (Momentum Eq.)} \quad (3)$$

$$\nabla\cdot(\rho\vec{u}T) = \nabla\cdot\left(\frac{k_f}{c_p}\nabla T\right)\,; \text{ (Energy Eq.)} \quad (4)$$

In the above energy equation, viscous heating term was omitted because the effect of viscous heating term is so small to be negligible.

For the fluid flow simulation, uniform velocity profile was applied at the channel inlet;

$$u = u_m,\ v = 0,\ w = 0 \quad \text{at} \quad x = 0 \quad (5)$$

On the other hand, Neumann condition was applied at the channel outlet, and no slip condition was applied at all solid boundaries. The water temperature at inlet was assumed to be uniform, that is about 24 ℃. Wall temperature was set to the measured temperatures except the temperature at top wall. The boundary condition used for the top wall was assumed to be adiabatic

The governing equations were discretized along the three spatial coordinates using finite volume method. The SIMPLE algorithm was applied to solve the momentum and continuity equations to obtain the velocity field. For the convective term UDS(Upward Difference Scheme) was used. The solution was regarded as convergent when the criterion of $\mathrm{Max}\left|\left(\phi^{i+1}-\phi^{i}/\phi^{i+1}\right)\right| \le 10^{-8}$ was satisfied, where ϕ represent any dependent variable and i is the iteration number. The numbers of grids used are 201 for the x-direction, 15 for y- and z-direction. More fine grid was used at the near wall.

5. RESULTS AND DISCUSSION

5-1 Experimental analysis

In Fig. 5, the temperature distributions along the 100 μm-width channel at different input powers are shown. This figure indicates that the higher the input power, the temperature of the device and the temperature gradient near the heater become higher. This temperature field indicates the case that natural convection mode presents. The temperature distributions under forced convection with different mass flow rate

of water are shown in Fig. 6(a). This figure shows that the chip temperature can be maintained below 75℃ with small mass flow rate of 4.07×10^{-3} kg/min(the corresponding Reynolds number is about 140). It can be found that the nonuniformity of the wall temperature along the channel reduces considerably when the forced convection mode operates, eventually the forced convection in microchannel is very efficient mode to remove the heat applied to the chip. The Nusselt number in laminar regime can be correlated by the following type of Peng and Peterson's relationship[8].

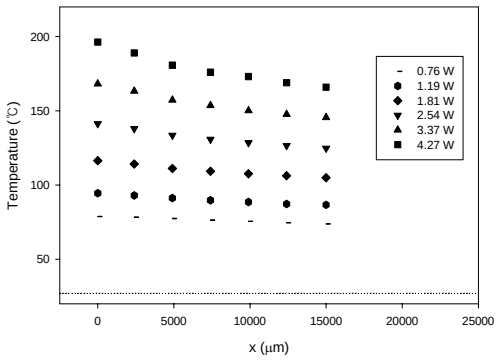


Fig. 5 Temperature distributions along the 100 μm-width channel for various input powers at natural convection mode.

$$\mathrm{Nu}=\frac{h\,D_h}{k_f}=A\left(\frac{D_h}{W_c}\right)^{0.48}\left(\frac{H}{W}\right)^{0.0054}\mathrm{Re}_{D_h}{}^{1.05}\,\mathrm{Pr}^{1/3}\quad(6)$$

where, A is 8.16×10^{-3} for 100 μm-width channel. As shown in Fig. 8, only a type of Peng and Peterson's correlation represents the Nusselt number data fairly. Indeed the geometrical factors such as D_h/W_c and H/W affect the heat transfer in the microchannels tested. The Reynolds numbers tested in this experiment were in the range between 55 and 218 for water which are certainly corresponding to laminar flow regime. In Fig. 9, convective heat transfer coefficients depending wall temperature at various driving pressure are shown. The maximum heat transfer coefficient obtained is about 9,000 W/m^{2}K at the wall temperature of 65℃ at the driving pressure of 175 kPa as illustrated in Fig. 7. Generally speaking, the heat transfer coefficients increase linearly as the wall temperature becomes higher except the case of lower Reynolds number. The convective heat transfer coefficients obtained in this study for microchannels turn out to be higher than those for minichannels[6].

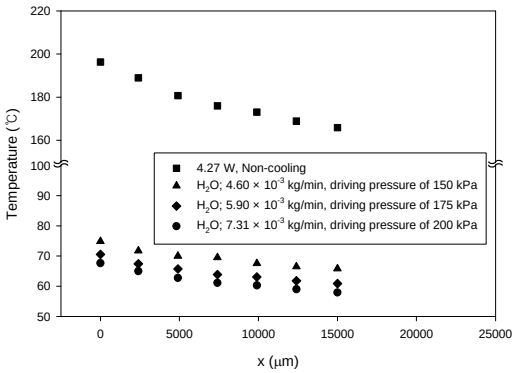


Fig. 6 Temperature distributions along the 100 μm-width channel for various flow rates at the heat input

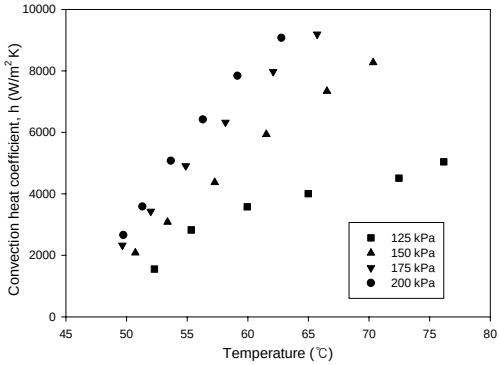


Fig. 7 Variation of heat transfer coefficients with wall temperature at different driving pressure.

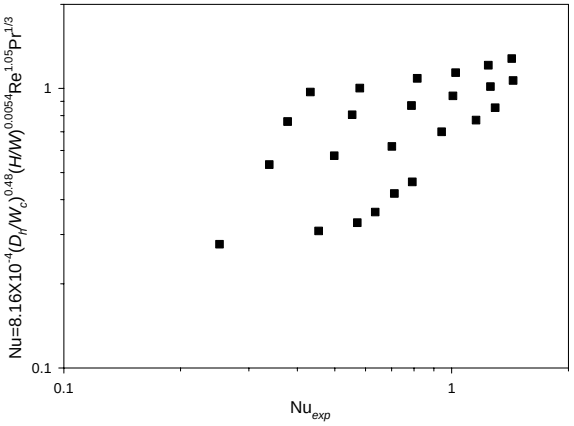


Fig. 8 Correlated Nusselt number versus measured Nusselt number for 100 μm-width microchannel.

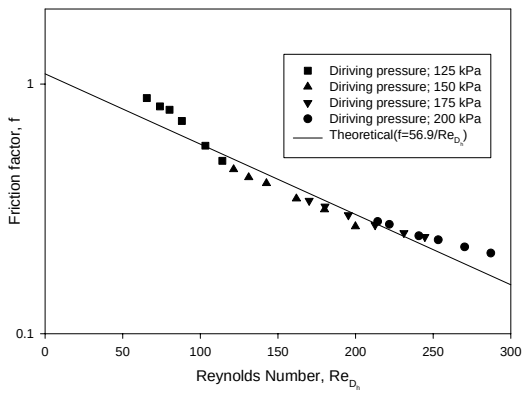
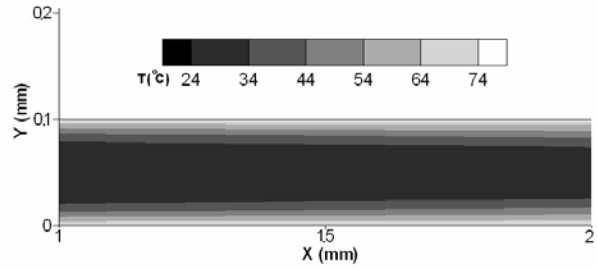


Fig. 9 Friction factors depending on Reynolds number for 100 μm-width channel with water.

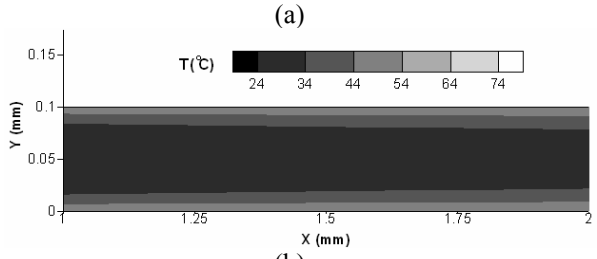
In Fig. 9, the friction factor obtained for the 100 μm-width channel at various driving pressure are shown. With this channel, the mass flow rate, correspondingly the Reynolds number at a given driving pressure increases as increasing the power input to the heater. This happens because the viscosity water decreases substantially as the liquid temperature increases. As can be seen in Fig. 9, the measured values of the friction factor are close to the theoretical value of $f = 56.9/\mathrm{Re}_{D_h}$. These friction factors obtained for microchannels with rectangular cross section are comparable to the previous measured values in microchannel[20,21].

5-2 Numerical Analysis

In this study, we performed numerical analyses under a driving pressure of 150 kPa with input powers of 4.27 W and 0.76 W. Temperature distributions at z =50 μm along the channel are shown in Fig. 10.



(a)

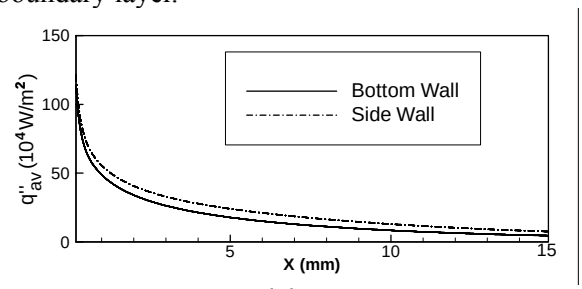


(b)

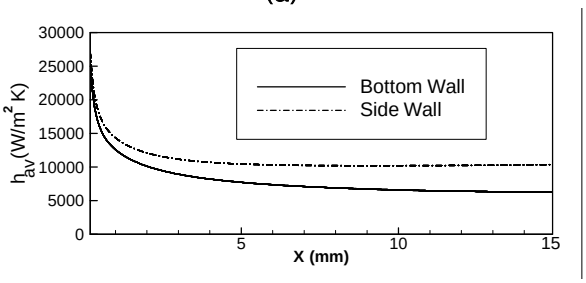
Fig. 10 Temperature contour at z =50 μm, x =1.0 mm to 2.0 mm; (a) 4.27 W, and (b) 0.76 W.

As shown in these figures, the thermal boundary layer is developed very well along the channel at the high power input so that the flow rate or the friction factor may change due to the reduction of liquid viscosity near wall. This fact was also confirmed by our experiments shown in Fig. 9. On the other hand the thermal boundary layer at lower power input turns out to be very thin.

The calculated heat flux along the wall and the corresponding heat transfer coefficients are shown in Fig. 11. The average heat transfer coefficient obtained at the power input of 4.76 W under the driving pressure of 150 kPa is about 8,000 W/m^2 K, which is close to the observed value of 8,200 W/m^2 K at the same conditions as shown in Fig. 7. The calculated pressure drop about 35.6 kPa, which is considerably less than the observed value of 47.6 kPa. This might be due to the overprediction of the temperature in the thermal boundary layer.



(a)



(b)

Fig. 11 Numerical results; (a) heat fluxes and (b) heat transfer coefficients along the channel at the input power of 4.27 W

6. CONCLUSION

An integrated microsystem consisting of microchannels, a localized heater, and an array of temperature sensors was fabricated on a single die. The microchannels tested has width of 100 μm, height of 100 μm, and length of 15 mm. Pressure drop, the temperature distribution along the microchannel, and the mass flow rate were measured at various power input to the heater in the microsystem. It has been found that the measured friction factor constants at laminar regime are comparable to the theoretical values and forced convection mode is an effective method to remove the heat applied to the microsystem. The convective heat transfer coefficients obtained in microchannels tested turn out to be higher than those from minichannels.

Nomenclature

C	friction flow constant
c_p	specific heat
D_h	hydraulic diameter
f	friction factor

h	heat transfer coefficient
H	height of a microchannel
k_f	conductivity of liquid
L	length of microchannel
Nu	Nusselt number
Pr	Prandtl number
Re	Reynolds number
T	temperature
u	fluid velocity in the channel
u_{av}	average velocity
v	y-direction fluid velocity
w	z-direction fluid velocity
W	width of a microchannel
μ	dynamic viscosity
ρ	density

Acknowledgements

This work has been supported by the grants from Korean Science and Engineering Foundation under Contract 1999-1-304-002-5.

References

1. Tuckerman, D.B., and Pease, R.F.W., "High-performance heat sinking for VLSI", IEEE Electronic Device Lett., Vol. EDL-2, 1981, pp.126-129.
2. Kishimoto, T., and Ohsaki, T., "VLSI packaging technique using liquid-cooled channels", IEEE Trans. On Components, Hybrids, and Manufacturing Tech., Vol. CHMT-9, 1986, pp.328-335.
3. Kovacs, G.T.A, "Micromachined Transducers Sourcebook", McGraw-Hill, New York, 1998.
4. Wu, P.Y., and Little, W.A., "Measurement of friction factors for the flow of gases in very fine channels used for microminiature Joule-Thompson refrigeration", Cryogenics, Vol. 23, 1983, pp.273-277.
5. Pfahler, J., Harley, J., Bau, H.H., and Zemal, J., "Liquid transport in micron and submicron channels", J. Sensors Actuators, Vol. 21, 1990, pp.431-434.
6. Wang, B.X., and Peng, X.F., "Experimental investigation on forced convection heat transfer through microchannels", Int. J. Heat Mass Transfer, Vol. 17, 1994, pp.73-82.
7. Peng, X.F., Peterson, G.P., and Wang, B.X., "Frictional flow characteristics of water flowing through rectangular microchannels," Exp. Heat Trans., Vol. 7, 1994, pp.249-264.
8. Peng, X.F., and Peterson, G.P., "Convective heat transfer and flow friction for water flow in microchannel structures", Int. J. Heat Mass Transfer, Vol. 39, 1996, pp.2599-2608.
9. Tuckerman, D.B., "Heat Transfer Microstructures for Integrated Circuits", Ph.D Thesis, Stanford University, 1984.
10. Peng, X.P., and Wang, B,-X, "Forced convection and flow boiling heat transfer for liquid flowing through microchannels", Int. J. Heat Mass Transfer, Vol. 36, 1993, pp.3421-3427.
11. Jiang, L., Wong, M., and Zohar, Y., "Forced convection boiling in a microchannel heat sink", J. Microelectromechanical Sys., Vol. 10, 2001, pp.80-87.
12. Harley, J., and Bau, H., "Fluid flow in micron and submicron size channels", IEEE Transactions, THO249-3, 1989, pp.25-28.
13. Choi, S.B., Barron, R.F., and Warrington, R.O., "Fluid flow and heat transfer in microtubes", Proceeding of ASME WAM, DSC-Vol. 32, 1991, pp.123-134.
14. Mala, G.M., and Li, D., "Flow characteristics of water in microtubes", Int. J. Heat Fluid Flow, Vol. 20, 1999, pp.142-148.
15. Qu, W., Mala, G.M., and Li, D., "Pressure-driven water flows in trapezoidal silicon microchannels", Int. J. Heat Mass Transfer, Vol. 43, 2000, pp.353-364.
16. Kawaji, M., Chung, P.M.-Y, and Kawahara, "Instantaneous velocity profiles and characteristics of pressure-driven flow in microchannels", Proceedings of 2001 ASME International Mechanical Engineering Congress and Exposition, 2001, IMECE 2001/HTD-24209.
17. Lee, J., Park, H., Kwak, H., and Jeon, J., "Bubble nucleation on micro line heaters", Proceedings of 2001 ASME International Mechanical Engineering Congress and Exposition, 2001, IMECE 2001/HTD-24215.
18. Jung, J.Y., Kwak, H.Y., "Fluid flow and heat transfer in microchannels with rectangular corss section", First International Conference on Microchannels and Minichannels, 2003, ICMM2003-1032.
19. Reid, R.C., Prausnitz, J.M., and Poling, B.E., "The properties of gases and liquids", McGraw-Hill, Fourth Ed., 1986, pp.439-456.
20. Pfahler, J., Harley, J., Bau, H.H., and Zemel, J., "Liquid and gas transport in small channels", Microstructures, Sensors and Actuators, Proceedings of ASME WAM, DSC-Vol. 19, 1990, pp.149-157.
21. Mala, G.M., and Li, D., "Flow characteristics of water in microtubes", Int. J. Heat Fluid Flow, Vol.20, 1999, pp.142-148.

Thermal Characterisation of an Ammonia-charged Pulsating Heat Pipe

R T Dobson and G Graf
Department of Mechanical Engineering, University of Stellenbosch,
Private Bag X1, MATIELAND 7602, South Africa.
Tel 27 21 8084268 Fax 27 21 808 4958 EMAIL rtd@maties.sun.ac.za

Abstract

This paper shows how a heat transfer coefficient may be defined and experimentally determined for an ammonia-charged pulsating heat pipe. The experimental apparatus consists of a 1.9 mm diameter closed loop pipe and a total length of 12.438 m pipe meandering back and forth between an electrically heated block of aluminium as the heat source and another water-cooled aluminium block as heat sink. Temperature and heat transfer rate response curves were obtained for different inclinations, electrical power inputs and liquid charge fill ratios. Examples of typical response curves are given and the sensitivity of the independent variables on the heat transfer rate investigated. It was found that when the heat source is positioned below the heat sink the heat transfer rate is proportional to the temperature difference. When the heat source is above the heat sink the response curves exhibited chaotic behaviour and larger excess temperature differences of up to 50 °C between the heat and sink are required for heat transfer to commence. Because at this time no mathematical model of a pulsating heat pipe is available the behaviour of a liquid-plug and two vapour-bubbles in a pipe is also investigated. This simple model is able to simulate chaotic behaviour but still needs to be extended before it can be considered as modelling an actual pulsating heat pipe. A useable correlation is obtained for the heat transfer coefficient for conditions when the heat source is below the heat sink. For conditions when the heat source is above the heat sink the as tested pulsating heat pipe is probably too erratic to be useful for the cooling of electronic equipment using an environment of about 20 °C as the heat sink.

Key words: Ammonia, heat transfer coefficient, pulsating heat pipes

1. INTRODUCTION

A pulsating heat pipe (PHP) is a relatively new and simple two-phase heat transfer device [1]. It is considered as being a potentially useful option in the thermal management and control of electrical and electronic devices [2]. A PHP has no moving parts, no wick structure and it can transfer heat even when the heat source, relative to gravity, is above the heat sink. It consists essentially of a relatively long but small diameter pipe meandering in a serpentine fashion between the heat source and the heat sink. The pipe is sealed, evacuated and then charged with a working fluid. Provided the diameter is small enough the fluid forms a system of discrete liquid plugs and vapour bubbles that move in a seeming random fashion back and forth between the heat source and the heat sink. *Figure 1* gives a typical representation of a transparent PHP.

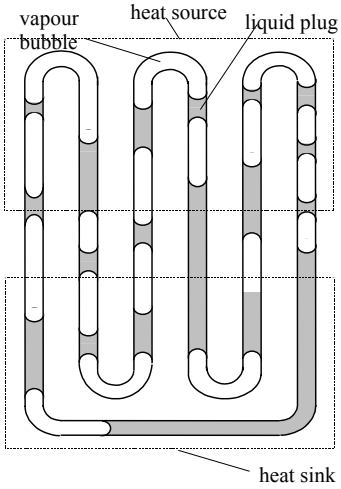


Figure 1 A pulsating heat pipe

A qualitative experimental analysis and flow visualisation of the movement of the liquid plugs and vapour bubbles in a PHP has been addressed [3]. A number of attempts have been made to mathematically model a PHP [4, 5, 6, & 7]. It is suggested that boiling and condensation contribute towards the motion of the bubbles and plugs; the major mode of heat transfer is not due to the latent heat transfer but rather due to sensible heat transfer between wall and the liquid plugs as they move back and forth in the pipe [8 & 9]. At this time however a comprehensive theory and reliable data or tools for the design of PHPs for a specific cooling application is as yet not available [10].

The object of this paper is to present the experimental test results of an ammonia-charged pulsating heat pipe. Such results are important because ammonia is a particularly efficient heat transfer fluid and no published results of it usage in a PHP was to be found. Further, in an attempt to better understand the functioning of a PHP, the thermal-fluid dynamics of a simple liquid plug and vapour bubble system will be theoretically modelled and investigated.

2. HEAT TRANSFER THEORY

The PHP may be modelled as a system of thermal resistances as shown in *figure 2*. The heat transfer coefficient between the ammonia working fluid and the inside wall of the PHP will vary as a function of position and time. At times there will be a liquid at other times vapour and yet at other times some two-phase combination of liquid and vapour. If however it is imagined that there is some average characteristic heat transfer coefficient which is the same for both the evaporator and the condenser i.e. $h_{ei} \approx h_{ci} = h_{PHP}$ then the heat transfer coefficient between the ammonia working fluid and the inside wall of the PHP, ignoring axial conduction in the wall, may be defined as

$$h_{PHP} = \frac{\dot{Q}_{PHP}}{T_e - T_c}\left(1/A_{ei} + 1/A_{ci} \right) \qquad \textbf{(1)}$$

where $A_{ei} = \pi d_i L_e$ and $A_{ci} = \pi d_i L_c$

The characteristic heat transfer coefficient as given by equation **(1)** will depend on a number of independent variables; heat flux, liquid charge fill ratio, inclination angle and working fluid temperature as well as the liquid-vapour two-phase flow pattern.

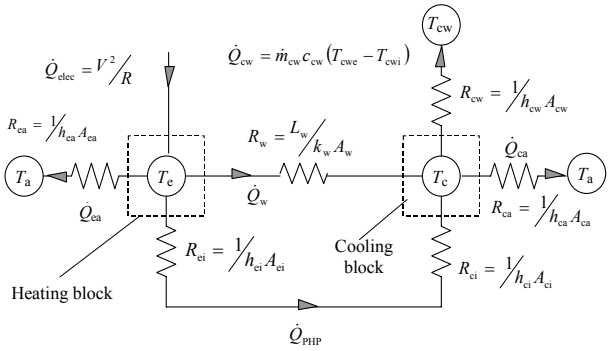


Figure 2 Thermal resistance model of a PHP

3. EXPERIMENTAL SETUP

An aluminium pipe was bent and supplied with two charge/discharge valves to form a close-loop as shown in *figure 3*. Each end of the closed-loop is embedded in matching grooves in an aluminium block. To ensure good thermal contact between heat pipe tin was cast into the space between the pipe and the block as shown in *figure 4*. One of the two blocks is supplied with grooves in which an electrical heating wire insulated with ceramic beads is fixed. Eleven equally spaced 5 mm diameter holes are drilled in the other aluminium block through which cooling water is circulated. The PHP and aluminium blocks are completely insulated with 12.7 mm thick foam rubber and mounted in a stand and can be rotated through 180° (about a horizontal axis through the two fill/discharge valves). Some important dimensions of the PHP are given in table 1. The temperature of each aluminium block is measured at the bottom of nine evenly spaced 2.0 mm holes drilled into the block using relatively thin T-type thermocouples.

Table 1 PHP dimensions

Total length of pipe	L_{PHP}	12.438 m
Evaporator length	L_e	4.955 m
Condenser length	L_c	4.923 m
Inside pipe diameter	d_i	0.00190 m
Outside pipe diameter	d_o	0.00318 m

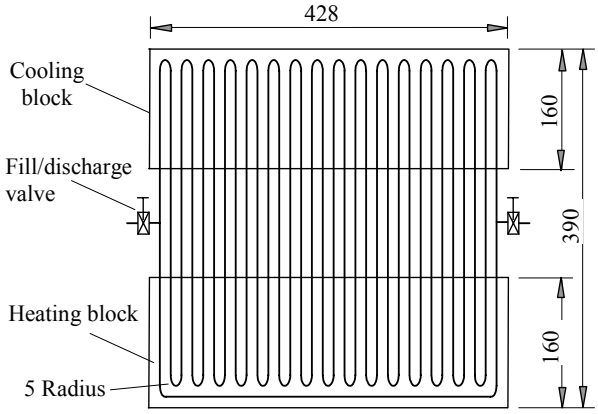


Figure 3 Experimentally tested PHP (dimensions in mm)

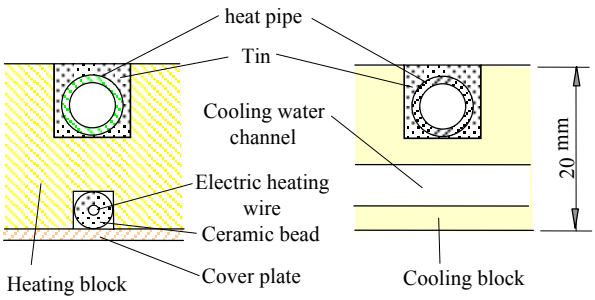


Figure 4 Construction details of the PHP

4. EXPERIMENTAL RESULTS

The heat transferred by the PHP $\dot{Q}_{PHP}$ referring to *figure 2* may be determined using either the

electrical power input to the evaporator or the heat removed from the condenser by the cooling water:

$$\dot{Q}_{\mathrm{PHP}} = \dot{Q}_{\mathrm{elec}} - \dot{Q}_{ea} - \dot{Q}_{\mathrm{w}} \qquad \textbf{(2)}$$

or

$$\dot{Q}_{\mathrm{PHP}} = \dot{Q}_{\mathrm{cw}} + \dot{Q}_{ca} - \dot{Q}_{\mathrm{w}} \qquad \textbf{(3)}$$

where $\dot{Q}_{\mathrm{elec}} = V^2/R$ and $\dot{Q}_{\mathrm{cw}} = \dot{m}c_{\mathrm{cw}}\left(T_{\mathrm{cwe}} - T_{\mathrm{cwi}}\right)$

The heat losses to the environment from the evaporator $\dot{Q}_{\mathrm{ea}}$ and condenser $\dot{Q}_{\mathrm{ca}}$ are determined experimentally and given and plotted as a function of temperature difference between the aluminium block and the environment in *figure 5*. The heat transferred though the wall of the PHP between the heating and cooling blocks was not experimentally determined but because it will be small is calculated using simple theory as

$$\dot{Q}_{\mathrm{w}} = k_{\mathrm{w}} \frac{\mathrm{n}\pi\left(d_{\mathrm{o}}^2 - d_{\mathrm{i}}^2\right)}{4}\frac{\left(\overline{T}_{\mathrm{e}} - \overline{T}_{\mathrm{c}}\right)}{L_{\mathrm{a}}}$$

$$= 204\frac{32\pi\left(0.00318^2 - 0.00190^2\right)}{4}\cdot\frac{\overline{T}_{\mathrm{e}} - \overline{T}_{\mathrm{c}}}{0.080}$$

$$= 0.415\left(\overline{T}_{\mathrm{e}} - \overline{T}_{\mathrm{c}}\right) \qquad \textbf{(4)}$$

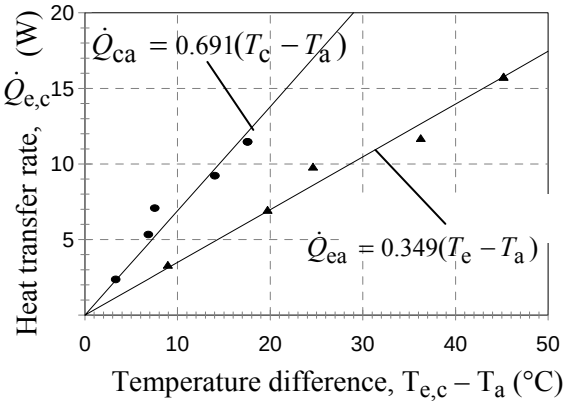


Figure 5 Experimentally determined heat loss from the aluminium blocks to the environment

Figure 6 shows a graph of the heat transferred by the PHP as reckoned from the electrical power supplied and the heat removed by the cooling water. The trend line shows a good correlation ($R^2 = 0.9214$) between the heat transfer rate of the PHP as reckoned using equations **(2)** and **(3)** but shows a small systematic deviation of about 5%.

Typical PHP heat transfer rate as a function of time for different inclinations are shown in *figure 7*. When the heat source is positioned below the heat sink (BHM or $0° < \phi < 90°$) the heat transfer rate is proportional to the temperature difference as can be seen in *figure 7(a)*. It can also bee seen that a steady state heat transfer rate is eventually attained. When the heat source is above the heat sink (THM or $-90° < \phi < 0°$) the response curves exhibited chaotic behaviour and larger excess temperature differences of up to 50 °C between the heat and sink are required before heat transfer commences as shown in *figure 7(b)*. Also, only in the time period from about 7000 to 10 000 s did some sort of *more-or-less* steady state heat transfer occur.

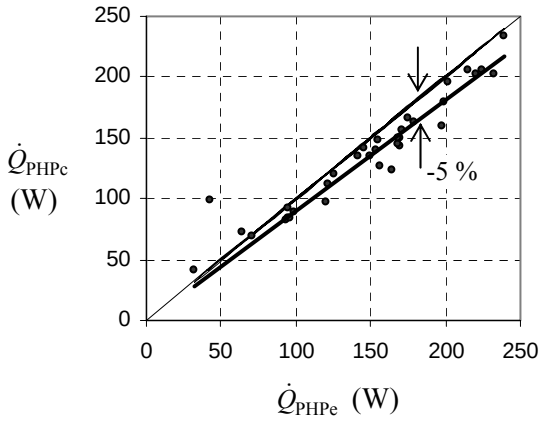


Figure 6 Comparison of heat transfer rate as calculated from electrical power input $\dot{Q}_{\mathrm{PHPe}}$ and as calculated from the cooling water $\dot{Q}_{\mathrm{PHPc}}$

A data set of heat transfer coefficients for steady state conditions using equation (1) was generated for heat transfer rates of 25 to 250 W, inclination angles of 90°, 45° and 0°, internal temperatures, defined as being approximately equal to $(T_e - T_c)/2$, and liquid charge fill ratios (liquid to total volume) of 33 to 80 %. THM results were excluded from this data set because in this operating mode no steady state operation occurred and/or the evaporator temperatures increased to unacceptably high (80 °C) levels before heat was transferred.

An idea of the effect of the various independent variables on the heat transfer rate is given in *figure 8*. For increasing temperature difference $(T_e - T_c)$ the heat transfer rate increases (as expected) but for a linear least squares approximation the correlation coefficient is only $R^2 = 0.5671$. For increasing inclination angle (BHM at +90° and THM at –90°) a similar tendency is noted but with an even lower $R^2 = 0.2332$. For liquid charge fill ratio $R^2 = 0.0470$ indicating that there is practically no dependency.

A multi-linear regression analysis was conducted and the following correlating equation for the heat transfer coefficient, as defined by equation **(1)**, was obtained:

$$h_{\mathrm{PHP}} = 5.23\dot{Q}^{0.943}T_{\mathrm{PHP}}^{0.025}\phi^{0.132}\left(V_\ell / V\right)^{-0.586} \qquad \textbf{(5)}$$

For this data set the most significant of the correlating coefficient is the heat transfer rate, followed by the average working fluid

temperature. The inclination angle played a small role whilst the liquid charge ratio played an insignificant role but is included in equation **(5)** for completeness. *Figure 9* shows the predicted heat transfer coefficients as a function of the experimental values.

5. BUBBLE-PLUG MODELLING

To investigate the thermal and fluid dynamics a single liquid plug in a pipe as shown in *figure 10* is mathematically simulated using a simple one-dimensional lumped parameter approach [4 & 6]. A vapour-bubble is assumed to behave as an ideal gas; its mass increases due to evaporation in the heated lengths whilst it decreases due to condensation in the cooled length. The rates of evaporation and condensation are assumed proportional to the temperature difference between the wall and the vapour

$$\dot{m}_{\mathrm{ve,vc}} = U_{\mathrm{e,c}}\pi d L_{\mathrm{e,c}}\left(T_{\mathrm{v}} - T_{\mathrm{e,c}}\right) \qquad \textbf{(6)}$$

The convective heat transfer between the wall and the vapour is assumed to be negligible. The temperature of the vapour-bubble is then determined *explicitly* by applying the conservation of energy as

$$T_{\mathrm{v}}^{t+\Delta t} = T_{\mathrm{v}}^{t} + \frac{\dot{m}_{\mathrm{vi}} i_{\mathrm{vi}} - \dot{m}_{\mathrm{ve}} i_{\mathrm{ve}} + P_{\mathrm{v}} A \Delta x_{\mathrm{p}} / \Delta t}{m_{\mathrm{v}} c_{\mathrm{vv}}}\Delta t \qquad \textbf{(7)}$$

where $A = \pi d^2/4$, $i_{\mathrm{vi}} = c_{\mathrm{p}} T_{\mathrm{vi}}$ and $i_{\mathrm{ve}} = c_{\mathrm{p}} T_{\mathrm{v}}$

The conservation of momentum is applied to the liquid plug to determine its velocity:

$$v_{\mathrm{p}}^{t+\Delta t} = v_{\mathrm{p}}^{t} + \frac{\sum F}{m_{\mathrm{p}}}\Delta t \qquad \textbf{(8)}$$

where ΣF are the sum of the pressure, shear, surface tension and gravity forces acting on the plug and hence the position as $x_{\mathrm{p}}^{t+\Delta t} = x_{\mathrm{p}}^{t} + v_{\mathrm{p}}^{t}\Delta t$.

The liquid plug temperature is determined as

$$T_{\ell\mathrm{p}}^{t+\Delta t} = T_{\ell\mathrm{p}}^{t} + \frac{\dot{Q}}{m_{\mathrm{p}} c_{\mathrm{vp}}} \qquad \textbf{(9)}$$

As the liquid plug moves out of the heated length it leaves behind it a thin trailing liquid film. If more evaporation than condensation is taking place the vapour pressure increases, and *visa versa*. If however the film dries up, evaporation ceases, and if condensation continues the pressure in the vapour bubble decreases at a faster rate and a relatively sudden change in liquid plug motion occurs. Predictions (using this theoretical model) of the liquid plug position and the amount of in the liquid film in the left hand evaporator length are given as a function of time in *figure 11* for the initial and operating conditions given in table 2. The vapour bubble-liquid plug motion in a PHP is regarded as being chaotic in nature [11]. The model presented here has been shown, by calculating the Lyapunov exponents of similar time series predictions, as being able to capture this chaotic behaviour [12].

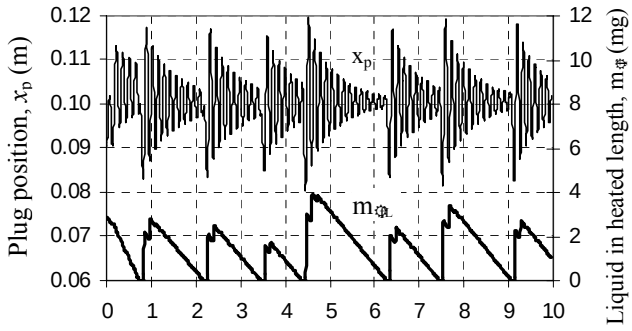


Figure 11 Liquid plug position and mass of liquid in the left hand heated length of the pipe as a function of time

Table 2 Numerical computer program values

L_{eL} = 0.09 m, L_{aL} = 0.001 m, L_{c} = 0.2 m,
$L_{\mathrm{aL}} = L_{\mathrm{aR}}$, L_{eR} = 0.10 m, L_{p} = 0.1 m,
d = 0.00334 m, $\delta_{\Phi,\mathrm{dep}}$ = 0.00003 m
T_{e} = 80 °C, T_{c} = 20 °C,
U_{e} = 1500 W/m^2°C, U_{c} = 1500 W/m^2°C
R_{v} = 461 J/kgK, c_{pv} = 1900 J/kg°C
$c_{\mathrm{vv}} = c_{\mathrm{pv}} - R_{\mathrm{v}}$
ρ_Φ= 1000 kg/m^3, $\sigma_\Phi = \sigma_{@(Th+Tc)/2}$
i_{fg} = 2.34 MJ/kg, $\mu_\Phi = \mu_{@(Th+Tc)/2}$ kg/ms,
Initial conditions: δ_Φ = 0.000003 m
x_{p0} = 0.09 m, T_{vL0} = 20 °C, $P_{\mathrm{vL0}} = P_{\mathrm{sat@}TvL0}$
$T_{\mathrm{vR0}} = T_{\mathrm{vL0}}$, $P_{\mathrm{vR0}} = P_{\mathrm{vL0}}$
and hence $V_{\mathrm{vL0}} = x_{\mathrm{p0}}\pi d^2/4$, and
$m_{\mathrm{vL0}} = (P_{\mathrm{vL0}} V_{\mathrm{vL0}})/(R_{\mathrm{v}}\,(T_{\mathrm{vL0}} + 273.15))$
$V_{\mathrm{vR0}} = (L - x_{\mathrm{p0}} - L_{\mathrm{p}})\pi d^2/4$, and
$m_{\mathrm{vR0}} = (P_{\mathrm{vR0}} V_{\mathrm{vR0}})/(R_{\mathrm{v}}\,(T_{\mathrm{vR0}} + 273.15))$

6. DISCUSSION AND CONCLUSIONS

- For BHM the heat transfer coefficient defined by equation **(1)** is predicted by equation **(5)** to within ±25 % of the experimentally determined values as shown in *figure 9*, the most significant correlating variable being the heat transfer rate or wall heat flux.
- In BHM heat is transferred to the condenser as soon as the evaporator is heated without any noticeable temperature *overshoot* as shown in *figure 7(a)*. In HHM however considerable temperature overshoot may occur before heat transfer commences as shown in *figure 7(b)*. In THM overshoot of unacceptably high levels always occurred. From this it is concluded that in BHM (in which the PHP is the same as a thermosyphon) that the PHP works well, however, the THM should be avoided. For conditions when the heat source is above the heat sink the as

tested pulsating heat pipe is probably too erratic to be useful for the cooling of electronic equipment using an environment of about 20 °C as the heat sink.

- The simple vapour bubble and liquid plug theoretical model tends to capture the oscillatory effect noticed in a transparent PHP. The model shows that when the bubble-plug system is in motion heat is transferred by evaporation and condensation. For water vapour temperatures up to 100 °C the ideal gas equation with a constant specific gas constant is good, for ammonia at these temperatures however a more advanced equation of state is needed. This simple model is able to simulate chaotic behaviour but still needs to be extended before it can be considered as modelling an actual pulsating heat pipe.
- It would be interesting to observe the operation of a PHP operating under different heating modes in a micro to zero gravity environment.

Nomenclature

A area, m^2
c specific heat, J/kgK
c_p specific heat at constant pressure, J/kgK
c_v specific heat at constant volume, J/kgK
C_f coefficient of friction
d diameter, m
F force, N
g gravitational constant, m/s^2
h heat transfer coefficient, W/m^2K
i enthalpy, J/kg
i_{fg} latent heat of vaporisation, J/kg
L length, m
m mass, kg
$\dot{m}$ mass flow rate, kg/s
n number
P pressure, Pa
$\dot{Q}$ heat transfer rate, W
R specific gas constant, J/kgK
R thermal resistance, °C/W
R^2 correlation coefficient
Re Reynolds number
T temperature, °C
t time, s
U overall heat transfer coefficient, W/m^2K
V volume, m^3 or voltage, Volts
v velocity, m/s
x displacement, m
δ thickness, m
ρ density, kg/m^3
μ viscosity, kg/ms
ϕ angle to the horizontal, °
τ shear stress, N/m^2
σ surface tension, N/m

subscripts

0 initial condition
a adiabatic
c condenser, cold
e exit, environment, evaporator
f film
g gravity
i inlet
L left hand side
P liquid
p plug
R right hand side
v vapour
σ surface tension
w water

References

1. Akachi, H. and Polášek, F. Pulsating Heat Pipes. *5th Int. Heat Pipe Symposium*, Melbourne, Australia, 17 - 20 November 1996.

2. Polášek, F and Zelko, M. Thermal control of electronic components by heat pipes and thermosyphons; A historical overview. *Proc. 10th Int. Heat Pipe Conf.,* Stuttgart, Germany, 21-25 September 1997.

3. Tong, B. Y, Wong, T N & Ooi, K T. Closed-loop pulsating heat pipe. *Applied Thermal Engineering* Vol 21 2001, pp 1845 – 1862.

4. Dobson, R T and Harms, T M. *Lumped parameter analysis of closed and open oscillatory heat pipes*. 1th Int. Heat Pipe Conf. Tokyo, 12-16 September 1999.

5. Wong, T N, et al. *Theoretical modelling of pulsating heat pipe*. 11th Int. Heat Pipe Conf. Tokyo, 12-16 September 1999.

6. Swanepoel, G, Taylor, A B & Dobson R T. Theoretical modelling of pulsating heat pipes. *6th International Heat Pipe Symposium.* Chiang Mai, Thailand, 5 - 9 November 2000.

7. Zou Z J, North M T & Ray L Combined pulsating and capillary heat pipe mechanism for cooling of high heat flux electronics. *Thermacore Inc, Web Page*.

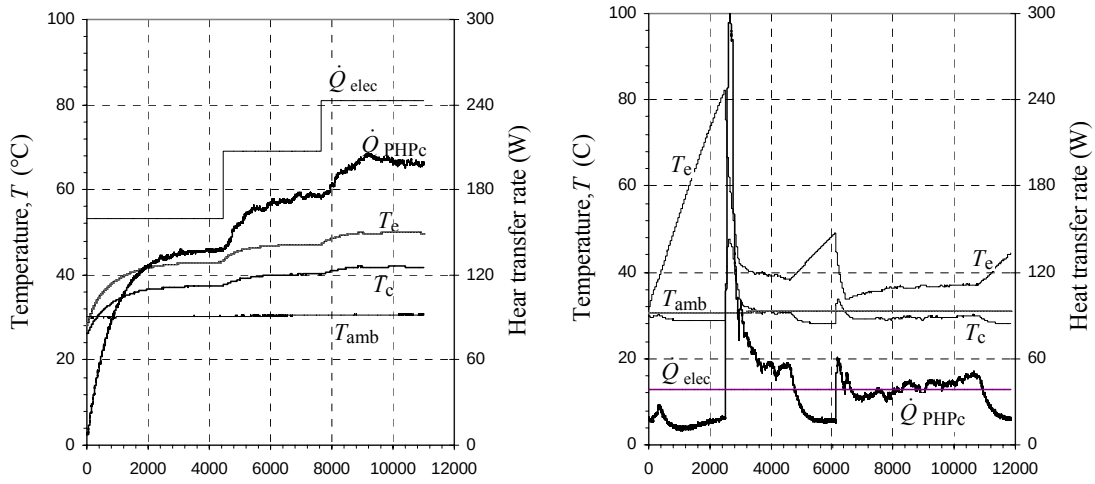
8. Shafii, M B, Faghri, A & Zhang, Y. Thermal modelling of Unlooped and looped pulsating heat pipes. *J Heat Transfer* Vol 123 December 2001, 1159-1172.

9. Zhang, Y and Faghri, A. Heat transfer in a pulsating heat pipe with open end. *Int. J Heat Mass Transfer*, Vol 45 (2002) 755 –764.

10. Khandekar S, Schneider M & Groll, M. Mathematical modelling of pulsating heat pipes: state of the art and future challenges, *5 th ASME/ISHMT joint Heat and Mass Transfer Conference*, Kolcata, India, 2002.

11. Maezawa, S. Izumi, T and Gi, K. *Experimental chaos in oscillatory tube heat pipes*. 10th International Heat Pipe Conference, Stuttgart, 21-25 September 1997.

12. Dobson, R T, Theoretical and experimental modelling of an open oscillatory heat pipe including gravity. *12th Int. Heat Pipe Conference*, Moscow, 19-24 May, 2002.



(a) $\phi = 90°$ (BHM), $V_f/V = 61\%$ (b) $\phi = 0°$ (HHM), $V_f/V = 61\%$

Figure 7 Temperature and heat transfer rate as a function of time for different inclination angles to the horizontal.

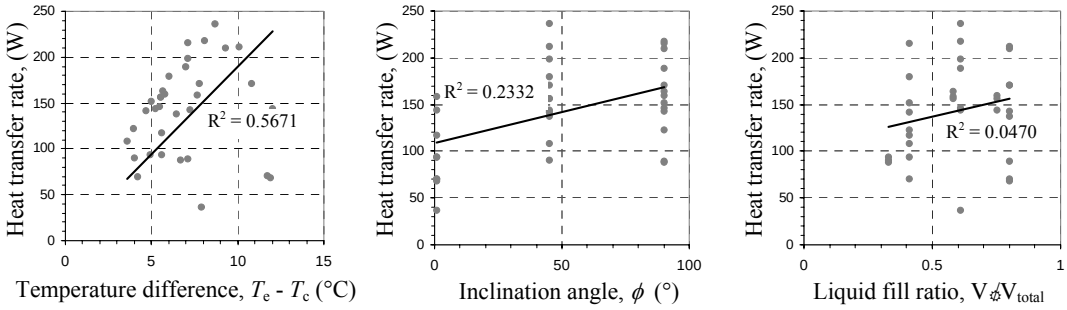


Figure 8 Effect of independent variables on the heat transfer rate

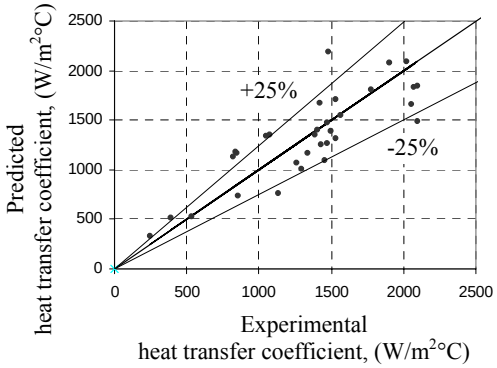


Figure 9 Predicted heat transfer coefficient using equation **(5)** as a function of the experimental values

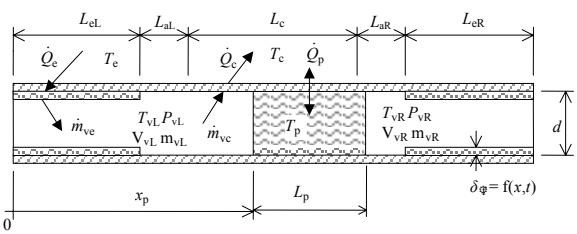


Figure 10 Vapour bubble-liquid plug model of PHP

Refrigerant Fluorinated Ethers and Self-Oscillating Heat Pipe Heat Exchanger for Peltier Cooling System

Saburo Maezawa and Keiyo Gi
Seikei University, Musashino-shi, Tokyo 180-8633 /Japan
TEL:0422-37-3718, FAX:0422-37-3871, E-mail: maezawa@me.seikei.ac.jp
Jun Sakiura , Naoya Yamazaki
Fujitu Ltd. Kawasaki-shi Kanagawa, 211-88/ Japan
TEL:044-754-3123, FAX:044-754-3588, E-mail: yamazaki.naoya@jp.fujitsu.com
T.Katoh, H. Akachi
TS-Heatronics Co. Yokohama-shi, kanagawa, 226-0011/Japan
TEL:045-937-6215, FAX:045-937-6265, E-mail: tkatoh@tsheatronics.co.jp

Abstract

This study is that basic tests for the new alternative substances HFE (hydrofluoroether) as refrigerant have been conducted with a two-phase closed thermosyphon, and their practical heat transfer performance have been also evaluated with a commercial self-oscillating heat pipe heat exchanger for a peltier cooling systems.

Key words: Fluorinated Ethers Refrigerant, HFE (hydrofluoroether), Two-phase closed thermosyphon, self-oscillating heat pipe heat exchanger

1. INTRODUCTION

Chlorofluorocarbons (CFCs), which are composed, of carbon, chlorine and fluorine are decomposed by ultraviolet in the stratosphere and react with ozone, leading to the destruction of the ozone layer, which protects the ecosystem on the earth by absorbing harmful ultraviolet rays. Based on the concern over this fact the world has agreed to phase out the uses of CFCs and TCA by the end of 1995, therefore the development of new alternative substances is urgently needed.

Hydrochlorofluorocarbones (HCFCs), which are composed of carbon, hydrogen, chlorine and fluorine, have begun to be used as emergency alternative materials. HCFCs, which have a hydrogen atom in their molecules, are not so stable in the troposphere. Consequently their lifetime are not so long, therefore they have lower impacts than CFCs on ozone depletion and global warming. But HCFCs still attack the ozone layer owing to the chlorine atom included in their molecules. Therefore, HCFCs are situated as provisional alternative substances now and had been regulated from the beginning of 1996. The development of the new alternative substance for HCFCs has not been achieved yet.

At RITE (Research Institute of Innovative Technology for the earth) in Japan, we conduct research into new refrigerant fluorinated ethers HFE (hydrofluoroether) that do not contain chlorine in the structure of molecule, and is the material that is different from CFCs and HCFCs completely. Refrigerant HFE do not deplete the ozone layer, thus preventing global warming problems and promoting the effective use for energy, and they have properties that were considered sufficiently to the earth environment as shown in the table.

This study is that basic tests for the new alternative substances HFE as refrigerant have been conducted, and their practical heat transfer performance have been also evaluated with a two-phase closed thermosyphon, and a prototype self-oscillating heat pipe heat exchanger for a peltier cooling, a cpu of desktop PC cooling system.

2. HEAT TRANSFER CHARACTERISTICS OF FLUORINATED ETHERS

2-1 Experiment Apparatus

Cross-sectional views of the experimental system and the dimension of the test thermosyphon are presented in Fig.1 and Fig.2 respectively.

The thermosyphon is formed by copper which has 27.8mm inner diameter, 31.8mm outer diameter and 800mm total length. The heating, adiabatic and cooling section are 250mm, 250mm, and 300mm individually.

Heat is transferred to the working fluid through the evaporator wall by means of an electric resistance

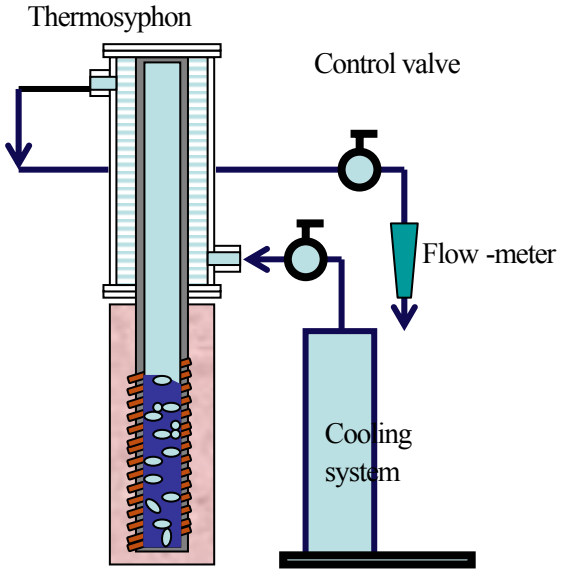


Fig.1 Experimental System

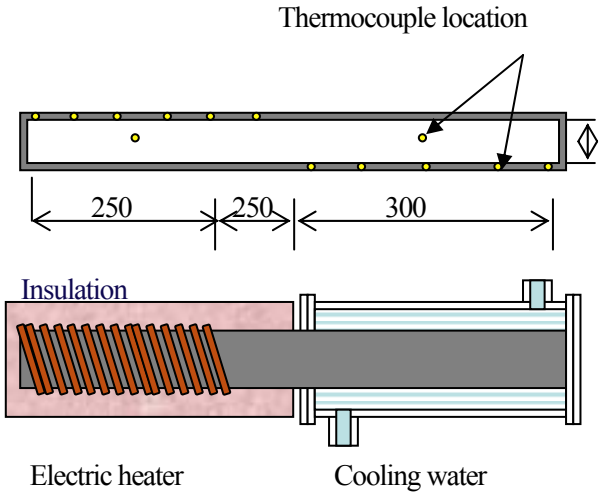


Fig.2 Dimension of Thermosyphon

heater around the outer wall of evaporator section. The heater, in turn, are surrounded by a thermal insulation to reduce heat leakage bellow a negligible level. The A.C. power supplied to the heater is controlled through a variable transformer, and measured with a wattmeter. In the condenser section, heat is carried away by means of cooling water controlled flow rate.

Temperature distributions along a thermosyphon tube wall are measured by copper-constantan located at appropriate points on tube wall and the surrounding thermal insulation. In addition, two thermocouple probes for measuring the vapor temperature inside thermosyphon are also installed. The thermocouple leads are connected to the scanning unit and personal computer. Operating temperatures are kept through the adjustment of cooling-water flow rate. A series of experimental data was taken with the operating temperature maintained constant 45℃ or 50℃.

Fig.2 shows an example of heat pipe dimension and thermocouples location.

2-2 New Refrigerant : HFEs

Authors estimate HFEs fine alternative to CFCs. What is needed as characteristics of alternatives? They must

not contribute to ozone layer depletion,
have properties similar to those of CFCs,
break down in the atmosphere soon after their useful life has ended,
be nonflammable, stable, and
have low global warming potential (GWP).

HFEs don't contain Chlorine atoms, as well as HFCs, which were also investigated as alternative candidate, so their ozone depleting potential are zero, but may potentially cause the global warming effect. Atmospheric lifetime is the key factor to determine GWP. Some of HFEs show shorter lifetime than HCFCs and HFCs. Too long lifetime causes global warming, and too short one does photochemical smog as VOC. We estimate HFEs fine, whose lifetime is between 1 and 5 year. HFEs described in table 1, fit this range.

These HFEs belong to perfluoroalkyl methyl ether, and are early known. They are easily producted from perfluoroalkyl ketone, dimethyl sulfate and KF (1,2,3,4). Range of their boiling point is between –25 and 35˚C, and fit refrigerant use. So we evaluated cyclic performance in a compression heat pump as refrigerant (5). COP (coefficient of performance) of some HFEs were equal to CFC-11 and CFC-114.HFEs described in table 1, were thermally stable, and were determined to be nontoxic in rat inhalation toxicity tests. So, we estimate HFEs practical alternative, which rank with natural alternatives, for example ammonia and hydrocarbon.

3. EXPERIMENTAL RESULTS AND DISCUSION

A series of heat transfer experiments were done at constant adiabatic wall temperatures 35, 40, 45, 50, 60℃. Fill charge ration 25% of the evaporator section volume for all working fluids.

Table 1 New refrigerant and emergency alternative materials

New refrigerant and emergency alternative materials			HFE-143m	HFE-245mc	HFE-347mmy	HFE-347mcc	HCFC-142b
Molecular formula			$C_2H_3F_3O$	$C_3H_3F_5O$	$C_4H_3F_7O$	$C_4H_3F_7O$	$C_2H_3C\ell F_2$
Structure			CF_3OCH_3	$CF_3CF_2OCH_3$	$(CF_3)_2CFOCH_3$	$CF_3CF_2CF_2OCH_3$	$CH_3CC\ell F_2$
Mean molecular weight			100.0	150.1	200.1	200.1	100.5
Boiling point		℃	-24.0	5.6	29.35	34.18	-9.7
Vapor pressure (25℃)		kPa	578.8	206.18	86.13	71.78	
Latent heat	L	kJ/kg	173.3 (25℃、pressure)	166 (25℃, pressure)	140 (25℃)	144 (25℃)	212
Solubility parameter (25℃)		$(cal/cm^3)^{1/2}$	6.30 (25℃,pressure)	6.76 (25℃, pressure)	6.58	6.66	
Specific heat	C_p(liquid)	kJ/kgK	1.415 (23℃,pressure)	1.297 (23℃, pressure)	1.208 (23℃)	1.246 (23℃)	1.197
Viscosity	μ(liquid)	mPaS	0.232 (23℃,pressure)	0.2847 (25℃, pressure)	0.4630 (23℃)	0.4707 (23℃)	0.32
Density	ρ(liquid)	kg/m^3	1089.3 (23℃,pressure)	1279.7 (23℃, pressure)	1420.1 (23℃)	1409.4 (23℃)	1110
	ρ(vapor)	kg/m^3		12.7 (23℃, pressure)			15.3
Kinematic viscosity	ν(liquid)	m^2/s	2.130E-07	2.225E-07	3.260E-07	3.340E-07	2.8829E-07
Surface tension	σ(liquid)	mN/m	8.51 (23℃pressure)	10.63 (21℃, pressure)	11.86 (23℃)	12.39 (23℃)	10.7 (30℃)
Thermal conductivity	λ(liquid)	W/mK	0.0769 (23℃,pressure)	0.0698(23℃, pressure)	0.0780 (23℃)	0.0754 (23℃)	0.119
Solubility for water		%	(unknown)	(unknown)	0.02	0.006	0.14
Specific inductive capacity	ε_r(liquid)		9.46 (23℃,pressure)	7.3 (21℃, pressure)	6.2 (23℃)	7.1 (23℃)	1.014
Flash point		℃	(unknown)	(unknown)	none	none	none
Critical point	temperature	℃	104.86	133.7	160.2	164.6	137.1
	pressure	k Pa	3627	2887	2553	2481	42
Ozone Depleting Potential	ODP		0	0	0	0	0.05
Global Warming Potential	GWP		750	580	330	480	2400
Atmospheric Life time			4.4	4.3	3.4	4.5	19
Merit Number	ρσL/μ	W/m^2	6.29E+09	7.93E+09	5.09E+09	5.34E+09	7.87E+9

***Names of New refrigerant HFE-143m, HFE-245mc etc. are the name at Research Institute of Innovative Technology for the earth (RITE).**

*Date noted "pressure" were measured under vapor-liquid equilibrium at indicated temperature.

*GWP is relative value[(each Refrigerant) / (CO_2)], and their time horizon are 100 years.

*GWP and Atmospheric Lifetime were quoted from IPCC's data (7) *Merit Number were calculated at 23+/-2℃, but in HCFC-142b,σ(liquid) at 30℃ was use.

In putting the experimental data in order, both condensation heat transfer coefficient α_c and boiling (evaporation) heat transfer coefficient α_e are defined following,

$$\alpha_c = \dot{q}/(T_{cv} - T_{cw}) \quad \alpha_e = \dot{q}/(T_{ew} - T_{ev}) \qquad (1)$$

Where T_{cv} and T_{cw} are vapor and wall temperatures at the condenser section, T_{ev} and T_{ew} are values at the evaporator section.

3-1 Experimental Correlation of HFEs

For comparison of the experimental results with the existing predicted equation. Those predicted equation is contained both old data[2] and new data.

(a) Condensation Heat Transfer

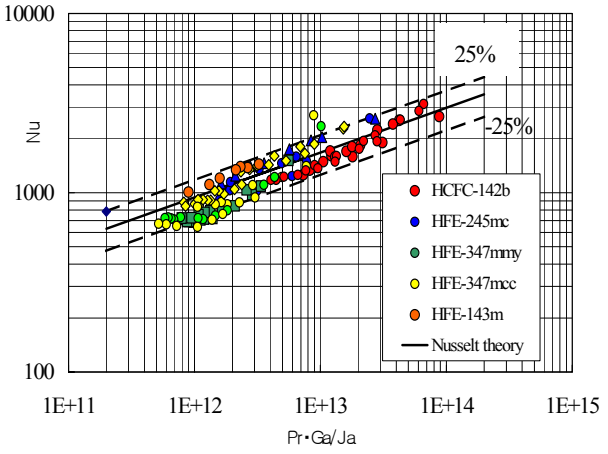
Nusselt's film condensation theory is used to compare with the condensation heat transfer coefficients.

$$\alpha_c = 0.943 X_c^{1/4}$$

$$X_c = \left(\frac{\rho_\ell (\rho_\ell - \rho_v) g h_{fg} \lambda_\ell^{\ 3}}{L_c \mu_\ell (T_{cv} - T_{cw})} \right) \qquad (2)$$

Fig.3 show that the comparison of the experimental results and Nusselts coreelation for all experimental results. It is evident that they are in agreement with the theoretical results of Nusselts theory.

Fig.3 Condensation heat transfer coefficients



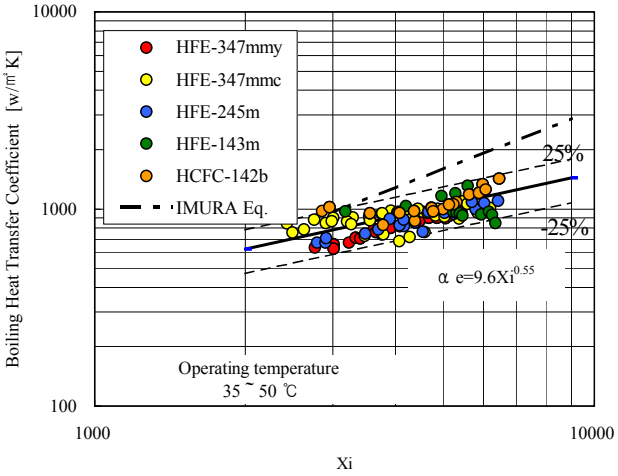
(b)*Boiling Heat Transfer*

For boiling heat transfer coefficients of a two-phase closed thermosyphon, there are many equations of correlated by Gross , Imura and Kaminaga etc[2].

Imura correlation agrees well with the data of alcohol. It is generally that CFCs values agree well Gross and Kaminaga correlation. Experimental values for water agree well with Gross's correlation.

In this study, we choose ***Imura correlation***[2] in which is widely noted to compare with HFEs experimental results.

As the results, experimental data were different from Imura's correlations, but it is possible to make a correlate equation between new refrigerant HFEs based on Imura's correlations. Rearranging data of HFEs, we could make a new correlation as shown in Fig.4. As the results, following correlated equation was obtained.



$$\alpha_e = 9.6 X_I^{\ 0.55}$$

$$X_I = \left(\frac{\rho_\ell^{\ 0.65} \lambda_\ell^{\ 0.3} C_{p\ell}^{\ 0.7} g^{0.2} \dot{q}_e^{\ 0.4}}{\rho_g^{\ 0.25} h_{fg}^{\ 0.4} \mu_\ell^{\ 0.1}} \right) \left(\frac{P_v}{P_a} \right)^{0.3} \qquad (3)$$

4. SELF-EXCITING OSCILLATION HEAT PIPE HEAT-EXCHANGER FOR PELTCIE, CPU DEVICE COOLING

Self-oscillating heat pipes, in which the working fluid does not circulate between the evaporator and the condenser, form of counter current liquid-vapor flow like conventional two-phased closed thermosyphon, but rather axially oscillates in the meandered capillary tubes. This oscillation movement of the working fluid is created by the vapor-liquid slug flow phenomenon. In this study, the self-oscillating heat pipe container consists of a flat aluminum extrusion whose external rectangular shape incorporates many parallel capillary channels inside as Fig. 5.

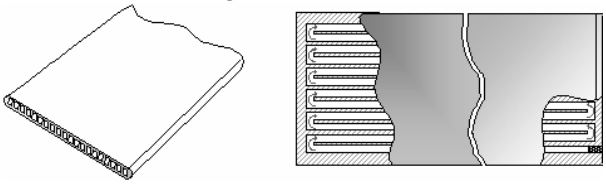


Fig.5 Flat plate self-oscillating heat pipe

A self-exciting oscillation heat pipe cooling system are made of a meandered flat aluminum plate and thin aluminum rubber fins installed inside a open cabinet. Heat pipe is soldered on the upper and bottom side of a cabinet and cooled by a small fan. The figure 6 is a dimension of heat pipe cooling system. And the photo1 shows a prototype cooling system with a peltie module. This cooling system is used for applications of a peltie module cooling and a CPU cooling of desk top personal computer etc.

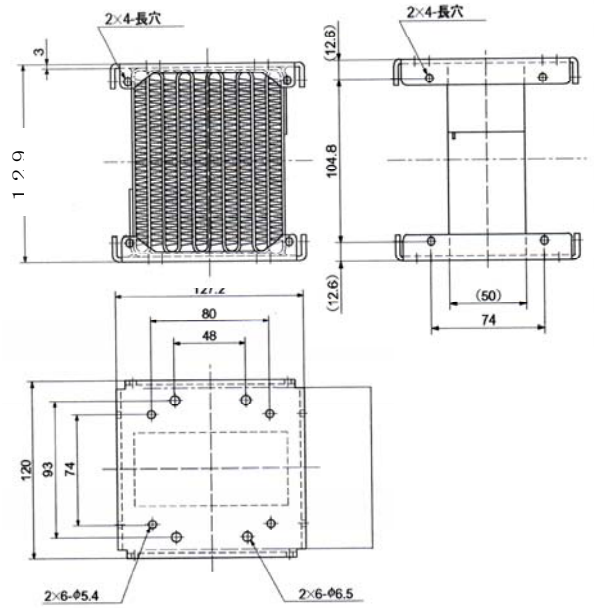


Fig.6 Self-exciting oscillation heat pipe cooling system



Photo 1. Pelture module with heat pipe cooling system

A schematic diagram of experimental set up is shown in figure 7. This cooling system is a prototype used for applications of a peltie module cooling and a CPU cooling of desk top personal computer, but in this experimental study, two electric heater are used as heating sources instead of peltie module. The temperature at the contact point between a heater and the heat pipe cooler , at the top of the heat pipe cooler and ambient air were measured with copper-constantan thermocouples and a data roger.

A heat transfer performance of the self-oscillating heat pipe cooler was evaluated due to the thermal resistance T_{th} as following definition,

$$R_{ht} = Q/(T - T_a)$$

where Q is out put heat from electric heater, T is temperature at contact point, and T_a is ambient air temperature.

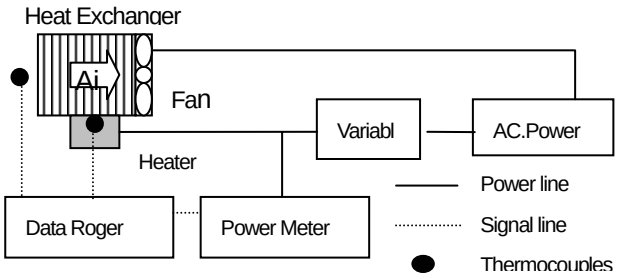


Fig.7 Set upped experimental equipments

In this experimental series, 4 HFE fluid were used as the working fluid in the Table2. And the refrigerant HFC134a was used also as commercial base in the Table2.

Table 2. Working fluid of heat pipe

Fluid	Boiling Point ℃	Critical Temp. ℃	Critical Pressure kPa	Latent Heat kJ/kg	Viscosity mPas
134a	-26.03	101.3	4135	177.9	0.202
143m	-24.0	104.8	3627	173.3	0.232
245mc	5	133.7	2887	166	0.247
347mmy	29.35	160.2	2553	140	0.463
347mcc	34.18	164.6	2481	144	0.471

5. EVALUATION RESULTS WITH PROTOTYPE DVICES

Fig 8 shows the temperature difference between the contact point of heater and ambient air as function of heat load from two electric heaters.

Figure8 becomes Fig.9 when the temperature difference and heat load is rewritten in a thermal resistance. In the figure 9, the thermal resistance decreases as increasing of heat road, and becomes constant value at high heat transfer rates.

When working fluid is compared respectively, a

thermal resistance becomes small in order of HFC-134a, HFE-143m, HFE-245mc, HFE-347mmy and HFE-347mcc, it is understood about that heat transfer performance increases.

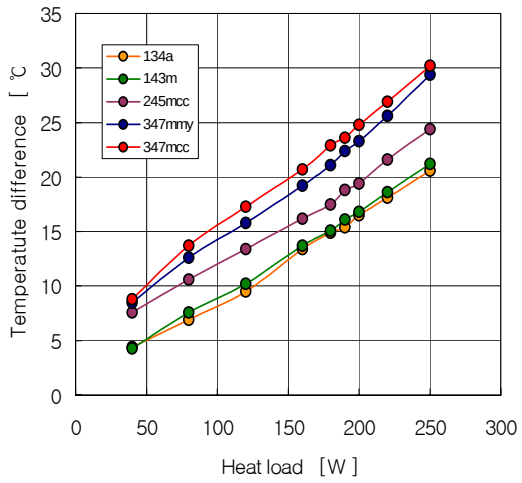


Fig.8 Temperature difference between contact point of heater and air

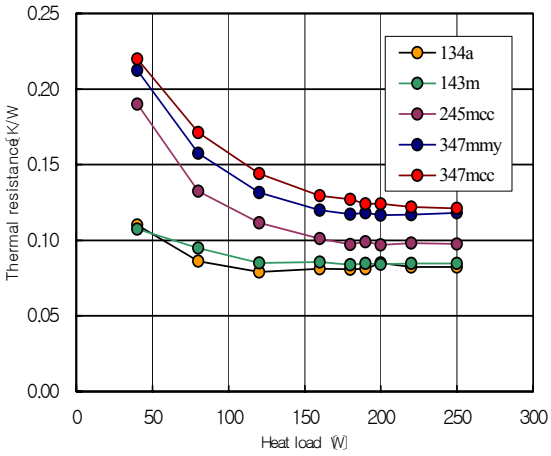


Fig.9 Thermal resistance

Fig.10 Comparison with HFC-134a

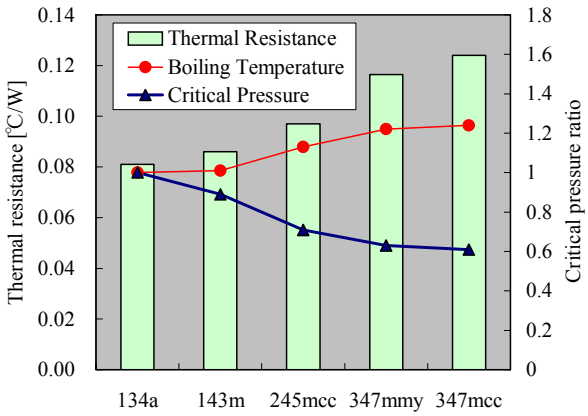


Fig.10 shows a comparison with HFE substances and alternative substance HFC-134a. In the figure, a thermal resistance of HFC-134a whose boiling point is the lowest and critical pressure is the highest, is the most efficient. And, for the continuation, it improves with HFE-143m, HFE-245mc, HFE-347mmy and HFE-347mcc in low order of boiling point.

6. CONCLUSION

New alternative substances HFE (hydrofluoroether) have been conducted by using a two-phase closed thermosyphon and prototype compact cooling system. As the results,

(1) The heat transfer performances become better in the order, HFE-143m, HFE-245mc, HFE-347mmy and HFE-347mcc, in low order of boiling point.

(2) Condensation heat transfer coefficients suggest an adequate correlation for Nusselts theory.

(3) Following experimental equation for boiling heat transfer was carried out by the Imura's correlation.

$$\alpha_e = 9.6 X_I^{0.55}$$

$$X_I = \left(\frac{\rho_\ell^{0.65} \lambda_\ell^{0.3} C_{p\ell}^{0.7} g^{0.2} \dot{q}_e^{0.4}}{\rho_g^{0.25} h_{fg}^{0.4} \mu_\ell^{0.1}} \right) \left(\frac{P_v}{P_a} \right)^{0.3}$$

Acknowledgement

The financial support of the New Energy and Industrial Technology Development Organization, who partly funded the research work presented in this paper, is gratefully acknowledged.

References

(1) Sekiya,A.;Misaki,S.,CHEMTECH, DECEMBER 1996, p44-48

(2)H.Imura, K.Sakamoto and S.Iltuposhi "Heat transfer in two-phase closed thermosyphon" Journal of JAHP, Vol.14,No.3 pp.5-13, (7.1995)

(2) "CLIMSATE CHANGE 2001 The Scientific Basis", Intergovernmental Panel on Climate Change 2001, p388 -90 (Table 6.7 and Table 6.8)

(4) S.Maezawa, K.Gi, K.Wakabayashi, N.Yamazaki, and J.Sakiura " Evaluation experiment of refrigerant fluorinated ethers by two-Phase closed thermosyphons" Heat Pipe Science Technology Application, Proceeding of 12th IHPC-Russia , pp.315-321 (5.2002)

Effects of Evaporator Section Lengths, Number of Turns and Working Fluid on Internal Flow Patterns of an Closed-End Oscillating Heat at Normal Operating Condition

S. Rittidech, P. Terdtoon*, M. Murakami**, P. Kamonpet*, and W. Jompakdee*
Faculty of Engineering Mahasarakham University, Thailand
Email: S_Rittidej @ hotmail.com
*****Department of Mechanical Engineering, Faculty of Engineering,
Chiang Mai University, Chiang Mai 50200 Thailand.
Tel. +66 53 944151 Ext. 911 Fax. +66 53 226014
******Institute of Engineering Mechanics and Systems
1-1-1 Tennodai,Tsukuba 305-8573 Japan

Abstract

A visual study of the flow patterns inside a closed-end oscillating heat pipe (CEOHP) at normal operating conditions for several evaporator section lengths, number of turns and working fluids has been conducted. The CEOHPs employed a glass tube with inside diameter of 2.03 mm. The lengths of evaporator of 150 and 50 mm (the lengths of evaporator, adiabatic and condenser section were equal) were employed with 10 and 28 turns. The inclination angle is 90^{o} from horizontal plane. R123 and R141b were used as the working fluids with filling ratio of 50% of internal volume of tube. The heat source temperature was controlled of 80 0C while the heat sink temperature was controlled at 20 0C. The evaporator section was heated by silicone oil and the condenser section was cooled by distilled water. The temperature at adiabatic section and the inlet-outlet of distilled water at condenser section were recorded. The photographs of flow patterns at specific times were recorded at evaporator section by a digital and three video cameras were used to observe the flow patterns at the evaporator section, condenser together with adiabatic sections and total part of CEOHP. It was found from the experiment that, as the evaporator section length decreases from 150 to 50 mm the main flow changes from the slug flow together with annular flow to slug flow with bubble flow. The length of vapor bubbles rapidly decreases. The velocity of vapor bubbles slightly increases. The frequency of temperature oscillation slightly increases as the amplitude rapidly decreases, the heat flux rapidly increases. Effect of number of turns cannot be clearly identified. If the working fluid changes from R141b to R123, the main flow changes from the slug flow with together annular flow to slug flow with bubble flow. The length of vapor bubbles rapidly decreases. The velocity of vapor bubbles rapidly increases. The frequency of temperature oscillation of working fluid slightly increases as the amplitude of temperature oscillation rapidly decreases, while the heat flux rapidly increases.

Key words: Closed-end oscillating heat pipe, Flow patterns

1. INTRODUCTION

As a heat transfer device for high heat load, conventional heat pipes have several limitations, such as the capillary limit when the diameter of the pipe is comparatively small, and the entrainment limit as the temperature difference is high. This problem becomes especially crucial when using heat pipes to cool electronic devices. Because of these limitations, other types of heat pipe with long capillary tubes are commonly employed. One such device is a closed-end oscillating heat pipe (CEOHP), as shown in Figure 1. The CEOHP consists of a single long section of meandering capillary tubing. The heat transfer of CEOHPs occurs because of self-excited oscillation which may be driven by fast fluctuating pressure waves caused by nucleate boiling and condensation of the working fluid. It is reported that capillary tube heat pipe with this serpentine structure is operated within the maximum inner diameter found by Maesawa et al. [1]

$$d_{max} \leq 2\sqrt{\frac{\sigma}{\rho g}} \qquad (1)$$

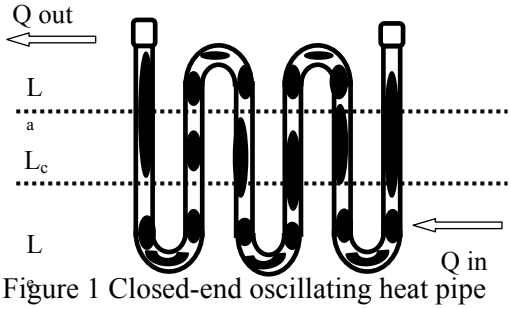


Figure 1 Closed-end oscillating heat pipe (CEOHP)

The advantages of CEOHPs are its property of transferring heat in any orientation, its quicker response, and its simpler wickless structure. In quantitative determining for the heat transfer characteristics of the CEOHP at the normal operating condition, Rittidech et al. [2] have conducted experiments with fill ratio 50% and working temperature of 50^{o}C. The variable parameters were the inclination angle, inner diameter of the tube, number of turn, working fluid and evaporator section length. It was found from the experimental results that when the inner diameter increased, the heat flux increased. As the evaporator section length increased, the heat flux conversely decreased. However, the heat flux increased when latent heat of vaporization of working fluid decreased.

Heat transfer characteristics of the CEOHP is directly affected by internal flow patterns. There are quite a number of research papers about flow behavior of the CEOHP. Gi et al. [3] have conducted experiments with R142b by varying the fill ratios and inclination angles. A CEOHP with an ID of 2 mm and a total length of 8020 mm was employed, with 10 turns and working temperature of 450 ^{o}C. They observed that the working fluid could not circulate thoroughly. The heat was transferred by the driving force due to the oscillation between heating and cooling section. The internal oscillation occurred at smaller inclination angle and smaller fill ratio. Lee et al. [4] conducted a visual study the flow visualization of closed-loop oscillating heat pipe with ethanol by varying the inclination angles, fill ratios and working temperatures. A CLOHP with 4 turns and a total length of 220 mm, The high-speed camera of 400 frame/sec was used to observe the flow visualization test. The shutter speed was set to 1/2000 sec and stroboscope was used as a light source. The circulation of working fluid cannot be clearly identified, and condensate returned to the evaporator section as a simple stratified or rivulet flow along the inner wall of channel. The oscillation of bubbles was caused by the nucleate boiling and vapor oscillation. The most active oscillation was observed at the fill ratio of 40-60% and at the inclination angle of 90 deg. Lee et al. [5] investigated the characteristics of pressure oscillation in self-excited oscillating heat pipe with R142b by varying the fill charge ratio and inclination angle. The test section was manufactured to the serpentine structure of loop type with flow channel of 10 turns by drilling the channel of length 220 mm, width 1.5mm and depth 1.5 mm on the surface of brass plate. The pressure tap was perforated to diameter 1.0 mm as flow channel of square of test section and sensors were installed to evaporating and condensing part and pressure was simultaneously measured. As the experimental results, the saturation pressure within oscillating heat pipe was also increased as the heat flux was increased. The charging ratio increased, the amplitude of pressure oscillation increased and when the inclination angles lied between 90 and 30 deg., the size of pressure and the variation of amplitude was not large. Irregular pressure oscillation phenomena occurred when the charging ratio of was 80% over and inclination was less than 30 deg. Heat transfer performance was excellent when pressure difference was decreased between evaporating and condensing part. Miyazaki et al. [6] concluded from their visual study of oscillatory flow in the oscillating heat pipe. The experimental results were compared with theoretical predictions. The theoretical predictions were based on an analytical model of self-excited oscillation, in which reciprocal excitation between pressure oscillation and oscillatory flow formed waves. The visualization model of an CEOHP consisted of a base plate of copper and a window plate of polycarbonate. The base plate was provided with a rectangular groove which was turned repeatedly at both ends to form 50 parallel grooves, and the grooves ends were connected as a loop. The working fluid of R142b, the working fluid was observed through the window and recorded by a digital video camcorder at 30 frames per second. It can be concluded from their results that the existence of the waves was confirmed in the visualization test, and the phase relationship and the wave velocity observed in the experiment were demonstrated to be predicted well by the proposed theory. They concerned with heat transfer characteristics and flow visualization of working fluid and the operation mechanism of CEOHP cannot be clearly identified. Therefore, in this study, it was intended to clearly visualize flow pattern according to the variation of evaporator section lengths, number of turns and working fluids. And, by the analysis of correlation between flow pattern and heat transfer characteristics, it was intended to obtain the basic data to make clear the operation mechanism of CEOHP. It is, therefore, the objective of this article to investigate the effects of evaporator section lengths, number of turns and working fluids on internal flow patterns of an CEOHP at normal operating conditions.

2. EXPERIMENTAL SETUP AND PROCEDURE

Figure 2 shows an experimental setup which consists of a CEOHP with the lengths of evaporator , adiabatic (which is equal to condenser

sections) were 150 and 50 mm respectively. The selected CEOHPs were made of the Pyrex glass tube with the internal diameter of 2.03 mm, The selected meandering turns (to observe the effect of number of turns) were 10 and 28. The evaporator section was heated by silicone oil, which was circulated from the hot bath (HAAKE: HS891000). The condenser section was cooled by distilled water, which was circulated from the cold bath (Bizer D7032, with an operating range of –20 to 20^0C). The heating and cooling jackets were made of high temperature glass to ensure the best visualization. The mass flow rate inside the cooling jacket was measured by floating rotameter (Platon PGB411) and 4 points of thermocouples (OMEGA type K) were installed at the inlet and outlet of condenser section to determine the heat transfer rate. The temperature probes were installed 2 points at high temperature glass of evaporator, 2 points condenser sections, and 1 point for ambient to determine the heat loss. The temperature recorder (Comark, C8510, with ±1 ^{o}C accuracy) was used to monitor all temperatures at specified time. Moreover, 2 points of the thermocouple were installed at the middle position of the 43^{th} and 44^{th} tube of adiabatic section starting from the left side. These two thermocouples were inserted inside the CEOHP by the special-designed probe. The thermocouples were connected to the chart recorder (Yokogawa, 4152 type, with ±0.5 ^{o}C accuracy) to measure the amplitude and oscillating of temperature of the working fluid at adiabatic section from which the internal saturated pressure can be observed. During the experiment the angle was set at 90 degrees from horizontal plane. Three video cameras (Sony CCD – TR618E) were employed to continuously record the flow patterns at the evaporator section, condenser together with adiabatic section, and total part of CEOHP. The digital camera (Sony DSC – S75) was used to record flow patterns of evaporator section at specified times. The scales were attached to the apparatus to measure the length and velocity of vapor bubble. The controlled parameters were:

Tube internal diameter of 2.03 mm

Working temperature of 500C

Filling ratio of 50% (by total volume)

The variable parameters were:

Evaporator section lengths of 150 and 50 mm

Working fluids R123 and R141b (since their boiling pressure are acceptable for the required temperature range)

Meandering turns of 28 and 10

The experiment was conducted as follows; Firstly, the CEOHP was filled with the working and set into the test rig. The temperature of the hot and cold baths were set at the required value, and the hot and cold fluids were supplied to the jackets of both the evaporator and the condenser section. After a steady state was reached, continuous movie were recorded by three video cameras while photographs were taken at specified times by digital camera. In the mean time, temperatures and heat transfer rates were monitored. The temperature oscillation of working fluid and amplitude were recorded to briefly observe the pressure oscillation of working fluid. Then the evaporator lengths, number of turns and working fluids were varied according to the required conditions.

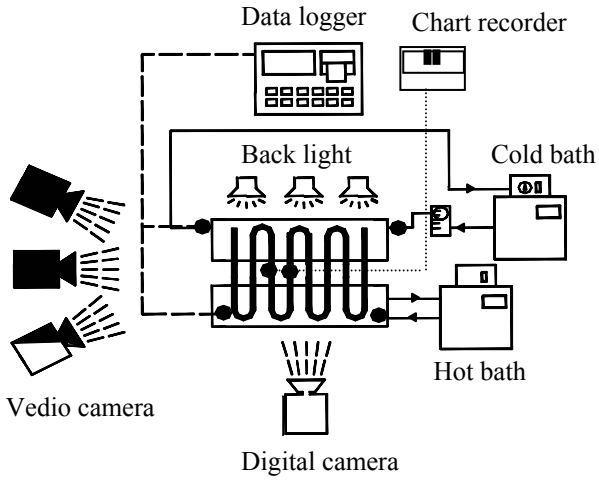


Figure 2 Experimental setup

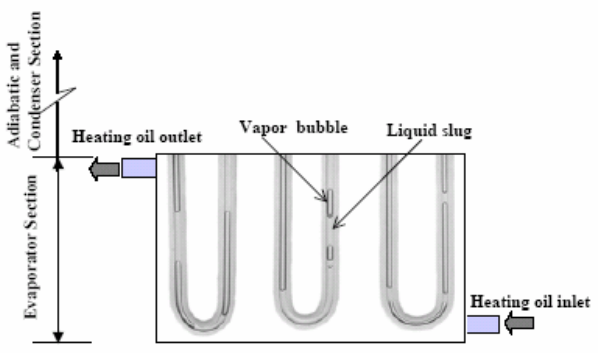


Figure 3 The inlet – outlet flow directions of silicon oil at evaporator section

3. RESULTS AND DISCUSSION

Visualization at the evaporator section was concentrated since the major phenomena occurred in this part. The total flow, which cannot be presented in the paper could, however, be observed by video movie. Figure 3 shows the inlet-outlet flow directions of silicon oil at evaporator section and all the experiment results will be referred with this figure. The vapor bubble length was measured as the length of the two ends of vapor bubble at

specified time. The expanding and shrinking ratio (in percentage) of vapor bubble were measured in comparison with the original length of vapor bubble at the original time. It can be concluded from the experimental results as follows;

3.1 Effect of evaporator section lengths

Figure 4 shows the flow pattern of the CEOHP with all same condiyion. Figure 4(A), shows the inside flow pattern of the CEOHP at the 150 mm evaporator length. It can be seen that slug flow is the main flow pattern with annular flow as frequently seen flow pattern . The length of vapor bubbles is approximately 1-10 mm. The annular flow tends to develop and flows separately from the lower to upper part at the right side of the evaporator with the length of vapor bubbles of 50-57 mm. However, bubble flow slightly occurs. The vapor bubbles oscillate from the left to right side with the frequency of 0.40 Hz. The total oscillation period cannot be clearly identified. The velocity of vapor bubbles at right side is about 0.52 m/s. The amplitude of temperature at the right side is about 2.7 and heat flux is 4578 W/m^2. The slug flow with very few nucleation sites appears at the bottom part of the evaporator. These vapor slugs subsequently expand to the middle parts of evaporator before moving up to the condenser section where they collapse and the heat is released. Figure 4(B), shows the inside flow pattern of the CEOHP with Le of 50 mm It can be seen that slug together with bubble flow still be the main flow pattern. The length of vapor bubbles is approximately 30-35 mm. At the middle part, bubble flow increasingly occurs with the length of vapor bubbles of 1-3 mm. The annular flow cannot be observed. The vapor bubbles oscillate from the left to right side with frequency of 0.48 Hz. However, the total oscillation period cannot be clearly identified. The velocity of vapor bubbles is about 0.50 m/s. The amplitude of temperature is about 0.32 and heat flux is 18189 W/m2. The slug flow with very few nucleation sites appears at the bottom part of the evaporator. These vapor slugs subsequently expand to the middle parts of evaporator before moving up to the condenser section where they collapse and the heat is released. From this study, it can be explained that the heat can be transferred by the following mechanism: as heat is supplied at the evaporator, the vapor bubbles originates in the evaporator section. Firstly the flow pattern of working fluid in the CEOHP is slug flow as the vapor bubbles is short. The bubbles grows irregularly. These bubbles move to condenser with very high speed. The frequency of temperature oscillation is very high but the amplitude is low. Most of the bubbles that flow into the condenser section collapse there where the absorbed latent heat is released, resulting in the lower void faction. The heat flux is, thus, transferred by this mechanism. These results agree with the results of Gi et al.[3], [4]. From which the results show that at 150 mm evaporator length, the vapor bubble grows to long vapor slug and the oscillation is low.

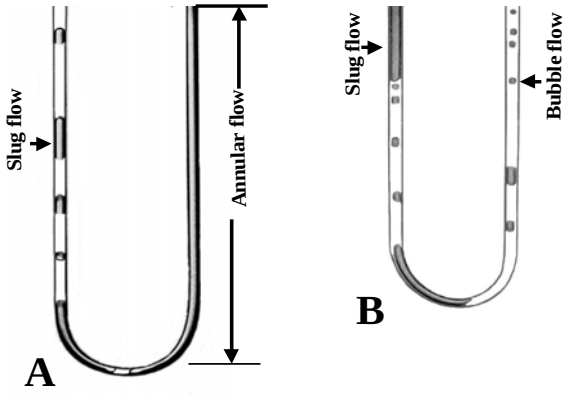


Figure	Le (mm)	Main flow plattern	Lv (mm)	Vs (m/s)	ω (Hz)	λ (°C)	q (W/m²)
A	150	Slug + Annular	50-57	0.40	0.31	3.22	4578
B	50	Slug + Bubble	1-35	0.45	0.38	0.36	18189

Figure 4 Internal flow pattern of CEOHP at Di 2.03mm, 10 Turns, Tv 50^{0}C, R123 and 90^0

It can be concluded that, if the evaporator length decreases from 150 to 50 mm, the main flow changes from the slug flow together with annular flow to slug flow together with bubble flow. The length of vapor bubble rapidly decreases. The velocity of vapor bubble slightly increases. The frequency of temperature oscillation slightly increases as the amplitude rapidly decreases. The heat flux rapidly increases.

3.2 Effect of number of turns

Figure 5 shows the flow pattern of the 2 CEOHPs with same condition. Figure 5 (A), shows the inside flow pattern of the CEOHP at the 28 turn. It can be seen that slug and bubble flow is the main flow pattern. The length of vapor bubbles is approximately 30-38 mm. At the middle part, the bubble flow increasingly occurs with the length of of 2-3 mm. The vapor bubbles oscillate from the left to right side with the frequency of 0.48 Hz. However, the total oscillation period cannot be clearly identified. The velocity of vapor bubble is about 0.53 m/s. The amplitude of temperature is about 0.33 ^{0}C and heat flux is 18102 W/m2. The slug flow with very few nucleation sites appears at the bottom part of the evaporator. These vapor slugs subsequently expand to the middle parts of evaporator before moving up to the condenser

section where they collapse and the heat is released. Figure 5(B), shows the inside flow pattern of the CEOHP at the 10 turn. It can be seen that slug together with bubble flow still be the main flow pattern. The length of vapor bubbles is approximately 30-35 mm. At the middle part, the bubble flow increasingly occurs with the length of vapor bubbles is approximately 1-3 mm. The annular flow cannot be observed. The vapor bubbles oscillate from the left to right side with the frequency of 0.48 Hz. However, the total oscillation period cannot be clearly identified. The velocity of vapor bubbles is about 0.50 m/s. The amplitude of temperature at right side is about 0.32 and heat flux is 18189 W/m2. The slug flow with very few nucleation sites appears at the bottom part of the evaporator. These vapor slugs subsequently expand to the middle parts of evaporator before moving up to the condenser section where they collapse and the heat is released.

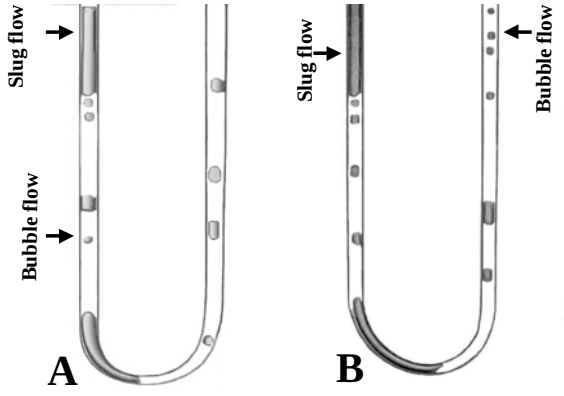


Figure	Turn	Main flow plattern	Lv (mm)	Vs (m/s)	ω (Hz)	λ (⁰C)	q (W/m²)
A	28	Slug + Bubble	2-38	0.43	0.41	0.33	18102
B	10	Slug + Bubble	1-35	0.45	0.38	0.36	18189

Figure 5 Internal flow pattern of CEOHP at Di 2.03mm, Le 50 mm, Tv 50^0C, R123 and 90^0

It can be concluded that, if the number of turns decreases from 28 to 10 mm, flow pattern remains at the slug flow with bubble flow. The length and velocity of vapor bubbles are nearly constant. The velocity of vapor bubbles is nearly constant. The frequency and amplitude of temperature oscillation are nearly constant. The heat flux is nearly constant. The effect of number of turn on the flow patterns cannot be clearly identified.

3.3 Effect of working fluids

Figure 6 shows the flow pattern of the CEOHP with working fluids of R141b and R123. It can be observed from Figure6(A) in which R141b is employed that, slug flow is the main flow pattern with annular flow some times seen. The length of vapor bubbles is approximately 10 mm. The annular flow tends to develop and flows separately from the lower to upper part at the right side of the evaporator with the length of vapor bubbles of 50 mm. At the middle part, bubble flow slightly occurs. The vapor bubbles oscillate from the left to right side with the frequency of 0.28 Hz. However, the total oscillation period cannot be clearly identified. The velocity of vapor is about 0.20 m/s. The amplitude of temperature is about 3.01 ⁰C and heat flux is 10804 W/m2. The slug flow with very few nucleation sites appears at the bottom part of the evaporator. These vapor slugs subsequently expand to the middle parts of evaporator before moving up to the condenser section where they collapse and the heat is released. Figure 6(B), shows the inside flow pattern of the CEOHP with R123 (Hfg of 160 kJ/kg, σ of 0.012 N/m). It can be seen that slug and bubble flow still be the main flow pattern. The length of vapor bubbles is approximately 30-38 mm. At the middle part the bubble flow increasingly occurs with the length of vapor bubbles is approximately 2-3 mm. The vapor bubbles oscillate from the left to right side with the frequency of 0.48 Hz. The velocity of vapor bubbles is about 0.53 m/s. The amplitude of temperature is about 0.33 ⁰C and heat flux is 18102 W/m2. The slug flow with very few nucleation sites appears at the bottom part of the evaporator. From this study, it can be explained that the heat can be transferred by the same mechanism as in section 3.1.

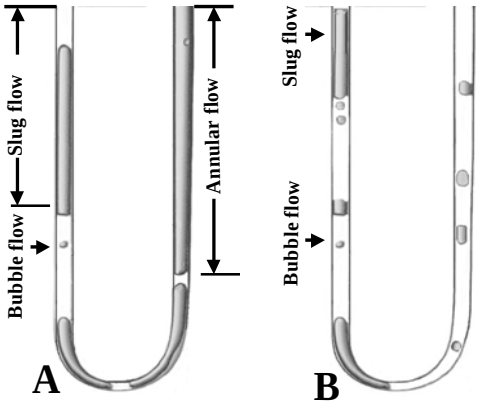


Figure	Hfg (kJ/kg)	Main flow plattern	Lv (mm)	Vs (m/s)	ω (Hz)	λ (⁰C)	q (W/m²)
A	213	Slug + Annular	1-50	0.35	0.38	2.02	10840
B	160	Slug + Bubble	2-38	0.43	0.41	0.33	18102

Figure 6 Internal flow pattern of CEOHP at Di 2.03mm, Le 50 mm, 28 Turns, Tv 50^0C, and 90^0

It can be concluded that, if working fluid is changed (for instance from the fluid of Hfg of 213 kJ/kg to the one with Hfg of 160 kJ/kg) the main flow changes from the slug flow with annular flow

to slug flow with bubble flow. The length of vapor bubbles rapidly decreases. The velocity of vapor bubbles rapidly increases. The frequency of temperature oscillation of working fluid slightly increases as the amplitude of temperature oscillation rapidly decreases, the heat flux rapidly increases.

4. CONCLUSIONS

From all experimental results, it can be concluded as follows:

The evaporator section length decreases from 150 to 50 mm. The main flow changes from the slug flow with annular flow to slug flow with bubble flow. The length of vapor bubbles rapidly decreases. The velocity of vapor bubbles slightly increases. The frequency of temperature oscillation slightly increases as the amplitude rapidly decreases, the heat flux rapidly increases. The number of turns decreases from 28 to 10 mm. The flow pattern remains at the slug flow with bubble flow. The length of vapor bubbles nearly constant. The velocity of vapor bubbles nearly constant. The frequency of temperature oscillation nearly constant as the amplitude nearly constant, the heat flux nearly constant.

The Hfg or σ . decreases (from 213 to 160 kJ/kg or from 0.015 to 0.012 N/m), the main flow changes from the slug and annular flow to slug and bubble flow. The length of vapor bubbles rapidly decreases. The velocity of vapor bubbles rapidly increases. The frequency of temperature oscillation of working fluid slightly increases as the amplitude of temperature oscillation rapidly decreases, the heat flux rapidly increases.

Nomenclature

hfg latent heat of vaporization (kJ/kg)
L_e evaporator section length (mm)
L_v length of vapor slug (mm)
q heat flux (W/m^2)
V_s velocity of vapor slug(m/s)
ω frequency of temperature oscillation (Hz)
λ amplitude of temperature oscillation (^0C)
σ surface tension (N/m)

Acknowledgments

The research has been supported by the Faculty of Engineering and Graduate School Chiang Mai University.

Reference

1. S. Maezawa, K. Gi, A. Minamisawa, H. Akachi, Themal performance of capillary tube thermosyphon, Proc. Of the IX international Heat Pipe Conference, Albuquerque New Maxico. Vol. II, 1996.
2. S. Rittidech, P. Terdtoon, M. Murakami, P. Kamonpet, and W. Jompakdee, Correlation to Predict Heat Transfer Characteristics of A Closed – End Oscillating Heat Pipe at Normal Operating Condition. Int. jour of Applied Thermal Engineering, Pergamon Press. U.K. (Submitted), 2001.
3. Gi, K, Sato, F, and Maezawa, S, Flow Visualization Experimental on Oscillating Heat Pipe. Proc. of the 11th International Heat Pipe Conference, Tokyo Japan, 1999.
4. W.H. Lee, J.S. Kim, J.H. Kim, H.S. Jung and I.S. Jang, Visualization of Oscillating Capillary Tube Heat Pipe. Proc. of the 11th International Heat Pipe Conference. Tokyo Japan, 1999.
5. W.H. Lee, J.S. Kim, J.H. Kim, and H.S. Jung, Characteristics of pressure Oscillation in Self–excited Oscillating Heat Pipe base on Experimental Study. Proc. of the 6th International Heat Pipe symposium, Chiang Mai Thailand, 2000.
6. Y. Miyazaki and M. Arikawa, Oscillatory Flow in the Oscillating Heat Pipe. Proc. of the 6th International Heat Pipe symposium, Chiang Mai Thailand, 2000.

Effect of Aspect Ratios and Internal Diameter on Performance Limit of A Closed-End Oscillating Heat Pipe Using Refrigerant Blend as Working Fluid

P. Anuchitchanchai, T. Wongratanaphisan, P. Kamonpet and P. Terdtoon

Department of Mechanical Engineering, Faculty of Engineering, Chiang Mai University
Tel. 66 53 994146 ext. 911, Fax. 66 53 94414, email: pradit@eng.cmu.ac.th

Abstract

This paper investigates the heat transfer characteristics at critical state of a closed-end oscillating heat pipe using refrigerant blends as working fluid. The selected working fluids were HP62 (or R-404a which is a near azeotropic blend of HFC125/HFC143a/HFC134a with 44/52/4% by weight) and MP39 (a blend of HPFC22/HFC152a/HCFC124 with 53/13/34% weight). Copper tubes with an ID of 0.66, 1.06 and 2.03 mm were employed with the selected evaporator length of 50, 100 and 150 mm. The selected filling ratio was 50% of total volume. The numbers of meandering turns were 5, 10 and 15. Experiments were conducted by setting the inclination angle at horizontal and vertical position with a controlled vapor temperature of 60±5°C. The effects of aspect ratios and Bond numbers on the heat transfer rate at critical state were experimentally determined. Good trends of systematic experimental results were found.

Key words: oscillating heat pipe, critical heat flux, aspect ratio, non-CFC refrigerant blend.

1. INTRODUCTION

Oscillating Heat Pipe (OHP) is a type of heat pipe made of a capillary tube bent around in meandering turns with inside working fluid partially filled. This device was recently invented by Akachi (1996). It has become increasingly popular owing to its simple construction, exceptionally high thermal conductivity, fast thermal response, and capability of operating in various orientations. With the working fluid partially filled, formation of alternating liquid slugs and and bubbles occurs inside the tube. The operational principle of the OHP is based on the oscillating movement and the phase change phenomena of the liquid slugs and bubbles allowing the heat to transfer from the hightemperature section to the low-temperature counterpart. The oscillation of the liquid slugs and bubbles is self-sustained by the evaporation of the liquid slugs and the condensation of the bubbles. The driving force of oscillation is generated by nucleate boiling and condensation of working fluid.

There are three basic types of OHP varying on its configuration: closed-loop OHP (CLOHP), closed-loop OHP with check valve, and closed-end OHP (CEOHP). In this study, the focus is on the heat transfer characteristics of the CEOHP as shown in Figure1.

Following are some definitions relating to CEHOP which will be encountered later in this paper.

aspect ratio: the ratio of the evaporator length, L_e to the inner diameter, D, of the tube.

filling ratio: the ratio of the volume of working fluid filled in the tube to the tube's total inside volume.

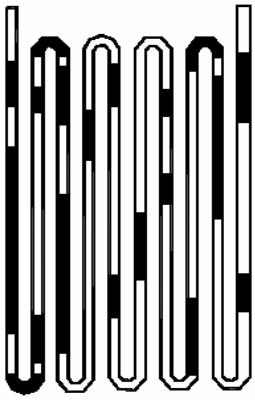


Figure 1 CEHOP

There have been a number of studies on heat transfer characteristics of OHP at normal operation [1,4,6,8]. Very few studies have investigated on its operating limitations some of which are mentioned as follows. Akachi et.al. (1996) found that an OHP with working fluid filled 50% of total inside volume will function effectively if the inner diameter of the tube is sufficiently small which is assessed by

$$D \le 2\sqrt{\frac{\sigma}{\rho_l g}}$$

Where D is the inner diameter of the tube, σ the surface tension of the working fluid, ρ_l the density of the working fluid and *g* the gravitational acceleration. This result indicates that there exists the lower limit at which the OHP can operate (transfer heat). Lin et. al. (2000) studied the relationship between the filling ratio and the heat flux of the CEOHP by using FC-72 and FC-75 as working fluids. It was found in their study that inadequate filling ratio could lead to dryout condition normally caused by insufficient quantity of the liquid in the evaporator section. Maezawa et. al. (1996) observed that, at a specific condition of their experimental works, the dryout occurred and the CEOHP did not function. It was also observed from the experimental works performed by Miyazaki et.al. (2000) that the dryout occurred by insufficient supply of liquid into the evaporator section. The solution by installing the check valve into the closed-loop oscillating heat pipe (CLOHP) was proposed.

In this study, the focus is on investigating the heat transfer characteristics of a CEOHP at upper operational limit condition, namely the critical state, in relation with the aspect ratios and inside tube diameters. Our hypothesis on the critical condition is explained by Figure 2. From past investigations, we establish that the dryout occurs at the evaporator section. When the OHP receives access amount of heat, the internal thermal resistance will increase rapidly. Accordingly, the heat flux can not be transferred from the evaporator to the condenser section. As a result, the inside vapor pressure becomes high and thus retards the liquid slug from returning back to the evaporator section. Finally, the amount of liquid in the evaporator section becomes too low and the dryout occurs at some part of the evaporator section. The state at which the dryout occurs is called the "critical state" of the OHP.

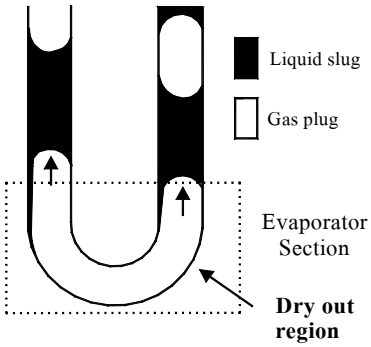


Figure 2 Hypothesis on critical state.

In the preliminary study, the CEOHP is chosen because its operating mechanism is not very complicated in comparison with the CLOHP. The main objectives are to experimentally investigate the effects of the aspect ratios and the tube internal diameters on heat transfer characteristics of a CEOHP at critical state. Two types of non-Chlorofluorocarbon (non-CFC) refrigerant blend, HP62 (or R-404a which is a near-azeotropic blend of HFC125/HFC143a/HFC134a with 44/52/4% by weight) and MP39 (a blend of HPFC22 /HFC152a/HCFC124 with 53/13/34% weight) were employed as working fluids. These non-CFC fluids were invented in an effort to replace or reduce the use of common CFC refrigerants which degrade the ozone in the atmosphere. Study on non-CFC refrigerants as working fluid has been rare. It is hope, therefore, that the results in this investigation will at least contribute to broaden the understanding in behaviors of these refrigerants when employed as working fluid.

2. EXPERIMENTAL SETUP

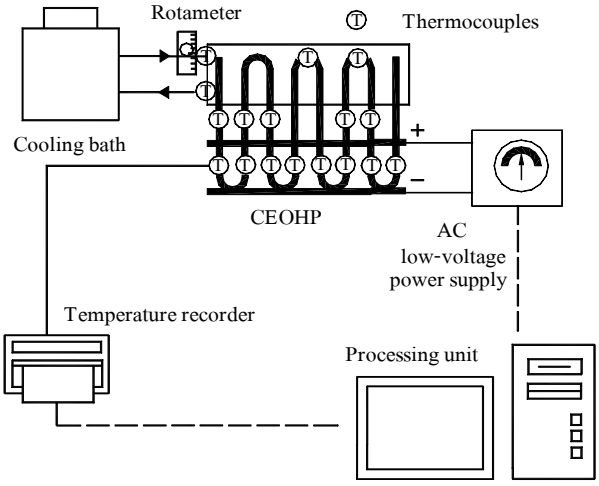


Figure 3 Diagram of the experimental setup

Figure 3 shows the diagram of the experimental setup. The CEOHP is made from a copper capillary tube bent to of a series of undulating turns. Attached by welding at its lower part are two copper bus bars separated by the distance that defines the evaporator length, L_e. Electric current supplied by a high-current low-voltage AC power supply is passed from the first bus bar to the second one through a series of parallel tubes in the evaporator section to provide heat. The cooling bath circulates a temperature-controlled one-to-one mixture of water and ethylene-glycol solution, used as cooling medium, through a cooling jacket which is installed at the condenser section to remove heat. The adiabatic section of the CEOHP is insulated. The amount of heat applied to the CEOHP is controlled by a variac.

The temperatures at various points are measured and recorded by data loggers (Comark, C8510, and 0.1°C). The flow rate of the cooling medium is measured by a rotameter (Platon, PGB411, and 0.1 lit/min).

In the experiment, a set of 27 CEHOPs was built in combination of following dimensions: internal diameters of 0.66, 1.06 and 2.03 mm, number of meandering turns of 5, 10 and 15, and evaporator lengths of 50, 100 and 150 mm. In all cases, the length of the adiabatic and condenser sections were set equal to the evaporator length to eliminate the heat transformer effect. The CEOHP was set to operate in bottom-heated-mode vertical orientation. Two working fluids, HP62, also known as R-404a, and MP39 were employed in the experiment. Twelve Chromel-Alumel thermo-couples (Omaga, K-type, 0.5°C) were attached on the outer surface of the tubes : ten at the middle of the evaporator section and two at the middle of the adiabatic section. Additional four thermocouples were used to measure the temperature of the cooling medium: two at the inlet and two at the outlet section of the condenser.

The steps for finding the heat flux at critical state were as follows. The heat was gradually added to the CEHOP at the evaporator section in small step. In each step, the temperature at the adiabatic section was controlled at 60±5°C by adjusting either the temperature of the cooling medium or its flow rate into the condenser section. Time was given for the temperature to settle down to steady-state. At steady state, the temperature reading at each point on the evaporator section was observed. If all readings stayed relatively close, the heat was added. These steps were repeated until the jump in temperature at one or more points at the evaporator section was detected. This means the CEHOP started to operate beyond the critical condition. The critical heat flux was taken as the heat flux as a step before the critical condition occurred. It was calculated by the calorific method from the heat being removed from the condenser section.

3. DATA AND DISCUSSION

3-1 Temperatures at Critical State

Figure 4 shows a profile sample of ten temperature readings at the evaporator section from the experiment data obtained from the CEOHP with D=2.03 mm., L_e=15 mm, turn=15 and using HP62 as a working fluid. The heat supplied to the evaporator section was increased with time in small step. At low temperature, all readings seemed to be in order. When the supplied heat was large enough, the CEOHP reached the critical state. At critical state, it can be seen that most of the readings rose rapidly. This means, according to our hypothesis, the vapor pressure at the evaporator section was so high that the liquid slug could not return from the condenser section. Consequently, the amount of liquid in the evaporator section was not enough and dryout occurred causing the temperature to rise up quickly. The corresponding heat flux profile is shown in Figure 5. It is evident that the maximum heat flux occurred at the critical state and dropped beyond it.

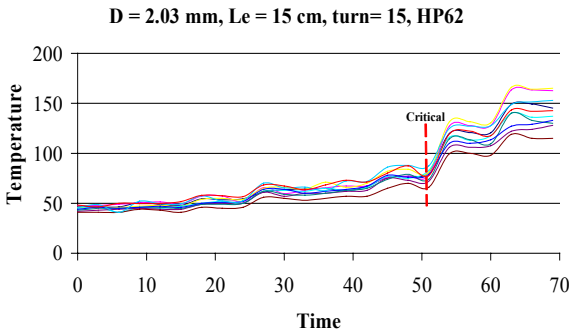


Figure 4 Temperature profile at evaporator section (D=2.03 mm., L_e = 15 mm, turn = 15, HP62)

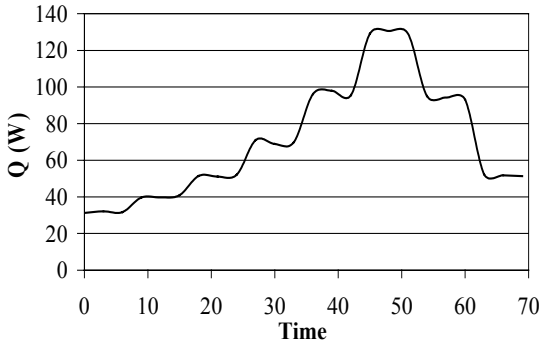


Figure 5 Heat transfer rate profile (D=2.03 mm., L_e = 15 mm, turn = 15, HP62)

It should be mentioned that of 27 CEOHPs that were prepared, data from only 12 of them give meaningful results. Those from the others (D=0.66 mm with all L_e and D=1.06 mm with L_e=50 and 150 mm) transferred very small amount of heat which was not higher than the accuracy of the measurement. This may be due to the combination of the selected dimension parameters and the working fluids employed. Data corresponding to this set are not concluded in the results that will be presented in the next section.

3-2 Effects of Aspect Ratio

Figure 6 shows the relationship between the critical heat flux and the aspect ratio (L_e/D) of the CEOHP with MP39 and HP62 as working fluids. The aspect ratios shown in the figure correspond to the evaporator length of 50, 100, 150 mm and the inner diameter of 1.06, 2.03 mm. All available data are included except the ones from CEHOPs with inner diameter of 0.66 mm due to the reason mentioned earlier.

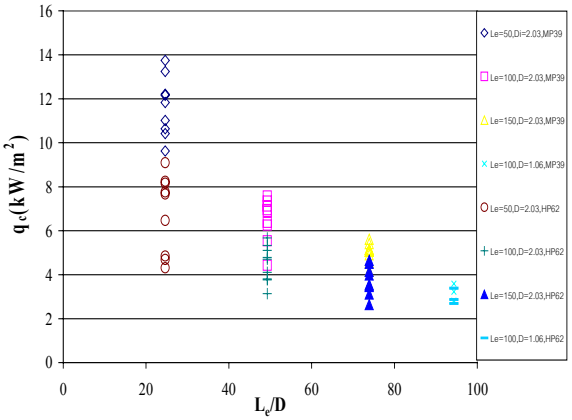


Figure 6 Relationship between critical flux and aspect ratio

From the figure, it can be seen that there is a trend in the relationship between the critical heat flux and the aspect ratio. The higher the aspect ratio the lower the critical heat flux value. From the available data, the critical heat flux decreased from about 10 kW/m^2 to about 3 kW/m^2 as the aspect ratio increased from 24 to 94 respectively.

3-2 Effects of Bond Number

The corresponding to diameter value can be represented by a dimensionless group of Bond number (Bo) which is a ratio of working fluid's buoyancy force to the surface tension force of the vapor bubble generated inside the CEOHP. Figure 7 shows the relationship between the critical heat flux and the Bond number. The Bond numbers in the figure correspond to CEHOP with inside dimension of 1.06 and 2.03mm with MP39 and HP62 employed as working fluids.

From the figure, the data points seem to scatter and there seems to be no clear conclusion on the relationship. This may be due to the fact that the number of data points available is too small since some of the data values do not pass the accuracy of the measurement and can not be included.

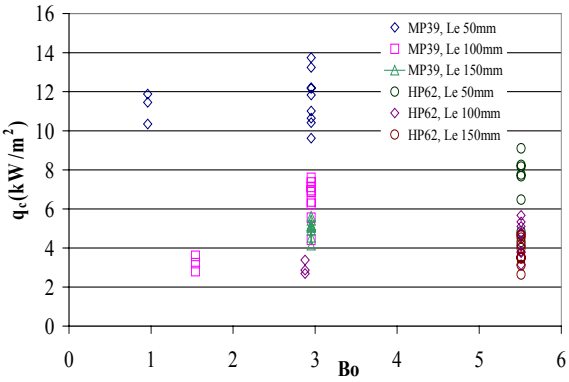


Figure 7 Relationship between critical heat flux and Bond number

For more insight into the relationship, more data points are needed. Either new conditions on dimension parameters should be set or other types of working fluid should be employed for additional data. However, the data seem to be orderly grouped and may be used for finding the correlation.

4. CONCLUSION

The effects of the aspect ratios and Bond numbers on the critical heat flux of the CEHOPs employed with two types of non-CFC refrigerant blend, MP29 and HP63, were studied in this paper. It can be concluded from the experimental results that the aspect ratio affects the critical heat flux in that as the aspect ratio increases, the critical heat flux decreases. From the available data obtained, the effects of Bond number on the critical heat flux with the chosen dimension parameters and working fluids are not conclusive. However, there seem to be an order in the data within the same group.

Acknowledgement

This research is supported by the Thai Research Fund agency under the contract no. BRG/06/2545.

Nomenclature

D	internal diameter, mm.
L_e	length of evaporator section, m
n	number of meandering turn
Q	heat transfer rate, W
q_c	critical heat flux, W/m^2
T_e	wall temperature at evaporator section

References

1. Akachi, H., Polasek, F., and Stulc, P.,1996 , "Pulsating Heat Pipe", Procs. of the 5th International Heat Pipe Symposium, Melbourne Australia.
2. Dunn, P. D. and Reay, D. A., 1982, *Heat Pipe*, Pergamon Press Ltd., 3rd edition.
3. Faghri, A., 1995, *Heat Pipe Science and Technology*, Taylor & Francis Pub.
4. Charoensawan, P., Terdtoon, P., Kamonpet, P., Ingsuwan, P., and Groll, M., "Effects of Inclination Angles, Filling Ratios and Total Lengths on Heat Transfer Characteristic of A Closed–Loop Oscillating Heat Pipe", 2000, Procs. of the 6th International Heat, Pipe Symposium. Chiang Mai Thailand.
5. Lin, L., Ponnappan, R. and Leland, J., 2000, "Experimental Investigation of Oscillating Heat Pipe", Procs. Of 35th Energy Conversion Engineering Conference and Exhibit, Vol. 2.
6. Maesawa, S., Gi, K.Y., Minamisawa, A., and Akachi, H., 1996, "Thermal Performance of Capillary Tube Thermosyphon", Procs. of the IX International Heat Pipe Conference, Albuquerque, USA. Vol. II.
7. Miyazaki, Y., Polasek, F. and Akachi, H., 2000, "Oscillating Heat Pipe with Check Valves", Procs. of the 6th International Heat Pipe Symposium, Chiang Mai, Thailand.
8. Ritidech,S., Terdtoon,P., Tantakom,P., Murakami,M., and Jompakdee,W., 2000, Effect of Inclination Angles, Evaporator Section lengthes and Working Fluid Properties on heat Transfer Characteristics of A Closed-End Oscillating Heat Pipe., Procs. of the 6th International Heat, Pipe Symposium. Chiang Mai, Thailand.

Experimental Study on Hydration Heat Control of The Mass Concrete Using Oscillating Capillary Tube Heat Pipe

*Jong Soo Kim, Bui Ngoc Hung, Tae Hoon Kim, Jae Hong Kim and Soo Jung Ha

**Myung Sik Kim,

*Faculty of Mechanical Engineering, Pukyong National University, Yongdang-dong, Namgu, Busan, Korea, 608-739

Tel : 82-51-620-1502, Fax : 82-51-611-6368, E-mail : jskim@pknu.ac.kr

**Department of Civil Engineering, Pukyong National University, Yongdang-dong, Namgu, Busan, Korea, 608-739

Abstract

In process of reinforced concrete(RC) box structures, the heat of hydration may cause serious thermal cracking problems.

In order to eliminate hydration heat of mass concrete, this paper reports results of hydration heat control in mass concrete using the OCHP(Oscillating Capillary tube Heat Pipe). Recently OCHP is drawn special attention from these points of low cost as well as short construction schedule for the manufacturing of heat exchanger, flexibility, simplification and high performance. There were three RC box molds (120 cm ×120 cm ×120 cm) which show a difference as compared with each other. One was not equipped with OCHP. While others were equipped with OCHP and these were cooled with air natural convection and spraying water respectively. The OCHP was composed of copper pipe with 12 turns (O.D 4 mm, I.D 0.28 mm). The working fluid was R-22 and its charging ratio was 30 (Vol. %). In order to analyze the distribution of temperature and index figure of the thermal crack in sequential placement of massive concrete, we used HYCON of computer program. As a result of the experiment, the peak temperature decreased about 15.6~23.4℃ than the general specimen and the probability of thermal crack generated in mass concrete decreased up to 0%.

Key words : Oscillating capillary tube heat pipe, Heat of hydration, Mass concrete, Thermal crack

1. INTRODUCTION

1.1 Objective and background of the study.

Heat generated for the chemical reaction between cement and water in the hardening process of concrete is called Hydration Heat. Hydration Heat depends on the kind of cement and chemical composition of concrete materials. And according to reference, about 353.6 kJ/kg Hydration Heat is generated in the hardening process of cement [1].The temperature rise due to this Hydration Heat generation affects the manifestation of intensity and the quality of a concrete. In addition it causes cracks.

Generally thin and polyhedral structures have no problems with temperature differences because those structures easily remove hydration heat from the inside to the outside. But in case of massive concrete structures, which have thick beams (more than 0.8~1.0m), Hydration Heat is caused a temperature difference between concrete inside and on the surface. So far only dams are classified as mass concrete, so their construction countermeasure is being considered as mass concrete. Recently the use of cement increased according to the scale and the high strength of the concrete structures. So, large structures such as footing beams, piers, reactor hangars and LNG tanks were built in abundance. When these structures were built, cracks in the concrete arose from Hydration Heat. Therefore, the question of the safety of structures remains unsettled.

Accordingly in this study, we would like to propose the new cooling method of mass concrete using the OCHP and the basic design data [2].

1.2 Previous study

So far, methods to remove Hydration Heat can be classified into two main categories: pre-cooling and post-cooling. Pre-cooling is the method which prevents cracks by reducing the concrete placing temperature after the concrete is placed. It gives a general name to the temperature reduction management from the material temperature of concrete to concrete mixture temperature and concrete placing temperature. This pre-cooling is basically divided into two methods. The first method is individually cooling the concrete materials using the cooling mediums of ice, cold water, cold blasts and liquid nitrogen. The second method is directly cooling concrete in a condition not set after production or during production.

Post-cooling is an effective means of reducing the Hydration Heat of concrete by arranging pipes in structures before the concrete placement and circulating cooling water in pipes immediately after the concrete is placed [3].

But both methods (pre-cooling and post-cooling) have the problems of construction, construction period and cost. The experiment of the removal of Hydration Heat using an Oscillating Capillary Tube Heat Pipe has never been studied in or out of the country so far.

2. EXPERIMENTAL SETUP AND METHODS

2.1 Experimental setup

The sketch of the experimental setup used in this study is shown in Fig. 1. The condition of the experiment (Fig. 1) is classified into three methods. The first method (a) is a general specimen, the second method (b) is the specimen equipped with the heat pipe. The third method (c) is spraying water on the surface of the condensing part of the heat pipe. Each temperature is measured by the data logger(DR-230, Yokogawa company) connected a T-type thermocouple [4]. The mold is made of a veneer board which is 125cm × 125 cm × 125 cm in size to secure the placing space of 120 cm × 120 cm × 120 cm. The top, bottom and sides of the specimen were insulated with 50 mm Styrofoam plate. The Oscillating Capillary Tube Heat Pipe is 12-turns copper tube which is 4 mm in outer diameter and 2.8 mm in inner diameter. It is adhered to the specimen in three rows. The vertical length of The Oscillating Capillary Tube Heat Pipe is 190 cm : the evaporative part of 120 cm is laid within the concrete structure and condensing part 70 cm is exposed outside the structure. As the heat transfer area ratio is 1.7 : 1, each heating surface area is 0.41 m^2, 0.24 m^2. The working fluid is R-22 and

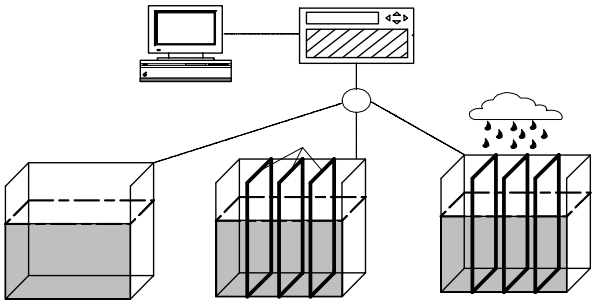


Fig. 1 Schematic diagram of experimental apparatus

Table. 1 Thermal Properties of Concrete [5]

Property \ Material	Concrete
Density(kg/m^3)	2300
Specific heat(kJ/kg·K)	1.046
Thermal conductivity(W/kg·K)	2.67
Design strength(kg/ cm^2)	210
Cement unit weight(kg/m^3)	313



(a) (b) (c)

Fig. 2 Photograph of test section

the charging ratio inside heatpipe is 30(Vol.%) [6].

2.2 Experimental methods

This study was mainly experimented about the temperature rise and distribution of concrete structures during hydration of concrete. Particularly we tried to interpret temperature cracks affected by internal restriction. We separately arranged 6 thermocouples in the general specimen and 11 thermocouples in the two

specimens equipped with the heat pipe like Fig. 3 in consideration of symmetry because the specimen is square [7]. After the concrete placement, temperature was measured during 60 hours at 10-minute intervals. The weight ratio of water to cement is 53% and cement unit weight is 313kg/m^3.

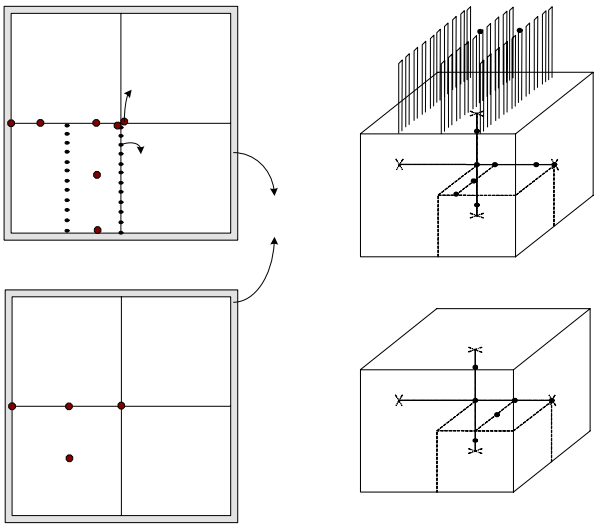


Fig. 3 Thermo-couple location in the concrete

3. RESULTS AND DISCUSSION.

3.1 Measurement results of mean temperature, overall heat transfer coefficient and hydration heat.

The variation of mean temperature in each time of the three experimental conditions is shown in Fig. (4). The peak temperature of method (a) appeared in 31 hours, that of method (b) and (c) appeared in 18 hours. The peak temperature reduced approximately 15.6℃ in the second method and reduced approximately 23.4℃ in the third method than that of the specimen.

Fig. 6 is a graph comparing the generation of calories per hour in each experimental condition. The generated heat rate of concrete was calculated by Eq. (1).

$$Q_m = m \cdot c \cdot (T_f - T_i) \qquad (1)$$

In Eq. (1), Q_m is measured heat rate in method (a), (b), (c) and the T_f, T_i is the mean temperature of each experimental condition. As a result of the Eq. (1), total measured heat transfer rate generated in the general specimen (a) was 125,241 kJ and was 65385 kJ in method (b) and was 34357 kJ in method (c). In total, in case of using heat pipes we could remove 47.8% heat and in the case of spraying water we could remove 72.6% of

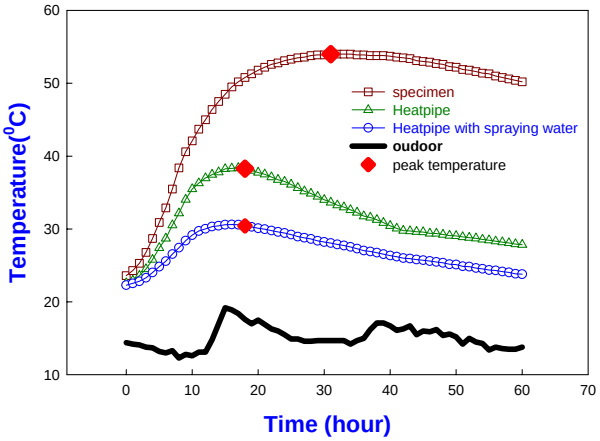


Fig. 4 Variation of mean temperature in the concrete

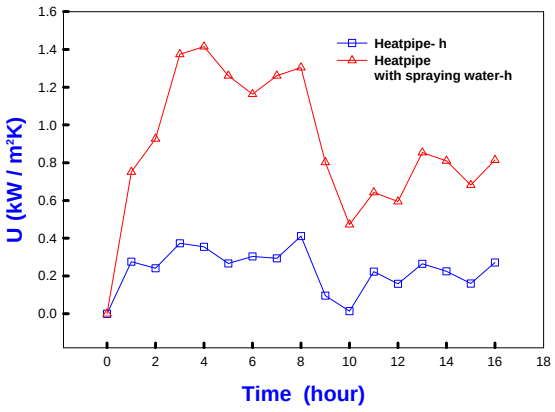


Fig. 5 Variation of overall heat transfer coefficient [9]

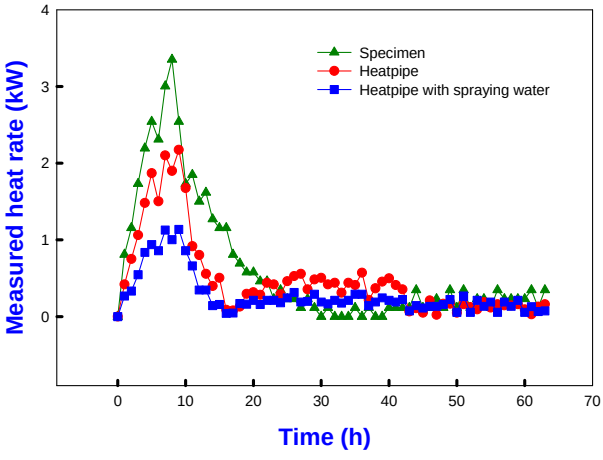


Fig. 6 Variation of measured heat rate

Styrofoam plate

generated heat rate. Fig. 5 shows the overall heat transfer coefficient of condensing part in the case of cooling method (b), (c). Therefore the heat transfer coefficient of method (b) is 233 W/ m^{2}K and that of method (c) is 889 W/ m^{2}K [8].

Table. 2 The comparison between Pipe Cooling and Heatpipe Cooling [10)]

	Pipe Cooling	Heatpipe Cooling	Heatpipe Cooling with spraying water
Temperature Lapse Effect	9~12℃	15.6℃	23.4℃
Crack initiation probability (The index figure of thermal crack)	45% (0.95~0.97)	11% (1.351)	0% (2.27)
Installation	Sufficient amount of water supply. The difficulty of construction. (Concrete has to be kept in pipe after placement.)	No water supply. Simple and easy construction.	A small amount of water supply. Simple and easy construction.

The overall heat transfer coefficient is calculated by Eq (2).

$$U = Q_c / A \cdot (T_{sur} - T_o) \qquad (2)$$

In Eq. (2), Q_c is the cooled heat transfer rate measured in every hour. T_{sur} is surface temperature of heatpipe and T_o is outdoor temperature.

3.2 The analysis for the crack with respect to Hydration Heat

We used a program called HYCON.FOR, developed in The Korean Advanced Institute of Science and Technology, to analyze of the concrete crack in this study.

The index figure of the thermal crack is calculated by Eq. (3) below.

$$\text{The index figure of the thermal crack} = 15/i \qquad (3)$$

i = The gap between the inside and the outside when the internal temperature is the highest(℃).

A general specimen shows the surface temperature of 36℃, the index of the temperature cracks of 0.833. Method (b) shows the surface temperature of 27.3℃, the index of the temperature cracks of 1.351. Method (c) shows the surface temperature of 24℃, the index of the thermal cracks of 2.27. It is possible to get the index figure of the thermal cracks with Fig.7. It shows 63% in the case of general specimen, 10% in the case of method (b), 0% in the case of method (c). Generally if crack is prevented, the index figure of thermal crack must be more than 1.5. Therefore the index of thermal crack of method (b), (c) using The Oscillating Capillary Tube Heat Pipe is very suitable in preventing generation of cracks.

3.3 The analysis and comparison between Pipe Cooling and Heatpipe Cooling.

The temperature lapse effect of conventional pipe cooling generally appeared in an average of 9~12℃, but the temperature lapse effect using heatpipe cooled with air appeared 15.6℃ and condition using heatpipe cooled with water appeared 23.4℃ [11)]. Also crack initiation probability of heatpipe was much lower than pipe cooling. A installation after pipe cooling is difficult because concrete has to grout in pipe, but it is simple and easy in condition of heatpipe because heatpipe is laid in that condition. Pipe cooling is compared with heatpipe in Table.2.

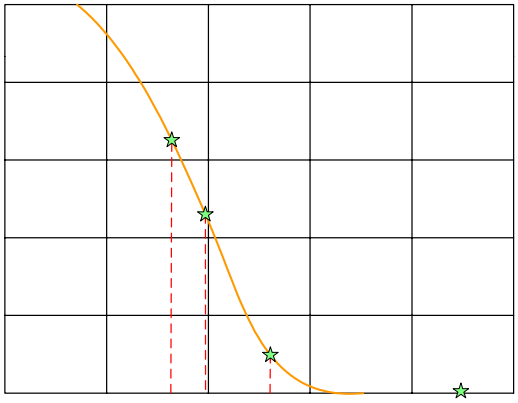


Fig. 7 The index figure of the thermal crack [12)]

4. CONCLUSIONS

We have studied performance of removing Hydration Heat and application probability using The Oscillating Capillary Tube Heat Pipe to mass concrete. We have found the following conclusions.

(1) The peak temperature in mass concrete with the heat pipe decreased 15.6℃, approximately 23.4℃ in the case of spraying water on the surface of the heat pipe than method (a).

(2) The index figure of the thermal crack with the heat pipe decreased 50%, and 63% in the case of spraying water on the surface of the condensing part of the heat pipe.

(3) Cooling performance of method (c) is one and a half times superior to that of method (b).

(4) We are convinced that performance of removing Hydration Heat and application probability using the Oscillating Capillary Tube Heat Pipe are good. It is possible to prevent thermal crack in the concrete as well.

Nomenclature

Q : Heat transfer rate [kW]
C : Specific heat [kJ/kg·K]
m : Mass of Concrete [kg]
T : Temperature [℃]
U : Overall heat transfer coefficient [W/ m^2·K]

Subscripts

hs: heatpipe surface
o : outdoor
f : final
i : initial
m : measured
c : cooled

References

1. Kim Jin-Keun, Noh Jae-Ho, Park Yon-Dong, “Hydration Heat Characteristics of Cement and Concrete”, Journal of the Korea Concrete Institute Vol. 7 No.3, 1995, pp 211-219

2. Ha Soo-Jung, “Development of Micro Cooling system for Telecommunication system using Oscillating Heatpipe”, Master thesis of Pukyong National University, 2003, pp 8~15
3. Kim, J, G, “A study on Technology for the Reduction on hydration heat in mass concrete structure”, KAIST, Ton gyang Inc. RP 39-52
4. An Sung-Jun, “Study on Optimal Thermal Design of Telecommunication Equipment using of Oscillating Capillary Tube Heat Pipe”, Master thesis of Pukyong National University, 2001, pp 23~28
5. Ministry of construction and Transportation of the Korea, Concrete Standard Specification, 2000
6. Lee Wook-Hyun, “Study on Heat Transfer and Flow Characteristics of Oscillating Capillary Tube Heat Pipe”, Doctor thesis of Pukyong National University, 2000, pp 8~14
7. Yunus A. Cengel, “Heat Transfer(A Practical Approach)”, Mc Graw Hill, 1997, pp 294-320
8. Frank P. Incropera, David P. Dewitt, “Introduction to Heat transfer(2^{nd} ed.)”, John Wiley & Sons. Inc, 1990, pp 7~11
9. Frank Kreith, Mark S. Bohn, “Principles of Heat Transfer-6^{th} ed”, Thomson, 2002, pp 74~83
10. Kim Sang-Chel, “Thermal Analysis Associated with the Application of Pipe Cooling System to a Massive Concrete Structure”, Proceeding of the Korea Concrete Institute 1998 autumn annual conference, 1998, pp 922~927
11. Park Chan-Kyu, “Hydration Heat Control with Closed Loop Pipe Cooling System”, Proceeding of the Korea Concrete Institute 2001 autumn annual conference, 2001, pp 403~408
12. A. Ghali. R. Faver, “Reinforced Concrete Structure”, pp 509-513

Internal Flow Patterns of a Closed-End Oscillating Heat Pipe at Normal Operating Condition: Effect of Internal Friction

N. Srihajong, P.Terdtoon, P. Kamonpet, W.Jompakdee and R Attabhanyo*

Department of Mechanical Engineering, Faculty of Engineering, Chiang Mai University, Chiang Mai, Thailand.
Tel: +66-53-944151, Fax: +66-53-226014 and E-mail Address: g4566427@cm.edu
*Department of Food Science and Technology, Faculty of Agro-industry, Chiang Mai University, Chiang Mai, Thailand.

Abstract

This paper aims at studying of the effect of internal wall friction on the inside flow patterns of closed-end oscillating heat pipe (CEOHP) at normal operating condition. Glass tube was used as a container of the heat pipe with the equaled length of evaporator, adiabatic and condenser sections of 50 mm. The internal diameter was 2 mm with 28 turns. The evaporator section was heated by silicone oil and the condenser section was cooled by distilled water. R123 was used as working fluid with filling ratio of 50 % of internal volume of tube. The heat source temperatures were controlled at 60, 70 and 80^{o}C while the heat sink temperature was controlled at 20^{o}C. The inclination angles were 0 - 90 degree from horizontal axis. The internal friction factors of the tubes were subsequently controlled at 0.00074 and 0.004. The temperatures at adiabatic section and the inlet - outlet of distilled water at condenser section were recorded. The photographs of flow patterns at evaporator section at specified time were recorded by digital camera and three video cameras were used to observe the flow patterns at the evaporator section, condenser together with adiabatic sections, and total part of CEOHP. It is found from the experiment that, as the heat source temperature increases, the main flow patterns are slug flow, the length of vapor bubble decreases as the heat transfer increases. The effect of inclination angle increases from 0-50 degree the internal flow patterns remain at the slug flow, the length of vapor bubble decreases but the heat transfer increases. However, as the angles increases further to 90 degree the flow patterns still be slug flow but the heat transfer gradually decreases. As the internal friction factor increases, the heat transfer rate increases the length of vapor bubble decreases. The internal flow patterns, however, remain at slug flow.

Key words: Closed-end oscillating heat pipe, flow patterns, internal friction.

1. INTRODUCTION

Akachi et al. (1996) [1] discovered that the oscillating heat pipe (OHP), which was a serpentine structure of closed-end type can transport heat without wick structure to return condensed liquid from condenser to evaporator section. The heat, however, was transported from evaporator to condenser sections by self–excited oscillation, occurred by pressure driving force from nucleate boiling and working fluid condensation in tube. The working fluid in OHP oscillates in the axial direction by the contraction and expansion of liquid and vapor, these contraction and expansion are due to the pressure wave caused by the formation and extinction of bubbles [3]. Among 3 types of OHP [4], closed-end OHP, or CEOHP, is the simplest type with magnificent heat transfer characteristics and the oscillation inside the CEOHP heat pipe occurs easily at small inclination angle [2] and small–medium fill charge ratio [2,5]. The heat transfer characteristics of the CEOHP strongly depended on its internal flow patterns [3]. Furthermore, the friction of internal wall can dramatically affect the internal flow patterns, and, accordingly, the heat transfer characteristic. In order to clarify such relationship this study aims at visual study of the effects of heat source temperature, inclination angles and internal wall friction on internal flow patterns of CEOHP.

2. EXPERIMENTAL APPARATUS AND METHODS

The experimental setup, which is schematically shown in Figure1, consists of the CEOHP with the length of evaporator, adiabatic (which is equal to condenser sections) is 50 mm.

It was made of the Pyrex glass tube with the internal diameter of 2.03 mm, outside diameter of 6 mm, with the selected meandering turn of 28. The evaporator section was heated by silicone oil which was circulated from the hot bath (HAAKE, HS891000). The condenser section was cooled by distilled water which was circulated from the cold bath (Bitzer D7032, with an operating rang of –20 to 20°C). The heating and cooling jackets were made of high temperature glass to ensure the best visualization.

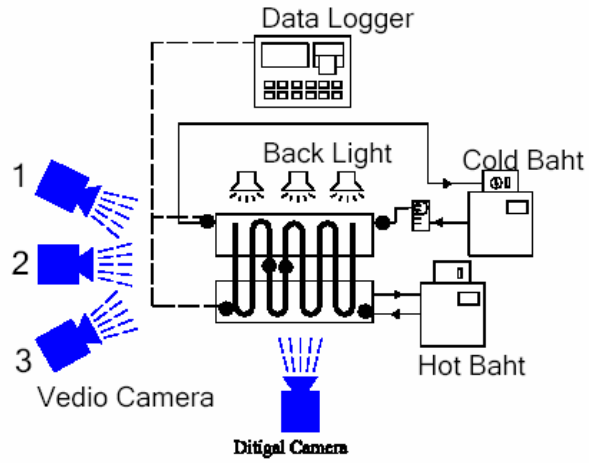


Figure 1: Experimental setup

The mass flow rate inside the cooling jacket was measured by rotameter (Platon, PGB411) and 4 points of thermocouples (OMEGA K type) were installed at the inlet and outlet of condenser section to determine the heat transfer rate. The temperature probes were installed 2 points at high temperature glass of evaporator, 2 points condenser sections, and 1 point for ambient respectively to determine the heat loss. The temperature recorder (Comark, C8510, with ±1°C accuracy) was used to monitor all temperatures at specified time. Moreover, 2 points of the thermocouple were installed at the middle position of the 43th and 44th tube of adiabatic section starting from the left side. These two thermocouples were inserted inside the CEOHP by the specially designed probe. The thermocouples were connected to the chart recorder (Yokogawa, 4152 type, with ±0.5°C accuracy) to measure the amplitude and oscillating of temperature of the working fluid at adiabatic section from which the internal saturated pressure can be observed. The internal friction of the CEOHP tube was accurately obtained by means of the apparatus shown in Figure 2. The air was passed through the long-serpentine CEOHP and the inlet, as well as outlets velocity with their pressure drop were simultaneously recorded using the anemometer (Testo-435 and Testo-454). The internal friction was obtained by the single-phase Moody's equation of friction. During the experiment the angle was set at 90 degree from horizontal plane. Three video cameras (Sony CCD-TR618E) were used to continuously record the flow patterns at the evaporator section, condenser together with adiabatic sections, and total part of CEOHP. The digital camera (Sony DSC-S75) was used to record flow patterns of evaporator section at specified times.

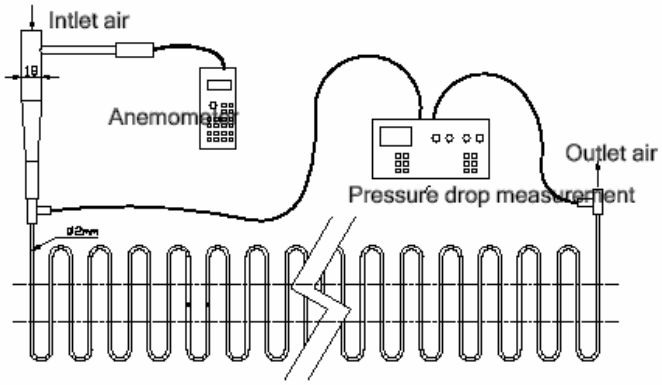


Figure 2: Measurement of velocity and pressure drop

The experiments were totally conducted with the controlled parameters as follow:

- The internal friction factors of the tubes were 0.00074 and 0.004.
- The working fluid was R123.
- The fitting ratio was 50% of total volume in capillary tube.
- The heat source temperature, Tso, were 60,70 and 80°C and the heat sink temperature, Tsi, was 20°C.
- The inclination angles were 0, 30, 50, 70, and 90 degree from horizontal position.

The experiment was conducted as follows; firstly, the CEOHP was filled with the working and set into the test rig. The temperature of the hot and cold baths were set at the required values, and the hot and cold fluids were supplied to the jackets of both the evaporator and condenser section. After a steady state was reached, continuous movies were recorded by three video cameras while photographs were taken at specified times by digital camera. In the mean time, temperatures and heat transfers were monitored. The temperature oscillation of working fluid and amplitude were recorded to briefly observe the pressure oscillation of working fluid. Then the heat source temperatures, inclination angles, internal wall frictions were varied according to the required conditions.

3. RESULTS AND DISCUSSION

Visualization at the evaporator section was concentrated since the major phenomena occurred in this part, the flow patterns of whole part of CEOHP which cannot be presented in the paper could, however, be observed by video movie. Figure 3 shows the inlet-outlet flow directions of silicon oil at evaporator section and all the experimental of experiment results will be referred to this figure. The vapor bubble length was measured as the length of the two ends of vapor bubble at specified time, and the vapor bubble edge is observed with solid lines in the working fluid in liquid phase. The expanding and shrinking ratio (in percentage) of vapor bubble were measured in comparison with the original length of vapor bubble at the original time. It can be concluded from the experimental results as follows;

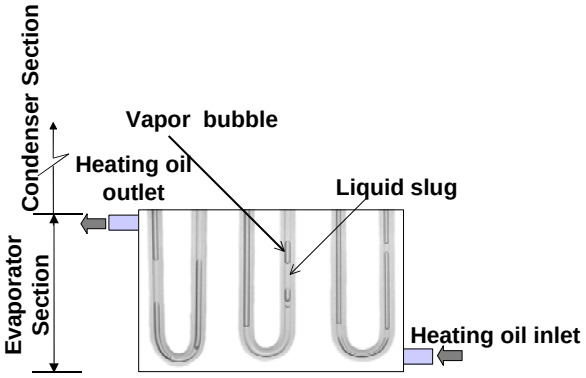


Figure 3: The inlet-outlet flow directions of silicon oil at evaporator section

3-1 Effects of the Temperature of Heat Source

Figure 4(A)-4(C) show the flow patterns of the heat source temperature of 60°C to 80°C, and the control parameters are friction factor of 0.0004, inclination angle of 50 degree.

At low temperature. In the case of low temperature, it can be concluded from the experimental data that, with the temperature of 60°C, slug flow is the main flow patterns of CEOHP at low temperature. Although, the slug flow can be mostly observed, the bubble flow happens occasionally with the frequency of 1-2 times per second. Few nucleation sites of 2-3 sites can be also seen at the bottom part of evaporator section. After evaporation the vapor bubbles merge together to form a long vapor slug with the average length of 5-100 mm. These vapor slugs subsequently occupy in both bottom and middle parts of evaporator before moving up to the condenser section where they collapse and the heat is released. Almost of the vapor slugs tend to move to the condenser section of the left glass tube with very few slugs move in the right tube (about 43%). It can be explained that, the heat transfer is absorbed by the vapor bubble originated in the evaporator section and the latent heat is the main mechanism. Most of the bubbles that flow into the condenser section collapse there where the absorbed latent heat is released, with the heat transfer of 242 W. The heat transfer is, thus, transferred by this mechanism. The frequency and amplitude of temperature oscillation of working fluid that indicate the working pressure oscillation are 0.45 cycle/sec and 4.5°C, respectively.

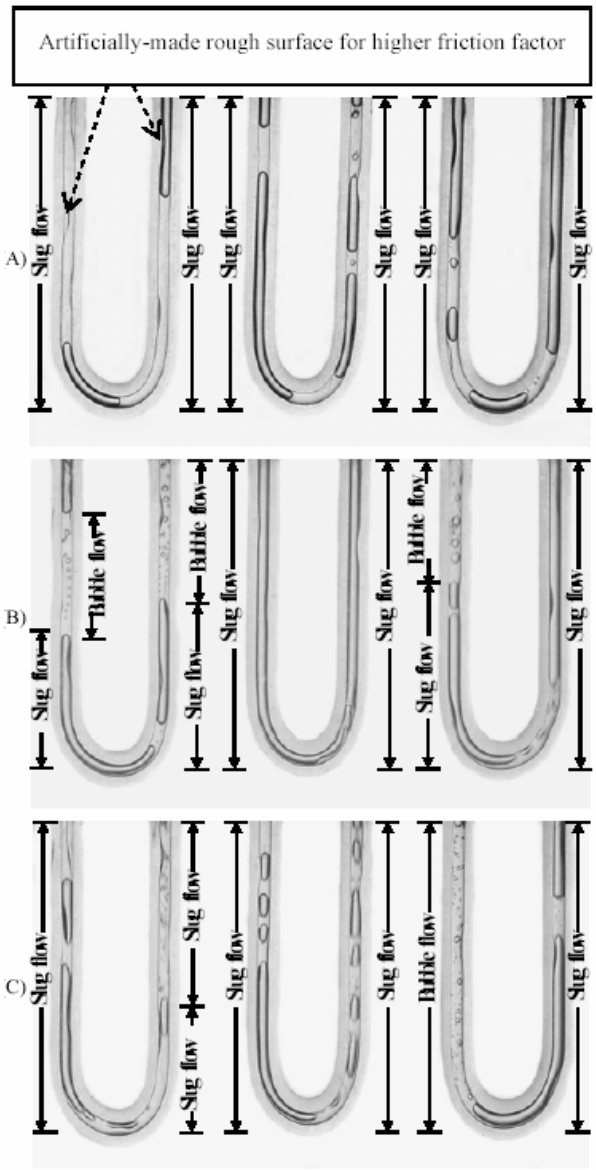


Fig	Tso °C	Tsi °C	Flow pattern	L_v mm	Frequency cycle/sec	Amplitude °C	Q W
(A)	60	20	Slug	5 - 100	0.45	4.5	242
(B)	70	20	Slug	3 – 80	0.48	3.0	283
(C)	80	20	Slug and Bubble	3 - 65	0.56	2.5	472

Figure 4: Flow patterns at any heat source temperatures of the CEOHP (f = 0.004, β = 50°)

At moderate temperature. It can be concluded from the experimental data that, with the temperature of 70°C, the internal flow patterns will unchanged with remain at the slug flow with moderate temperature. Although, the slug flow can be mostly observed, the bubble flow happens occasionally with the frequency of 2-3 times per second. The nucleation sites of 5-6 sites can be also seen at the bottom and middle parts of evaporator section. After evaporation the vapor bubbles merge together to form a long vapor slug with the average length of 3-80 mm. These vapor slugs subsequently occupy in the bottom to upper parts of evaporator before moving up to the condenser section where they collapse and the heat is released. Almost of the vapor slugs tend to move to the condenser section of the left glass tube with slugs move in the right tube (about 49%), the frequency and amplitude of temperature oscillation of working fluid are 0.48 cycle/sec and 3°C, respectively.

At higher temperature. It can be concluded from the experimental data that, with the temperature of 80°C, the internal flow patterns will unchanged with remain at the slug flow with higher temperature. Although, the slug flow can be mostly observed, the bubble flow happens occasionally with the frequency of 4-5 times per second. The nucleation sites of 8-9 sites can be also seen at the bottom and middle parts of evaporator section. After evaporation the vapor bubbles merge together to form a long vapor slug with the average length of 3-65 mm. These vapor slugs subsequently occupy in the bottom to upper parts of evaporator before moving up to the condenser section where they collapse and the heat is released. Almost of the vapor slugs tend to move to the condenser section of the left glass tube with slugs move in the right tube (about 57%), the frequency and amplitude of temperature oscillation of working fluid are 0.56 cycle/sec and 2.5°C, respectively.

It can be found that, when the heat source temperature increases from 60°C to 80°C, the length of vapor bubbles decreases of 20-30 mm or 40% of the original vapor length, bubble flow will increasingly occur. Furthermore, the temperature oscillation of working fluid increases from 0.45 to 0.56 cycle/sec as the amplitude of temperature decreases from 4.5 to 2.5°C. And the heat transfer increases from 242 to 472 W. This may be since when the heat source temperature increases, the pressure at the evaporator section increases and the vapor bubble is driven to move up extremely. Thus the vapor bubble splits in to the small vapor bubble that move to the condenser section for transferring higher latent heat. Therefore, the high temperature boiling in confined channel, therefore high heat transfer. But at low temperature, boiling is pool boiling, therefore low heat transfer. These findings agree with the results of Gi et al. (1999) [2]. It was seen that, when the temperature of heat source increased, the length of vapor bubbles decreased, and slug flow is the main flow pattern in the CEOHP.

It can be concluded that, the heat source temperature increases, the main flow patterns are slug flow, the length of vapor bubble decreases as the heat transfer increases.

3-2 Effects of the Inclination Angle

At an inclination angle of 0 degree. Figure 5(A) shows the internal flow patterns of CEOHP with an inclination angle of 0 degree, heat source temperature of 60°C, friction factor of 0.00074. It can be concluded from the experimental data that, with the inclination angle of 0 degree, slug flow is the main flow patterns of CEOHP without any bubble flow. Few nucleation sites of 1-2 sites can be also seen at the bottom part of evaporator section. After evaporation the vapor bubbles merge together to form a long vapor slug with the average length of 60-100 mm. These vapor slugs subsequently occupy in both bottom part of evaporator before moving up to the condenser section where they collapse and the heat is released. Almost of the vapor slugs tend to move to the condenser section of the right glass tube with slugs move in the lift tube (about 36%). It can be explained that, the heat transfer is absorbed by the vapor bubble originated in the evaporator section and the latent heat is the main mechanism. Most of the bubbles that flow into the condenser section collapse there where the absorbed latent heat is released, with the heat transfer of 102.3W. The heat transfer is, thus, transferred by this mechanism. The frequency and amplitude of temperature oscillation of working fluid are 0.51 cycle/sec and 3.5°C, respectively.

At an inclination angle of 50 degree. Figure 5(B) shows the internal flow patterns of CEOHP with an inclination angle of 50 degree, heat source temperature of 60°C, friction factor of 0.00074. It can be concluded from the experimental data that, with the inclination angle of 50 degree, slug flow is the main flow patterns of CEOHP. Although, the slug flow can be mostly observed, the bubble flow happens occasionally with the frequency of 5-6 times per second. The nucleation sites of 5-6 sites can be also seen at the bottom part of evaporator section. After evaporation the vapor bubbles merge together to form a long vapor slug with the average length of 5-40 mm. These vapor

slugs subsequently occupy in both bottom and middle parts of evaporator before moving up to the condenser section where they collapse and the heat is released, with the heat transfer of 223W. Almost of the vapor slugs tend to move to the condenser section of the left glass tube with very few slugs move in the right tube (about 53%). The frequency and amplitude of temperature oscillation of working fluid are 0.87 cycle/sec and 1.5°C, respectively.

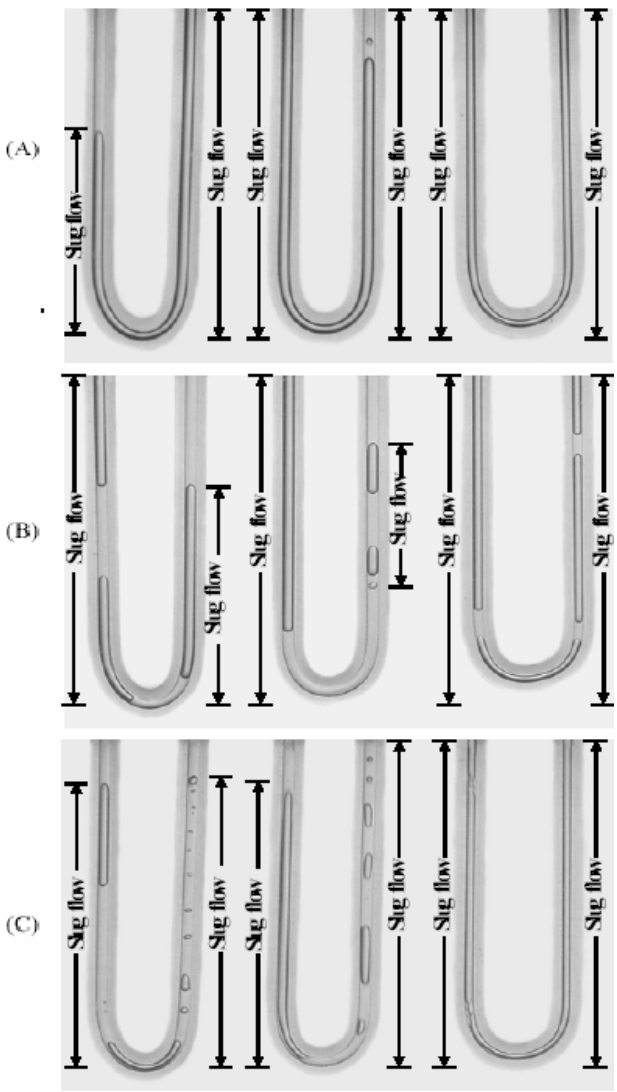


Fig	β deg	Flow pattern	L_v mm	Frequency cycle/sec	Amplitude °C	Q W
(A)	0	Slug	60 - 100	0.51	3.5	102.3
(B)	50	Slug	5 - 40	0.87	1.5	223.0
(C)	90	Slug	3 - 70	0.60	3.0	185.4

Figure 5: Internal flow patterns at any inclination angles of the CEOHP (T_{so} = 60°C, T_{si} = 20°C, f = 0.00074)

At an inclination angle of 90 degree. Figure 5(C) shows the internal flow patterns of CEOHP with an inclination angle of 90 degree, heat source temperature of 60°C, friction factor of 0.00074. It can be concluded from the experimental data that, with the inclination angle of 90 degree, slug flow is the main flow patterns of CEOHP. Although, the slug flow can be mostly observed, the annular flow happens occasionally with the frequency of 4-5 times per second. The nucleation sites of 4-5 sites can be also seen at the bottom and middle parts of evaporator section. After evaporation the vapor bubbles merge together to form a long vapor slug with the average length of 3-70 mm. These vapor slugs subsequently occupy in both bottom and middle parts of evaporator before moving up to the condenser section where they collapse and the heat is released, with the heat transfer of 185.4W. Almost of the vapor slugs tend to move to the condenser section of the left glass tube with very few slugs move in the right tube (about 48%). The frequency and amplitude of temperature oscillation of working fluid are 0.85 cycle/sec and 3°C, respectively.

It can be found that, when increasing the inclination angles from 0 to 50 degree, the flow patterns will unchanged is remain at the slug flow. The length of vapor bubbles decreases of 40 mm or 33% of original vapor length. The frequency of temperature oscillation of working fluid increases from 0.51 to 0.87 cycle/sec as the amplitude of temperature decreases from 3.5 to 1.5°C and the heat transfer rate increases from 102.3 to 223 W. After, when the inclination angles are more than 50 degree, the length of vapors increases about 10-20 mm or 28% of original vapor length. The frequency of temperature oscillation of working fluid is nearly constant as amplitude of temperature increases from 1.5 to 3°C and the heat transfer rate decreases from 223 to 185.4 W. Because at this inclination angle, the amount of liquid that returns to evaporator section is appropriate value rapidly generate boiling. Thus the velocity of vapor increase, the vapor bubble expansion and the length of vapor bubble decrease. And it is able to transfer higher heat with condensation of working fluid at the condenser section. Therefore, the inclination angle of 50 degree boiling in confined channel, therefore high heat transfer. But at an inclination angle of 0 and 90 degree, boiling is pool boiling, therefore low heat transfer. These findings agree with the results of Gi et al. [2]. It was seen that, at the inclination angles of 30 to 60 degrees, slug flow is the main flow pattern in the CEOHP, the length of vapor bubble decreases.

It can be concluded that, when the inclination angle increases, the remain flow patterns are slug flow, the length of vapor bubble decreases, and the heat transfer rate increases with maximum value is occurred at inclination angle 50 degree.

3-3 Effect of the Internal Friction

At the friction factor of 0.00074. Figure 6(A) shows the internal flow patterns of CEOHP with the heat source temperature of 80°C, inclination angle of 50 degree. It can be concluded from the experimental data that, with the friction factor of 0.00074, slug flow is the main flow patterns of CEOHP. Although, the slug flow can be mostly observed, the annular flow happens occasionally with the frequency of 1-2 times per second. Few nucleation sites of 2-3 sites can be also seen at the bottom part of evaporator section. After evaporation the vapor bubbles merge together to form a long vapor slug with the average length of 5-130 mm. These vapor slugs subsequently occupy in both bottom and middle parts of evaporator before moving up to the condenser section where they collapse and the heat is released, with the heat transfer of 392W. Almost of the vapor slugs tend to move to the condenser section of the left glass tube with very few slugs move in the right tube (about 51%). It can be explained that, the heat transfer is absorbed by the vapor bubble originated in the evaporator section and the latent heat is the main mechanism. Most of the bubbles that flow into the condenser section collapse there where the absorbed latent heat is released, resulting in the lower void fraction. The heat transfer is, thus, transferred by this mechanism. The frequency and amplitude of temperature oscillation of working fluid are 0.38 cycle/sec and 4°C, respectively.

At the friction factor of 0.004. Figure 6(B) shows the internal flow patterns of CEOHP with a friction factor of 0.004, heat source temperature of 80°C, inclination angle of 50 degree. It can be concluded from the experimental data that, with the friction factor of 0.004, slug flow is the main flow patterns of CEOHP. Although, the slug flow can be mostly observed, the bubble flow happens occasionally with the frequency of 4-5 times per second. The nucleation sites of 8-9 sites can be also seen at the bottom and middle parts of evaporator section. After evaporation the vapor bubbles merge together to form a long vapor slug with the average length of 3-65 mm. These vapor slugs subsequently occupy in both bottom and middle parts of evaporator before moving up to the condenser section where they collapse and the heat is released, with the heat transfer of 472W. Almost of the vapor slugs tend to move to the condenser section of the left glass tube with very few slugs move in the right tube (about 57%). The frequency and amplitude of temperature oscillation of working fluid are 0.56 cycle/sec and 2°C, respectively.

It can be found that, when friction factor increases from 0.00074 to 0.004, the length of vapor bubble decreases of 30-40 mm or 30% of original vapor length. The fraction of bubble flow

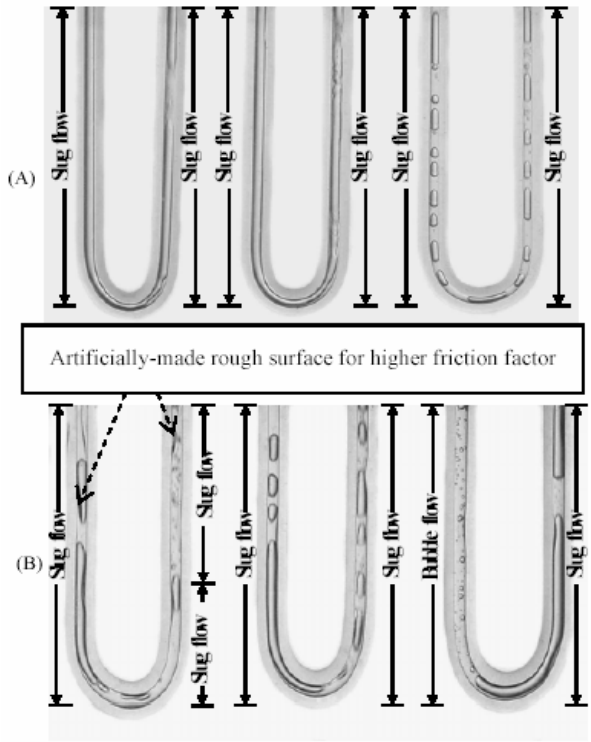


Fig	Friction factor	Flow pattern	L_v mm	Frequency cycle/sec	Amplitude °C	Q W
(A)	0.00074	Slug	5 - 130	0.38	4	392
(B)	0.004	Slug and bubble	3 - 65	0.56	2.5	472

Figure 6: Internal flow patterns at any friction factors of the CEOHP (T_{so} = 80°C, T_{si} = 20°C, $\beta = 50^{o}$)

increases and the heat transfer increases from 392 of 472 W. It can be seen (form the temperature oscillating of working fluid) that, (when the friction factor increases) the frequency of temperature oscillating of working fluid increases from 0.38 to 0.56, as the amplitude of temperature decreases from 4 to 2.5°C. Because when the friction factor of inner surface of tube increases, the internal surface of tube is also higher rough. The merging of vapor bubble will be hardly occurred then the vapor size is small. And at a friction factor of 0.004 boiling in confined channel, therefore high heat transfer. But at a friction factor of 0.00074, boiling is pool boiling, therefore low heat transfer. Because this research is new research that can not be compared with other research, but it will tendency for further research.

It can be concluded that, when the internal friction factor increases, the remain flow patterns are slug flow, the length of vapor bubble decreases as the heat transfer rate increases.

3-4 Flow pattern map

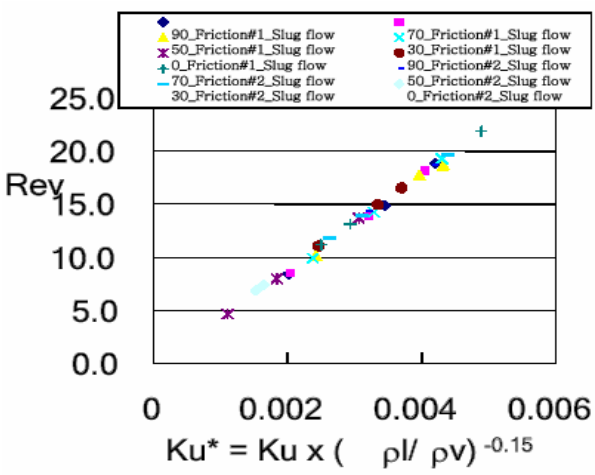


Figure7: Flow pattern map of the internal flow of CEOHP

Figure7 shows flow pattern map which is the relationship of Ku* and Re_V It can be seen that, the data points have a linear relationship on the flow pattern map and their flow patterns were only slug flow. Although other boundary cannot be identified that of any type flow pattern. Because the this research is new research that can not be compared with other research, but they can be used as reference for further research. It can be concluded that, the internal flow pattern map is sample between Ku* and Re_v which apply with every working fluid.

4. CONCLUSIONS

From all experimental results, it can be concluded as follows:

4.1 The heat transfer increases when friction factor and heat source temperature increases. The maximum heat transfer, which is 472 W, is occurred at friction factor of 0.004, heat source temperature of 80°C and inclination angle of 50 degree.

4.2 For all of friction factor, heat source temperature and inclination angle, the majority flow pattern of working fluid within the CEOHP is slug flow and the bubble flow that slightly occurs mixing with slug flow.

4.3 For friction factor of 0.004 and inclination angle 50 degree, (when the heat source temperature increases), the frequency of temperature oscillation increase from 0.45 to 0.56 cycle/sec as the amplitude of temperature decrease from 4.5 to 2.5°C.

4.4 At the inclination angles of 50 degree, the minimum length of vapor bubble is 3-65 mm, the maximum frequency of temperature oscillation of working fluid is 0.55 cycle/sec and the minimum amplitude of temperature is 2.5°C occur.

4.5 For the heat source temperature of 80°C and inclination angle of 50 degree, (when the friction factor increases), the length of vapor bubble from 5-130 mm to 3-65 mm and amplitude of temperature decrease form 0.38 to 0.56 cycle/sec as the frequency of temperature oscillation increases from 4 to 2.5°C.

Acknowledgement

This research was conducted under the Faculty of Engineering and, Chiang Mai University, Chiang Mai, Thailand. The authors would like to express their sincere appreciation for all of the support provided.

References

1. Akachi H., Polasek F. and Stulc P., 1996, "Pulsating Heat Pipe," Proc, 5th. Int. Heat Pipe Symp., Melbourne, Australia.
2. Gi K., Sato F. and Maezawa S., 1999, "Flow Visualization Experimental on Oscillating Heat Pipe," Procs. 11th Int. Heat Pipe Conf., Tokyo, Japan.
3. Lee W., Jung H. and Kim J. S., 1999, "Flow Visualization of Oscillating Capillary Tube Heat Pipe," Proc. 11th Int. Heat Pipe Conf., Tokyo, Japan.
4. Maezawa S., Gi K., Minamisawa A. and Akachi H., 1996, "Thermal Performance of Capillary Tube Thermosyphon," Proc. 4th Int. Heat Pipe Conf., Albuquerque, USA, Vol. II.
5. Rittidech S., Terdtoon P., Tantakom P., Murakami M. and Jompakdee W., 2000, "Effect of Inclination Angles, Evaporator Section Lengths and Working Fluid Properties on Heat Transfer Characteristics of Closed-End Oscillating Heat Pipe, Proc. 6th Int. Heat Pipe Symp., Chiang Mai, Thailand.

Nomenclature

f Friction factor
Rev Reynolds number of vapor, $\rho_v vd / \mu_v$
Ku Kutateladze number, $(q/\{h_{fg}\rho_v[\sigma g(\rho_l - \rho_v)/\rho_v^2]^{1/4}\})$
Ku* Modified Kutateladze number, $Ku(\rho_l/\rho_v)^{-0.15}$
Tsi Heat sink temperature, °C
Tso Heat source temperature, °C
β Inclination angle, degree

Effects of Evaporator Lengths, Number of Turns and Working Fluids on Internal Flow Patterns of a Vertical Closed-Loop Oscillating Heat Pipe

P. Charoensawan, P. Terdtoon, P. Kamonpet and P. Ingsuwan
Department of Mechanical Engineering, Faculty of Engineering, Chiang Mai University, Chiang Mai, Thailand.
Tel: +66-53-944151, Fax: +66-53-226014 and E-mail Address: g4366428@cm.edu

Abstract

A visual study of flow patterns inside a vertical closed-loop oscillating heat pipe has been conducted. The article describes the details of the flow patterns varying with evaporator lengths, numbers of turns and working fluids. The tested CLOHPs were made of Pyrex tubes with 2 mm ID and 6 mm OD. The numbers of turns of CLOHPs were 10 and 28 turns. The evaporator, adiabatic and condenser sections were of equal length, viz. 50 and 150 mm for each number of turns. The selected working fluids were R123 and R141b with 50% filling ratio. The CLOHPs operated at vertical orientation and the adiabatic temperature was controlled at 50^{o}C. Flow phenomena were recorded with a digital still camera and three video cameras, and the corresponding heat transfer rate was also monitored. It was found that when the evaporator length decreased from 150 mm to 50 mm, the main flow patterns remained at the slug flow slightly mixing with bubble flow, as the sub flow patterns were the annular flow that increasingly happened from 1 to 2 times per second. The collapsing ratio of vapor slugs in condenser section increased from 500% to 1300% and the heat flux increased from 3001 to 8313 W/m^2. When the number of turns decreased from 28 to 10, although the main flow patterns remained at the slug flow slightly mixing with bubble flow, the annular flow increasingly happened from 1.5 to 2 times per second. The collapsing ratio of vapor slugs in condenser section increased from 800% to 1300% and the heat flux increased from 7603 to 8313 W/m^2. When the latent heat decreased from 214 kJ/kg to 161 kJ/kg or using R123 instead of R141b, the main flow patterns remained at the slug flow, as the sub flow patterns were the annular flow that increasingly happened from 1.25 to 1.5 times per second. The collapsing ratio of vapor slugs in condenser section increased from 700% to 800% and the heat flux increased from 7202 to 7603 W/m^2. In addition, the average length and velocity of vapor slugs and the amplitude and frequency of temperature oscillation were investigated.

Key words: closed-loop oscillating heat pipe, internal flow patterns, evaporator length, number of turns, working fluid

1. INTRODUCTION

A closed-loop oscillating heat pipe (CLOHP) is a heat transfer device with very high thermal performance. The CLOHP is used for cooling the CPU of notebook personal computer and the small electronic devices. Firstly, Akachi et al. (1996) proposed that the basic operational principle of CLOHP was the oscillating movement of working fluid and phase change phenomena. Thereafter, the visualization studies were conducted to obtain the internal flow phenomena of CLOHP to understand its heat transfer mechanism. Gi et al. (1999) studied a CLOHP that was made of a Teflon tube with a 2 mm inside diameter and 10 turns. Lt, Le, La, and Lc were 8200, 150, 100, and 150 mm, respectively. The CLOHP was tested from 30o to 90o from horizontal axis. The working fluid was R142b with the filling ratio of 30% to 70%. It was seen that the best heat transfer performance resulted of the moderate oscillation phenomena, movement velocity of vapor bubble, size of vapor bubble and liquid slug, amplitude and frequency of pressure fluctuation of working fluid. Miyazaki et al. (1999) studied the visualization model of a top heat mode CLOHP that consisted of a base plate of copper and a window plate of polycarbonate. The base plate was provided with a rectangular groove, which was turned repeatedly to form 50 parallel grooves. The working fluid was R142b. It was found that liquid and vapor were almost separated into two parts in the individual turns. The liquid flow into the heating section and the vapor flow into the cooling section were accomplished due to the liquid column oscillation. As the heat load increased, the oscillation of liquid column became higher and the liquid overflowed into neighboring turns. Hosoda et al. (1999) studied the CLOHP at bottom heat mode. The CLOHP was made of a glass tube with a 2.4 mm inner diameter and 10

turns. L_e, L_a, and L_c were 58, 174, and 58 mm, respectively. The working fluid was distilled water. It was observed that only two vapor plugs existed separately in adjacent turns, and one of them started to shrink when the other started to grow. When the shrinking plug disappeared, a new vapor plug appeared in the turn adjacent to the turn including the grown-up vapor plug. This vapor-plug propagation phenomenon induced liquid flow between the heating and cooling sections. Lee et al. (2000) studied the pressure oscillation of CLOHP that was made of brass and acrylic plate with 20 rectangular channels and using R142b as working fluid. It was found that the heat transfer performance was excellent when the amplitude of pressure oscillation was small and the frequency of pressure oscillation was large. Recently, Qu et al. (2002) investigated the semi-visualization setup of CLOHP, which was mainly made of small copper tubes. The visualization window was located at adiabatic section. It was seen that the working fluid oscillated accompanying with intermission-stop. This was similar to the result of Khandekar et al. (2002). With increasing the transfer power and inclination angle, the oscillation frequency of evaporator temperature and the frequency of oscillating flow increased as the intermission-stop waiting time decreased. Most of the researches mentioned above investigated the internal flow pattern of a CLOHP with a specific shape and working fluid. Moreover, the internal flow patterns have not been clearly explained.

It is therefore the objective of this paper to investigate the effects of evaporator lengths, number of turns and working fluids on the internal flow patterns of the CLOHP at vertical orientation with bottom heat mode.

2. EXPERIMENTAL SETUP AND PROCEDURE

Most of the previous researches mentioned above studied the tested CLOHP that was made of a base plate of metal covered by a window plate. The internal flow patterns, which were observed from this flat plate CLOHP, were compromisingly good because of the problem of light position and the reflection of metal plate. In order to clearly observe the internal flow patterns of CLOHP in our research, the evaporator, adiabatic and condenser sections were made of Pyrex tubes with 2 mm inside diameter and 6 mm outside diameter. The Pyrex tubes were connected each other by brazing to form a tested CLOHP as shown in Figure 1.

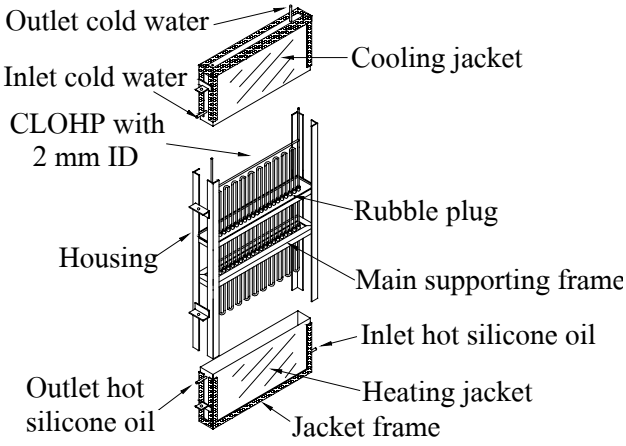


Figure 1 Glass CLOHP

Two aluminum sheets were used to support the Pyrex tubes CLOHP and two glass boxes were used to be the jackets of the evaporator and condenser sections. The number of turns of CLOHP was 10 turns. The evaporator, adiabatic and condenser sections were 150 mm. The filling ratio maintained at 50% of total volume within the tube. The CLOHPs operated at 90 degree inclination angle from horizontal axis or vertical orientation and the adiabatic temperature was controlled at 50°C.

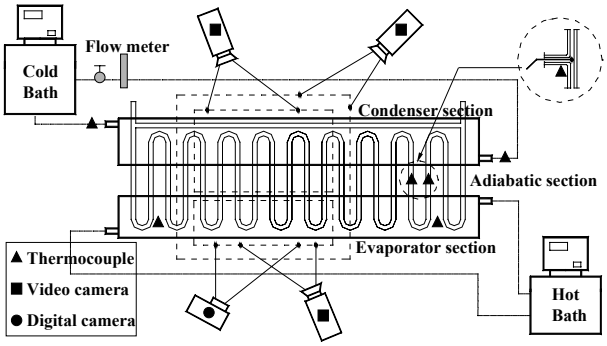


Figure 2 Experimental setup

The experimental setup, which is schematically shown in Figure 2, consists of a CLOHP with the length of evaporator, adiabatic (which is equal to condenser sections) were 50 and 150 mm, respectively. The CLOHPs were made of the Pyrex glass tube with the internal diameter of 2 mm and the selected meandering turns of 10 and 28. The evaporator section was heated by silicone oil, which was circulated from the hot bath (HAAKE, 8N3-B, and ±0.03°C). The condenser section was cooled by distilled water, which was circulated from the cold bath (Bitzer, D7032, and ±0.1°C). The heating and cooling jackets were made of high temperature glass to ensure the best visualization. The mass flow rate

inside the cooling jacket was measured by a rotameter (Platon, PGB411 with ±0.1 l/min accuracy) and 4 points of thermocouples (OMEGA type K) were installed at the inlet and outlet of condenser section to determine the heat transfer rate. The Temperature probes were installed 2 points at high temperature glass of evaporator, 2 points condenser sections, and 1 point for ambient respectively to determine the heat loss. The temperature recorder (Comark, C8510, and ±1°C) was used to monitor all temperatures at specified time. Moreover, 2 points of the thermocouple were installed at the middle position of the 17th and 18th tube of adiabatic section starting from the left side. These two thermocouples were inserted inside the CLOHP by the specially–designed probe. The thermocouples were connected to the chart recorder (Yokogawa, 4152, 2-pen, and ±0.5°C) to measure the amplitude and oscillating of temperature of the working fluid at adiabatic section from which the internal saturated pressure can be observed. During the experiment the angle was set at 90 degree from horizontal plane. Three video cameras (Sony, CCD-TR618E) were used to continuously record the flow patterns at the evaporator section, condenser together with adiabatic sections, and total part of CLOHP. The digital camera (Sony, DSC–S75) was used to record flow patterns of evaporator section at specified times. The scale was attached to the apparatus to measure the length and velocity of vapor bubble.

The controlled parameters were:

- Tube internal diameter of 2 mm
- Working temperature of 50°C
- Filling ratio of 50% (by total volume)

The variable parameters were:

- Evaporator section lengths of 50 and 150 mm (to observe the effects at these lengths)
- Working fluids of R123 and R141b (since their boiling pressure are acceptable for the required temperature range and their latent heat of vaporization are totally difference)
- Meandering turns of 10 and 28 (to observe the effect of number of turns)

The experiment was conducted as follows; firstly, the CLOHP was filled with the working fluid and set into the test rig. The temperature of the hot and cold baths were set at the required values, and the hot and cold fluids were supplied to the jackets of both the evaporator and condenser sections. After a steady state was reached, continuous movies were recorded by three video cameras while photographs were taken at specified times by digital camera. In the meantime, the temperatures and heat transfer rates were monitored. The temperature oscillation of working fluid and amplitude were recorded to briefly observe the pressure oscillation of working fluid. Then the evaporator lengths, numbers of turns and working fluids were varied according to the required conditions.

3. RESULTS AND DISCUSSION

Since the major phenomena occurred in the evaporator section, the visualization at this part was concentrated. Therefore all of the flow patterns that are shown in this paper are the internal flow patterns at evaporator section which are especially recorded by a digital still camera. The flow of whole part of CLOHP could, however, be observed by video movie. Figure 3 shows the inlet–outlet flow directions of silicon oil at evaporator section and all experimental results will be referred by this figure. And the vapor slug edge is observed with solid lines in the working fluid in liquid phase. In this visualization study, the internal flow concerned with flow patterns, vapor slug length, vapor velocity, rate of merging stage, collapsing ratio(the collapsing ratio is the average value. After the vapor bubble break into several bubbles in the condenser part, I measure the bubble length. After the vapor bubbles collape, i measure the bubble length again. So the collapsing ration is the ratio of bubble length after to before the collapsing of vapor bubble in condenser part.), frequency and amplitude of temperature oscillation of working fluid. The vapor slug length was measured from the length of the two ends of vapor slug at specified time. The vapor slug velocity was measured from the distance that the one end of vapor slug moved in one second. The merging stage was observed from the internal flow, which changed from slug flow into annular flow. The collapse ratio (in percentage) of vapor bubble was measured in comparison with the original length of vapor bubble at the original time. The frequency and amplitude of temperature oscillation were measured from graph between adiabatic temperature in y-axis and time in x-axis.

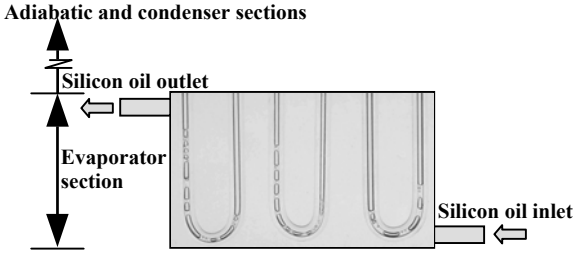


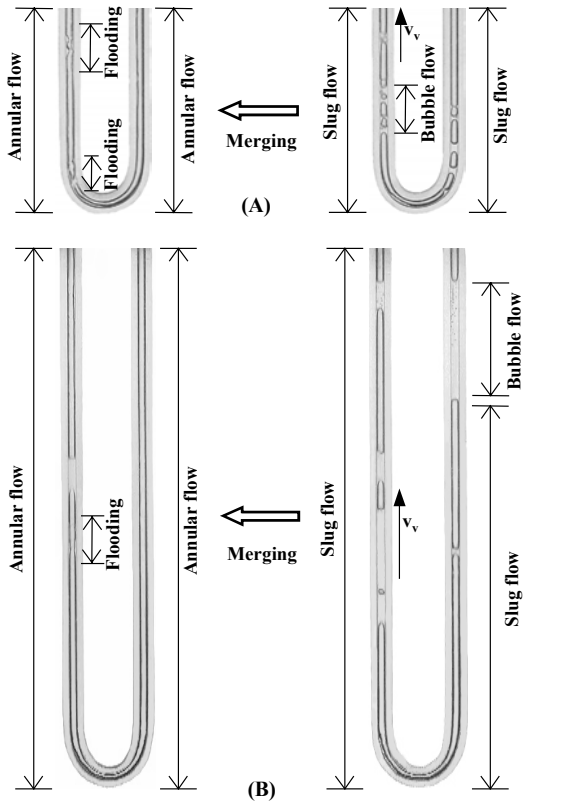
Figure 3 The inlet–outlet flow directions of silicon oil at evaporator section

Because of the working fluid within CLOHP is saturated fluid, the temperature oscillation was used to estimate the pressure oscillation. For a thorough understanding of all of the effects of evaporator length, number of turns, and the working fluids, the internal flow at specific number of turns and working fluid will be presented with respect to increasing the evaporator length first. Second, the internal flow at specific evaporator length and working fluid will be presented with respect to increasing the number of turns. After that, comparison of internal flow patterns at the same evaporator length and number of turns for two working fluids will be made.

3-1 Effect of the Evaporator Length

At a short evaporator length of 50 mm. Figure 4 (A) shows the effect of evaporator length on internal flow patterns of CLOHP with 2 mm inner diameter, 10 turns, and R123 as working fluid. It can be concluded from the experimental data that, the slug flow slightly mixing with bubble flow is the main flow patterns of CLOHP with low evaporator length. Although the slug flow can be mostly observed, the annular flow occasionally happens with the frequency of 2 times per second. When the annular flow occurs within the tube, the flooding phenomena can be often observed in both bottom and middle parts of evaporator section. After evaporation the vapor bubbles merge together to form a long vapor slug with the average length of 20 mm. These vapor slugs subsequently occupy in both bottom and middle parts of evaporator before moving up with the average velocity of 0.5 m/s to the condenser section. While these vapor slugs are moving up, they coalesce again to form a longer vapor slug with the average length more than 100 mm. Thus all parts of evaporator are fully filled with the vapor in the core of tube and the liquid film at the inner wall of tube. Although all of the vapor slugs generally move to the condenser section in the left glass tube, they sometimes move in the right glass tube. After that these vapor slugs collapse with the collapsing ratio of 1300% and the heat is released with the heat flux of 8313 W/m^2. The frequency and amplitude of temperature oscillation of working fluid that indicate the working pressure oscillation are 0.41 cycle/sec and 0.28^{o}C, respectively.

At a high evaporator length of 150 mm. Figure 4 (B) shows the effect of evaporator length on internal flow patterns of CLOHP with the same size, number of turns and working fluid mentioned above. It can be concluded that, the



CLOHP with 10 turns using R123 as working fluid					
Phenomena	Fig. A	Fig. B	Phenomena	Fig. A	Fig. B
L_e (mm)	50	150	Collapse (%)	1300	500
Merging (times/sec)	2	1	Frequency (cycle/sec)	0.41	0.46
L_v (mm)	20	50	Amplitude (^{o}C)	0.28	0.72
v_v (m/s)	0.5	1.13	q (W/m^2)	8313	3001

Figure 4 Effect of evaporator lengths on internal flow patterns of CLOHP

main flow patterns of CLOHP with high evaporator length remain at the slug flow slightly mixing with bubble flow. In addition, the annular flow occasionally happens with the frequency of 1 time per second. As the annular flow occurs within the tube, the flooding phenomena can be also observed in middle part of evaporator section. After evaporation the vapor bubbles merge together to form a long vapor slug with the average length of 50 mm. These vapor slugs subsequently occupy in both bottom and middle parts of evaporator before moving up with the average velocity of 1.13 m/s to the condenser section. While these vapor slugs are moving up, they coalesce again to form a longer vapor slug with the average length more than 300 mm. Thus almost of the evaporator part are filled with the vapor in the core of tube and the liquid film at the inner wall of tube. Although all of the vapor slugs generally move to the condenser section in the left glass tube, they sometimes move in the right glass tube. After that these vapor slugs collapse with

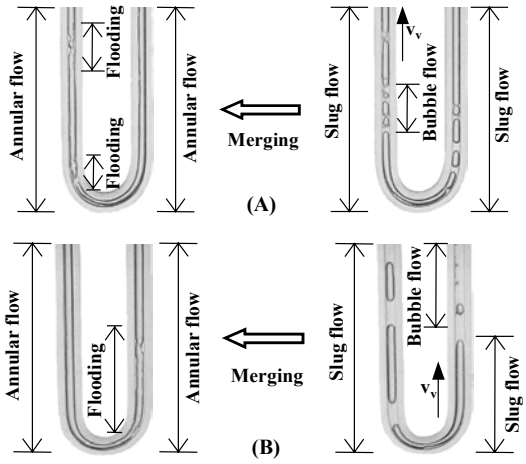
the collapsing ratio of 500% and the heat is released with the heat flux of 3001 W/m^2. The frequency and amplitude of temperature oscillation are 0.46 cycle/sec and 0.72^{o}C, respectively.

It can be found that, when the evaporator length decreases, the movements of vapor slugs to the condenser section increasingly occur from 1 to 2 times per second and the collapsing ratio also increases from 500% to 1300%. Thus the heat flux increases. At the same time, the average length of vapor slug decreases from 50 mm to 20 mm, the vapor velocity decreases from 1.13 m/s to 0.5 m/s and the amplitude of temperature oscillation or the working pressure difference decreases from 0.72^{o}C to 0.28^{o}C. These indicate that the vapor slugs of short evaporator part can easily move to the condenser section and have a sufficient time to transfer a latent heat. However, the frequencies of pressure oscillation for all evaporator lengths are not different. Although this experimental result can not be compared with the previous researches that mentioned above because their tested CLOHP only has a specific evaporator length, this result has a similar trend with the result of Gi et al. (1999). It was found from their experiment that the best heat transfer performance resulted of the moderate oscillation phenomena, movement velocity of vapor bubble, size of vapor bubble and liquid slug, amplitude and frequency of pressure fluctuation of working fluid.

It can be concluded that, with decreasing the evaporator length from 150 mm to 50 mm, the main flow patterns remain at the slug flow slightly mixing with bubble flow, as the sub flow patterns are the annular flow that increasingly happens from 1 to 2 times per second. In addition, the average length and velocity of vapor slug and the amplitude of temperature oscillation decrease. The collapsing ratio of vapor slugs in condenser section increases from 500% to 1300%. The heat flux increases from 3001 to 8313 W/m^2.

3-2 Effect of the Number of Turns

At a number of turns of 10. Figure 5 (A) shows the effect of number of turns on internal flow patterns of CLOHP with 2 mm inner diameter, 50 mm evaporator length, and R123 as working fluid. It can be found from the experimental data that, the slug flow slightly mixing with bubble flow is the main flow patterns of CLOHP with small number of turns. Although the slug flow can be mostly observed, the annular flow occasionally happens with the frequency of 2 times per second. When the annular flow occurs within the tube, the flooding phenomena can be often observed in both bottom and middle parts of evaporator section. After evaporation the vapor bubbles merge together to form a long vapor slug with the average length of 20 mm. These vapor slugs subsequently occupy in both bottom and middle parts of evaporator before moving up with the average velocity of 0.5 m/s to the condenser section. While these vapor slugs are moving up, they coalesce again to form a longer vapor slug with the average length more than 100 mm. Thus all parts of evaporator are fully filled with the vapor in the core of tube and the liquid film at the inner wall of tube. Although all of the vapor slugs generally move to the condenser section in the left glass tube, they sometimes move in the right glass tube. After that these vapor slugs collapse with the collapsing ratio of 1300% and the heat is released with the heat flux of 8313 W/m^2. The frequency and amplitude of temperature oscillation of working fluid are 0.41 cycle/sec and 0.28^{o}C, respectively.



CLOHP with 50 mm L_e using R123 as working fluid					
Phenomena	Fig. A	Fig. B	Phenomena	Fig. A	Fig. B
N (turns)	10	28	Collapse (%)	1300	800
Merging (times/sec)	2	1.5	Frequency (cycle/sec)	0.41	0.44
L_v (mm)	20	25	Amplitude (^{o}C)	0.28	1.09
v_v (m/s)	0.5	0.63	q (W/m^2)	8313	7603

Figure 5 Effect of numbers of turns on internal flow patterns of CLOHP

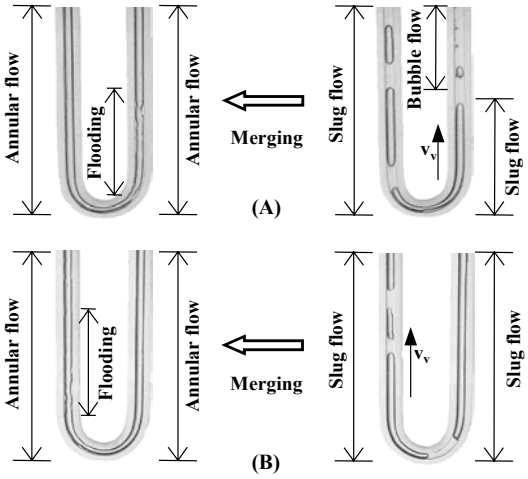
At a number of turns of 28. Figure 5 (B) shows the effect of number of turns on internal flow patterns of CLOHP with the same size and working fluid mentioned above. It can be concluded that, the main flow patterns of CLOHP with large number of turns remain at the slug flow slightly mixing with bubble flow. In addition, the annular flow occasionally happens with the frequency of 1.5 time per second. As the annular flow occurs within the tube, the flooding phenomena can be also observed in both bottom

and middle parts of evaporator section. After evaporation the vapor bubbles merge together to form a long vapor slug with the average length of 25 mm. These vapor slugs subsequently occupy in both bottom and middle parts of evaporator before moving up with the average velocity of 0.63 m/s to the condenser section. While these vapor slugs are moving up, they coalesce again to form a longer vapor slug with the average length more than 100 mm. Thus all of the evaporator parts are filled with the vapor in the core of tube and the liquid film at the inner wall of tube. All of the vapor slugs tend to move to the condenser section in the left glass tube as much as in the right glass tube. After that these vapor slugs collapse with the collapsing ratio of 800% and the heat is released with the heat flux of 7603 W/m^2. The frequency and amplitude of temperature oscillation of working fluid are 0.44 cycle/sec and 1.09^{o}C, respectively.

It can be found that, when the number of turns decreases, the movements of vapor slugs to the condenser section increasingly occur from 1.5 to 2 times per second and the collapsing ratio also increases from 800% to 1300%. Thus the heat flux increases. At the same time, the average length of vapor slug decreases from 25 mm to 20 mm, the vapor velocity decreases from 0.63 m/s to 0.5 m/s and the amplitude of temperature oscillation decreases from 1.09^{o}C to 0.28^{o}C. These indicate that the vapor slugs of small number of turns can easily move to the condenser section and have a sufficient time to transfer a latent heat. However, the frequencies of pressure oscillation for all numbers of turns are not different. This result can not be also compared with the previous researches that mentioned above because their tested CLOHP only has a specific number of turns. Nevertheless this result has a same direction with the results of Lee et al. (1999) and Lee et al. (2000). It was found from their experiments that the flooding phenomena by the collision or friction between liquid and vapor were observed and the heat transfer performance was excellent when the amplitude of pressure oscillation was small.

It can be concluded that with decreasing the number of turns from 28 to 10, although the main flow patterns remain at the slug flow slightly mixing with bubble flow, the annular flow increasingly happens from 1.5 to 2 times per second. In addition, the average length and velocity of vapor slug and the amplitude of temperature oscillation decrease. The collapsing ratio of vapor slugs in condenser section increases from 800% to 1300%. The heat flux increases from 7603 to 8313 W/m^2.

3-3 Effect of the Working Fluid



CLOHP with 50 mm L_e and 28 turns					
Phenomena	Fig. A R123	Fig. B R141b	Phenomena	Fig. A R123	Fig. B R141b
h_{fg} (kJ/kg)	160.96	213.98	Collapse (%)	800	700
Merging (times/sec)	1.5	1.25	Frequency (cycle/sec)	0.44	0.50
L_v (mm)	25	35	Amplitude (^{o}C)	1.09	1.67
v_v (m/s)	0.63	0.75	q (W/m^2)	7603	7202

Figure 6 Effect of working fluids on internal flow patterns of CLOHP

At R123 as working fluid. Figure 6 (A) shows the effect of working fluid on internal flow patterns of CLOHP with 2 mm inner diameter, 50 mm evaporator length and 28 turns. It can be found from the experimental data that, the slug flow slightly mixing with bubble flow is the main flow patterns of CLOHP with R123 as working fluid. Although the slug flow can be mostly observed, the annular flow occasionally happens with the frequency of 1.5 times per second. When the annular flow occurs within the tube, the flooding phenomena can be often observed in both bottom and middle parts of evaporator section. After evaporation the vapor bubbles merge together to form a long vapor slug with the average length of 25 mm. These vapor slugs subsequently occupy in both bottom and middle parts of evaporator before moving up with the average velocity of 0.63 m/s to the condenser section. While these vapor slugs are moving up, they coalesce again to form a longer vapor slug with the average length more than 100 mm. Thus all parts of evaporator are fully filled with the vapor in the core of tube and the liquid film at the inner wall of tube. All of the vapor slugs tend to move to the condenser section in the left glass tube as much as in the right glass tube. After that these vapor slugs collapse with the collapsing

ratio of 800% and the heat is released with the heat flux of 7603 W/m^2. The frequency and amplitude of temperature oscillation of working fluid are 0.44 cycle/sec and 1.09^{o}C, respectively.

At R141b as working fluid. Figure 6 (B) shows the effect of working fluid on internal flow patterns of CLOHP with the same size and number of turns mentioned above. It can be concluded that, the main flow patterns of CLOHP with R141b as working fluid are only the slug flow. In addition, the annular flow occasionally happens with the frequency of 1.25 time per second. As the annular flow occurs within the tube, the flooding phenomena can be often observed in both bottom and middle parts of evaporator section. After evaporation the vapor bubbles merge together to form a long vapor slug with the average length of 35 mm. These vapor slugs subsequently occupy in both bottom and middle parts of evaporator before moving up with the average velocity of 0.75 m/s to the condenser section. While these vapor slugs are moving up, they coalesce again to form a longer vapor slug with the average length more than 100 mm. Thus all of the evaporator parts are filled with the vapor in the core of tube and the liquid film at the inner wall of tube. All of the vapor slugs tend to move to the condenser section in the left glass tube as much as in the right glass tube. After that these vapor slugs collapse with the collapsing ratio of 700% and the heat is released with the heat flux of 7202 W/m^2. The frequency and amplitude of temperature oscillation of working fluid are 0.50 cycle/sec and 1.67^{o}C, respectively.

It can be found that, when the latent heat of vaporization decreases or using R123 instead of R141b, the movements of vapor slugs to the condenser section increasingly occur from 1.25 to 1.5 times per second and the collapsing ratio also slightly increases from 700% to 800%. Thus the heat flux fairly increases. At the same time, the average length of vapor slug decreases from 35 mm to 25 mm, the vapor velocity decreases from 0.75 m/s to 0.63 m/s and the amplitude of temperature oscillation decreases from 1.67^{o}C to 1.09^{o}C. These indicate that the vapor slugs of R123 can easily move to the condenser section and have a sufficient time to transfer heat. However, the frequencies of pressure oscillation for all numbers of turns are not different. It was found from the research of Khandekar et al. (2002) that a flat plate CLOHP properly operated when a working fluid must not have a substantial difference between the leading and lagging contact angles. For our research, these patterns are not seen for all working fluids, because the leading and lagging contact angles of each working fluid in glass tube are not difference. Thus the heat flux of R123 is fairly higher than the heat flux of R141b.

It can be concluded that with decreasing the latent heat from 214 kJ/kg to 161 kJ/kg or using R123 instead of R141b, the main flow patterns remain at the slug flow. The sub flow patterns are the annular flow that increasingly happens from 1.25 to 1.5 times per second. In addition, the average length and velocity of vapor slug and the amplitude of temperature oscillation decrease. The collapsing ratio of vapor slugs in condenser section increases from 700% to 800%. The heat flux increases from 7202 to 7603 W/m^2.

4. CONCLUSIONS

From visual study of the effects of evaporator lengths, number of turns and working fluids on the internal flow patterns of Vertical CLOHP, it can be concluded that:

4.1 With decreasing the evaporator length from 150 mm to 50 mm, the main flow patterns remain at the slug flow slightly mixing with bubble flow, as the sub flow patterns are the annular flow that increasingly happens from 1 to 2 times per second. In addition, the average length and velocity of vapor slug and the amplitude of temperature oscillation decrease. The collapsing ratio of vapor slugs in condenser section increases from 500% to 1300%. The heat flux increases from 3001 to 8313 W/m^2.

4.2 With decreasing the number of turns from 28 to 10, although the main flow patterns remain at the slug flow slightly mixing with bubble flow, the annular flow increasingly happens from 1.5 to 2 times per second. In addition, the average length and velocity of vapor slug and the amplitude of temperature oscillation decrease. The collapsing ratio of vapor slugs in condenser section increases from 800% to 1300%. The heat flux increases from 7603 to 8313 W/m^2.

4.3 With decreasing the latent heat from 214 kJ/kg to 161 kJ/kg or using R123 instead of R141b, the main flow patterns remain at the slug flow. The sub flow patterns are the annular flow that increasingly happens from 1.25 to 1.5 times per second. In addition, the average length and velocity of vapor slug and the amplitude of temperature oscillation decrease. The collapsing ratio of vapor slugs in condenser section increases from 700% to 800%. The heat flux increases from 7202 to 7603 W/m^2.

Acknowledgement

This research was conducted under the Royal Golden Jubilee Scholarships of the Thailand Research Fund (Contract No. 1.M.CM/43/A.1). The authors would like to express their sincere appreciation for all of the support provided.

References

1. Akachi H., Polášek F. and Štulc P., 1996, "Pulsating Heat Pipes," Proc. 5th Int. Heat Pipe Symp., Melbourne, Australia, ISBN 0-08-042842-8, pp. 208-217.
2. Gi K., Sato F. and Maezawa S., 1999, "Flow Visualization Experiment on Oscillating Heat Pipe," Proc. 11th Int. Heat Pipe Conf., Tokyo, Japan, pp. 373-377.
3. Hosada M., Nishio S. and Shirakashi R., 1999, "Meandering Closed-Loop Heat-Transport Tube (Propagation Phenomena of Vapor Plug)," Proc. 5th Int. ASME-JSME Thermal Engineering Joint Conf., USA.
4. Khandekar S., Schneider M., Schäfer P., Kulenovic R. and Groll M**.,** 2002, "Thermofluiddynamic Study of Flat Plate Closed Loop Pulsating Heat Pipes," Microscale Thermophysical Engineering, Taylor and Francis, ISSN 1089-3954, pp. 303-318, Vol. 6, No. 4.
5. Lee W., Jung H., Kim J. and Kim J., 1999, "Flow Visualization of Oscillating Capillary Tube Heat Pipe," Proc. 11th Int. Heat Pipe Conf., Tokyo, Japan, pp.355-360.
6. Lee W., Jung H., Kim J. and Kim J., 2000, "Characteristics of Pressure Oscillation in Self-excited Oscillating Heat Pipe based on Experimental Study," Proc. 6th Int. Heat Pipe Symp., Chiang Mai, Thailand, pp.394-403.
7. Qu W. and Ma T., 2002, "Experimental Investigation on Flow and Heat Transfer of a Pulsating Heat Pipe," Proc. 12th Int. Heat Pipe Conf., Moscow, pp.226-231.
8. Miyazaki Y. and Arikawa M., 1999, "Oscillatory Flow in the Oscillating Heat Pipe," Proc. of the 11th Int. Heat Pipe Conf., Tokyo, Japan, pp.367-372.

Nomenclature

h_{fg}	latent heat of vaporization, kJ/kg
L_a	length of adiabatic section, m
L_c	length of condenser section, m
L_e	length of evaporator section, m
L_t	total length of capillary tube, m
L_v	average length of vapor bubble, m
N	number of turns, turns
N_v	amount of vapor bubble, bubbles/turn
q	radial heat flux, W/m^2
v_v	vapor velocity, m/s

Effect of Number of Turns and Working Fluids on Heat Transfer Characteristics of a Closed-End Oscillating Heat pipe at Critical State

T. Katpradit, T. Wongratanaphisan, P. Kamonpet, P. Terdtoon and A. Akbarzadeh*

Department of Mechanical Engineering, Faculty of Engineering
Chiang Mai University, Chiang Mai, Thailand.
Tel. +66 53 544151, Fax. +66 53 226014, E-mail: K_thanad@hotmail.com

*Faculty of Engineering, Royal Melbourne Institute of Technology
Melbourne, Victoria, Australia

Abstract

This paper investigates the heat transfer characteristics of a closed-end oscillating heat pipe (CEOHP) at critical state. The CEOHPs were made of copper tube having the internal diameter of 2 mm and thickness of 1 mm with number of meandering turns of 5, 10 and 15. Both ends of the tubing are separately sealed. The evaporator length of 50 mm was employed. R123, ethanol and water were used as working fluids with the filling ratio of 50 percent by volume. The tubes were set to be in vertical orientation. In the experiment, high-current low-voltage AC power supply was employed as a heat source to the evaporator section. The cooling medium, a mixture of water and ethylene - glycol 50 percent by volume, was used to transfer heat out of the condenser. The operating temperature was controlled at 600C at the adiabatic section. The effects of the number of meandering turns and working fluids on the heat transfer rate at critical state were experimentally determined. It was found from the experiment that as the number of meandering turn increases, the critical heat flux of each working fluid also increases. The maximum critical heat flux of each working fluid was obtained at the maximum turn of 15. These values were 17.98, 20.60 and 23.95 kW/m2 for R123, ethanol and water respectively.

Key words: closed–end oscillating heat pipe, heat transfer characteristics at critical state

1. INTRODUCTION

Heat pipe is a heat transfer device with very high thermal conductivity that transfers heat by the evaporation and condensation of working fluid. However, when the diameter of the tube is too small, capillary limit and countercurrent flow limit become problems. A new type of heat pipe called “oscillating heat pipe (OHP)” has been developed to solve this problem by connecting bundle of parallel capillary tubes without internal wick into a single undulating series [1]. In this undulating pipe, working fluid is partially filled causing formation of liquid slugs and bubbles. When the evaporator receives heat, the oscillation of the liquid and bubble occurs. The movement of working fluid due to the oscillation allows heat to transfer to the condenser. The driving force that causes the oscillation is produced by nucleate boiling and condensate of working fluid. The oscillation is self-sustained by the evaporation of the liquid slugs and the condensation of the bubbles. The OHP has advantages over conventional heat pipe in that it can be easily made with low cost, has good heat transfer performance, has fast thermal response, is capable of operating in any position and has operational flexibility. It is found that the OHP can successfully operate when the amount of working fluid filled is 50% of total volume within the tube and the inner diameter of the capillary tube is sufficiently small [5].

In the design of OHP for the applications, the heat transfer characteristic at normal operation has been studied actively [1, 4, 6, 8]. However, few of them realized that there was an upper limit of heat transfer mechanism involved with the OHP, namely the critical state of OHP. Maezawa et. al. (1996) observed in their experimental works that, at a specific condition,

the dryout occurred and the closed-end oscillating heat pipe (CEOHP) failed to operate. Lin et. al. (2000) studied the relationship of filling ratio and heat flux of the CEOHP by using the FC-72 and FC-75 CEOHP. There was two condenser sections with only one evaporator section (located at the middle section) in their experimental setup. The working temperature was 75 – 85 C. It was found from their experiments that, in case of FC – 72 CEOHP, the filling ratio of only 32% would cause the dryout condition even with very low heat input of 200 W. In case of FC – 75, the heat flux was much higher (800 W at 38% of filling ratio). Inadequate filling ratio easily led to the dryout condition because it was caused by insufficient amount of liquid inside the evaporator section. It was observed from the experimental works of Miyazaki et. al. (2000) that, the dryout occurred by insufficient supply of liquid into the evaporator section. It was also suggested that, installing of check valve into the closed-loop oscillating heat pipe (CLOHP) could alleviate such phenomena even at top heat mode. It can be fully observed from past studieds that, dryout will occur at evaporator section and the phenomena of dryout can be illustrated in Figure 1.

The following hypothesis can be established to explain such phenomenon. When the OHP is heated to some degree, the internal thermal resistance will rapidly increase. Accordingly, the heat flux from the evaporator to condenser section cannot be transferred. The inside vapor pressure is subsequently high. This high vapor pressure will retard the liquid slug from returning back to the evaporator section. The liquid amount in the evaporator section is accordingly low causing the dryout at some part of the evaporator. The state at which the dryout occurs is called "Critical State" of OHP.

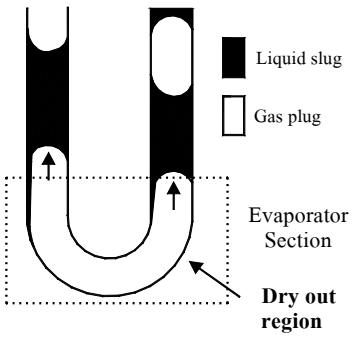


Figure 1.Dryout occurred at evaporator section

The CEOHP is selected in this investigation at critical state due to the operating phenomena of CEOHP is not complicated compared with the CLOHP. The relationships between of the number of turns, working fluids and the heat transfer rate at the critical state which are important in OHP design have not been reported. The main objective of this research is therefore to experimentally investigate the effects of the number of turns and working fluids on heat transfer characteristics of CEOHP at critical state.

2 EXPERIMENTAL SETUP AND PROCEDURE

The construction of the CEOHP for the experiment is shown by the diagram in Figure 2 . The CEOHPs were made of a copper tube having the internal diameter of 2 mm and 1 mm thickness with number of meandering turns of 5, 10 and 15. To easily monitor the temperature at evaporator section at critical state, small turns of 5, 10 and 15 are selected. The evaporator length was selected at 50 mm. Both ends of the tube were sealed separately. At the lower part of the CEOHP, two copper bus bars were welded some distance apart onto the CEOHP to form the evaporator section. The current from a high-current AC power supply was passed from one bus bar, through the copper tube, to the other bus-bar, the process by which heat was generated. R123, ethanol and water were used as working fluids with the filling ratio of 50 percent by volume. In the condenser section, the cooling jacket was installed and the mixture of water and ethylene- glycol 1:1 or 50% by volume was used as cooling medium. The schematic diagram of the experimental setup is shown in

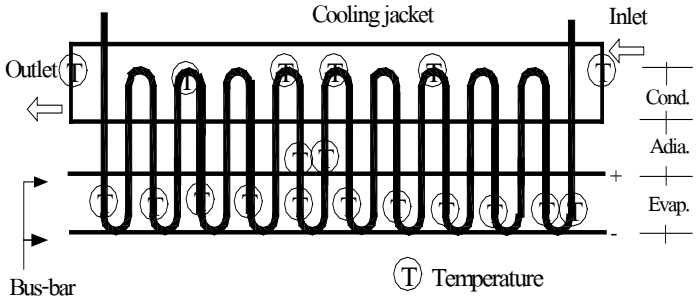


Figure 3.

Figure 2. Closed-end oscillating heat pipe (CEOHP)

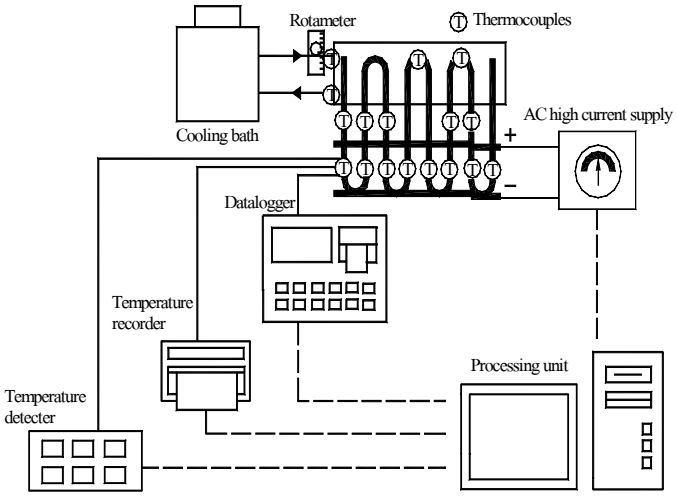


Figure 3. The experimental apparatus

The setup consists of the CEOHP, a high - current low-voltage AC power supply, a cooling bath, a data logger (Comark, C8510, and ± 0.1 ^{o}C), and a flow meter (Platon, PGB411, and ± 0.1 lit/min). The evaporator section of the CEOHP was connected to the AC power supply. The contact surface of copper bus-bars was cleaned before the experiment. The adiabatic and condenser sections of the CEOHP were well insulated. Several Chromel-Alumel thermocouples (Omaga, K type, $\pm 0.5^{o}$C) were attached on the outer surface of the tubes at different locations. Sixteen thermocouples were placed on the CEOHP wall: ten in middle of the evaporator section, two in middle of the adiabatic section and four in the condenser section. In addition, four points of thermocouples were used to measure the temperature of the cooling solution, two points at the inlet and two points at the outlet section of condenser. The procedure for finding the critical state of the operation is as follows. The heat was gradually added to the tubes at evaporator section and the operating temperature at adiabatic section was controlled at 60^{o}C $\pm 5^{o}$C. When the temperature at the evaporator section increases rapidly with increasing of heat but at same time, the condenser temperature does not increase, the critical state occurs. The critical heat flux can be calculated from the difference between the inlet and the outlet water at condenser section by the calorific method. The experiment was started by switching on the coolant circulation system and setting flow rate. The heating at the evaporator section was produced after turning on the power supply. Heat is added to the tube at evaporator section in steps by a variac and the heat was removed at the condenser section by a calorific jacket with cooling substance. The CEOHP operating temperature indicated by the temperature of adiabatic section was maintained at 60^{o}C by adjusting the flow rate and cooling temperature for different the input power. After the system reached steady state, the temperature, flow rate and input power were recorded. The wall temperatures in each tube of evaporator section were compared. The supplying heat will be continually added in steps until one or more wall-temperature at the evaporator section start increasing rapidly.

3. RESULT AND DISCUSSION

3-1 Temperature at evaporator and condenser section of CEOHP at critical state

When the heat was supplied to the CEOHP, the temperatures of wall at evaporator increased to some degree and became constant when the steady state was reached. Figure 4 shows the wall temperatures of the evaporator sections.

After the critical state was reached, since the dryout occured inside the evaporator section, the temperature of the evaporator increased rapidly. At the same time, the wall temperature of condenser section decreased. This implies that the heat could not transferred to the condenser section. In addition, it was found from the experiment that the dryout phenomenon occur mostly near both ends of the CEOHP. One of the reasons may be that at both ends in the evaporator section, the vapor was accumulated and the pressure continually increased.

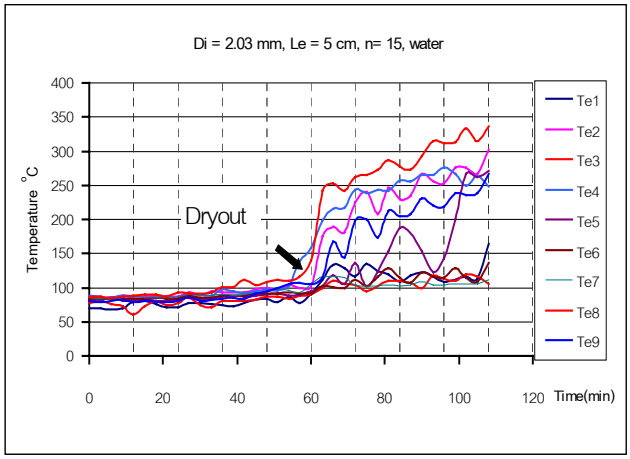


Figure 4. The temperature of tube wall at the evaporator at critical state

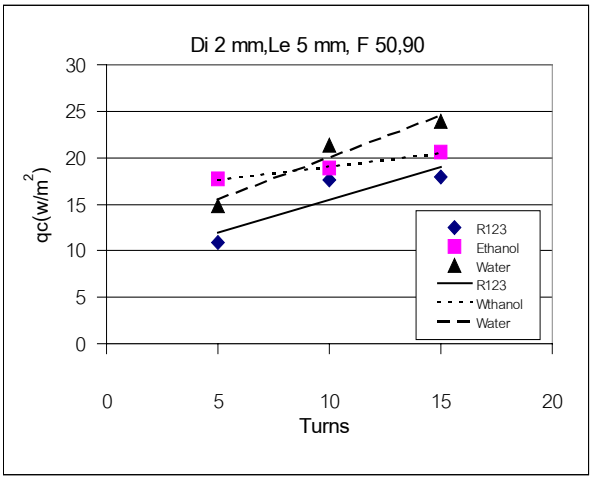


Figure 5. Relationship of meandering turns and critical heat flux of CEOHP

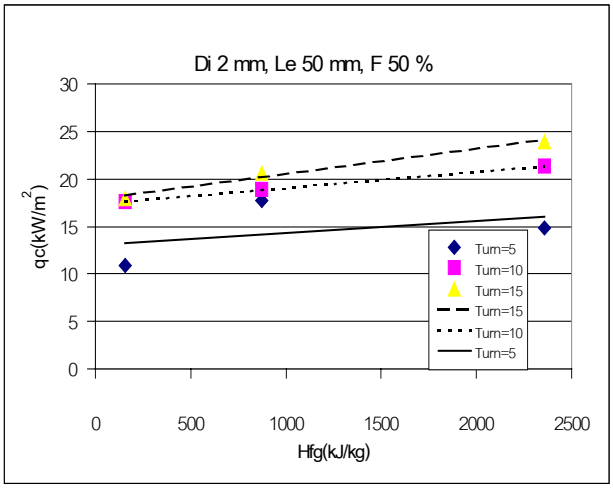


Figure 6. Relationship between the latent heat of vaporization and the critical heat flux of CEOHP

3-2 Effect of number of turns at critical state

Figure 5 shows the relationship between the number of meandering turns and the critical heat flux. R123, ethanol and water were used as working fluids with an evaporator length of 50 mm. The internal diameter of 2 mm was employed. It was found from the experiment that as the number of turns increased from 5 to 15 turns the critical heat flux increased from 10.87 to 17.98 kW/m^2, 14.85 to 20.60 kW/m^2 and 14.85 to 23.95 kW/m^2 for R123, ethanol and water respectively.

The maximum critical heat flux of each working fluid was obtained at the maximum turn of 15. These values are 17.98, 20.60 and 23.95 kW/m^2 for R123, ethanol and water, respectively. This maybe because, when number of turns increases, it is easier for the working fluid to form into slug- train. For this reason, the liquid slugs and gas plugs in the tube with more number of turns are easily moved by self-excited oscillation flow. Then, more liquid in the condenser section can be stably supplied to the evaporator than in the case of smaller turn, causing the heat flux at the critical state to be higher.

3-3 Effect of working Fluid at critical state

Figure 6 shows the relationship between the latent heat and the critical heat flux. It was found from the experiment that as the latent heat increased from 156 to 2356 kJ/kg, the critical heat flux increased from 10.87 to 14.98 kW/m^2, 17.62 to 21.33 kW/m^2 and 17.98 to 23.95 kW/m^2 for the number of turns of 5, 10 and 15 respectively.

From the result, R123 has lower critical heat flux when compared with ethanol and water. When heat is supplied to the tube, R123 will be easily vaporized with more vapor pressure at the evaporator section. The working fluid in condenser section will be retarded by high vapor pressure at evaporator section. Then sufficiently amount of working fluid can not return to the evaporator causing dryout to occur.

4. CONCLUSIONS

The experiment on the heat transfer characteristics at critical state of a CEOHP was conducted. It can be briefly concluded that the meandering of turn and the working fluid have effects on the critical heat flux. In details, as the number of meandering turn increases, the critical heat flux of each working fluid increases. The maximum critical heat flux of each working fluid was obtained at the maximum turn of 15. As the latent heat increase from 156 to 2356 kJ/kg the critical heat flux increased from 10.87 to 14.98 kW/m^2, 17.62 to 21.33 kW/m^2 and 17.98 to 23.95 kW/m^2 for the number of turns of 5, 10 and 15, respectively.

Acknowledgement

This research was conducted under Thailand Research Fund (contract No. BRG/06/2545). The authors would like to express their sincere appreciation for all of the support provided.

Nomenclature

D_i internal diameter, mm.
F Filling ratio
Hfg latent heat of vaporization, J/kg
L_e length of evaporator section, m
mm millimeter
n number of meandering turn
q_c critical heat flux, W/m^2
Te wall temperature at evaporator section

References

1. Akachi, H., Polasek, F., and Stulc, P.,1996 , "Pulsating Heat Pipe", Procs. of the 5th International Heat Pipe Symposium, Melbourne Australia.
2. Dunn, P. D. and Reay, D. A., 1982, *Heat Pipe*, Pergamon Press Ltd., 3rd edition.
3. Faghri, A., 1995, *Heat Pipe Science and Technology*, Taylor & Francis Pub.
4. Charoensawan, P., Terdtoon, P., Kamonpet, P., Ingsuwan, P., and Groll, M., "Effects of Inclination Angles, Filling Ratios and Total Lengths on Heat Transfer Characteristic of A Closed–Loop Oscillating Heat Pipe", 2000, Procs. of the 6th International Heat, Pipe Symposium. Chiang Mai Thailand.
5. Lin, L., Ponnappan, R. and Leland, J., 2000, "Experimental Investigation of Oscillating Heat Pipe", Procs. Of 35th Energy Conversion Engineering Conference and Exhibit, Vol. 2.
6. Maesawa, S., Gi, K.Y., Minamisawa, A., and Akachi, H., 1996, " Thermal Performance of Capillary Tube Thermosyphon", Procs. of the IX International Heat Pipe Conference, Albuquerque, USA. Vol. II.
7. Miyazaki, Y., Polasek, F. and Akachi, H., 2000, "Oscillating Heat Pipe with Check Valves", Procs. of the 6th International Heat Pipe Symposium, Chiang Mai, Thailand.
8. Ritidech, S., Terdtoon,P., Tantakom,P., Murakami,M., and Jompakdee,W., 2000, Effect of Inclination Angles, Evaporator Section lengthes and Working Fluid Properties on heat Transfer Characteristics of A Closed – End Oscillating Heat Pipe., Procs. of the 6th International Heat, Pipe Symposium. Chiang Mai, Thailand.
9. P., Terdtoon.,1993, *Heat Pipe*, Department of Mechanical Engineering, Chaing Mai University, Thailand (in thai).

Mathematical Modeling of a Closed-Loop Oscillating Heat Pipe at Normal Operating Condition

P. Sakulchangsatjatai, P. Kamonpet, T. Wongratanapaisan, P. Terdtoon and M. Murakami**

Department of Mechanical Engineering, Faculty of Engineering
Chiang Mai University, 50200, Thailand
Tel. +66 5394 4151 ext 911 Fax. +66 5322 6014
Email: phrut235@yahoo.com
**Institute of Engineering Mechanics and Systems, University of Tsukuba
Tsukuba-shi, Ibaraki, Japan

Abstract

The heat transfer characteristics of a closed-loop oscillating heat pipe (CLOHP) are modeled by explicit finite element method. The CLOHP was modeled under adiabatic condition. The parameters affecting the heat transfer of CLOHP at top heat mode was analytically investigated. The principles and theories of internal friction flow, basic governing equations and finite difference scheme were applied to evaluate the heat transfer rate. Subsequently, the heat transfers of the CLOHP were predicted by using the model compared with the existing systematic experimental data. The effect of working fluid, evaporator length and inner diameter on the heat transfer characteristics of CLOHP was also investigated.

Key words: closed-loop oscillating heat pipe, top heat mode, heat transfer characteristics

1. INTRODUCTION

The heat pipes have been utilized in many cooling applications. It is a heat transport devices, that transfer heat from hot to cold region with small temperature difference. The oscillating heat pipe (OHP) is a one type of it, which has a very effective heat transfer [1]. It has a very simple structure and operates rapidly without external force. The OHP consists of a continuous long capillary tube bent into many turns and filled with some of the working fluid. However, there is no wick structure to return the condensate liquid from the condenser section to the evaporator section. In the some definition of the OHP, the condensate liquid will flow from the condenser section to the evaporation section by the capillary action. In contrast, a thermosyphon or wickless heat pipe, which returns the condensate liquid by utilizing the gravitational force, and heat transfer can take place only in upwards direction. The inner diameter of the OHP is important. It must be small enough so that under operational conditions liquid slugs and vapor plugs can be formed. If the diameter is too large, the liquid and vapor inside a tube will stratify and operation cannot be established.

The basic heat transfer mechanism of OHP is the self-excited oscillating movement of the liquid slug and the phase changes of working fluid inside tube. Although OHP is very useful, its working principle still cannot be clearly explained and the flow phenomena within the OHP are very complicated too.

There are three types of OHP as shown in fig. 1. First is a closed-end oscillating heat pipe (CEOHP) which is closed both ends in each. Second is a closed-loop oscillating heat pipe (CLOHP) which is connected at both ends of tube to form loop. Final is a closed-loop oscillating heat pipe with check valve (CLOHP/CV) that is connected at both ends of tube to form loop and installed check valve at the loop. Basically the CLOHP has higher heat transfer rate than the CEOHP. The studies on modeling the OHP are very few such as the research of Dobson et al. [4]. They studied the lumped parameter analysis of a closed and open oscillatory heat pipe. They assumed that the effect of surface tension was negligible and that no heat transfer occurred between the liquid and its surroundings. Wong et al. [11] studied a theoretical model of a OHP by using a formulation based on the Lagrangian method. It was shown that the pressure and velocity varied with time. Recently, Shafii et al. [9] presented an analytical model for a symmetric CEOHP and a CLOHP with two turns based on the explicit finite element method. It was concluded that the numbers of liquid slugs were always reduced to that of the number of heating sections. Although the above models can be used with some degree of prediction, they considered

OHP with very few meandering turns, e.g. 2 turns. It is widely accepted that, the higher the number of turns, the better the heat transfer characteristics of the OHP's. For the top heat mode, the number of turns must be more than 40. So it can be seen that the above models can not to be applied to use exactly applications because the meandering turns is very small. Moreover it is not consider adiabatic condition and comparison with exactly experimental data. The objectives of this study are to modify such models under adiabatic condition with a higher number of turns and to quantitatively compare the results of such models with the systematic result of Charoensawan et al. [3] by most equations refer from Shafii et al. [9].

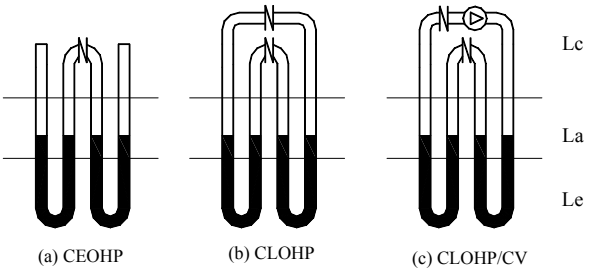


Fig 1. Type of oscillating heat pipe

2. THEORETICAL MODEL

Fig. 2(a) shows a schematic diagram of a CLOHP, the system may be represented one-dimensionally. The evaporator section of the OHP is above the condenser section or top heat mode. The continuous equation, momentum equation and energy equations for each vapor plug and liquid slug are as follows:

Continuous equation

$$\frac{dm_{vi}}{dt} = \dot{m}_{in,vi} - \dot{m}_{out,vi} \quad (1)$$

$$\frac{dm_{li}}{dt} = \dot{m}_{in,li} - \dot{m}_{out,li} \quad (2)$$

Momentum equation

$$\frac{d\left(m_{li}v_{li}\right)}{dt} = \left(P_{vi} - P_{v(i+1)}\right)A - \pi d L_{li}\tau_{li} - m_{li}g \quad (3)$$

Energy equations

$$m_{vi}C_v\frac{dT_{vi}}{dt} = \left(\dot{m}_{in,vi} - \dot{m}_{out,vi}\right)RT_{vi} - P_{vi}A\frac{dX_{vi}}{dt} \quad (4)$$

$$\frac{1}{\alpha_{li}}\frac{dT_{li}}{dt} = \frac{d^2T_{li}}{dX^2} - \frac{h_{li}\pi d}{k_l A}\left(T_{li} - T_w\right) \quad (5)$$

The ideal gas equation is:

$$P_{vi}V_{vi} = m_{vi}R(T_{vi} + 273.15) \quad (6)$$

Where the appropriate inner diameter of CLOHP should be small enough and can be calculated by using the equation of Maezawa et al. [7]

$$d_{\max} \le 2\sqrt{\frac{\sigma}{\rho_l g}} \quad (7)$$

The assumptions used in this model are as follows:

1.Evaporative and condensation heat transfer coefficients are assumed to be constants.

2.The liquid slug is assumed to be incompressible fluid and the vapor plugs assumed to behave as ideal gas.

3.The pressure in the each vapor plug is constant and pressure losses at the each bends can be neglected so it can be assumed that the CLOHP are straight (see Fig. 2(b)).

4.The amount of liquid slugs corresponds to the number of turns [9]. The length of the liquid slug along the centerline of the tube is dependant on the filling ratio.

5.The layer of liquid film can be neglected.

6.The initial mass of the vapor plug and liquid slug are calculated from the properties of working fluid and the obtained lengths of vapor plug and liquid slug.

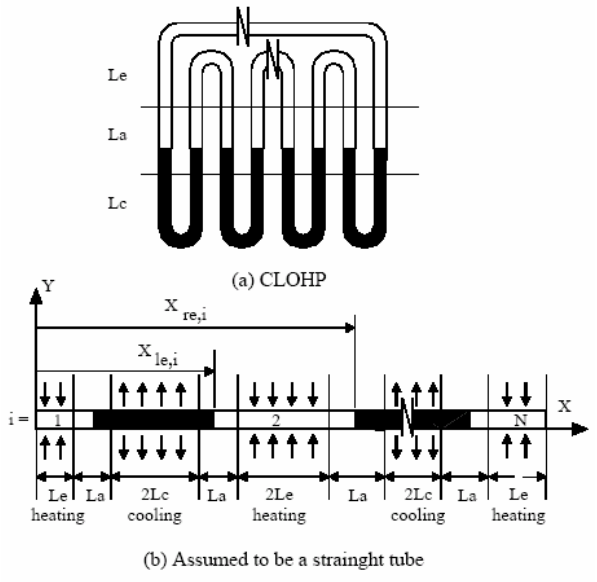


Fig. 2 Model of oscillating heat pipe

The rate of change of mass of the vapor plug and liquid slug can be found from the difference between the mass flow rate due to the the evaporation $\dot{m}_{in,vi}$ and the mass flow rate due to the condensation $\dot{m}_{out,vi}$ and can be expressed as

$$\dot{m}_{in,vi} = U_e\pi d Le_{vi}\left(T_h - T_{vi}\right)/h_{fg} \quad (8)$$

$$\dot{m}_{out,vi} = U_c\pi d Lc_{vi}\left(T_{vi} - T_c\right)/h_{fg} \quad (9)$$

Where Le_{vi}, Lc_{vi} is the length of the vapor plug that in the evaporator section and condenser

section respectively. Assuming appropriate values for the evaporative overall heat transfer coefficient, U_e, and the condensation overall heat transfer coefficient, U_c. Shafii et al [9]. present the rate of change of mass of liquid slug is equal to the average changes in mass of its adjacent vapor plugs.

$$\frac{dm_{li}}{dt} = \frac{1}{2}\left(\frac{dm_{vi}}{dt} + \frac{dm_{v(i+1)}}{dt} \right) \tag{10}$$

In the momentum equation, the gravity force can be determined by measuring the difference in level between both ends of the liquid slug because it is assumed that the OHP is a straight tube. Moreover, the wall shear stress (τ) of liquid slug is calculated and its direction is opposite to the motion direction.

$$\tau_{li} = \frac{1}{2} C_{li} \rho_l v_{li}^2 \tag{11}$$

where the friction coefficient [4] may be approximated by

$$C_{li} = \begin{cases} \dfrac{16}{\mathrm{Re}} & \mathrm{Re} \le 1180 \\ 0.078\,\mathrm{Re}^{-0.25} & \mathrm{Re} > 1180 \end{cases} \tag{12}$$

In the energy equation for vapor plug

$$m_{vi} C_v \frac{dT_{vi}}{dt} = \left(\dot{m}_{in,vi} - \dot{m}_{out,vi} \right) R T_{vi} - P_{vi} A \frac{dX_{vi}}{dt} \tag{13}$$

Using the ideal gas equation can determinate the pressure of vapor plug. In the final energy equation, for liquid slug, it can be solving and determinate heat transfer between the tube wall and the liquid slugs.

$$\frac{1}{\alpha_{li}} \frac{dT_{li}}{dt} = \frac{d^2 T_{li}}{dX^2} - \frac{h_{li} \pi d}{k_l A} \left(T_{li} - T_w \right) \tag{14}$$

Where the boundary conditions of the liquid slug temperature is:

$$\begin{aligned} X &= X_{re,i} \quad ; \quad T_{li} = T_{vi} \\ X &= X_{le,(i+1)} \quad ; \quad T_{li} = T_{v(i+1)} \end{aligned} \tag{15}$$

The convection heat transfer coefficient (h_{li}) of liquid slug is calculated within three regimes, i.e. laminar, transient and turbulent regions. For small Reynolds, laminar regime, Nusselt number is considered as thermally developing Hagen-Poiseuille flow

Laminar regions $\left|\mathrm{Re}\right| < 2200$

$$Nu = \frac{1}{4L_l^*} \ln\left(\frac{1}{\theta_m^*} \right) \tag{16}$$

where $$\theta_m^* = 8 \sum_{n=0}^{\alpha} \frac{G_n}{\lambda_n^2} \exp\left(-2\lambda_n^2 L_l^* \right) \tag{17}$$

$$L_l^* = \frac{L_{li}/d}{\mathrm{Re}_d\,\mathrm{Pr}} \tag{18}$$

The eigenvalues, λ_n, and the constants, G_n, can be found in Bejan., [2].

Transition regions $2200 < \left|\mathrm{Re}\right| < 10000$

$$Nu = 0.012\left(\left|\mathrm{Re}\right|^{0.87} - 280 \right) \mathrm{Pr}^{0.4} \left(\frac{\mu_{li}}{\mu_w} \right)^{0.11} \left[1 + \left(\frac{d}{L_{li}} \right)^{2/3} \right] \tag{19}$$

Turbulent regions $\left|\mathrm{Re}\right| > 10000$

$$Nu = 0.0236 \left|\mathrm{Re}\right|^{0.8} \mathrm{Pr}^{0.43} \left(\frac{\mu_{li}}{\mu_w} \right)^{0.25} \tag{20}$$

Heat transfer in the CLOHP is defined as the total heat transferred from the evaporator sections to the condenser sections. It can be divided into 2 parts, first the heat transfer is due to the evaporation and condensation of the working fluid at vapor phase. So the heat transferred into and out of the vapor plug is

$$\dot{Q}_{in,vi} = \dot{m}_{in,vi} h_{fg} \tag{21}$$

$$\dot{Q}_{out,vi} = \dot{m}_{out,vi} h_{fg} \tag{22}$$

Second, the heat transfer between the tube wall and the liquid slugs. The total heat transferred into and out of the liquid slug between the wall of the tube and the liquid slug is

$$\dot{Q}_{out,li} = \int_{X_{re,i}}^{X_{le,(i+1)}} \pi d h_X \left(T_{li,X} - T_w \right) dX \;;\; T_{li} > T_w \tag{23}$$

$$\dot{Q}_{in,li} = \int_{X_{re,i}}^{X_{le,(i+1)}} \pi d h_X \left(T_w - T_{li,X} \right) dX \;;\; T_{li} \le T_w \tag{24}$$

The total heat transferred into and out of the CLOHP can be defined as

$$\dot{Q}_{total,in} = \sum_{i=1}^{N} \dot{Q}_{in,vi} + \sum_{i=1}^{N-1} \dot{Q}_{in,li} \tag{25}$$

$$\dot{Q}_{total,out} = \sum_{i=1}^{N} \dot{Q}_{out,vi} + \sum_{i=1}^{N-1} \dot{Q}_{out,li} \tag{26}$$

3. NUMERICAL SOLUTION

An explicit finite difference scheme was used to solve the governing equation for the vapor and liquid phase except Eq. (5), is solved using an implicit finite difference scheme [8] by the total number of nonuniform grids chosen was 400. The time step used in all numerical simulations are

10^{-5} s because when varying the time step to 10^{-6} s the result is less than 0.3 percent in the location of the liquid slug.

The new values at time step t+Δt can be determined from the old values at time t by

$$m_{vi}^{new} = m_{vi} + \left(\dot{m}_{in,vi} - \dot{m}_{out,vi}\right)\Delta t \quad (27)$$

$$T_{vi}^{new} = T_{vi} + \frac{\left(\dot{m}_{in,vi} - \dot{m}_{out,vi}\right)RT_{vi}\Delta t - P_{vi}A\Delta X_{vi}}{m_{vi}^{new}C_v} \quad (28)$$

$$P_{vi}^{new} = \frac{m_{vi}^{new}R(T_{vi}^{new} + 273.15)}{V_{vi}^{new}} \quad (29)$$

$$m_{li}^{new} = m_{li} + \frac{1}{2}\left[\begin{array}{l}\left(\dot{m}_{in,vi} - \dot{m}_{out,vi}\right) + \\ \left(\dot{m}_{in,v(i+1)} - \dot{m}_{out,v(i+1)}\right)\end{array}\right]\Delta t \quad (30)$$

$$v_{li}^{new} = \left[m_{li}v_{li} + \left[\begin{array}{l}\left(P_{vi} - P_{v(i+1)}\right)A - \\ \pi dL_{li}\tau_{li} - m_{li}g\end{array}\right]\Delta t\right] \Big/ m_{li}^{new} \quad (31)$$

The new valves replaced the old valves and the procedure was repeated for the next time step until steady state. The locations of the vapor plug CLOHP can be known by the location of their ends.

The new position of each vapor plug in CLOHP can be defined as:

$$\begin{aligned} X_{re,i}^{new} &= X_{re,i} + v_{li}\Delta t \\ X_{le,i}^{new} &= X_{le,i} + v_{l(i-1)}\Delta t \end{aligned} \quad (32)$$

$$\begin{aligned} X_{re,i}^{new} &= X_{re,i}^{new} - L \quad ; X_{re,i}^{new} > L \\ X_{le,i}^{new} &= X_{le,i}^{new} - L \quad ; X_{le,i}^{new} > L \end{aligned} \quad (33)$$

$$\begin{aligned} X_{re,i}^{new} &= X_{re,i}^{new} + L \quad ; X_{re,i}^{new} < 0 \\ X_{le,i}^{new} &= X_{le,i}^{new} + L \quad ; X_{le,i}^{new} < 0 \end{aligned} \quad (34)$$

Where the length difference in Eq. (4) can be defined as:

$$\begin{aligned} \Delta X_{re,i} &= X_{re,i}^{new} - X_{re,i} \\ \Delta X_{le,i} &= X_{le,i}^{new} - X_{le,i} \end{aligned} \quad (35)$$

$$\Delta X_{vi} = \Delta X_{re,i} - \Delta X_{le,i} \quad (36)$$

4. RESULTS

4.1 Comparison with the existing model and experimental data

In order to verify the present model, calculation result from this model will be compared with the existing result of prediction from Shafii et al. [9] at same condition. Fig. 3(a) and 3(b) show the displacement of the right end of the first vapor plug as a function of time of present model and Shafii's model, respectively. It can be seen that the results obtained by using the present model agreed very well with Shafii's model. The present model can be, therefore correctly applied to other conditions. It is sometimes acknowledged that the oscillation phenomena of the OHP is a kind of non-linear one, but the linear from of translation is presumed in this model due to its simplicity of calculation. Moreover, the graph of predicted internal pressure at any specified time could be easily obtained from the model. The experimental results, however, cannot show since there is no pressure monitoring in our apparatus.

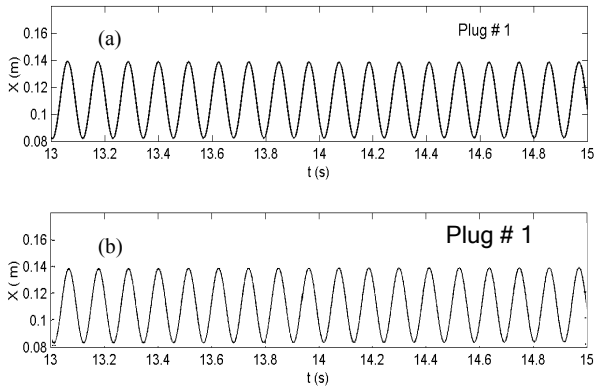


Fig. 3 Comparison of the position of first vapor plug variation with time:
(a) present model (b) Shafii et al.'s model [9]

In order to compare with existing experimental data of CLOHP [3], the following parameters are defined.

- CLOHP operate at vertical, top heating mode.
- Working fluids water, ethanol and R123.
- Evaporator length 50, 100 and 150 mm. evaporator, adiabatic and condenser lengths are kept equal in a given configuration.
- Tube inner diameter of 0.66, 1.06 and 2.03 mm.

Figure 4 shows the comparison of the predicted heat flux from the model with the experimental data at the same condition which detail of apparatus and testing condition could be seen at Charoensawan et al, [3]. It was found that the heat fluxes from prediction can loosely fit with those of the heat flux from experiment. However, all data tends to follow the trend line of one power function which implies that the present model is quite closed to reality. However, more

assumption must be made to improve the model in very near future. Corrective expression of heat flux of CLOHP can firstly be found from this comparison as;

$$q_{\exp} = 8\times10^{-5} q_{prd}^{2.335} \qquad (37)$$

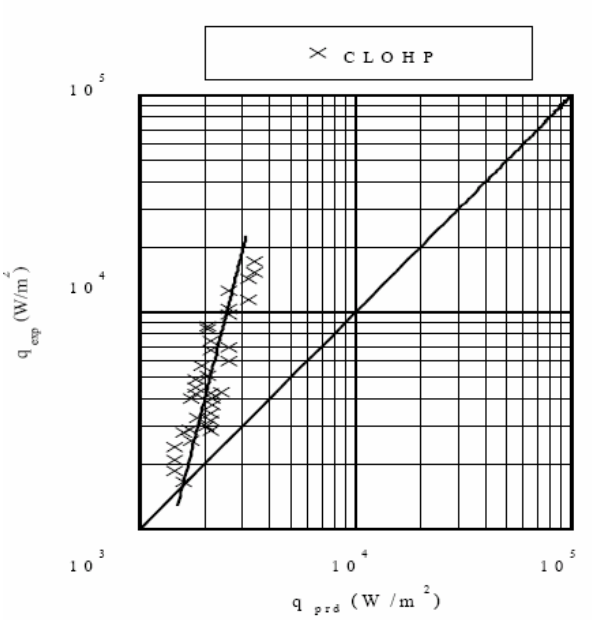


Fig. 4 Comparison of heat transfers of prediction and of experiment

After applying such corrective expressions the exact heat flux can be calculated from the heat flux of prediction of the model. The comparison of heat fluxes from the prediction and the heat fluxes from the experimental data is, again, shown in Fig. 5. It can be seen that all data trended to distribute in the exact line with the standard deviation of 23.77%. The data that exceeded the standard variation may be happened from two reasons. First, the heat flux of the OHP at top heat mode from the experiment is rather low. So the temperature difference between the coolant that flows across the condenser section compared to the accuracy of measurement is relatively small. Second, it is necessary to add more assumptions for the formulation of the mathematical model in order to correspond with the real operational condition.

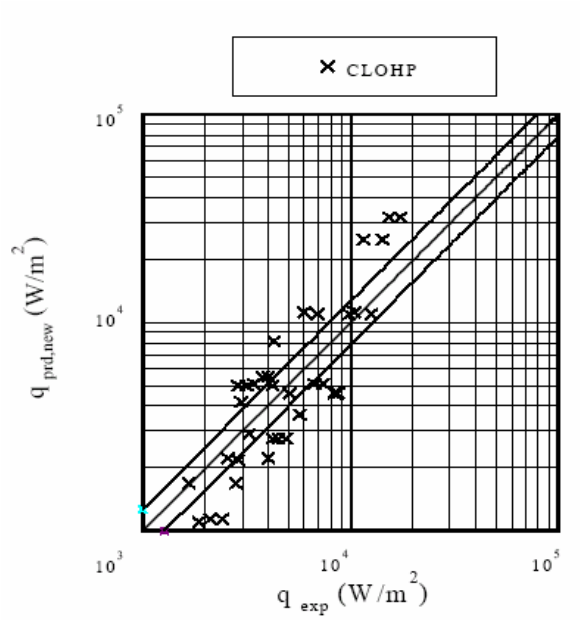


Fig. 5 Comparison of heat transfers from the new prediction and from experiment

4.2 Effect of Evaporator Length

Figure 6 shows the comparison heat flux obtained from the model and from the experiments with respect to the evaporator lengths of CLOHP and CEOHP at the same condition. The abcissa represents the evaporator length between 0 and 200 mm. It can be seen that when increasing the evaporator length, heat flux will decrease. This is because when the evaporator length is long, the amplitude of motion of vapor plug and liquid slugs will increase but the frequency will decrease. Thus the heat flux is low [3]. Moreover the heat flux of CLOHP and CEOHP are had same tend. However the heat flux of CLOHP more than heat flux of CEOHP because influence of the loop of CLOHP which can be balance pressure of both end of CEOHP

From the effect evaporator length, it can be concluded that the present model is reliable and its prediction is systematic.

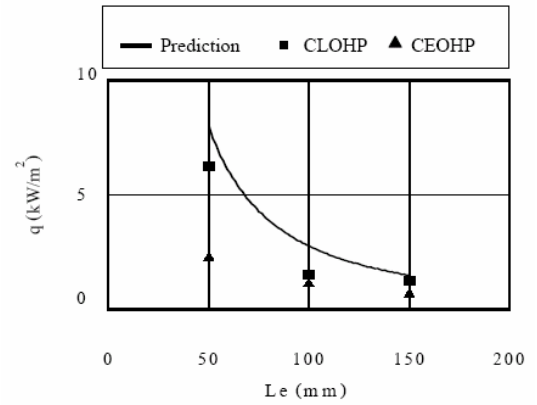


Fig. 6 Comparison of effect of evaporator length (Di of 2.03 mm, and water as the working fluid.)

4.3 Effect of Tube Inner Diameter

Figure 7 shows the heat flux obtained from the model and from the experiments with respect to the inner diameters of CLOHP and CEOHP at the same condition. The abcissa represents the inner diameter between 0 and 2.5 mm. It can be seen that with increasing the inner diameter, heat flux will increase. This is because in the case of big inner diameter, the boiling phenomena will be like the pool boiling phenomena, but in the case of small inner diameter, the boiling phenomena will be like the confined channel boiling phenomena, which its heat transfer coefficient is lower. Moreover the heat flux of CLOHP and CEOHP are had same tend. However the heat flux of CLOHP are more than heat flux of CEOHP.

From the effect inner diameter, it can be concluded that the present model is reliable and its prediction is systematic.

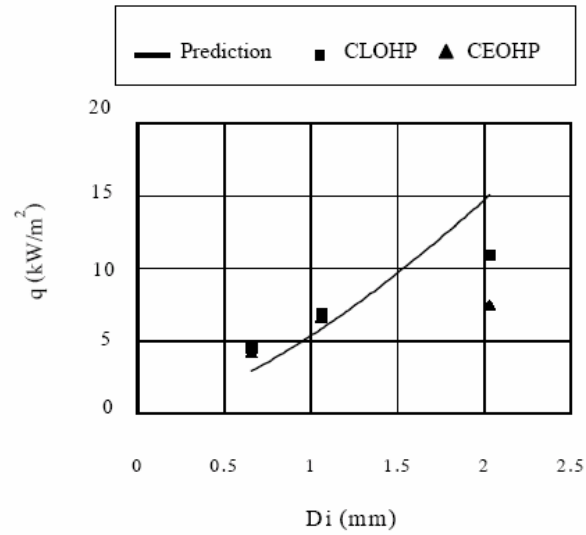


Fig. 7 Comparison of effect of inner diameter (Le of 50 mm and R123 as the working fluid)

4.4 Effect of type of Working Fluid

The main property that will represent fluid property is the latent heat of vaporization, which strongly affects the motion of liquid slug and vapor plug with in the tube and the heat transfer of the CLOHP. Figure 8 shows the heat flux obtained from the model and from the experiments with respect to the latent heat of the working fluids within CLOHP and CEOHP at the same condition. The abcissa represents the latent heat of the working fluid between 0 and 2500 kJ/kg. It can be seen that the working fluid can be arranged from the minimum heat flux to the maximum heat flux as: water, ethanol and R123. This is because when the latent heat decreases, the phase change of vapor plug in the condenser and evaporator sections becomes increasingly active. Furthermore, it can be seen that the trend of heat flux from the prediction is more than that of the experiment. This is because the heat transfer rate calculated from model results of the vaporization latent heat has an effect on the mass transfer of vapor plug and the saturated working pressure has an effect on the velocity of liquid slug. The heat transfer rate from the model increases when the vaporization latent heat decreases and the saturated working pressure increases. In fact, in practical operation, the CLOHP may be strongly affected by other properties such as velocity profile at the bends. So the heat flux of this model are loosely fit with the heat flux of experiment. Moreover the heat flux of CLOHP and CEOHP are had same tend. However the heat flux of CLOHP are more than heat flux of CEOHP.

From the effect of vaporization latent heat of the working, it can be concluded that the present model is reliable and its prediction is systematic.

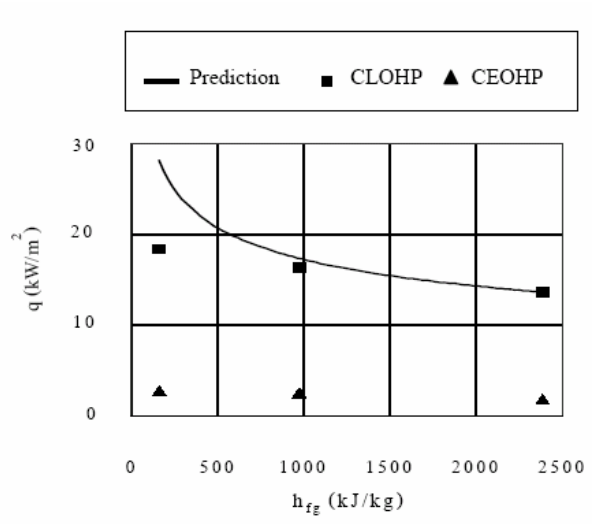


Fig. 8 Comparison of effect of latent heat of vaporization of working fluid (Le of 50 mm, Lt of 15 m, and Di of 2.03 mm)

5. CONCLUSION

By comparing the experimentally determined heat flux with theoretically determined heat flux it is seen that the theoretical model reasonably represent the behavior of the close-loop oscillating heat pipe.

Acknowledgments

This research was conducted under Thailand Research Fund (Contract No. PHD/0046/2546). The authors would like to express their sincere appreciation for all of the support provided.

Nomenclature

A	area (m^2)
C	friction coefficient
C_v	specific heat (J/kgK)
Di	inner diameter (m)
d	ordinary differential
g	gravitational constant (m/s^2)
h	heat transfer coefficient (W/m^2K)
h_{fg}	latent heat of vaporization (J/kg)
k	thermal conductivity (W/mK)
L	length (m)
La	length of adiabatic section (m)
Lc	length of condenser section (m)
Le	length of evaporator section (m)
m	mass (kg)
n	number of tube
N	number of parallel plug
Nu	Nusselt number
$\dot{Q}$	heat transfer rate (W)
P	pressure (N/m^2)
Pr	Prandtl number = $C_p\mu / k$
R	specific gas constant (J/kgK)
Re	Reynolds number = $\rho vd / \mu$
T	temperature (K)
t	time (s)
U	overall heat transfer coefficient (W/m^2K)
V	volume (m^3)
v	velocity (m/s)
X	distance (m)

Greek letters

α	thermal diffusivity (m^2/s)
Δ	difference
μ	dynamic viscosity (kg/ms)
σ	surface tension (N/m)
ρ	density (kg/m^3)
τ	shear stress (N/m^2)

Subscripts

a	adiabatic
c	cold, condenser
e	evaporator
exp	experimental value
f	friction
g	gas
h	hot
in	inlet
l	liquid
li	i th liquid plug
le	left end
out	outlet
prd	prediction value
re	right end
vi	i th vapor plug
w	wall tube
X	horizontal coordinate

Superscripts

new	new value

Reference

1. Akachi H., Polášek F. and Štulc, P., Pulsating Heat Pipe, Procs. of the 5th International Heat Pipe Symposium, Melbourne, Australia, 1996, ISBN 0-08-042842-8, pp. 208-217.
2. Bejan, B., Convection Heat Transfer, 2nd edition, John Wiley & Sons, Inc., New York, 1995.
3. Charoensawan, P., Terdtoon, P., Tantakom, P., Ingsuwan, P., and Manfred, G., Effect of Inclination Angles, Filling Ratios and Total Lengths on Heat Transfer Characteristic of A Closed-loop Oscillating Heat Pipe, Procs. of the 6th International Heat Pipe Symposium, Chiang Mai, Thailand, 2000, pp. 422-430
4. Dobson, R.T., and Harms, T.M., Lumped Parameter Analysis of Closed and Open Oscillatory Heat Pipe, Procs. of the 11th International Heat Pipe Conference, Tokyo, Japan , 1999, pp. 361-366
5. Dunn, P. D., and Reay, D. A., Heat Pipe, Pergamon Press Ltd., 3rd edition, 1982.
6. Faghri, A., Heat Pipe Science and Technology. Taylor & Francis Pub., 1995.
7. Maezawa, S., Gi, K.Y., Minamisawa, A., and Akachi, H., Thermal Performance of Capillary Tube Thermosyphon, Procs. of the 9th International Heat Pipe Conference, Albuquerque, USA. Vol. 2, 1996, pp. 791-795
8. Patankar, S. V., Numerical Heat Transfer and Fluid Flow, McGraw-Hill, New York, 1980.
9. Shafii, M.B., Faghri, A., and Zhang, Y., Thermal Modeling of Unlooped and Looped Pulsating Heat Pipes, Heat Transfer, Vol. 123, 2001, pp. 1159-1172
10. Terdtoon, P., Heat Pipe, Department of Mechanical Engineering, Chiang Mai University, Thailand, 1993.
11. Wong, T. N., Tong, B. Y., Lim, S. M., and Oci, K. T., Theorytical Modeling of Pulsating Heat Pipe, Procs. of the 11th International Heat Pipe Conference, Musashinoshi, Tokyo, Japan, 1999, pp. 378-392.

KEYWORD INDEX

Aeroponic system, 232
Air handling unit (AHU), 209
Anti-gravity, 83, 182
Aspect ratio, 88, 343
Axial grooved heat pipe, 114, 133, 209, 224

Bakery ovens, 193
Baking chamber, 193
Boiling heat transfer coefficient, 88

Capillary
    flow, 269
    limit, 114, 276
    pressure, 114
    structure, 157
Capillary Pumped Loop (CPL), 1
CDMA, 252
Combine buoyancy, 70
Combustion chamber, 193
Communication satellite, 216
Control volume, 288
Convection
    forced convection, 319
    marangoni convection, 70
    thermocapillary convection, 70
Copper
    foil plate, 294
    copper net, 294
CPU, 157, 238, 276, 282
    cooling, 238
    future thermal solution, 1
Creep Behavior, 100

Double-condenser, 151
Double-diffusive convection, 70
Dryer, 175

Electronic cooling, 282
Energy saver, 232
Enthalpy efficiency, 209
Evacuated tube solar collector (ETSC), 243
Evaporation, 94, 288
    flash evaporation, 163
Evaporator
    length, 360
    orientation, 182

Fill charge ratio, 94, 104
Fin
    aero, 209
    integral, 209
Film type heat pipe (FTHP), 294
Flat type heat pipe, 306
    flat evaporator, 157
    flat strip, 300
    micro, 269, 276

Glass-to-copper direct sealing, 243
Green house, 232
Groove
    curved triangular groove, 312
    internal, 94
    open channel, 264
    rectangular, 300

Heat control, 133
Heat exchanger
    heat pipe, 209
    loop thermosyphon, 9
    mini channel, 257
    oscillating heat pipe, 331
    remote, 204
Heat flux, 94
    critical, 169, 343
Heat of hydration, 384
Heat pipe, 75, 114, 127, 133, 140, 193, 204, 220, 238, 243 252, 257, 264
    chemical Reactor, 19
    embedded panel, 220
    family, 1
    heat exchanger, 209
    heating roller (HPHR), 199
    medium temperature, 146
Heat pump dryer (HPD), 175
Heat sink, 204, 238, 247, 252
Heat spreader, 204, 247, 269
Heat transfer, 204, 247, 319
    characteristics, 119, 127, 146, 343, 374
    characteristics at critical state
    coefficient, 104,157, 276, 325,
    condensation heat transfer coefficient, 88, 94
    limit, 282

maximum heat transfer capacity, 276
maximum heat transfer rate, 169
Heat transport
maximum heat transport capacity, 306
maximum heat transport rate, 312
High density polyethylene (HDPE), 100, 110
thermosyphon, 110
High-speed two-phase flow, 163

Imbalance test, 151
Impingement jet cooling, 257
Intermittent heat transporting device, 163
Internal flow pattern, 119, 360
Internal friction, 353

Japan Association for Heat Pipe (JAHP), 63

Laser printer, 199
Liquid-vapor interfacial shear stress, 264
Longan, 175
Longitudinal acceleration, 306
Loop heat Pipe (LHP), 1, 151, 157
application, 31
background, 31
classification, 31
startup, 182
Loop thermosyphon (LTS), 9, 83, 169, 175
closed two-phase, 104, 187
heat exchanger (LTHE), 9

Mass concrete, 348
MAXI (monitor of all-sky x-ray image), 151
Measurement method for standardization, 63
Meniscus, 114
Extended meniscus region, 288
Micro
channel, 288, 319
chip cooling, 257
flat type micron heat pipe, 269, 276
heat pipe, 269, 282, 306, 312
temperature sensor, 319
Mini channel heat exchanger (MCHE), 257
Modeling, 312
Modified Shah Method, 264, 312
Mole fraction, 140
Multi-heat source, 300

Non-condensable gas (NCG), 9, 127, 133
Number of turns, 360

Operating limit, 163
Operating temperature, 94
Oscillating heat pipe, 48, 343
closed-end oscillating heat pipe (CEOHP), 48, 331, 337, 353, 368
closed-loop oscillating heat pipe (CLOPH), 360, 373
chaotic heat pipe, CHP, 48
pulsating heat pipe (PHP), 48, 325
looped capillary heat pipe (LCHP), 1
self-exciting mode oscillating heat pipe (SEMOS), 1
oscillating capillary tube heat pipe, 348
flat plate self-oscillating heat pipe, 331
self-oscillating heat pipe heat exchanger, 331
Oscillation, 151

Permeability, 252
Phase change, 288
Pressure drop, 319
Publications, 63

Radially rotating heat pipe (RRHP), 119
Radius of curvature, 114

Solar domestic hot water system (SDHWS), 187
Space application, 151, 220, 224
Start-up, 151
Steady-state behavior, 157
Surface tension gradient flow, 70
Switching valve, 83
System on chip (SOC), 1, 276

Tensile strength, 110
Thermal characteristics, 88
Thermal crack, 348
Thermal optimization, 312
Thermal resistance, 104, 140
Thermosyphon, 75, 83, 94, 193, 232
gas assisted oven, 193
two-phase closed, 88, 331
theoretical model, 75
Thin packaging, 282
Top heating, 83, 373
Two-phase thermal control system, 216
active, 216

Vaccum diffusion welding, 294
Variable conductance heat pipe, 127, 133
Vapor accumulation, 163
Vapor chamber, 204, 247

Visualization, 119, 163, 337, 353, 360
flow patterns, 337, 353

Wall temperature profile, 169
Waste heat recovery, 9
Water spray, 209
Wetting angle, 114
Working fluid, 127,146, 360
ammonia, 325
binary mixture, 140
dowtherm-A, 146
ethanol-water, 140
fluorinated Ethers Refrigerant, 331
HFE (Hydrofluoroether), 331
non-CFC refrigerant blend, 343
water, 75, 133

AUTHOR INDEX

Akachi, H., 331
Akbarzadeh, A., 9, 257, 368
Andrews, J., 9
Anuchitchanchai, P., 343
Attabhanyo, R., 353

Baek, B.J., 238
Bartenev, V., 216
Baungartner, R., 193
Bintoro, J.S., 257
Boo, J.H., 140, 243, 300
Booddachan, K., 100, 110
Byun, G.S., 114
Byun, Y.S., 209

Cao, J., 182, 224
Chang, K.C., 146
Charoensawan, P., 360
Cho, D.H., 94
Choi, J.S., 220
Choi, S.G., 209
Chun, W.G., 187
Chung, K.T., 133
Chung, W.B., 140, 243

Do, K.H., 264, 312
Dobson, R.T., 325
Dorokhov, V., 216
Dube, V., 9
Dvirnyi, V., 216

Feroz, C., 169

Gi, K., 331
Graf, G., 325
Gruzdova, N.L., 156

Ha, S.J., 348
Han, K.I., 94
Homma, Y., 276, 306
Hong, J.K., 209
Hosoya, N., 276
Hou, Z., 182
Hung, B.N., 348
Hwang, G., 282

Ichinomiya, T., 83
Imura, H., 83, 247
Ingsuwan, P., 360

Jalilvand, A., 306
Jang, Y.S., 146
Jompakdee, W., 337, 353
Jung, E.G., 140
Jung, J.Y., 319

Kadoguchi, K., 163
Kalaei, M.H., 88
Kaminaga, F., 169
Kamonpet, P., 100, 110, 119, 175, 232, 337, 343, 353, 360, 368, 373
Kang, C.H., 114
Kang, M.C., 187
Kang, S.W., 294
Kang, Y.H., 187
Karng, S.W., 319
Katoh, T., 331
Katpradit, T., 368
Katsuta, M., 1, 276, 306
Khoshnoodi, M., 88
Kim, C.J., 104
Kim, H.B., 199
Kim, J.H., 348
Kim, J.R., 146
Kim, J.S., 348
Kim, K.S., 156, 199
Kim, M.S., 348
Kim, S.J., 264, 312
Kim, T.H., 348
Kim, Y.T., 282
Kimura, Y., 276
Kiseev, V.M., 156
Klongpanich, W., 175
Ko, S.C., 282
Kobayashi, Y., 100, 110
Koito, Y., 83, 247
Kwak, H.Y., 140, 243
Kwak, H.Y., 319

Lallemand, M., 269
Landa, H.G., 193
Lee, J.H., 70

Lee, K.J., 127
Lee, K.S., 288
Lee, K.W., 127, 133, 199
Lee, K.W., 199
Lee, S.H., 94
Lee, S.P., 220
Lee, W.H., 127
Lee, Y.P., 319
Lee, Y.S., 146
Lefevre, F., 269
Li, T., 224
Lin, Y.H., 294
Loganov, A., 216
Lopes, A., 193
Lv, W., 224

Maezawa, S., 119, 331
Mantelli, M.B.H., 193
Martins, G.J.M., 193
Mashiko, K., 204
Matsumoto, S., 63
Matsumura, K., 169
Matsuoka, M., 151
Maydanik, Y., 31
Mi, M., 224
Miao, J., 224
Mochizuki, M., 9, 204, 247, 257
Moon, S.H., 282
Moon, W.S., 238
Motomatsu, K., 247
Murakami, M., 151, 337, 373
Muto, M., 151

Nagai, H., 151
Nakamura, Y., 276
Nepomnyashy, A.S., 156
Nguyen, T., 204, 257
Nguyen, T., 204
Noie, S.H., 88

Ohyama, T., 232
Ong, K.S., 75

Pak, B.C., 238
Park, J.H., 220
Park, J.U., 94
Park, K.H., 127, 133
Park, K.W., 288
Park, S.Y., 300
Park, Y.J., 104
Park, Y.S., 133
Phaphuangwittayakul, W., 175
Preechawuttipong, I., 100

Raghavan, G.S.V., 175
Revellin, R., 269
Rittidech, S., 337
Ruamrungsri, S., 232

Saito, Y., 204, 247
Sakiura, J., 331
Sakulchangsatjatai, P., 373
Seo, J.K., 264, 312
Shao, X., 224
Shindo, T., 276
Sotani, J., 276
Srihajong, N., 232, 353
Suh, J.S., 114, 127, 133
Sutjaritakul, T., 110

Tao, H., 252
Terdtoon, P., 48, 100, 110, 119, 175, 232, 337, 343, 353, 360, 368, 373
Tsai, M.C., 294

Ueno, S., 151

Vorayos, N., 175

Wang, Z., 19
Waowaew, N., 119
Watanabe, H., 169
Won, M.H., 238
Wongratanapaisarn, T., 119, 243, 368, 373
Woo, H.J., 220
Wu, X.P., 204
Wuttijumnong, V., 204

Yamamoto, T., 63
Yamazaki, M., 163
Yamazaki, N., 331
Yang, H., 224
Yang, K.O., 209
Yoo, B.O., 104

Zhang, H., 19, 252
Zhuang, J., 19, 252
Zimmerman, R., 193

HEAT PIPE TECHNOLOGY
Theory and Applications

ISBN 89-950046-3-0 93520